A Theoretical and Experimental Investigation of a Photochromic RAFT Agent and the Photoiniferter Effect

by

Oskar Majewski

Thesis
Submitted to Flinders University
for the degree of

Doctor of Philosophy

College of Science and Engineering

9 / 3 / 2019

Abstract

Reversible Fragmentation Chain Transfer (RAFT) polymerisation is increasingly utilised in research and industrial applications due to its ability to polymerise monomers with diverse reactivity and functionality across a wide range of polymerisation conditions with both conventional and photoinitiator systems. Two key limitations exist; tailoring the class of RAFT agent to the reactivity of the monomer being polymerised and polymerising monomers of sequentially lower reactivity during block copolymer synthesis.

In this thesis, the feasibility of a model photochromic RAFT agent whose reactivity towards radical addition and fragmentation can be switched remotely through a photoswitchable Z group was explored.

Density Functional Theory level quantum chemical studies showed that spirooxazine based RAFT agents (xanthate and dithiocarbamate) displayed changes to both their LUMO energy levels and electron density within the RAFT moiety, indicating potential changes in reactivity. Thermodynamic parameters used to qualitatively predict RAFT agent reactivity based on *ab initio* theory confirmed that the closed and open states of both spiro-RAFT compounds will have different reactivity towards radical addition and fragmentation, enabling controlled polymerisation of Less Activated Monomers (LAMs) and More Activated Monomers (MAMs) respectively.

A novel spirooxazine based xanthate (spiro-XEP) and its non-photochromic analogue (PXEP) were synthesised and tested in the polymerisation of methyl acrylate (MA), a typical MAM and vinyl acetate (VAc) a typical LAM under typical RAFT conditions both with and without UV irradiation.

The rate of MA polymerisation in the dark initiated by AIBN was the same for both PXEP and spiro-XEP. Irrespective of the presence of AIBN, with UV irradiation the polymerisation rate of MA increased by 10x and 2.67x for PXEP and spiro-XEP, respectively. Good agreement between the expected and obtained molecular weights and narrow dispersities ($D < 1.25$) were obtained with both RAFT agents, indicating control was maintained. Chain extension kinetics with a spiro-XEP macroinitiator replicated these trends, demonstrating living characteristics and that the main RAFT equilibrium reaction dominated polymerisation behaviour.

For VAc polymerisation with PXEP under UV irradiation, an enhancement was observed but it was only 1.15x higher than the AIBN alone. With spiro-XEP severe rate retardation was seen, only being 2% that obtained with PXEP under equivalent dark conditions. Furthermore, the polymerisation rate did not change with UV irradiation. In both cases there was good agreement between expected and obtained molecular weights, with dispersities being narrower with spiro-XEP. Solutions containing

spiro-XEP underwent a series of colour changes when in the presence of UV and/or thermally generated radicals species. For polymerisations, the intensity of the colour changes depended on the monomer used and conversion attained. The evidence suggests that these colours arise due to radical reactions with the spiro-XEP compound which are non-reversible in nature.

Modelling the polymerisations of MA and VAc with PXEP in Predici revealed that for MA the dominant photolysis pathway and thus primary source of initiating radicals was the reversible photolysis of RAFT capped species, whilst for VAc it was the photolysis of AIBN. Under UV irradiation the model revealed that for both polymerisation systems the RAFT mechanism was responsible for molecular weight and dispersity regulation, with no evidence of propagation from the thiyl radical generated through the photolysis of RAFT species.

Finally, the limitations on leveraging the photoiniferter effect to synthesise block copolymers with block orders that are "forbidden" by the RAFT process was investigated. This involved the synthesis of copolymers with blocks comprised of methyl methacrylate (MMA), styrene (Sty), MA, and VAc. A variety of RAFT agents with identical R groups including PXEP, spiro-XEP and a trithiocarbonate were used to investigate the effect of RAFT agent class. Initiation systems ranging from a combination of conventional thermal initiation and purely photoinitiated systems, including different monomer orders, were tested to find the limits of this approach. It was found that PXEP was the superior RAFT agent in all cases and that only moderate reversals against the conventional block order were possible. Furthermore, dilute reaction mixtures featuring lower concentrations of initiating species gave superior consumption of starting macroinitiators and narrower molecular weight distributions.

Declaration

I certify that this thesis does not incorporate without acknowledgment any material previously submitted for a degree or diploma in any university; and that to the best of my knowledge and belief it does not contain any material previously published or written by another person except where due reference is made in the text.

Oskar Majewski, Bachelor of Science (Honours) (Nanotechnology)

Date: 9 / 3 / 2019

Table of Contents

Table of Figures

Table of Equations

Table of Schemes

Table of Tables

Glossary

AIBN	2,2’-azobisisobutyronitrile
AT	Atom – Transfer
ATRP	Atom Transfer Radical Polymerisation
CSIRO	Commonwealth Scientific and Industrial Research Organisation
CTA	Chain Transfer Agent
DC	Dissociation – Combination
DECET	S-1-dodecyl-S’-((2-ethoxycarbonyl)-ethyl) trithiocarbonate
DFT	Density Functional Theory
DT	Degenerative Chain Transfer
EDTS	Energy-Directed Tree Search
FRP	Free Radical Polymerisation
GPC	Gel Permeation Chromatography
HOMO	Highest Unoccupied Molecular Orbital
Iniferter	Initiator Transfer Terminator
LAM	Less Activated Monomer
LED	Light Emitting Diode
LRP	Living Radical Polymerisation
LUMO	Lowest Unoccupied Molecular Orbital
MA	Methyl Acrylate
MADIX	Macromolecular Design via Interchange of Xanthates
MAM	More Activated Monomer
MMA	Methyl Methacrylate
Mn	Number average molecular weight
Mw	Weight average molecular weight

NMP	Nitroxide Mediated Polymerisation
NMR	Nuclear Magnetic Resonance
NVC	N-Vinylcarbazole
NVP	N-Vinylpyrrolidone
PXEP	2-((phenoxycarbonothioyl)thio) ethyl propanoate
RAFT	Reversible Addition Fragmentation Chain Transfer
RDRP	Reversible Deactivation Radical Polymerisation
RSE	Radical Stabilisation Energy
Spiro-XEP	9'-((ethyl 2-propanoate carbonothioyl) thio)-1,3,3-trimethyl-spiro[indoline-2,3'-[3H]naphtha[2,1-b][1,4]oxazine]
Sty	Styrene
TCT	Thiocarbonyl thio
UV	Ultraviolet
UV-Vis	Ultraviolet – Visible
VAc	Vinyl Acetate

Acknowledgements

First and foremost, I want to acknowledge and thank my supervisor Prof. David Lewis; without your guidance and support this project simply would not have come into being. By allowing me to decide my own problem to investigate along with the decision to pursue a rather unconventional and challenging solution ultimately lead to the extraordinary journey that has been this PhD. I have learned an incredible amount from you regarding how to approach problems, how to know if I am asking the right questions, and most of all, how to manage the uncertainty that comes with being a research scientist. To my co-supervisor Prof. Jamie Quinton, thank you for all the help and moral support over the years. Your ability to listen patiently and give constructive, non-judgemental and practical advice helped me many times, and for that I am grateful.

I feel incredibly privileged to have worked with both Dr. Graeme Moad and Prof. Michelle Coote. Michelle, your enthusiasm and willingness to contribute to the quantum chemistry within this thesis gave me and this project much needed encouragement early on. Graeme, thank you for sharing your wealth of polymer knowledge, for facilitating my use of the Predici software, and for your concise and direct feedback. A big thank you to Dr. Guoxin Li for taking the time to run polymer samples through the GPC, without which the last chapter of this thesis would have been impossible. Thank you also to Dr. Greg Simpson who was instrumental in introducing me to the wonderful people at CSIRO.

Thank you also to Dr. Daniel Keddie and Dr. Richard Evans for your help in getting this project underway with practical suggestions and discussions, especially early on when I was lacking direction. Thank you to Assoc. Prof. Martin Johnston for training me on the Spartan modelling software and for help with NMR experiments. To all the members of the Lewis research group and colleagues in the College of Science and Engineering; thank you for all your feedback, your support, and your friendship. A big thank you to all the library staff who were instrumental in delivering the papers from obscure journals I often requested.

This PhD would have been impossible without the unwavering love and support of my parents, Anna and Dariusz. Thank you for believing in me, especially when I doubted myself. To Dr. Sian La Vars, I feel privileged that we could share this journey together. I am eternally thankful that we were there for each other through the highs and the lows.

This work has been supported by the CSIRO through a Top Up Scholarship.

Publication List

Journal articles

A manuscript based on the combined work presented in Chapters 3 and 7 is in preparation.

A manuscript based on the combined work presented in Chapters 5 and 6 is in preparation.

A manucript based on the work presented in 8 is in preparation.

Oral Presentations

Oskar Majewski, Daniel J. Keddie, Michelle Coote, David A. Lewis, *Exploring the impact of UV irradiation on traditional RAFT systems*, 36th Australasian Polymer Symposium, Lorne, Australia (2016).

Oskar Majewski, Daniel J. Keddie, Michelle Coote, David A. Lewis, *Exploring the capabilities of novel photochromic RAFT agents with photoswitchable reactivity*, The International Chemical Congress of Pacific Basin Societies 2015, Hawaii, USA (2015). Awarded best student presentation at the symposium titled "Advances in Precision Polymer Synthesis Using Reversible Deactivation Radical Polymerisation".

Oskar Majewski, Daniel J. Keddie, Michelle Coote, David A. Lewis, *Towards RAFT agents with photoswitchable reactivity*, 35th Australasian Polymer Symposium, Gold Coast, Australia (2015).

Oral presentations listed below are based on work undertaken during this PhD however are outside the scope of this thesis.

Oskar Majewski, Daniel Mangos, David A. Lewis, *Elucidating the structure and function of silica nanoparticles directly functionalized with chain transfer agents for use in RAFT polymerisation*, Royal Australian Chemical Institute (RACI) National Congress 2014, Adelaide, Australia (2014).

Oskar Majewski, Daniel Mangos, David A. Lewis, *A Simple and Facile Approach to Functionalizing Silica Nanoparticles for use in RAFT Polymerisation to Make Functional Polymer-Hybrid Nanoparticles*, ICONN 2014 International Conference of Nanoscience and Nanotechnology, Adelaide, Australia (2014).

Poster Presentations

Oskar Majewski, Graeme Moad, David A. Lewis, *Discerning the influence of the photo-iniferter effect on RAFT polymerisation – experimental and modelling approaches*, Flinders Institute for Nanoscale Science and Technology 7th Annual Conference, Adelaide, Australia (2017).

Oskar Majewski, David A. Lewis, Jamie Quinton, Daniel Keddie, Greg Simpson, Richard Evans, Michelle Coote, *Towards the design, synthesis and testing of light switchable agents for Reversible Addition Fragmentation Chain Transfer (RAFT) polymerisation*, Flinders Institute for Nanoscale Science and Technology 3rd Annual Conference, Adelaide, Australia (2013).

Oskar Majewski, Jamie Quinton, David A. Lewis, *Towards novel light sensitive agents for RAFT polymerisation*, Flinders Institute for Nanoscale Science and Technology 2nd Annual Conference, Adelaide, Australia (2012).

The poster presentation listed below is based on work undertaken during this PhD however this work is outside the scope of this thesis.

Oskar Majewski, Daniel Mangos, David A. Lewis, *Elucidating the structure and function of silica nanoparticles directly functionalized with chain transfer agents for use in RAFT polymerisation*, Flinders Institute for Nanoscale Science and Technology 4th Annual Conference, Adelaide, Australia (2014).

1 Introduction

1.1 Project Context

Thiocarbonyl thio (TCT) compounds can function as chain transfer agents (CTAs) in free radical polymerisations, with this process being called Reversible Addition Fragmentation Chain Transfer (RAFT) polymerisation. Owing to their unique structure, upon irradiation at the appropriate wavelength of light they can also undergo initiation, transfer and termination, with this process termed photoiniferter polymerisation.

Despite their broad applicability in both techniques, this does not make TCT compounds universal polymerisation control agents; both polymerisation mechanisms impose limitations on which TCT compounds can be used. In RAFT, specific classes of TCT compounds must be employed in the polymerisation of vinyl monomers with disparate reactivities and the order of block placement in block copolymer synthesis is restricted. To date, no truly universal RAFT agent which can control the polymerisation of all vinyl monomers exists. The development of such an agent is highly desirable due to it streamlining the RAFT process and potentially allowing the synthesis of block copolymers where the blocks are made from monomers of dissimilar reactivity.

In photoiniferter polymerisations, the control obtained over both polymerisation kinetics and the final polymers formed is typically inferior to RAFT polymerisation. Recent advances in the selection of TCTs, reaction conditions including a trend towards lower energy light sources, have led to significant improvements in this field. Regarding the use of TCTs in a photoiniferter context, the relative contribution of the RAFT and photoiniferter mechanisms to the control of the polymerisation process remains unknown.

The primary objective of this research is to investigate the design, synthesis and testing of a RAFT agent with a photoswitchable Z group to potentially allow its reactivity in the RAFT process to be modulated by light. The potential consequences of irradiation leading to the photoiniferter mechanism and its impact on the polymerisation process are also investigated, along with how the photoiniferter effect can be subsequently used in overcoming the limitations of block copolymer synthesis imposed by the RAFT mechanism.

1.2 Project Aims

- To design RAFT agents with photochromic Z groups that change structure upon irradiation to influence the reactivity of the RAFT moiety, and to test the validity of such a concept *via* quantum chemical calculations
- To synthesise a photochromic RAFT agent and test it in the RAFT polymerisation of monomers with disparate reactivities, namely methyl acrylate and vinyl acetate, under both tradiational RAFT and photoiniferter polymerisation conditions
- To explore how the photoiniferter process potentially influences a photochromic RAFT agent by testing and comparing a non-photochromic analogue via experimental and modelling methods
- To test if a photochromic RAFT can overcome the limitation of needing to polymerise monomers of sequentially greater reactivty (thus generating more stable radicals) in block copolymer synthesis as dictated by the RAFT mechanism, and to determine whether this is a result of a fundamental change in the reactivity of the RAFT agent or simply the result of the photoiniferter mechanism
- To investigate how monomer and RAFT agent class along with the initiation mechanism influence the photoiniferter process as applied to block copolymer synthesis

1.3 Thesis Structure

Chapter 2: An introduction to the mechanisms and kinetics governing free radical polymerisation and reversible deactivation radical polymerisation processes is provided. The RAFT process is explored in detail, including its advantages and disadvantages, how they arise mechanistically, their consequences regarding RAFT agent design and selection for certain monomer classes, application of reaction conditions and the synthesis of block copolymers. Alternative approaches that have been employed to overcoming these limitations are explored in detail. Due to certain unanswered aspects of the photoiniferter mechanism with TCT compounds, this is explored in detail after the kinetic basis for free radical polymerisation and the RAFT process have been covered. The inherent similarities between the two methods, relevant points of overlap along with their potential implications for the influence of side reactions and practical considerations are also explored. A general introduction to photochromism, the main families of photochromic molecules and the prior application of spirooxazines in polymer science is briefly covered due to the vast scope of this field. A general introduction to quantum chemistry is provided, along with a detailed explanation of the process for

the *in silico* assessment of a range of RAFT agents. This includes the thermodynamic parameters computed and their mechanistic significance. A brief introduction to the Predici modelling program is given, including its application to the modelling and investigation of the RAFT process and its application to other areas of polymer science is also briefly covered. General synthetic approaches to the synthesis of both RAFT agents and spirooxazines are briefly covered under the relevant sections. Finally, the practical aspects of the characterization of the polymerisation process and the polymer products obtained is covered. This includes commonly employed analytical techniques, their underlying principles, method of operation, advantages, limitations and complementary nature.

Chapter 3: This chapter deals with the design strategy and rationale behind a new family of photochromic spirooxazine based RAFT agents. Several of these compounds are then evaluated at both *ab initio* and DFT levels of computational theory, including calculations of a series of thermodynamic descriptors of RAFT agent activity. The DFT calculations explore interesting trends in the computed properties based on patterns of RAFT agent substitution and establish the necessity for further exploration of this concept at a higher level of computational assessment. Thermodynamic descriptors were computed for two photochromic spirooxazine based RAFT agents where the difference lies in the position of the RAFT moiety on the parent spirooxazine. These are compared to several RAFT agents examined previously within literature and confirm that on this theoretical basis the synthesis and testing of these photoswitchable RAFT agents is worth pursuing experimentally. The computational procedures for both levels of theory are also covered here.

Chapter 4: This chapter summarises all the procedures utilised throughout the experimental sections of this thesis, including the synthesis of various RAFT agents, synthesis and chain extension of a range of RAFT polymers, RAFT and photo-RAFT polymerisation conditions, purification, isolation and characterization of both polymer and non-polymer products. This includes the successful synthesis of a photochromic xanthate and progress towards a photochromic dithiocarbamate.

Chapter 5: This chapter details the experimental and theoretical investigation of the photoiniferter effect as applied to the polymerisation of methyl acrylate (MA) under conditions optimised for the RAFT process. MA is polymerised under 3 sets of conditions, which are also applied to the chain extension of a poly(MA) macro-RAFT agent. To elucidate the mechanistic origins of the experimental phenomena seen, a comprehensive Predici model that includes all the features of conventional free radical polymerisation, the RAFT equilibrium and a range of potential photolysis effects was constructed. Several possible photolysis scenarios are presented by means of sensitivity analysis of the model to the parameters for the respective phenomena. These include the effect of photolysis of the conventional free radical initiator AIBN, direct radical generation within the reaction

mixture by photolysis of monomer and the core photoiniferter principle, namely the reversible photolysis of the RAFT agent. The simulated results are critically analysed on their realistic probability by comparison to literature precedent for the parameters used and by comparing the model output to the experimental phenomena seen. Furthermore, the relative importance of degenerative chain transfer within photoiniferter polymerisation under these conditions is explored; this is accomplished by selectively deactivating these reactions within the Predici model.

Chapter 6: This chapter details the experimental and theoretical investigation of the photoiniferter effect as applied to the polymerisation of vinyl acetate (VAc) under conditions optimised for the RAFT process. As for the MA case in the previous chapter, VAc is polymerised under 3 sets of conditions, which are also applied to the chain extension of a poly(VAc) macro-RAFT agent. The same Predici model from the previous chapter is used, appropriately adjusted for the different reaction conditions and kinetic parameters implemented. The modelling scenarios and subsequent analysis is repeated, with particular attention paid to the drastically different behaviour of VAc polymerisation seen under UV irradiation as compared to MA polymerisation. Theories for the vast differences seen between the two monomers are put forth and explored further in the modelling.

Chapter 7: This chapter details the systematic testing of a novel photochromic spirooxazine based xanthate. This includes kinetic testing under identical conditions to the kinetic investigations undertaken in chapters 5 & 6 with the non-photochromic xanthate analogue. The living characteristics of several of the polymers created with this RAFT agent are confirmed under various experimental conditions, and the potential significance and mechanistic implications of the colour changes seen is probed, with several potential explanations put forth.

Chapter 8: This chapter explores the potential for a photochromic xanthate to be used in the synthesis of block copolymers with the monomer sequence running contrary to that which is traditionally allowed by the RAFT mechanism. This concept is explored further *via* the photoiniferter technique using the non-photochromic xanthate and a commonly used trithiocarbonate. The effect of utilising a range of light sources with different emission wavelengths and monomers of different reactivities is investigated. This gives further insight into the influence of the degenerative transfer mechanism that operates in both RAFT and photoiniferter polymerisations conducted with TCT compounds, and how this fundamentally suggests that certain limits on monomer sequence control cannot be overcome by employing a photolysis-based reaction.

Chapter 9: This is a summary which re-iterates the key findings as established throughout this thesis. followed by a short statement outlining the prospects for future work with the concepts, compounds and approaches explored throughout this thesis.

2 Literature Review

2.1 Free Radical Polymerisation

2.1.1 Historical Context

Free radical polymerisation (FRP) has become of great commercial interest in the past half century due to its utility in creating large quantities of high value polymer products to suit an incredibly diverse range of applications. Aerospace, automotive, defence, medical and consumer goods now commonly contain high percentages of polymer materials [1]. The ability to control polymer properties arises through the careful selection of monomers, reaction conditions and a plethora of additives such as thermal stabilisers, antioxidants, cross linkers and plasticizing agents [2]. Furthermore, compared to anionic and cationic polymerisation methods which are extremely sensitive to reagent purity and reaction conditions, FRP processes show remarkable tolerance to reagent impurities and reaction conditions including the ability to conduct polymerisations in aqueous media [3]. Despite all these advantages, there are fundamental limitations bought about by aspects of the FRP mechanism that have by necessity lead to the development of reversible deactivation radical polymerisation (RDRP) techniques which impart "living" characteristics to the FRP process [4]. Fundamentally, regardless of the RDRP method, the goals of all RDRP techniques has been to give polymer scientists the ability to control, with as much precision as possible, the molecular architecture of the polymers formed. This includes overall polymer structure (linear, branched, dendritic, brush, crosslinked etc), monomer composition (multiblock synthesis) chain end functionality, targeted molecular weight and a narrow dispersity of the molecular weight distribution. Historically this has resulted in the development of the 5 main RDRP techniques; the Iniferter process in 1982 [5], nitroxide mediated polymerisation (NMP) in 1984-85 [4], Atom Transfer Radical Polymerisation (ATRP) in 1995 [6], Reversible Addition Fragmentation Chain Transfer (RAFT) in 1998 [7] and Macromolecular Design via Interchange of Xanthates (MADIX, often considered a subset of the RAFT technique) also in 1998 [8]. Collectively the RDRP techniques now dominate research in polymer science; however, despite their many advantages over FRP there are still fundamental limitations arising from their respective mechanisms that need to be overcome.

2.1.2 Kinetics and Mechanisms of Free Radical Polymerisation (FRP) Processes

An understanding of the mechanisms and kinetics underpinning the FRP process is essential before adding the complexities of the RDRP techniques discussed above. Historically, a lot has been

published in this area, from Flory's pioneering work [9] in 1953 to the present day [10-14]. As nomenclature of kinetic rate coefficients and kinetic definitions can vary between publications, the most commonly employed nomenclature has been used, with notation chosen such as to not conflict with rate coefficients used later in this thesis. Despite the underlying approximations of the the steady state assumption and the fact that under certain conditions it is not strictly applicable; as it is standard practice within the literature it has also been used here. It nevertheless works very well for describing most FRP processes [11] and simplifies the mathematical description significantly. In summary, these are the general assumptions underpinning the kinetic analysis explained in the following sections:

- That all kinetic rate coefficients are independent of chain length and conversion.
- That there is an instantaneous establishment of a steady-state free radical concentration, meaning that radical pairs are created at the same rate at which they are destroyed.
- That the monomer (M) consumed as the reaction progresses is only due to chain propagation and not due to the initiation process or to chain transfer reactions. This is important as it allows the rate of monomer consumption to be equated directly with the rate of polymerisation.
- That all reactions are irreversible in nature, i.e. depolymerisation does not occur.
- That the effective concentration of initiator derived free radicals is essentially constant over the course of the polymerisation.

For explanations of the kinetics of pseudo-stationary and non-stationary polymerisation systems as they apply to pulsed laser polymerisation and other unique systems, please refer to [11] and [15].

2.1.2.1 Initiation

The definition of initiation is the generation of primary radicals (I*) that then add to the carbon-carbon double bond of the monomer (M), which leads to the formation of initiating radicals (M*) in the proceeding step. The process is summarised in Scheme 2.1.

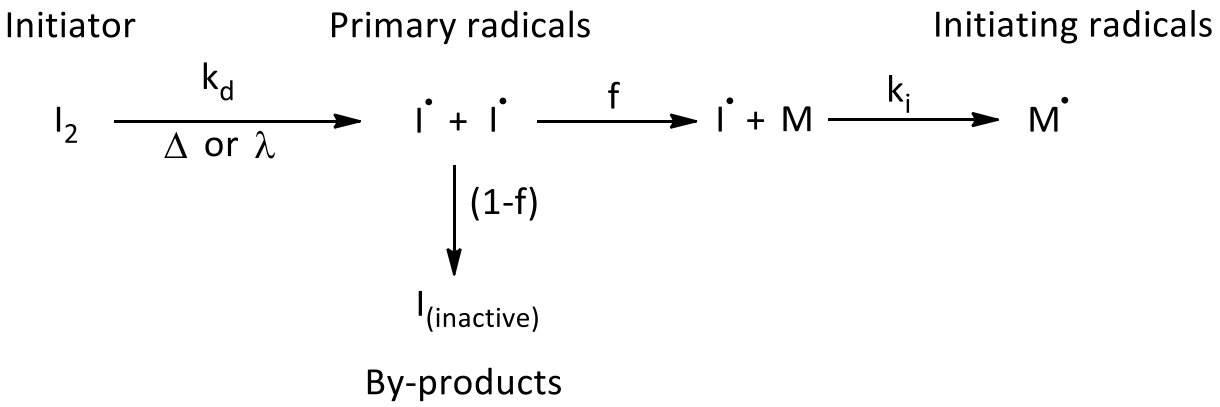

Scheme 2.1: Summary of pathways operating during the dissociation of a radical initiator.

When sufficient energy is provided to a radical initiator (I_2) a pair of primary radicals is created and this occurs with the rate coefficient for dissociation, k_d. This mechanism for the initial generation of primary radicals is applicable to both thermal and photochemical pathways, with the rate of initiator disappearance (R_{Id}) being described by Equation 2.1:

$$R_{Id} = -\frac{d[I_2]}{dt} = k_d \cdot [I_2]$$

Equation 2.1: Rate equation for decrease of initiator concentration.

Integration of Equation 2.1 yields Equation 2.2 that describes the decreasing concentration of initiator $[I_2]$ as a function of time (t) at a given temperature, starting from an initial initiator concentration of $[I_2]_0$.

$$[I_2] = [I_2]_0 \cdot e^{-k_d \cdot t}$$

Equation 2.2: Integrated rate equation for decrease of initiator concentration.

From Equation 2.1 and Scheme 2.1, another key relationship can be derived; the rate of generation of primary radicals which can then initiate polymerisation. This is defined as R_g and shown in Equation 2.3.

$$R_g = \frac{d[I^*]}{dt} = -2 \cdot f \cdot \frac{d[I_2]}{dt} = 2 \cdot f \cdot k_d \cdot [I_2]$$

Equation 2.3: Rate equation for the generation of primary radicals capable of initiating polymerisation.

For the thermal dissociation of initiators, k_d can be calculated from the Arrhenius equation; thus k_d is strongly temperature dependent. For thermal initiators, the parameters of E_a and A are fundamentally linked to the chemical structure of the radical initiator. For azo initiators, k_d has also been shown to vary by up to a factor of 2 with the nature of the solvent in which the initiator is used [12].

As is evident from Scheme 2.1, not all primary radicals that are generated go on to become "useful" or initiating radicals; this is evident by a fraction of all radical pairs becoming consumed via side reactions to form by-products. These are often a range of stable and/or unstable species, some of which can degrade further to release secondary radicals of different reactivity to the primary radicals [12, 16], however for simplicity and by the definition of initiator efficiency (f), they are treated as inactive species in Scheme 2.1. These by-products arise from radicals needing to first escape the solvent cage before they can react with monomer and this has been shown to be a diffusion controlled process. The consequences of this are that the cage effect is likely to increase with decreased reaction temperature and increase with increased conversion as the polymerisation progresses due to the formation of polymer in the reaction medium increasing viscosity, however the extent of this is also

dependent on the molecular weight of the polymer being formed. Furthermore, termination reactions of the primary radicals with other radicals in the system and transfer to initiator can also reduce the initiator efficiency. All these effects are accounted for in Scheme 2.1 by the inclusion of the efficiency factor; for thermal initiators, this typically has a value ranging from 0.3 to 0.8 depending on reaction conditions and can decrease quite severely over the course of a polymerisation for reasons described previously [17]. It is useful to define the initiator efficiency, f, as the ratio shown in Equation 2.4 which relates the number of moles of radicals generated per mole of initiator molecules (n) to the rate of initiation of propagating chains (R_i, from here on referred to simply as the "the rate of initiation") and previously defined parameters as shown in Equation 2.4:

$$f = \frac{(Rate\ of\ initiation\ of\ propagating\ chains)}{n \cdot (Rate\ of\ initiator\ disappearance)} = \frac{R_i}{n \cdot R_{Id}}$$

Equation 2.4: Definition of initiator efficiency (f).

From Scheme 2.3 and Scheme 2.1 it becomes clear that for the case of unsymmetrical initiators, the primary radicals in each generated primary radical pair will have different reactivities and thus different initiation rate coefficients (k_i). For two non-identical primary radicals (I_a* and I_b*), this can be summarised as shown in Scheme 2.2.

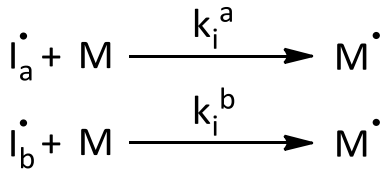

Scheme 2.2: Initiation by two radicals of differing reactivity.

Where the rate of initiation (R_i) will be determined by an average of the two separate initiation rate coefficients (k_i^a and k_i^b), as shown in Equation 2.5.

$$R_i = \frac{d[M^*]}{dt} = -\frac{d[I_a^*]}{dt} - \frac{d[I_b^*]}{dt} = k_i^a \cdot [I_a^*] \cdot [M] + k_i^b \cdot [I_b^*] \cdot [M]$$

Equation 2.5: Rate of initiation for the case when an unsymmetrical radical initiator is used.

Equation 2.5 can be simplified such that:

$$R_i = k_i \cdot [I^*] \cdot [M]$$

Equation 2.6: Expression for the rate of initiation (R_i) in a FRP system with a radical initiator present.

Where for unsymmetrical initiators Equation 2.7 applies:

$$k_i = \frac{k_i^a + k_i^b}{2} \quad and \quad [I_a^*] = [I_b^*] = \frac{[I^*]}{2}$$

Equation 2.7: Definition of composite terms for the case of an unsymmetrical radical initiator is used.

It should be noted that Equation 2.5 and Equation 2.7 also apply in the case of a symmetrical initiator where the side products of initiator breakdown lead to unstable species which further degrade to radicals with different reactivities from the primary radicals. For symmetrical initiators, Equation 2.6 is used as given.

Finally, if we assume that k_d is the rate limiting step in the initiation process such that $k_i >> k_d$, then it becomes clear that the rate of initiation of propagating chains (R_i) can be directly equated to the rate of primary radical generation (R_g) such that:

$$R_i = k_i \cdot [I^*] \cdot [M] = 2 \cdot f \cdot k_d \cdot [I_2]$$

Equation 2.8: Definition of the rate of initiation of by a thermal radical initiator.

Under the same assumption, this relationship can also be neatly obtained by the rearrangement of the definition for initiator efficiency (Equation 2.4).

For photoinitiated process, the equivalent definition of the combined term of $k_d f$ in Equation 2.8 is more complicated. Firstly, irrespective of the type of photoinitiator that is employed (Type 1 or 2), a practical definition of the quantum yield (Φ) is given by Equation 2.9.

$$\Phi = \frac{(Yield\ of\ initiating\ radicals)}{n \cdot (Photons\ absorbed)}$$

Equation 2.9: Practical definition of quantum yield in the context of photoinitiators used in FRP processes.

In this way, quantum yield is analogous to the term $k_d \cdot f$ for the case of thermal initiation, and Equation 2.9 is analogous to Equation 2.4, and likewise can be equated to the rate of initiation:

$$\Phi = \frac{(Rate\ of\ initiation)}{n \cdot (Intensity\ of\ incident\ irradiation\ absorbed)} = \frac{R_i}{n \cdot I_{abs}}$$

Equation 2.10: Rate of initiation (R_i) for a photoinitiator as a function of quantum yield.

Where:

$$I_{abs} = Intensity\ of\ incident\ irradiation\ absorbed$$

Which is directly governed by the Beer–Lambert law; this directly relates I_{abs} to the total incident light intensity (I_0):

$$\frac{I_{abs}}{I_0} = 1 - 10^{\varepsilon \cdot c \cdot l}$$

Equation 2.11: Beer-Lambert law.

Where:

$\varepsilon = molar\ extinction\ coefficient$

$c = concentration\ of\ photoinitiator\ [I_2]$

$l = pathlength\ of\ the\ sample$

Thus combining Equation 2.10 and Equation 2.11 gives a complete expression for the rate of initiation (R_i) by a photoinitiator, where n = 2 as is the case for thermal initiation (see Scheme 2.1):

$$R_i = 2 \cdot \Phi \cdot I_0 \cdot (1 - 10^{\varepsilon \cdot l \cdot [I_2]})$$

Equation 2.12: Definition of the rate of initiation by a photoinitiator.

2.1.2.2 Types of Free Radical Initiators

The generation of primary radicals is almost exclusively achieved via the thermal or photochemical decomposition of a specialty class of compounds called radical initiators, however direct generation of radicals from the monomer itself is also possible [18], and a multitude of multicomponent initiating systems have also been devised [10, 19]. The most common class of thermal initiators are the azo class of compounds; these feature weak C-N bonds which decompose via homolytic cleavage upon heating to release two carbon centred radicals and a molecule of nitrogen (Scheme 2.3, A). The interesting feature of azo initiators is that they can also behave as photoinitiatiors, whereupon the absorption of a photon of correct energy they can undergo cis-trans isomerisation around the nitrogen double bond or direct photolysis [20].

Photoinitiators have come into prominence in the fields of FRP and LRP due to the ability to tailor their absorption profiles and reactivity of the generated radicals by careful design of the photoinitiator [21], along with giving the potential for spatial and temporal control over radical generation [22]. Photoinitiators are characterised as being one of two Types. Type 1 photoinitiators typically absorb in the UV region and have bonds capable of undergoing unimolecular bond scission; examples include the symmetrical bis thiocarbonylthio disulfides (which can also have thermally labile bonds) and unsymmetrical thiocarbonylthio compounds as utilised in photoiniferter systems (Scheme 2.3, C & D). Type 2 photoinitiators typically absorb in the UV and visible regions and require the interaction of the excited triplet state of the photoinitiator with a co-initiator molecule [23]. These co-initiators are often alcohols or amines as these tend to have readily abstractable hydrogens [23]; the commonly

used UV initiator benzophenone is an example of a Type 2 photoinitiator and is illustrated in Scheme 2.3, B.

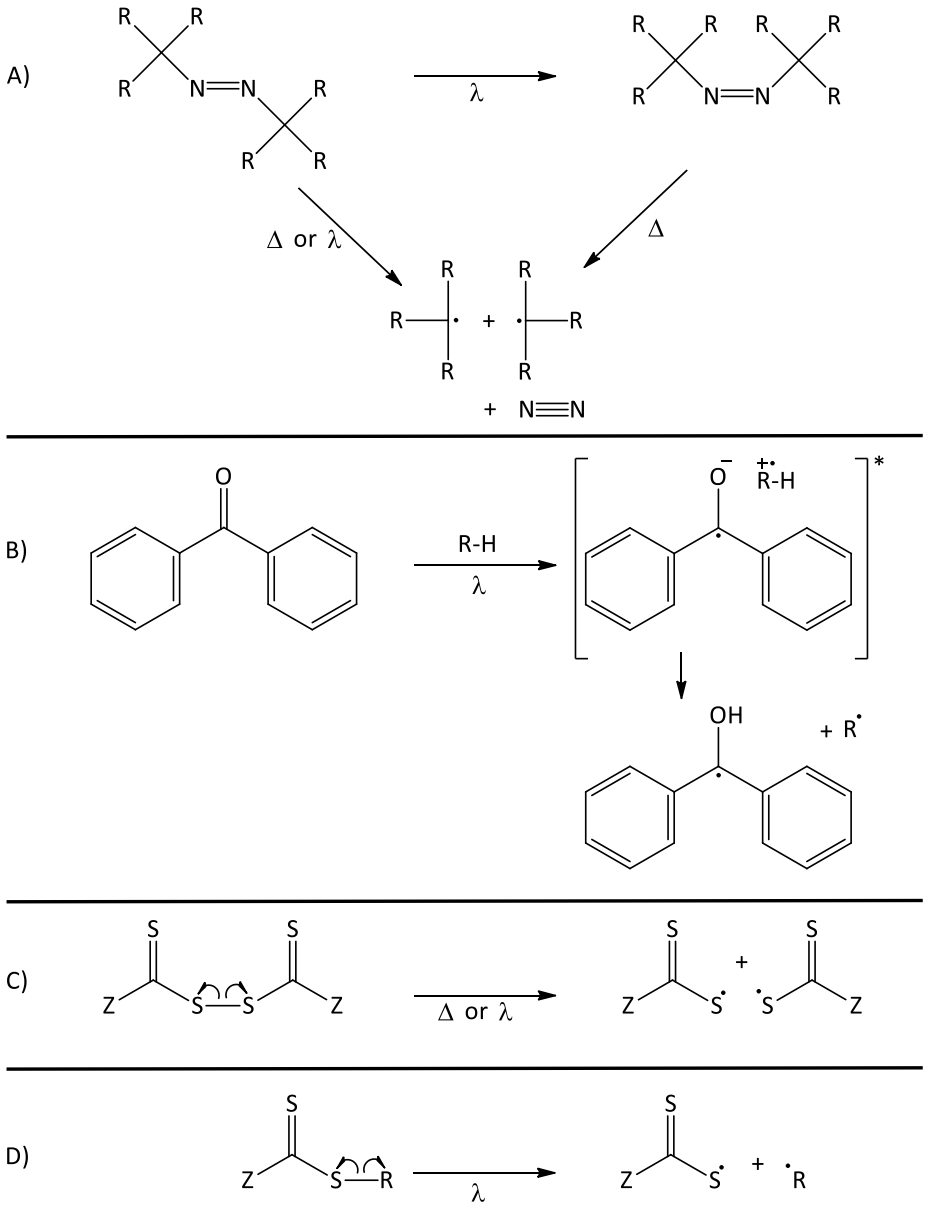

Scheme 2.3: Summary of initiators commonly encountered in FRP and living radical polymerisation techniques.

2.1.2.3 Reactivity of radicals & classification of monomers

Since both FRP and RDRP techniques function entirely by radical mechanisms, a general primer as to the factors that influence both the reactivity of radicals and monomers is provided here. 1,1-disubstituted (A = H) and 1,1,2-trisubstituted alkenes of the general form CHA=CXY (where A, X & Y are variable substituents) are by far the most common monomers that are employed in FRP and RDRP techniques; the process of addition of a radical (R*) to such an alkene is shown in Figure 2.1.

Figure 2.1 has been removed due to copyright restrictions.

Figure 2.1: General representation of the energy profile showing the reaction of a radical (R*) with a alkene of the general form CHA=CXY, taken from [24].

The addition of a radical to a double bond is potentially a reversible reaction as polymerisation is not entropically favoured [13], however due to its exothermic nature arising from the replacement of a π bond with a σ bond [24] it is thermodynamically favoured until the depolymerisation temperature is reached [25]. The depolymerisation temperature is typically significantly higher than commonly employed polymerisation temperatures hence this phenomenon is not of concern in most instances. The rate coefficient for radical addition (k) to a double bond can be described by the Arrhenius equation (Equation 2.13):

$$k = A \cdot e^{\frac{-E_a}{R \cdot T}}$$

Equation 2.13: Arrhenius equation.

Where:

$A = Frequency\ factor\ (M^{-1}s^{-1})$

$E_a = Activation\ energy\ for\ dissociation\ (kJ\ mol^{-1})$

$R = Gas\ constant\ (8.314\ kJ\ K^{-1}\ mol^{-1})$

$T = Temperature\ (K)$

For polyatomic radicals, the frequency factor spans a narrow range of around 2 orders of magnitude ($6.5 < \log A < 8.5$) [24], however the rate constant for addition can vary by many orders of magnitude. From this it can be concluded that the greatest effect on the rate coefficient comes from the activation energy (E_a) which is the height of the energy barrier in Figure 2.1 and corresponds to the energy required to form the transition state. The main influences on the activation energy are a combination of steric, resonance, enthalpic and polarity factors [24]. Regardless of the primary mechanistic factor at work, the rate coefficient for radical addition is most strongly influenced by the chemical substituents on either the site of radical attack on the alkene or at the radical centre itself; remote substituents generally only show a minor influence on the stereochemistry and regiospecificity of radical addition [26]. Bulky substituents on the alkene are responsible for decreasing the frequency factor while subsequently raising the activation energy. Enthalpic factors describe the stabilising or destabilising effects of substituents on all species (radical, alkene and transition state) and generally decrease with increased exothermicity of the reaction [24]. Polar factors are thought to be very significant and can be explained as a an energetically favourable alignment of the singly occupied

molecular orbital (SOMO) of the radical and with either the lowest or highest occupied molecular orbital (LUMO or HOMO) of the alkene [24].

From the perspective of RDRP techniques it is important to notice that the reactivity of a propagating radical and that of the monomer are close to opposite of one another; in general the most stable monomers form very reactive radicals and *vice versa* [27]. In the context of RAFT polymerisation especially, this has led to monomers being broadly characterised as belonging to one of two groups. Namely, there are the More Activated Monomers (MAMs) and the Less Activated Monomers (LAMs). Their succinct definitions are as such [28]:

- MAMs: monomers in which the double bond is conjugated to an aromatic ring (e.g. styrene), a carbonyl group (e.g. methyl methacrylate, methyl acrylate or acrylamide) or a nitrile (e.g. acrylonitrile). Due to possible resonance and delocalisation of the radical, these monomers form very stable and thus quite unreactive monomeric and polymeric radicals. This makes them poor attacking groups and good leaving groups.
- LAMs: monomers in which the double bond is adjacent to a saturated carbon, an oxygen or nitrogen lone pair (e.g. vinyl acetate or N-vinylpyrrolidone) or the heteroatom in an aromatic ring (e.g. N-vinylcarbazole). Due to limited opportunity to delocalise the radical or stabilise it via conjugation, these monomers form very unstable and thus very reactive radical species. This makes them very good attacking groups and very poor leaving groups.

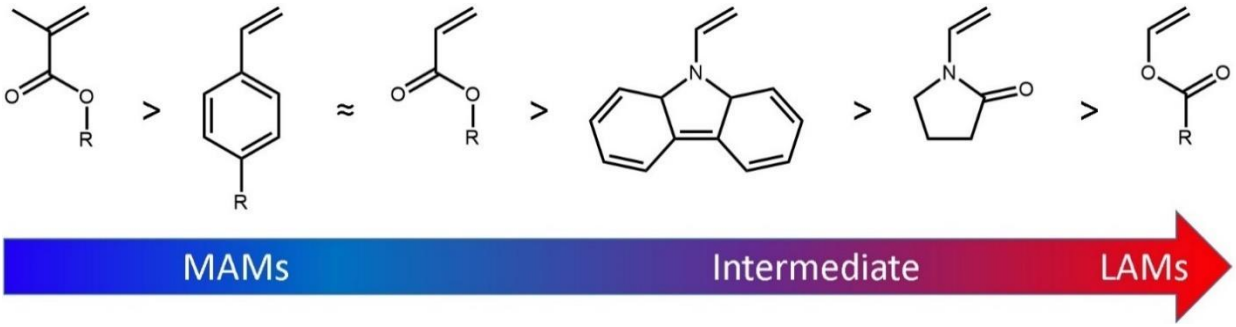

Figure 2.2: General classification of common monomers used in RAFT polymerisation.

2.1.2.4 Propagation

The factors affecting the rate of monomer propagation are the same factors that govern the reactivity of all free radicals, and this have covered previously in section 2.1.2.2. From a practical and theoretical perspective, the accurate determination of the propagation rate coefficients (k_p) for commonly used monomers is of critical importance to researchers. Efforts guided by the International Union of Pure and Applied Chemistry (IUPAC) have been made to systematically collate, analyse and verify the values of k_p for various monomers [11, 29-32]. The modern method of choice for the

determination of k_p values has categorically been Pulsed Laser Polymerisation (PLP) and subsequent analysis of the resulting molecular weight distributions (MWDs) [33]. Although the PLP technique is considered accurate and state of the art, the values of k_p determined by this technique often do not represent the "actual" k_p under realistic experimental conditions. This arises due to two main reasons which occur under normal FRP and LRP conditions but are either entirely absent or minimised in PLP experiments:

- For acrylate monomers, the propagating radical tends to form tertiary midchain radicals (MCRs) through inter and intra-molecular branching. These MCRs have a markedly lower k_p relative to the terminal radicals which are secondary in nature. Thus the "effective" k_p under FRP and LRP conditions is always lower than the k_p determined by PLP [31].
- Several monomers including vinyl chloride, vinyl acetate and other allyl esters tend to have non-negligible rates of addition where the propagating radical does not add in the usual "head to tail" manner and instead adds to the "head" of the monomer in a "head to head" manner [29, 34, 35]. Due to steric, polar and resonance factors, the usual mode of addition of monomer to a growing polymeric radical is in "head to tail" manner [13]. The resulting radicals once again have different k_p values. Both these effects are illustrated in Scheme 2.4.

1) Formation of tertiary midchain radicals in acrylate systems

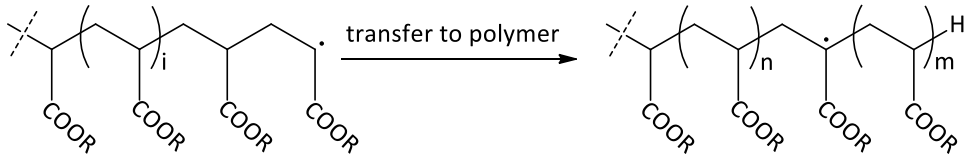

2) Possble modes of monomer addition in FRP systems

A) Head to tail

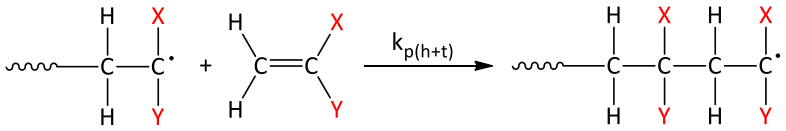

B) Head to head

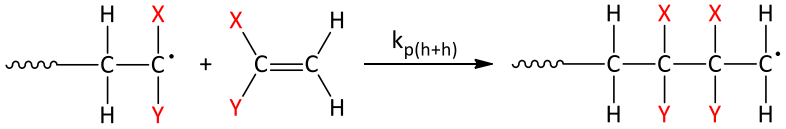

C) Tail to head

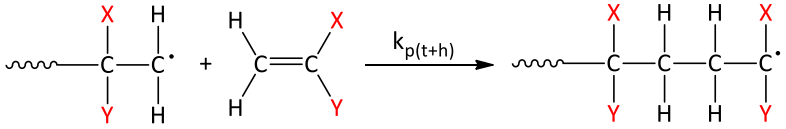

D) Tail to tail

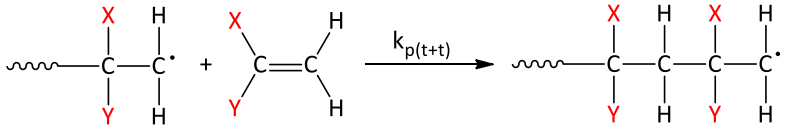

Scheme 2.4: Illustrated mechanisms for the formation of midchain radicals in acrylate systems (1, recreated from [31]) and modes of addition available to monomers in FRP systems (2, recreated from [29]).

The assumption that k_p is chain length independent is somewhat valid; there is experimental evidence that the rate of monomer addition reaches a constant value of k_p after an oligomeric chain length of n ≈ 4 [13], however a gradual plateauing of k_p at higher chain lengths has also been seen for a range of common monomers [36]. This assumption has practical utility as FRP processes tend to generate chain lengths in the range of 100 to 15000 monomer units long, depending on reaction conditions, monomer and additives present. This assumption is supported by the fact the propagation reaction is considered to be under chemical control [11], i.e. controlled by thermodynamics and not kinetics until very high conversion (conv. > 80%) when viscosity becomes a major influence. This arises from the consideration that at room temperature the rate of collisions between monomers is ≈ 10^{12} s^{-1} whilst most monomers have a k_p of ≈ 10^3 s^{-1}, thus implying only ≈ 1 in every 10^9 collisions leads to propagation. A further consequence of this is that the value of k_p is essentially independent of monomer concentration, i.e. does not change significantly as a function of conversion. That is not to

say that solvent effects are totally negligible; specific monomer solvent pairs show some influence on the value of k_p and this is attributed to the interaction between the propagating radical and the electron accepting ability of the solvent [37], with an extreme example being the FRP of methacrylic acid in aqueous systems [38]. The FRP of methyl methacrylate (MMA) seems to exemplify all these complex behaviours; studies indicate a significantly higher k_p for PMMA oligomers (up to a factor of 10x) [39] and a significant decrease in k_p at very high conversions during bulk MMA polymerisation. Situations where the kinetics of single monomer unit insertion (SUMI) [40] or the synthesis of oligomers [41] of chain length smaller than 10 units long are being studied require chain length dependent k_p values to be considered.

Fundamentally, from the perspective of kinetic analysis, the rate coefficient (k_p) for the addition of monomer to the initiating radical (M*) is considered the same as for a polymeric radical of chain length P_n adding further monomer to propagate further, as shown in Scheme 2.5.

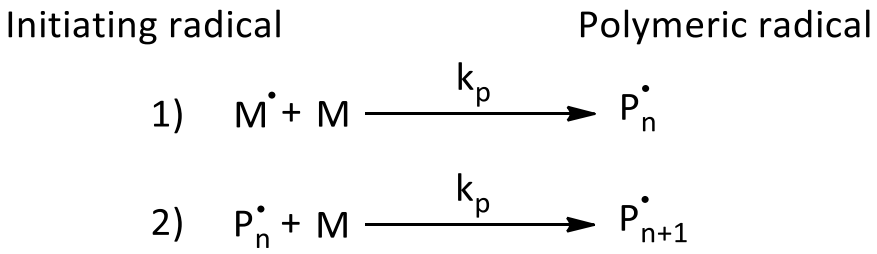

Scheme 2.5: Summary of propagation reactions within a FRP system

From the fact that any initiating radical, regardless of chain length (n), is considered to have an identical k_p as shown in Scheme 2.5, it is possible to conclude that the overall rate of propagation (R_p) is given by:

$$R_p = -\frac{d[M]}{dt} = \sum_{n=1}^{n} k_p \cdot [P_n^*] \cdot [M]$$

Equation 2.14: Definition of the rate of propagation.

If we assume that the chain length of the polymers formed is significant (i.e. n > 1000), then consistent with the assumptions listed in section 2.1.2 is the assumption that in Scheme 2.5 the number of monomers consumed in step 1 << those consumed in step 2. Thus, it follows that the rate of propagation (R_p) directly equals the rate of polymerisation.

2.1.2.5 Termination

Collectively, the termination reactions that determine the final fate of free radicals in a FRP process are overall the most complicated to describe and model, whilst having the most profound

consequences on the kinetics and the resulting polymers formed. The process of termination can fundamentally only proceed by one of two mechanisms; via the combination or disproportionation of radicals. Combination and disproportionation reactions have their own rate coefficients, k_{tc} and k_{td} respectively. These processes are illustrated with generic propagating polymer radicals in Scheme 2.6.

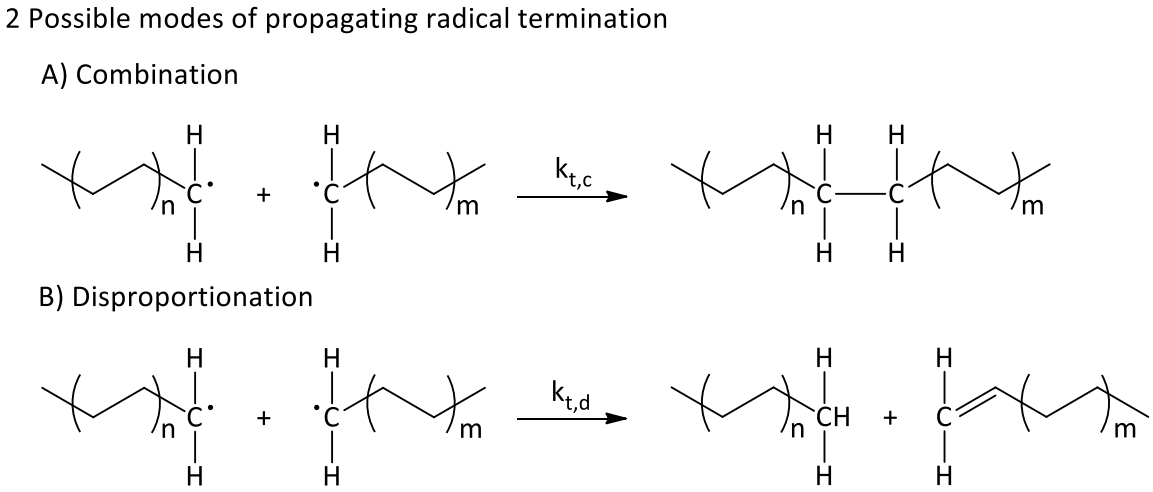

Scheme 2.6: Combination reactions as they apply to propagating polymer radicals.

$$k_t = k_{t,c} + k_{t,d}$$

Equation 2.15: Definition of the overall termination rate coefficient.

For every FRP system, the overall termination rate coefficient (k_t) is defined as the sum of two respective contributions. Equation 2.15 also leads to the definition for the contribution of disproportionation to the overall termination rate coefficient as a ratio:

$$\delta = \frac{k_{t,d}}{k_{t,c} + k_{t,d}}$$

Equation 2.16: Relative contribution of disproportionation to the overall rate coefficient for termination.

The size of the contribution due to disproportionation is largely determined by the repeat unit of the polymeric radical; as a general rule the contribution from disproportionation is greater for radicals that are sterically hindered or have abstractable β hydrogens [16]. There is evidence that the ratio of δ can change as a function of temperature, however the effect is not consistent in favour of a particular mechanism with an increase in temperature [16].

From a more "classical" analysis of FRP, the rates of termination between propagating polymeric radicals and both initiating radicals and primary radicals is considered to be negligible, hence the overall reaction scheme for termination is as shown in Scheme 2.7.

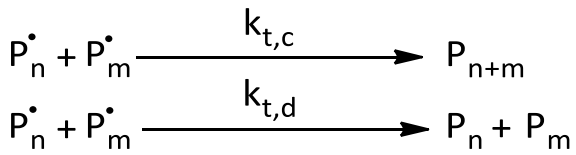

Scheme 2.7: Simplified kinetic scheme for termination as portrayed in a classical kinetic analysis of FRP processes.

Using the general expression that the overall rate coefficient is a sum of the two terms $k_{t,d}$ and $k_{t,c}$, and all termination rate coefficients are chain length independent (assume $P_n = P_m$), the overall rate of termination (R_t) can be summarised as:

$$R_t = -\frac{d[P_n^*]}{dt} = 2 \cdot k_t \cdot [P_n^*]^2$$

Equation 2.17: Overall rate of termination in a FRP process.

From here, the kinetic treatment of FRP processes can be finalised to yield some useful relationships by applying the assumptions outlined previously in section 2.1.2. One key assumption is that there is a steady state concentration of radicals; this implies that the rate of radical generation (R_i) is equal to the rate of termination (R_t), hence combining Equation 2.8 with Equation 2.17 gives:

$$\frac{d[P_n^*]}{dt} = R_i - R_t = 0$$
$$\therefore 2 \cdot f \cdot k_d \cdot [I_2] = 2 \cdot k_t \cdot [P_n^*]^2$$
$$\therefore [P_n^*] = \left(\frac{f \cdot k_d}{k_t}\right)^{0.5} \cdot [I_2]^{0.5}$$

Equation 2.18: Concentration of propagating radicals as a function of fundamental parameters and initiator concentration.

Substituting the result of Equation 2.18 result into Equation 2.14 gives an expression for the overall rate of polymerisation (R_p) as a function of fundamental reaction parameters and quantities such as initiator concentration and monomer concentration which can be measured experimentally.

$$R_p = k_p \cdot \left(\frac{f \cdot k_d}{k_t}\right)^{0.5} \cdot [I_2]^{0.5} \cdot [M]$$

Equation 2.19: Rate of polymerisation defined without the concentration of any radical species.

The first order dependence of the rate of polymerisation on the monomer concentration and a square root dependence on the initiator concentration has been confirmed in multiple polymerisation systems [9, 11]. There are however complications to this: Equation 2.19 is expected to hold if f is unity or close to unity. If f is substantially less than unity, this can lead to a direct correspondence between f and [M]. In this case, the rate of polymerisation should vary with $[M]^{1.5}$ as a result of the fact that the

propagating radical concentration becomes a function of $[M]^{0.5}$ [9]. Deviations from the $[I_2]^{0.5}$ dependence can arise from the chain length dependent nature of rate coefficients or primary radical termination effects. Furthermore, extreme dilution of monomer can lead to deviations from the dependence of Rp from both [M] and $[I_2]$ in much the same way as for the case when f is substantially less than unity, as explained previously. From a more practical standpoint, Equation 2.19 is easily integrated and yields an expression that correlates monomer conversion (c) to the "apparent" rate coefficient (k_{app}) of polymerisation of a reaction as a function of time (t). This results in the typical "pseudo first order" kinetic plot that is ubiquitous in polymer science publications, where $[M]_t$ and $[M]_0$ are the monomer concentration at time t and t = 0 respectively.

$$ln\left(\frac{1}{1-c}\right) = \ln\left(\frac{[M]_0}{[M]_t}\right) = k_{app} \cdot t \quad and \quad k_{app} = k_p \cdot \left(\frac{f \cdot k_d}{k_t}[I_2]\right)^{0.5}$$

Equation 2.20: Pseudo first order kinetics for FRP processes, relating the observe rate coefficient for polymerisation.

The assertion that a straight-line pseudo first order kinetic plot implies that a polymerisation shows "living" characteristics is often stated in the LRP literature. Considering the closer analysis of the equations presented here, at best, the statement can be made that the overall radical concentration is constant if a straight-line pseudo first order kinetic plot is obtained. Statements such as "linear pseudo first order kinetics prove the "living" nature of a LRP process" are misleading and should not be used; this was reiterated in a recent article by Stenzel & Barner-Kowollik [42].

Several other relationships can be obtained from the kinetic analysis as outlined above, namely the average kinetic chain length ($\bar{\nu}$) of the polymer formed:

$$\bar{\nu} = \frac{R_p}{R_t} = \frac{R_p}{R_i} = \frac{k_p \cdot [M]}{(2 \cdot k_d \cdot f \cdot [I_2] \cdot k_t)^{0.5}}$$

Equation 2.21: Definition of the average kinetic chain length formed during the FRP process.

An alternate expression for $\bar{\nu}$ relates the ratios of the rate coefficient for propagation and termination relative to the overall rate of polymerisation [9]:

$$\bar{\nu} = \frac{k_p^2 \cdot [M]^2}{2 \cdot k_t \cdot R_p}$$

Equation 2.22: Alternate expression for the average kinetic chain length formed during the FRP process.

From Equation 2.22 it can be seen that if the rate of polymerisation for two separate monomers is the same, the value of ($\bar{\nu}$) can be related back to the ratio of (k_p^2/k_t); as an example, for equivalent values of R_p, the average kinetic chain length for vinyl acetate is approximately 180x that for styrene due to

the greater speed of propagation relative to termination in vinyl acetate [9]. Hence under equivalent values of R_p, the value of $\bar{\nu}$ can give insight into the reactivity of the propagating radical species.

In reality the termination process is incredibly complex; this translates into complexity surrounding how the k_t rate coefficient is implemented within simulations and models for FRP and LRP processes. The process of termination is best explained when one considers that for two polymeric radicals to terminate, the following series of events must occur (shown in Figure 2.3) [14]:

1. Translation of polymer chains towards each other through the reaction medium; this is also known as centre of mass diffusion and is shown in Figure 2.3 (A).
2. Segmental diffusion of the radical chain ends until they reach close proximity to one another; this is shown in Figure 2.3 (B).
3. Actual reaction between the two radicals via one of the two pathways; combination or disproportionation, shown in Figure 2.3 (C).

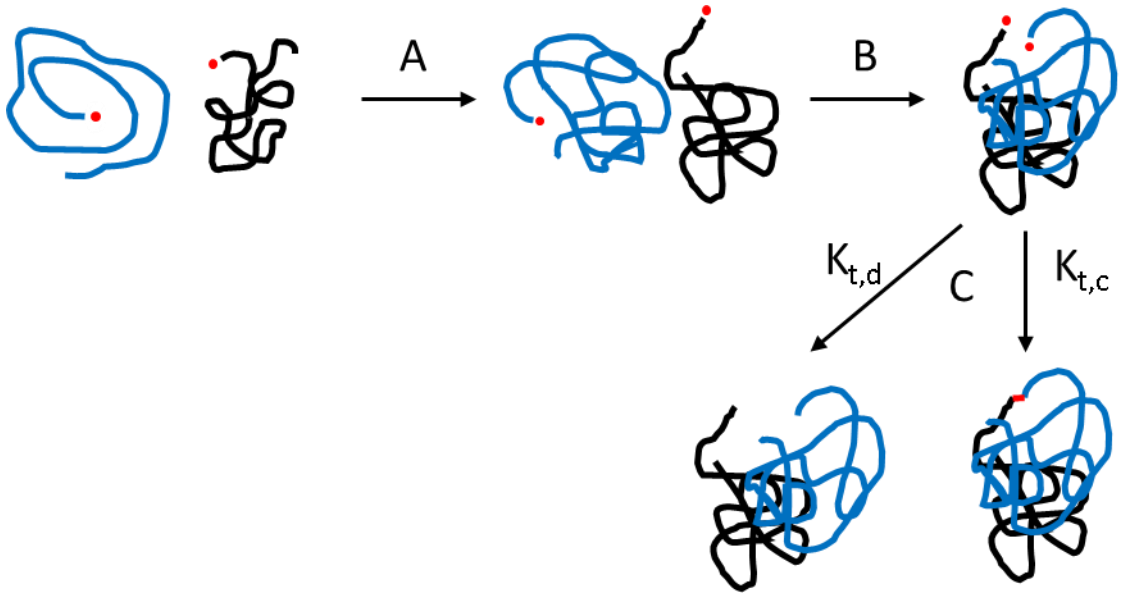

Figure 2.3: Summary of the termination process for two propagating polymeric chains. Recreated from [14].

The rate coefficient for bimolecular termination between two small carbon centred radicals is in the order of $\approx 10^9$ M^{-1} s^{-1} [16], however there is incontrovertible evidence that the average rate coefficient for termination (often designated as $\langle k_t \rangle$) between polymeric radicals is diffusion controlled even at very low conversion and shows far more complex behaviour [43]. The evidence for this is that k_t decreases with system viscosity as expected for a diffusion controlled process [14], and hence this is dependent on both the chain length of the propagating species and the conversion as these both directly influence the system viscosity. Furthermore, the value of k_t can vary by many orders of magnitude depending on the nature of the monomer [11] and is not identical to that of analogous

small radical models whose rate constants can be predicted by the Smoluchowski equation [14]. For most common monomers the overall rate of the termination reaction is believed to be limited by segmental diffusion at low and intermediate conversion (A in Figure 2.3) with it becoming limited by centre of mass diffusion (B in Figure 2.3) at a certain chain length called the critical chain length (i_{crit}) or crossover length [43]. The interplay between these phenomena result in the value of $\langle k_t \rangle$ that changes as a function of chain length *i*, as shown in Figure 2.4.

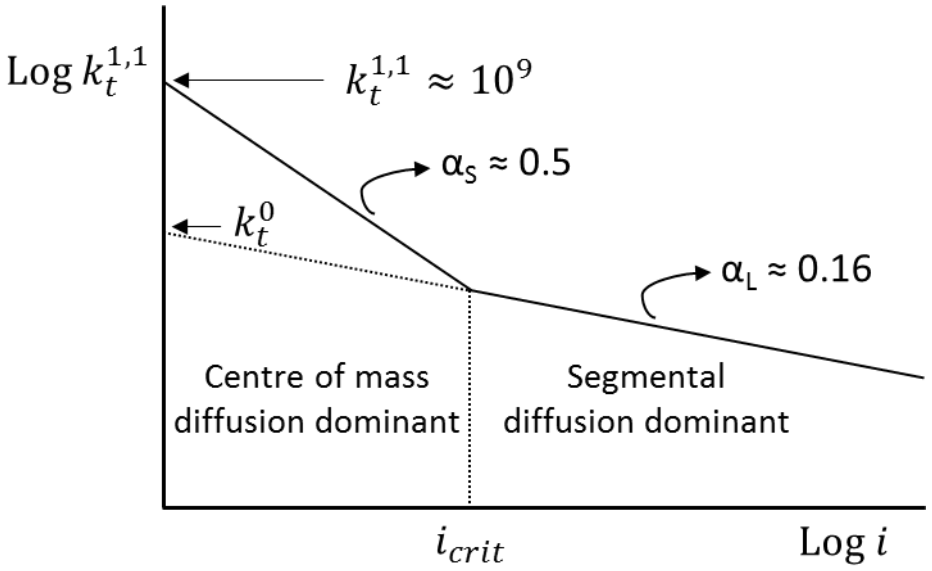

Figure 2.4: General relationship between the overall rate of termination ⟨k_t⟩ and the propagating chain length of the terminating radicals (*i*). Recreated from [43].

From Figure 2.4, an accurate description of the termination rate coefficient for two propagating chains, both of length *i*, is given by:

$$k_t^{i,i} = k_t^{1,1} \cdot i^{-\alpha_S} \quad for\ i \leq i_{crit}$$
$$k_t^{i,i} = k_t^{1,1} \cdot (i_{crit})^{-(\alpha_S - \alpha_L)} \cdot i^{-\alpha_l} = k_t^0 \cdot i^{-\alpha_l} \quad for\ i > i_{crit}$$

Equation 2.23: Expression for the termination rate coefficient as a function of propagating chain length.

For the case when the chains are of two different lengths, (*i* & *j*), the rate of cross termination is given by:

$$k_t^{i,j} = \sqrt{(k_t^{i,i} \cdot k_t^{j,j})}$$

Equation 2.24: Expression for the rate coefficient of cross termination between propagating chains of various lengths.

The full treatment for termination as given by Equation 2.23 and Equation 2.24 is sometimes simplified for simulation purposes of FRP and LRP processes, and the average termination rate coefficient is often implemented as shown in Equation 2.25:

$$\langle k_t \rangle = k_t^0 \cdot i^{-\alpha}$$

Equation 2.25: Expression for the average rate coefficient for termination as a function of chain length.

Where k_t^0 is the starting value of termination at chain length of ≈ 0, i.e. essentially $k_t^0 = k_t^{1,1}$ as seen in Figure 2.4. In reality k_t^0 is often slightly different for different monomers and values have been determined experimentally, however as a first approximation k_t^0 can be set equal to ≈ 10^9 M^{-1} s^{-1}.

2.1.2.6 Molecular weight definitions and distributions

The degree of polymerisation of a polymer (X_n, also referred to as the degree of polymerisation (DP_n)) is directly equal to the number of monomer units (n) in the polymer chain. The end groups are neglected in this number; however, the overall molecular weight includes the molecular weight of the end groups. The expression for the number molecular weight is given by:

$$M_n = X_n \cdot M_0$$

Equation 2.26: Definition for the number molecular weight of a polymer.

Where in this case the assumption is made that the polymer contains only one type of monomer which has a molecular weight of M_0. This however is not a commonly used or useful definition, as polymer chains, regardless of by which process they are made, are not all the same length but invariably a distribution of lengths with the spread of values denoted by the dispersity, D. This leads to the 3 fundamental definitions of the molecular weight of a polymer, all of which are considered average values for the respective quantities. These are the number average molecular weight (M_n), the weight average molecular weight (M_w) and the Z average molecular weight (M_z, from the German word for centrifuge (zentrifuge)). From a mathematical perspective, due to being average values, the values should be denoted as $\overline{M_n}, \overline{M_w}$ and $\overline{M_z}$, however the non-accented versions are more common in the literature and the two are used. The definitions are as shown in Equation 2.27:

$$\overline{M_n} = \frac{\sum n_n \cdot X_n}{\sum n_n} \cdot M_0$$

$$\overline{M_w} = \frac{\sum w_n \cdot X_n}{\sum w_n} \cdot M_0 = \frac{\sum n_n \cdot X_n^2}{\sum n_n} \cdot M_0$$

$$\overline{M_z} = \frac{\sum n_n \cdot X_n^3}{\sum n_n \cdot X_n^2} \cdot M_0$$

Equation 2.27: Definitions for the most commonly used descriptors for the molecular weight of a polymer.

Where n_n is the concentration of chains of length *n* (monomer units) and w_n is the weight of chains of length *n*. Another useful definition is that of the moments of the chain length distribution, where the *j*th moment is defined as:

$$\lambda^j = \sum n_n \cdot X_n^j$$

Equation 2.28: Definition for the moment of a chain length distribution.

From this, the zeroth moment can be defined as the total concentration of polymer chains and the first moment is the total concentration of repeat or monomer units in those chains:

$$\lambda^0 = \sum n_n \quad and \quad \lambda^1 = \sum n_n \cdot X_n = \sum w_n$$

Equation 2.29: Definition for the zeroth and first moments of a chain length distribution.

From these definitions, the breadth or spread of the molecular weight distribution, called the dispersity index can be defined as given in Equation 2.30. This is designated in most texts as Đ or D, but is also commonly referred to as the polydispersity index (PDI).

$$Đ = \frac{M_w}{M_n} = \frac{X_w}{X_n} = \frac{\lambda^0 \cdot \lambda^1}{(\lambda^1)^2}$$

Equation 2.30: Interchangeable definitions for the dispersity of a distribution of polymer molecular weights.

As stated by Moad and Solomon [14], in calculations the moments are effectively treated as concentrations, and kinetic simulations of FRP processes often involve the calculation of the dispersity by evaluating the moments rather than the complete distribution. It must be stressed this is only accurate if the kinetics of the process being simulated are independent of chain length, which is often not the case.

The distribution of the molecular weights within a polymer sample is critically linked to the interplay between the various reactions occurring during the polymerisation process, as has been outlined in the previous sections. The statistical treatment of FRP processes was originally proposed by Schulz and elaborated upon by Flory [9] and others [44]. This leads to the definition that the probability of a

propagation event (∅) is described as the ratio of the propagation rate relative to the sum of all other competing reactions, such that:

$$\emptyset = \frac{R_p}{R_p + R_t + R_{tr}}$$

Equation 2.31: Definition of the probability of propagation.

Where R_p and R_t are the rates of propagation and termination respectively, as defined previously, and R_{tr} is the rate of chain transfer in the presence of a chain transfer agent as defined in the following section (2.1.2.7). A given chain will undergo (i – 1) propagation steps, each with a probability of (∅), before terminating with a probability of (1 – ∅).

If termination occurs solely by chain transfer or by disproportionation, it can be shown [9] that the chain length distribution is given by the Schultz-Flory distribution:

$$n_i = \emptyset^{i-1} \cdot (1 - \emptyset)$$

Equation 2.32: Schultz-Flory distribution.

Applying this to the definitions for moments of the molecular weight distribution gives:

$$X_n = \frac{1}{1-\emptyset} \quad , \quad X_w = \frac{1+\emptyset}{1-\emptyset} \quad and \quad Đ = \frac{X_w}{X_n} = 1 + \emptyset$$

Equation 2.33: Expressions for M_w, M_n and Đ using the Schultz-Flory distribution.

For long chains, as $\emptyset \rightarrow 1$, $D \rightarrow 2$ as given by Equation 2.33.

The other situation that must be considered is where termination occurs only by combination; this was first described by Bamford *et al.* [44]. It can be shown that under these conditions the number distribution is given by:

$$n_i = (i-1) \cdot (1 - \emptyset)^2 \cdot \emptyset^{i-1}$$

Equation 2.34: Chain length distribution when combination is the sole mode of termination.

Once again, applying the definitions for moments of the molecular weight distribution gives:

$$X_n = \frac{2}{1-\emptyset} \quad , \quad X_w = \frac{2+\emptyset}{2-\emptyset} \quad and \quad Đ = \frac{X_w}{X_n} = 2 + \emptyset$$

Equation 2.35: Expressions for M_w, M_n and Đ applying the termination by combination distribution.

For long chains, as $\emptyset \rightarrow 1$, $D \rightarrow 1.5$ as given by Equation 2.35.

A comparison of both these termination modes and the resulting number and GPC distributions are illustrated in Figure 2.5.

Figure 2.5 has been removed due to copyright restrictions.

Figure 2.5: Illustrated number (a) and GPC distributions (b) for two polymers both with an Xn = 100. The number distribution of chains formed by disproportionation or chain transfer (dotted line, sum n_i = 1.0, Xw/Xn= 2.0) is calculated by Equation 2.33. The number distribution of chains formed by combination (solid line, sum n_i = 1.0, Xw/Xn = 1.5) is calculated using Equation 2.35. Taken from [14].

2.1.2.7 Chain transfer

Chain transfer is the process by which an active radical can be transferred to a non-radical species during the polymerisation by interaction with a chain transfer agent (CTA). This process is summarised in Scheme 2.8, where k_{tr} is the rate coefficient for chain transfer and $k_{re\text{-}in}$ is the rate coefficient for re-initiation by the transferred radical. Chain transfer is also unique in the sense that it is not strictly propagation and not strictly termination. Indeed, the effect of chain transfer on the kinetics and the X_n and D of the polymers obtained can vary widely between these two extremes due to the complex interplay of the various rate coefficients that underpin the process (k_{tr} and $k_{re\text{-}in}$) with the other fundamental parameters that characterise the polymerisation such as k_p, k_i and k_t. For this reason, the chain transfer step is typically not covered under a traditional kinetic analysis of FRP kinetics. This is not to say that chain transfer is avoidable or potentially insignificant. Even in the simplest scenario where only monomer, solvent and initiator are present, chain transfer can occur between growing radicals and all these species or even with the growing polymer itself. This was evident in Section 2.1.2.4 for the case of acrylates forming MCRs during propagation. The extent of these reactions is situation specific.

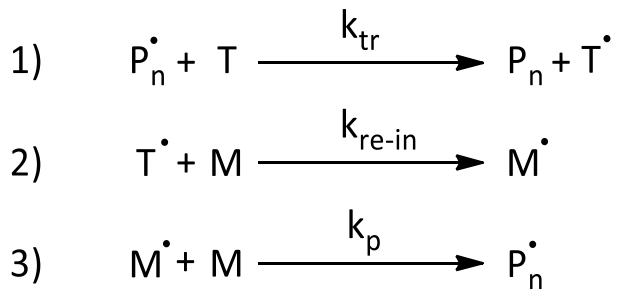

Scheme 2.8: Summary of the chain transfer process including further propagation.

From Scheme 2.8 the chain transfer rate (R_{tr}) can be defined as:

$$R_{tr} = -\frac{d[T]}{dt} = k_{tr} \cdot [P_n^*] \cdot [T]$$

Equation 2.36: Definition of the chain transfer rate.

Furthermore, a common definition that is useful for determining the effectiveness of a CTA under a given set of polymerisation conditions is the chain transfer constant (C_{tr}), which is formally defined as the ratio of the chain transfer coefficient to the propagation coefficient:

$$C_{tr} = \frac{k_{tr}}{k_p}$$

Equation 2.37: Definition of the chain transfer constant.

There are 4 important key scenarios concerning chain transfer to consider [11]:

- Scenario #1: when $k_p >> k_{tr}$ and $k_{re\text{-}in} \approx k_p$ this leads to "normal" chain transfer which is characterised by a decrease of the X_n of the polymer chains formed proportional to the amount of chain transfer agent added. This also does not lead to a decrease in the overall rate of polymerisation (R_p).
- Scenario #2: when $k_p << k_{tr}$ and $k_{re\text{-}in} \approx k_p$ this leads to telomerisation [45], which means that there is a severe decrease the X_n of the polymer formed such that only oligomers can form (n < 10 units). This scenario does not impact on R_p.
- Scenario #3: when $k_p >> k_{tr}$ and $k_{re\text{-}in} < k_p$ this leads to a decrease of the X_n, and as the rate coefficient for re-initiation is significantly reduced relative to the rate coefficient for propagation, an overall decrease in R_p is seen.
- Scenario #4: when $k_p << k_{tr}$ and $k_{re\text{-}in} < k_p$ this leads to a large decrease in the X_n and once again as in Case #3, an overall decrease in R_p is seen. This is termed degenerative chain transfer as due to $k_p << k_{tr}$ this process happens frequently between species.

There is also the special scenario for inhibition, although which strictly speaking is not always a transfer process, can nevertheless be adequately described by the case where when $k_p << k_{tr}$ and $k_{re\text{-}in} \approx 0$ in Scheme 2.8. From here we can see that if the generated radical (T*) is sufficiently unreactive and sufficiently stable, the polymerisation will effectively be halted until all of T is consumed.

A well-designed RAFT reaction is a hybrid combination of scenarios #1 and # 4, where, roughly speaking, $k_p < k_{tr}$ or $k_p \approx k_{tr}$ and $k_{re\text{-}in} > k_p$ or $k_{re\text{-}in} \approx k_p$. This leads to a situation where degenerative transfer should occur rapidly, the X_n is controlled by [T] and the R_p is essentially that for a FRP without added transfer agent.

The effect of the addition of a chain transfer agent on the number average degree of polymerisation obtained during a polymerisation is illustrated in Figure 2.6.

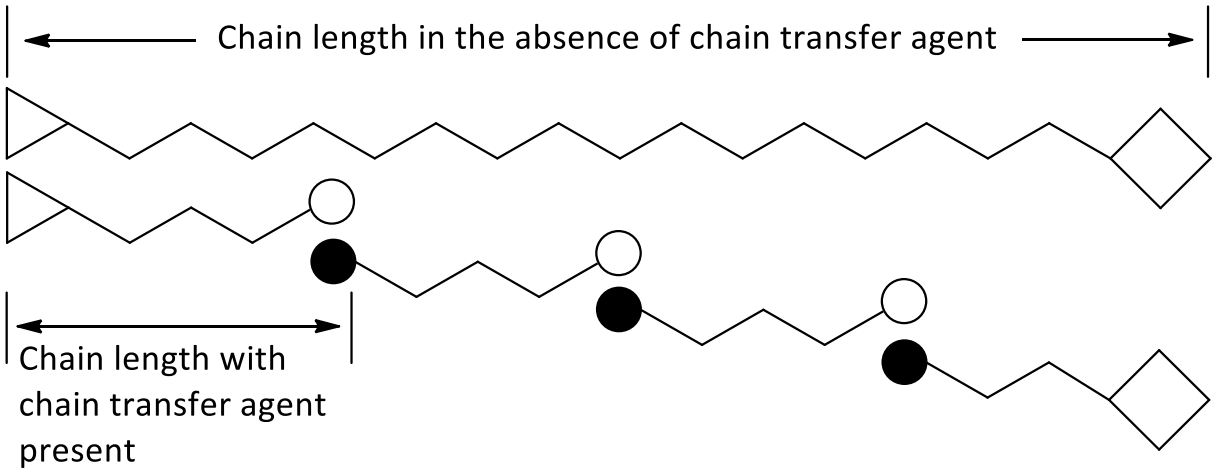

Figure 2.6: A schematic description of chain transfer on the average polymer chain length in FRP process: Δ and ◊ are end groups present without a chain transfer agent (typically initiator fragments), ● and ○ represent end groups derived from the chain transfer agent (typically initiator fragments), ● and ○ represent end groups derived from the chain transfer agent. Recreated from [16].

In a practical sense, the effect off chain transfer on X_n can be quantified by the Mayo method, which is effectively the process by which X_n is measured as a function of chain transfer agent concentration added to the FRP reaction mixture. This results in the Mayo equation:

$$\frac{1}{X_{n,0}} = \frac{1}{X_{n,T}} + \frac{C_{tr} \cdot [T]}{[M]}$$

Equation 2.38: Mayo equation.

Where:

$X_{n,0} = number\ average\ degree\ of\ polymerization\ without\ CTA$

$X_{n,T} = number\ average\ degree\ of\ polymerization\ with\ CTA$

2.2 Reversible deactivation radical polymerisation

2.2.1 Criteria and classification of "living" vs "controlled" polymerisation methods

There has been a long running and passionate academic debate as to which criteria need to be strictly met for a polymerisation to be classified as "living" in nature and whether RDRP processes meet these criteria [46]. The general criteria for a living system are as follows [47]:

1. Polymerisation proceeds until all monomer is consumed and restarts when fresh monomer is added. A stricter interpretation of this includes that the number of living chains remains constant. This also implies if other monomers are added sequentially that the synthesis of multi-block copolymers is possible.

2. If the molecular weight of the polymer formed increases linearly as a function conversion. Traditional FRP fails this criterion, while FRP in the presence of a conventional chain transfer agent satisfies this criterion whilst not giving other living characteristics.
3. That the total concentration of both active and dormant species remains constant, which should result in a linear pseudo first order kinetic plot. Non-living conventional FRP processes can meet this criterion whilst certain RDRP can fail this criterion.
4. That a "narrow" molecular weight distribution is obtained; this is subjective however a well-designed RDRP process can yield polymers with D < 1.2 and even close to 1.05 or lower. That is however not to say that a narrow dispersity implies the absence of side reactions. Similarly, a RDRP process that yields a higher dispersity whilst satisfying other living criteria should not be considered a failure from the "living" perspective.
5. That the end groups of the polymer are those imparted to it by the specific control agent used, irrespective of the RDRP process chosen.

Even amongst disagreement, it is now common to refer to a RDRP process as living if it satisfies most if not all, even if not perfectly, the criteria listed above.

2.2.2 Mechanisms and advantages of common RDRP processes

Fundamentally, the value of a well optimised RDRP system is that it displays the advantageous "living" characteristics as listed in the preceding section, and likewise yields polymers with the same desirable properties. The living characteristics of RDRP processes arise from kinetic consequences of the complex interplay between the rate coefficients for activation and deactivation of the propagating chains and other fundamental rate coefficients such as those for propagation and termination. The most general schematic for an RDRP process is shown in Scheme 2.9.

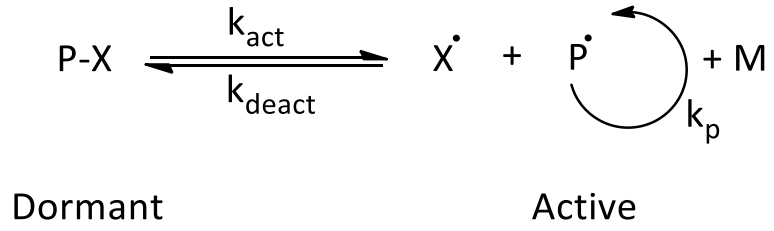

Scheme 2.9: General scheme showing a Reversible Deactivation Radical Polymerisation., adapted from [48].

The main RDRP processes, including RAFT, the Iniferter technique, ATRP and NMP, can be categorised into one of the 3 mechanisms shown in Scheme 2.10 [48].

a) Dissociation-Combination (DC)

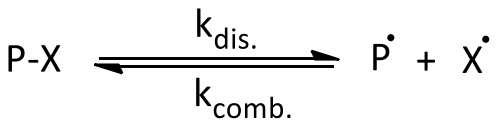

b) Atom Transfer (AT)

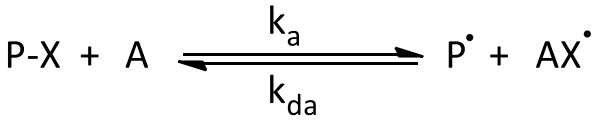

c) Degenerative Chain Transfer (DT)

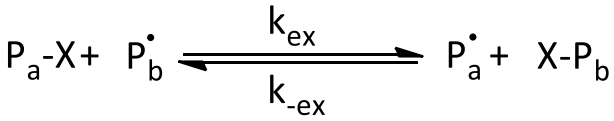

Scheme 2.10: Summary of simplified LRP mechanisms, recreated from [48].

Relevant in this context is that iniferter polymerisation with thiocarbonylthio compounds is thought to potentially obtain control from both the DC mechanism and the DT mechanism [49-52], whilst RAFT polymerisation functions exclusively via the DT mechanism [53, 54]. For a DC system, the equilibrium constant is defined as [48]:

$$K_{eq} = \frac{k_{dis.}}{k_{comb.}}$$

Equation 2.39: Definition of the equilibrium constant for a DC system.

It is interesting to note that this definition is somewhat the opposite to that for a DT system in the sense that it is the ratio of the activation to deactivation, whilst for RAFT this is essentially reversed as described in section 2.3.2.

In a typical FRP reaction which may be hours in duration, the average lifetime of a propagating radical is in the order of 1 second; in this brief time initiation, propagation and termination happen, giving an average X_n of around $10^3 – 10^4$ and a dispersity dependent on the method of termination. The rate coefficients in Scheme 2.9 are pseudo first order in nature, meaning that every dormant chain activates once every k_{act}^{-1} seconds and has an average active lifetime during which propagation can occur of k_{deact}^{-1} seconds [48]. In successful RDRP systems, the value of k_{act}^{-1} is in the order of $10 – 10^3$ s and k_{deact}^{-1} = 0.1 – 1 ms; this has the practical effect that the cumulative lifetime of propagating radicals in an RDRP system is significantly higher than then average lifetime of a propagating radical in a FRP system [48]. Importantly, the same rate coefficients that allow this behaviour to occur also results

in the rate of exchange between dormant (P-X) and active species (P*) being high relative to termination and initiation, and that at any given time, the ratio [P*]/[P-X] < 10^{-5} [48]. Ultimately this means that for most of the time, the living polymer chain is in the dormant state, which allows the propagating radicals to all grow intermittently at roughly the same rate and thus achieve a lower dispersity for the molecular weight distribution. For the two RDRP techniques of interest (Iniferter & RAFT), expressions can be derived for the expected kinetic behaviours of these systems, the number average molecular weight and dispersity of the molecular weight distributions. For a thorough analysis and derivation of these the reader is referred to [48, 55], however the following expressions have been taken from [47]. These expressions assume ideal conditions i.e. chain length independent rate coefficients and negligible influence of side reactions including initiation from other sources and conventional termination reactions.

For a dissociation combination system such as in the iniferter case, the number average molecular weight is given by:

$$M_n = \frac{([M]_0 - [M]_t)}{[P-X]_0} \cdot M_0 + M_{P-X}$$

Equation 2.40: Expression for the number average molecular weight obtained via an ideal dissociation combination process.

Where:

$[M]_0 - [M]_t = \ monomer\ consumed$

$[P-X]_0 = concentration\ of\ iniferter\ agent\ at\ t = 0$

$M_0 = molecular\ weight\ of\ monomer$

$M_{P-X} = molecular\ weight\ of\ iniferter$

$$Đ = \frac{X_w}{X_n} = 1 + \frac{1}{X_n} + \left(\frac{2-c}{c}\right) \cdot \frac{k_p \cdot [P-X]}{k_{comb.}}$$

Equation 2.41: Expression for the dispersity obtained via an ideal dissociation combination process.

Where k_c is the rate constant for combination of the dormant and active radicals, and all other constants are as defined previously.

$$ln\frac{[M]_0}{[M]_t} = \frac{3}{2} \cdot k_p \cdot \left(\frac{K_{eq} \cdot [P-X]_0}{3 \cdot k_t}\right)^{1/3} \cdot t^{2/3}$$

Equation 2.42: Expression for the expected kinetic behaviour obtained via an ideal dissociation combination process.

Where $K_{eq} = \frac{k_{dis.}}{k_{comb.}}$ and all other constants are as defined previously.

For a degenerative transfer process such as RAFT, the expression for the number average molecular weight is the same as that for a DC system (Equation 2.40) with the trivial substitution that $[P-X]_0$ is replaced by the initial concentration of CTA ($[CTA]_0$).

The expression for dispersity for a DT system is also very similar to that of a DC system:

$$Đ = \frac{X_w}{X_n} = 1 + \frac{1}{X_n} + \left(\frac{2-c}{c}\right) \cdot \frac{1}{C_{tr}}$$

Equation 2.43: Expression for the dispersity obtained via an ideal degenerative chain transfer process.

From Equation 2.41 and Equation 2.43, the key difference between the DT and DC mechanism is that the dispersity is not expected to be directly influenced by the initial concentration of control agent for the DT case.

In a DT system such as in RAFT, the initiating radicals generated come from a radical initiator with the assumption that the process of chain transfer does not retard the rate of polymerisation. Thus the kinetic description is identical to that of a conventional FRP process, the rate is given by Equation 2.20, which can also be re-written as:

$$\ln\left(\frac{[M]_0}{[M]_t}\right) = k_p \cdot \left(\frac{R_i}{k_t}\right)^{\frac{1}{2}} \cdot t$$

Equation 2.44: Expression for the expected kinetic behaviour obtained via an ideal degenerative chain transfer process, identical to that for a conventional free radical polymerisation.

2.3 Reversible Addition Fragmentation Chain Transfer (RAFT) Polymerisation

2.3.1 Fundamentals of the RAFT mechanism

As for the FRP case, the terminology regarding the RAFT mechanism varies across publications; the rate coefficients were kept as consistent as possible with the latest literature but altered where necessary to make differentiation in the Predici model easier. Irrespective of ongoing debate over the significance of potential side reactions, the overall mechanism of RAFT is not disputed [56] and is widely reported in the literature in the form as in Scheme 2.11.

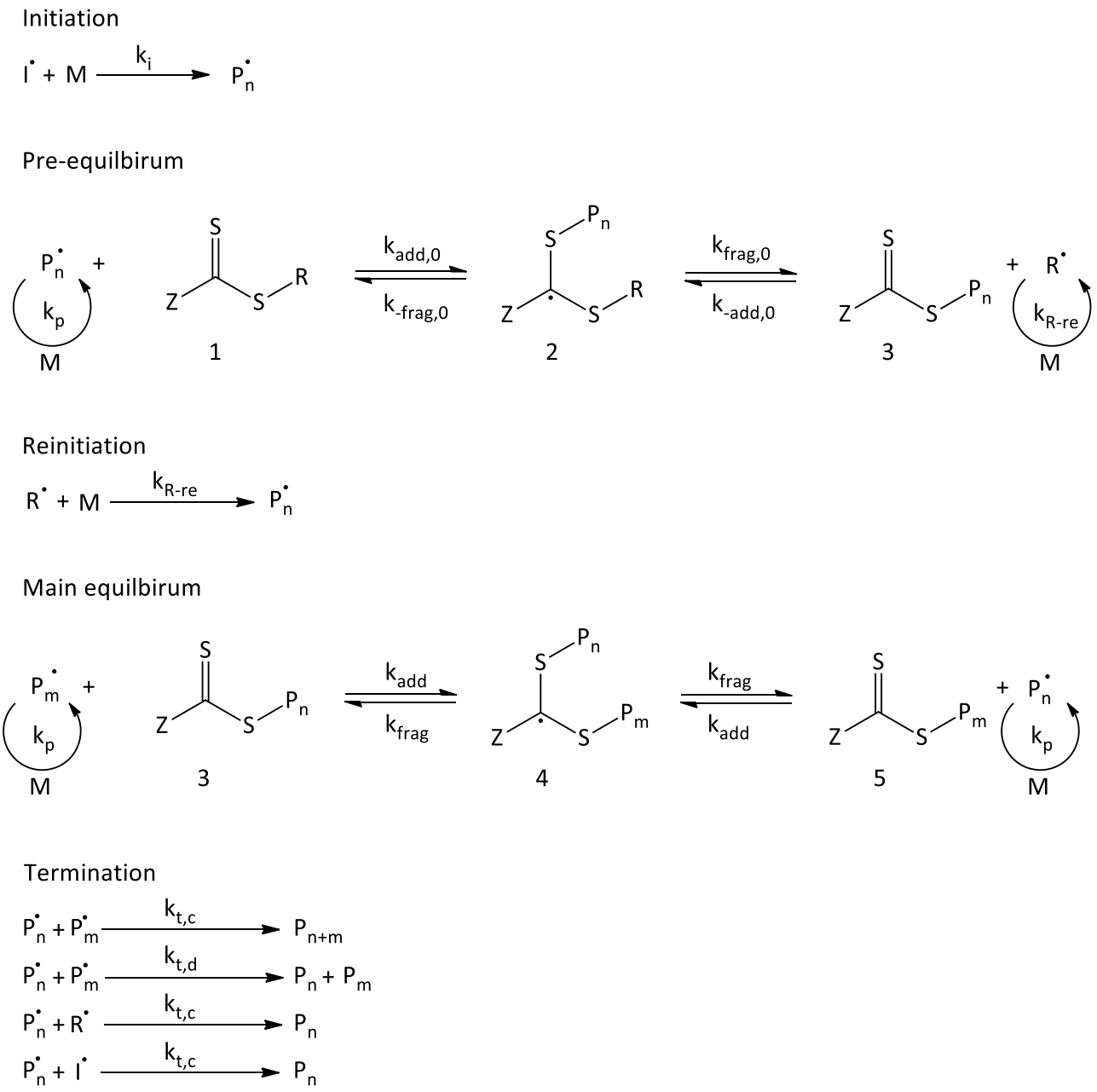

Scheme 2.11: The RAFT mechanism as it appears in literature; numbers in subsequent description relate to the numbered species in this scheme.

As implied in the name, the process of Reversible Addition Fragmentation Chain Transfer (RAFT) relies on a chain transfer process that operates when a RAFT agent is added to a conventional FRP system. This means that the RAFT mechanism operates concurrently with all the steps present within a FRP process, including initiation, propagation and termination. RAFT begins like any FRP, with initiator derived primary radicals adding to monomer, forming propagating polymeric radicals of chain length n (P_n^*). These radicals then add to the sulfur of the C=S double bond of the RAFT agent (1), forming the pre-equilibrium adduct radical (2). Radical attack on the carbon in the C=S bond is thermodynamically preferred, however a vastly greater kinetic preference for addition to the sulfur

ensures this is the dominant pathway [57, 58]. The pre-equilibrium adduct can then fragment via beta scission "back" to reform the polymeric radical and the RAFT agent (1), or fragment "forward" to release the R group radical (R*) and creating a macro-RAFT agent (3) in the process. The R* then reinitiates polymerisation by adding to the monomer, forming a propagating polymer radical of length m (P_m^*). The P_m^* adds to the macro-RAFT agent (3), forming the equilibrium adduct radical (4) which for chain lengths n ≈ m then has an equal probability of fragmentation to either side; this is the dynamic equilibrium that forms the core of the RAFT process. The process comes to a halt and "dead" polymer is formed when radicals terminate by any of the termination mechanisms shown. Several key conditions need to be fulfilled for the RAFT process to function efficiently and not result in scenarios #2 or #3 occurring as described earlier in section 2.1.2.7; these include [59]:

- The RAFT agent (1) and the macro-RAFT agent (3) need to have a reactive C=S bond (high $k_{add,0}$ and k_{add}).
- The adduct radicals (2 & 4) should fragment rapidly via beta scission and not participate in any side reactions (high $k_{frag,0}$ and k_{frag}).
- The pre-equilibrium adduct radical (2) needs to fragment preferentially in favour of the right-hand side of the reaction to release the R group radical (R*) ($k_{frag,0} \geq k_{-add,0}$) .
- The R group radical should be able to efficiently reinitiate the polymerisation by adding rapidly to the monomer ($k_{R-re} \geq k_p$).

2.3.2 Definitions of key relationships governing the RAFT process

The conditions described in the preceding section are general guidelines; to allow a more qualitative description of the RAFT process several important relationships have been defined. These, along with common methods for how they can be calculated or estimated are covered here.

2.3.2.1 Relating to the pre-equilibrium

The pre-equilibrium in the RAFT process is arguably the most complex step mechanistically, with profound consequences for both the kinetic behaviour seen and how closely the molecular weight of the polymer formed matches that of the theoretically predicted molecular weight. Two pre-equilibrium constants can be defined [54]:

$$K = \frac{k_{add,0}}{k_{-frag,0}} \quad and \quad K_\beta = \frac{k_{-add,0}}{k_{frag,0}}$$

Equation 2.45: Definitions for pre-equilibrium constants in the RAFT mechanism.

K describes the fragmentation of the pre-equilibrium adduct back to the starting RAFT agent and the P_n radical whilst K_β describes the fragmentation to release the R group radical and generate the initial macro-RAFT agent (3). Which fragmentation pathway is more likely to occur is directly reflected in how the pre-equilibrium adduct is partitioned between products and starting materials. This leads to the combination of intrinsic rate coefficients being lumped together to give "apparent" transfer rate coefficients which are defined by the partition coefficient (ϕ) [60]:

$$k_{tr,0} = k_{add,0} \cdot \frac{k_{frag,0}}{k_{frag,0} + k_{-frag,0}} = k_{add,0} \cdot \phi$$

$$k_{-tr,0} = k_{-add,0} \cdot \frac{k_{-frag,0}}{k_{frag,0} + k_{-frag,0}} = k_{-add,0} \cdot (1 - \phi)$$

Equation 2.46: Definitions for transfer rate coefficients in the pre-equilibrium of the RAFT mechanism.

The overall rate of consumption of the RAFT agent is directly related to the relative reactivity of the propagating radical (P_n^*) and the expelled radical (R^*) [54]; these are respectively quantified by initial chain transfer constants as:

$$C_{tr,0} = \frac{k_{tr,0}}{k_p} \quad and \quad C_{-tr,0} = \frac{k_{-tr,0}}{k_{R-re}}$$

Equation 2.47: Definitions for chain transfer constants in the pre-equilibrium of the RAFT mechanism.

A common method developed by the team at CSIRO for estimating $C_{tr,0}$ involves directly measuring the consumption of the RAFT agent as a function of monomer consumption [61]. If the rate of transfer back to the macro-RAFT agent (3) is assumed to be is negligible such that $C_{-tr,0} \approx 0$, the following equation is employed:

$$C_{tr,0} \approx \frac{d\ln([CTA])}{d\ln([M])}$$

Equation 2.48: Approximation for the estimation of the initial chain transfer constant via the CSIRO method [61].

For RAFT agents with high initial chain transfer constants ($C_{tr,0} > 100$), this method becomes problematic as the RAFT agent is entirely consumed within the first few % of monomer conversion [60]. Thus, this technique can only be reliably applied to RAFT agents with low to medium initial chain transfer constants [54, 60].

Polymerisations run with RAFT agents with low initial chain transfer constants tend to exhibit hybrid behaviour that does not initially behave like a well-controlled RAFT polymerisation; this is characterised by an initial spike in the molecular weight at the start of the polymerisation [54]. This

fact has been utilized by Barner Kowollik and co-workers [62] to develop a method for estimating $C_{tr,0}$ which requires determining the molecular weight of the polymer formed as a function of conversion and extrapolating the intercept to c = 0, thus giving the molecular weight of the polymeric species before it reacts with the RAFT agent. This gives the expression:

$$X_n^0 \approx \frac{[M]_0}{C_{tr,0} \cdot [RAFT]_0} + 1$$

Equation 2.49: Approximation for estimating the initial chain transfer constant as developed by Barner Kowollik *et al* [62].

2.3.2.2 Relating to the main equilibrium

The dynamic exchange of propagating species in the main equilibrium occurs with an equal probability of fragmentation and addition to either side of the equilibrium ($\phi = 0.5$) once the chain lengths of the two propagating species reach a sufficient length or are inherently similar at the onset, such that n ≈ m (Scheme 2.11). This leads the equilibrium constant, chain transfer constant and chain transfer coefficients having definitions [60]:

$$K_{eq} = \frac{k_{add}}{k_{frag}} \quad and \quad C_{tr} = \frac{k_{tr}}{k_p} \quad with \quad k_{tr} = k_{add} \cdot \frac{k_{frag}}{k_{frag} + k_{frag}} = k_{add} \cdot 0.5$$

Equation 2.50: Definitions for relationships relating to the main RAFT equilibrium.

The equilibrium constant for the main equilibrium ultimately determines the relative concentrations of the propagating species and the dormant species in the form of the RAFT adduct radical; this value has been theoretically predicted to range over many orders of magnitude and is strongly influenced by RAFT agent structure [63]. The chain transfer constant C_{tr} reflects the relative reactivity of the macro-RAFT agent to the rate of propagation; this essentially determines how many monomer units can add during each activation cycle. A simple and thus commonly used method for determining C_{tr} from experimental measurements of D, Xn and c was developed by Goto and Fukuda [48]:

$$Đ \approx 1 + \frac{1}{X_n} + \frac{2 - c}{c \cdot C_{tr}}$$

Equation 2.51: Approximation for estimating the chain transfer constant developed by Goto and Fukuda [48].

For a comprehensive review and comparison of other techniques for determining both initial and main chain transfer constants in RAFT polymerisation, the reader is referred to the excellent review by Derboven *et al.* [60], along with recent pioneering work from the same research group by De Rybel *et al.* [64].

2.3.3 Structure property relationship of RAFT agents

The kinetic descriptors and ratios thereof that define the various constants in the preceding sections are determined by the reactivity of the RAFT agent, the propagating radical and thus the combination of the two in the form of the RAFT adduct radical. This is fundamentally linked to the chemical structure of both the initial RAFT agent and the propagating radical. The success of a RAFT polymerisation relies critically not only on the selection of the reaction conditions, but most importantly, the selection of the correct RAFT agent for the desired monomer to be polymerised.

2.3.3.1 Role of the Z group

The key factor in determining the reactivity of a RAFT agent is the chemical nature of the Z group. The Z group directly affects the electron density and electron delocalisation of the C=S bond, which directly impacts its reactivity towards radical addition. After experimental observations that the Z group was critical to the control obtained during a polymerisation [7, 65], several key studies [66-68] systematically determined the effect of the Z group by using a series of RAFT agents with fixed R groups and varying Z groups in the polymerisation of various monomers. The overwhelming experimental evidence showed that as the electron withdrawing ability of the Z group increased, there was an observed increase in the apparent chain transfer constant. These results were used to establish that the rates of radical addition and subsequent rate of fragmentation follow the trends shown in Scheme 2.12.

Scheme 2.12 has been removed due to copyright restrictions.

Scheme 2.12: For Z, the rate of addition (k_{add}) decreases and the rate of fragmentation (k_{frag}) increases when going from left to right. The dashed lines indicate partial control over the polymerisation, meaning control over molecular weight but poor control over dispersity or substantial retardation in the case of VAc, NVP or NVC. Taken from [56].

These conclusions are ultimately based on the rationale that if the R group is reactive enough to efficiently reinitiate polymerisation ($k_{R-re} \geq k_p$), then the differences in chain transfer constant must fundamentally arise due to parameters associated with the Z group and subsequently the rate coefficients on the left-hand side of the RAFT pre-equilibrium. Furthermore, the rate of fragmentation is influenced by the Z group; this can arise due to the Z group stabilising the RAFT agent formed after fragmentation or destabilising the RAFT adduct radical along with decreasing the double bond character of the initial RAFT agent [69].

The lower activity and subsequently lower chain transfer constants (for a given monomer as compared to other RAFT agents) for xanthates and dithiocarbamates can be qualitatively rationalised due to the

ability of these moieties to delocalise the electron density by virtue of the formation of their canonical forms via the following mechanism [66] as shown in Scheme 2.13:

Scheme 2.13: Canonical forms of dithiocarbamates (left) and xanthates (right). Adapted from [66].

This subsequently reduces the double bond character of the C=S bond whilst simultaneously stabilising the RAFT agent, both these factors reducing their overall reactivity towards radical addition [65, 66].

The trend of dithiocarbamates and xanthates having lower reactivity can be somewhat reversed by careful modification of the Z group with electron withdrawing substituents, further reinforcing the general trends found across various Z groups and the importance of the canonical forms. This is illustrated with studies by Adamy *et al.* [70], Chiefari *et al.* [67] and Destarac *et al.* [71] which all showed greater control over the M_n and Đ for MAMs such as styrene and ethyl acrylate with xanthates as the electron withdrawing ability of the Z group was increased. Similarly, Destarac *et al.* showed similar behaviour for cyclic and N,N-disubstituted dithiocarbamates, which can be applied with limited success to both styrene and vinyl acetate polymerisation, with moderate control over Đ in the former and significant retardation for the later [72]. For the polymerisation of LAMs like vinyl acetate, the opposite is seen; Stenzel *et al.* reported that for xanthates where Z were a series of phenol derivatives, the inhibition times increased as the electron withdrawing ability of the Z substituent was increased [69].

A seemingly inverse dichotomy exists; RAFT agents suitable for MAMs either inhibit and/or retard the polymerisation of LAMs, whilst RAFT agents suitable for LAMs show little to no control in the polymerisation of MAMs. For the two classes of monomers, this can be summarised if the RAFT mechanism is viewed as two fundamentally competing steps, namely those on either side of the RAFT pre-equilibrium as shown in Scheme 2.14.

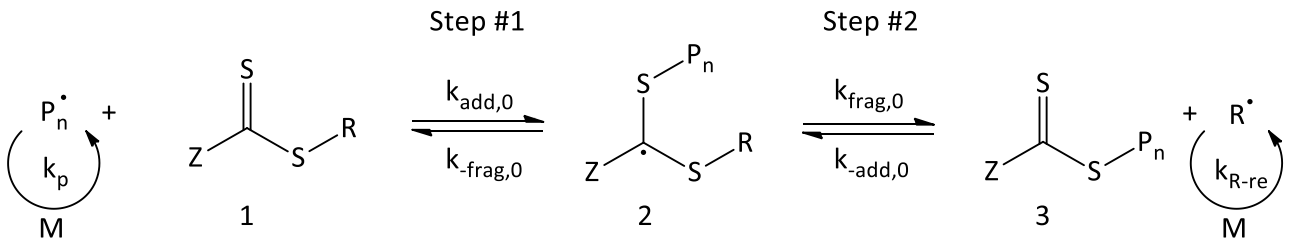

Scheme 2.14: RAFT pre-equilibrium.

- For MAMs, the P_n radical is relatively stable and thus unreactive, hence the Z group needs to be chosen such that step #1 needs to be promoted. Z needs to either destabilise the starting RAFT agent (1) to make it more susceptible to radical attack or stabilise the radical adduct (2).
- For LAMs, the P_n radical is relatively unstable and thus more reactive, hence step #1 is not the limiting factor and it is step #2 that needs to be promoted. The radical adduct (2) cannot accumulate in significant quantities as this can cause retardation or inhibition. The Z group needs to promote fragmentation by either destabilise the RAFT adduct radical (2) or stabilise the RAFT agent formed after fragmentation (3).

2.3.3.2 Role of the R group

The role of the R group has been explored with an identical approach to that of the Z group; experimental studies have utilised a series of RAFT agents with a fixed Z group and varying R groups. The influence on M_n and Đ along with kinetic behaviour can be related back to the RAFT mechanism using the same rationale; namely that if the Z group is chosen such that $k_{add,0}$ & $k_{add} \geq k_p$, then any subsequent effects must arise from the R group. The stability and re-initiating ability of the R directly influences the rate coefficients on the right-hand side of the RAFT pre-equilibrium, which impacts the overall chain transfer constant by affecting the partition coefficient. These assertions were experimentally confirmed by the pioneering work of Chong *et al.*, who used a series of dithiobenzoates with varying R groups for the polymerisation of methyl methacrylate, styrene and butyl acrylate [73]. Their results confirm the rate of addition to the RAFT agent is not strongly influenced by the R group, however it has major implications on the chain transfer constant and the subsequent overall control seen. This includes the presence of so called "hybrid behaviour" typified by an initial spike in the molecular weight [74] and on the dispersity of the polymer obtained. Similar results were obtained by Favier *et al.* who saw hybrid behaviour in the polymerisation of N-acryloylmorpholine with carboxymethyl dithiobenzoate, which was attributed to the significantly poorer leaving ability of the carboxymethyl R group relative to the propagating N-acryloylmorpholine (NAM) radical [75]. Furthermore, these observations extend to the less active RAFT agents such as

dithiocarbamates and xanthates albeit with a caveat, especially when they are used to polymerise MAMs. In this case the R group can mitigate the size of the initial spike in molecular weight however not prevent it entirely as this is caused by a mismatch between the reactivity of the RAFT agent (as dictated by the Z group) and the reactivity of the propagating radical. Furthermore a "correct" choice of R group will narrow the dispersity of the polymer obtained as a function of conversion however often in a limited fashion, i.e. it might be the difference between a dispersity of 2 or 1.7 upon reaching high conversion. These were essentially the findings of Destarac *et al.*, who using a series of O-ethyl xanthates in the polymerisation of styrene saw an increase in the chain transfer constant and better agreement between the obtained and expected molecular weight as the radical stabilisation ability of the R group increased [76].

The phenomenon of incredibly slow polymerisation that can resemble total inhibition has been extensively investigated by McLeary *et al.* for St [77, 78] and MA [79] polymerisations with dithiobenzoates and by Pound *et al.* for VAc and NVP polymerisation with xanthates [80]. Preferential consumption of the RAFT agent to form a single monomer addition product followed by conversion to higher molecular weight species was observed. The rate of RAFT agent consumption and thus the extent of the inhibition period was found to vary with the identity of the R group. The more stable R group fragmented preferentially and had a lower $k_{R\text{-}re}$ than k_p, thus leading to preferential conversion of the RAFT agent into a single monomer product. Combined, these experimental findings have led to the general guideline that the R group should be selected such that it gives a radical of equal or slightly greater stability and thus equal or greater re-initiation efficiency than that of the propagating radical [56]. The various R groups and the monomers to which they can be applied is seen in Scheme 2.15:

Scheme 2.15 has been removed due to copyright restrictions.

Scheme 2.15: For R, fragmentation rates decreases from left to right. The dashed lines indicate partial control over the polymerisation, meaning control over molecular weight but poor control over dispersity or substantial retardation in the case of VAc, NVP or NVC. Taken [56].

Various theoretical studies [81] have shown that the sufficiently electron withdrawing R groups can influence RAFT agent reactivity towards radical addition by destabilising the RAFT agent and the RAFT adduct radical. This occurs when the resonance effect shown in Scheme 2.16 is minimised, however the possible contribution of this effect is dwarfed by the effect of the Z group as described previously.

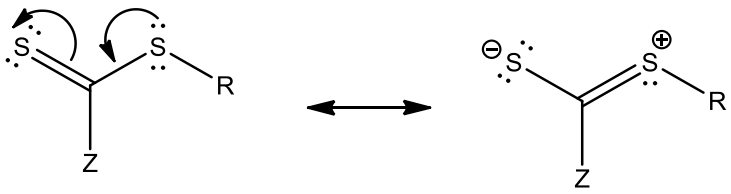

Scheme 2.16: Resonance effects of R group on RAFT agent structure.

2.3.4 Rate retardation and inhibition during polymerisation with dithiobenzoates

Owing to their high reactivity and thus ability to control the most stable of the MAMs including the methacrylate class of monomers, dithiobenzoates are a popular class of RAFT agent. However, over the years seemingly contradictory reports have arisen over rate retardation and inhibition periods observed when dithiobenzoates are used for the polymerisation of MMA, MA and styrene [73, 74, 82]. Stemming from an initial publication outlining these discrepancies [83], a whole field of inquiry has arisen [84, 85], including studies hunting for the elusive stable radical intermediates [86, 87], suggested evidence of a missing step in the RAFT mechanism [88, 89] and *ab initio* evidence for slow fragmentation of the RAFT adduct radical [58]. Besides the slow fragmentation hypothesis, all other explanations fall into the categories of either irreversible and reversible termination of the RAFT adduct radical. For a comprehensive and current review on the matter, the reader is referred to a recent review by Moad [90].

2.3.5 Key advantages of RAFT polymerisation

As described in the preceding sections, a well-designed RAFT polymerisation has the key advantages of a living polymerisation technique; namely the ability to target specific molecular weights by changing RAFT agent concentration, a narrow dispersity of chain lengths for the resulting polymer and high-end group fidelity. However, these are not the only characteristics that make RAFT appealing for polymer synthesis for research and commercial applications. The thiocarbonylthio moiety is not solely reactive towards radicals but can also undergo a wide range of chemical transformations, which make RAFT terminated polymers attractive substrates for further derivatisation. These processes are summarised in Figure 2.7. For a general overview of available processes, the reader is referred to the comprehensive reviews by Moad *et al.* [91, 92] and Willcock & O'Reilly [93]. Articles and reviews by Boyer *et al.* focus more on tandem RAFT group transformations coupled with thiol-ene click chemistry and the biomedical and biological applications of these polymer conjugates [94-98]. The photochemistry and associated photochemical transformations possible with thiocarbonylthio compounds is covered in later sections of this chapter. The advantages of the presence of the RAFT group in polymer analysis is also covered later.

Figure 2.7 has been removed due to copyright restrictions.

Figure 2.7: Processes for RAFT end group transformations, where R'· = radical, H = hydrogen donor and M = monomer. Taken from [91].

RAFT polymerisation does not have inherent limitations on monomers bearing halogens or carboxylic acid functionality due to these functionalities not interfering with the core RAFT mechanism; this is not the case for ATRP where these monomers require specific reaction conditions [99]. Furthermore, the absence of heavy metal catalysts in the RAFT process simplifies purification of polymers and allows their use in biomedical and biological settings [95, 100]. Indeed, presence of RAFT end group functionality does not necessarily increase the cytotoxicity of the polymer, and in any case, it can be removed by a multitude of simple approaches [100]. Lastly, a plethora of RAFT agents are commercially available from Sigma Aldrich, along with several companies like Lubrizol and Boron Molecular able to synthesise RAFT agents in commercial multi-ton quantities.

Figure 2.8 has been removed due to copyright restrictions.

Figure 2.8: A summary of polymer architectures accessible by RAFT polymerisation. Taken from [101].

A key advantage of RAFT is the ability to access a wide range of polymer architectures, and these are depicted in Figure 2.8. For comprehensive reviews of these, the reader is referred to [56, 102-104]. One of the primary areas of research within the RAFT field and within this thesis is overcoming the specific limitations that arise when RAFT is applied to the synthesis of polymers and copolymers of monomers with disparate reactivities, namely on opposite ends of the reactivity spectrum. This is discussed in detail in the following section.

2.3.6 Limitations of RAFT in the synthesis of block copolymers

Diblock and multiblock copolymer synthesis via chain extension of a macro-RAFT agent brings with it same challenges as explained previously regarding correct Z and R group selection, however in this case the R group is polymeric in nature. Furthermore, as the RAFT mechanism does not eliminate termination, the starting macro-RAFT agent will never retain 100% RAFT end group functionality and will always contain some dead chains. Assuming 100% chain end fidelity, the RAFT mechanism for block copolymer formation is shown in Scheme 2.17. In Scheme 2.17, it is evident that due to termination, alongside the desired A-B copolymer with RAFT end group functionality (blue rectangle) that a range of undesired biproducts can occur (red rectangle). These are termed "dead" polymer species as they no longer retain the RAFT moiety which gives them their "living" characteristics. These include A-B-A triblock copolymers, A-B diblock copolymers and B

homopolymer. If the RAFT end group is to be removed post polymerisation or further chain extension with a third monomer is not desired, the formation of A-B copolymer without the RAFT end group becomes less of a concern.

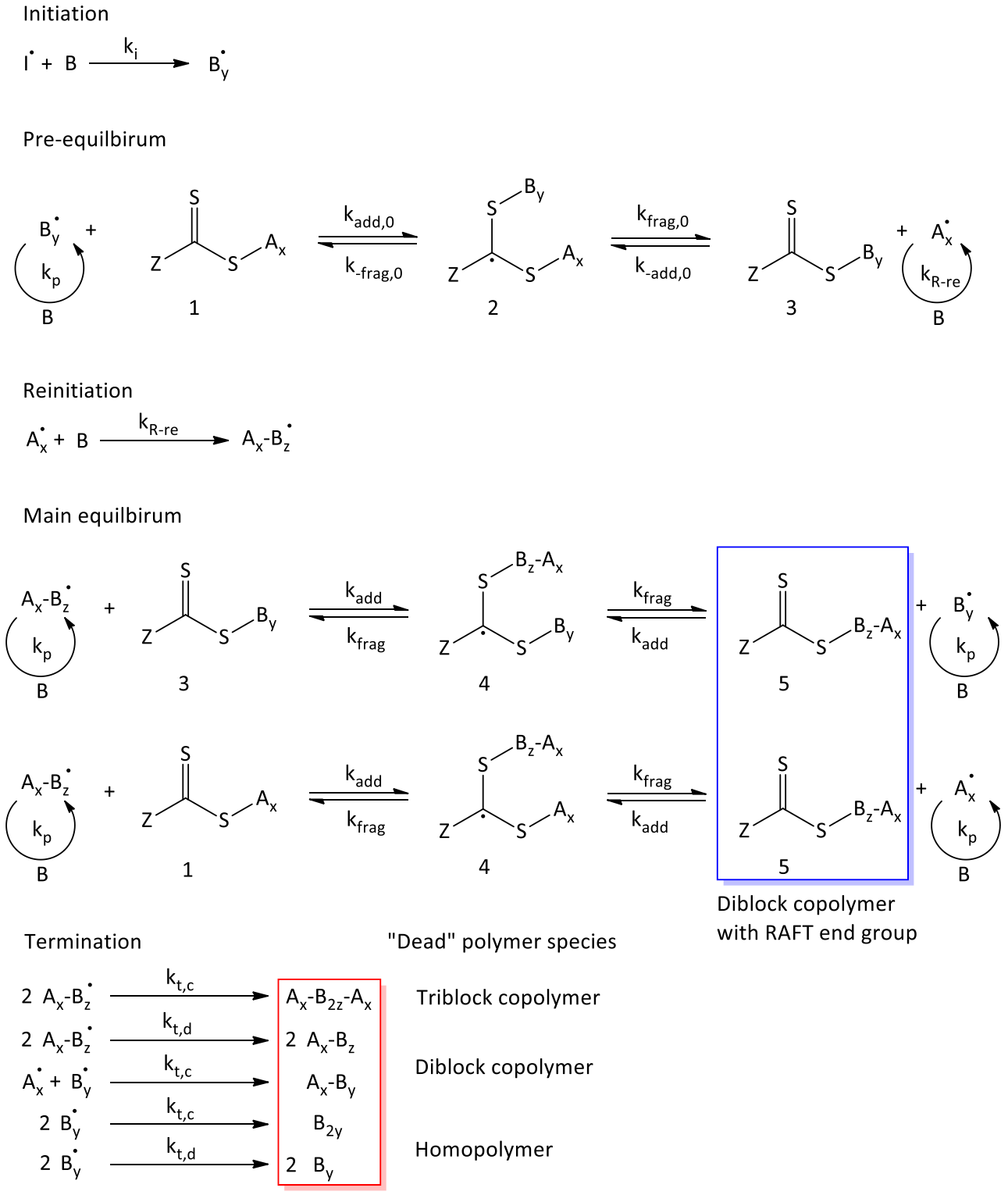

Scheme 2.17: RAFT mechanism for the synthesis of block copolymers of the form A_x-B_z. Adapted from [103].

Due to the nature of the monomers and the stability of the radicals that they form (as has been explained previously), it is very difficult to make poly(MAM-b-LAM) copolymers and essentially impossible to make poly(LAM-b-MAM) copolymers. In the former case, this arises from the fact a Z group suitable for the synthesis of the starting polyMAM macro-RAFT agent will be reactive enough to trap LAM radicals but can prevent their efficient fragmentation. In the latter case, the Z group suitable for the initial polyLAM block will be unreactive enough to efficiently trap MAM radicals. Furthermore, once a MAM radical is trapped by the polyLAM macro-RAFT agent, it will preferentially fragment in the "wrong" direction to release the MAM radical, as polyLAM radicals are very poor leaving groups with respect to polyMAM radicals. This leads to the observation that polyLAM derived macro-RAFT agents tend to have very low chain transfer constants in MAM polymerisations [56]. It is always recommended to polymerise the more "MAM like" monomer first, especially when dealing with methacrylate monomers. Surprising exceptions to this rule have been reported; this includes copolymers of N-isopropylacrylamide (NIPAAm) with methyl methacrylate [105] and with methacrylic acid [106]. Observations in the preceding studies did include a broadening of the molecular weight distribution and some unreacted macro-RAFT agent and trace quantities of secondary homopolymer [106]. Examples where the differences in monomer reactivity are less extreme include interchangeable sequences of styrene with butyl acrylate [107] and with 4-vinylbenzylchloride [108]. A comprehensive tutorial article outlining these concepts and guidelines for the synthesis of block copolymers via RAFT has been written by Keddie [109].

2.3.7 Avenues to overcoming the limitations of block copolymer synthesis with RAFT

5 general categories of approaches have been devised to overcome these limitations in block copolymer synthesis; the include:

1. Altering the reactivity and radical trapping properties of the RAFT agent via reversible chemical modification of the Z group.
2. The design of a "universal" RAFT agent that can in principle be applied to the polymerisation of any polymerisable 1,1-disubstituted and 1,1,2-trisubstituted alkenes.
3. Use of non-standard RAFT polymerisation conditions to synthesise oligomers where the placement of individual monomers can be controlled [40].
4. Circumventing the limitations of the RAFT mechanism by utilising a dual functional RAFT agent that can be used in conjunction with another CRP method [110, 111].
5. The synthesis of the two blocks separately by RAFT and/or another CRP, followed by a method of covalent linkage, typically via a highly efficient "click" chemistry approach [112, 113].

The first two approaches will be covered in greater detail in the forthcoming sections as they relevant in the context of this thesis.

A completely standalone approach is the manipulation of the reactivity of the monomer being polymerised to effectively change the "MAM or LAM" character of the monomer. In a first in the RAFT context, Liu *et al.* used 2-cyanoprop-2-yl-1-dithionaphthalate (CPDN) to polymerise N-vinylpyrrolidone (NVP) in the presence of 1,1,1,3,3,3-hexafluoro-2-propanol (HFIP) [114]. NVP is a LAM and CPDN is suited to the polymerisation of MAMs, a range of solvents were used, however only in the presence of HFIP were acceptable dispersity values (~ 1.3) achieved along with a pronounced acceleration of the polymerisation rate. Crucially, with HFIP as solvent, poly(NVP-b-PS) and poly(NVP-b-PMA) block copolymers were synthesised with ~ 75% consumption of the starting polyNVP macro-RAFT agent. The authors attribute this behaviour to a hydrogen bonding interaction between the NVP monomer and HFIP changing the reactivity of the alkene double bond, and provided ^{1}H NMR evidence to support this claim.

2.3.7.1 Acid/base switchable dithiocarbamates

Benaglia *et al.* first reported a series of N-(4-pyridinyl)-N-methyl dithiocarbamate RAFT agents which could be switched reversibly by protonation of the pyridinyl Z group with a strong acid [115]. In their protonated form, the dithiocarbamates give good control over MAMs such as MMA, MA, BA and St, whilst retarding LAMs such as NVC. Protonation followed by neutralisation with N,N-dimethylaminopyridine (DMAP) allowed the synthesis of poly(MMA-b-VAc) and poly(MA-b-NVC). Expanding on this, Benaglia *et al.* refined the approach by making poly(St-b-MA-VAc) after high dispersities (~2) and significant inhibition times (~ 4 h) were seen when the direct synthesis of poly(St-b-VAc) was attempted using a deprotonated PS macro-RAFT agent [116]. Keddie *et al.* successfully polymerised DMAm in aqueous solution and subsequent chain extension with NVC, VAc and NVP in organic solvents yielded several well defined monodisperse block copolymers [117]. Key findings from several publications include that a non-protic Lewis acids such as aluminum triflate could also be used, however best results are always obtained when a strong organic acid such as p-tolusulfonic acid is used in stoichiometric quantities relative to the RAFT agent [117, 118]. The final iteration of this concept was further manipulation of the reactivity of the Z group by using N-aryl-N-pyridyl dithiocarbamates with varying aryl substituents by Keddie *et al.* [119]. The key finding of a direct linear correlation between the Hammett parameter of the aryl substituent and the apparent chain transfer coefficient explains the overall better control over MA polymerisation in the protonated form and higher retardation in VAc polymerisation with an increase in the electron withdrawing ability of the substituent. This is summarised in Figure 2.9.

Figure 2.9 has been removed due to copyright restrictions.

Figure 2.9: Reactivity trends with the acid/base switchable dithiocarbamates developed by CSIRO. Taken from [119].

2.3.7.2 A universal RAFT agent – the "Holy Grail" of RAFT

A truly revolutionary approach came from Coote & Henry, who used thermodynamic descriptors of RAFT agent reactivity calculated from *ab initio* calculations to design an entirely new class of RAFT agent, namely a fluoro dithioformate where the Z group is a fluorine atom [120]. Theis *et al.* synthesised benzyl fluoro dithioformate (BFDF, R = 5 in Scheme 2.18), however in initial tests it showed hybrid behaviour when applied to styrene polymerisation [121]. Upon further theoretical investigation into R group selection for the new class of F-RAFT agents by Coote *et al.* [122], Busch *et al.* synthesised and briefly tested isopropyl fluoro dithioformate (IFDF, R = 4 in Scheme 2.18) for the high-pressure polymerisation of ethylene [123]. Results indicated improved control over the control experiment in the absence of any control agent, however hybrid behaviour was once again seen.

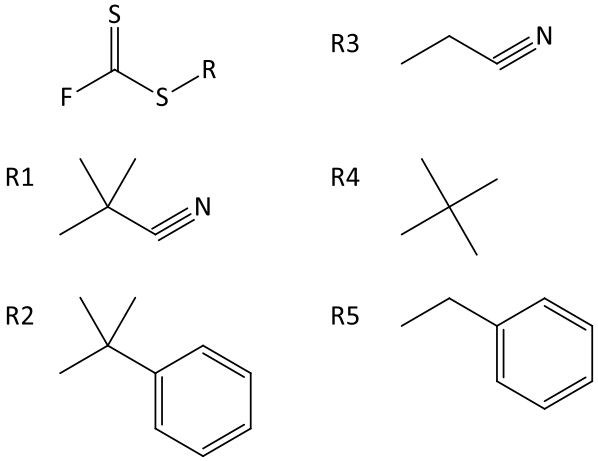

Scheme 2.18: Generic F-RAFT agent (top left), with varying R substituents giving hypothetical F-RAFT agents R1--3. RAFT agents R = 4 and R = 5 were synthesised, being IFDF and BFDF respectively. Compiled from [121] [122, 123].

Although Destarac *et al.* first claimed cyclic and N,N-disubstituted dithiocarbamates could behave as "universal" RAFT agents in 2000 [72], as described previously in section 2.3.3.1, the results obtained were sub-optimal and far from what would be expected of a true universal RAFT agent. Building upon this original work, others have however had greater success with dithiocarbamates as general if not truly "universal" RAFT agents. Malepu *et al.* reported that malonate N,N-diphenyl dithiocarbamate was applicable to both VAc, MA and t-BA, giving dispersities less than 1.5 in all cases even at high targeted M_n values. Poly(MA-b-VAc) was synthesised and the block order was again affirmed to be crucial to successful block copolymer formation [124]. Dayter *et al.* expanded

on the original work with MDP-DTC which allowed the synthesis of PS-b-PVAc copolymer with a considerable range of PS to PVAc block lengths whilst maintaining monomodal molecular weight distributions with reasonable dispersities (~1.5 for most cases) [125].

Gardiner *et al.* have recently improved on previous studies to provide a more complete picture of how subtle variations in the Z group gives dithiocarbamates a broad range of activity, as summarised in Figure 2.10 [126, 127].

Figure 2.10 has been removed due to copyright restrictions.

Figure 2.10: Effect of dithiocarbamate groups on RAFT agent activity. Taken from [127].

The ability to synthesise copolymers from both MAMs and LAMs, including DMA with MMA and MMA with VAc was demonstrated, however the observation was made that only narrow dispersity polymers are possible if some of the more active comonomer remains, and for the DMA/MMA case the reactivity ratios differed significantly to literature values [126]. Synthesis of quasi-block copolymers, where the first monomer is polymerised almost to completion followed by addition of the second monomer, was undertaken with 3,5-dimethyl-1H-pyrazole based dithiocarbamates. Both poly(DMA-b-VAc) and poly(DMA-b-MA) were synthesised; in the former case, complete consumption of the PDMA macro-RAFT was seen along with some PVAc homopolymer formation. In the latter case some residual PDMA macro-RAFT was observed along with a higher molecular weight shoulder in the block copolymer, attributed to side reactions inherent to acrylate reactivity [126]. In the subsequent publication, a further two 4-Halogeno-3,5-dimethyl-1H-pyrazole-1-carbodithioates (halogens tested = chlorine & bromine) were investigated and provided better control over both MAM and LAM polymerisations thus showing this substituent increases their reactivity, albeit with slower polymerisation of VAc. The quasi-block copolymer poly(DMAm-b-VAc) was synthesised, however showed a broader dispersity and a higher molecular weight shoulder; when the same block copolymer was made with an acid base switchable dithiocarbamates, the dispersity was better and no such artefacts were evident [127].

2.4 Initiator Transfer Terminator (Iniferter) polymerisation

2.4.1 Iniferter mechanism with TCT compounds

The idea of using a one component polymerisation system, where a single reagent causes the Initiation, Transfer and Termination reactions with monomer was termed the Iniferter approach by Otsu & Yoshida in 1982 [5, 128]. The idea of TCT as initiators of polymerisation was explored much earlier by Ferington & Tobolsky [129], Walter & Reding [130] and Okawara *et al.* [131]. An iniferter

should thermally or photochemically dissociate into two radicals; one which is reactive enough to add to monomer and is responsible for initiation (A*), and another radical that is much more stable, long lived, and primarily responsible for reversible termination with propagating radicals (B*) [49]. These compounds fall into two different categories, namely unsymmetrical A-B type iniferters where the two constituent radicals have significantly different reactivities, and symmetrical C-C type iniferters which release two identical radicals of the same reactivity. Upon either photolysis or thermal breakdown, A* and B* radicals are formed and 2 C* radicals respectively, and in the presence of monomer (M), the process forms polymers as is illustrated in Scheme 2.19.

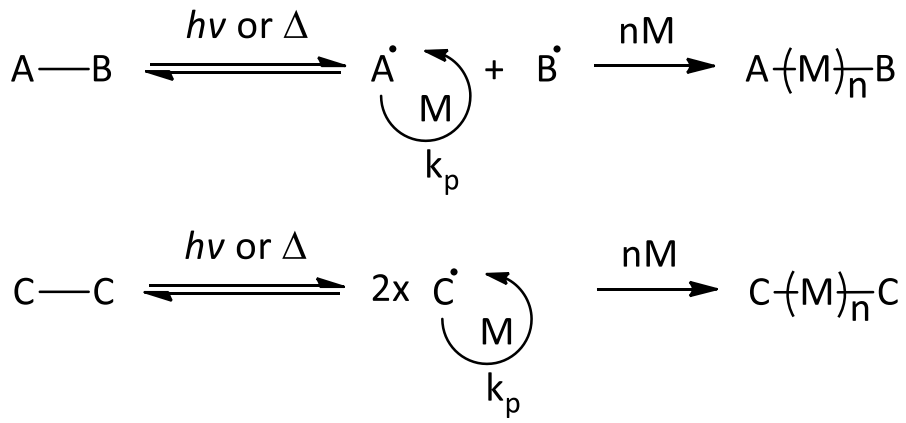

Scheme 2.19: Illustrated function of A-B and C-C type iniferters. Adapted from [49].

For the case of TCT compounds, it is commonly accepted that the significantly less reactive thiyl radical functions as the stable long-lived species, whilst the R group radical functions to reinitiate the polymerisation, just like in the RAFT mechanism. Thus, for simple TCT compounds as used in RAFT, in an iniferter context they behave as an A-B type iniferter. The process of a C-C iniferter is more complicated, as upon addition of monomer the reactivity of the propagating radical will change, and it is possible for a C-C iniferter convert to an A-B type iniferter by the very nature of its function. Symmetrical bis thiocarbonylthio disulfides fall into this category.

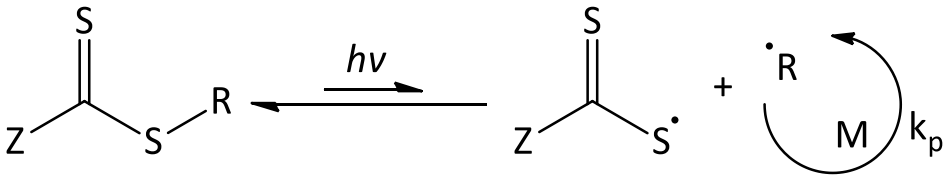

Scheme 2.20: Summary of simplified photoiniferter mechanism with TCT compounds.

The iniferter mechanism with TCT compounds was initially thought to follow strictly a dissociation combination pathway (Scheme 2.20), however as TCT compounds are utilised in RAFT, the possibility arises for degenerative chain transfer to occur [132], essentially leading to a hybrid RAFT mechanism (Scheme 2.21) [133].

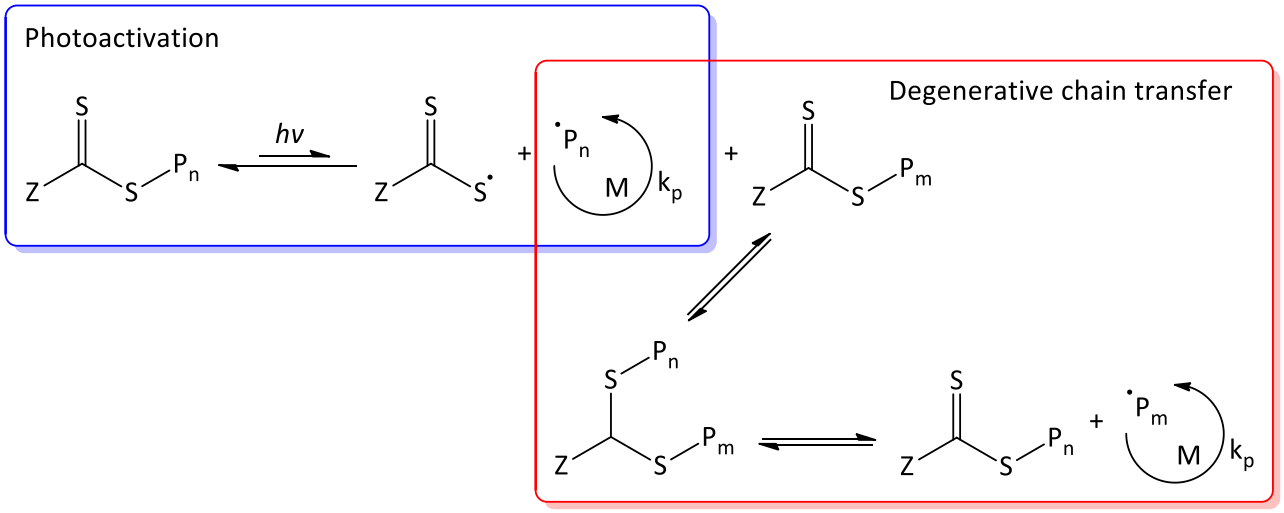

Scheme 2.21: Iniferter mechanism with degenerative chain transfer included. Adapted from [133].

The reactions shown here are idealised process; like in an RDRP process, termination still occurs in a dissociation combination mechanism. As described by Goto & Fukuda [48, 55], a typical DC polymerisation is characterised by the persistent radical effect and at the start, there are no radicals present. When the A-B molecule dissociates, initially the concentrations of A* and B* increase linearly with time; A* can add monomer and propagate but is treated as being kinetically identical to the starting A* species. As the [A*] and [B*] continue to increase, at a certain point the reactions between propagating A*s and A* and B* will start to become significant. Self-termination of propagating A*s leads to a decrease in [A*] relative to [B*], eventually leading to the establishment of a quasi-equilibrium, where the rate of deactivation equals the rate of dissociation. After this point is reached, the [A*] reaches a maximum and continues to decrease due to self-termination; in the absence of secondary initiation sources, this eventually leads to an incredibly slow polymerisation that essentially stops the reaction.

2.4.2 Reactivity of thiyl radicals towards monomer addition

There is an ongoing debate about the actual reactivity of thiyl radicals towards the addition of various monomers; early work by Otsu & coworkers showed that thiyl radicals derived from the photolysis of various bis thiocarbonylthio disulfides could be used to initiate polymerisation [5, 134, 135]. Lambrinos *et al.* also made similar observations, however noted the slow and often incomplete consumption of the starting N,N-diethyldithiocarbamate even as high molecular weight polymers formed, implying the thiyl radicals generated have very low reactivity towards monomer addition [136].

Lalevée *et al.* have investigated the respective roles of both the initiating and thiyl radicals within iniferter polymerisation using a range of compounds (see Figure 2.14) for the polymerisation of MMA and 1,6-hexane diol diacrylate. Key findings were that the thiyl radicals are indeed primarily the cause for reversible termination as per a DC mechanism, having high dissociation rate coefficients (~ 10^8 M^{-1} s^{-1}) and long lifetimes greater than 20 μs in solution [137, 138]. Furthermore, it was found that an increase in the quantum yield for dissociation was not directly related to an increase in the polymerisation rate. An upper limit of ~ 10^3 M^{-1} s^{-1} was proposed for the rate coefficient of MMA addition to a range of thiyl radical species, with the more reactive the thiyl radical species, the poorer the overall control seen [137, 139]. This supported the earlier work of Bertin *et al.* [140].

2.4.3 The role of degenerative chain transfer in TCT mediated iniferter polymerisation

Matyjaszewski surmised that the prominent characteristics of polymerisations seen in the early iniferter investigations [5, 128, 134, 135] can be described as typical hybrid behaviour as it applies to RAFT polymerisation, where the choice of monomer and RAFT agent are suboptimal to achieve good control [141]. There has been ongoing debate of the importance of degenerative chain transfer in iniferter polymerisation relative to the control obtained via a DC mechanism.

The work of Niwa *et al.* showed varying degrees of hybrid behaviour for the polymerisation of MA and MMA with bis(isopropy1xanthogen) disulfide [142, 143], including a decrease of degree of polymerisation with increased reaction time. Kilambi *et al.* studied the polymerisation of hexyl acrylate with tetraethylthiuram disulfide (TED), only considering chain transfer to the TCT compound as being a termination reaction and non-reversible in nature. Based on this, it was concluded that at room temperature chain transfer contributed more to the termination rate than combination with dissociated thiyl radicals [144]. Lalevée *et al.* saw hybrid behaviour in all their investigations, however attributed the initial spike in molecular weight to termination events and not a poor chain transfer efficiency, having not included chain transfer in their reaction schemes [137-139].

You *et al.* polymerised St, MMA and BA with dibenzyl trithiocarbonates under UV irradiation, seeing satisfactory control in all cases, and showed the formation of a PMA-b-PS-b-PMA copolymer with the trithiocarbonate moiety at its centre [145]. They explicitly claim that the control seen was a combination of the RAFT and iniferter mechanisms. Hong *et al.* used the same trithiocarbonate to polymerise acrylic acid under gamma radiation from a ^{60}Co source; they proposed the same combined mechanism of control [146]. Barner-Kowollik *et al.* challenged these claims with the finding that a reaction mixture containing a dithiobenzoate with styrene could be irradiated with gamma radiation

and left for a period of 1 h at room temperature without any polymerisation occurring. However, after removal of the radiation source and heating to 60 °C, slow polymerisation was seen, indicating the presence of a radical or non-radical initiation source which could not be conclusively identified [147].

Quinn *et al.* showed polymerisation of MMA with a dithiobenzoate with a secondary R group under constant gamma irradiation yields essentially constant M_n and D with time. When a dithiobenzoate with a tertiary R group was used, traditional RAFT behaviour was seen, including agreement between the obtained and theoretical M_n values [148]. In a separate study, Quinn *et al.* investigated identical MMA dithiobenzoate systems but under constant UV irradiation which gave effectively the same findings as to the work conducted with gamma irradiation [149]. Based on these results it was claimed that the degenerative chain transfer mechanism was operative and solely responsible for the behaviour seen. However, it must be noted that in both studies the control experiments conducted with no dithiobenzoate gave an equivalent yield of polymer, which indicates the majority of the radicals in the system arise due to direct initiation of the monomer and not photolysis/initiation of the dithiobenzoate. Based on this, it is expected that the RAFT mechanism would be operative.

Overall it is clear that most likely both the DC and degenerative chain transfer mechanism are responsible for the control seen in iniferter systems, with several authors most recently remarking that the extent of the DC mechanism is most likely experiment specific [150, 151]. Indeed, recent publications [152] tend to show a hybrid scheme featuring both the iniferter and RAFT mechanisms merged together, akin to Scheme 2.21.

2.4.4 Photochemistry of dithioester compounds

TCT compounds tend to have vibrant colours often characteristic to their class; trithiocarbonates, dithiocarbamates and xanthates tend to be bright shades of yellow or orange, whilst dithiobenzoates are often bright red or pink. This is a direct result of the C=S bond in the thiocarbonylthio moiety which has a non-bonding MO on the sulfur atom (n), a π bonding MO and a π* antibonding MO. The ground state is designated as S_0, and the two excited states are n π* and π π*, both able to exist as either a singlet (S_1 & S_2) or triplet state (T_1 or T_2), thus 5 possible electronic transitions exist [153]. The two transitions seen in the UV-Vis spectrum for a TCT compound are the π → π* and n → π* transitions. Being spin allowed, the π → π* transition occurs around 300 nm for most TCT compounds, regardless of structure, and has a large absorption coefficient (8000 – 20000 L mol^{-1} cm^{-1}). Conversely the spin forbidden n → π* transition typically have much smaller absorption coefficients (15 – 120 L mol^{-1} cm^{-1}) and can occur anywhere from 360 – 540 nm depending on the

class of TCT studied [133, 154]. Even though it is a much weaker, the n → π* transition is what gives RAFT agents their intense and characteristic colours [133, 155]. This is summarised in Figure 2.11.

Figure 2.11 has been removed due to copyright restrictions.

Figure 2.11: Illustrated electronic transitions available to TCT compounds and the corresponding UV-Vis spectrum of a generic RAFT agent showing these transitions. Taken from [133].

Due to the large absorption coefficient, the π → π* transition is often used to quantify the amount of RAFT agent attached to a polymer post polymerisation, which can be reasonably reliable for M_w of 100,000 g/mol or below [154]. The disappearance of these transitions has been the primary method for determining the extent of TCT photolysis described in the following sections, and the same principle is often used to prove either qualitative or quantitatively the success of reactions designed to remove the TCT moiety [156-158].

In a similar fashion, UV-Vis information can be used to investigated mechanistic aspects of the RAFT process. Vana *et al.* reported seeing a colour change during the polymerisation of styrene with cumyl phenyldithioacetate, which gradually changed from orange to yellow in appearance, and was attributed to the formation of a single monomer adduct [159]. Similarly, Lu *et al.* saw a blue shift in the UV-Vis absorbance of S, S′-bis(R,R′-dimethyl-R″-acetic acid) trithiocarbonate when polymerising MA, attributing it to the formation of a single monomer adduct with a larger absorption coefficient [160].

2.4.4.1 Photolytic stability of dithioester compounds & effect of irradiation wavelength

The ability of thiocarbonylthio to undergo photochemical dissociation into radical species has been known for over 50 years [131] and is essential to their ability to function as iniferters. Depending on the wavelength of light used, UV light always decomposes the weakest bond in an initiator, and this depends on both length (and thus strength) and bond energy [161]. The key questions investigated include what extent of photolysis is acceptable to maintain living polymerisation behaviour, what wavelength of light should be used, and how iniferter structure and monomer selection dictate theprevalence of undesired decomposition pathways.

An early report on the photolysis of sodium N,N-dimethyldithiocarbamate and hexamethylene ammonium hexamethylenedithiocarbamate showed considerable degradation of both compounds in a matter of minutes during photolysis, resulting in the generation of carbon disulfide [162]. Niwa *et al.* reported seeing almost complete decomposition of the xanthate moiety in telechelic isopropyl xanthate-terminated polystyrene over a period of 60 mins of UV irradiation, and this followed 1st

order kinetics up to 80% decomposition. Using the non-symmetrical benzyl O-ethyl xanthate, Niwa *et al.* found that the preference for bond dissociation followed the ratio a:b = 1:5, which lead to rapid degradation (Figure 2.12).

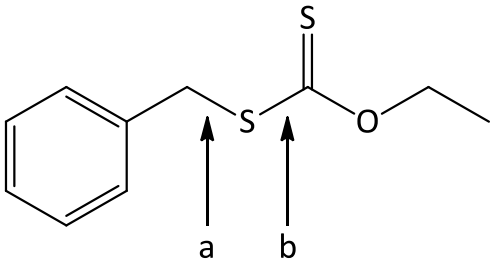

Figure 2.12: Location of bond dissociation under photolysis of benzyl O-ethyl xanthate. Recreated from [163].

Similar possibilities of bond scission locations were summarised by Zard in his review of xanthate chemistry [155], but depended on the structure of the xanthate. These findings for xanthates however are contradicted by recent investigations, such as those of Veetil *et al.* who found exclusive C-S bond fragmentation corresponding to the bond location a in Figure 2.12 when studying the photolysis of S-phenacyl xanthates [164]. These differences most like arise from both the wavelengths and intensities of light used during photolysis. Indeed, various studies have recommended to use the highest wavelength (and thus lowest energy) of UV light possible in order to induce photolysis, with better living characteristics and less TCT compound degradation seen at higher wavelengths [160, 165, 166]. Most recent studies primarily use LED light sources due to their specific wavelength output, lower emission intensities, low cost and ease of use [50, 133, 150, 167]. Recent structure property studies of TCT stability under irradiation have revealed that under photolysis, TCT compounds tend to show photolytic stability that mirrors their ability to fragment via the RAFT mechanism as determined by the radical stability of the R group. McKenzie *et al.* tested a series of trithiocarbonates and found conventionally correct R group selection reduced the inhibition times seen in the polymerisation of MA, and that post initiation, all compounds showed effective photolysis and roughly the same rates of polymerisation [168]. A similar pattern of photolytic stability was found earlier for xanthates by Ham *et al.* where even compounds which were photolytically stable showed degradation upon conversion in poly(VAc) macro-initiators [169]. These results are summarised in Figure 2.13.

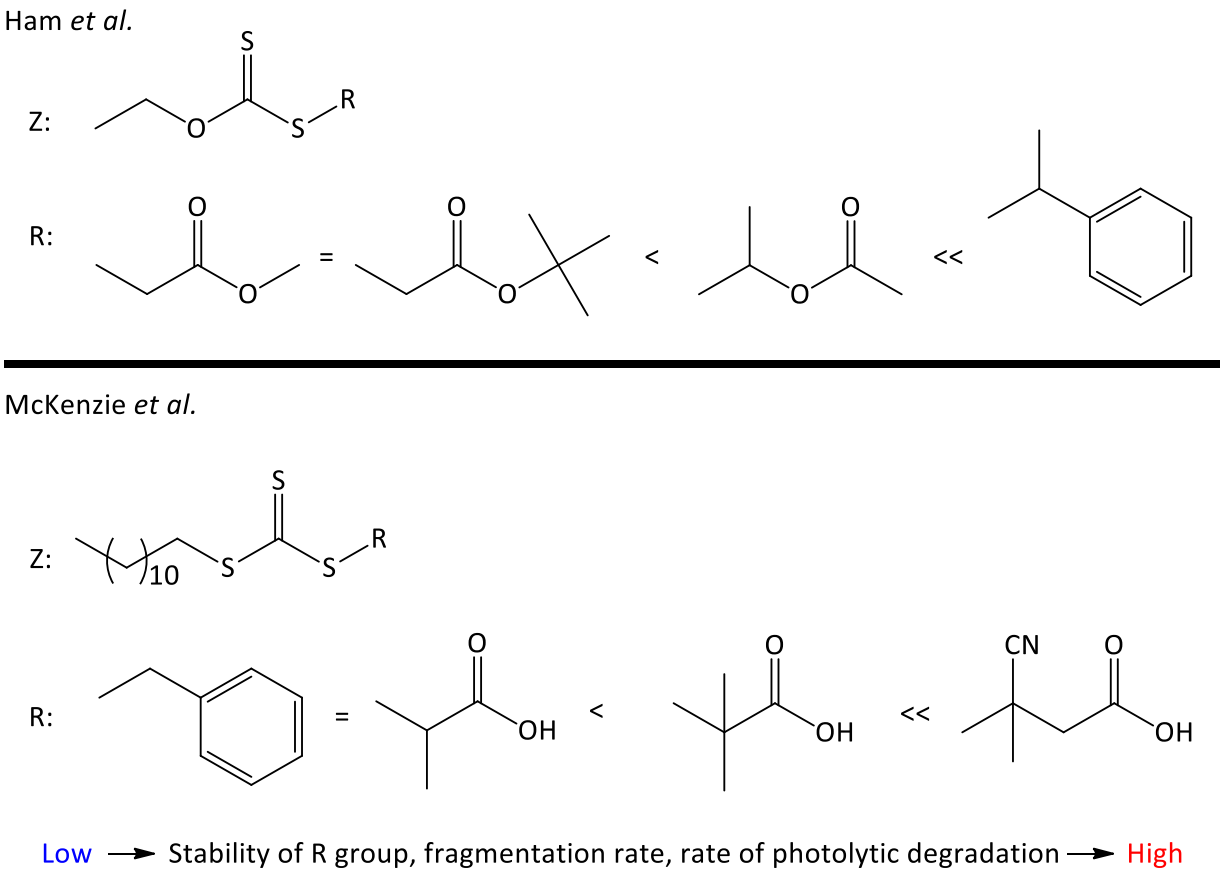

Figure 2.13: Summary of photolytic stability and fragmentation rate as found by Ham *et al.* [169] and McKenzie *et al.* [168].

Poly *et al.* found that the incorporation of a short terminal NVC block into a poly(VAc) macro-initiator acted as a chromophore and enhanced its photolytic decomposition; the rate of decomposition for a poly(VAc-b-NVC) polymer was significantly greater than the starting poly(VAc) macro-initiator [170]. A similar phenomenon as applying to the starting TCT compound was found by Kitchin *et al.* studied two dithiobenzoates, one with a conventional cyanoisopropyl R group (compound J, Figure 2.14) and another with a chromophore modified R group (compound K, Figure 2.14). They found the cyanoisopropyl R group lead to a 10-fold increase in the quantum yield and thus a 10 fold increase in the rate of photochemical degradation [171].

The negative effects of different bond scission location has been investigated by several authors; Turner & Blevins noted the formation of CS_2 during photolysis of PMMA terminated with a dithiocarbamate [172]. Dika Manga *et al.* studied the degradation of butyl-2-(N,N-diethyldithiocarbamyl) propionate and found significant elimination of the R group to yield the symmetrical byproduct TED, along with a series of other by-products. This occurred both with and without the presence of BA monomer [173]. A follow up study found that a loss of control of the polymerisation at higher conversions was associated with extensive degradation of the TCT moiety

[174]. Similar results were seen by Lambrinos *et al.* who saw evidence of side reactions due to decomposition of TCT at other bond locations [136]. Doi *et al.* found evidence that decompositions occurred at different bond locations depending on which end of a bifunctional polymer made with TED was photolysed. Rates of bond scission varied, with non-preferred bond scission being directly linked to a decrease in "livingness" seen during polymerisation [175]. These side reactions are summarised in Scheme 2.22.

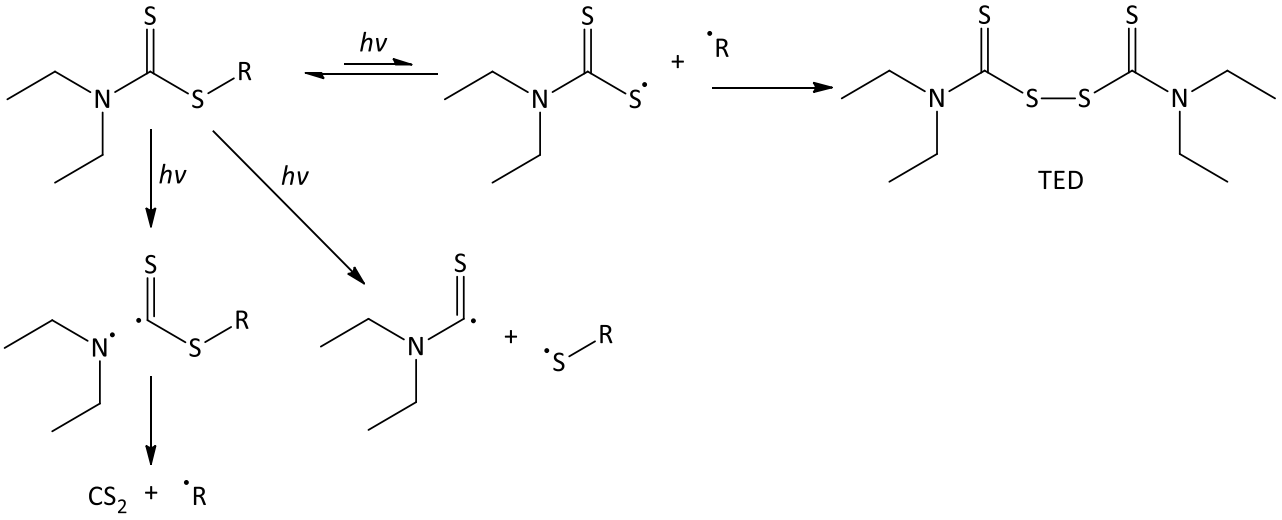

Scheme 2.22: Summarised alternative breakdown pathways from the photolysis of dithiocarbamates. Adapted from [47].

2.4.4.2 Quantum yield for photolysis of thiocarbonylthio compounds

A brief summary of quantum yields for various TCT compounds is provided blow, showing structures in Figure 2.14 and compiled data in Table 2.1.

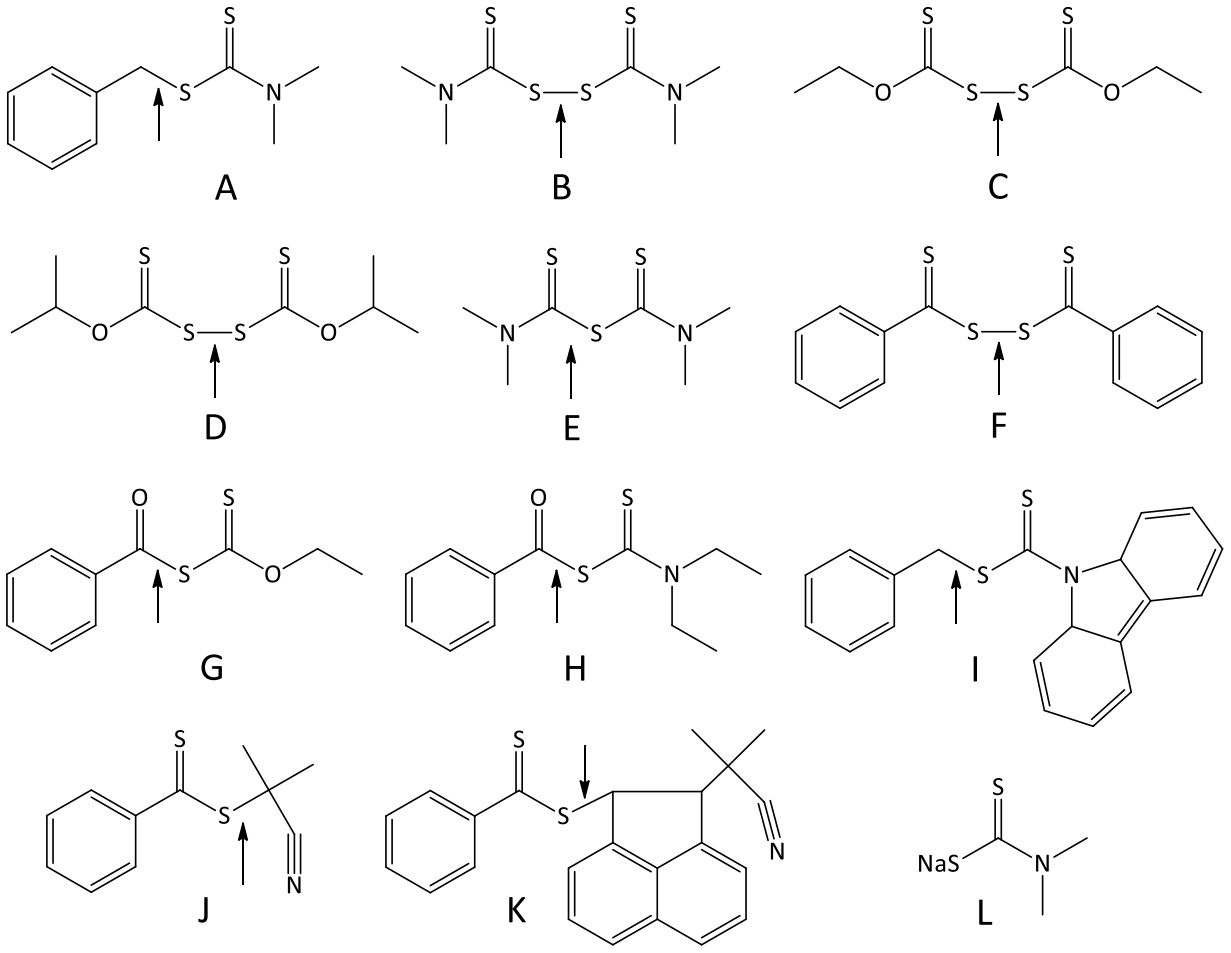

Figure 2.14: Summary of TCT compounds showing location of bond fracture, corresponding data summarised in Table 2.1.

Table 2.1: Summary of a selection of TCT compounds and associated quantum yields as gathered from sources listed therein.

Thiocarbonylthio compound	Quantum yield	Reference
A	0.45, polychromatic radiation	[137, 139]
B	0.9, polychromatic radiation	[137]
C	0.4, polychromatic radiation	[137]
D	0.097 – 0.247 for St and 0.047 – 0.607 for MMA. Found to vary with TCT concentration, polychromatic radiation.	[143]
D	0.38, polychromatic radiation.	[137]
E	0.25, polychromatic radiation.	[137]
F	0.27, polychromatic radiation.	[137]
G	0.12, polychromatic radiation.	[139]
H	0.17, polychromatic radiation.	[139]
I	0.04, polychromatic radiation.	[139]
J	0.8 @ 300 nm	[171]
K	0.07 @ 300 nm	[171]
L	0.11, polychromatic radiation.	[162]

It is clear that structural trends in the symmetrical TCT are somewhat hard to define, with a simple change of methyl (compound C) to isopropyl Z group (compound D) decreasing the quantum yield by a factor of 4. This is interesting given the isopropyl Z group for xanthates was identified to be responsible for an alternate fragmentation pathway during RAFT polymerisation [176], hence if chain transfer after photolysis were to occur, fragmentation via this method might arise. Similarly, compound B, designated TED, has previously been shown to be stable under photolysis conditions [173]; this could potentially arise due to different light sources being used.

2.4.4.3 Selective RAFT group removal during photolysis of thiocarbonylthio compounds

Carmean *et al.* recently reported on the ability to remove the RAFT moiety from thrithiocabonates, dithiobenzoates, dithiocarbamates and xanthates in a rapid and facile manner. This was achieved by irradiating a polymer solution with mild 365 nm light, with N-ethylpiperidine hypophosphite being added as a hydrogen donor [177]. This illustrates that solvent selection is important during photoiniferter polymerisations with TCT compounds. Any solvent that is a good hydrogen donor could become problematic in the terminal stages of a polymerisation when monomer is depleted by facilitating this reaction.

2.4.5 Block copolymer synthesis via the iniferter method

Block, multi-block, random and star copolymers synthesis received significant attention in the early iniferter literature as the iniferter mechanism was one of the first FRP techniques to allow these types of polymers to be made successfully. Conventional TCT compounds as used in RAFT were rarely used in the early literature [135], whilst symmetrical or multifunctional TCTs were more commonly employed [135, 142, 143, 172]. A selection of RAFT agents used are shown in Figure 2.15. The early iniferter literature contains the most extensive studies of polymerisation where the block order is considered sub-optimal as per the RAFT mechanism. Niwa *et al.* undertook polymerisations with bis(isopropylxanthogen) (BX) to form poly(Sty-b-MMA), poly(Sty-b-MA), poly(MMA-b-MA) and poly(MMA-b-Sty). Only the conversion of monomer was provided, with the yield of copolymer, homopolymer from the second monomer along with molecular weight distributions not detailed [143]. Subsequently, it was found that higher concentrations of poly(Sty) macro-initiator caused bimodal distributions when polymerising MMA, which did not occur when MA was used [142]. In both cases, the authors postulate that the properties of the monomer, including its propensity to undergo chain transfer with the macro-initiator and primary radical termination are potentially the cause for this behaviour [142, 143].

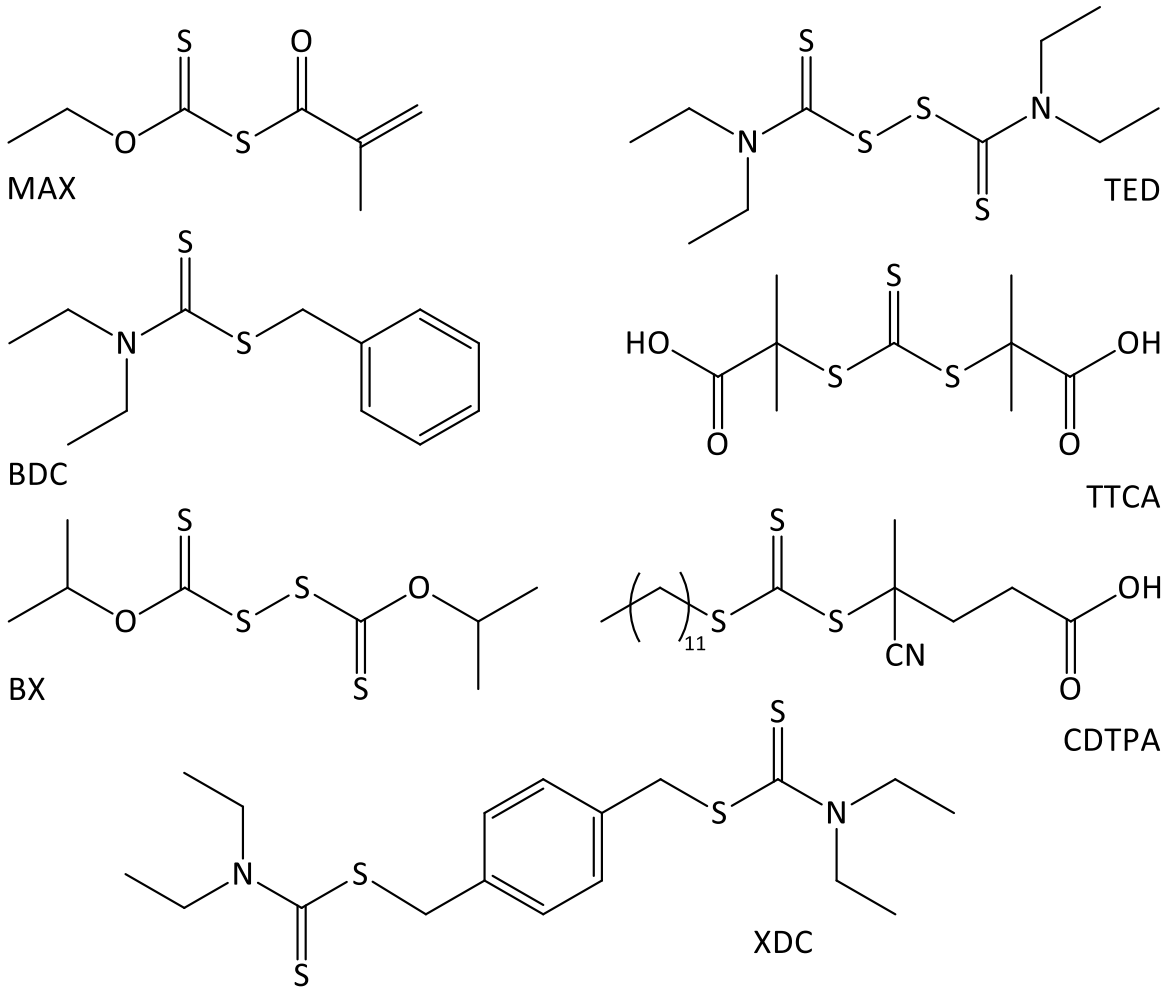

Figure 2.15: Summary of RAFT agents commonly employed in the synthesis of block copolymers via the photo-iniferter method.

Similar behaviour of incomplete macro-initiator consumption was seen by Turner & Blevins [172], who found preparation of PS-b-PMMA to be far more successful than when the synthesis was attempted in reverse in order to make poly(MMA-b-Sty) as evidenced by much higher dispersity values (> 4) being observed in the latter case [172]. Van Kerckhoven *et al.* synthesised poly(Sty-b-MMA) with TED, with the low yield of this copolymer being attributed to the low quantum yield of photolysis and strong absorption at the irradiation wavelength by the PS chain [178]. Interestingly, Otsu *et al.* claim a very high efficiency of converting poly(Sty) into poly(Sty-b-VAc) using benzyl N,N-diethyldithiocarbamate (BDC) based iniferters; however molecular weight characterization or confirmation of retention of the RAFT moiety was not provided [179]. Wang *et al.* recently attempted the synthesis of the reverse poly(VAc-b-Sty) using 1-Cyano-1-methylethyl diethyldithiocarbamate in the conventional RAFT manner with thermal initiator with only limited success [180]. The initial poly(VAc) had a dispersity of 1.61 and the resulting block copolymers were not sufficiently resolved by GPC from the starting macroinitiator. Van Kerckhoven *et al.* synthesised poly(Sty-b-EA) with BDC that was reasonably successful as evidenced by a large percentage of EA in the block copolymer

[178]. A non-exhaustive summary of copolymers formed by the photo-iniferter method using Sty, MMA and n-BA is given in Table 2.2.

Conventional ordering of monomer blocks as recommended for the RAFT mechanism is more common within the recent literature, with Ran & Wan synthesising poly(Sty-b-BA-Sty) with S,S'-bis (α,α'-dimethyl-α''-acetic acid) trithiocarbonate (TTCA) [181]. 4-cyano-4-[(dodecylsulfanylthiocarbonyl) sulfanyl] (CDTPA) has been used by both Xu *et al.* who used it to synthesise poly(GMA-b-MMA) [152], while Rubens *et al.* synthesised a range of methacrylate block copolymers in a flow reactor, yielding excellent chain end fidelity and good dispersity values [182].

Table 2.2: Selection of copolymers featuring Sty, MMA and n-BA as synthesised by the iniferter method within literature. Homo 1 and Homo 2 refer to unreacted macro-initiator and homopolymer formed from the second monomer respectively. Reproduced from [173].

TCT compound	1st Monomer	2nd Monomer	Block (%)	Homo 1 (%)	Homo 2 (%)	Reference
BDC	Sty	MMA	74	13	16	[183]
BDC	MMA	Sty	41	31	28	[183]
XDC	Sty	MMA	90	2	8	[183]
XDC	MMA	Sty	62	14	23	[183]
TED	Sty	MMA	67	5	28	[172]
TED	MMA	Sty	75	10	15	[172]
TED	Sty	n-BA	100	N/A	0	[172]
XDC	n-BA	MMA	79	0	20	[136]

A unique class of photoiniferters bearing polymerisable double bonds, sometimes called inimers, have been investigated by multiple researchers for the purposes of selectively making graft [184] and branched polymer networks [185, 186]. Interestingly, MMA and Sty appear to display unique patterns of reactivity in the presence of the iniferter S-methacryloyl O-ethyl xanthate (MAX). At an irradiation wavelength of 350 nm, MMA in benzene could be polymerised successfully [187] whilst polymerisation of bulk styrene and styrene diluted in benzene gave gel polymers and polymers with a constant molecular weight as a function of conversion respectively [188]. This behaviour was theorised to arise from the interaction of MAX with the electron rich styrene double bond which facilitated a donor-acceptor interaction, thus leading to MAX behaving as both a monomer and an iniferter [188]. Using MAX as the starting iniferter, both poly(MMA-b-MA) [188] and poly(MMA-b-Sty) [187] could be synthesised, but it was noted that the irradiation wavelength needed to be decreased below 300 nm in order to allow this polymerisation to occur. MAX could behave like a monomer to form random block copolymers with MMA and Sty with conventional AIBN initiation. Styrene was photo-grafted from poly(MAX-co-MMA) and MMA was photo-grafted from poly(MAX-co-Sty) under 350nm irradiation. In both cases the crosslinked homolpolymers generated

by direct monomer photolysis remained at 6% or less and these were separated from the graft copolymers by soxhlet extraction [189].

Based on their experimental work with symmetrical TCT capped macro-initiators, Otsu & Yoshida [5] postulated that double photolysis could occur. This can lead to the formation of a polymer chain that propagates at both ends before being reversibly terminated (Scheme 2.23), however can also lead to bond scission at other non-ideal locations.

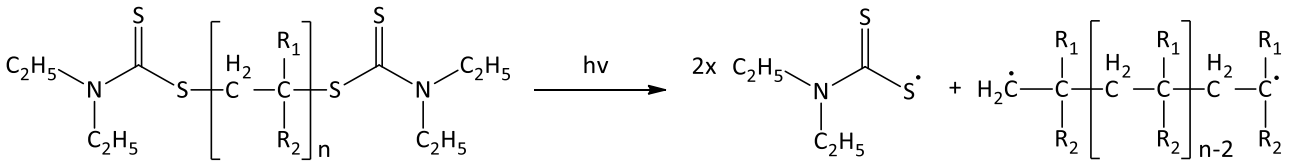

Scheme 2.23: Formation of block copolymers with symmetrical TCT macro-initiator. Reproduced from [5].

Otsu & Kuriyama reported triblock copolymers both of the form C-B-A-B-C and A-B-C which included various combinations of blocks of Sty, MMA, VAc, isobutene (IB), vinyl chloride (VC) and butadiene (BD). Furthermore, alternating copolymers featuring St, DEF, MAn and IBVE were also synthesised [135]. Almost always the yield of the desired copolymer was less than 90 %, with homopolymers of the last block often forming in significant quantities (~ 15 – 20 %) and unreacted macro-initiator remaining in all cases.

Overall it can be concluded that most block copolymers reported within the photoiniferter literature suffer from broader molecular weight distributions, incomplete consumption of the starting macroinitiator and sometimes significant formation of secondary homopolymer formation. These are all issues that could potentially be resolved through further investigation of

2.5 Computational quantum chemistry

2.5.1 General introduction

As computational quantum chemistry is not the candidate's specialty or the sole focus of this thesis, a general introduction compiled from several publications [63, 190, 191] is given. For a detailed exploration of quantum chemistry as it applies to radical polymerisation and radical chemistry, the reader is referred to reviews by Coote [191] and Fischer & Radom [24]. Furthermore, a detailed description of Density Functional Theory (DFT) and Ab Initio Molecular Orbital theory are provided in the review by Coote [191].

Computational quantum chemistry is fundamentally based on solving a non-relativistic version of the Schrödinger equation, which equates the total kinetic and potential energy (E) of the system with its corresponding wavefunction (Ψ), expressed via the Hamiltonian operator:

$$\hat{H} \cdot \psi = E \cdot \psi$$

Equation 2.52: Schrodinger equation.

In principle, only the masses and charges of the nuclei and electrons that make up a molecule, along with some fundamental physical constants are required to solve the Schrodinger equation; therefore, computational quantum chemistry is often referred to as an "*ab initio*" technique, meaning "without assumptions". The problem arises that no analytical solution for the multi-electron Schrodinger equation exists; algorithms that approximate solutions to this equation have been developed. However, the greater the accuracy of these approximations, the greater the required computing power and thus time that is needed to implement them. Computational quantum chemistry is an incredibly powerful technique as applied to polymerisation and radical reactions as it allows the evaluation of potential reactions without recourse to kinetic or mechanistic assumptions. It is possible to compute the thermodynamic barrier, the enthalpy, the kinetic rate constants for the reaction along with the geometries of the products, reactants and transition structures. Furthermore, a range of other useful parameters for all the species involved can be obtained, including bond lengths, atomic charges, ionization energies, electron affinities, singlet-triplet gaps of the reactants and radical stabilization energies. Since computational cost scales exponentially with the number of non-hydrogen atoms within the system being computed, and polymer molecules being incredibly large (hundreds to many thousands of atoms), model systems that only compute the active site of a radical reaction are used. This need to compute larger molecules has led to the development of hybrid computational models which feature two levels of theory; both molecular mechanics (MM) and quantum theory (QM) [192]. MM is computationally far less demanding as it does not require the solving the Schrödinger equation, instead using empirical models and approximations to compute van der Waals interactions, electrostatic interactions, along with torsions and small amplitude vibrations around bonds. This is the basis for the widely used ONIOM model [193]; this allows the active site of the reaction to be computed at higher levels of QM theory while the periphery of the molecule(s) are optimised at much lower levels of QM or even MM theories, thus drastically reducing computing time.

2.5.2 Quantum chemistry as applied to RAFT polymerisation and dithioester compounds

A range of studies focusing on the RAFT mechanism and the chemistry of dithioester compounds which are used in RAFT and iniferter polymerisations have been undertaken. These range in

complexity from qualitative structure property relationship calculations to analysis of fundamental mechanistic pathways within the RAFT mechanism by high level *ab initio* methods. Often, quantum chemistry is used in conjunction with experimental investigations to provide supporting evidence for mechanisms or experimental trends. Most of the examples presented here fall into this category and the experimental findings of these studies are explained in the relevant sections within this chapter.

2.5.2.1 Low computational cost studies

The advantage of low cost computational quantum chemistry approaches is that it can be conducted on computers of modest processing power in a reasonable timeframe. Graphical user interface (GUI) programs such as GaussView [194] used in tandem with a program such as Gaussian 09 [195] which performs the necessary calculations has enabled researchers to gain insight into various structure property relationships with relative ease. Programs such as Spartan '16 [196] simplify the process further by combining both the GUI and computational elements into one package.

The experimental observations about Z group effects by Chiefari *et al.* were supplemented by a AM1 calculations for a range of parameters [67]. These included the relative heats of formation for methyl radical addition to the RAFT agent, defined as the change in enthalpy between the RAFT agent and a methyl radical and the methyl group as part of the RAFT adduct radical. Negative linear correlations between the LUMO energy and the natural logarithm of the measured chain transfer constant and the charge on the sulfur in the C=S were found, along with a positive linear correlation between the LUMO energy and the relative heat of formation of the RAFT adduct radical. Similar AM1 calculations were used by Benaglia *et al.* and Moad *et al.* in their pioneering work on acid base switchable RAFT agents to show a decreased C=S bond length upon protonation, thus supporting the idea that the canonical forms of the RAFT agent directly impact the C=S bond strength [115, 118]. The observation was made that the HOMO and LUMO levels for the acid base switchable dithiocarbamates would vary greatly depending on the nature and position of the counterion [118]. These results support the assertion that more active RAFT agents retain their C=S double bond character to a greater extent, and that this makes radical addition to these RAFT agents thermodynamically more favourable.

In a companion publication on the effect of the R group, Chong *et al.* [73] found a lowered influence of the R group on the rate of radical addition, as evidenced by only slight variations in the HOMO and LUMO levels and the charges on the sulfur atoms in the RAFT moiety as the R group was varied. Matyjaszewski & Poli compared various R groups for a range of RAFT agents, however found that there was no consistent trend in the charge on the sulfur in the C-S bond of the RAFT agent. Unsurprisingly, the carbon adjacent to this sulfur on the R group showed a trend to become more

positively charged as the substituents became more electronegative [197]. Furthermore, their work also featured the bond dissociation energy (BDE) for various R group and RAFT combination, with the general trend seen that the more exothermic the BDE, the more favourable fragmentation process.

Structure property relationships at lower levels of theory have also been applied in a limited fashion to the study of photoiniferter systems. Lalevée *et al.* found two correlations to an increase in spin density on the sulfur of a thiyl radical; this increased the reactivity towards radical addition, however the overall control over the polymerisation decreased [139]. Ajayaghosh & Francis used AM1 calculations to show a potential electron donor-acceptor interaction between a xanthate photoiniferter with the double bond in two monomers. This was postulated to explain the preferential polymerisation by this photoiniferter of St which is electron rich and not MMA which is comparatively electron poor [188]. Liu *et al.* used a similar approach to show that electron density around the double bond of the NVP monomer changes significantly when in the presence of HFIP molecules; this supports their ^{1}H NMR experimental data which is consistent with this claim [114].

2.5.2.2 Higher computational cost studies

A pioneering investigation by Coote [198] into scenarios under which a RAFT polymerisation mediated by dithiobenzoates or dithioesters either experiences a regular or retarded polymerisation rate lead to significant theoretical insights into the relative roles of the Z and R groups of the RAFT agent and their mechanistic and kinetic effects. An investigation by Coote into the addition of model radicals for styrene and methyl acrylate polymerisations to a range of prototypical RAFT agents (Z = CH_3, phenyl or benzyl, R = CH_3, benzyl, MA and cyanoisopropyl) concluded that analysis of radical additions for the RAFT process was a technically challenging exercise and required careful consideration of many factors [199]. It was found that the rate coefficient for addition (k_{add}) varied by an enormous 11 orders of magnitude whilst the rate coefficient for fragmentation (k_{frag}) by less than an order of magnitude. This further reinforced the notion that the rate of radical addition is primarily determined by the Z group, however R groups which are bulky and can destabilise the breaking S-R bond of the adduct radical or have radical stabilising substituents still have non-trivial effects on the fragmentation rate, with entropic factors sometimes being more important than the RSE energies. This work also reinforced previous findings about the superior reactivity of the C=S bond [57, 200], with the rate of radical addition to the C=S bond being around 10^3 times faster than to the corresponding alkene. This was attributed to the lower singlet-triplet gap of the C=S bond which is a reflection of the lower π bond character of the typically longer C=S bond.

The radical stabilisation energy (RSE) is a measure of radical stability which is applicable in the analysis of general radical chemistry and RDRP techniques including RAFT. The RSE is defined as the difference in energy upon the transfer of a hydrogen as shown in Scheme 2.24 [201]:

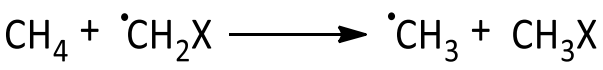

Scheme 2.24: Hydrogen transfer during a radical reaction used in the definition of the radical stabilization energy.

Applying the RSE concept to RAFT agent stability has lead the Coote group to formulate a comprehensive set of parameters (ΔH_{stab}, ΔH_{frag} and RSE values) that can calculate the reactivity of RAFT agents with the prototypical methyl radical [81]. Key *ab initio* findings using these parameters from several works of the Coote group [81, 127, 202] have given fundamental insights into the structure reactivity trends observed experimentally in the past. Figure 2.16 shows the effect of Z group selection as ranked by the parameter ΔH_{frag}; Z groups to the left of the blue line will retard the polymerisation of unstable radicals by preventing fragmentation from the RAFT adduct radical, whilst those to the right will not.

Figure 2.16 has been removed due to copyright restrictions.

Figure 2.16: Summary of the *ab initio* parameter ΔH_{frag} as a measure of RAFT agent suitability. Taken from [127].

An analogous comparison was made regarding the ΔH_{stab} parameter, shown in Figure 2.17. Z groups to the left of the blue line give RAFT agents of sufficient reactivity to effectively moderate the polymerisation of the more stable propagating radicals, whilst Z groups to the right of the blue lie give RAFT agents that are too stable and will give poor control over the polymerisation of MAMs.

Figure 2.17 has been removed due to copyright restrictions.

Figure 2.17: Summary of the *ab initio* parameter ΔH_{stab} as a measure of RAFT agent suitability. Taken from [127].

The design strategy for the F-RAFT agents pioneered by Coote & Henry (see section 2.3.7.2) focused on a Z substituent that destabilises the RAFT adduct radical without stabilising the C=S double bond [120], thus allowing efficient fragmentation as well as radical addition. Substituents adjacent to a radical centre which are π (or pseudo π) accepting or lone pair donating are known to stabilise carbon centred radicals. This makes destabilising the RAFT adduct radical a challenging prospect due to the two sulfur atoms adjacent to the radical centre being capable of lone pair donation. When Z = fluorine in a RAFT moiety, the sigma withdrawing effect dominates over the counteracting stabilising effects of lone pair donation [120]. The RSE values obtained showed that an F-RAFT agent (R = CH_3) should be more destabilising for prototypical methyl radicals than a dithioester or xanthate, but slightly more stable than a xanthate for VAc radicals. A further study [122] by Coote *et al.* determined that k_{add} to F-RAFT agents for styrene radicals is comparable to that of a dithioester and even faster than addition to a xanthate for vinyl acetate radicals. Rates of fragmentation were faster for styrene radicals compared to from dithioesters but slower for vinyl acetate radicals compared to from xanthates. A series of suggested R groups for styrene, vinyl acetate and ethylene polymerisation were also put forth based on these quantum chemical calculations (see Scheme 2.18 in section 2.3.7.2).

The theoretical descriptors of RAFT agent reactivity were applied in the work of Gardiner *et al.* where *ab initio* calculations showed the enhanced reactivity of 4-chloro-3,5-dimethyl-1H-pyrazole-1-carbodithioate arises due to a lower RAFT adduct stability [127].

2.6 Modelling with Predici software

The RAFT polymerisation process has been modelled via various mathematical approaches [64, 203-205], however the Predici program is a powerful tool frequently utilised in this field and will be covered here. Predici is a solver program based on a discrete Galerkin h-p method coupled with a special time discretization method for approximating and solving the system of differential equations that can mathematically describe a polymerisation process. The basis for this method was originally published in 1996 [206]. For an explanation of the mathematical underpinnings of Predici, the reader is referred to a comprehensive review [207] written by the author of the Predici program, Dr. Michael Wulkow. This review lays out in detail the system of equations, mathematical assumptions and overall structure of the program, how it functions and the modular system of reactions that make it applicable to a range of polymerisation scenarios. The great utility of Predici comes from its modular and adaptable nature; the current version (Predici 11, version 11.15.5) features an almost exhaustive range of reactions from which the user then constructs the desired model for the polymerisation system at hand. All aspects of the polymerisation process can be controlled; this includes the ability

to set up multiple heterogenous phases, multiple reactors with output and inputs of reagents and products at desired flow rates, the ability to implement kinetic parameters and species parameters based on thermodynamic data, the ability to include temperature changes and the ability to modify kinetic parameters and model outputs with custom user defined scripts. As always with any modelling procedure, it must be stressed that the accuracy of the modelling results is primarily determined by three things:

1. Knowing which reactions are significant regarding what information is desired.
2. Directly determining for the system being modelled as many rate coefficients as possible; this is preferable to obtaining or calculating them from literature values.
3. Knowing which kinetic parameters have the greatest influence on the kinetics; some parameters that govern the various stages of the RAFT process can be varied over many orders of magnitude without significant kinetic effects whilst fundamental parameters such as k_d, f, k_i, k_p and k_t are very sensitive parameters in dictating the kinetic behaviour seen.

2.6.1 Implementing the RAFT pre-equilibrium in Predici

Publications which pioneered the implementation of the RAFT mechanism into Predici usually represented the pre-equilibrium as a single transient reaction with no potential for a reverse reaction [70, 208, 209] (reaction 1 in Table 2.3). A more comprehensive approach by Vana *et al.* [210] included the fully reversible pre-equilibrium consisting of addition and fragmentation reactions, including the reaction of the fragmented R* with initial RAFT agent (reactions 2 &3 in Table 2.3). This model had the advantage that it enabled the manipulation of both forward and reverse fragmentation parameters for both sides of the pre-equilibrium and main equilibrium, thus allowing the effective establishment of radical "sinks" in the form of the intermediate RAFT radical. Recently Derboven *et al.* also modelled the process as a transient step (reaction 4 in Table 2.3) using the pseudo-steady-state assumption [60] as was originally proposed by Moad & Barner-Kowollik [54]. McLeary *et al.* tracked all individual species to a chain length of n = 3 monomers in the pre-equilibrium, with a model too detailed to show here; it featured no less than 86 equations with 22 rate coefficients [41]. A similarly complex approach was employed by Houshyar *et al.* [40].

Table 2.3: Implementations of the RAFT pre-equilibrium found in the Predici literature.

Reaction	Pre-equilibrium model	Ref.
1	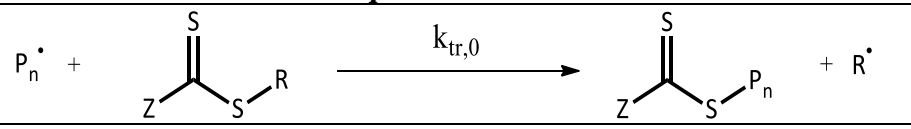	[70, 208, 209]
2	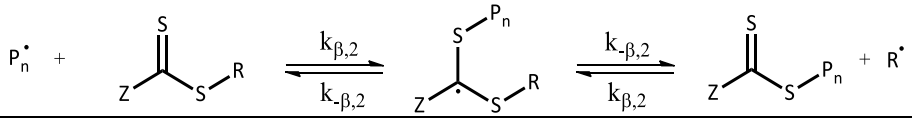	[210]
3	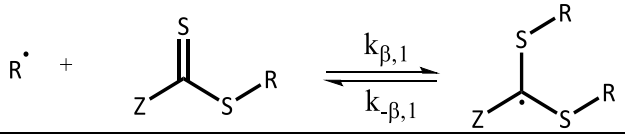	[210]
4	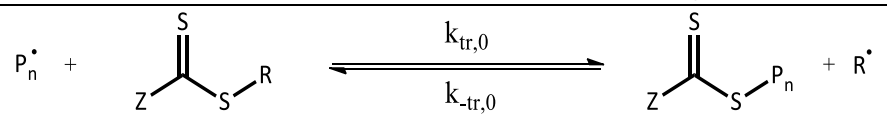	[60]

2.6.2 Implementing the main RAFT equilibrium in Predici

As a consequence of the RAFT mechanism and the need to keep track of the two chain length distributions of the intermediate RAFT radical in the main equilibrium, two new fictive species (Q1 and Q2) are required [209]. They can be essentially thought of as one and the same species that is duplicated as necessitated by the two potential fragmentation pathways (one towards the reactants and the other towards the products). There are two important consequences of this; firstly, the value of k_{-tr} implemented into the model needs to be half of the actual k_{-tr} value calculated from experimental data or the desired k_{-tr} value as it is duplicated in four separate reactions (reactions 6- 9 in Table 2.4) instead of two reactions as per the reality of the RAFT model. Secondly, adjusting the value of the k_{-tr} value gives the possibility of adjusting the rate of polymerisation by effectively creating a radical "sink" in the form of the intermediate RAFT radical species, just as in the complete implementation of the pre-equilibrium. The implementation of the chain length memory for the RAFT equilibrium adduct radical has been thoroughly explored and conclusively proven to be a correct and mathematically accurate in an article by Wulkow *et al.* [209], after objections were raised by Zhu *et al.* as to the accuracy of implementing the RAFT mechanism into Predici [85]. Furthermore, the ability of Predici to accurately reproduce results obtained by other mathematical modelling methods has been verified extensively by Pallares *et al.* with the key finding being that the model implementation is more important that how it is computed [205]. As in the pre-equilibrium, the main equilibrium can also be simplified into a transient step [60, 70].

Table 2.4: Implementations of the RAFT equilibrium found in the Predici literature.

Reaction	Main equilibrium	Ref.
5	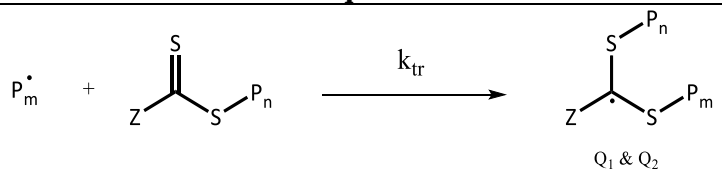	[208-210]
6	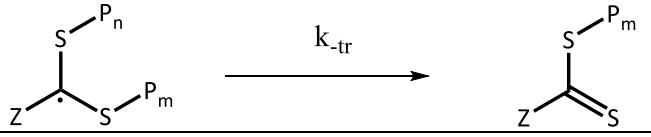	
7	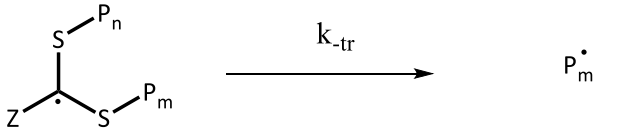	
8	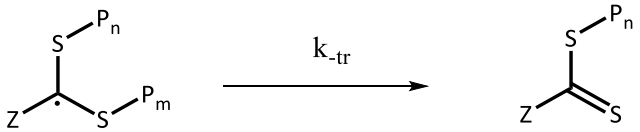	
9	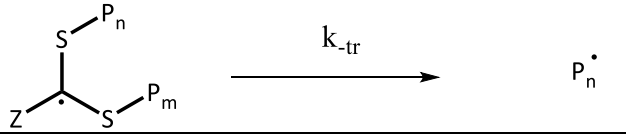	
10	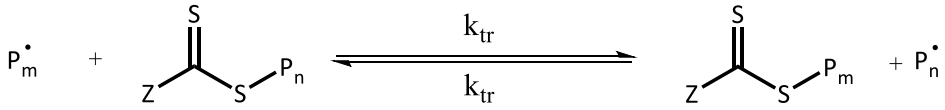	[60, 70]

2.6.3 Applications of Predici modelling: RAFT processes & related kinetic parameter investigations

Barner-Kowollik *et al.* first used Predici to supplement the experimental investigation of the polymerisation of styrene with cumyl dithiobenzoate. They reported that a large (~10^7) equilibrium constant for the main equilibrium simulated the experimental data well, and that this factor was the reason the polymerisation rate dropped markedly as the concentration of RAFT agent was increased [208]. Vana *et al.* undertook a comprehensive exploration of the RAFT process [210]; they found that slow fragmentation can adequately explain the inhibition period seen when the values of $k_{-\beta,2}$ and

$k_{-\beta,1}$ are smaller than the value of $k_{-\beta,}$ in the main equilibrium. Inhibition was also more sensitive to a decreased value of $k_{-\beta,2}$ as this reaction consumes the starting RAFT agent, whilst the reaction governed by $k_{-\beta,1}$ does not as it is degenerate in nature. Slow fragmentation gave a "normal" rate of polymerisation after the inhibition period, whilst lowering $k_{R\text{-}re}$ to simulate poor R group re-initiation gave a retarded rate of polymerisation throughout. Varying k_β and $k_{-\beta}$ over several orders of magnitude while keeping $K_{eq} \approx 10^7$ showed that k_β needs to be at least ~10^3, otherwise loss of control characterised by very large dispersity values occurs. Finally, there is an upper limit to the control that can be obtained; increasing $K_{eq} >> 10^7$ does not yield better a better dispersity; this is rationalised as

the limit given by the Poisson distribution. This investigation highlighted the advantage of the model that enabled the manipulation of both forward and reverse fragmentation parameters for both sides of the pre-equilibrium and main equilibrium, allowing the effective formation of a radical "sink". Barner-Kowollik *et al.* modelled the cumyl phenyldithioacetate mediated polymerisations of St and MMA and found that the modelling was far less sensitive to the values of k_{β} and $k_{-\beta}$ if hybrid behaviour was significant, as was the case for the MMA system [74]. An experimental investigation of the thioketone mediated polymerisation of nBA as a case study for the existence of stable RAFT adduct radicals was modelled by Junkers *et al.* [87].

A basic Predici model for estimating RAFT agent consumption during the polymerisation of styrene with xanthates was put forth by Adamy *et al.* [70], and curiously, unlike in other publications, the authors stated that chain transfer to both solvent and monomer must be accounted for, otherwise inaccurate simulated results are obtained. McLeary *et al.* tracked individual species to chain length of n = 3 monomers within the RAFT pre-equilibrium by modelling selective initialisation period seen in the cyanoisopropyl dithiobenzoate mediated polymerisation of styrene; the model provided close agreement to experimental data [41]. Furthermore, Coote *et al.* modelled the same experimental data using a slightly simplified model, however with rate coefficients calculated from *ab initio* calculations, providing an even better fit to the experimental data, thus supporting the validity of this combined approach [211]. Houshyar *et al.* modelled the process of Single Monomer Unit Insertion (SUMI) into a trithiocarbonate RAFT agent to form a styrene-N-isopropylacrylamide (NIPAM) co-dimer macro-RAFT [40], further confirming the limitations on monomer sequence control in RAFT. Once again, very good correlation between the modelling data and experimental data was seen.

To predict the behaviour of novel F-RAFT agents in ethylene polymerisation, Coote *et al.* [122] employed the previously described RAFT model of Wulkow *et al.* [209] superimposed upon the model for ethylene polymerisation as published by Busch [212]. Jaramillo-Soto *et al.* also investigated various reaction parameters for the polymerisation of ethylene in supercritical CO_2 with parameters for a "generic" RAFT agent [213].

Predici has been extensively used to investigate various kinetic rate coefficients via the RAFT Chain Length Distribution (RAFT-CLD technique); Vana *et al.* reported a simple way of modelling the chain length dependence of the termination rate coefficient using differential scanning calorimetry (DSC) data from styrene polymerisation mediated by cumyl phenyldithioacetate [159]. This method has also been applied to the termination rate coefficient of MA by Theis *et al.* [62, 214]. The specific characteristics of the termination process during polymerisation of VAc has also been modelled by

Monyatsi *et al.* who investigated the effect of head-to-head termination [34] and by Theis *et al.* who looked at transfer reactions and chain length dependence [215].

2.7 Modelling of Iniferter polymerisations

Investigations into photoiniferter polymerisations mediated by TCT compounds has been somewhat limited. Ward & Peppas investigated the influence of a generic TCT iniferter on both linear and crosslinked polymer networks by a percolation model that considered the probability of polymerisation events based on a raw % of occurrence [216]. They found that too rapid a dissociation of the iniferter will raise the dispersity in both systems. Rahane et al. modelled iniferter polymerisations of MMA from a silicon wafer functionalised with a dithiocarbamate, neglecting degenerative chain transfer as a mechanism [217]. Through parameter estimation, several key kinetic parameters were approximated and able to reproduce general experimental trends seen. The authors acknowledge that the surface tethered nature of the polymerisation presents unique challenges in regard to model complexity reflecting experimental reality, with several factors such as surface initiator grafting density being key, however their effect was not modelled. Vivaldo-Lima & Mendoza-Fuentes provided a comprehensive model for a generic iniferter polymerisation that included a multitude of reactions including thermal self-initiation, transfer to iniferter and monomer and generative transfer between growing chains. Simulations showed diffusion controlled propagation was found to reduce the living behaviour seen, whilst diffusion controlled termination increased the living behaviour seen [218]. Two experimental iniferter polymerisations were simulated, however only moderate agreement was seen between experimental and simulated data, most likely arising from inadequate parameter selection. Krajnc & Golob simulated the tetraphenyl biphosphine mediated polymerisation of MMA under UV irradiation which was an iniferter system, with the authors stating that chain transfer was an important mechanism [219]. There was limited evidence for this, and the dispersity of all polymers was ~ 2, with M_n values decreasing as a function of conversion, indicating poor control.

More studies exist that have explored the behaviour and characteristics of other polymerisation mechanisms which are mediated by the DC mechanism, with the potential role of the DT mechanism investigated where applicable. Arguably, these have typically have been far more comprehensive and useful in understanding the relative contributions and parameters governing successful control with the DC and DT mechanisms, and can be potentially applied to the study of iniferter polymerisations conducted with TCT compounds.

Souaille & Fischer modelled the DC mechanism with a series of 4 equations with full analytical solutions, and investigated the conditions under which living and controlled polymerisation occurs in the quasi equilibrium regime [220] using typical literature values for NMP polymerisations of styrene. Similar to the results pertaining to the RAFT equilibrium as later obtained by Vana *et al.* [210], it was found the absolute equilibrium constant was not as important as the actual values of $k_{dis.}$ and $k_{comb.}$. Fischer reviewed the persistent radical effect and simulated a number of scenarios relevant to unique DC systems such as NMP and ATRP [221]. Souaille & Fischer [222] found that secondary initiation could be used to markedly accelerate the reaction, leading a decrease in the concentrations of both the reactive and persistent radicals derived from the iniferter, with a minimal impact on polymer dispersity, however at the cost of polymer chain end fidelity. Removal of the persistent radicals from the system increases the rate of polymerisation and decreases the time taken for the establishment of the quasi equilibrium; conversely adding an excess of the stable radical species at the start of the reaction lowers the polymerisation rate and increases control.

Vana & Goto used Predici to implement a model featuring both the DC and DT mechanism for Reversible Chain Transfer Catalyzed Polymerisation, and found that for a typically successful system that gives good control over M_n and $Đ$, the influence of the DT mechanism is small [223].

2.8 Synthetic protocols for TCT compounds utilised in RAFT and Iniferter polymerisations

The protocol chosen for RAFT agent synthesis primarily depends on the class of RAFT agent required, however certain generic approaches have emerged which are applicable to multiple classes of RAFT agents. For a comprehensive review on RAFT agent synthesis, please refer to the excellent review by Keddie *et al.* [28]. The two approaches primarily utilised within this thesis are highlighted in Scheme 2.25.

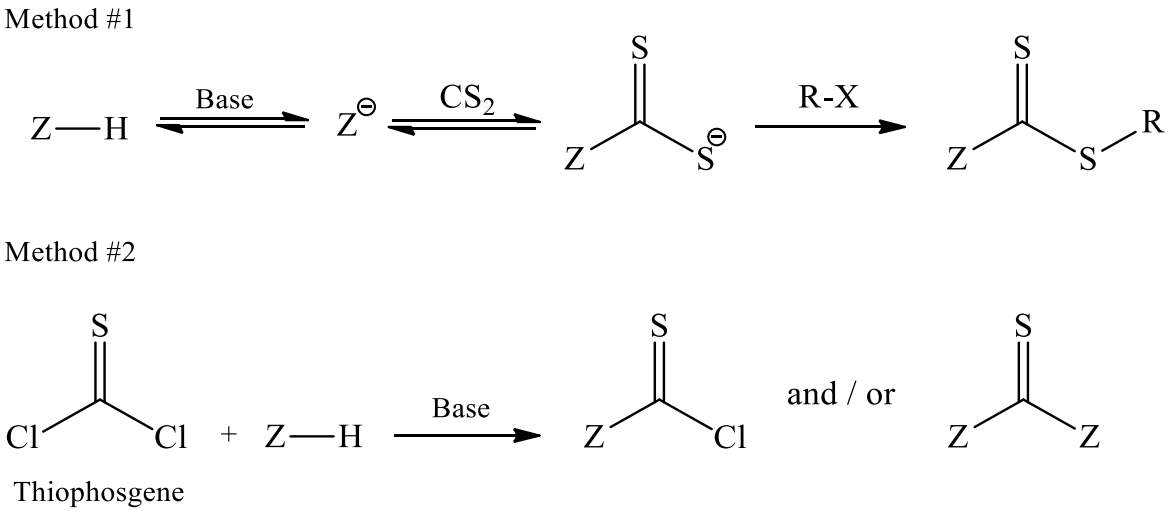

Scheme 2.25: Key strategies utilised for RAFT agent synthesis within this thesis.

Method #1 in Scheme 2.25 is by far the most commonly utilised method for RAFT agent synthesis due to its applicability to all classes of RAFT including xanthates, trithiocarbonates, dithiocarbamates and dithioesters [28]. This synthesis is typically done with the Z group first, with the choice of base being determined by the nucleophilicity of the starting compound (Z-H) to yield the carbodithioate salt, however stronger bases typically give higher yields [224]. The next step involves the addition of carbon disulfide which is typically done in a dropwise manner as this reaction is exothermic [225]; the quantity of CS_2 added varies from stoichiometric equivalents [224, 226] to large excesses where it is used as the solvent [227]. The alkylating agent is similarly added in a dropwise manner. Due to steric limitations, this approach should be avoided for tertiary R groups [66], however secondary and primary R groups often give high yields [224, 228]. Leaving group ability of the alkylating agent and overall nucleophilicity of the carbodithioate salt determine overall yield.

Method #1 can fail for several reasons; this includes the equilibrium concentration of the carbodithioate salt being very low due to the starting Z group being very weakly nucleophilic and lacking a sufficiently acidic proton. Furthermore, even if formed, the nucleophilicty of the intermediate carbodithioate salt can be the limiting factor, especially if the R group is very weakly electrophilic in nature. In instances such as this, method #2 provides a viable alternative. Utilising a very electrophilic compound such as thiophosgene allows for synthesis of RAFT agent starting with weakly nucleophilic Z groups that in turn created weakly nucleophilic carbodithioate ions. The primary drawbacks of this approach include the high toxicity of thiophosgene which requires extreme care when handling [28] coupled with the possibility of double addition to yield symmetrical TCT compounds which may not be desired [229].

2.9 Photochromism

2.9.1 General introduction

A molecule in its ground state will have electrons primarily in the lowest electronic state, however when irradiated with a suitable wavelength of light, the electrons within certain bonds are excited, which in turn leads to the molecule entering a higher energy level [230]. The molecule can then undergo a range of processes including intersystem crossing between singlet and triplet states (as described previously for TCT compounds in section 2.4.4), non-radiative decay, fluorescence and phosphorescence [230]. Another broad category of pathways after excitation available to certain molecules is that of photochromism. Photochromism can be defined as the reversible transformation of a chemical species between two states which have observable differences in their UV-Vis absorbance spectra, with the transformation being induced at least in one direction by the direct interaction of the chemical species with electromagnetic radiation [231]. Unimolecular photochromic systems are by the most common, with a simplified system being described by Scheme 2.26.

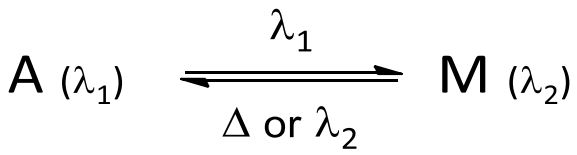

Scheme 2.26: Interconversion between two states of a generalised unimolecular photochromic system. Recreated from [231].

Generally, the wavelength of light required to switch the photochromic from state A to state M falls in the UV region (250 – 400 nm), however systems with activation wavelengths in the visible region (400 – 800 nm) also exist. The back reaction to transform M to A can either be exclusively driven by irradiation with a different wavelength of light (referred to as "S" type systems) or by a combination of thermal and photochemical reactions (referred to as "T" type systems) where the thermal reaction is normally predominant [231]. As shown in Figure 2.18, the defining characteristic of photochromic molecules is that upon conversion from state A (Figure 2.18, yellow trace) to state M (Figure 2.18, blue trace), there is a marked difference in the absorption spectra of the two species. Depending on the family of photochromic molecule and thus the associated mechanism that allows the photochromic switch, there can be several physical and chemical changes in the properties of the two states (A and M). These can include shifts in the dipole moment and thus electronic distribution, refractive index and geometrical structure of the molecule [232].

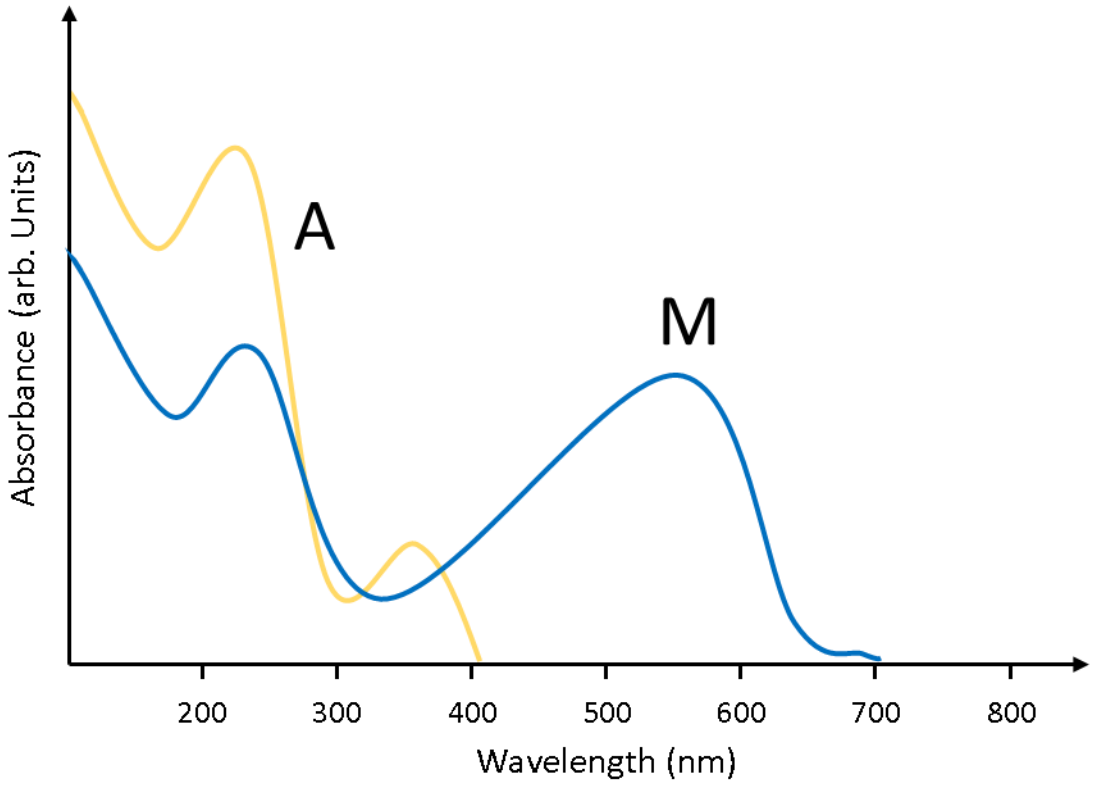

Figure 2.18: Generalised absorption spectra showing the photoisomerization of a photochromic molecule between two isomeric forms (A and B). Adapted from [233].

The chemical processes facilitating photochromism in organic photochromic molecules are pericyclic reactions along with intramolecular transfer reactions involving functional groups, electrons and bond dissociation processes [233, 234]. The most common classes of organic photochromic molecules used within the polymer science field and in commercial applications are summarised in Figure 2.19.

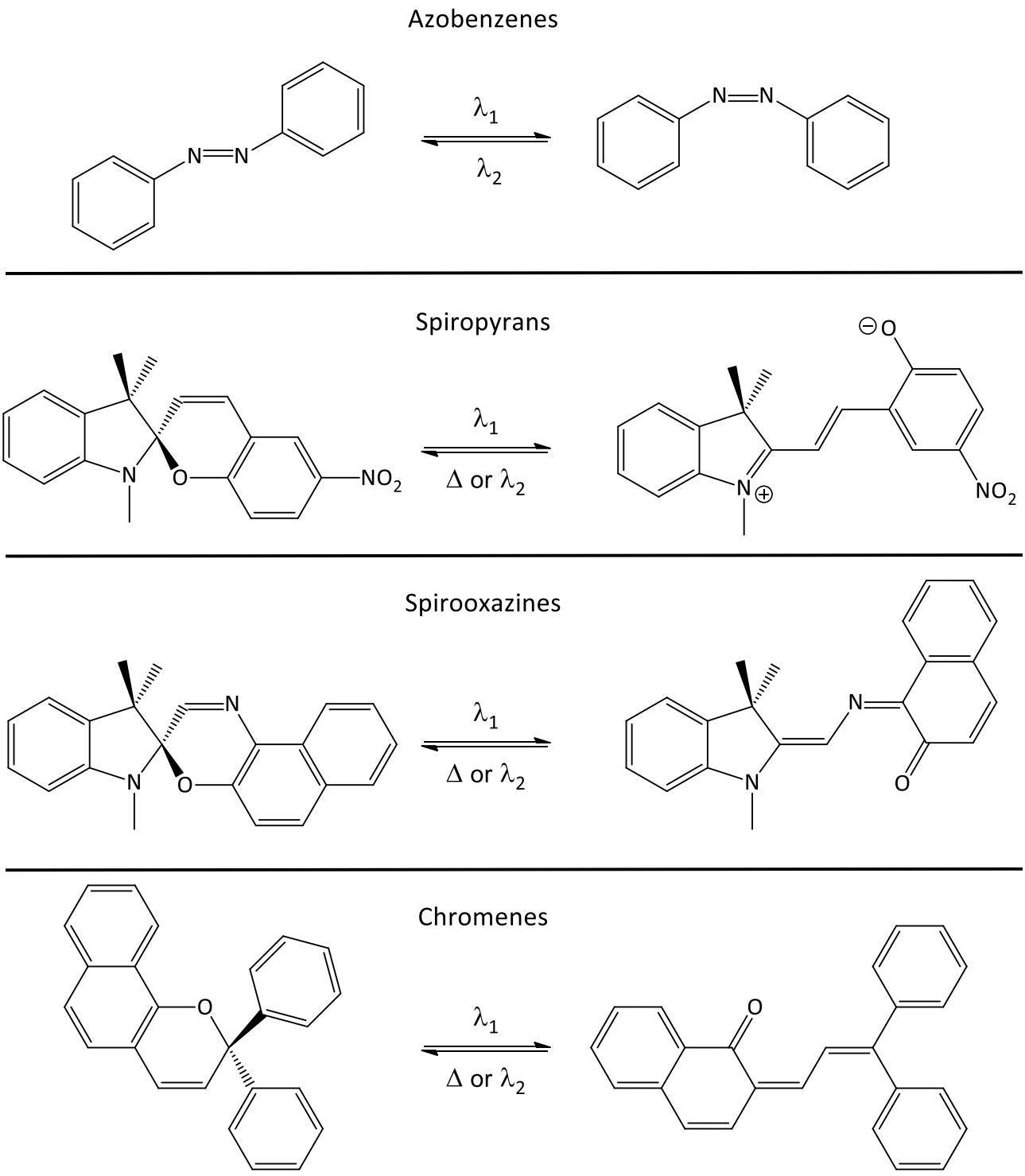

Figure 2.19: Main photochromic families used in polymer science and commercial applications. Adapted from [235].

Azobenzenes have seen extensive incorporation into polymeric materials including photo and thermoresponsive copolymers [236, 237], into polyelectrolyte mixtures [238] and photoresponsive polymer gels [239]. Their use in commercial applications is however typically limited to novelty items, with compounds such as spirooxazines and chromenes being more commercially significant.

2.9.2 Spirooxazines and spiropyrans

Spirooxazines and spiropyrans are composed of two distinct “halves” connected by a spiro carbon; these are the indole half and the naphthalene (for spirooxazines) or the salicylaldehyde (for spiropyrans) half. In the closed spirooxazine form these two halves are electronically isolated from one another and as a result the UV-Vis absorption spectrum for this form is effectively a superposition of the two constituent components [240, 241]. Upon irradiation with light of sufficient energy, the spirooxazine is raised to an excited state (A* in Figure 2.20), with evidence suggesting this is a triplet state for spiropyrans and a singlet state for spirooxazines [234]. This breaks the C-O bond connecting the two halves of the spirooxazine, leading to the formation of a highly unstable cis-cisoid isomer (B* in Figure 2.20), which then becomes a planar structure with distinct zwitterionic character (B in Figure 2.20). The zwitterionic isomer rearranges to form a distribution of planar merocyanine isomers of varying structures (Figure 2.21) of different stabilities [242, 243], with the most stable isomer (TTC) shown as M in Figure 2.20.

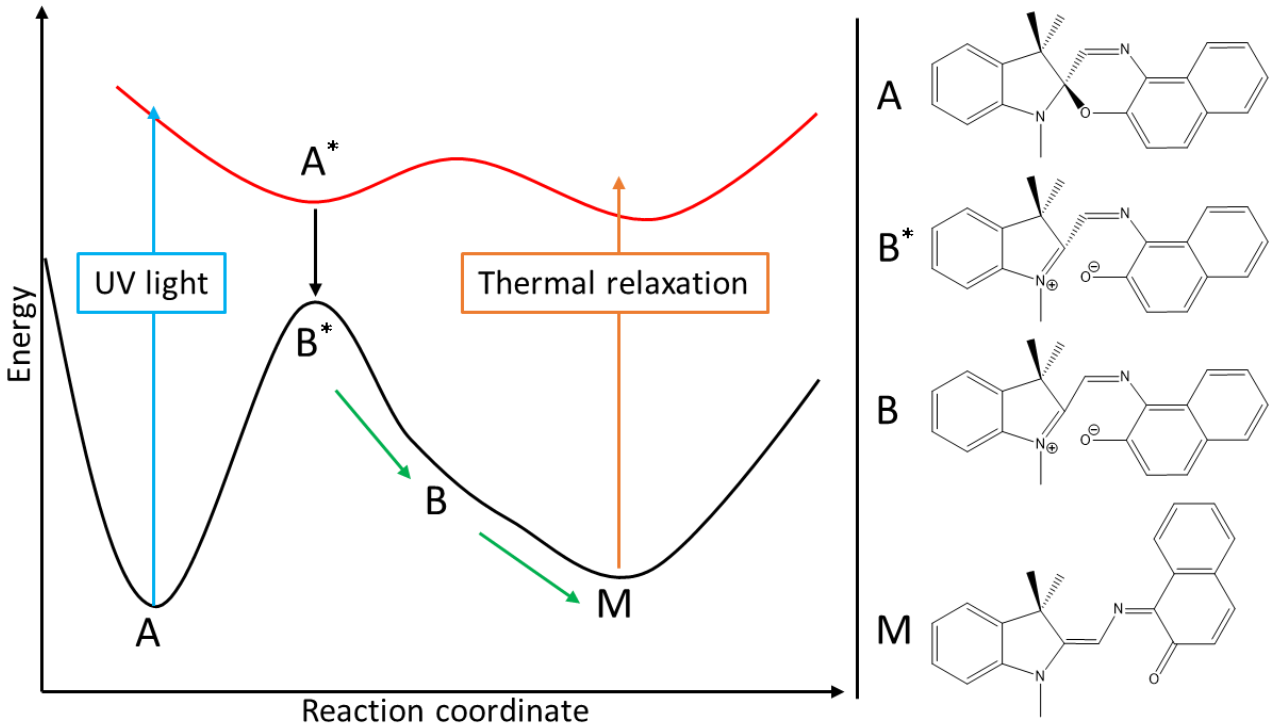

Figure 2.20: Generalised potential energy curve of photochromic reaction pathways with spirooxazines. Adapted from [244].

By effectively extending the conjugation pathway within the spirooxazine and thus shifting the absorption maximum of these species well into the visible region, these merocyanine isomers are the source of the intense colour changes seen after UV irradiation of spirooxazines [245]. Belonging to the T class of dyes, the merocyanine isomers revert to the closed spirooxazine form either thermally

or under irradiation with visible light. Whilst the exact times for the transitions between A → A* → B* → B → M vary between compounds and testing conditions [234, 244, 246], these transitions are nevertheless incredibly rapid (femtosecond to picoseconds) relative to the thermal back conversion to the spirooxazine form which occurs over second to minutes [247]. Furthermore, the back reaction is known to be affected by both solvent polarity [234, 247], temperature [248] and environmental constraints such as free volume and mobility within polymer matrix materials [235, 249-251].

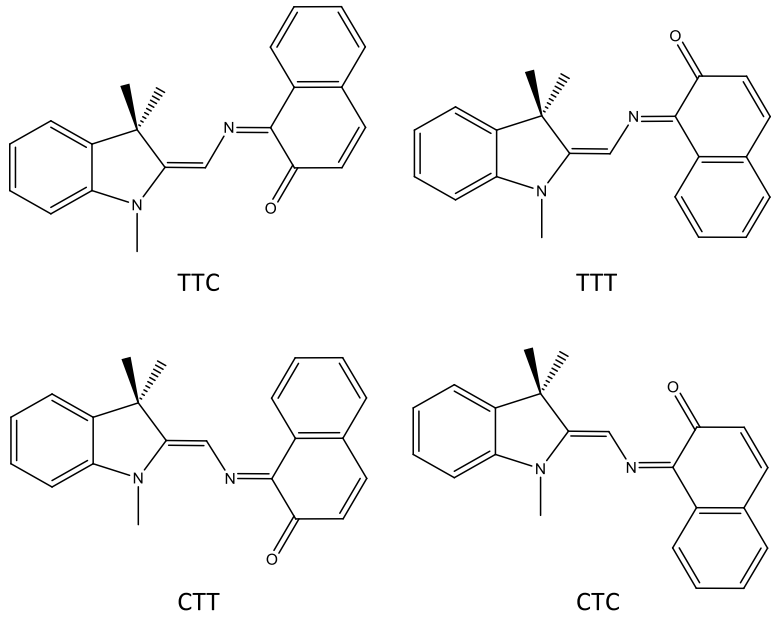

Figure 2.21: Spirooxazines isomers of the planar merocynanine form. Stability decreases in the order TTC > CTC > TTT > CTT. Recreated from [243].

An idealised photochromic process for spirooxazines is shown in Scheme 2.27, however this can be significantly more complicated by photodegradation processes which lead to loss of photochromic properties [234]. Evidence for different photodecomposition pathways exists for both spiropyrans [234] and spirooxazines [252-256], with this covered further in sections 7.1and 7.6.3 in chapter 7. Spirooxazines are more resistant to photodegradation [245] including under constant irradiation as shown by Baillet *et al.* [252], with this being a key reason why they are generally favoured over spiropyrans for research and commercial applications [245].

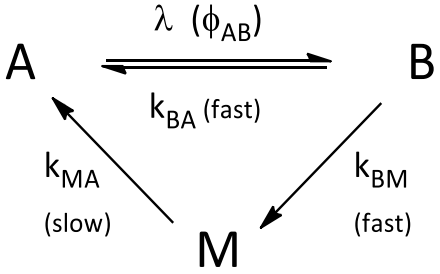

Scheme 2.27: Generalised isomerization pathways for a T type photochromic molecule such as a spirooxazine. Species labels correspond to those shown in Figure 2.20.

2.9.3 Spirooxazine and spiropyran derivatives in polymer science

By far the greatest monetary value of these compounds comes from their use as reversible darkening agents in polymer based ophthalmic lens technology as pioneered by the Carl Zeiss company in the form of "Transitions Lenses" products. To this end, significant research over the past 20 years has investigated the relationship between how these compounds are derivatised in relation to their key properties such as colour upon switching and their switching speed and fade rate back from the darkened state within polymer matrices [242, 257-259].

In interesting research applications, both spiro families have been utilised as logic systems to detect the presence of acids, bases and even CO_2 gas in solution[260, 261], for increasing sensitivity in detecting changes in thermally sensitive stimulus responsive copolymers [262], as reversible memory systems [232, 263] to name but a few. Furthermore, it is clear from the extensive derivatisation of both families of spiro compounds into polymerisable derivatives that they are reasonably resistant to radical attack and can survive the polymerisation process [107, 250, 262, 264].

2.10 Synthetic protocols for the synthesis of spirooxazines

The two most common methods of spirooxazine synthesis are shown in Scheme 2.28. The popularity and advantage of these methods arises from the fact the two constituent halves of the molecule can usually be purchased, and the reaction conditions are usually straightforward. Method 1 involves the reaction of either 1-methylene-2,3,3-trimethylindoline (R = CH_3, Fischer's base) or other commercially available indoline derivatives indoline with the desired 1-nitroso-2-naphthol derivative by refluxing in an organic solvent, usually an alcohol, for a short period of time under an inert atmosphere [265]. This method works well if the indoline in question is not too sensitive to oxidation [266].

Method 2 is useful when other functionality is required on the nitrogen on the indole half of the spirooxazine; 2,3,3-trimethylindolenine provides a useful starting material which can be reacted with the desired alkylating agent to generate the quaternary indolenium salt. The purification of indolenium salts prior to the condensation step is rarely attempted due to their amphiphilic nature, sensitivity to bases and hygroscopic nature [267]. Selection of a sufficiently strong organic base to generate the indoline compound in situ is essential [267].

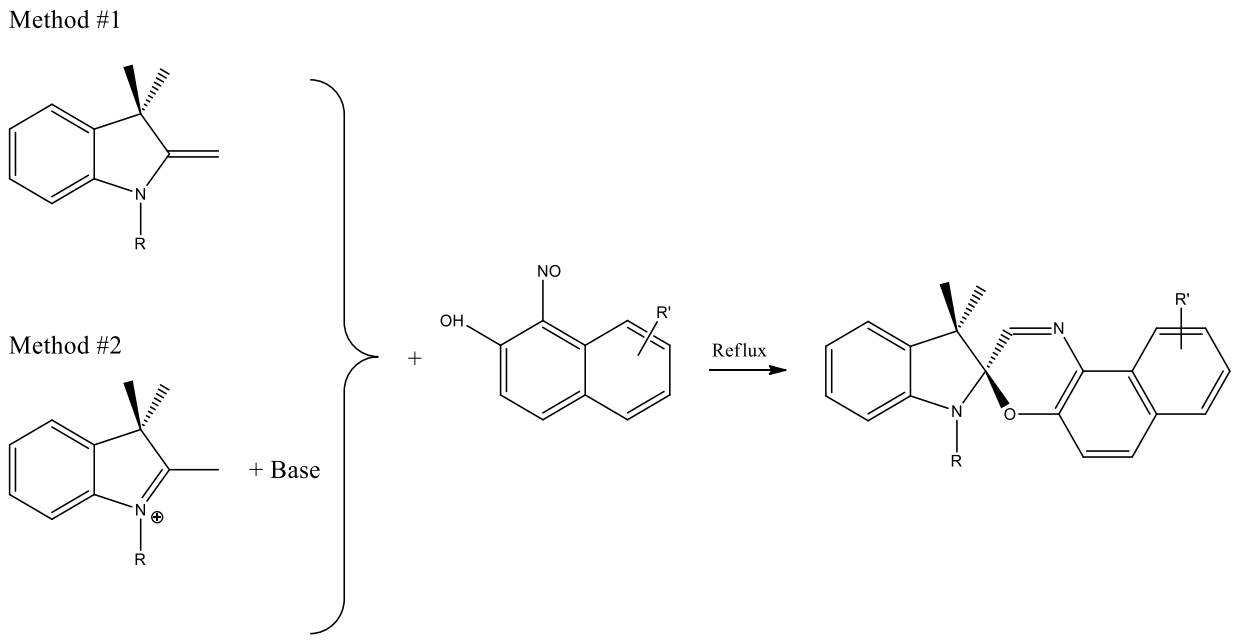

Scheme 2.28: Two common methods for the synthesis of spirooxazines. R and R' are generic substituents. Adapted from [268].

Pottier *et al.* postulated that spirooxazines are formed via the mechanism [265] shown in Scheme 2.29.

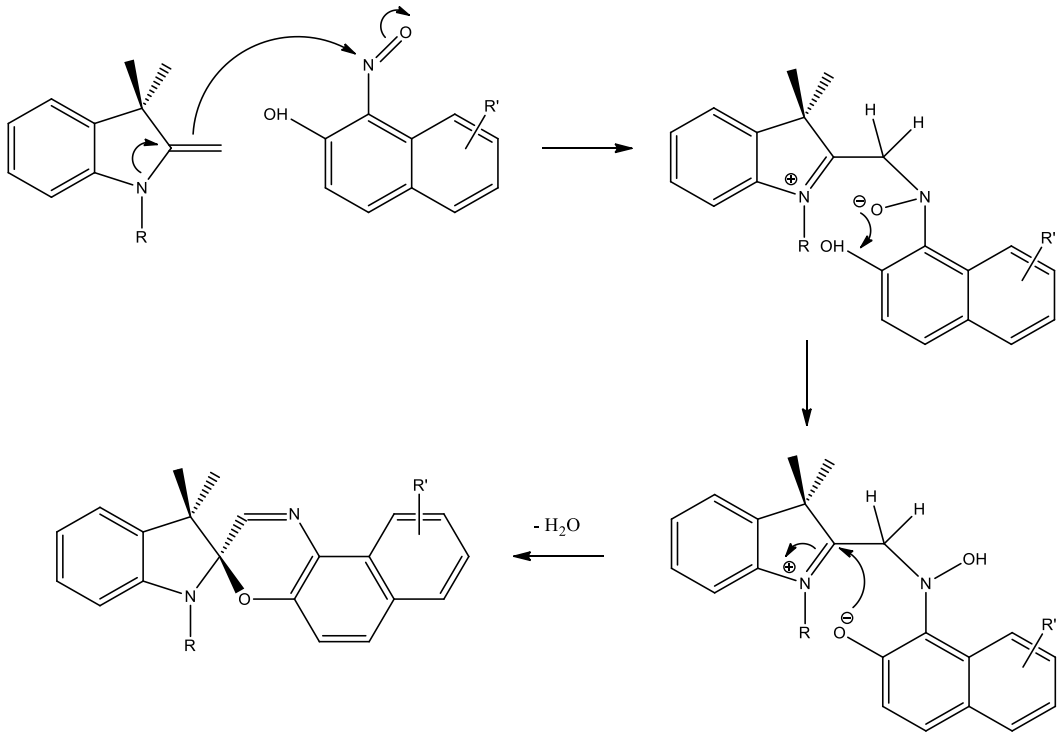

Scheme 2.29: Proposd mechanism for spirooxazine formation. Adapated from [265].

2.11 Key experimental techniques for characterization of polymers

In brief, the theoretical and practical basis for the key techniques most relevant to the characterization of polymerisation processes and of the resulting polymers formed will be covered here. Due to their unique structure, being somewhat between a molecule in chemical terms and an ensemble of nanoparticles due to their dispersity of chain lengths and thus subsequent size, the characterization of polymers requires a slightly nuanced approach when using traditional analytical chemistry techniques. The techniques described here are by far the most commonly encountered within the polymer literature and the ones that are utilised within this thesis. Techniques which either historically held greater importance (osmometry, viscometry, fractional separation) or newer techniques (MALDI-ToF spectroscopy) which were not employed in this thesis are not covered.

2.11.1 Nuclear Magnetic Resonance (NMR) Spectroscopy

NMR spectroscopy works on the principle that nuclei which have a net nuclear spin of ½ (such as ^{1}H and ^{13}C) will experience an alignment of their spin vectors either parallel or antiparallel when placed in a strong magnetic field. Furthermore, the nuclei can absorb a photon with a characteristic frequency that allows the energy barrier to be overcome between flipping the orientation of this spin; in NMR, this is achieved by a radio frequency pulse. Once the excitation pulse is removed, the nuclei then relax back to their previous spin, emitting a photon of identical wavelength to that which was absorbed to allow this transition to occur. This is what is detected by the NMR spectrometer and is characteristic of the nuclei being excited. Within a molecule, the substituents surrounding a nucleus have a direct bearing on the magnitude of the magnetic field experienced by the nucleus, hence the different absorption frequencies (chemical shifts in practical terms) and subsequent splitting patterns observed which allow structural determinations to be made [269].

NMR spectroscopy is a very useful tool for characterising the RAFT polymerisation process in regard to both kinetic analysis and the analysis of the final products formed. The determination of conversion by ^{1}H NMR is achieved by integrating the resonances attributed to either the alkene protons and/or the pendent functionality of the monomer to those of the polymer, often the resonances from the alkane backbone that arise due to consumption of the alkene bond. Any resonances that can be resolved between the monomer and those arising solely due to the polymer formation can be used, such that even resonances from the R group that shift upon conversion to polymer can be integrated. An internal or external standard can also be used in this process. Comparison of such ratios prior to the start of the reaction to those at a desired time point allows fractional conversion of the monomer to be determined. Examples are ubiquitous in the literature [117, 119, 270, 271].

The practical considerations with this approach include effectively halting the reaction to prevent further conversion prior to ^{1}H NMR analysis. Exposing the reaction mixture to atmospheric oxygen is often sufficient as this converts propagating radicals into alkoxy radicals [272], which are typically much less reactive [24]. Cooling the reaction mixture in liquid nitrogen or in a freezer is also recommended; the safest approach is adding a small amount of radical inhibitor such as those present in commercially obtained monomers. Dilution of the reaction mixture by the addition of a deuterated solvent is required to allow for proper locking and shimming of the sample by the NMR spectrophotometer. Proper sample handling should ensure no removal of the often-volatile monomer and that the polymer is soluble in the deuterated solvent added. In a ^{1}H NMR experiment, significant peak broadening arises for the polymer resonances from the multitude of chemical environments in a polymer chain, resulting in structurally analogous protons from the backbone each having a unique resonance. Also contributing to this is the inherent decrease in polymer mobility due to a rise in viscosity as high molecular weight polymers form [77].

In-situ ^{1}H NMR polymerisation experiments are an ideal method for the quantification of the apparent chain transfer coefficient by measuring the disappearance of the RAFT agent as a function of monomer conversion (see CSIRO method, section 2.3.2.1) [119], and to probe the intricacies of the RAFT pre-equilibrium [40, 41, 77-80, 273].

For purified RAFT polymers obtained by conventional experiment, the estimation of the number average molecular weight (M_n) of the polymer is achieved by integration of the unique resonances that arise from the RAFT agent (if possible, from both the protons on the Z and R groups) relative to resonances associated with the alkane backbone and/or the functionality present on the pendent monomer units. This number can easily be influenced by the presence of initiator derived chains [42] which are unavoidable in a RAFT process. Discrepancies between the M_n obtained by this method as compared to the theoretically expected M_n can be used to estimate chain end functionality [54].

It is also not trivial to accurately determine the percentage of polymer chains capped with the RAFT agent, as for this, careful 2D correlation experiments such as diffusion ordered spectroscopy (DOSY) are needed, and this requires significant NMR experience [42]. Furthermore, ^{1}H NMR analysis, irrespective of the experiment, does not give any information as to the dispersity of the polymer, as it does not give information as to the length of each polymer chain.

As highlighted by Stenzel & Barner-Kowollik [42], care must be taken in the NMR characterization of block copolymers made by RAFT. Analysis of a simple ^{1}H spectrum cannot differentiate between two separate polymer blocks (polyA & polyB) in solution and a single poly(A-b-B) copolymer. Furthermore, even if analysing a single poly(A-b-B) copolymer the relative intensities of the peaks

can be altered due to differing relaxation times; this arises due to differences in the mobility of the segments in different solvents and can give a false indication of the relative number of monomers in each block [274]. DOSY experiments can also confirm the successful conversion of a polyA macro-RAFT agent to form a poly(A-b-B) RAFT polymer, as evidenced by the work of Gardiner *et al.* [126].

NMR characterization is complemented greatly by Gel Permeation Chromatography (GPC) as will be comprehensively outlined in the next section.

2.11.2 Gel Permeation/ Size Exclusion Chromatography(GPC/SEC)

The terms GPC and SEC are often used interchangeably in the literature; GPC is used throughout this thesis. GPC is the most common technique for the characterization of the molecular weight and dispersity of polymer samples both for industrial and research applications. Analysis of most synthetic polymers obtained by RAFT or other RDRP polymerisation methods requires a separation column filled with semi-porous crosslinked polymer beads and HPLC purity organic solvents as the mobile phase in which the polymers are readily soluble. The remainder of a GPC system is essentially a conventional high-performance liquid chromatography (HPLC) system that includes an isocratic pump and solvent degasser, an autosampler and a column oven to allow for sample analysis at different temperatures. GPC is fundamentally different from other chromatographic methods in that it does not rely on direct chemical interactions of the analyte with the column packing, and any such interactions should be minimised [275]. A limitation of GPC is that it is not an absolute method of molar mass determination, as the molar mass is not related to any physical quantity that can be directly measured [275]. Instead the molecular weight is determined indirectly as the polymer chains are separated based on their hydrodynamic volume; the exact details of the mechanism by which this occurs is still a topic of investigation [10]. Nevertheless, the process is commonly explained as such: the smallest polymer chains have the smallest hydrodynamic volume and thus have a greater residence time within the pores of the column material, whilst the larger polymer chains with a larger hydrodynamic volume cannot enter as many pores. If the polymer chains are sufficiently large, they elute at the same rate as the solvent; this is also the reason why every column has a recommended range of molecular weights to which it is suited. This process is graphically shown in Figure 2.22.

Figure 2.22 has been removed due to copyright restrictions.

Figure 2.22: Schematic of the separation process for two polymers of differing hydrodynamic volume within a GPC column as a function time. Taken from https://polyanalytik.com/resource-centre/theory/what-is-size-exclusion-gel-permeation-chromatography.

The detector through which the sample passes after separation on the column is the key distinguishing feature between GPC systems. The most common due to applicability and cost are Refractive Index (RI) detectors that measure the difference between the RI of the mobile phase and the sample. The second most common are photo-diode array (PDA) detectors which essentially function like a conventional UV-Vis spectrophotometer, measuring the absorbance of light through the sample as a function of wavelength. A PDA detector is useful for determining the presence of RAFT end groups within a polymer, especially when block copolymers are synthesised [118, 127, 276]. An online viscometer in conjunction with an RI detector allows for a universal calibration to be established, whilst a system with a multiangle light scattering (MALS) detector has the advantage of being able to determine molecular size and molecular weight without the need for standards. Operating multi-detector systems brings with it technical challenges including peak broadening and peak shifting between detectors [277].

The most common approach is the calibration of a GPC system with commercially available narrow dispersity polymer standards, where the retention time and thus retention volume is known as a function of molecular weight. By measuring the retention time of an unknown polymer sample, the molecular weight given as molecular weight equivalents of the polymer standard is obtained. This however can be misleading; as depending on polymer structure and functionality, two polymers of equivalent molecular weight can have vastly different hydrodynamic volumes in the same solvent. The hydrodynamic volume of a polymer is directly related to its radius of gyration in solution, which is in turn linked to their intrinsic viscosity by the Flory-Fox equation [277]:

$$\langle r_g^2 \rangle^{3/2} = \frac{[\eta] \cdot M}{6^{3/2} \cdot \Phi}$$

Equation 2.53: Flory-Fox equation.

Where:

$\langle r_g^2 \rangle = radius\ of\ gyration$

$[\eta] = intrinsic\ viscosity$

$M = molecular\ weight$

$\Phi = \text{constant inverse proportionality factor}$

The intrinsic viscosity $[\eta]$ of a polymer can be related to its molecular weight (M) by the use of Mark-Houwink-Kuhn-Sakurada (MHKS) equation, where K and α are parameters that can be determined by viscosity measurements:

$$[\eta] = K \cdot M^{\alpha}$$

Equation 2.54: MHKS equation relating intrinsic viscosity to molecular weight for a polymer.

The observation that if the chromatographic retention time of two separate polymers is identical ($T_{R1} = T_{R2}$) then their hydrodynamic volumes must also be identical, along with the MHKS equation, gives an expression that allows the direct determination of the "true" molecular weight of the polymer being measured relative to that of the standards that were used to calibrate the system:

$$K_1 \cdot {M_1}^{1+\alpha_1} = K_2 \cdot {M_2}^{1+\alpha_2}$$

Equation 2.55: Equating the intrinsic viscosities of two polymers of equivalent retention time.

$$\log(M_2) = \frac{\log\left(\frac{K_1}{K_2}\right)}{1+\alpha_1} + \frac{1+\alpha_1}{1+\alpha_2} \cdot \log(M_1)$$

Equation 2.56: Relationship between the MHKS parameters for two polymers of equivalent retention time.

Considerable effort has been made to determining MHKS parameters for a range of polymers under various analytical conditions, however the spread of values is significant [278]. Gruendling *et al.* have circumvented some of the major drawbacks of universal calibration curves made with MHKS parameters by coupling supplementary methods of polymer characterization to GPC measurements of a range of polymers commonly encountered in research applications [277].

2.11.3 Ultraviolet Visible (UV-Vis) spectroscopy

UV-Vis spectroscopy is a technique that measures the interaction of radiation in the ultraviolet to visible region by molecules within solution. A molecule can absorb a photon of light in this wavelength range if it possesses a chromophore which is a moiety or structure which has an electronic transition between the HOMO and LUMO electronic levels corresponding to that energy [279]. The absorption of light by a sample is dependent on the molar absorptivity (quantified by the extinction coefficient) at the given wavelength, the concentration in solution and the path length. This is given by the Beer–Lambert law (Equation 2.11), however it is often expressed in the logarithmic format as a function of the light absorbed by the sample:

$$\log_{10}\left(\frac{I_0}{I_0 - I_{abs}}\right) = A = \varepsilon \cdot c \cdot l$$

Equation 2.57: Logarithmic form of the Beer-Lambert law as used in UV-Vis spectroscopy.

Where:

$A = absorbance$

$\varepsilon = molar\ extinction\ coefficient$

$c = concentration\ of\ analyte$

$l = pathlength\ of\ the\ sample$

$I_0 = intensity\ of\ incident\ radiation$

$I_{abs} = intensity\ of\ absorbed\ radiation$

Practical considerations include taking a blank reference spectrum in order to account for absorption by the solvent in which the analyte is dissolved, and for any light that may be absorbed or reflected by the cuvette housing the sample. Furthermore, using concentration ranges for analysis that give an absorbance less than ~ 1.5 is essential as above this range the Beer-Lambert law ceases to be strictly valid and non-linear relationships between analyte concentration and absorbance can become significant. This behaviour arises due to inter-molecular interactions influencing the electronic properties of individual analyte molecules.

2.11.4 Gravimetric analysis

Gravimetric analysis in polymer science is the equivalent to isolated yield in organic chemistry; this can give an indication of the overall conversion obtained upon completion of the reaction. For FRP and RDRP processes such as RAFT, the overall yield cannot be used to infer any information about the molecular weight distribution. This is because in the former case molecular weight is not predicted by monomer conversion alone, and in the latter case, is directly correlated with monomer conversion only under theoretically perfect conditions. Gravimetric analysis involves a direct comparison between the mass of the obtained purified polymer and the mass of the starting monomer. Removal of unreacted monomer, initiator and RAFT agent is required for this to be strictly valid. The most common purification methods are the precipitation of the polymer by adding the reaction mixture slowly into a ~ 10-fold volume excess of a solvent chosen such that it is a poor solvent for the polymer but a good solvent for the monomer. This process can be repeated several times; care must be taken to ensure product is not lost, and that the polymer is dried thoroughly. Another option is drying the polymer sample under high vacuum. This only works if the monomer is relatively volatile, if complete consumption of RAFT agent has occurred and the amount of initiator is low, and/or the polymer will not be used in chain extension experiments. Other more elaborate purification methods such as soxhlet extraction and diffusion through membranes with a well-defined molecular weight cut off can also be used.

2.12 References

1. Cunningham, M.F. and R. Hutchinson, *Industrial Applications and Processes*, in *Handbook of Radical Polymerization*. 2003, John Wiley & Sons, Inc. p. 333-359.
2. Coleman, E.A., *23 - Plastics Additives A2 - Kutz, Myer*, in *Applied Plastics Engineering Handbook*. 2011, William Andrew Publishing: Oxford. p. 419-428.
3. Matyjaszewski, K., *General Concepts and History of Living Radical Polymerization*, in *Handbook of Radical Polymerization*. 2003, John Wiley & Sons, Inc. p. 361-406.
4. Gigmes, D., *Nitroxide Mediated Polymerization: From Fundamentals to Applications in Materials Science*. 2015: Royal Society of Chemistry.
5. Otsu, T. and M. Yoshida, *Role of initiator-transfer agent-terminator (iniferter) in radical polymerizations: Polymer design by organic disulfides as iniferters.* Die Makromolekulare Chemie, Rapid Communications, 1982. **3**(2): p. 127-132.
6. Wang, J.S. and K. Matyjaszewski, *Controlled/"living" radical polymerization. atom transfer radical polymerization in the presence of transition-metal complexes.* Journal of the American Chemical Society, 1995. **117**(20): p. 5614-5615.
7. Chiefari, J., et al., *Living Free-Radical Polymerization by Reversible Addition−Fragmentation Chain Transfer: The RAFT Process.* Macromolecules, 1998. **31**(16): p. 5559-5562.
8. Corpart, P., et al., *Method for block polymer synthesis by controlled radical polymerisation*. 1998, Google Patents.
9. Flory, P.J., *Principles of Polymer Chemistry*. 1953, Ithaca, New York: Cornell University Press. 672.
10. Ravve, A., *Principles of Polymer Chemistry*. 3rd ed. 2012, New York: Springer.
11. Barner-Kowollik, C., P. Vana, and T.P. Davis, *The Kinetics of Free-Radical Polymerization*, in *Handbook of Radical Polymerization*. 2003, John Wiley & Sons, Inc. p. 187-261.
12. Moad, G. and D.H. Solomon, *3 - Initiation*, in *The Chemistry of Radical Polymerization (Second Edition)*. 2005, Elsevier Science Ltd: Amsterdam. p. 49-166.
13. Moad, G. and D.H. Solomon, *4 - Propagation*, in *The Chemistry of Radical Polymerization (Second Edition)*. 2005, Elsevier Science Ltd: Amsterdam. p. 167-232.
14. Moad, G. and D.H. Solomon, *5 - Termination*, in *The Chemistry of Radical Polymerization (Second Edition)*. 2005, Elsevier Science Ltd: Amsterdam. p. 233-278.
15. Smith, G.B., J.P.A. Heuts, and G.T. Russell, *New Paradigms in Free-Radical Polymerization Kinetics.* Macromolecular Symposia, 2005. **226**(1): p. 133-146.
16. Yamada, B. and P.B. Zetterlund, *General Chemistry of Radical Polymerization*, in *Handbook of Radical Polymerization*. 2003, John Wiley & Sons, Inc. p. 117-186.
17. Buback, M., et al., *Initiator efficiencies in 2,2'-azoisobutyronitrile-initiated free-radical polymerizations of styrene.* Macromolecular Chemistry and Physics, 1994. **195**(6): p. 2117-2140.
18. Chong, Y.K., E. Rizzardo, and D.H. Solomon, *Confirmation of the Mayo mechanism for the initiation of the thermal polymerization of styrene.* Journal of the American Chemical Society, 1983. **105**(26): p. 7761-7762.

19. Fouassier, J.P. and J. Lalevée, *Multicomponent Photoinitiating Systems*, in *Photoinitiators for Polymer Synthesis*. 2012, Wiley-VCH Verlag GmbH & Co. KGaA. p. 269-282.

20. Engel, P.S., *Mechanism of the thermal and photochemical decomposition of azoalkanes.* Chemical Reviews, 1980. **80**(2): p. 99-150.

21. Fouassier, J.P. and J. Lalevée, *Reactivity and Efficiency of Radical Photoinitiators*, in *Photoinitiators for Polymer Synthesis*. 2012, Wiley-VCH Verlag GmbH & Co. KGaA. p. 367-397.

22. Fouassier, J.P. and J. Lalevée, *Basic Principles and Applications of Photopolymerization Reactions*, in *Photoinitiators for Polymer Synthesis*. 2012, Wiley-VCH Verlag GmbH & Co. KGaA. p. 1-1.

23. Fouassier, J.P. and J. Lalevée, *Two-Component Photoinitiating Systems*, in *Photoinitiators for Polymer Synthesis*. 2012, Wiley-VCH Verlag GmbH & Co. KGaA. p. 199-268.

24. Fischer, H. and L. Radom, *Factors Controlling the Addition of Carbon-Centered Radicals to Alkenes—An Experimental and Theoretical Perspective.* Angewandte Chemie International Edition, 2001. **40**(8): p. 1340-1371.

25. Ivin, K.J., *Thermodynamics of addition polymerization.* Journal of Polymer Science Part A: Polymer Chemistry, 2000. **38**(12): p. 2137-2146.

26. Moad, G. and D.H. Solomon, *2 - Radical Reactions*, in *The Chemistry of Radical Polymerization (Second Edition)*. 2005, Elsevier Science Ltd: Amsterdam. p. 11-48.

27. Heuts, J.P.A., *Theory of Radical Reactions*, in *Handbook of Radical Polymerization*. 2003, John Wiley & Sons, Inc. p. 1-76.

28. Keddie, D.J., et al., *RAFT Agent Design and Synthesis.* Macromolecules, 2012. **45**(13): p. 5321-5342.

29. Barner-Kowollik, C., et al., *Critically Evaluated Rate Coefficients in Radical Polymerization – 8. Propagation Rate Coefficients for Vinyl Acetate in Bulk.* Macromolecular Chemistry and Physics, 2017. **218**(1): p. n/a-n/a.

30. Kockler, K.B., F. Fleischhaker, and C. Barner-Kowollik, *Free Radical Propagation Rate Coefficients of N-Containing Methacrylates: Are We Family?* Macromolecules, 2016. **49**(22): p. 8572-8580.

31. Barner-Kowollik, C., et al., *Critically evaluated rate coefficients in radical polymerization - 7. Secondary-radical propagation rate coefficients for methyl acrylate in the bulk.* Polymer Chemistry, 2014. **5**(1): p. 204-212.

32. Junkers, T., et al., *Determination of Propagation Rate Coefficients for Methyl and 2-Ethylhexyl Acrylate via High Frequency PLP−SEC under Consideration of the Impact of Chain Branching.* Macromolecules, 2010. **43**(24): p. 10427-10434.

33. Barner-Kowollik, C., et al., *Critically evaluated termination rate coefficients for free-radical polymerization: Experimental methods.* Progress in Polymer Science, 2005. **30**(6): p. 605-643.

34. Monyatsi, O., A.N. Nikitin, and R.A. Hutchinson, *Effect of Head-To-Head Addition on Vinyl Acetate Propagation Kinetics in Radical Polymerization.* Macromolecules, 2014. **47**(23): p. 8145-8153.

35. Morin, A.N., et al., *Effect of Head-to-Head Addition in Vinyl Acetate Controlled Radical Polymerization: Why Is Co(acac)2-Mediated Polymerization so Much Better?* Macromolecules, 2013. **46**(11): p. 4303-4312.

36. Olaj, O.F., et al., *Is the rate constant of chain propagation kp in radical polymerization really chain-length independent?* Macromolecular Rapid Communications, 2000. **21**(13): p. 913-920.

37. Matsumoto, A. and Y. Mohri, *Effects of solvent as an electron-pair acceptor on propagation reactions during radical polymerization and copolymerization of polar vinyl monomers.* Journal of Polymer Science Part A: Polymer Chemistry, 1999. **37**(15): p. 2803-2814.

38. Beuermann, S., et al., *Propagation Kinetics of Free-Radical Methacrylic Acid Polymerization in Aqueous Solution. The Effect of Concentration and Degree of Ionization.* Macromolecular Symposia, 2007. **248**(1): p. 23-32.

39. Gridnev, A.A. and S.D. Ittel, *Dependence of Free-Radical Propagation Rate Constants on the Degree of Polymerization.* Macromolecules, 1996. **29**(18): p. 5864-5874.

40. Houshyar, S., et al., *The scope for synthesis of macro-RAFT agents by sequential insertion of single monomer units.* Polymer Chemistry, 2012. **3**(7): p. 1879-1889.

41. McLeary, J.B., M.P. Tonge, and B. Klumperman, *A Mechanistic Interpretation of Initialization Processes in RAFT-Mediated Polymerization.* Macromolecular Rapid Communications, 2006. **27**(15): p. 1233-1240.

42. Stenzel, M.H. and C. Barner-Kowollik, *The living dead - common misconceptions about reversible deactivation radical polymerization.* Materials Horizons, 2016. **3**(6): p. 471-477.

43. Heuts, J.P.A., et al., *The Importance of Chain-Length Dependent Kinetics in Free-Radical Polymerization: A Preliminary Guide.* Macromolecular Symposia, 2007. **248**(1): p. 12-22.

44. Bamford, C.H., et al., *The Kinetics of Vinyl Polymerization by Radical Mechanisms*. 1958, London: Butterworths.

45. McNaught , A.D. and A. Wilkinson, *IUPAC Compendium of Chemical Terminology*. 2nd. ed. 1997, Oxford, UK.: Blackwell Scientific Publications.

46. Darling, T.R., et al., *Living polymerization: Rationale for uniform terminology.* Journal of Polymer Science Part A: Polymer Chemistry, 2000. **38**(10): p. 1706-1708.

47. Moad, G. and D.H. Solomon, *9 - Living Radical Polymerization*, in *The Chemistry of Radical Polymerization (Second Edition)*. 2005, Elsevier Science Ltd: Amsterdam. p. 451-585.

48. Goto, A. and T. Fukuda, *Kinetics of living radical polymerization.* Progress in Polymer Science, 2004. **29**(4): p. 329-385.

49. Otsu, T., *Iniferter concept and living radical polymerization.* Journal of Polymer Science Part A: Polymer Chemistry, 2000. **38**(12): p. 2121-2136.

50. Yeow, J., O.R. Sugita, and C. Boyer, *Visible Light-Mediated Polymerization-Induced Self-Assembly in the Absence of External Catalyst or Initiator.* ACS Macro Letters, 2016. **5**(5): p. 558-564.

51. Chen, M., M. Zhong, and J.A. Johnson, *Light-Controlled Radical Polymerization: Mechanisms, Methods, and Applications.* Chemical Reviews, 2016. **116**(17): p. 10167-10211.

52. Wang, H., et al., *Real-Time and in Situ Investigation of "Living"/Controlled Photopolymerization in the Presence of a Trithiocarbonate.* Macromolecules, 2013. **46**(7): p. 2576-2582.

53. Moad, G., et al., *New Features of the Mechanism of RAFT Polymerization*, in *Controlled/Living Radical Polymerization: Progress in RAFT, DT, NMP & OMRP*. 2009, American Chemical Society. p. 3-18.

54. Moad, G. and C. Barner-Kowollik, *The Mechanism and Kinetics of the RAFT Process: Overview, Rates, Stabilities, Side Reactions, Product Spectrum and Outstanding Challenges*, in *Handbook of RAFT Polymerization*. 2008, Wiley-VCH Verlag GmbH & Co. KGaA. p. 51-104.

55. Fukuda, T., A. Goto, and Y. Tsujii, *Kinetics of Living Radical Polymerization*, in *Handbook of Radical Polymerization*. 2003, John Wiley & Sons, Inc. p. 407-462.

56. Moad, G., E. Rizzardo, and S.H. Thang, *Living Radical Polymerization by the RAFT Process - A Third Update.* Australian Journal of Chemistry, 2012. **65**(8): p. 985-1076.

57. Henry, D.J., et al., *Comparison of the Kinetics and Thermodynamics for Methyl Radical Addition to CC, CO, and CS Double Bonds.* Journal of the American Chemical Society, 2004. **126**(6): p. 1732-1740.

58. Coote, M.L. and L. Radom, *Ab Initio Evidence for Slow Fragmentation in RAFT Polymerization.* Journal of the American Chemical Society, 2003. **125**(6): p. 1490-1491.

59. Moad, G., E. Rizzardo, and S.H. Thang, *Living Radical Polymerization by the RAFT Process - A First Update.* Australian Journal of Chemistry, 2006. **59**(10): p. 669-692.

60. Derboven, P., et al., *Chain Transfer in Degenerative RAFT Polymerization Revisited: A Comparative Study of Literature Methods.* Macromolecular Theory and Simulations, 2016. **25**(2): p. 104-115.

61. Moad, G., et al., *Initiating free radical polymerization.* Macromolecular Symposia, 2002. **182**(1): p. 65-80.

62. Theis, A., et al., *Access to Chain Length Dependent Termination Rate Coefficients of Methyl Acrylate via Reversible Addition−Fragmentation Chain Transfer Polymerization.* Macromolecules, 2005. **38**(7): p. 2595-2605.

63. Coote, M.L., E.H. Krenske, and E.I. Izgorodina, *Quantum-Chemical Studies of RAFT Polymerization: Methodology, Structure-Reactivity Correlations and Kinetic Implications*, in *Handbook of RAFT Polymerization*. 2008, Wiley-VCH Verlag GmbH & Co. KGaA. p. 5-49.

64. De Rybel, N., et al., *An Update on the Pivotal Role of Kinetic Modeling for the Mechanistic Understanding and Design of Bulk and Solution RAFT Polymerization.* Macromolecular Theory and Simulations, 2017. **26**(1): p. n/a-n/a.

65. Mayadunne, R.T.A., et al., *Living Radical Polymerization with Reversible Addition−Fragmentation Chain Transfer (RAFT Polymerization) Using Dithiocarbamates as Chain Transfer Agents.* Macromolecules, 1999. **32**(21): p. 6977-6980.

66. Moad, G., et al., *Living free radical polymerization with reversible addition – fragmentation chain transfer (the life of RAFT).* Polymer International, 2000. **49**(9): p. 993-1001.

67. Chiefari, J., et al., *Thiocarbonylthio Compounds (SC(Z)S−R) in Free Radical Polymerization with Reversible Addition-Fragmentation Chain Transfer (RAFT Polymerization). Effect of the Activating Group Z.* Macromolecules, 2003. **36**(7): p. 2273-2283.

68. Bicciocchi, E., et al., *Substituent Effects on RAFT Polymerization with Benzyl Aryl Trithiocarbonates.* Macromolecular Chemistry and Physics, 2010. **211**(5): p. 529-538.

69. Stenzel, M.H., et al., *Xanthate Mediated Living Polymerization of Vinyl Acetate: A Systematic Variation in MADIX/RAFT Agent Structure.* Macromolecular Chemistry and Physics, 2003. **204**(9): p. 1160-1168.

70. Adamy, M., et al., *Influence of the Chemical Structure of MADIX Agents on the RAFT Polymerization of Styrene.* Macromolecules, 2003. **36**(7): p. 2293-2301.

71. Destarac, M., et al., *Xanthates as Chain-Transfer Agents in Controlled Radical Polymerization (MADIX): Structural Effect of the O-Alkyl Group.* Macromolecular Rapid Communications, 2002. **23**(17): p. 1049-1054.

72. Destarac, M., et al., *Dithiocarbamates as universal reversible addition-fragmentation chain transfer agents.* Macromolecular Rapid Communications, 2000. **21**(15): p. 1035-1039.

73. Chong, Y.K., et al., *Thiocarbonylthio Compounds [SC(Ph)S−R] in Free Radical Polymerization with Reversible Addition-Fragmentation Chain Transfer (RAFT Polymerization). Role of the Free-Radical Leaving Group (R).* Macromolecules, 2003. **36**(7): p. 2256-2272.

74. Barner-Kowollik, C., et al., *Kinetic Investigations of Reversible Addition Fragmentation Chain Transfer Polymerizations: Cumyl Phenyldithioacetate Mediated Homopolymerizations of Styrene and Methyl Methacrylate.* Macromolecules, 2001. **34**(22): p. 7849-7857.

75. Favier, A., et al., *Study of the RAFT Polymerization of a Water-Soluble Bisubstituted Acrylamide Derivative. 1. Influence of the Dithioester Structure.* Macromolecules, 2002. **35**(22): p. 8271-8280.

76. Destarac, M., et al., *Macromolecular Design via the Interchange of Xanthates (MADIX): Polymerization of Styrene with O-Ethyl Xanthates as Controlling Agents.* Macromolecular Chemistry and Physics, 2002. **203**(16): p. 2281-2289.

77. McLeary, J.B., et al., *Beyond Inhibition: A 1H NMR Investigation of the Early Kinetics of RAFT-Mediated Polymerization with the Same Initiating and Leaving Groups.* Macromolecules, 2004. **37**(7): p. 2383-2394.

78. McLeary, J.B., et al., *A 1H NMR Investigation of Reversible Addition−Fragmentation Chain Transfer Polymerization Kinetics and Mechanisms. Initialization with Different Initiating and Leaving Groups.* Macromolecules, 2005. **38**(8): p. 3151-3161.

79. McLeary, J.B., et al., *Initialisation in RAFT-mediated polymerisation of methyl acrylate.* Chemical Communications, 2004(17): p. 1950-1951.

80. Pound, G., et al., *In-Situ NMR Spectroscopy for Probing the Efficiency of RAFT/MADIX Agents.* Macromolecules, 2006. **39**(23): p. 7796-7797.

81. Krenske, E.H., E.I. Izgorodina, and M.L. Coote, *An Ab Initio Guide to Structure—Reactivity Trends in Reversible Addition Fragmentation Chain Transfer Polymerization*, in *Controlled/Living Radical Polymerization*. 2006, American Chemical Society. p. 406-420.

82. Perrier, S., et al., *Origin of Inhibition Effects in the Reversible Addition Fragmentation Chain Transfer (RAFT) Polymerization of Methyl Acrylate.* Macromolecules, 2002. **35**(22): p. 8300-8306.

83. Barner-Kowollik, C., et al., *Mechanism and kinetics of dithiobenzoate-mediated RAFT polymerization. I. The current situation.* Journal of Polymer Science Part A: Polymer Chemistry, 2006. **44**(20): p. 5809-5831.

84. Barner-Kowollik, C., et al., *The reversible addition-fragmentation chain transfer process and the strength and limitations of modeling: Comment on "the magnitude of the fragmentation rate coefficient".* Journal of Polymer Science Part A: Polymer Chemistry, 2003. **41**(18): p. 2828-2832.

85. Wang, A.R., et al., *A difference of six orders of magnitude: A reply to "the magnitude of the fragmentation rate coefficient".* Journal of Polymer Science Part A: Polymer Chemistry, 2003. **41**(18): p. 2833-2839.

86. Hawthorne, D.G., et al., *Living Radical Polymerization with Reversible Addition−Fragmentation Chain Transfer (RAFT): Direct ESR Observation of Intermediate Radicals.* Macromolecules, 1999. **32**(16): p. 5457-5459.

87. Junkers, T., et al., *Thioketone-Mediated Polymerization with Dithiobenzoates: Proof for the Existence of Stable Radical Intermediates in RAFT Polymerization.* Macromolecular Rapid Communications, 2012. **33**(11): p. 984-990.

88. Kwak, Y., A. Goto, and T. Fukuda, *Rate Retardation in Reversible Addition−Fragmentation Chain Transfer (RAFT) Polymerization: Further Evidence for Cross-Termination Producing 3-Arm Star Chain.* Macromolecules, 2004. **37**(4): p. 1219-1225.

89. Buback, M., et al., *A Missing Reaction Step in Dithiobenzoate-Mediated RAFT Polymerization*, in *Radical Polymerization*. 2007, Wiley-VCH Verlag GmbH & Co. KGaA. p. 158-167.

90. Moad, G., *Mechanism and Kinetics of Dithiobenzoate-Mediated RAFT Polymerization – Status of the Dilemma.* Macromolecular Chemistry and Physics, 2014. **215**(1): p. 9-26.

91. Moad, G., E. Rizzardo, and S.H. Thang, *End-functional polymers, thiocarbonylthio group removal/transformation and reversible addition–fragmentation–chain transfer (RAFT) polymerization.* Polymer International, 2011. **60**(1): p. 9-25.

92. Moad, G., et al., *Advances in RAFT polymerization: the synthesis of polymers with defined end-groups.* Polymer, 2005. **46**(19): p. 8458-8468.

93. Willcock, H. and R.K. O'Reilly, *End group removal and modification of RAFT polymers.* Polymer Chemistry, 2010. **1**(2): p. 149-157.

94. Boyer, C., V. Bulmus, and T.P. Davis, *Efficient Usage of Thiocarbonates for Both the Production and the Biofunctionalization of Polymers.* Macromolecular Rapid Communications, 2009. **30**(7): p. 493-497.

95. Boyer, C., et al., *Bioapplications of RAFT Polymerization.* Chemical Reviews, 2009. **109**(11): p. 5402-5436.

96. Boyer, C. and T.P. Davis, *One- pot synthesis and biofunctionalization of glycopolymersviaRAFT polymerization and thiol-ene reactions.* Chemical Communications, 2009(40): p. 6029-6031.

97. Boyer, C., et al., *Modification of RAFT-polymers via thiol-ene reactions: A general route to functional polymers and new architectures.* Journal of Polymer Science Part A: Polymer Chemistry, 2009. **47**(15): p. 3773-3794.

98. Boyer, C., et al., *RAFT Polymer End-Group Modification and Chain Coupling/Conjugation Via Disulfide Bonds.* Australian Journal of Chemistry, 2009. **62**(8): p. 830-847.

99. Matyjaszewski, K., *Atom Transfer Radical Polymerization (ATRP): Current Status and Future Perspectives.* Macromolecules, 2012. **45**(10): p. 4015-4039.

100. Fairbanks, B.D., P.A. Gunatillake, and L. Meagher, *Biomedical applications of polymers derived by reversible addition – fragmentation chain-transfer (RAFT).* Advanced Drug Delivery Reviews, 2015. **91**(Supplement C): p. 141-152.

101. Moad, G., E. Rizzardo, and S.H. Thang, *Living Radical Polymerization by the RAFT Process.* Australian Journal of Chemistry, 2005. **58**(6): p. 379-410.

102. Gregory, A. and M.H. Stenzel, *Complex polymer architectures via RAFT polymerization: From fundamental process to extending the scope using click chemistry and nature's building blocks.* Progress in Polymer Science, 2012. **37**(1): p. 38-105.

103. Stenzel, M.H., *Complex Architecture Design via the RAFT Process: Scope, Strengths and Limitations*, in *Handbook of RAFT Polymerization*. 2008, Wiley-VCH Verlag GmbH & Co. KGaA. p. 315-372.

104. Takolpuckdee, P., et al., *Polymer Architectures via Reversible Addition Fragmentation Chain Transfer (RAFT) Polymerization.* Macromolecular Symposia, 2004. **216**(1): p. 23-36.

105. Tang, T., et al., *Thermo-responsive Poly(methyl methacrylate)-block-poly(N-isopropylacrylamide) Block Copolymers Synthesized by RAFT Polymerization: Micellization and Gelation.* Macromolecular Chemistry and Physics, 2006. **207**(19): p. 1718-1726.

106. Yang, C. and Y.L. Cheng, *RAFT synthesis of poly(N-isopropylacrylamide) and poly(methacrylic acid) homopolymers and block copolymers: Kinetics and characterization.* Journal of Applied Polymer Science, 2006. **102**(2): p. 1191-1201.

107. Such, G.K., R.A. Evans, and T.P. Davis, *The Use of Block Copolymers to Systematically Modify Photochromic Behavior.* Macromolecules, 2006. **39**(26): p. 9562-9570.

108. Save, M., et al., *Synthesis by RAFT of Amphiphilic Block and Comblike Cationic Copolymers and Their Use in Emulsion Polymerization for the Electrosteric Stabilization of Latexes.* Macromolecules, 2005. **38**(2): p. 280-289.

109. Keddie, D.J., *A guide to the synthesis of block copolymers using reversible-addition fragmentation chain transfer (RAFT) polymerization.* Chemical Society Reviews, 2014. **43**(2): p. 496-505.

110. Tong, Y.Y., et al., *Synthesis of Well-Defined Poly(vinyl acetate)-b-Polystyrene by Combination of ATRP and RAFT Polymerization.* Macromolecules, 2008. **41**(20): p. 7339-7346.

111. Huang, C.F., et al., *Homopolymerization and Block Copolymerization of N-Vinylpyrrolidone by ATRP and RAFT with Haloxanthate Inifers.* Macromolecules, 2009. **42**(21): p. 8198-8210.

112. Tasdelen, M.A., *Diels-Alder "click" reactions: recent applications in polymer and material science.* Polymer Chemistry, 2011. **2**(10): p. 2133-2145.

113. Quemener, D., et al., *RAFT and click chemistry: A versatile approach to well-defined block copolymers.* Chemical Communications, 2006(48): p. 5051-5053.

114. Liu, Q., et al., *RAFT polymerization of N-vinylpyrrolidone mediated by cyanoprop-2-yl-1-dithionaphthalate in the presence of a fluoroalcohol: the possibility of altering monomer properties by hydrogen bonding?* Polymer Chemistry, 2016. **7**(11): p. 2015-2021.

115. Benaglia, M., et al., *Universal (Switchable) RAFT Agents.* Journal of the American Chemical Society, 2009. **131**(20): p. 6914-6915.

116. Benaglia, M., et al., *Polystyrene-block-poly(vinyl acetate) through the Use of a Switchable RAFT Agent.* Macromolecules, 2009. **42**(24): p. 9384-9386.

117. Keddie, D.J., et al., *Switchable Reversible Addition–Fragmentation Chain Transfer (RAFT) Polymerization in Aqueous Solution, N,N-Dimethylacrylamide.* Macromolecules, 2011. **44**(17): p. 6738-6745.

118. Moad, G., et al., *Block Copolymer Synthesis through the Use of Switchable RAFT Agents*, in *Non-Conventional Functional Block Copolymers*. 2011, American Chemical Society. p. 81-102.

119. Keddie, D.J., et al., *Chain Transfer Kinetics of Acid/Base Switchable N-Aryl-N-Pyridyl Dithiocarbamate RAFT Agents in Methyl Acrylate, N-Vinylcarbazole and Vinyl Acetate Polymerization.* Macromolecules, 2012. **45**(10): p. 4205-4215.

120. Coote, M.L. and D.J. Henry, *Computer-Aided Design of a Destabilized RAFT Adduct Radical: Toward Improved RAFT Agents for Styrene-block-Vinyl Acetate Copolymers.* Macromolecules, 2005. **38**(13): p. 5774-5779.

121. Theis, A., et al., *A Synthetic Approach to a Novel Class of Fluorine-Bearing Reversible AdditionFragmentation Chain Transfer (RAFT) Agents: F-RAFT.* Australian Journal of Chemistry, 2005. **58**(6): p. 437-441.

122. Coote, M.L., et al., *Addition-Fragmentation Kinetics of Fluorodithioformates (F-RAFT) in Styrene, Vinyl Acetate, and Ethylene Polymerization: An Ab Initio Investigation.* Macromolecules, 2006. **39**(13): p. 4585-4591.

123. Busch, M., et al., *The Use of Novel F-RAFT Agents in High Temperature and High Pressure Ethene Polymerization: Can Control be Achieved?* Australian Journal of Chemistry, 2007. **60**(10): p. 788-793.

124. Malepu, V., et al., *RAFT Polymerization of Vinyl Acetate, Styrene and Acrylates Using N,N-Dithiocarbamates*, in *Controlled/Living Radical Polymerization: Progress in RAFT, DT, NMP & OMRP*. 2009, American Chemical Society. p. 37-47.

125. Dayter, L.A., K.A. Murphy, and D.A. Shipp, *RAFT Polymerization of Monomers with Highly Disparate Reactivities: Use of a Single RAFT Agent and the Synthesis of Poly(styrene-block-vinyl acetate).* Australian Journal of Chemistry, 2013. **66**(12): p. 1564-1569.

126. Gardiner, J., et al., *Dithiocarbamate RAFT agents with broad applicability - the 3,5-dimethyl-1H-pyrazole-1-carbodithioates.* Polymer Chemistry, 2016. **7**(2): p. 481-492.

127. Gardiner, J., et al., *4-Halogeno-3,5-dimethyl-1H-pyrazole-1-carbodithioates: versatile reversible addition fragmentation chain transfer agents with broad applicability.* Polymer International, 2017. **66**(11): p. 1438-1447.

128. Otsu, T., M. Yoshida, and T. Tazaki, *A model for living radical polymerization.* Die Makromolekulare Chemie, Rapid Communications, 1982. **3**(2): p. 133-140.

129. Ferington, T.E. and A.V. Tobolsky, *Organic Disulfides as Initiators of Polymerization: Tetramethylthiuram Disulfide.* Journal of the American Chemical Society, 1955. **77**(17): p. 4510-4512.

130. Walter, E.R. and F.P. Reding, *Organic Polysulfides as Polymerization Initiators.* Journal of Polymer Science, 1957. **21**(99): p. 559-561.

131. Okawara, M., et al., *Photochemical Behavior of O-Ethyl S-Benzyl Xanthate as a Model Compound for a Photosensitive Resin.* The Journal of Organic Chemistry, 1965. **30**(6): p. 2025-2029.

132. Moad, G. and D.H. Solomon, *6 - Chain Transfer*, in *The Chemistry of Radical Polymerization (Second Edition)*. 2005, Elsevier Science Ltd: Amsterdam. p. 279-331.

133. McKenzie, T.G., et al., *Visible Light Mediated Controlled Radical Polymerization in the Absence of Exogenous Radical Sources or Catalysts.* Macromolecules, 2015. **48**(12): p. 3864-3872.

134. Kuriyama, A. and T. Otsu, *Living Radical Polymerization of Methyl Methacrylate with a Tetrafunctional Photoiniferter: Synthesis of a Star Polymer.* Polym J, 1984. **16**(6): p. 511-514.

135. Otsu, T. and A. Kuriyama, *Polymer Design by Iniferter Technique in Radical Polymerization: Synthesis of AB and ABA Block Copolymers Containing Random and Alternating Copolymer Sequences.* Polym J, 1985. **17**(1): p. 97-104.

136. Lambrinos, P., et al., *The mechanism of the polymerization of n.butyl acrylate initiated with N,N-diethyl dithiocarbamate derivatives.* European Polymer Journal, 1990. **26**(10): p. 1125-1135.

137. Lalevée, J., et al., *Controlled photopolymerization reactions: The reactivity of new photoiniferters.* Journal of Polymer Science Part A: Polymer Chemistry, 2007. **45**(12): p. 2436-2442.

138. Lalevée, J., X. Allonas, and J.P. Fouassier, *A New Efficient Photoiniferter for Living Radical Photopolymerization.* Macromolecules, 2006. **39**(24): p. 8216-8218.

139. Lalevée, J., et al., *New Photoiniferters: Respective Role of the Initiating and Persistent Radicals.* Macromolecules, 2008. **41**(7): p. 2347-2352.

140. Bertin, D., et al., *Polymérisation radicalaire vivante du mma en présence de dérivés piperidino-dithiocarbamates comme photoiniferters.* European Polymer Journal, 1998. **34**(1): p. 85-90.

141. Matyjaszewski, K., *A Commentary on "Role of Initiator-Transfer Agent-Terminator (Iniferter) in Radical Polymerizations: Polymer Design by Organic Disulfides as Iniferters" by T. Otsu, M. Yoshida (Macromol. Rapid Commun. 1982, 3, 127–132).* Macromolecular Rapid Communications, 2005. **26**(3): p. 135-142.

142. Niwa, M., Y. Sako, and M. Shimizu, *Block Polymerizations of Vinyl Monomers Initiated by Telechelicisopropyl Xanthate-Terminated Polymers as Macrophotoinitiator. Design Of Block Copolymers. 2.* Journal of Macromolecular Science: Part A - Chemistry, 1987. **24**(11): p. 1315-1332.

143. Niwa, M., T. Matsumoto, and H. Izumi, *Kinetics of the Photopolymerization of Vinyl Monomers by Bis(Isopropylxanthogen) Disulfide. Design of Block Copolymers.* Journal of Macromolecular Science: Part A - Chemistry, 1987. **24**(5): p. 567-585.

144. Kilambi, H., S.K. Reddy, and C.N. Bowman, *Kinetic and Mechanistic Studies of Photopolymerizations of Acrylates in the Presence of Iniferters.* Macromolecules, 2007. **40**(17): p. 6131-6135.

145. You, Y.Z., et al., *Photo-Initiated Living Free Radical Polymerization in the Presence of Dibenzyl Trithiocarbonate.* Macromolecular Chemistry and Physics, 2002. **203**(3): p. 477-483.

146. Hong, C.Y., et al., *Controlled polymerization of acrylic acid under 60Co irradiation in the presence of dibenzyl trithiocarbonate.* Journal of Polymer Science Part A: Polymer Chemistry, 2001. **39**(22): p. 3934-3939.

147. Barner-Kowollik, C., et al., *Long-lived intermediates in reversible addition–fragmentation chain-transfer (RAFT) polymerization generated by γ radiation.* Journal of Polymer Science Part A: Polymer Chemistry, 2002. **40**(8): p. 1058-1063.

148. Quinn, J.F., et al., *Living Free Radical Polymerisation Under a Constant Source of Gamma Radiation – An Example of Reversible Addition-Fragmentation Chain Transfer or Reversible Termination?* Macromolecular Rapid Communications, 2002. **23**(12): p. 717-721.

149. Quinn, J.F., et al., *Reversible Addition−Fragmentation Chain Transfer Polymerization Initiated with Ultraviolet Radiation.* Macromolecules, 2002. **35**(20): p. 7620-7627.

150. McKenzie, T.G., et al., *Beyond Traditional RAFT: Alternative Activation of Thiocarbonylthio Compounds for Controlled Polymerization.* Advanced Science, 2016. **3**(9): p. n/a-n/a.

151. Carmean, R.N., et al., *Ultra-High Molecular Weights via Aqueous Reversible-Deactivation Radical Polymerization.* Chem, 2017. **2**(1): p. 93-101.

152. Xu, J., et al., *Catalyst-Free Visible Light-Induced RAFT Photopolymerization*, in *Controlled Radical Polymerization: Mechanisms*. 2015, American Chemical Society. p. 247-267.

153. Fouassier, J.P. and J. Lalevée, *One-Component Photoinitiating Systems*, in *Photoinitiators for Polymer Synthesis*. 2012, Wiley-VCH Verlag GmbH & Co. KGaA. p. 127-197.

154. Skrabania, K., et al., *Examining the UV-vis absorption of RAFT chain transfer agents and their use for polymer analysis.* Polymer Chemistry, 2011. **2**(9): p. 2074-2083.

155. Zard, S.Z., *On the Trail of Xanthates: Some New Chemistry from an Old Functional Group.* Angewandte Chemie International Edition in English, 1997. **36**(7): p. 672-685.

156. Xu, J., et al., *Thermal Decomposition of Dithioesters and Its Effect on RAFT Polymerization.* Macromolecules, 2006. **39**(11): p. 3753-3759.

157. Qiu, X.P. and F.M. Winnik, *Facile and Efficient One-Pot Transformation of RAFT Polymer End Groups via a Mild Aminolysis/Michael Addition Sequence.* Macromolecular Rapid Communications, 2006. **27**(19): p. 1648-1653.

158. Chong, Y.K., et al., *Thiocarbonylthio End Group Removal from RAFT-Synthesized Polymers by Radical-Induced Reduction.* Macromolecules, 2007. **40**(13): p. 4446-4455.

159. Vana, P., T.P. Davis, and C. Barner-Kowollik, *Easy Access to Chain-Length-Dependent Termination Rate Coefficients Using RAFT Polymerization.* Macromolecular Rapid Communications, 2002. **23**(16): p. 952-956.

160. Lu, L., et al., *Toward Rapid and Well-Controlled Ambient Temperature RAFT Polymerization under UV−Vis Radiation: Effect of Radiation Wave Range.* Macromolecules, 2006. **39**(11): p. 3770-3776.

161. Šebenik, A., *Living free-radical block copolymerization using thio-iniferters.* Progress in Polymer Science, 1998. **23**(5): p. 875-917.

162. Yamase, T., H. Kokado, and E. Inoue, *The Photolysis of Sodium N,N-Dimethyldithiocarbamate and Hexamethyleneammonium Hexamethylenedithiocarbamate.* Bulletin of the Chemical Society of Japan, 1970. **43**(3): p. 934-935.

163. Niwa, M., et al., *Molecular design of block and graft copolymers by vinyl-substituted xanthates.* Die Makromolekulare Chemie, 1988. **189**(9): p. 2187-2199.

164. Tazhe Veetil, A., et al., *Photochemistry of S-Phenacyl Xanthates.* The Journal of Organic Chemistry, 2011. **76**(20): p. 8232-8242.

165. Zhang, H., et al., *Ambient-Temperature RAFT Polymerization of Styrene and Its Functional Derivatives under Mild Long-Wave UV−vis Radiation.* Macromolecules, 2007. **40**(26): p. 9252-9261.

166. Nemoto, Y. and Y. Nakayama, *Optimal irradiation wavelength in iniferter-based photocontrolled radical polymerization.* Journal of Polymer Science Part A: Polymer Chemistry, 2008. **46**(13): p. 4505-4512.

167. Shanmugam, S., J. Xu, and C. Boyer, *Living Additive Manufacturing.* ACS Central Science, 2017. **3**(2): p. 95-96.

168. McKenzie, T.G., et al., *Investigation into the photolytic stability of RAFT agents and the implications for photopolymerization reactions.* Polymer Chemistry, 2016. **7**(25): p. 4246-4253.

169. Ham, M.K., et al., *Photoinitiated RAFT polymerization of vinyl acetate.* Journal of Polymer Science Part A: Polymer Chemistry, 2012. **50**(12): p. 2389-2397.

170. Poly, J., et al., *Polymers synthesized by RAFT as versatile macrophotoinitiators.* Polymer Chemistry, 2015. **6**(31): p. 5766-5772.

171. Kitchin, A.D., et al., *Photophysics of a dithioester RAFT polymerization agent and the acenaphthenyl model light-harvesting chromophore.* Photochemical & Photobiological Sciences, 2007. **6**(8): p. 853-856.

172. Turner, S.R. and R.W. Blevins, *Photoinitiated block copolymer formation using dithiocarbamate free radical chemistry.* Macromolecules, 1990. **23**(6): p. 1856-1859.

173. Dika Manga, J., et al., *Mechanism of the polymerization of n-butyl acrylate initiated by N,N-diethyldithiocarbamate derivatives. Part 1. Photolysis of butyl-2-(N,N-diethyldithiocarbamyl)propionate and oligomerization of butyl acrylate.* Polymer International, 1998. **45**(1): p. 14-21.

174. Dika Manga, J., et al., *Mechanism of the polymerization of n-butyl acrylate initiated by N,N-diethyldithiocarbamate derivatives. Part 2. Investigation of the reaction mechanism.* Polymer International, 1998. **45**(3): p. 243-254.

175. Doi, T., A. Matsumoto, and T. Otsu, *Elucidation of mechanism for living radical polymerization of styrene with N,N-diethyldithiocarbamate derivatives as iniferters by the use of spin trapping technique.* Journal of Polymer Science Part A: Polymer Chemistry, 1994. **32**(12): p. 2241-2249.

176. Coote, M.L. and L. Radom, *Substituent Effects in Xanthate-Mediated Polymerization of Vinyl Acetate: Ab Initio Evidence for an Alternative Fragmentation Pathway.* Macromolecules, 2004. **37**(2): p. 590-596.

177. Carmean, R.N., et al., *Catalyst-Free Photoinduced End-Group Removal of Thiocarbonylthio Functionality.* ACS Macro Letters, 2017. **6**(2): p. 185-189.

178. Van Kerckhoven, C., et al., *Dithiocarbamate telechelic polymers: Synthesis and block copolymerization.* Die Makromolekulare Chemie, 1991. **192**(1): p. 101-114.

179. Otsu, T., et al., *Features of living radical polymerization of vinyl monomers in homogeneous system using N,N-diethyldithiocarbamate derivatives as photoiniferters.* European Polymer Journal, 1995. **31**(1): p. 67-78.

180. Wang, M., et al., *Facile synthesis of poly(vinyl acetate)-b-polystyrene copolymers mediated by an iniferter agent using a single methodology.* Polymer Chemistry, 2017. **8**(38): p. 5918-5923.

181. Ran, R., Y. Yu, and T. Wan, *Photoinitiated RAFT polymerization in the presence of trithiocarbonate.* Journal of Applied Polymer Science, 2007. **105**(2): p. 398-404.

182. Rubens, M., P. Latsrisaeng, and T. Junkers, *Visible light-induced iniferter polymerization of methacrylates enhanced by continuous flow.* Polymer Chemistry, 2017.

183. Otsu, T. and A. Kuriyama, *Living mono- and biradical polymerizations in homogeneous system synthesis of AB and ABA type block copolymers.* Polymer Bulletin, 1984. **11**(2): p. 135-142.

184. Qin, S.H. and K.Y. Qiu, *A new polymerizable photoiniferter for preparing poly(methyl methacrylate) macromonomer.* European Polymer Journal, 2001. **37**(4): p. 711-717.

185. Ishizu, K. and A. Mori, *Synthesis of hyperbranched polymers by self-addition free radical vinyl polymerization of photo functional styrene.* Macromolecular Rapid Communications, 2000. **21**(10): p. 665-668.

186. Ishizu, K. and A. Mori, *Solution properties of hyperbranched polymers and synthetic application for amphiphilic star-hyperbranched copolymers by grafting from hyperbranched macroinitiator.* Polymer International, 2002. **51**(1): p. 50-54.

187. Ajayaghosh, A. and R. Francis, *Narrow Polydispersed Reactive Polymers by a Photoinitiated Free Radical Polymerization Approach. Controlled Polymerization of Methyl Methacrylate.* Macromolecules, 1998. **31**(4): p. 1436-1438.

188. Ajayaghosh, A. and R. Francis, *A Xanthate-Derived Photoinitiator that Recognizes and Controls the Free Radical Polymerization Pathways of Methyl Methacrylate and Styrene.* Journal of the American Chemical Society, 1999. **121**(28): p. 6599-6606.

189. Francis, R. and A. Ajayaghosh, *Minimization of Homopolymer Formation and Control of Dispersity in Free Radical Induced Graft Polymerization Using Xanthate Derived Macro-photoinitiators.* Macromolecules, 2000. **33**(13): p. 4699-4704.

190. Coote, M.L., *Quantum-Chemical Modeling of Free-Radical Polymerization.* Macromolecular Theory and Simulations, 2009. **18**(7-8): p. 388-400.

191. Coote, M.L., *Computational Quantum Chemistry for Free-Radical Polymerization*, in *Encyclopedia of Polymer Science and Technology*. 2006, John Wiley & Sons, Inc.

192. Lin, H. and D.G. Truhlar, *QM/MM: what have we learned, where are we, and where do we go from here?* Theoretical Chemistry Accounts, 2006. **117**(2): p. 185.

193. Vreven, T. and K. Morokuma, *Investigation of the S0-S1 excitation in bacteriorhodopsin with the ONIOM(MO:MM) hybrid method.* Theoretical Chemistry Accounts, 2003. **109**(3): p. 125-132.

194. Dennington, R., T.A. Keith, and J.M. Millam, *GaussView*. 2016, Semichem Inc: Shawnee Mission, KS.

195. Frisch, M.J., et al., *Gaussian 09, Revision C.1*. 2009, Gaussian, Inc., Wallingford CT.

196. *Spartan '16*. 2016, Wavefunction, Inc.: Irvine, CA.

197. Matyjaszewski, K. and R. Poli, *Comparison of Bond Dissociation Energies of Dormant Species Relevant to Degenerative Transfer and Atom Transfer Radical Polymerization.* Macromolecules, 2005. **38**(19): p. 8093-8100.

198. Coote, M.L., *Ab Initio Study of the Addition−Fragmentation Equilibrium in RAFT Polymerization: When Is Polymerization Retarded?* Macromolecules, 2004. **37**(13): p. 5023-5031.

199. Coote, M.L., *The Kinetics of Addition and Fragmentation in Reversible Addition Fragmentation Chain Transfer Polymerization: An ab Initio Study.* The Journal of Physical Chemistry A, 2005. **109**(6): p. 1230-1239.

200. Coote, M.L., G.P.F. Wood, and L. Radom, *Methyl Radical Addition to CS Double Bonds: Kinetic versus Thermodynamic Preferences.* The Journal of Physical Chemistry A, 2002. **106**(50): p. 12124-12138.

201. Coote, M.L., *Reliable Theoretical Procedures for the Calculation of Electronic-Structure Information in Hydrogen Abstraction Reactions.* The Journal of Physical Chemistry A, 2004. **108**(17): p. 3865-3872.

202. Coote, M.L., E.H. Krenske, and E.I. Izgorodina, *Computational Studies of RAFT Polymerization–Mechanistic Insights and Practical Applications.* Macromolecular Rapid Communications, 2006. **27**(7): p. 473-497.

203. Wang, A.R. and S. Zhu, *Modeling the reversible addition–fragmentation transfer polymerization process.* Journal of Polymer Science Part A: Polymer Chemistry, 2003. **41**(11): p. 1553-1566.

204. Fortunatti, C., et al., *Modeling of RAFT Polymerization using Probability Generating Functions. Detailed Prediction of Full Molecular Weight Distributions and Sensitivity Analysis.* Macromolecular Reaction Engineering, 2014. **8**(12): p. 781-795.

205. Pallares, J., et al., *A Comparison of Reaction Mechanisms for Reversible Addition-Fragmentation Chain Transfer Polymerization Using Modeling Tools.* Journal of Macromolecular Science, Part A, 2006. **43**(9): p. 1293-1322.

206. Wulkow, M., *The simulation of molecular weight distributions in polyreaction kinetics by discrete Galerkin methods.* Macromolecular Theory and Simulations, 1996. **5**(3): p. 393-416.

207. Wulkow, M., *Computer Aided Modeling of Polymer Reaction Engineering—The Status of Predici, I-Simulation.* Macromolecular Reaction Engineering, 2008. **2**(6): p. 461-494.

208. Barner-Kowollik, C., et al., *Modeling the reversible addition–fragmentation chain transfer process in cumyl dithiobenzoate-mediated styrene homopolymerizations: Assessing rate coefficients for the addition–fragmentation equilibrium.* Journal of Polymer Science Part A: Polymer Chemistry, 2001. **39**(9): p. 1353-1365.

209. Wulkow, M., et al., *Implementing the reversible addition–fragmentation chain transfer process in PREDICI.* Journal of Polymer Science Part A: Polymer Chemistry, 2004. **42**(6): p. 1441-1448.

210. Vana, P., T.P. Davis, and C. Barner-Kowollik, *Kinetic Analysis of Reversible Addition Fragmentation Chain Transfer (RAFT) Polymerizations: Conditions for Inhibition, Retardation, and Optimum Living Polymerization.* Macromolecular Theory and Simulations, 2002. **11**(8): p. 823-835.

211. Coote, M.L., et al., *Quantum Chemical Mapping of Initialization Processes in RAFT Polymerization.* Macromolecular Rapid Communications, 2006. **27**(13): p. 1015-1022.

212. Busch, M., *Modeling Kinetics and Structural Properties in High-Pressure Fluid-Phase Polymerization.* Macromolecular Theory and Simulations, 2001. **10**(5): p. 408-429.

213. Jaramillo-Soto, G., et al., *Simulation of RAFT Dispersion Polymerization in Supercritical Carbon Dioxide.* Macromolecular Theory and Simulations, 2008. **17**(6): p. 280-289.

214. Theis, A., et al., *Mapping Chain Length and Conversion Dependent Termination Rate Coefficients in Methyl Acrylate Free Radical Polymerization.* Macromolecules, 2005. **38**(24): p. 10323-10327.

215. Theis, A., et al., *Probing the reaction kinetics of vinyl acetate free radical polymerization via living free radical polymerization (MADIX).* Polymer, 2006. **47**(4): p. 999-1010.

216. Ward, J.H. and N.A. Peppas, *Kinetic Gelation Modeling of Controlled Radical Polymerizations.* Macromolecules, 2000. **33**(14): p. 5137-5142.

217. Rahane, S.B., S.M. Kilbey, and A.T. Metters, *Kinetic Modeling of Surface-Initiated Photoiniferter-Mediated Photopolymerization in Presence of Tetraethylthiuram Disulfide.* Macromolecules, 2008. **41**(24): p. 9612-9618.

218. Vivaldo-Lima, E. and A. de Jesús Mendoza-Fuentes, *Development Of A Kinetic Model For Iniferter Controlled/"Living" Free-Radical Polyerization Considering Diffusion-Controlled Effects.* Polymer Reaction Engineering, 2002. **10**(4): p. 193-226.

219. Krajnc, M., I. Poljanšek, and J. Golob, *Kinetic modeling of methyl methacrylate free-radical polymerization initiated by tetraphenyl biphosphine.* Polymer, 2001. **42**(9): p. 4153-4162.

220. Souaille, M. and H. Fischer, *Kinetic Conditions for Living and Controlled Free Radical Polymerizations Mediated by Reversible Combination of Transient Propagating and Persistent Radicals: The Ideal Mechanism.* Macromolecules, 2000. **33**(20): p. 7378-7394.

221. Fischer, H., *The Persistent Radical Effect: A Principle for Selective Radical Reactions and Living Radical Polymerizations.* Chemical Reviews, 2001. **101**(12): p. 3581-3610.

222. Souaille, M. and H. Fischer, *Rate Enhancement and Retardation Strategies in Living Free Radical Polymerizations Mediated by Nitroxides and Other Persistent Species: A Theoretical Assessment.* Macromolecules, 2002. **35**(1): p. 248-261.

223. Vana, P. and A. Goto, *Kinetic Simulations of Reversible Chain Transfer Catalyzed Polymerization (RTCP): Guidelines to Optimum Molecular Weight Control.* Macromolecular Theory and Simulations, 2010. **19**(1): p. 24-35.

224. Aoyagi, N. and T. Endo, *Functional RAFT agents for radical-controlled polymerization: Quantitative synthesis of trithiocarbonates containing functional groups as RAFT agents using equivalent amount of CS2.* Journal of Polymer Science Part A: Polymer Chemistry, 2009. **47**(14): p. 3702-3709.

225. Farnham, W., *Synthesis of trithiocarbonates*. 2007, Google Patents.

226. Ponnusamy, K., R.P. Babu, and R. Dhamodharan, *Synthesis of block and graft copolymers of styrene by raft polymerization, using dodecyl-based trithiocarbonates as initiators and chain transfer agents.* Journal of Polymer Science Part A: Polymer Chemistry, 2013. **51**(5): p. 1066-1078.

227. D'Amico, J.J. and F.G. Bellinger, *Derivatives of 3-(2-hydroxyethyl)2-benzothiazolinone and related compounds.* Journal of Heterocyclic Chemistry, 1988. **25**(6): p. 1601-1605.

228. Movassagh, B. and M. Soleiman-Beigi, *Triethylamine-catalyzed one-pot synthesis of trithiocarbonates from carbon disulfide, thiols, and alkyl halides in water.* Monatshefte für Chemie - Chemical Monthly, 2008. **139**(8): p. 927-930.

229. Sharma, S., *Thiophosgene in Organic Synthesis.* Synthesis, 1978. **1978**(11): p. 803-820.

230. Atkins, P. and J. de Paula, *Atkins' Physical Chemistry*. 8th ed. 2006: Oxford University Press.

231. Crano, J.C. and R.J. Guglielmetti, *Introduction & Index*, in *Organic Photochromic and Thermochromic Compounds - Volume 1 - Main Photochromic Families*, J.C. Crano and R.J. Guglielmetti, Editors. 2002, Kluwer Academic Publishers: New York.

232. Ercole, F., T.P. Davis, and R.A. Evans, *Photo-responsive systems and biomaterials: photochromic polymers, light-triggered self-assembly, surface modification, fluorescence modulation and beyond.* Polymer Chemistry, 2010. **1**(1): p. 37-54.

233. Ercole, F., *Photochromic Polymers - The Application and Control of Photochromism through its Interaction with Polymers*. 2011, University of New South Wales.

234. Malatesta, V., *Photodegradation of Organic Photochromes,* in *Organic Photochromic and Thermochromic Compounds - Volume 2 - Physicochemical Studies, Biological Applications and Thermochromism*, J.C. Crano and R.J. Guglielmetti, Editors. 2002, Kluwer Academic Publishers: New York. p. 65-166.

235. Such, G., et al., *Factors Influencing Photochromism of Spiro-Compounds Within Polymeric Matrices.* Journal of Macromolecular Science, Part C, 2003. **43**(4): p. 547-579.

236. Yoshida, T., S. Kanaoka, and S. Aoshima, *Photo-responsive copolymers with azobenzene side groups synthesized by living cationic polymerization: Efficient amplification of photosensitivity in aqueous photo-switching system.* Journal of Polymer Science Part A: Polymer Chemistry, 2005. **43**(21): p. 5337-5342.

237. Sugiyama, K. and K. Sono, *Characterization of photo- and thermoresponsible amphiphilic copolymers having azobenzene moieties as side groups.* Journal of Applied Polymer Science, 2001. **81**(12): p. 3056-3063.

238. Lee, C.T., K.A. Smith, and T.A. Hatton, *Photoreversible Viscosity Changes and Gelation in Mixtures of Hydrophobically Modified Polyelectrolytes and Photosensitive Surfactants.* Macromolecules, 2004. **37**(14): p. 5397-5405.

239. Deshmukh, S., L. Bromberg, and T.A. Hatton, *Responsive Azobenzene-Containing Polymers and Gels*. 2005: Massachusetts Institute of Technology, Cambridge.

240. Tyer, N.W. and R.S. Becker, *Photochromic spiropyrans. I. Absorption spectra and evaluation of the .pi.-electron orthogonality of the constituent halves.* Journal of the American Chemical Society, 1970. **92**(5): p. 1289-1294.

241. Lenoble, C. and R.S. Becker, *Photophysics, photochemistry and kinetics of indolinospiropyran derivatives and an indolinothiospiropyran.* Journal of Photochemistry, 1986. **34**(1): p. 83-88.

242. Yee, L.H., et al., *Photochromic Spirooxazines Functionalized with Oligomers: Investigation of Core−Oligomer Interactions and Photomerocyanine Isomer Interconversion Using NMR Spectroscopy and DFT.* The Journal of Organic Chemistry, 2010. **75**(9): p. 2851-2860.

243. Maeda, S., et al., *The molecular design and applications of spirooxazines.* Molecular Crystals and Liquid Crystals. **246**: p. 223-230.

244. Tamai, N. and H. Miyasaka, *Ultrafast Dynamics of Photochromic Systems.* Chemical Reviews, 2000. **100**(5): p. 1875-1890.

245. Maeda, S., *Spirooxazines,* in *Organic Photochromic and Thermochromic Compounds - Volume 1 - Main Photochromic Families*, J.C. Crano and R.J. Guglielmetti, Editors. 2002, Kluwer Academic Publishers: New York. p. 85-109.

246. Antipin, S.A., et al., *Femtosecond transient absorption spectroscopy of non-substituted photochromic spirocompounds.* Chemical Physics Letters, 2000. **331**(5–6): p. 378-386.

247. Deniel, M.H., D. Lavabre, and J.C. Micheau, *Photokinetics under Continuous Irradiation,* in *Organic Photochromic and Thermochromic Compounds - Volume 2 - Physicochemical Studies, Biological Applications and Thermochromism*, J.C. Crano and R.J. Guglielmetti, Editors. 2002, Kluwer Academic Publishers: New York. p. 167-209.

248. Lokshin, V. and A. Samat, *Thermochromism of Organic Compounds,* in *Organic Photochromic and Thermochromic Compounds - Volume 2 - Physicochemical Studies, Biological Applications and Thermochromism*, J.C. Crano and R.J. Guglielmetti, Editors. 2002, Kluwer Academic Publishers: New York. p. 415-466.

249. Hou, L. and H. Schmidt, *Thermal decoloration kinetics of spirooxazines in Ormocer coatings prepared via sol-gel processing.* Journal of Materials Science, 1996. **31**(13): p. 3427-3434.

250. Such, G.K., R.A. Evans, and T.P. Davis, *Control of Photochromism through Local Environment Effects Using Living Radical Polymerization (ATRP).* Macromolecules, 2004. **37**(26): p. 9664-9666.

251. Evans, R.A., et al., *The generic enhancement of photochromic dye switching speeds in a rigid polymer matrix.* Nature Materials, 2005. **4**: p. 249.

252. Baillet, G., G. Giusti, and R.J. Guglielmetti, *Comparative photodegradation study between spiro[indoline-oxazine] and spiro[indoline-pyran] derivatives in solution.* Journal of Photochemistry and Photobiology A: Chemistry, 1993. **70**: p. 157-161.

253. Baillet, G., *Dealkylation of N-substituted Indolinospironaphthoxazine Photochromic Compounds Under UV Irradiation.* Journal of Photochemistry and Photobiology A: Chemistry, 1994. **83**(2): p. 147-151.

254. Baillet, G., G. Giusti, and R.J. Guglielmetti, *Study of the Fatigue Process and Yellowing of Polymeric Films Containing Spirooxazine Photochromic Compounds*. Vol. 68. 1995. 1220-1225.

255. Malatesta, V., R. Millini, and L. Montanari, *Key Intermediate Product of Oxidative Degradation of Photochromic Spirooxazines. X-ray Crystal Structure and Electron Spin Resonance Analysis of Its 7,7,8,8-Tetracyanoquinodimethane Ion-Radical Salt.* Journal of the American Chemical Society, 1995. **117**(23): p. 6258-6264.

256. Malatesta, V., et al., *Reductive Degradation of Photochromic Spiro-Oxazines. Reaction of the Merocyanine Forms with Free Radicals.* The Journal of Organic Chemistry, 1995. **60**(17): p. 5446-5448.

257. Malic, N., et al., *Controlling Molecular Mobility in Polymer Matrices: Synchronizing Switching Speeds of Multiple Photochromic Dyes.* Macromolecules, 2010. **43**(20): p. 8488-8501.

258. Larkowska, M., M. Wuebbenhorst, and S. Kucharski, *Spirooxazine Photoisomerization and Relaxation in Polymer Matrices.* International Journal of Polymer Science, 2011.

259. Malic, N., et al., *Fast switching immobilized photochromic dyes.* Journal of Polymer Science Part A: Polymer Chemistry, 2011. **49**(2): p. 476-486.

260. Darwish, T.A., et al., *CO2 Triggering and Controlling Orthogonally Multiresponsive Photochromic Systems.* Journal of the American Chemical Society, 2010. **132**: p. 10748-10755.

261. Darwish, T.A., R.A. Evans, and T.L. Hanley, *Spiropyran, chromene and spirooxazine, mélange á trois: Molecular logic systems through selective and reversible deactivation of photochromism mediated by CO2 gas.* Dyes and Pigments, 2012. **92**(2): p. 817-824.

262. Ercole, F., et al., *The application of a photochromic probe to monitor the self-assembly of thermosensitive block copolymers.* Soft Matter, 2011. **7**(6): p. 2687-2696.

263. Kawata, S. and Y. Kawata, *Three-Dimensional Optical Data Storage Using Photochromic Materials.* Chemical Reviews, 2000. **100**(5): p. 1777-1788.

264. Such, G.K., R.A. Evans, and T.P. Davis, *Tailoring Photochromic Performance of Polymer-Dye Conjugates Using Living Radical Polymerization (ATRP).* Molecular Crystals and Liquid Crystals, 2005. **430**(1): p. 273-279.

265. Pottier, E., et al., *Synthese De Quelques Spiro[indoline-naphthoxazines] et Spiro[indolinepyridobenzoxazines] Photochromiques - Application De La Methodologie De La Recherche Experimentale.* Bulletin Des Societes Chimiques Belges, 1992. **101**(8): p. 719-739.

266. Robinson, B., *The Autoxidation of 2-Hydroxy-1,3,3-Trimethyl-2-T-Butlyindoline and 1,3,3-Trimethyl-2-Methylenenindoline.* Journal of The Chemical Society, 1963: p. 586-590.

267. Bertelson, R.C., *Spiropyrans*, in *Organic Photochromic and Thermochromic Compounds - Volume 1 - Main Photochromic Families*, J.C. Crano and R.J. Guglielmetti, Editors. 2002, Kluwer Academic Publishers: New York. p. 11-83.

268. Rasheed, A., *Molecular Modelling Aided Design and Synthesis of Photochromic Dyes Containing a Permanent Chromophore*

in *School of Textiles and Design*. 2008, Heriot-Watt University.

269. Clayden, J., et al., *Organic Chemistry*. 2000: Oxford University Press.

270. Couture, G. and B. Améduri, *Kinetics of RAFT homopolymerisation of vinylbenzyl chloride in the presence of xanthate or trithiocarbonate.* European Polymer Journal, 2012. **48**(7): p. 1348-1356.

271. Stace, S.J., et al., *The effect of Z-group modification on the RAFT polymerization of N-vinylpyrrolidone controlled by "switchable" N-pyridyl-functional dithiocarbamates.* Polymer Chemistry, 2015. **6**(40): p. 7119-7126.

272. Corrigan, N.A., et al., *Oxygen Tolerance in Living Radical Polymerization: Investigation of Mechanism and Implementation in Continuous Flow Polymerization.* Macromolecules, 2016. **49**(18): p. 6779-6789.

273. van den Dungen, E.T.A., et al., *Initialization behavior at various target molecular weight RAFT-mediated methyl acrylate polymerizations.* Journal of Polymer Science Part A: Polymer Chemistry, 2008. **46**(7): p. 2500-2509.

274. Hales, M., et al., *Shell-Cross-Linked Vesicles Synthesized from Block Copolymers of Poly(d,l-lactide) and Poly(N-isopropyl acrylamide) as Thermoresponsive Nanocontainers.* Langmuir, 2004. **20**(25): p. 10809-10817.

275. Podzimek, S., *Truths and myths about the determination of molar mass distribution of synthetic and natural polymers by size exclusion chromatography.* Journal of Applied Polymer Science, 2014. **131**(7): p. n/a-n/a.

276. Bowes, A., J.B. McLeary, and R.D. Sanderson, *AB and ABA type butyl acrylate and styrene block copolymers via RAFT-mediated miniemulsion polymerization.* Journal of Polymer Science Part A: Polymer Chemistry, 2007. **45**(4): p. 588-604.

277. Gruendling, T., et al., *Mark–Houwink Parameters for the Universal Calibration of Acrylate, Methacrylate and Vinyl Acetate Polymers Determined by Online Size-Exclusion Chromatography—Mass Spectrometry.* Macromolecular Chemistry and Physics, 2010. **211**(5): p. 520-528.

278. *Polymer Data Handbook*. 1999: Oxford University Press.

279. Carey, F. and R. Guilian, *Organic Chemistry*. 2011, New York, USA: McGraw-Hill.

3 Design and theoretical assessment of spirooxazine based RAFT agents

3.1 Introduction

The rate of radical addition to the C=S bond of the RAFT agent and the rate at which the RAFT abduct can fragment to release the R group radical are the two kinetic parameters that determine the success or failure of a RAFT polymerisation. The mechanistic definition of parameters of ΔH_{stab}, ΔH_{frag} and RSE introduced briefly in Chapter 2, section 2.5.2.2 which are used to describe the effect of Z group selection of the reactivity of a RAFT agent are illustrated in Scheme 3.1. Although these are fundamentally thermodynamic parameters, previous work has shown they can be used in a semi-quantitative fashion to study the substituent effects on resulting kinetic rate coefficients which govern the RAFT equilibrium [1-4].

Effect of Z on RAFT agent stability (ΔH_{stab})

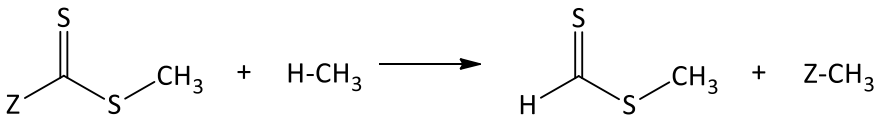

Effect of Z on RAFT adduct radical stability (RSE)

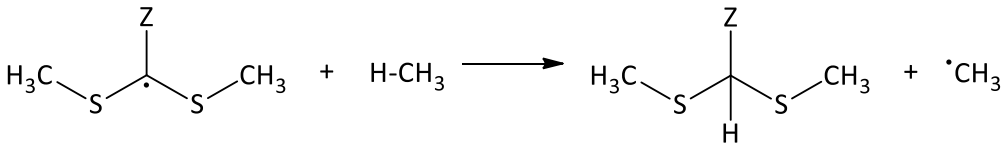

Effect of Z on fragmentation efficiency (ΔH_{frag})

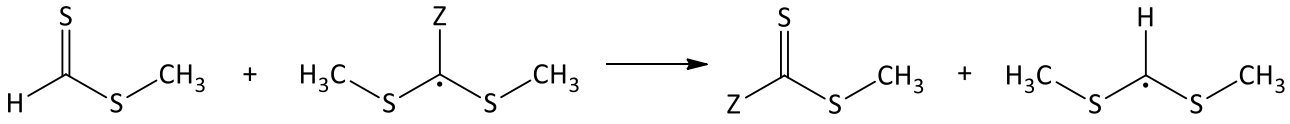

Scheme 3.1 Summary of parameters for computing RAFT agent properties as pioneered by the Coote group [4]

The chemical structure of the Z group influences both the stability of the RAFT agent and thus its reactivity towards radical addition, and the stability of the RAFT adduct radical. Decoupling these two effects is essential as RAFT agent stability described by the value of ΔH_{stab} has the most dramatic impact on the kinetics of radical addition while the stability of the RAFT adduct radical described by the RSE only has a minimal effect [4].

The descriptor ΔH_{stab} is designed to assess the effect of the Z group on the stability of the C=S bond of the RAFT agent relative to the reference compound with Z = H and has been shown in prior studies to provide an excellent correlation with RAFT agent reactivity towards radical addition [4]. Less reactive RAFT agents such as xanthates and dithiocarbamates have values of the order of 80 - 100 kJ mol^{-1}, while more active trithiocarbonates and dithioesters typically have values of ~ 60 kJ mol^{-1} and ~ 40 kJ mol^{-1} respectively [4]. Thus, as a general rule, the more endothermic the ΔH_{stab} value, the more stable the starting RAFT agent and the less reactive towards radical addition it will be.

Closely related to the RAFT agent stability is the stability of the RAFT adduct radical, which is known as the RSE; this parameter is mainly used to evaluate the potential contribution of the stability of the adduct radical towards the overall kinetic rate of radical addition. As the RSE for the RAFT adduct radical is a measure of its stability, the more endothermic the value the more stable the RAFT adduct radical.

The second critical descriptor of RAFT agent applicability is ΔH_{frag} which measures the effect of the Z group on the enthalpy of the fragmentation reaction relative to a reference compound with Z = H. Understanding ΔH_{frag} is crucial as this value determines whether a given propagating radical can successfully fragment from the RAFT adduct radical, and this is reflected in the fact this value spans a range of nearly 100 kJ mol^{-1} across the various classes of RAFT agents [4]. The more exothermic the value of ΔH_{frag} the more easily a given leaving group will undergo fragmentation. This is reflected in that the most exothermic values occur with xanthates and dithiocarbamates which can promote the fragmentation of most propagating radicals. Conversely, the most endothermic values occur with π-acceptor Z groups such as phenyl and cyano which retard fragmentation of LAM radicals and are only suitable for highly stabilised MAM radicals. Previous experimental [5] and theoretical findings [6] show that the unique class of F-RAFT agent is somewhat suitable for the polymerisation of both MAMs and LAMs.

This chapter explores the design of RAFT agents based on the spirooxazine family of photochromics, from here on referred to as “spiro-RAFT” or spiro-dithio. and spiro-xan. for the dithiocarbamate and xanthate versions respectively. The theoretical and practical considerations pertaining to the placement of the RAFT moiety and synthetic accessibility of these molecules is considered. To evaluate the potential reactivity and thus utility of several candidate spiro-RAFT agents in both their open and closed states, using Density Functional Theory (DFT) level quantum chemical calculations were undertaken for these molecules. A selection of non-photochromic analogues from the main classes of RAFT agents were also computed, which allows comparisons to be made using a previously established qualitative relationship between the charge on the sulfur of the C=S bond and the

molecule's LUMO energy level. A newly discovered highly linear relationship between the charge on the central carbon in the RAFT moiety and the length of the C-Z bond also neatly categorises the RAFT agents by applicability to monomer class. Comparisons using both relationships showed that the spiro-RAFT agents have different electronic properties on the RAFT moiety in their closed and open states, thus validating the need for further analysis at a higher level of *ab initio* theory.

Two candidate spiro-RAFT molecules along with the acid/base switchable dithiocarbamate developed by CSIRO [7, 8] were subjected to a higher level of computational analysis by the research group of Prof. Michelle Coote. Accessing the parameters of ΔH_{stab}, ΔH_{frag} and RSE allows an in-depth comparison into the expected properties and reactivity of these compounds in relation to an extensive catalogue of conventional RAFT agents. The results obtained from this analysis indicate noticeably different reactivities of these spiro-RAFT agents depending on whether they are in the open or closed state. This evidence motivated the attempted synthesis of two spiro-RAFT agents and this is described in detail in the following chapter.

3.2 Design of spirooxazine based RAFT agents

3.2.1 Origin of the concept

To date there are only two types of switchable RAFT agents and they belong to the dithiocarbamate family, being the 4-pyridinyl-N-methyldithiocarbamates [7] and N-aryl-N-pyridyl dithiocarbamates [9] as shown in Scheme 3.2, A. In their neutral state, the double bond character of the central carbon sulfur double bond within the RAFT moiety is naturally reduced. This is due to the ability of the dithiocarbamate nitrogen to be quaternarised due to resonance (Scheme 3.2, A), which gives these dithiocarbamates equivalent reactivity to conventional dithiocarbamates, making them suitable for controlling the polymerisation of LAMs. When treated with a stoichiometric equivalent of a strong organic acid or non-protic Lewis acid, the protonation of the pyridyl nitrogen effectively shifts this resonance between the nitrogen on the pyridyl moiety and the nitrogen on the dithiocarbamate (Scheme 3.2, A) [10]. This effectively preserves the double bond character of the central carbon sulfur double bond within the RAFT moiety, which in turn results in the protonated dithiocarbamate having reactivity towards radical addition comparable to a trithiocarbonate. Adding an excess of a base such as sodium bicarbonate after polymerisation followed by purification allows this process to be fully reversible [8]. The limitations of this process include the need for stoichiometric equivalents of a strong acid [11], the need for strict purification of products after switching [11] and poor solubility of the protonated RAFT agent in organic solvents including monomers [9].

Based on these limitations, the concept of a photoswitchable RAFT agent whose reactivity towards radical addition and ability to undergo radical fragmentation can be reversibly altered by the application of light is appealing for several reasons. Firstly, unlike an acid/base switch, using light as a switching stimulus theoretically allows the switch to be achieved much faster and in an external fashion without the need to add reagents. Secondly, depending on the family of photochromic chosen as the parent molecule, this switch can be reversed by the application of either another wavelength of light or heat.

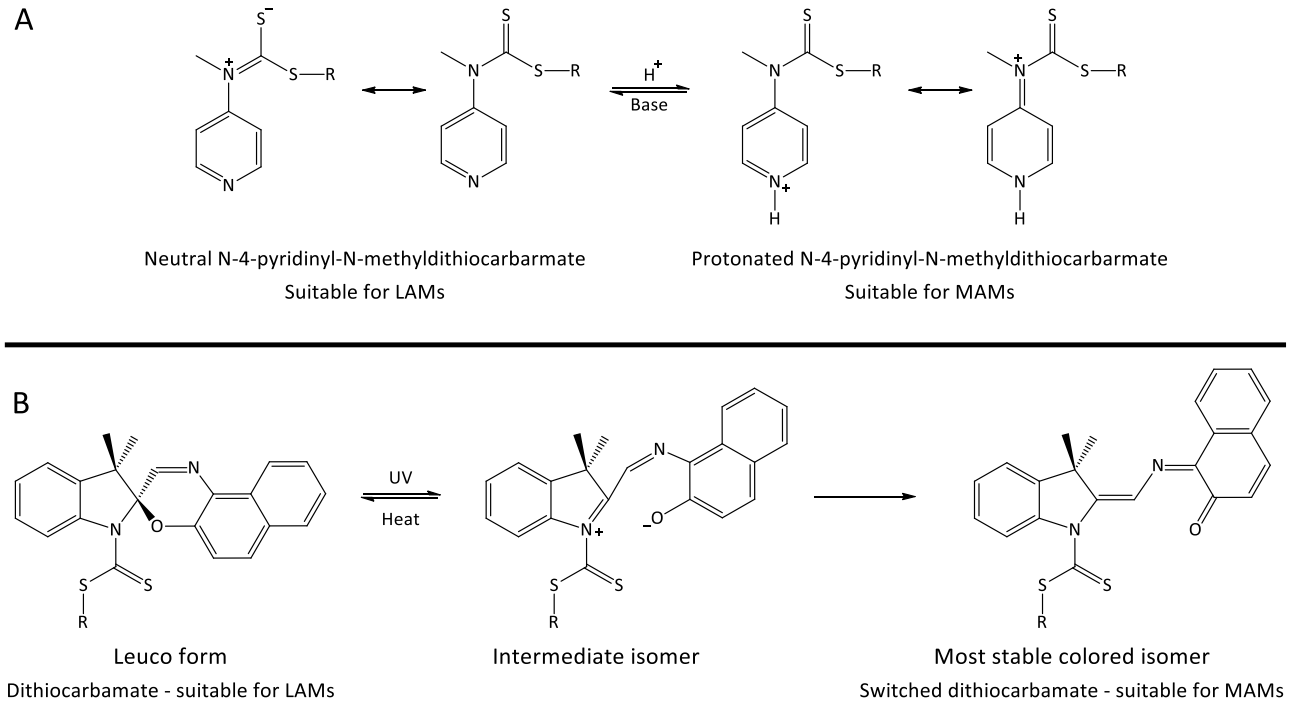

Scheme 3.2: Comparison of CSIRO acid/base switchable dithiocarbamates (A) and photo-switchable spirooxazine dithiocarbamates (B).

As can be seen in Scheme 3.2 (B), a spirooxazine based dithiocarbamate should effectively allow a change of the electronic properties of the RAFT moiety. A positive charge originates on the nitrogen within the dithiocarbamate structure upon photochromic ring opening of the spirooxazine, which rearranges to the planar merocyanine form. This leads to a change in electron density and associated increase in conjugation pathlength which are the key properties that make the merocyanine form highly coloured [12]. This was the key reason the spirooxazine family of photochromics was chosen as the parent molecule for the design, synthesis and theoretical testing of photochromic RAFT agents. As described in Chapter 2, section 2.9.2, this decision was also based on the positive attributes of spirooxazines in relation to both chemical and photochromic properties, numerous spirooxazine systems having useful synthetic "handles" for further derivatisation and prior applications of spirooxazines within polymer science including with RAFT polymerisation.

3.2.2 Theoretical and practical considerations for the design of spiro-RAFT molecules

As is evident from the CSIRO acid/base switchable dithiocarbamates, conjugation between the RAFT moiety and the active mechanism of switching is essential to the reversible modulation of the reactivity of the RAFT moiety. By logical extension this also applies to any photoswitchable RAFT systems designed; any change in electron distribution of the parent molecule must be able to affect the electronic properties of the RAFT moiety by being directly linked to it. This means that long chain alkyl or other spacers should not be used to separate the photochromic and RAFT components of the spiro-RAFT agents designed.

The switchable RAFT agent should traverse a useful range of reactivity towards both MAM and LAM propagating radicals. Ideally it should be at least moderately applicable to both types of monomers in one of the two states without inhibiting propagation.

Based on these considerations, the idealised targets selected for synthesis can be seen in Scheme 3.4. Two xanthates were also designed based off the commercially available 9-hydroxy-1,3,3-trimetylspiro [indoline-2,3'-[3H] naphtha [2,1-b][1,4] oxazine]. This was done due to the consideration that generation of a spirooxazine with a pendent hydrogen on the indole nitrogen might not be possible due to synthetic difficulties or that this species might be unstable or unable to be isolated once generated. Isomerisation of such a species which may prevent synthesis of the RAFT moiety in the desired location is also a concern, as shown in Scheme 3.3.

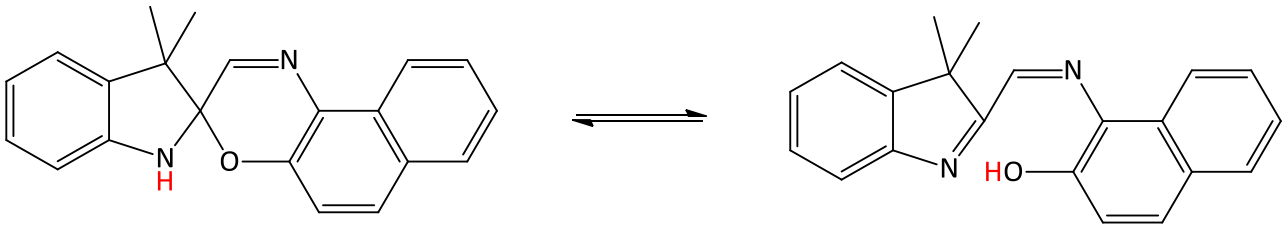

Scheme 3.3: Possile isomerisation of a NH terminated spirooxazine, with the pendant hydrogen shown in red.

This is based on an almost complete absence of these types of photochromics appearing in the literature, with only three references to similar compounds bearing such a pendent hydrogen being found [13]. These references were themselves inaccessible due to being in the Japanese patent literature.

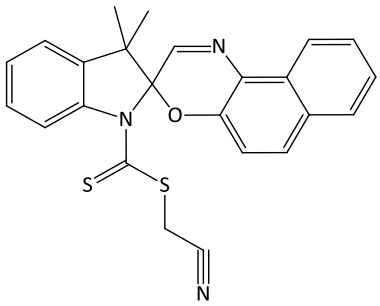

Spiro-dithio. A (R = cyanomethyl)

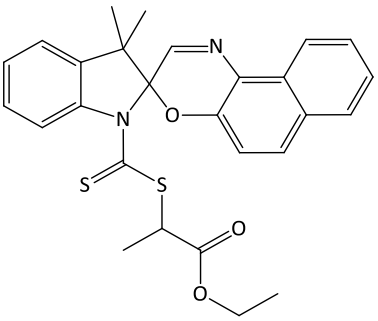

Spiro-dithio. B (R = ethyl propanoate)

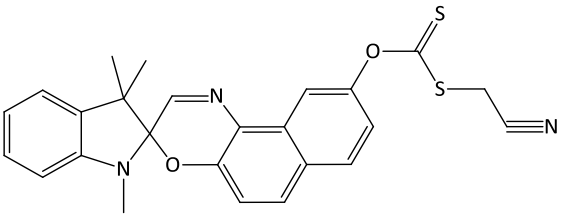

Spiro-xan. A (R = cyanomethyl)

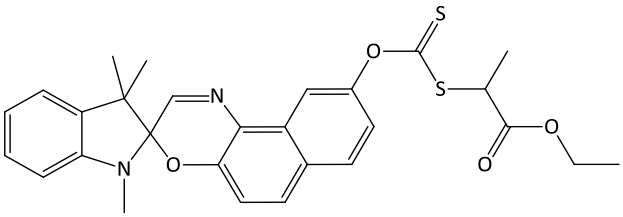

Spiro-xan. B (R = ethyl propanoate)

Scheme 3.4: Spirooxazine based RAFT agents selected for modelling.

The two R groups selected were the cyanomethyl and ethyl propanoate groups. The cyanomethyl group was chosen as an R group as it is highly efficient at adding to all common monomers [14] and is suitable for a range of both LAMs and MAMs in that it will preferentially fragment from the RAFT abduct radical [15]. The ethyl propanoate group was considered as a contingency if the parent spiro-NH or spiro-OH compounds are insufficiently nucleophilic when deprotonated to allow the synthesis of the RAFT agent via the CS_2 and nucleophilic substitution route. This was designed as an alternative to attempting to attach the cyanomethyl R group using the thiophosgene route as this would require the synthesis and handling of thioacetonitrile, which is extremely reactive and prone to spontaneous and violent detonation [16].

3.3 DFT Study

3.3.1 Computational methods

All molecules within this section were computed using a 64-bit Windows version of Spartan '16 V2.0.7 [17]. The molecules were initially constructed with the general structure and orientation of Z and R groups as shown in Figure 3.1.

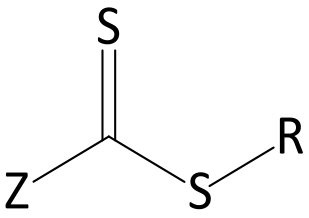

Figure 3.1 Orientation of Z and R groups used in constructing RAFT agents for modelling.

The molecule was then optimised by using the inbuilt "Minimize" function, followed by a calculation to optimise the molecule to the equilibrium geometry at the Semi-Empirical level using the AM1 basis set. This was followed by optimisation to the equilibrium geometry using Density Functional Theory (DFT) at the B3LYP/6-31G* basis set level, with the "Orbitals & Energies" and "Charges & Bond orders" options selected.

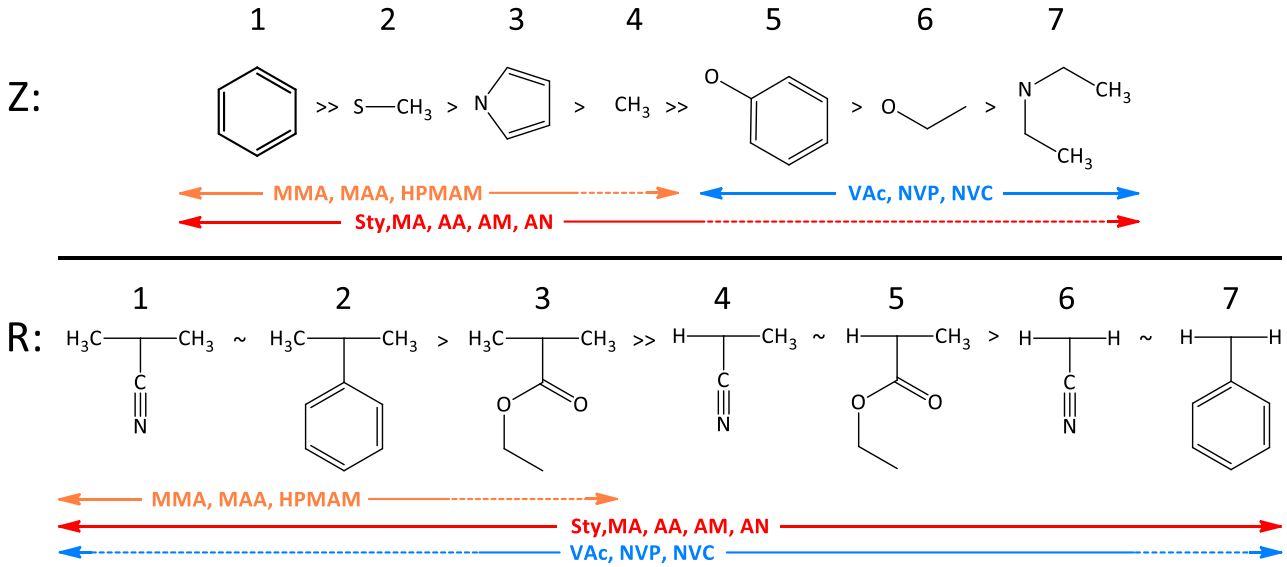

Scheme 3.5: Z and R groups used to construct RAFT agents for DFT level theoretical assessment by modelling. Solid lines indicate the group is suitable for use with the designated monomer, dashed line indicates only partial compatibility. Numbers above groups are used as shorthand notation to simplify graphing the resulting data. Adapted from [18].

Only combinations of Z and R groups (shown in Scheme 3.5) that gave "practical" RAFT agents which are applicable to 3 different groups of monomers were modelled (listed in Table 3.1), along with the spiro-RAFT agents as shown in Scheme 3.4.

Table 3.1 Summary of RAFT agents computed at lower levels of theory, and the range of monomers to which they are theoretically applicable in RAFT polymerisation. Applicability of RAFT agents is colour coded in the far-right column to match the colours used in Scheme 3.5. AN = acrylonitrile, AM = acrylamide, HPMAM = N-2-hydroxypropyl methacrylamide

Z Groups	R Groups	Applicable to monomers	
1, 2, 3	1, 2	MMA, MAA, HPMAM	
1, 2	3, 7	Sty, MA, AA, AM, AN	
4	1, 3, 7		
5, 6, 7	4, 5, 6	VAc, NVP, NVC	

The simulation data that was collated included the HOMO and LUMO energy levels (in eV), dipole moment (in Debye), the bond lengths (in Angstroms) and Natural charges on all atoms on the RAFT moiety as shown in Figure 3.1. For a complete summary of this data, please see Table A1 in the Appendix.

3.3.2 DFT Results

The correlations that were analysed from the available data were the LUMO vs natural charge on S in C=S and the linear correlation that was found for the C-Z bond length vs natural charge on C in C=S which is an implicit measure of the electron density on this sulfur. This data leads to the segregation of RAFT agents by applicability to 2 distinct classes of monomers; namely the LAMs (blue data points, Figure 3.2) and the MAMs (red and orange data points, Figure 3.2). In general, RAFT agents suited to LAMs have greater electron density on the sulfur in the C=S bond, leading to a charge on the sulfur that is more negative than – 0.07, with the exceptions being Z = 5 with R = 4 & 6. There is overlap between the RAFT agents applicable to the two classes of the most reactive monomers (most “MAM” like, orange data points) and the moderately reactive monomers (red data points). This is unsurprising, as for example a RAFT agent suited to the polymerisation of MMA would also be applicable to MA, albeit with the potential of rate retardation and or an inhibition period [19, 20].

In their closed leuco form the spiro-RAFT compounds all lie within the scatter of data points seen for the conventional RAFT agents computed. Specifically, the spiro-dithio. A (light green square, Figure 3.2) lies near the general separation between RAFT agents suited to LAMs and MAMs, while spiro-dithio. B (dark green square, Figure 3.2 lies firmly in the range of RAFT agents suited to MAMs. In this closed leuco form, the change in natural charge on the sulfur within the C=S bond with a change in R group is much less dramatic for the spiro-xan. compounds, with spiro-xan. B being almost identical to the trithiocarbonates with Z = 2 with R = 2 & 7. Spiro-xan. A is almost identical to the xanthates with the phenol Z group (Z = 5) with R = 4 & 6. Relative to the spiro-dithio. agents, the

change in electron density on the sulfur in the C=S bond is smaller in absolute terms between the two R groups for the two spiro-xan. agents.

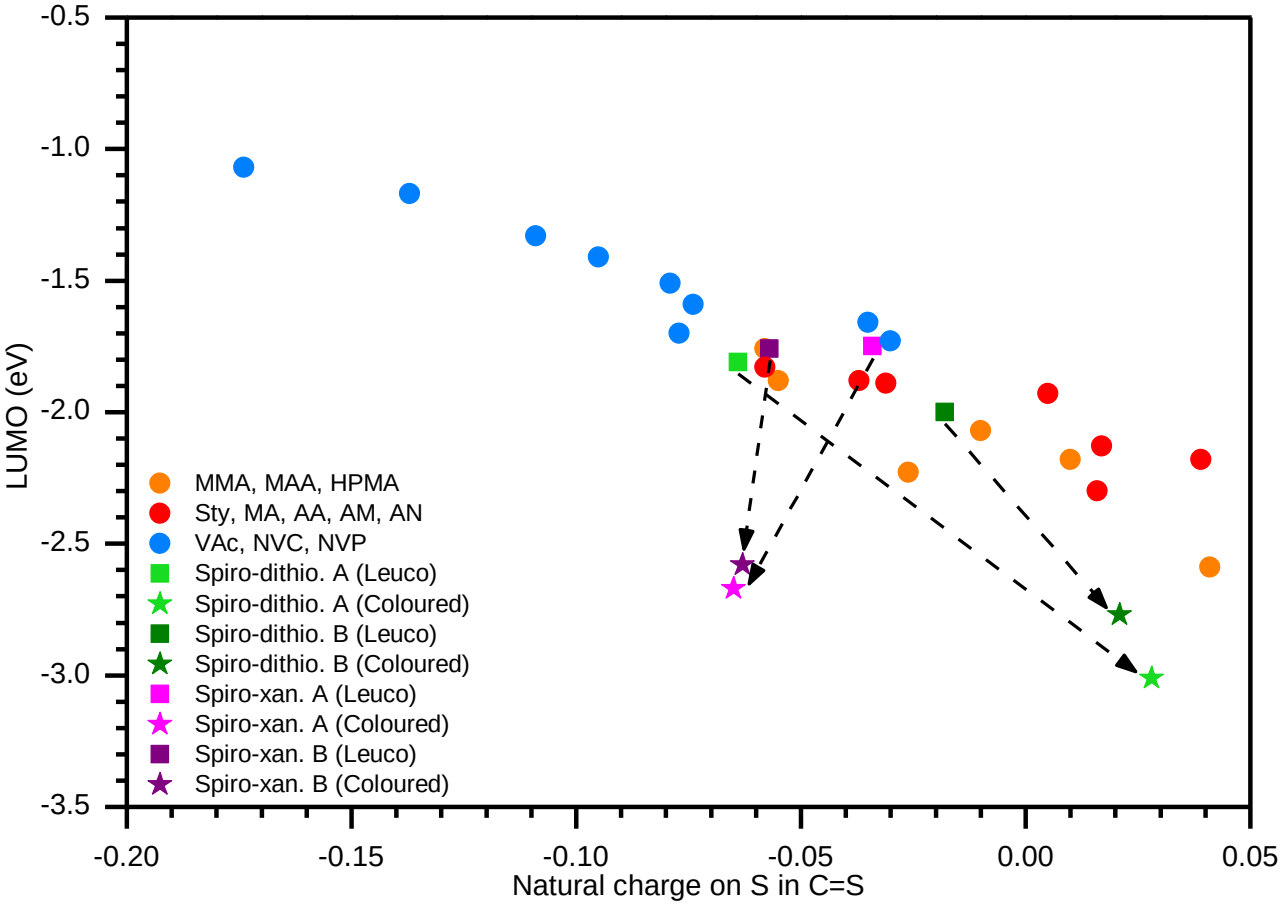

Figure 3.2: Correlation of LUMO vs natural charge on S in C=S for a range of RAFT agents simulated at a DFT level of theory.

In their most stable coloured form, all spiro-RAFT agents show a significant decrease in their LUMO energy. The spiro-dithio. agents both show a significant shift in the electron density on the sulfur within the C=S bond, which results in a change from a negative natural charge on the sulfur in the leuco form to a positive natural charge on the sulfur in the open coloured form (green stars, Figure 3.2). Interestingly for both spiro-xan. agents, the electron density on the sulfur in the C=S bond increases after conversion into the coloured form. For both classes of spiro-RAFT agents, the relative difference in electron density on the sulfur in the C=S bond between the two R groups selected is smaller in the coloured form than in the leuco form. Overall this results in an almost parallel arrangement of values for the spiro-RAFT agents in their coloured open forms to the main linear grouping seen for conventional RAFT agents, which is itself intriguing.

The general inverse relationship seen in Figure 3.2 for the LUMO energy vs natural charge on the sulfur in the C=S bond closely matches the trend as reported by Chiefari *et al.* [21] who computed a

similar series of RAFT agents but with a simple methyl R group at a lower level of theory. The clustering of xanthates and dithiocarbamates based on a greater electron density on the sulfur in the C=S bond is possible due to the existence of the resonance structures as shown previously for the neutral CSIRO acid/base switchable dithiocarbamates (Scheme 3.2, A).

Based on their positions within the dataset, these results suggest that in their closed leuco form both spiro-dithio. agents along with spiro-xan. B should have an electron density on the sulfur in the C=S bond that would make them applicable to the polymerisation of both moderately and highly reactive MAMs (red and orange data points respectively, Figure 3.2). The location of spiro-xan. A while in the leuco state within the dataset implies it could potentially be applicable to both moderately reactive MAMs and LAMs (red and blue data points respectively, Figure 3.2).

The increase in electron density on the sulfur in the C=S bond upon opening for the spiro-xan. agents is unexpected, as the extended conjugation pathway over the whole spiro-xan. molecule should allow the desired minimisation of the isomerization reaction to still occur. This result suggests that any changes in electron density to the RAFT moiety as translated from the spirooxazine ring opening are proximal in nature to the location of bond scission that allows the ring opening to occur. This implies that the location of the RAFT moiety on the parent spirooxazine can potentially influence the magnitude of any switch in reactivity between the two states of the spiro-RAFT agent.

The problem arises that while the relationship explored in Figure 3.2 is based on guidelines of general RAFT agent reactivity, it is not directly related to any experimental data that can be used to directly assess the potential performance of novel spiro-RAFT agents. Chiefari *et al.* did find a weak logarithmic correlation between the measured chain transfer constant in the bulk thermally initiated polymerisation of styrene and the computed LUMO energy for their respective series of similar RAFT agents [21]. Due to the spiro-RAFT agents in their coloured open states deviating from the general trend seen in Figure 3.2 it in a parallel fashion, and that styrene is not indicative of the reactivity of other monomer classes, any comparisons made in this fashion are inherently limited in predicting the reactivity of the spiro-RAFT agents towards monomers of different reactivities.

Further investigation revealed a near inversely linear relationship between the length of the C-Z bond and the natural charge on the central carbon in the C=S bond as shown in Figure 3.3. This can be rationalised as representing the stability of the RAFT agent, as a shorter C-Z implies a stronger bond. This in turn is again facilitated by the resonance structures that exist within xanthates and dithiocarbamates, which are known to be more stable RAFT agents [22]. It is interesting to note that just as in Figure 3.2, the conventional RAFT agents are segregated quite neatly depending on which

of the 3 classes of monomer they are intended to be used with. There is similar considerable overlap between RAFT agents applicable to both classes of MAMs (orange and red data points, Figure 3.3).

The spiro-dithio. agents in the closed state (green rectangles, Figure 3.3) align on the intersection of the LAM and MAM applicable RAFT agents, whilst in the open coloured state (green stars, Figure 3.3) the length of the C-Z bond increases. This is consistent with the desired switch having occurred in the RAFT moiety, indicating the RAFT agent should now be more suitable for the polymerisation of MAMs. For the spiro-xan. compounds, there is seemingly no difference in both the charge on the central carbon and the C-Z bond length, again most likely due to the further proximity of the RAFT moiety from the active site where the parent spirooxazine molecule undergoes ring opening and rearrangement around the spiro carbon.

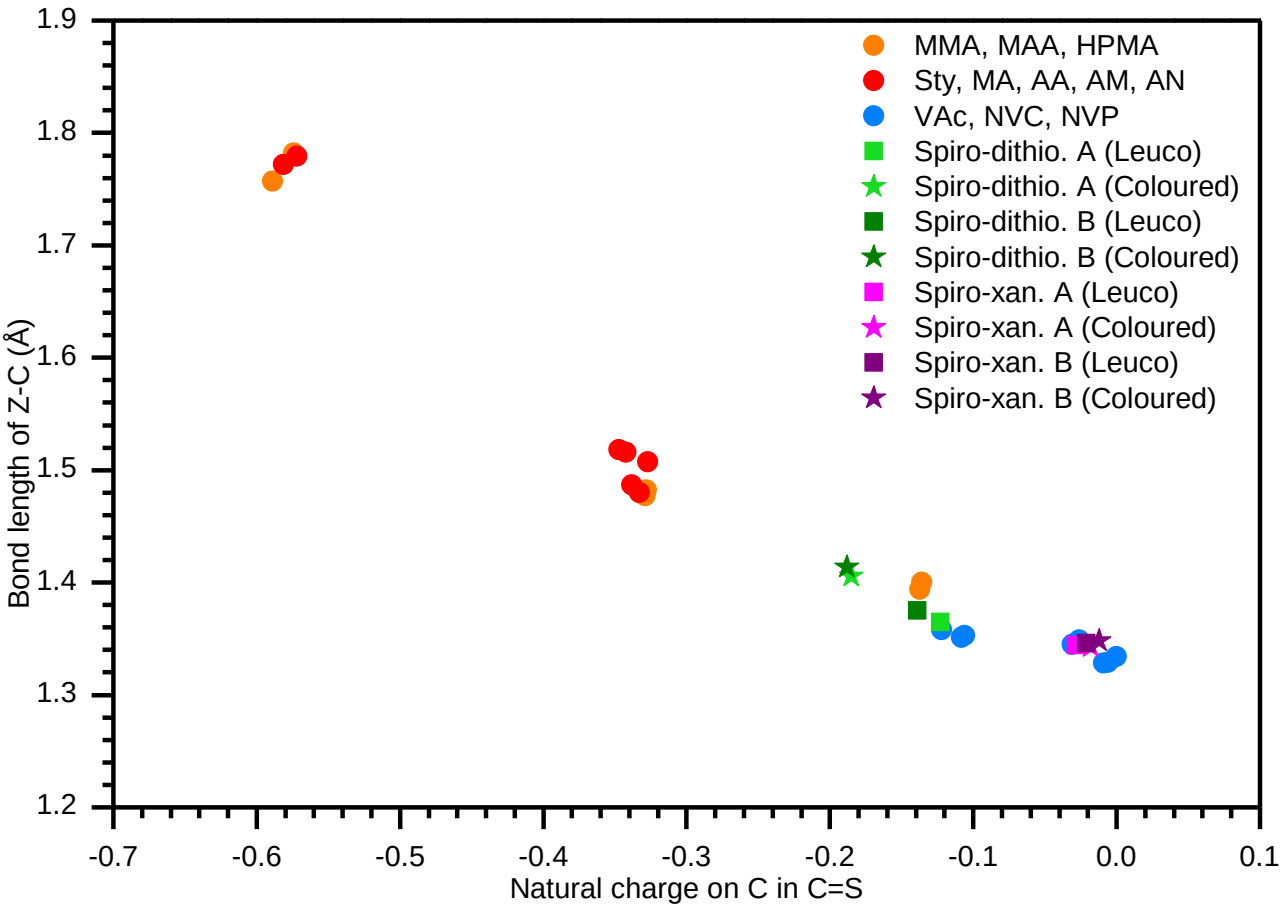

Figure 3.3: Correlation of C-Z bond length vs natural charge on C in C=S for a range of RAFT agents simulated at a DFT level of theory.

These results are all indicative of a probable change in the reactivity of the spiro-RAFT compounds towards radical addition once they are switched from the leuco to the coloured form. This is consistent with the initial hypothesis that they should function in a similar manner to the CSIRO acid/base

switchable dithiocarbamate by altering the electron density on the sulfur in the C=S bond which in turn modulates the reactivity of the RAFT agent towards radical addition.

Since the relationships explored with this level of theory are only qualitative and cannot predict the actual reactivity of a RAFT agent towards radical addition along with its stability and fragmentation efficiency, higher level calculations were required to answer these questions. This was facilitated by a collaboration with Prof. Michelle Coote and her research team as described in section 3.4.

3.4 High level *ab initio* molecular orbital theory calculations

3.4.1 Computational methods

The interpretation of the data presented in this section (3.4) was undertaken in collaboration with Prof. Michelle Coote, with all calculations undertaken by Prof. Michelle Coote & Dr.Ching-Yeh Lin. Compilation of all Figures from the resulting data as well as from literature sources cited herein along with the description of the results was undertaken by the candidate.

For all molecules computed within this section, *ab initio* molecular orbital theory and DFT calculations were performed using the software programs Q-Chem 4.0 [23], Gaussian 09 [24] and Molpro 2009.1 [25]. Optimisation of molecular structure to a global conformational minimum was undertaken using the energy-directed tree search (EDTS) algorithm [26] and optimised at the B3-LYP level of theory using the 6-31G(d) basis set. Scaled frequency calculations were also performed at this level.

For the CSIRO acid/base switchable dithiocarbamate, more accurate energies were calculated at the G3(MP2)-RAD level of theory. Due to its large size and conjugated structure, more accurate energies for the spiro-xanthate were computed at the M062X/6-31G* level of theory. An assessment study that validates this approach can be found in section A1.1.1 in the Appendix.

For the spiro-dithiocarbamate, improved energies were calculated using ONIOM-G3(MP2)-RAD with the ROMP2/G3MP2Large basis set, with the core system (shown in red in Scheme 3.6, B) being calculated using the RI-ROMP2/G3MP2Large with cc-pVTZ auxiliary basis set to speed up the calculation [27].

The values of ΔH_{stab}, ΔH_{frag} and RSE were calculated using the standard definitions for these parameters as described in the literature [4] using the energies calculated at the highest level of theory available for each respective molecule computed.

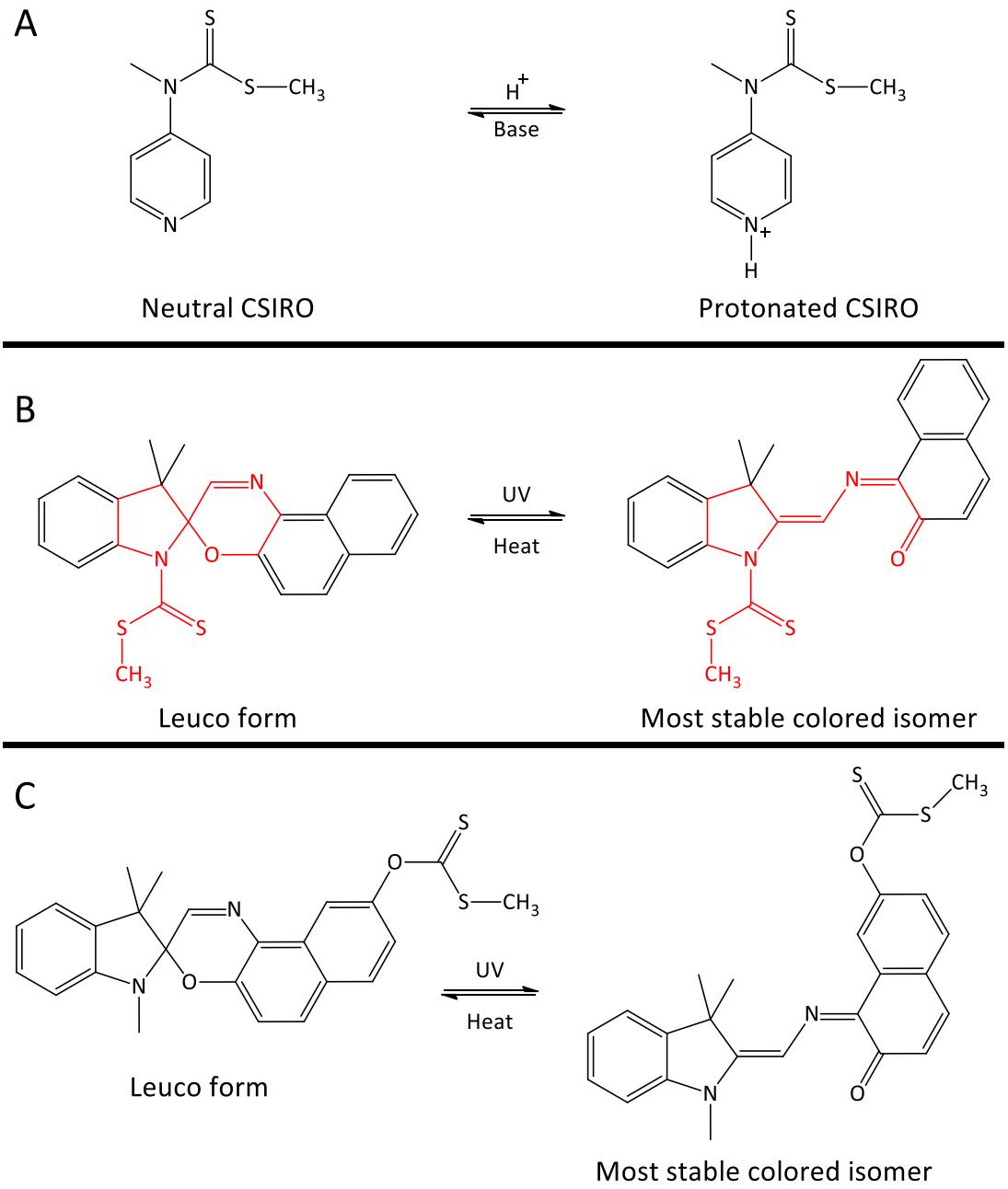

Scheme 3.6: Structures used in *ab initio* calculations: CSIRO acid/base switchable dithiocarbamate (A), spiro-dithiocarbamate (B) and spiro-xanthate (C).

3.4.2 High level *ab initio* results for the assessment of radical addition to spiro-RAFT agents

It should be stressed that the reactivity of monomers towards radical addition and the stability of the resulting monomer propagating radicals is a gradual scale determined by many complex and often competing factors [28]. Due to this reality, in the context of discussing the classification of RAFT agents based on applicability, this broadly refers to LAMs which give "unstable" propagating radicals and MAMs which tend to give "stable" propagating radicals. Demarcation limits for both ΔH_{stab} and

ΔH_{frag} parameters allow classification of RAFT agents based on their applicability to stable and unstable radicals.

Ample experimental evidence shows that xanthates and dithiocarbamates are only suited for highly reactive radicals derived from LAMs [29, 30] whilst trithiocarbonates [31] and dithiobenzoates [32] are sufficiently reactive to control unreactive monomers. Taking the midpoint of the ΔH_{stab} value calculated for dithiocarbamates and trithiocarbonates gives a cut off at ~ 70 kJ mol^{-1}; theoretically any RAFT agents with a ΔH_{stab} value higher than this should be applicable to LAMs, whilst any those with lower ΔH_{stab} values should be applicable to most monomers.

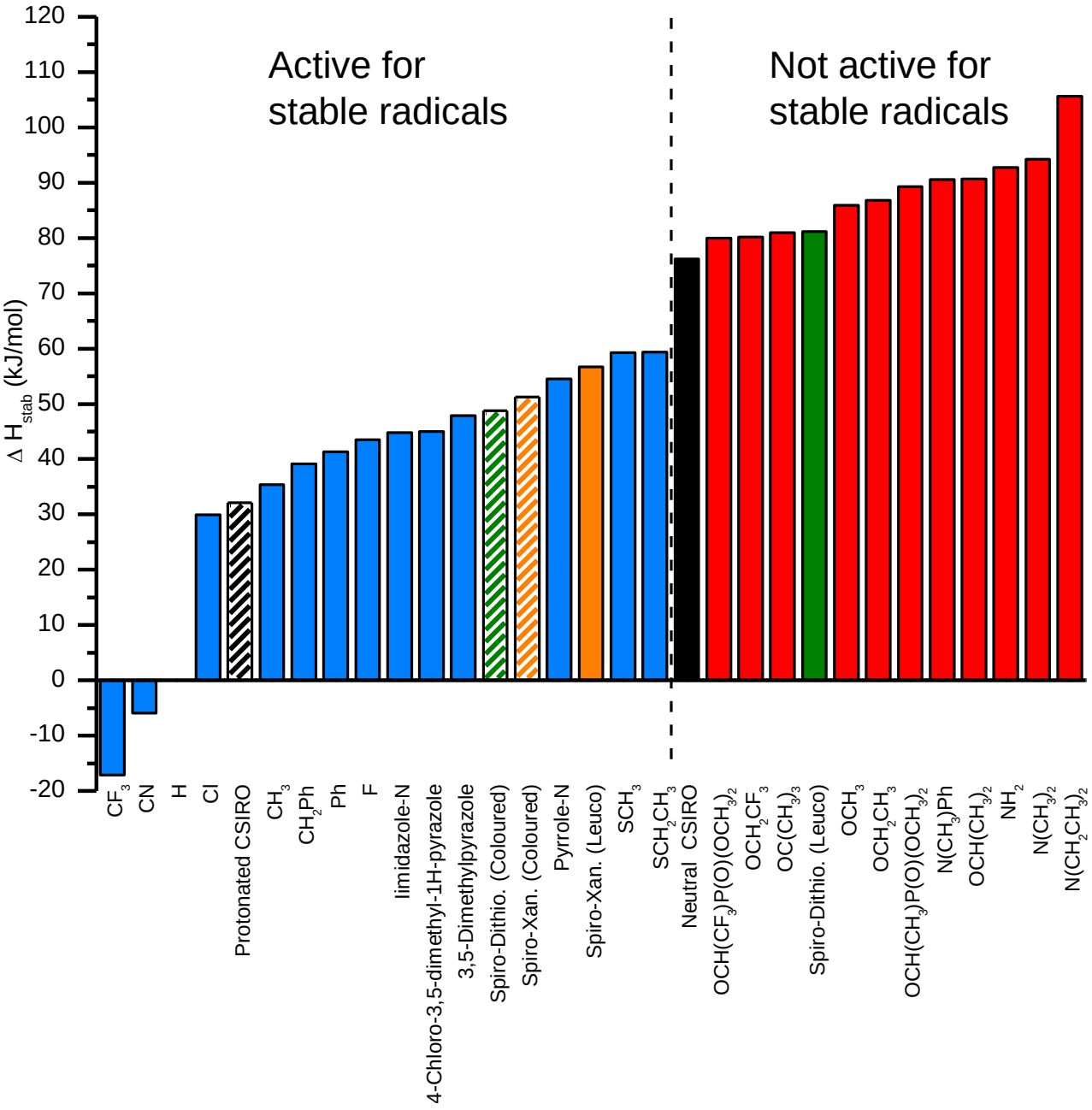

Figure 3.4: Values of ΔH_{stab} computed in the present study compared to values compiled for a selection of RAFT agents compiled from previous studies (data in red and blue) [4, 33]. R = methyl in all cases.

The CSIRO acid/base switchable dithiocarbamate in its neutral form (solid black bar, Figure 3.4) falls above the cut off value, while the protonated form (striped black bar, Figure 3.4) shows a significant decrease in ΔH_{stab} value which is now comparable to that of a dithioester. This prediction for an increase in reactivity towards radical addition upon protonation is consistent with experimental studies that show adequate control over the polymerisation of MAMs in the protonated state but poor control in the neutral state [8, 9].

The spiro-dithio. agent in the closed leuco state (solid green bar, Figure 3.4) has a ΔH_{stab} value above the cut off value and comparable to some of the less stable xanthates. This indicates it should be stable enough to allow the polymerisation of unstable radicals, which simultaneously makes it unreactive enough to control the polymerisation of stable radicals. Upon switching to the coloured open state, the stability decreases to below the cut off value, with the ΔH_{stab} value now being comparable to that of a 3,5-dimethylpyrazole based RAFT agent which is suitable for stable radicals derived from MAMs. The magnitude and positioning of this switch is comparable to that for the CSIRO acid/base switchable RAFT agent; this strongly suggests the original idea that a spiro-dithio. agent should function in an analogous manner is correct.

Interestingly, the spiro-xan. agent has a ΔH_{stab} value in the closed leuco state (solid orange bar, Figure 3.4) comparable to a trithiocarbonate and somewhere between that of a 3,5-dimethylpyrazole and N-pyrrole based RAFT agent in open coloured state (striped orange bar, Figure 3.4). This difference in stability between states is a lot smaller compared to differences seen between the switched states for both the spiro-dithio. and CSIRO acid/base switchable RAFT agents. Both ΔH_{stab} values fall below the cut off value which implies that in both states the spiro-xan. agent will be reactive enough to add both stable and unstable propagating radicals, thus potentially giving it universal applicability. This however is strictly dependent on the ability of successful fragmentation after radical addition, which is explored further via the results for the ΔH_{frag} values in section 3.4.3.

These results are consistent with the DFT calculations which showed smaller changes in the measured parameters (Figure 3.2 and Figure 3.3) between the closed leuco and open coloured states for the spiro-xan. agent relative to the spiro-dithio. agent. This also shows that while the DFT calculations generate non-quantitative correlations, they nevertheless accurately predicted the correct change in reactivity of the spiro-RAFT agents between the open and closed forms.

3.4.3 High level *ab initio* results for the assessment of radical fragmentation from spiro-RAFT agents

The ability of the RAFT adduct radical to fragment and release a propagating radical is described by the parameter ΔH_{frag}. Calculating this parameter is crucial, as efficient fragmentation of the RAFT adduct radical is essential to prevent complete inhibition or severe rate retardation of the polymerisation. Previous experimental [5] and theoretical findings [6] show that the unique class of F-RAFT agent is suitable for the polymerisation of unstable radicals generated from LAMs, whilst trithiocarbonates cause inhibition and are thus not suitable. The midpoint of the ΔH_{frag} for these two classes of RAFT agents is ~ -17 kJ mol^{-1}. RAFT agents with higher ΔH_{frag} values are expected to retard the polymerisation by effectively preventing the fragmentation of unstable radicals, whilst those with lower ΔH_{frag} facilitate the fragmentation of propagating radicals of diverse reactivities.

Analysis of the CSIRO acid/base switchable dithiocarbamate (solid and striped black bars, Figure 3.5) reveals that in the neutral state it should not retard the fragmentation of unstable radicals, which is consistent with its experimental success in the polymerisation of VAc [8, 9]. Upon protonation however, it is expected that it would effectively halt the polymerisation of monomers giving unstable propagating radicals. This prediction is consistent with the fact only an oligomeric product was obtained in the polymerisation of NVC (which gives moderately unstable propagating radicals) when the dithiocarbamate was used in its protonated state [8].

Both the spiro-dithio. and spiro-xan. agents have negative ΔH_{frag} values (solid green and orange bars respectively, Figure 3.5) in the closed leuco state, meaning both should allow for the fragmentation of most types of propagating radicals. In the switched coloured state, both spiro-RAFT agents show an endothermic ΔH_{frag} (striped green and orange bars, Figure 3.5) meaning they should both retard the fragmentation of unstable propagating radicals.

Taken together, the values of ΔH_{stab} and ΔH_{frag} suggest that in the closed leuco form the spiro-xan. agent could potentially function as a universal RAFT agent in its own right, although compared to its open coloured form it is better suited to less stable monomers. In practical terms the magnitude of the switch in reactivity after opening upon irradiation is predicted to be smaller than the pH switch in CSIRO's acid/base switchable dithiocarbamate, but the switch is nonetheless predicted to be sufficient to effect control of both classes of monomer.

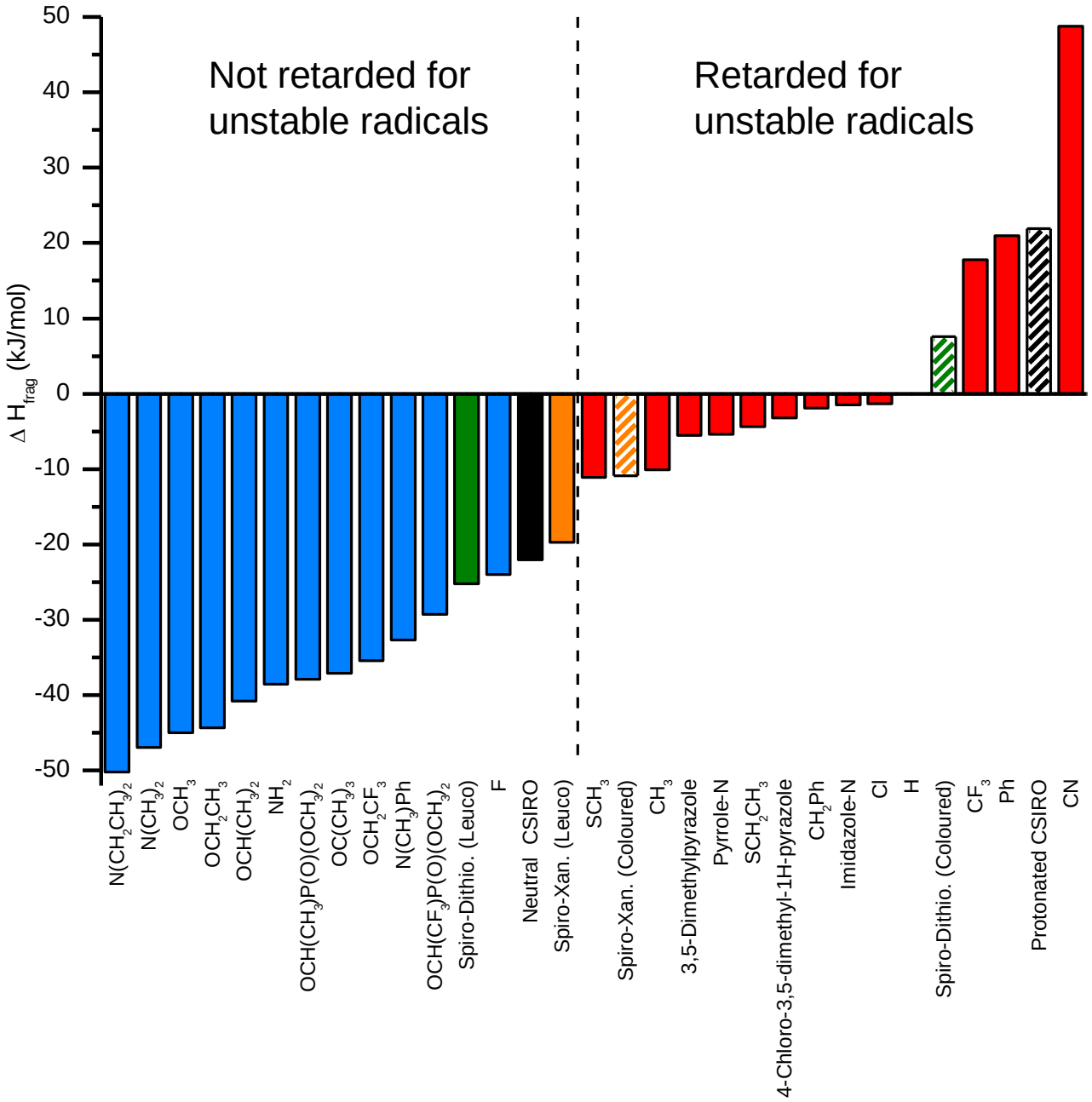

Figure 3.5: Values of ΔH_{frag} computed in the present study compared to values compiled for a selection of RAFT agents compiled from previous studies (data in red and blue) [4, 33]. R = methyl in all cases.

While the difference in ΔH_{stab} values between the two states of both the spiro-dithio. and CSIRO acid/base switchable dithiocarbamate are comparable, the difference in the stability of the RAFT adduct radicals as denoted by the RSE is significantly higher for the spiro-dithio. agent as shown in Figure 3.6. It is interesting to note that for the spiro-xan. agent the trend is reversed, with the RSE of the adduct radical being marginally smaller in the open coloured state. This effect could arise from relative proximity of the RAFT moiety to the location of the bond scission in the spirooxazine compound, or differences in how the heteroatom is integrated into the spiro-RAFT molecule. For the spiro-dithio. agent the nitrogen is integral to the ring structure of the indole half of the molecule which

could allow more successful conjugation, whilst in the spiro-xan. agent the oxygen is pendent off the naphthalene half of the molecule.

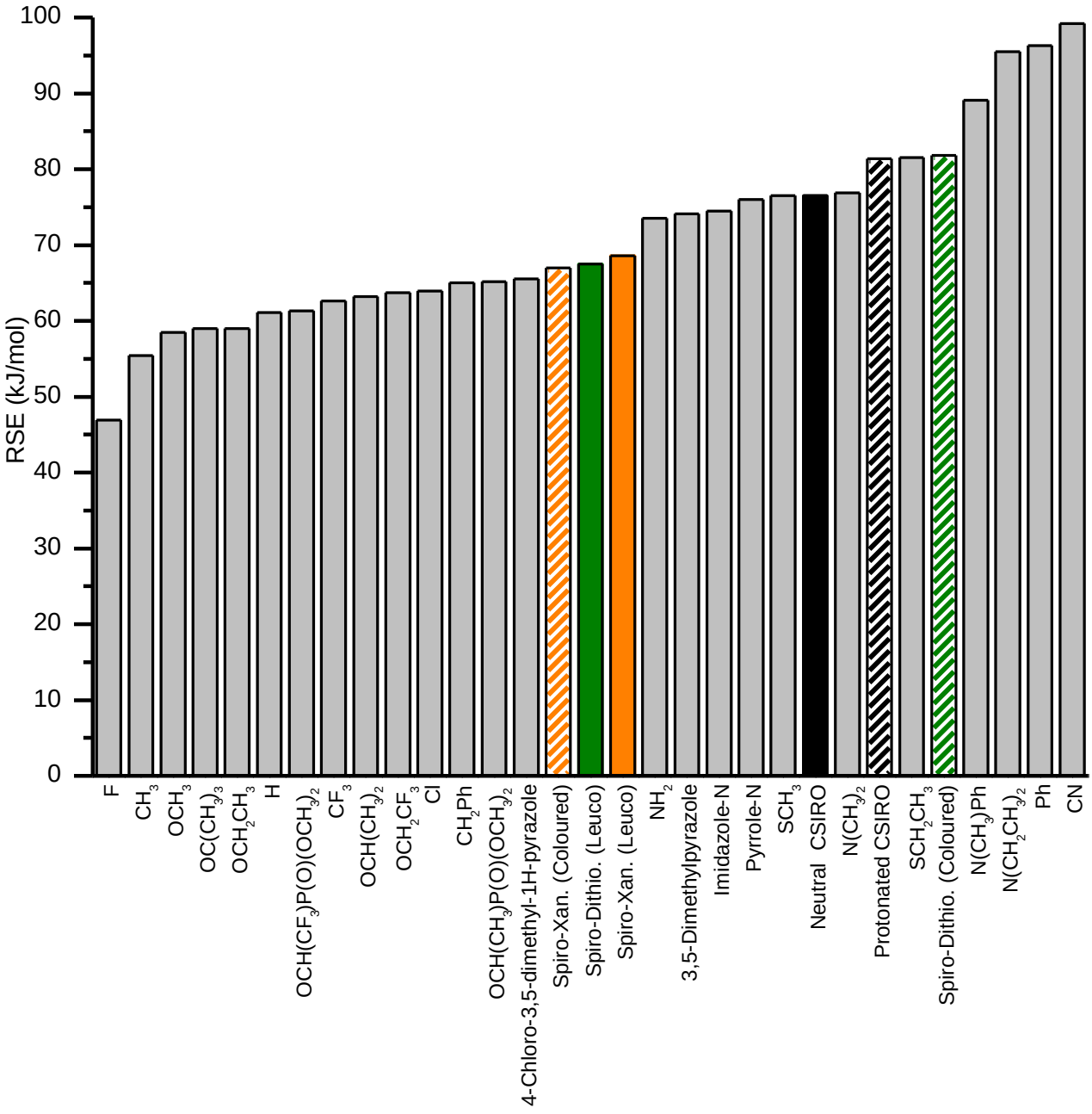

Figure 3.6: Values of radical stability (RSE) computed in the present study compared to values compiled for a selection of RAFT agents compiled from previous studies (grey data) [4, 33]. R = methyl in all cases.

3.5 Conclusions

4 novel RAFT agents were designed to explore the possibility of altering the properties of the RAFT agents in a reversible manner via the photoswitchable nature of the parent spirooxazine family of photochromic molecules. Two locations of placing the RAFT moiety on the spirooxazine were investigated, along with two potential R groups suited to most common monomers. This results in a

spiro-dithiocarbamate where the RAFT moiety is directly bonded to the nitrogen which is integral in the indole half of the spirooxazine, and a spiro-xanthate where the RAFT moiety is bonded to a pendent oxygen on the naphthalene half of the spirooxazine.

A series of DFT level quantum chemical calculations were undertaken for an assortment of conventional RAFT agents applicable to most common alkene monomers of interest by selecting a range of varied Z and R groups. Analysis revealed that the computed electron density on the sulfur in the C=S bond within the RAFT moiety of the conventional RAFT agents result in a segregation based on RAFT agent applicability. The 4 target spiro-RAFT molecules were also computed in both the closed lueco state and the open coloured state. Comparisons using the relationship between several molecular properties were undertaken between the two states of the spiro-RAFT agents and their conventional RAFT analogues which revealed differences suggestive of different reactivity in RAFT polymerisation.

High level *ab initio* calculations were undertaken for the CSIRO acid/base switchable dithiocarbamate in both their neutral and protonated states, along with a model spiro-dithio. and spiro-xan. agent in both the open and closed states. The calculated thermodynamic parameters used to evaluate the function of RAFT agents revealed that in both cases the spiro-RAFT agents are expected to have different stabilities and thus reactivity towards radical addition. Furthermore, the stability of the RAFT adduct radicals and subsequent ability to fragment are sufficiently different between the open and closed forms. This should allow these RAFT agents to theoretically be applicable to both stable and unstable propagating radicals when they are in the open and closed states respectively. The magnitude of the switch in reactivity is smaller than for the CSIRO acid/base switchable dithiocarbamate. Encouragingly the descriptors indicate the spiro-xan. agent in the closed state could potentially be applicable to monomers with a wide range of stabilities, essentially making it universal in nature.

These findings validate the idea of a spirooxazine based RAFT agent with photoswitchable reactivity, hence the synthesis of the desired compounds was imperative to allow for experimental testing. The synthesis of these compounds and several non-photochromic RAFT agents is covered in Chapter 4.

3.6 References

1. Coote, M.L., *Ab Initio Study of the Addition−Fragmentation Equilibrium in RAFT Polymerization: When Is Polymerization Retarded?* Macromolecules, 2004. **37**(13): p. 5023-5031.

2. Coote, M.L. and D.J. Henry, *Effect of Substituents on Radical Stability in Reversible Addition Fragmentation Chain Transfer Polymerization: An ab Initio Study*. Macromolecules, 2005. **38**(4): p. 1415-1433.

3. Izgorodina, E.I. and M.L. Coote, *Reliable Low-Cost Theoretical Procedures for Studying Addition−Fragmentation in RAFT Polymerization.* The Journal of Physical Chemistry A, 2006. **110**(7): p. 2486-2492.

4. Krenske, E.H., E.I. Izgorodina, and M.L. Coote, *An Ab Initio Guide to Structure—Reactivity Trends in Reversible Addition Fragmentation Chain Transfer Polymerization*, in *Controlled/Living Radical Polymerization*. 2006, American Chemical Society. p. 406-420.

5. Busch, M., et al., *The Use of Novel F-RAFT Agents in High Temperature and High Pressure Ethene Polymerization: Can Control be Achieved?* Australian Journal of Chemistry, 2007. **60**(10): p. 788-793.

6. Coote, M.L., et al., *Addition-Fragmentation Kinetics of Fluorodithioformates (F-RAFT) in Styrene, Vinyl Acetate, and Ethylene Polymerization: An Ab Initio Investigation.* Macromolecules, 2006. **39**(13): p. 4585-4591.

7. Benaglia, M., et al., *Polystyrene-block-poly(vinyl acetate) through the Use of a Switchable RAFT Agent.* Macromolecules, 2009. **42**(24): p. 9384-9386.

8. Benaglia, M., et al., *Universal (Switchable) RAFT Agents.* Journal of the American Chemical Society, 2009. **131**(20): p. 6914-6915.

9. Keddie, D.J., et al., *Chain Transfer Kinetics of Acid/Base Switchable N-Aryl-N-Pyridyl Dithiocarbamate RAFT Agents in Methyl Acrylate, N-Vinylcarbazole and Vinyl Acetate Polymerization.* Macromolecules, 2012. **45**(10): p. 4205-4215.

10. Moad, G., et al., *Block Copolymer Synthesis through the Use of Switchable RAFT Agents*, in *Non-Conventional Functional Block Copolymers*. 2011, American Chemical Society. p. 81-102.

11. Keddie, D.J., et al., *Switchable Reversible Addition–Fragmentation Chain Transfer (RAFT) Polymerization in Aqueous Solution, N,N-Dimethylacrylamide.* Macromolecules, 2011. **44**(17): p. 6738-6745.

12. Maeda, S., *Spirooxazines*, in *Organic Photochromic and Thermochromic Compounds - Volume 1 - Main Photochromic Families*, J.C. Crano and R.J. Guglielmetti, Editors. 2002, Kluwer Academic Publishers: New York. p. 85-109.

13. Dürr, H. and H. Bouas-Laurent, *Photochromism : molecules and systems*. 1990, Amsterdam; New York; New YorK, NY, U.S.A.: Elsevier ; Distributors for the U.S. and Canada, Elsevier Science Pub. Co.

14. Fischer, H. and L. Radom, *Factors Controlling the Addition of Carbon-Centered Radicals to Alkenes—An Experimental and Theoretical Perspective.* Angewandte Chemie International Edition, 2001. **40**(8): p. 1340-1371.

15. Keddie, D.J., et al., *RAFT Agent Design and Synthesis.* Macromolecules, 2012. **45**(13): p. 5321-5342.

16. Gaumont, A.C., L. Wazneh, and J.M. Denis, *Thiocyanohydrins, a new class of compounds, precursors of unstabilized thiocarbonyl derivatives.* Tetrahedron, 1991. **47**(27): p. 4927-4940.

17. *Spartan '16*. 2016, Wavefunction, Inc.: Irvine, CA.

18. Moad, G., E. Rizzardo, and S.H. Thang, *Living Radical Polymerization by the RAFT Process - A Third Update.* Australian Journal of Chemistry, 2012. **65**(8): p. 985-1076.

19. Chong, Y.K., et al., *Thiocarbonylthio Compounds [SC(Ph)S−R] in Free Radical Polymerization with Reversible Addition-Fragmentation Chain Transfer (RAFT Polymerization). Role of the Free-Radical Leaving Group (R).* Macromolecules, 2003. **36**(7): p. 2256-2272.

20. Barner-Kowollik, C., et al., *Kinetic Investigations of Reversible Addition Fragmentation Chain Transfer Polymerizations: Cumyl Phenyldithioacetate Mediated Homopolymerizations of Styrene and Methyl Methacrylate.* Macromolecules, 2001. **34**(22): p. 7849-7857.

21. Chiefari, J., et al., *Thiocarbonylthio Compounds (SC(Z)S−R) in Free Radical Polymerization with Reversible Addition-Fragmentation Chain Transfer (RAFT Polymerization). Effect of the Activating Group Z.* Macromolecules, 2003. **36**(7): p. 2273-2283.

22. Moad, G., et al., *Living free radical polymerization with reversible addition – fragmentation chain transfer (the life of RAFT).* Polymer International, 2000. **49**(9): p. 993-1001.

23. Shao, Y., et al., *Advances in methods and algorithms in a modern quantum chemistry program package.* Physical Chemistry Chemical Physics, 2006. **8**(27): p. 3172-3191.

24. Frisch, M.J., et al., *Gaussian 09, Revision C.1*. 2009, Gaussian, Inc., Wallingford CT.

25. Werner, H.J., et al., *MOLPRO, a package of ab initio programs*. http://www.molpro.net.

26. Izgorodina, E.I., C.Y. Lin, and M.L. Coote, *Energy-directed tree search: an efficient systematic algorithm for finding the lowest energy conformation of molecules.* Physical Chemistry Chemical Physics, 2007. **9**(20): p. 2507-2516.

27. Feyereisen, M., G. Fitzgerald, and A. Komornicki, *Use of Approximate Integrals in Abinitio Theory - an Application in Mp2 Energy Calculations.* Chemical Physics Letters, 1993. **208**(5-6): p. 359-363.

28. Coote, M.L., *3.03 - Radical Reactivity by Computation and Experiment A2 - Matyjaszewski, Krzysztof*, in *Polymer Science: A Comprehensive Reference*, M. Möller, Editor. 2012, Elsevier: Amsterdam. p. 39-58.

29. Destarac, M., et al., *Macromolecular Design via the Interchange of Xanthates (MADIX): Polymerization of Styrene with O-Ethyl Xanthates as Controlling Agents.* Macromolecular Chemistry and Physics, 2002. **203**(16): p. 2281-2289.

30. Mayadunne, R.T.A., et al., *Living Radical Polymerization with Reversible Addition−Fragmentation Chain Transfer (RAFT Polymerization) Using Dithiocarbamates as Chain Transfer Agents.* Macromolecules, 1999. **32**(21): p. 6977-6980.

31. Mayadunne, R.T.A., et al., *Living Polymers by the Use of Trithiocarbonates as Reversible Addition−Fragmentation Chain Transfer (RAFT) Agents: ABA Triblock Copolymers by Radical Polymerization in Two Steps.* Macromolecules, 2000. **33**(2): p. 243-245.

32. Moad, G., *Mechanism and Kinetics of Dithiobenzoate-Mediated RAFT Polymerization – Status of the Dilemma.* Macromolecular Chemistry and Physics, 2014. **215**(1): p. 9-26.

33. Gardiner, J., et al., *4-Halogeno-3,5-dimethyl-1H-pyrazole-1-carbodithioates: versatile reversible addition fragmentation chain transfer agents with broad applicability.* Polymer International, 2017. **66**(11): p. 1438-1447.

4 Materials, Methods, Experimental Techniques and Formulas

This chapter details the experimental and theoretical approaches taken throughout this thesis. Included are explanations of the quantum chemical methods employed in both simplified and in-depth calculations to deduce structure property relationships of the target molecules under investigation. The synthesis, purification and characterization of the RAFT agents investigated, along with their precursors and intermediates is detailed. Synthetic progress towards ultimately unrealised photochromic RAFT agent targets is also explored, along with potential explanations for the synthetic difficulties encountered. Polymerisation procedures and subsequent purification and analysis of all polymers is detailed, along with all equipment used for any characterization undertaken. Furthermore, any calculations and methods employed for various analyses are also detailed.

4.1 Materials

Table 4.1 below shows the compounds used within this project, their commercial source and purity.

Table 4.1 Summary of chemical compounds utilised throughout this thesis

Chemical	Supplier	Purity & notes
1,2-dichloroethane	Sigma Aldrich	Anhydrous, 99.8 %
1,8-Diazabicyclo[5.4.0]undec-7-ene (DBU)	Sigma Aldrich	> 99 %
1-nitroso-2-napthol	Aldrich	98 %
2,2'-azobisisobutyronitrile	TCI	See 4.1.1.3
2,3,3-Trimethylindolenine	Aldrich	98 %
2,7-dihydroxynaphthalene	Aldrich	97 %
2-Methylene-1,3,3-trimethylindoline	Aldrich	97 %, See 4.1.1.1
Acetic acid	Merck	Glacial, 99.7 %
Acetonitrile	Sigma Aldrich	HPLC grade, > 99.9 %
Ammonium chloride	Sigma Aldrich	ACS grade, > 99.5 %
Ammonium chloride sat. solution	N/A	Made using ammonium chloride
Benzyl bromide	Aldrich	Reagent grade, 98 %
Bromoacetonitrile	Aldrich	97 %
Carbon disulfide	Chem-Supply	ACS grade, 99.9 %
Celaton FW60 (Celite 545)	Chem-Supply	Technical grade
Chloroacetonitrile	Aldrich	99 %
Chloroform	RCI Labscan Ltd.	ACS grade, 99.8 %
Deuterated DMSO (DSMSO – d6)	Sigma Aldrich	100 %, 99.9 atom % D
Deuterochloroform ($CDCl_3$)	Sigma Aldrich	> 99 %, 99.8 atom % D
Dichloromethane (DCM)	Chem-Supply	AR grade, 99.8 %
Diisopropylethyl amine (DIEA)	Sigma Aldrich	> 99 %
Dimethylformamide (DMF)	Chem-Supply	AR, 99.8 %

Dimethylsulfoxide (DMSO)	Sigma Aldrich	ACS grade, > 99.9 %
Dodecanethiol	Aldrich	> 98 %
Ethanol	Scharlau	ACS grade, > 99 %
Ethyl 2-bromopropionate	Sigma Aldrich	99 %
Ethyl 2-mercaptopropionate	Aldrich	> 95 %
Ethyl acetate	RCI Labscan Ltd.	99.8 %
Hexane (mixture of isomers)	ChemSupply	Drum grade, distilled prior to use
Hydrochloric acid	RCI Labscan Ltd.	32 % w/w in water
Hydroquinone	Sigma	99 %
Methanol	Chem-Supply	99.8 %
Methyl acrylate (MA)	Aldrich	99 %, See 4.1.1.2
Methyl methacrylate (MMA)	Sigma Aldrich	99 %, See 4.1.1.2
Neutral alumina	Aldrich	Activated, neutral, Brockmann I, Standard grade, ~ 150 mesh
Palladium on Carbon (10 % w/w)	Aldrich	99 %
Phenol	Chem-Supply	99 %
Piperidine	Sigma Aldrich	99 %
Potassium hydroxide	Merck	AR grade, > 85 %
Potassium hydroxide solution	N/A	Made using potassium hydroxide
Potassium tert-butoxide (K tert-butoxide)	Sigma Aldrich	Reagent grade, > 98 %
Silica gel	San Pont	230 – 400 mesh
Sodium bicarbonate	Chem-Supply	ACS grade, > 99.7 %
Sodium bicarbonate solution	N/A	Made using sodium bicarbonate
Sodium chloride	Sigma Aldrich	ACS grade, > 99 %
Sodium chloride sat. solution (brine)	N/A	Made using sodium chloride
Sodium nitrite	Sigma Aldrich	Reagent plus, > 99 %
Sodium sulfate	Chem-Supply	AR grade, anhydrous, 99 %
Styrene (Sty)	Acros Organics	99.5 %, See 4.1.1.2
Tetrahydrofuran (THF)	Chem-supply	AR grade, 99.8 %, stabilised with BHT
Thiophosgene	Aldrich	97 %
Toluene	Sigma Aldrich, Honeywell Burdick & Jackson	Anhydrous, HPLC grade
Vinyl acetate (VAc)	Aldrich	99 %, See 4.1.1.2
Water	Labconco filtration unit	MilliQ grade,18.2 M Ohm

4.1.1 Special procedures relating to specific compounds in Table 4.1

4.1.1.1 Use of 2-methylene-1,3,3-trimethylindolenine

Regardless of supplier and stated purity, straight from the container the purity will most likely be poor due to the extremely air sensitive nature of this compound. Using flame dried glassware that had

been flushed with dry nitrogen prior to use, this compound was distilled under reduced pressure immediately prior to use. The dark red compound that remains at the end is the main impurity by mass and is the oxidised form of the original indolenine. The freshly distilled indolenine can be stored in flame dried Schlenk flask under dry nitrogen in the freezer for several weeks; during this time, it will change in colour from clear to bright pink and eventually to dark red. When light pink in colour, this compound is acceptable to use, however when dark red it needs to be re-distilled as described.

4.1.1.2 Removal of inhibitors from liquid monomers

The liquid monomers used (methyl acrylate, methyl methacrylate, vinyl acetate and styrene) were all stored under nitrogen in the freezer when not in use. Prior to use, they were gradually warmed to room temperature without opening the container, then the desired amount of monomer was passed through a short column (~10 cm in a disposable glass pipette) of neutral alumina under gentle back pressure with nitrogen.

4.1.1.3 Recrystallization of 2,2'-azobisisobutyronitrile (AIBN)

Due to the age and subsequently poor purity of the starting AIBN, this reagent was purified by a two-stage recrystallization procedure. AIBN was firstly dissolved in hot ethanol with vigorous stirring and the insoluble solids filtered off under gravity. The filtrate was cooled to room temperature before being placed in a freezer overnight. The resulting crystals were vacuum filtered and immediately recrystallised a second time from larger volume of ethanol, this time without heating to minimise decomposition. The solution was placed in the freezer overnight, the crystals vacuum filtered and dried under vacuum at room temperature for 4 h. The obtained product was > 99% pure based on ^{1}H NMR analysis where the resonance from AIBN at 1.88 ppm had an integration value of 1000 compared to the other resonances from impurities at 3.50 and 1.06 ppm which integrated for 1.43 and 2.16 respectively.

4.2 Nuclear magnetic resonance (NMR) spectroscopy & analysis methods

4.2.1 NMR instrumentation & data processing

NMR experiments were conducted on a Bruker Avance 600 Ultrashield spectrophotometer. Spectra were calibrated relative to the residual solvent peak from the deuterated solvent used. Raw data from the instrument was initially processed by applying a Fourier transform and phase correcting directly in Bruker TopSpin software using the "FT" and "APK" commands in sequence. Subsequent baseline

correction, manual phase correction, calibrating the spectrum, integration and labelling of peaks and exporting data in ASCII format was undertaken using ACD Labs NMR Processor, Academic Edition.

4.2.2 NMR spectroscopy of organic compounds and purified polymers

Sample preparation for all organic compounds and purified polymer samples was straightforward; a small amount of the compound was placed directly in a Bruker NMR tube (rated to 800 MHz) and ~ 0.7 mL of the appropriate deuterated solvent was added. The choice of solvent ($CDCl_3$, DMSO-d_6 or acetonitrile-d_3) is specified in the synthesis of the individual compounds/polymers in the following sections.

4.2.3 Determination of monomer conversion by ^{1}H NMR

The conversion for all polymerisations was determined by ^{1}H NMR. The formulas used to calculate conversion are provided along with exemplary spectra featuring PXEP and PXEP derived macroinitiators after the details for each respective polymerisation in section 4.5. Spectra for polymerisations conducted with other RAFT agents are not shown for clarity and conciseness. If more detailed ^{1}H NMR analysis for a polymerisation was necessary, the results and subsequent analysis are detailed in the relevant chapter. An external standard added to $CDCl_3$ was used for simplifying the integration process; two solutions using different standards were employed depending on the polymerisation mixture being analysed. These are as follows:

- For analysis of polymerisation solutions from methyl acrylate or methyl methacrylate polymerisations, a stock solution of 4.95 mL of $CDCl_3$ spiked with 50 µm of 1,2 – dichloroethane was made. The samples for ^{1}H NMR analysis were made by adding 0.55 mL of this solution to 50 µL of each aliquot of polymerisation mixture.
- For analysis of polymerisation solutions from vinyl acetate or styrene polymerisations, a stock solution of 4.95 mL of $CDCl_3$ spiked with 50 µL of dichloromethane was made. The samples for ^{1}H NMR analysis were made by adding 0.55 mL of this solution to 50 µL of each aliquot of polymerisation mixture.

In all cases, all samples and solvents were handled by micropipette.

After the ^{1}H NMR spectra had been phase and baselined corrected along with calibration relative to the deuterated solvent as per section 4.2.1, the reference peak (1,2 – dichloroethane at 5.3 ppm shift or dichloromethane at 3.7 ppm shift) was then integrated for a fixed value of 1000. All other peaks of interest were then integrated along with the region in the spectrum from 3 – 0.5 ppm, referred to as the “aliphatic region”. In certain exemplary spectra, proton resonances attributed to penultimate

units have been identified; these peaks are denoted with a (p) after the respective proton assignment. These peaks are not significant in that they do not influence the determination of conversion.

4.3 Synthesis and characterization of RAFT agents, precursors and intermediates thereof

The labelling system for the molecules within this section was kept consistent with prior literature, with extra labels added where necessary to simplify assignments. For each molecule, the NMR assignments correspond directly to the labels used in the scheme describing its synthesis.

4.3.1 Attempted synthesis of cyanomethyl (phenoxycarbonothioyl) xanthate

Phenol was chosen as a model system to optimise the synthesis of several xanthates, as unlike 9'-hydroxy-1,3,3-trimethyl-spiro[indoline-2,3'-[3*H*]naphtha[2,1-b][1,4]oxazine], phenol is cheap, does not require synthesis or purification and should have similar reactivity. The synthesis of cyanomethyl (phenoxycarbonothioyl) xanthate was attempted via 4 different methods adapted from literature (shown in Scheme 4.1). For full details please see section A1.2.1 in the Appendix.

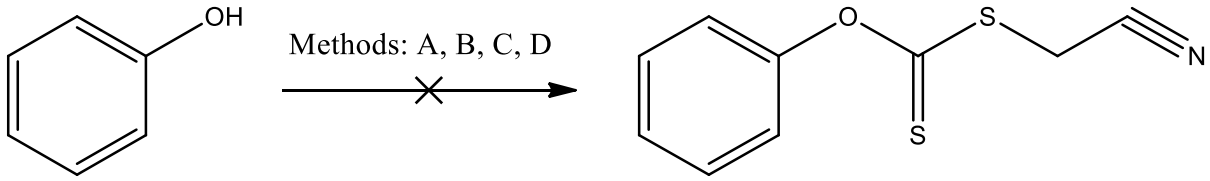

A: DMSO, KOH sol. (30% w/v, 1.0 eq.), CS_2 (1.51 eq.), $ClCH_2CN$ (1.0 eq.)
B: Dry DMF, K tert-butoxide (1.23 eq.), CS_2 (1.47 eq.), $ClCH_2CN$ (0.98 eq.)
C: DMSO, KOH sol. (30% w/v, 1.0 eq.), CS_2 (1.09 eq.), $BrCH_2CN$ (1.10 eq.)
D: Dry toluene, K tert-butoxide (1.12 eq.), CS_2 (1.07 eq.), $BrCH_2CN$ (1.05 eq.)

Scheme 4.1 Attempted synthesis of cyanomethyl (phenoxycarbonothioyl) xanthate.

In both methods **A** and **B**, the organic extracts were separated by column chromatography on silica gel and analysed by ^{1}H NMR. In both cases the fractions more non-polar than phenol were not the desired product as evidenced by the complete absence of the resonances from the cyanomethyl R group, coupled with the very faint off-white colour which indicates an absence of the RAFT moiety. Separation of the main yellow fractions that were more polar than phenol gave pungent smelling yellow residues that were not the desired product as determined by ^{1}H NMR. Methods **C** & **D** used bromoacetonitrile which provides a better leaving group over chloroacetonitrile, however this seemingly made no difference, with the outcome of the reactions giving similar results by both TLC

and ^{1}H NMR analysis. From these results it is concluded that the intermediate xanthate anion which forms is not sufficiently nucleophilic to allow these substitution reactions to occur.

4.3.2 Synthesis of 2-((phenoxycarbonothioyl)thio) ethyl propanoate

After the unsuccessful attempts at the synthesis of cyanomethyl (phenoxycarbonothioyl) xanthate, a more forceful approach was taken to the synthesis of 2-((phenoxycarbonothioyl)thio) ethyl propanoate via the use of thiophosgene (Scheme 4.2). The necessity of this approach is supported by the first reported synthesis of this compound (after this work was undertaken) utilising phenyl chlorodithioformate being reacted with ethyl 2-mercaptopropionate [1].

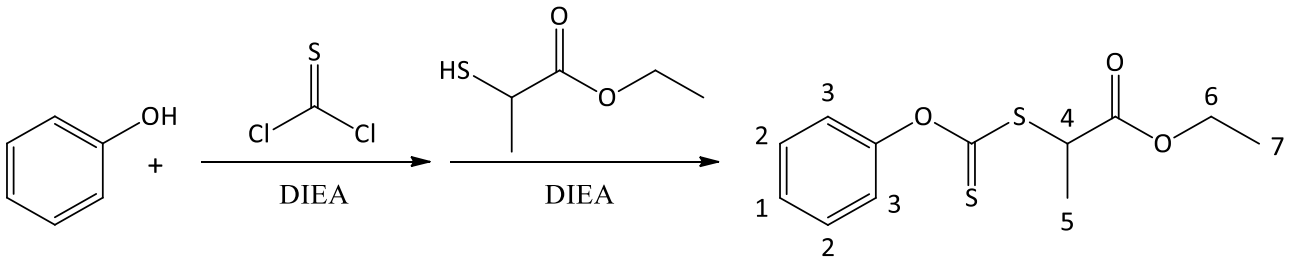

Scheme 4.2: 2-((phenoxycarbonothioyl)thio) ethyl propanoate.

Into a flame dried 250 mL two neck round bottom flask equipped with a stirrer bar and a nitrogen inlet was placed thiophosgene (5 mL, 6.52 x10^{-2} moles, 1.00 eq.) and 20 mL of anhydrous toluene. The reaction vessel was chilled in an ice bath. A mixture of phenol (6.149 g, 6.53 x10^{-2} moles, 1.00 eq.) and DIEA (8.4440 g, 6.53 x10^{-2} moles, 1.00 eq.) in 30 mL anhydrous toluene was added via dropping funnel over a period of 1 h with rapid stirring. A mixture of ethyl 2-mercaptopropionate (13.1446 g, 9.79 x10^{-2} moles, 1.50 eq.) and DIEA (12.6437 g, 9.78 x10^{-2} moles, 1.50 eq.) in 40 mL of anhydrous toluene was added via a dropping funnel over a period of 1 h with rapid stirring. The reaction was left to stir overnight for a period of 24 h which allowed a gradual increase back up to room temperature. The reaction mixture was then washed twice with ~ 150 mL of 5 % (w/w) potassium hydroxide solution followed by washing with ~ 100 mL of brine. The aqueous phase was back extracted twice times with 75 mL of DCM. The organic extracts were combined and dried with sodium sulfate, filtered under gravity and the solvent removed under vacuum. Purified by column chromatography over silica gel using a mixture of hexane : ethyl acetate (88 : 12 (v/v), Rf = 0.33) with the solvent removed under vacuum. Obtained 2.9174 g (16.5 % yield) of a viscous bright yellow oil. ^{1}H NMR (600 MHz, $CDCl_3$) δ ppm: 1.31 (t, J = 7.1 Hz, 3 H, *7 H*), 1.67 (d, J = 7.3 Hz, 3 H, 5 *H*), 4.245 (dq, J = 3.7 Hz, 2 H, *6 H*), 4.495 (q, J = 7.3 Hz, 1 H, *4 H*), 7.1 (d, J = 8.5 Hz, 2 H, *3 H*), 7.31 (t, J = 7.3 Hz, 1 H, *1 H*), 7.44 (t, J = 7.7 Hz, 2 H, *2 H*). ^{13}C NMR (600 MHz, $CDCl_3$) δ ppm: 14.13, 16.91, 48.52, 61.91, 121.99, 126.73, 129.58, 154.29, 171.11 (C=O), 212.07 (C=S).

4.3.3 Synthesis of 1-nitroso-2,7-dihydroxynaphthalene

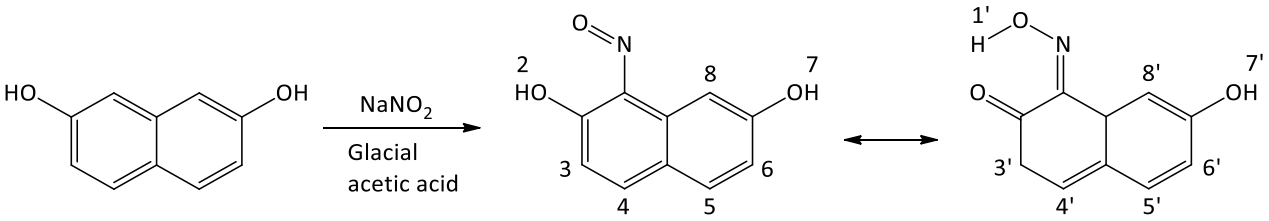

Scheme 4.3: Synthesis of 1-nitroso-2,7-dihydroxynaphthalene, with isomerization shown.

In a 250 mL beaker equipped with a stirrer bar and chilled in an ice bath, 2,7-hydroxynaphthalene (20.0185 g, 1.25 x10^{-1} moles, 1 eq.) was dissolved in 20 mL of water and 160 mL (2.795 moles, 22.36 eq.) of glacial acetic acid. Sodium nitrite (10.035 g, 1.45 x10^{-1} moles, 1.16 eq.) was dissolved in 12 mL of water, and this was added dropwise to the chilled solution over a period of 2 h, then the reaction mixture was left to stir for a further 2 h at room temperature. The reaction mixture was then poured into 500 mL of water with rapid stirring, followed by vacuum filtration. The dark red brown product was washed extensively with ~ 2.5 L of water, then placed on a pre-weighed watch glass and dried in a 50 °C oven overnight. Obtained 23.0178 g (97.35 % yield) of a crunchy dark brown compound. The ^{1}H NMR spectra obtained in DMSO-d6, acetonitrile-d3 and $CDCl_3$ were quite complex, with multiple broad and often overlap resonances being seen in all cases. This is attributed to the isomerization between the nitroso and oxime tautomers (Scheme 4.3), which is known to occur for both nitrosophenol [2] and nitrosonaphthol [3] compounds. For this reason, the ^{1}H NMR data is not presented here, however the purity of the compound was sufficient to yield pure 9'-hydroxy-1,3,3-trimethyl-spiro[indoline-2,3'-[3*H*]naphtha[2,1-b][1,4]oxazine] in the subsequent condensation reaction.

4.3.4 Synthesis of 9'-hydroxy-1,3,3-trimethyl-spiro[indoline-2,3'-[3*H*]naphtha[2,1-b][1,4]oxazine], spiro-OH

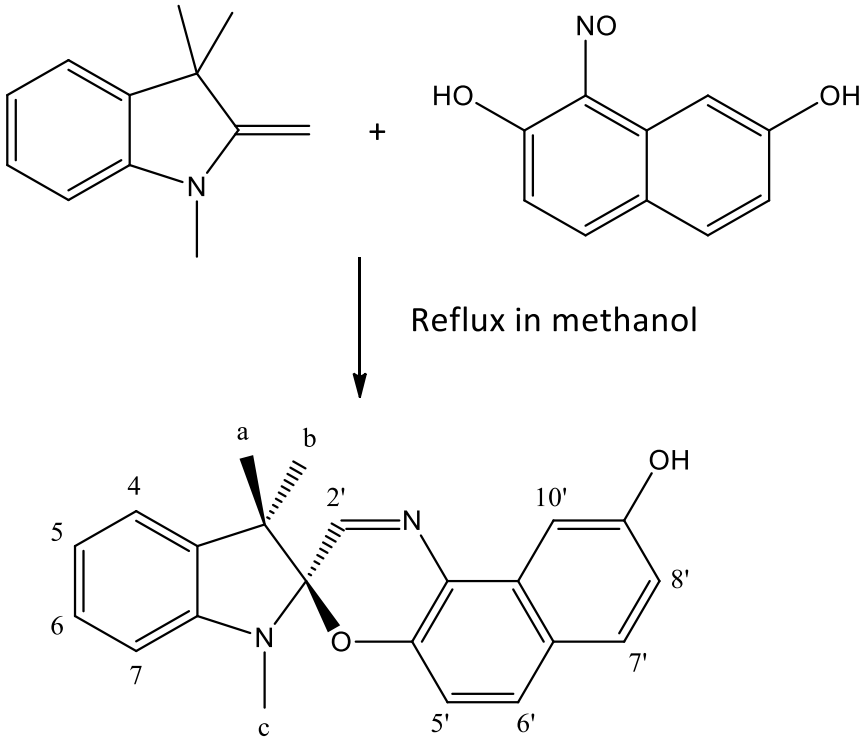

Scheme 4.4: Synthesis of 9'-hydroxy-1,3,3-trimethyl-spiro[indoline-2,3'-[3*H*]naphtha[2,1-b][1,4]oxazine].

In a 150 mL round bottom flask equipped with a stirrer bar, freshly distilled 1-methylene-2,3,3-trimethylindoline (5.5359 g, 3.195 x10^{-2} moles, 1.21 eq.) was added to 1-nitroso-2,7-dihydroxynaphthalene (5.0031 g, 2.645 x10-2 moles, 1 eq.). 70 mL of methanol that was sparged with nitrogen for 1 h prior to use was added as solvent and set to gently stir; a reflux condenser was then equipped and the reaction heated to reflux under nitrogen for a period of 6 h. Upon completion of the reflux, the reaction mixture was exposed to air and left to cool to room temperature overnight to allow the product to precipitate out. The precipitate was filtered under vacuum and washed extensively with a hexane : ethyl acetate (70 : 30, v/v) mixture until the dark red impurities were removed and the resulting product was a beige grey colour. The product was transferred onto a pre-weighed watch glass and dried in a 50 °C oven overnight. Obtained 3.8759 g (42.55 % yield) of a powdery beige compound. ^{1}H NMR (600 MHz, $CDCl_3$) δ ppm: 1.365 (d, J = 2.8 Hz, 6 H, *a + b H*), 2.77 (s, 3 H, *c H*), 5.35 (broad, , 1H, *OH*), 6.585 (d, J = 7.9 Hz, 1 H, *7 H*), 6.855 (d, J = 8.8 Hz, 1 H, *5' H*), 6.91 (t, J = 7.4 Hz, 1 H, *5 H*), 7.025 (dd, J = 8.8, 2.6 Hz, 1 H, *8' H*), 7.095 (d, J = 7.3 Hz, 1 H, *4 H*), 7.23 (t, J = 7.6 Hz, 1 H, *6 H*), 7.585 (d, J = 8.8 Hz, 1 H, *6' H*), 7.665 (d, J = 8.8 Hz, 1 H, *7' H*), 7.71 (s, 1 H, *2' H*), 7.86 (d, J = 2.2 Hz, 1 H, *10' H*). ^{13}C NMR (600 MHz, $CDCl_3$) δ ppm: 20.78,

25.43, 29.61, 51.76, 98.6, 103.74, 107.1, 114.23, 115.68, 119.81, 121.47, 122, 124.72, 127.99, 129.98, 130.12, 132.43, 135.87, 144.93, 147.58, 150.27, 154.89.

Notes on purification: if the reaction mixture does not precipitate upon cooling, removal of approximately half the solvent under reduced pressure and leaving to chill in a refrigerator can induce precipitation. Purification by column chromatography on silica, loaded with dichloromethane and run with hexane : ethyl acetate (70 : 30, v/v) gives acceptable results, however streaking of bands is common even under moderate loading. If further purification of the precipitate is desired, washing with ice cold methanol is sufficient.

4.3.5 Synthesis of ethyl propanoate chlorodithioformate

During the synthesis of 2-((phenoxycarbonothioyl)thio) ethyl propanoate via the use of thiophosgene (Scheme 4.5), the presence of other yellow compounds containing the ethyl propanoate R group was detected by TLC and ^{1}H NMR analysis. To avoid possible complications, the alkylating agent ethyl propanoate chlorodithioformate was synthesised. This can be reacted with various weakly nucleophilic compounds to generate RAFT agents that would otherwise be difficult if not impossible to synthesise via other synthetic methodologies. Due to health and safety reasons associated with the extremely reactive thioacetonitrile [4], the synthesis of an alkylating agent with a cyanomethyl group using the thiophosgene route was not pursued.

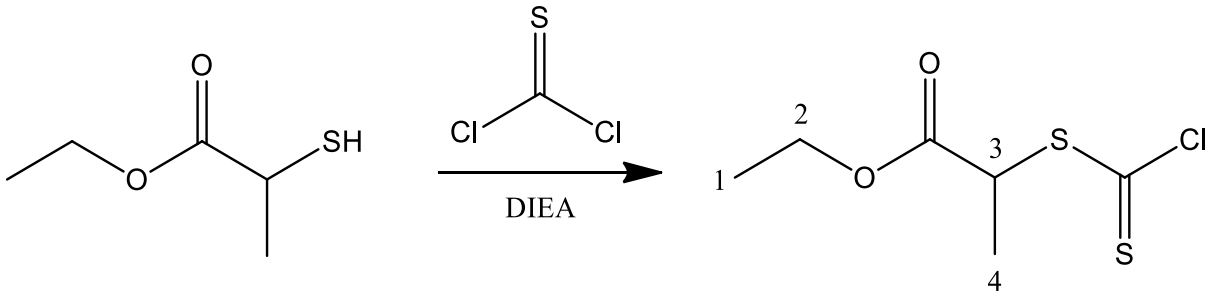

Scheme 4.5: Synthesis of ethyl propanoate chlorodithioformate.

Into a flame dried 250 mL two neck round bottom flask equipped with a stirrer bar and a nitrogen inlet was placed thiophosgene (3 mL, 3.94 x10^{-2} moles, 1.11 eq.) and 100 mL of anhydrous toluene. The reaction vessel was chilled in an ice bath with NaCl added (~ -14 °C). A mixture of ethyl 2-mercaptopropionate (4.585 mL, 3.52 x10^{-2} moles, 1 eq.) and DIEA (6.135 mL, 3.52 x10^{-2} moles, 1 eq.) in 100 mL of anhydrous toluene was added dropwise via a dropping funnel over a period of 2.5 h with rapid stirring. The reaction was left to stir overnight for a period of 24 h which allowed a gradual increase back up to room temperature. The reaction mixture was then washed twice with ~ 150 mL of saturated sodium bicarbonate solution, with the aqueous phase being back extracted three

times with 50 mL of DCM. The organic extracts were combined and dried with sodium sulfate, filtered under gravity and the solvent removed under vacuum. Purified by column chromatography over silica gel using a mixture of hexane : ethyl acetate (90 : 10 (v/v), Rf = 0.43), with the solvent removed under vacuum. Obtained 5.7067 g (76.17 % yield) of a light orange oil with a viscous consistency and a pungent fruity odour. ^{1}H NMR (600 MHz, $CDCl_3$) δ ppm: 1.3 (t, J = 7.1 Hz, 3 H, *1 H*), 1.64 (d, J = 7.3 Hz, 3 H, *4 H*), 4.23 (dq, J = 7.1, 2.8 Hz, 2 H, *2 H*), 4.395 (q, J = 7.3 Hz, 1 H, *3 H*). ^{13}C NMR (600 MHz, $CDCl_3$) δ ppm: 14.06, 16.03, 51.92, 62.24, 169.83 (C=O), 195.21 (C=S).

4.3.6 Synthesis of 9'-((ethyl 2-propanoate carbonothioyl) thio)-1,3,3-trimethyl-spiro[indoline-2,3'-[3H]naphtha[2,1-b][1,4]oxazine], spiro-XEP

Two methods were used to synthesise spiro-XEP to attempt to minimise the formation of undesired impurities (Scheme 4.6). Initially method A and variations thereof was used, followed by the synthesis of ethyl propanoate chlorodithioformate and its utilisation in method B. For both synthetic methods, light was excluded as much as possible by using brown glassware and wrapping adapters and stoppers in aluminium foil.

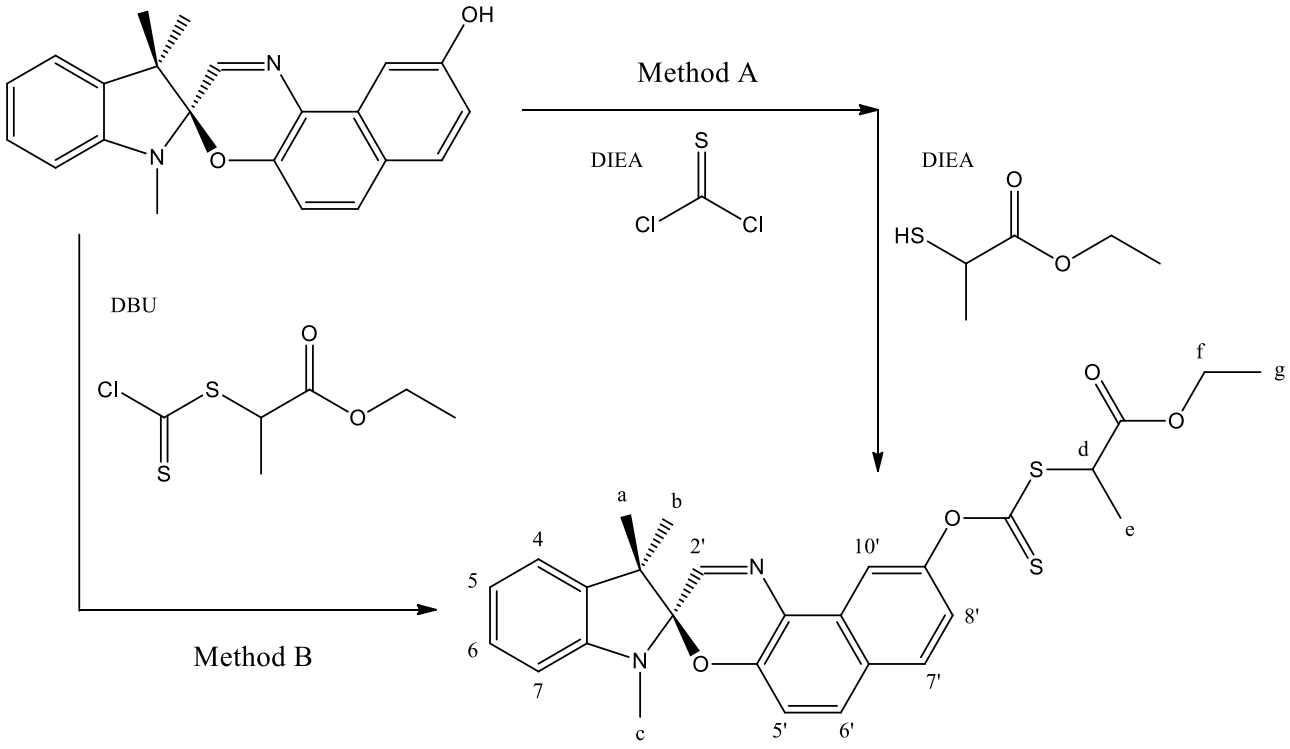

Scheme 4.6: Two methods used to synthesise spiro-XEP.

Method A: Into a brown glass flame dried 250 mL two neck round bottom flask equipped with a stirrer bar and a nitrogen inlet was placed thiophosgene (0.8 mL, 1.04 x10^{-2} moles, 1.05 eq.) and 20 mL of DCM, with the reaction vessel being chilled in an ice bath. A mixture of spiro-OH (3.4037 g,

9.88 x10^{-3} moles. 1 eq.) and DIEA (1.27624 g, 9.87 x10^{-3} moles. 1 eq.) in 150 mL of DCM was added dropwise over a period of 30 mins. The reaction was warmed to room temperature and left to stir for 24 h. A mixture of ethyl 2-mercaptopropionate (1.9898 g, 1.48 x10^{-2} moles, 1.5 eq.) and DIEA (1.9158 g, 1.48 x10^{-2} moles, 1.5 eq.) in 10 mL of DCM was added dropwise over a period of 10 mins with rapid stirring and left to stir for a further 24 h. The solvent was then removed under vacuum and purified by column chromatography over silica gel using toluene (Rf = 0.37).

Other attempts at the synthesis of 2-((phenoxycarbonothioyl)thio) ethyl propanoate revealed that using DBU as the organic base resulted in no product forming, thus DIEA was used in method A whilst DBU could successfully be used as the base in method B. Furthermore, several variations of method A were tried including using toluene as the solvent, however this did not diminish the quantity of by-products formed as determined by ^{1}H NMR analysis to be ~ 25 %. Another complication arises from the nature of the starting spiro-OH compound. Washing the reaction mixture with basic solutions (5 % KOH w/w or saturated sodium bicarbonate) during the workup to remove any unreacted ethyl 2-mercaptopropionate resulted in the formation of an intractable dark foam that could not be recovered due to it being only sparingly soluble in most organic solvents (toluene, chloroform, DCM or THF) and being insoluble in water.

Method B: Into a brown glass flame dried 250 mL two neck round bottom flask equipped with a stirrer bar and a nitrogen inlet was placed ethyl propanoate chlorodithioformate (1.8158 g, 8.54 x10^{-3} moles, 1.09 eq.) with 30 mL of anhydrous toluene. A mixture of spiro-OH (2.678 g, 7.78 x10^{-3} moles, 1 eq.) and DBU (1.35 mL, 9.04 x10^{-3} moles, 1.16 eq.) in 60 mL of anhydrous toluene was added dropwise via a dropping funnel over a period of 5 mins, then rinsed in with a further 10 mL of anhydrous toluene. Left to stir for a period of 24 h, after which it was washed sequentially with water and brine. The aqueous phase was extracted with toluene, the organic extracts combined and dried with sodium sulfate, filtered under gravity and the solvent removed under vacuum. This mixture was loaded on a chromatotron plate (2mm thick, standard recipe) with toluene and eluted with toluene to yield a sticky green - yellow compound, which after drying under vacuum has a hard toffee-like texture.

^{1}H NMR (600 MHz, $CDCl_3$) δ ppm: 1.26 – 1.30 (m, 0.75 H, *impurity 1 + A H*), 1.33 (t, J = 7.1 Hz, 3 H, *g H*), 1.37 (s, 6 H, *a + b H*), 1.62 (dd, J = 7.4, 2.0 Hz, 0.50 H, *impurity E H*), 1.71 (d, J = 7.4 Hz, 3 H, *e H*), 2.77 (s, 3 H, *c H*), 3.61 (dq, J = 7.2, 3.7 Hz, 0.05 H, *impurity 4 H*), 4.19 – 4.24 (m, 0.5 H, *impurity 2 + B H*), 4.25 – 4.30 (m, 2 H, *f H*), 4.545 (q, J = 7.4 Hz, 1 H, *d H*), 4.785 (dq, J = 7.3, 4.6 Hz, 0.15 H, *impurity D H*),

6.595 (d, J = 7.9 Hz, 1 H, *7 H*), 6.96 (dt, J = 7.7, 0.8 Hz, 1 H, *5 H*), 7.03 (d, J = 8.8 Hz, 1 H, *8' H*), 7.105 (dd, J = 6.6, 0.7 Hz, 1 H, *5' H*), 7.155 (dd, J = 8.8, 2.4 Hz, 1 H, *4 H*), 7.235 (dt, J = 6.4, 1.3 Hz, 1 H, *6 H*), 7.68 (d, J = 8.8 Hz, 1 H, *6' H*), 7.73 (s, 1 H, *2' H*), 7.79 (d, J = 8.8 Hz, 1 H, *7' H*), 8.27 (d, J = 2.4 Hz, 1 H, 10*' H*). ^{13}C NMR (600 MHz, $CDCl_3$) δ ppm: 14.03 (impurity, A), 14.15, 16.86 (impurity, E), 1696 (impurity, E), 17.04, 20.71, 25.39, 29.60, 47.19, 48.37 (impurity, D), 48.43 (impurity, D), 48.55, 51.89, 61.40, 61.94, 98.85, 107.14, 113.59, 117.10, 119.29, 119.91, 122.98, 127.54, 128.02, 129.41, 130.06, 131.78, 135.75, 144.88, 147.49, 150.93, 150.95, 153.29, 170.77 (impurity, C), 170.83 (impurity, C), 171.13 (C=O), 212.07 (C=S).

4.3.7 Synthesis of impurities formed during the synthesis of spiro-XEP

To identify the by-products formed during the synthesis of spiro-XEP that could not be removed by purification, another reaction was run under similar conditions to that of the synthesis of ethyl propanoate chlorodithioformate. An excess of ethyl 2-mercaptopropionate was used to generate the symmetrical diethoxycarbonylethyl trithiocarbonate, which also resulted in the synthesis of the symmetrical bis ethyl 2-mercaptopropionate disulfide as shown in Scheme 4.7.

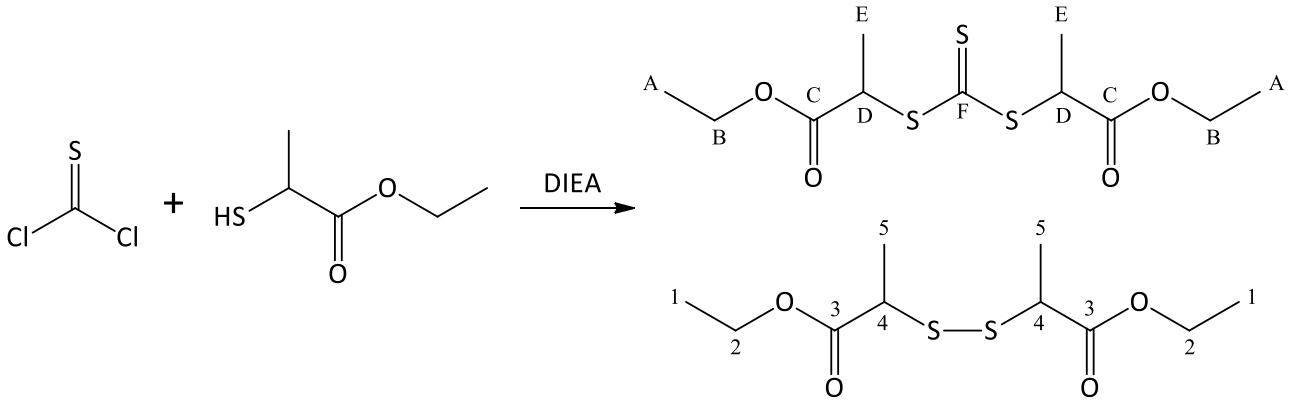

Scheme 4.7: Synthesis of impurities formed during the synthesis of spiro-XEP.

Into a flame dried 100 mL two neck round bottom flask equipped with a stirrer bar and a nitrogen inlet was placed thiophosgene (0.5 mL, 6.52 x10^{-2} moles, 1.00 eq.) and 10 mL of anhydrous toluene, with the reaction vessel chilled in an ice bath. A mixture of ethyl 2-mercaptopropionate (1.8421 g, 1.37 x10^{-2} moles, 2.10 eq.) and DIEA (1.7752 g, 1.37 x10^{-2} moles, 2.10 eq.) in 15 mL of anhydrous toluene was added dropwise over ~ 5 mins, then left to stir for 12 h. The reaction mixture was washed twice with ~ 50 mL of sodium bicarbonate solution, with the aqueous phase extracted with twice with ~ 50 mL of DCM. The organic extracts were combined, dried with sodium sulfate, filtered under gravity and the solvent removed under vacuum. Purified by column chromatography over silica gel using a mixture of hexane : ethyl acetate (85 : 15 (v/v)). 2 distinct yellow bands were separated; the

first being that of ethyl propanoate chlorodithioformate with a yield of 94.5 mg with the second band being most of the product by mass at 902 mg. Given the similar structure of diethoxycarbonylethyl trithiocarbonate and bis ethyl 2-mercaptopropionate disulfide and thus assuming both have similar solubilities in $CDCl_3$, the second band was identified by ^1H NMR analysis as consisting of approximately 51.6 % of the trithiocarbonate and 48.4 % of the disulfide. Due to both compounds existing as a mixture of diastereomers which leads to the resonances from several protons from both compounds overlapping, the J splitting values could not be determined for all resonances. ^1H NMR (600 MHz, $CDCl_3$) δ ppm: 1.26 – 1.31 (m, 6 H, *1* + *A H*), 1.495 (dd, J = 7.1, 2 Hz, 3 H, *5 H*), 1.60 (dd, J = 7.3, 2 Hz, 3 H, *E H*), 3.595 (dq, J = 7.2, 3.7 Hz, 1 H, *4 H*), 4.17 – 4.23 (m, 4 H, *2* + *B H*), 4.77 (dq, J = 4.4, 3.0 Hz, 1 H, *D H*). ^{13}C NMR (600 MHz, $CDCl_3$) δ ppm: 14.03 (A), 14.05 (A), 14.13 (1), 16.69 (5), 16.75 (5), 16.84 (E), 16.95 (E), 47.19 (4), 48.01 (4), 48.36 (D), 48.43 (D), 61.39 (2), 61.93 (B), 170.76 (C), 170.82 (C), 172.05 (3), 172.11 (3), 219.61 (F), 219.7 (F).

4.3.8 Purification of spiro-XEP & identification of impurities

A sample of spiro-XEP (0.7 mL, 35 mg/mL in $CDCl_3$) was titrated with a solution containing the mixture of impurities (25 uL aliquots, 50.1 mg/mL in $CDCl_3$) and observing the ^1H resonances. Upon the addition of the first aliquot of impurities (Figure 4.1, blue trace), the resonances (labelled D, 2, B, E, 5, A & 1 in Figure 4.1) attributed to these impurities in the original spectrum for spiro-XEP (Figure 4.1, black trace) simply increased in size and did not show further splitting. These resonances only increased further when the second aliquot was added (Figure 4.1, magenta trace) as is to be expected. This confirms what was initially suspected, that the impurities in the spiro-XEP sample that could not be purified out by various approaches (see below) are indeed a mixture of diethoxycarbonylethyl trithiocarbonate and bis ethyl 2-mercaptopropionate disulfide. Assuming that spiro-XEP and these impurities have comparable solubility in $CDCl_3$, the relative abundance of all 3 compounds was estimated by comparing the integrations for the resonances corresponding to the same proton present on the R group (peaks D, d & 4 in Figure 4.1). Based on this calculation, it is estimated that the spiro-XEP sample contained approximately 91.3 % of spiro-XEP, 7.0 % of the trithiocarbonate and 1.7 % of the disulfide.

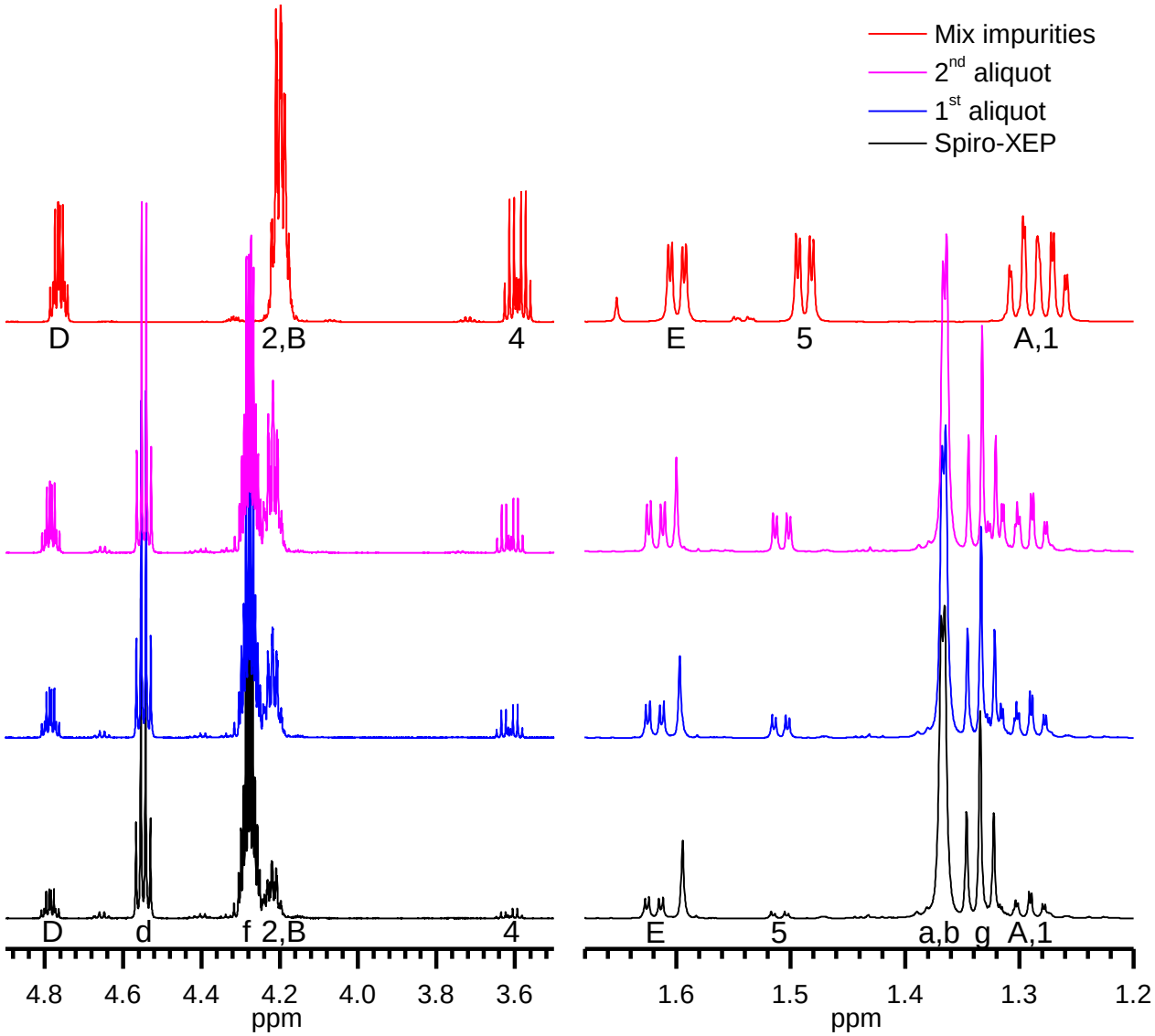

Figure 4.1: ^{1}H NMR spectra for the titration of the spiro-XEP sample with the synthesised trithiocarbonate and disulfide impurities.

Figure 4.2: Silica TLC plate developed in toluene showing a comparison of spiro-XEP (label P) with synthesised impurities; 1st band (label 1) and 2nd band (label 2).

When purifying spiro-XEP, separating the small amount of the ethyl propanoate chlorodithioformate that remains unreacted is straightforward due to it being the 1st band that elutes (Figure 4.2, label 1). However it becomes clear that the mixture of impurities (Figure 4.2, label 1) has essentially the same Rf value as that of spiro-XEP (Figure 4.2, label P). The tendency of spiro-XEP to undergo ring opening causes the band to smear out; this occurred on silica gel and on the chromatotron plate, even when the separations were performed at night in the dark under a red light with a UV cut off. Forcing the spiro-XEP to switch on the chromatotron plate by irradiating it with the same UV lamp as used in the kinetic experiments (370nm, 2 mW/cm^2) in order delay its elution did not aid separation. Ultimately, the most effective method of purifying the reaction mixture in regard to time taken, volume of solvent used and purity of the obtained spiro-XEP was found to be loading onto a dry chromatotron plate (2mm thick, standard recipe) with toluene and elution with toluene.

4.3.9 Synthesis of 1-benzyl-2,3,3-trimethylindolenium bromide, benzylated indole salt

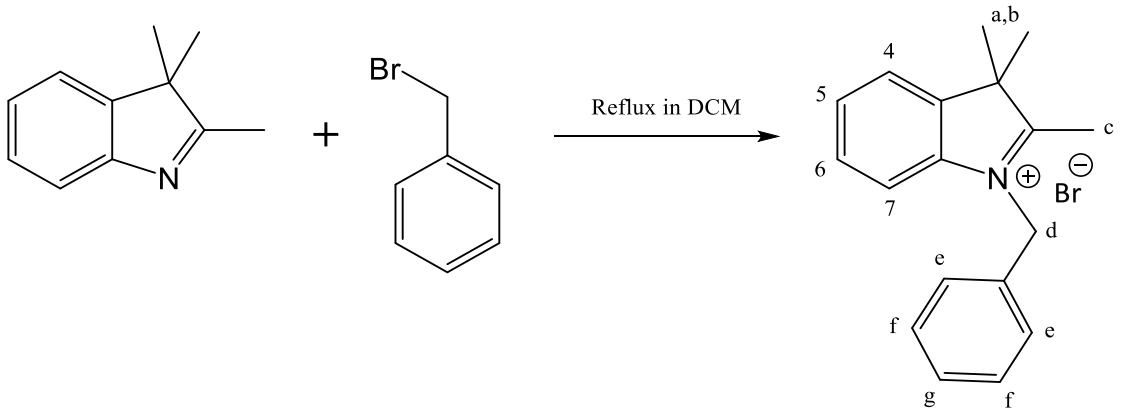

Scheme 4.8: Synthesis of 1-benzyl-2,3,3-trimethylindolenium bromide.

2,3,3-Trimethylindolenine (7.6992 g, 4.835 x10^{-2} moles, 1 eq.) was placed into a 50 mL round bottom flask equipped with a stirrer bar, to which benzyl bromide (12.0795 g, 7.063 x10^{-2} moles, 1.46 eq.) was then added. 10 mL of DCM was added as solvent and set to gently stir; a reflux condenser was then equipped, and the reaction heated to reflux under nitrogen for a period of 18 h. Upon completion of the reflux, the reaction mixture was transferred to a pre-weighed 250 mL round bottom flask and blown over with a nitrogen stream for a period of 24 h to evaporate most of the excess benzyl bromide and the DCM. Despite further extensive drying under vacuum for a period of 8 h, obtained 18.4254 g (115. 4 % yield) of a dark purple, incredibly sticky and dense compound that was difficult to handle due to its hygroscopic nature. The greater than 100 % yield indicates incomplete drying, however this is inconsequential as this compound was used in its crude form and in significant excess in the subsequent synthetic step. ^{1}H NMR (600 MHz, $CDCl_3$) δ ppm: 1.68 (s, 6 H, *a,b H*), 3.14 (s, 3 H, *c*

H), 6.03 (s, 2 H, *d H*), 7.32 – 7.41 (multi, 5 H, *e,f,g H*), 7.48 – 7.51 (multi, 1 H, *5 H*), 7.55 (dt, J = 7.6, 0.9 Hz, 1 H, *6 H*), 7.585 (dd, J = 7.5, 0.8 Hz, 1 H, *4 H*), 7.61 (d, J = 7.9 Hz, 1 H, *7 H*). ^{13}C NMR (600 MHz, $CDCl_3$) δ ppm: 16.56, 22.9, 46.14, 54.72, 115.65, 123.18, 126.74, 129.1, 129.4, 129.6, 129.96, 141.42, 141.46, 197.53.

4.3.10 Synthesis of 1-benzyl-3,3-trimethylspiro[indoline-2,3'-[3*H*]naphtha[2,1-b][1,4]oxazine], benzylated spirooxazine

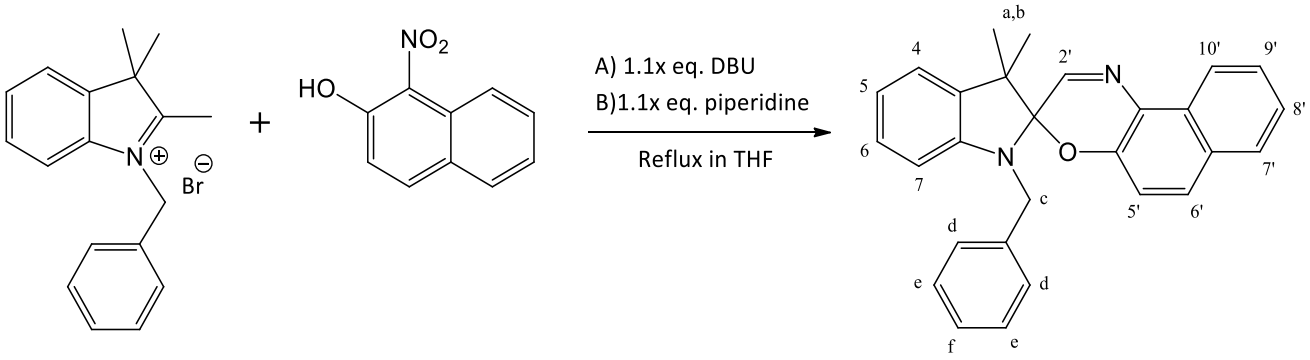

Scheme 4.9: Synthesis of 1-benzyl-3,3-trimethylspiro[indoline-2,3'-[3H]naphtha[2,1-b][1,4]oxazine].

Due to difficulties in handling as explained previously, the benzylated indole salt was solvated in ~ 100 mL of chloroform and divided approximately in half into two pre-weighed 100 mL round bottom flasks. The chloroform was then removed under vacuum and the remaining indole salt dried to get an approximate measurement of the amount used. Two reactions were run, differing in the strength of the organic based used:

Method A: to the indole salt (9.06077g, 2.909 x10^{-2} moles, 1.09 eq.) was added 1-nitroso-2-napthol (3.2713 g, 2.679 x10^{-2} moles, 1 eq.) and 50 mL of THF that had been sparged with nitrogen for 1 h prior to use along with a stirrer bar. DBU (4.1976 g, 2.757 x10^{-2} moles, 1.03 eq.) was weighed out in a separate scintillation vial, then added dropwise to the reaction mixture before being rinsed in with a further 20 mL of THF.

Method B: to the indole salt (10.008 g, 3.030 x10^{-2} moles, 1.10 eq.) was added 1-nitroso-2-napthol (3.3717 g, 2.761 x10^{-2} moles, 1 eq.) and 50 mL of THF that had been sparged with nitrogen for 1 h prior to use along with a stirrer bar. Piperidine (2.5943 g, 3.047 x10^{-2} moles, 1.10 eq.) was weighed out in a separate scintillation vial, and then added drop wise to the reaction mixture before being rinsed in with a further 20 mL of THF.

Both reaction vessels were fitted with a reflux condenser and heated to reflux under nitrogen for a period of 18 h with stirring. After the elapsed time, the volatiles were removed under vacuum. Both reaction mixtures were purified by column chromatography over silica gel using a mixture of toluene

: hexane (75 : 25 , v/v), Rf = 0.6. Further purification was achieved by recrystallisation from ethanol, followed by washing with cold methanol. The resulting compound was beige green and dried in a 50 °C oven overnight. For reaction A, obtained 1.6936 g (15.6 % yield) of compound, whilst for reaction B 1.8323 g (16.4 % yield) of compound was obtained. Characterisation of the purified compound from both batches showed identical ^{1}H NMR signals with only the trace amounts of impurities seen. ^{1}H NMR (600 MHz, $CDCl_3$) δ ppm: 1.435 (d, J = 42.3 Hz, 6 H, *a,b H*), 4.39 (dd, J = 96.5, 16.5 Hz, 2 H, *c H*), 6.38 (d, J = 7.9 Hz, 1 H, *7 H*), 6.9 (dt, J = 7.4, 0.9 Hz, 1 H, *5 H*), 7.035 (d, J = 8.8 Hz, 1 H, *5' H*), 7.1 (dt, J = 7.7, 1.3 Hz, 1 H, *6 H*), 7.125 (d. J = 7.2 Hz, 1 H, *4 H*), 7.25 (t, J = 7 Hz, 1 H, *f H*), 7.28-7.33 (multi, 4 H, *d,e H*), 7.4 (dt, J = 7.75, 1.1 Hz, 1 H, *8' H*), 7.56 (dt, J = .75, 1.1 Hz, 1 H, *9' H*), 7.685 (d, J = 9 Hz, 1 H, *6' H*), 7.755 (d, J = 8.1 Hz, 1 H, *7' H*), 7.78 (s, 1 H, *2' H*), 8.51 (d, J = 8.3 Hz, 1 H, *10' H*). ^{13}C NMR (600 MHz, $CDCl_3$) δ ppm: 20.8, 25.55, 48.44, 52.28, 108.08, 116.79, 120.04, 121.51, 121.53, 122.77, 124.18, 126.75, 127.1, 127.13, 127.73, 127.85, 128.58, 130.28, 134.77, 135.79, 138.17, 142.44, 143.94, 145.18, 147.13, 150.88.

4.3.11 Attempted synthesis of N-H terminated spirooxazine by de-benzylation of 1-benzyl-3,3-trimethylspiro[indoline-2,3'-[3*H*]naphtha[2,1-b][1,4]oxazine]

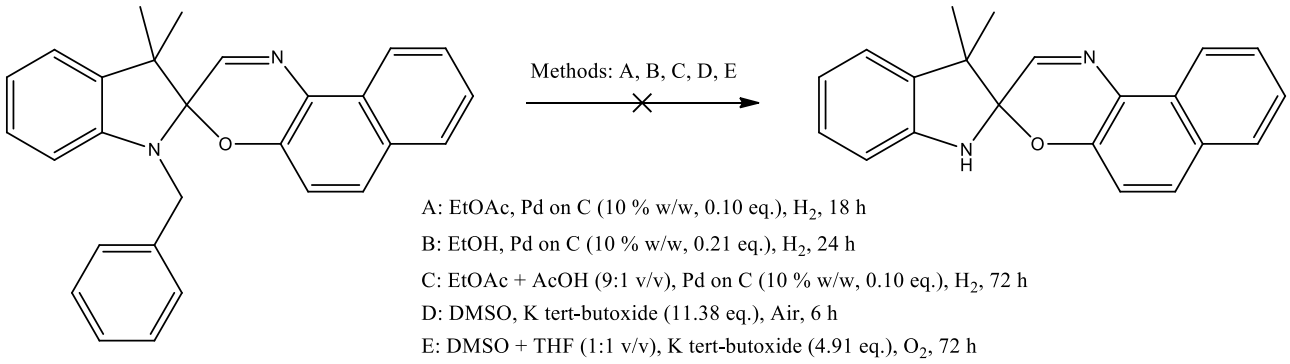

Scheme 4.10: Attempted de-benzylation of 1-benzyl-3,3-trimethylspiro[indoline-2,3'-[3*H*]naphtha[2,1-b][1,4]oxazine].

Regardless of the solvent used, methods **A** and **B** returned unreacted starting material as evidenced by ^{1}H NMR spectra before and after the reaction. Extending the reaction time and employing acetic acid as a catalyst (method **C**) did not overcome this issue, as only starting material was recovered as determined by ^{1}H NMR analysis. Method **D** conversely destroyed the starting material as evidenced by a large exotherm being observed upon the addition of the potassium tert-butoxide, with no starting material or any other photochromic products being detected by TLC analysis. This was confirmed by ^{1}H NMR analysis of the reaction mixture after drying, which showed many resonances covering large sections of the spectral window, making identification of individual components impractical. To try and prevent this, method **E** used only a stoichiometric equivalent of k tert-butoxide, however it was

evident that even after 36 h and the addition of a further equivalent of k tert-butoxide there was still starting material remaining as determined by TLC. After the addition of a further 2.93 equivalents of k tert-butoxide and 36 h of reaction time, all the starting material had been consumed. The two organic fractions (red and orange) extracted from the reaction mixture were both determined not to be the desired N-H terminated spirooxazine as determined by ^{1}H NMR. It is suspected that this treatment degraded the benzylated spirooxazine into derivatives of its constituent halves; this was evidenced by the red fraction still retained resonances clearly attributed to the benzyl group, while the orange fraction did not have all the resonances attributed to the indole half of the molecule. Furthermore, none of these fractions showed any photochromic properties. For full details of these reactions, please see section A1.2.2 in the Appendix.

Further investigations into the synthesis of a spirooxazine based dithiocarbamate were not pursued due to the difficulties encountered here, and due to spirooxazine based xanthates being much more synthetically accessible.

4.3.12 Synthesis of S-1-dodecyl-S'-((2-ethoxycarbonyl)-ethyl) trithiocarbonate (DECET)

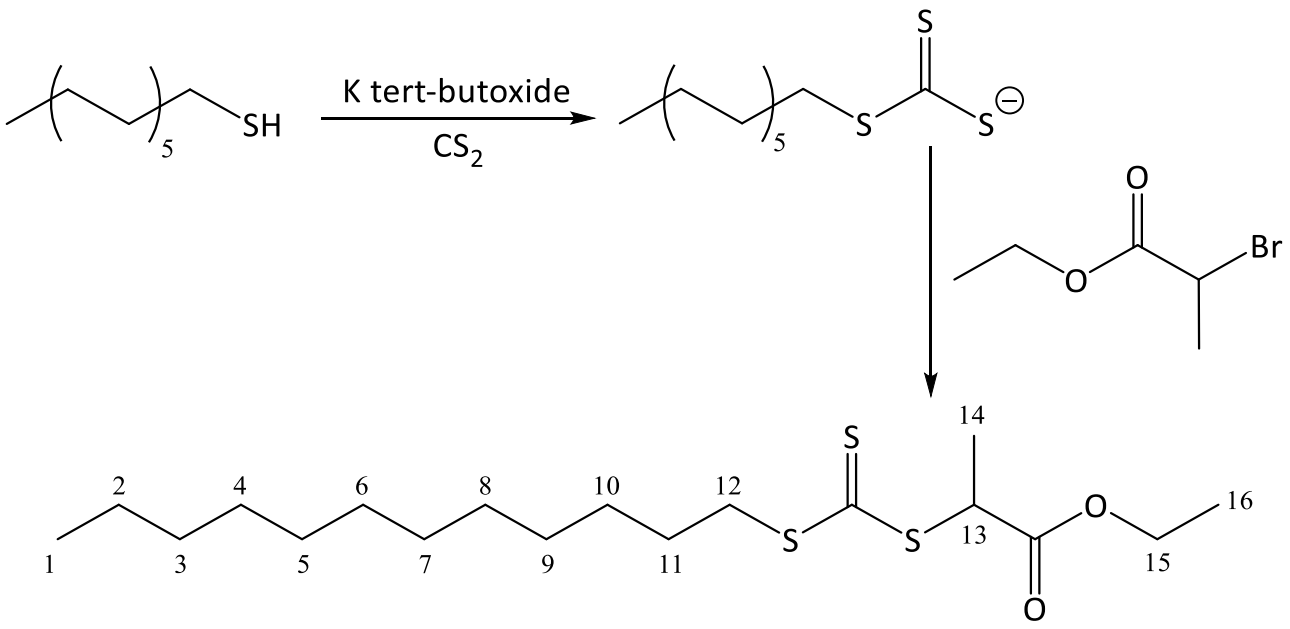

Scheme 4.11: Synthesis of S-1-dodecyl-S'-((2-ethoxycarbonyl)-ethyl) trithiocarbonate (DECET).

Into a flame dried 250 mL two neck round bottom flask equipped with a stirrer bar and a nitrogen inlet was placed potassium tert-butoxide (1.5662 g, 1.396 x10^{-2} moles, 1.11 eq.) along with 130 mL of anhydrous toluene. Dodecane thiol (2.5459 g, 1.25 x10^{-2} moles, 1.00 eq.) was mixed with 10 mL of anhydrous toluene in a scintillation vial, then added dropwise to the reaction vessel which was left to stir for 1 h. Carbon disulfide (2.8583 g, 3.75 x10^{-2} moles, 2.98 eq.) was mixed with 10 mL of

anhydrous toluene in a scintillation vial, then added slowly dropwise to the reaction vessel over a period of 5 minutes, causing a colour change to bright yellow. The reaction was left to stir at room temperature for a further 18 h. Ethyl 2-bromopropionate (4.5648 g, 2.52 x10^{-2} moles, 2.00 eq.) was mixed with 10 mL of anhydrous toluene in a scintillation vial, then added dropwise to the reaction mixture which intensified in colour to a darker yellow. This was left to stir at room temperature for a further 24 h, after which the reaction was halted by washing with ~ 200 mL of water, followed by washing with 50 mL of 5 % HCl solution to neutralise any remaining base. The organic layer was then washed with ~ 200 mL of saturated sodium bicarbonate solution, then with 200 mL brine to aid in separation. The aqueous washings were combined and back extracted with 2x of 75 mL of chloroform; the organic fractions were then combined and dried with sodium sulfate, filtered under gravity and the remaining solvent removed under vacuum. The product was purified by column chromatography over silica gel using a mixture of hexane : ethyl acetate (95 : 5, v/v), Rf = 0.33. Obtained 3.8507 g (80.85 % yield) of a viscous bright yellow oil. ^{1}H NMR (600 MHz, $CDCl_3$) δ ppm: 0.89 (t, J = 7.2 Hz, 3 H, *1 H*), 1.27-1.32 (multi, 19 H, *2-9,16 H*), 1.4 (q, J = 7.3 Hz, 2 H, *10 H*), 1.605 (d, J = 7.4 Hz, 3 H, *14 H*), 1.7 (q, J = 7.5 Hz, 2 H, *11 H*), 3.36 (t, J = 7.5 Hz, 2 H, *12 H*), 4.205 (dq, J = 7.2, 2.2 Hz, 2 H, *15 H*), 4.825 (q, J = 7.3 Hz, 1 H, *13 H*). ^{13}C NMR (600 MHz, $CDCl_3$) δ ppm: 14.08, 14.1, 16.96, 22.68, 27.89, 28.89, 29.08, 29.33, 29.42, 29.54, 29.62, 31.9, 37.23, 48.02, 61.85, 171.13 (C=O), 222.15 (C=S).

4.4 Use of light sources for polymerisation and characterization thereof

Two different light sources were employed in this work and they were selected based on spectral output, price and availability.

4.4.1 Characterisation of output spectrum of light sources used

Characterisation of the spectral output of both light sources was undertaken using an Ocean Optics Jaz Spectrometer, equipped with a JAZ-PX module and a pulsed xenon lamp (200 – 1100 nm operating range) operating in reflectance mode with a 10 msec integration time. All characterization of light sources was done in a room with blinds over the windows and all electronic light sources besides the required computer turned off. The dark reference was obtained in the manner as recommended in the instrument manual; the forked fibre optic cable was detached from the light source but left connected to the detector to collect data. This ensures that the dark reference is the level of ambient light in the room under which the light sources were characterised. The white reference was taken by reattaching the detector to the forked fibre optic cable and placing it directly

onto a Spectralon reference standard. As can be seen in Figure 4.3, the resulting spectrum is prone to significant noise in the < 250 nm region. For this reason, when plotting UV-Vis data within this thesis, data below 250 nm was omitted. Spectral characterization data for both lamps is presented where relevant in subsequent chapters.

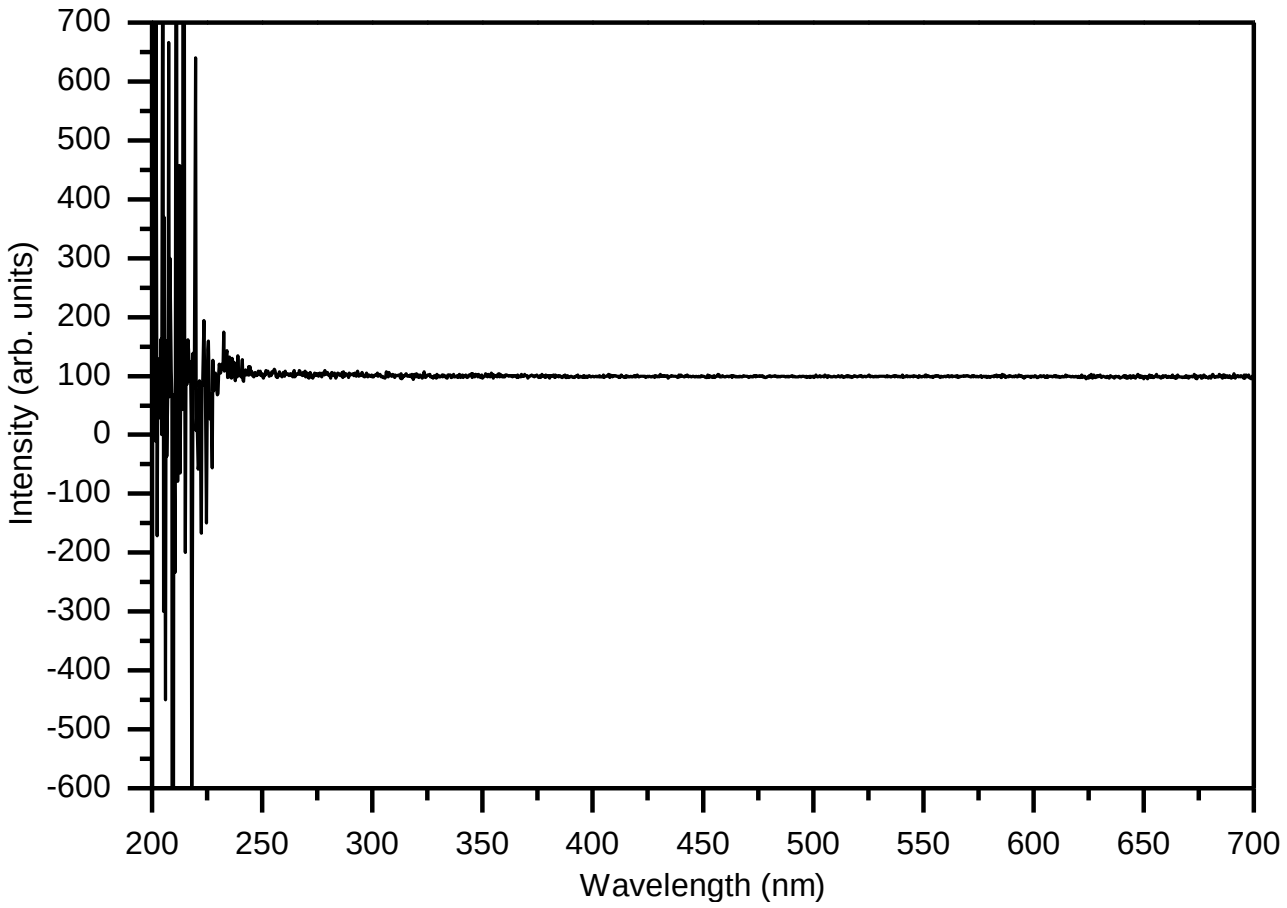

Figure 4.3: Emission intensity spectrum taken from the Spectralon white reference.

4.4.2 Characterisation of power output of light sources used

The power output of the 6W UV lamp was quantified using a Dymax ACCU-CAL ™ 50-LED (PN 40519), a self-contained LED radiometer with measuring probe which was used in peak intensity mode. The probe was placed in line with the face of the UV lamp at a distance of ~ 1 cm in the same manner as a Young's flask; this returned a reading of 2 mW/cm^2. Placing a Pyrex dish (same brand/thickness as the oil bath used) in between the detector and the UV lamp did not decrease this reading. The power output of the LED reactor (peak emission intensity at ~ 470 nm) could not be quantified as this radiometer has a spectral range of 360 – 450 nm.

4.4.3 Use of 6W UV lamp with traditional RAFT conditions

A Spectroline E-Series (Model ENF-260C) dual wavelength 6W UV lamp with a LONGLIFE™ filter assembly (part no. 2F006) was used for irradiation of polymerisation solutions. It was used exclusively in the 365 nm mode and placed perpendicular to the side of the oil bath at a distance of approximately 1 cm in order to illuminate the contents of the Young's flasks as is shown in Figure 4.4 (B). This was the setup used for reactions run under light + AIBN and light only polymerisation conditions. As stated previously, the peak emission was found to be 370nm with an overall power of 2 mW/cm^2 within the UV range. The stirring rate was set to ~ 350 – 400 rpm in all cases.

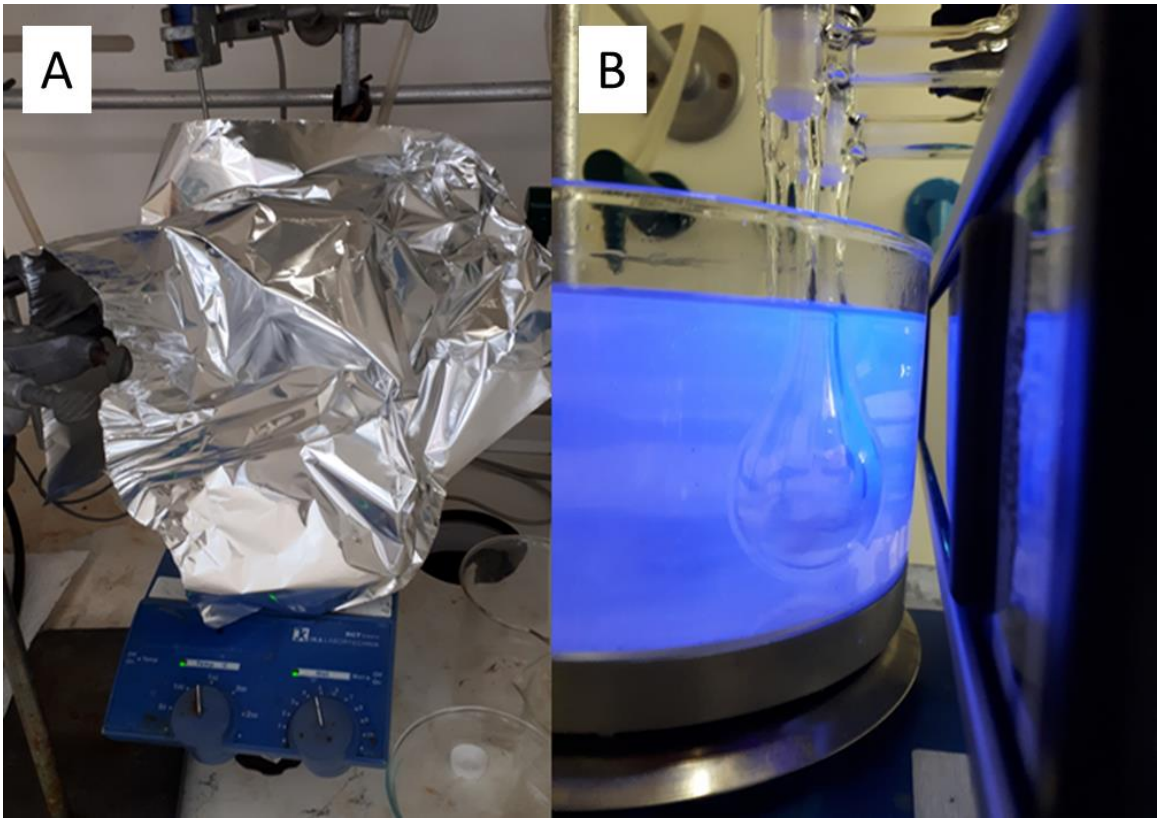

Figure 4.4: Reaction conditions employed; dark + AIBN (A) & under UV irradiation (light on + AIBN, light only) (B).

4.4.4 Construction and use of blue LED photochemical reactor at room temperature

A blue LED photochemical reactor was made by wrapping a 5 m long LED strip comprised of 300 individual 3528 SMD LEDs on the inside of a 2L glass beaker (internal diameter = 13 cm). This gave a spiral of LEDs that was distributed evenly over a height of 15 cm within the beaker. The power source was a 12 v DC transformer with an output of 2 A. The LED power consumption was listed as 4.8 W/m, which for the 5 m strip gives a total power of 24 W, or equivalent to the total output of the DC transformer. The luminous flux was stated to be 180-240 lumens/m. A complete specifications

sheet for this type of LED was obtained from Wayjun Technology [5] and can be found in the Appendix.

The LED strip and AC/DC transformer were purchased as a complete setup from eBay Australia. Aluminium foil was wrapped along the outside in order to maximise light intensity by allowing internal reflection of any stray light and to prevent interference from external light sources. This was then placed on top of an IKA hotplate to allow for stirring of the solutions when placed in the reactor, as shown in Figure 4.5.

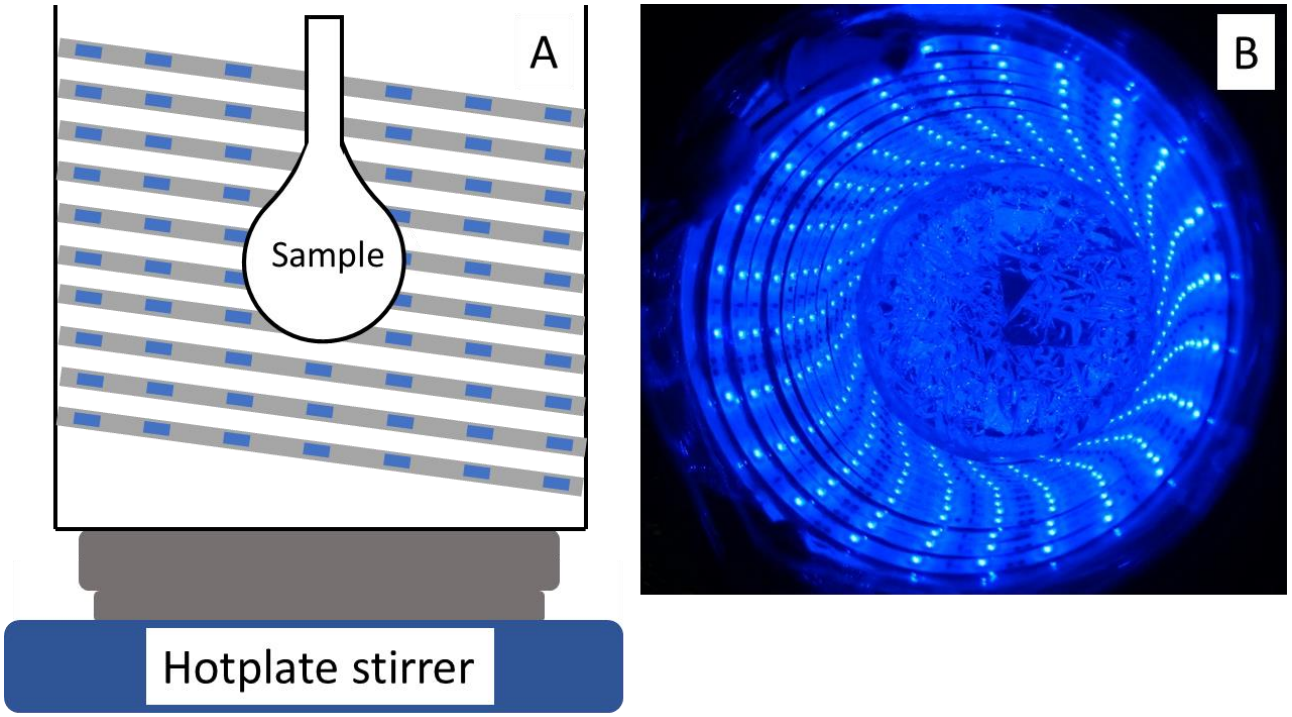

Figure 4.5: LED photo-reactor constructed for photoiniferter polymerisations at room temperature shown in schematic view (A) and top down view (B).

4.5 Polymer synthesis & purification of polymers

All polymerisations undertaken within this thesis followed the general procedures for making, handling and degassing of polymerisation solutions as outlined in sections 4.5.1 and 4.5.2.

An explanation of the formulas used to determine conversion by ^{1}H NMR analysis is provided later in section 4.2. The actual conversion attained for polymerisation experiments is provided in the relevant chapters and discussed where appropriate. Likewise, an explanation of the gel permeation chromatography (GPC) systems used in the molecular weight characterization of polymers is given in section 4.6, with the molecular weights obtained being discussed where relevant in the appropriate chapters.

4.5.1 General procedure for preparation and handling of polymerisation solutions

All polymerisation solutions were prepared in pre-weighed volumetric flasks. All liquid monomers had the inhibitor removed as described previously in section 4.1.1.2. The chosen RAFT agent/macroinitiator was weighed directly into the volumetric flask, followed by the monomer. For reactions requiring AIBN as initiator, a stock solution of AIBN was made using the given reaction solvent in a separate 5 mL volumetric to a known concentration, usually in the range of 4 – 5 mg/mL. Based on the absolute amount of AIBN required, the appropriate volume of stock initiator solution was then added to the volumetric flask containing RAFT agent and monomer by micropipette. When the required quantity of AIBN was large enough (> 20 mg), it was weighed out normally instead of a stock solution being made. The volumetric flask was then filled to the mark with the reaction solvent, stoppered and homogenised by gently inverting several times. A 0.5 mL aliquot of this stock polymerisation solution was extracted and placed in a freezer in a HPLC vial for subsequent NMR and UV-Vis analysis. The remaining mixture was then partitioned by glass pipette as evenly as possible between the required number of Young's flasks which were equipped with a small magnetic stirrer bar.

4.5.2 General freeze pump thaw (FPT) procedure

The Young's flasks were connected to a vacuum manifold capable of maintaining a pressure in the 5 – 8 x 10^{-3} mbar range. In pairs the flasks were then immersed in liquid nitrogen until frozen solid, then opened to vacuum for a period of ~ 20 minutes. Once the vacuum reading had stabilised, the flasks was sealed, allowed to warm to room temperature naturally, then the process repeated a further two times. On the third and final cycle prior to warming to room temperature, the flasks were backfilled with nitrogen that had been passed through a Drierite™ cartridge, then sealed and disconnected from the manifold.

4.5.3 Standard procedure for dark + AIBN conditions

For kinetic experiments where a series of 5 samples all from the same stock solution had to be polymerised under identical conditions in the dark, the Young's flasks were immersed in the oil bath 4 at a time, and the oil bath covered with aluminium foil in order to block out ambient light as shown in Figure 4.4, A. Once the first sample was withdrawn, the 5th and final sample was put in its place.

4.5.4 Standard procedure for light + AIBN and light only conditions with UV irradiation

For kinetic experiments where a series of 5 samples all from the same stock solution had to be polymerised under identical conditions under UV irradiation, at any one time only two samples were placed into the oil bath. This was done to ensure even irradiation, with extra care taken to place them equidistant (maintained at ~ 1 cm) from the surface of the UV lamp (370nm, 2 mW/cm^2). While waiting to be placed in the oil bath, the other samples were stored at room temperature in the dark to prevent inadvertent polymerisation. During the polymerisation, the oil bath was once again covered with aluminium foil as shown in Figure 4.4, A. For light only conditions, the procedure was the same however AIBN was omitted when making the stock polymerisation solution.

4.5.5 Standard procedure for simultaneous AIBN with/without UV irradiation conditions

For chain extension experiments which often required half of the polymerisation stock solution to be polymerised under dark + AIBN and the other under light + AIBN conditions; this was achieved by directly wrapping one flask in aluminium foil. The rest of the experimental procedure followed was as in sections 4.5.3 and 4.5.4.

4.5.6 RAFT polymerisation under blue LED irradiation

AIBN was omitted during the making of the stock polymerisation solution. The Young's flask was placed into the centre of the home-made LED reactor as shown in Figure 4.5 (A), with the stirring rate set to ~ 500 rpm. A stream of compressed air was blown into the centre of the reactor for the duration of the reaction to offset the effect of the LEDs naturally heating up during prolonged use, thus ensuring the reaction temperature inside the reactor was maintained at ~ 25 °C as measured by a thermometer suspended in the middle of the reactor next to the Young's flask.

4.5.7 Post polymerisation procedures

After the required amount of time had elapsed, the polymerisations were halted by removal from the oil bath and cooling to room temperature whilst simultaneously exposing the reaction mixture to air. Immediately after, 0.5 mL of the reaction mixture was withdrawn for NMR and UV-Vis analysis (placed in a HPLC vial in the freezer). The stirrer bar was removed. Processing the reaction mixture at this point depended on the reaction being conducted.

4.5.7.1 Recovery of samples from kinetic polymerisations of MA & VAc & homopolymer chain extension experiments thereof

Volatiles were removed under high vacuum to prevent further polymerisation. Once completely dry, the samples were re-solvated in ~ 15 mL of dichloromethane before being placed in 20 mL scintillation vials. The solvent was then primarily removed by blowing over with a stream of nitrogen, followed by drying in a vacuum oven overnight at 40 °C, ~ 35 mbar.

4.5.7.2 Recovery of samples from the synthesis of starting macroinitiators with MA and VAc

Depending on the viscosity of the reaction mixture, it was diluted with anywhere from 5 to 15 mL of dichloromethane. This was then precipitated into a 10-fold excess of a chilled hexane with rapid stirring in a beaker which was then covered will aluminium foil and left to chill in a freezer overnight. Given the low molecular weights of these macroinitiators, the collected polymer had a stringy glue-like consistency which made clean precipitation impossible. The hexane was then removed by slow decantation, with the remaining polymer washed gently with more chilled hexane which was also discarded. The polymer was then scraped into a pre-weighed scintillation vial, with any remaining polymer solvated out with dichloromethane and transferred accordingly. Removal of solvent and drying was achieved as in section 4.5.7.1.

4.5.7.3 Recovery of samples from the synthesis of starting macroinitiators with Sty

Same process of dilution as in section 4.5.7.1, with a 10-fold excess of chilled methanol used for precipitation. Samples were recovered by filtering the precipitate through a 0.45 μm PTFE filter under vacuum followed by rinsing with a further ~ 50 mL of chilled methanol. The polymer was then scraped off the filter on a pre-weighed watch glass and dried in a vacuum oven overnight at 40 °C, ~ 35 mbar.

4.5.7.4 Recovery of samples from the synthesis of poly(Sty-b-MMA) block copolymers

Due to the ease of precipitation of poly(Sty-b-MMA) block copolymers in methanol, the same procedures were followed as in section 4.5.7.3.

4.5.7.5 Recovery of samples from the synthesis of block copolymers with poly(MA) and poly(VAc) starting macroinitiators

This also applies to the synthesis of poly(MA-b-VAc), poly(VAc-b-MA) and poly(MA-b-MMA) block copolymers. Due to the difficulty in precipitation and recovering of starting poly(MA) and poly(VAc) macroinitiators, the same procedure was followed as in section 4.5.7.1. This ensured these

samples when analysed by GPC do not falsely appear to have an absence of the starting macroinitiator if it was not entirely consumed in the chain extension process.

4.5.8 Kinetic polymerisations of MA under standard conditions

These conditions were taken directly from a previous publication by Keddie *et al.* [6]. The ratio of reagents was maintained at [MA] : [RAFT] : [AIBN] = 6975 : 34: 1 which gives a theoretical M_n at 100 % conversion of 17800 g/mol. All kinetic experiments conducted under these conditions used the quantities of reagents as shown in Table 4.2. The stock solution was made to a volume of 10 mL using acetonitrile as solvent and the reaction temperature was 70 °C. Polymers were recovered as per section 4.5.7.1. Conversion was determined by using a ratio of proton resonances as shown in Equation 4.1, with an exemplary comparison of ^{1}H NMR spectra used for this purpose with annotated resonances shown in Figure 4.6.

Table 4.2: Summary of reagents used in the kinetic polymerisations of MA under standard conditions.

Kinetic polymerisations of MA with PXEP							
Conditions	Time (h)	MA (g)	[MA] (M)	RAFT (mg)	RAFT (mM)	AIBN (mg)	[AIBN] (mM)
Dark + AIBN	6	2.4126	2.80	37.0	13.68	0.66	0.40
Light + AIBN	6	2.4023	2.79	36.4	13.46	0.66	0.40
Light only	6	2.4038	2.79	36.8	13.61	N/A	N/A
Light only (short)	0.42	2.4129	2.80	37.2	13.76	N/A	N/A
Kinetic polymerisations of MA with Spiro-XEP							
Conditions	Time (h)	MA (g)	[MA] (M)	RAFT (mg)	RAFT (mM)	AIBN (mg)	[AIBN] (mM)
Dark + AIBN	6	2.4018	2.79	70.8	13.60	0.66	0.40
Light + AIBN	6	2.4075	2.80	70.8	13.60	0.66	0.40

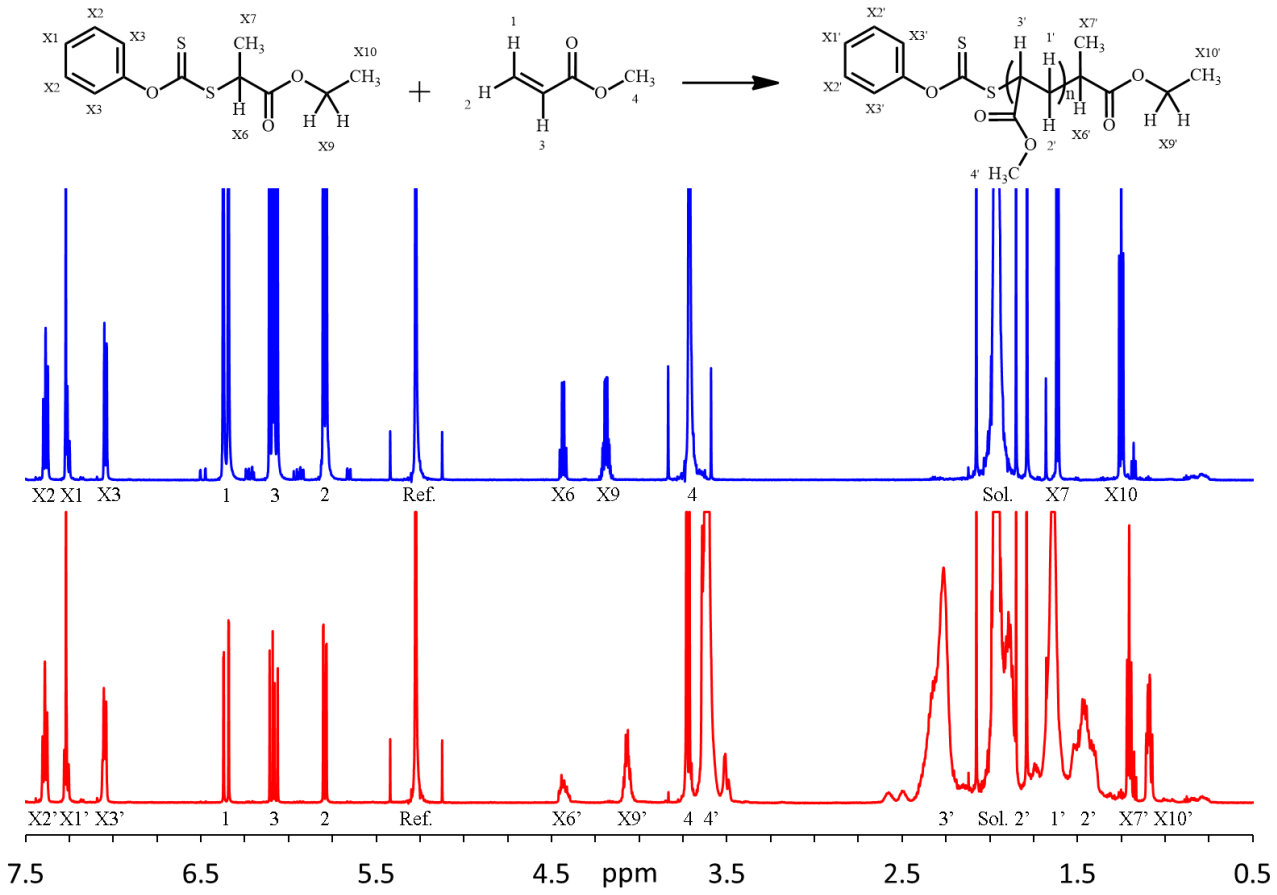

Figure 4.6: Exemplary ^{1}H NMR spectra for a polymerisation of MA with PXEP with annotated proton peaks; top spectrum is from the t = 0 h sample, bottom spectrum is from the t = 6 h sample. Scheme for polymerisation with annotated peak shown at top.

$$\%\ monomer\ remaining\ = \frac{\frac{\int(Peaks\ 1+2+3)\ @\ t=x}{\int_{0.5pm}^{3ppm}(Aliphatic\ region)\ @\ t=x}}{\frac{\int(Peaks\ 1+2+3)\ @\ t=0}{\int_{0.5pm}^{3ppm}(Aliphatic\ region)\ @\ t=0}}$$

$$\therefore\ \%\ monomer\ conversion = 100 - \%\ monomer\ remaining$$

Equation 4.1 Ratio of proton resonances used to calculate conversion for polymerisations of MA.

4.5.9 Synthesis of poly(MA) macroinitiator with PXEP for use in kinetic chain extension experiments with MA

PXEP (408.2 mg, 1.51 x 10^{-3} moles), MA (3.0161 g, 3.50 x 10^{-2} moles) and the appropriate amount of AIBN stock solution (in acetonitrile) to give 7.60 mg of AIBN. All reagents mixed to a total volume of 10 mL using acetonitrile. The resulting ratio of [MA]:[RAFT]:[AIBN] = 756.5 : 32.6 : 1 gives a

theoretical M_n at 100 % conversion of 2000 g/mol. Polymerisation time was 18 h under dark conditions and the reaction temperature was 70 °C. Purified and dried as in section 4.5.7.2. M_n = 2700 g/mol, M_w = 3210 g/mol and Đ = 1.18. Conversion determined using the same formula and proton resonances as shown in section 4.5.8.

4.5.10 Kinetic chain extension polymerisations of poly(MA) derived from PXEP under standard conditions

These conditions were analogous to those used previously in section 4.5.8, with the poly(MA) macroinitiator synthesised in section 4.5.9 used in place of PXEP. The ratio of reagents was maintained at [MA] : [poly(MA)] : [AIBN] = 7069.6 : 34: 1 which gives a theoretical M_n at 100 % conversion of 20606 g/mol. All kinetic experiments conducted under these conditions used the quantities of reagents as shown in Table 4.3. The stock solution was made to a volume of 10 mL using acetonitrile as solvent and the reaction temperature was 70 °C. Polymers were recovered as per section 4.5.7.1. Conversion determined using the same formula and proton resonances as shown in section 4.5.8.

Table 4.3: Summary of reagents used in the kinetic chain extension polymerisations of MA under standard conditions.

Kinetic polymerisations of MA with poly(MA) macroinitiator derived from PXEP							
Conditions	Time (h)	MA (g)	[MA] (M)	Poly(MA) (g)	Poly(MA) (mM)	AIBN (mg)	[AIBN] (mM)
Dark + AIBN	6.5	2.4149	2.81	0.3464	13.49	0.65	0.40
Light + AIBN	6	2.4212	2.81	0.3687	13.64	0.55	0.34
Light only	6	2.4188	2.81	0.3654	13.52	N/A	N/A

4.5.11 Synthesis of poly(MA) macroinitiator with Spiro-XEP for use in chain extension experiments with MA

Spiro-XEP (187.2 mg, 3.60 x 10^{-4} moles), MA (0.7198 g, 8.36 x 10^{-3} moles) and the appropriate amount of AIBN stock solution (in acetonitrile) to give 1.75 mg of AIBN. All reagents mixed to a total volume of 3 mL using acetonitrile. The resulting ratio of [MA]:[RAFT]:[AIBN] = 783.3 : 33.7 : 1 gives a theoretical M_n at 100 % conversion of 2000 g/mol. Polymerisation time was 18 h under light + AIBN conditions and the reaction temperature was 70 °C. Purified and dried as in section 4.5.7.2. M_n = 2300 g/mol, M_w = 2700 g/mol and Đ = 1.17. Conversion determined using the same formula and proton resonances as shown in section 4.5.8.

4.5.12 Chain extension polymerisations of poly(MA) derived from Spiro-XEP under standard conditions

These conditions were analogous to those used previously in section 4.5.8, with the poly(MA) macroinitiator synthesised in section 4.5.11 used in place of PXEP. Poly(MA) (84.6 mg, 3.65 x 10^{-5} moles), MA (1.2050 g, 1.40 x 10^{-2} moles) and the appropriate amount of AIBN stock solution (in acetonitrile) to give 0.14 mg (8.87 x 10^{-7} moles) of AIBN. All reagents mixed to a total volume of 5 mL using acetonitrile. The resulting ratio of [MA]:[RAFT]:[AIBN] = 15777.4 : 41.5 : 1 gives a theoretical M_n at 100 % conversion of 35014 g/mol. The polymerisation solution was divided in half; half was polymerised under dark + AIBN conditions whilst the other half was polymerised under light + AIBN conditions. In both cases polymerisation time was 18 h and the reaction temperature was 70 °C. Polymers were recovered as per section 4.5.7.1. Conversion determined using the same formula and proton resonances as shown in section 4.5.8.

4.5.13 Kinetic polymerisations of VAc under standard conditions

These conditions were taken directly from the same publication by Keddie *et al.* [6]. The ratio of reagents was maintained at [VAc] : [RAFT] : [AIBN] = 1764 : 10: 1 which gives a theoretical M_n at 100 % conversion of 15200 g/mol. All kinetic experiments conducted under these conditions used the quantities of reagents as shown in Table 4.4. The stock solution was made to a volume of 10 mL using acetonitrile as solvent and the reaction temperature was 70 °C. Polymers were recovered as per section 4.5.7.1. Conversion was determined by using a ratio of proton resonances as shown in Equation 4.2, with an exemplary comparison of ^{1}H NMR spectra used for this purpose with annotated resonances shown in Figure 4.7.

Table 4.4: Summary of reagents used in the kinetic polymerisations of VAc under standard conditions.

Kinetic polymerisations of VAc with PXEP							
Conditions	Time (h)	VAc (g)	[VAc] (M)	RAFT (mg)	RAFT (mM)	AIBN (mg)	[AIBN] (mM)
Dark + AIBN	6	5.4607	6.34	98.4	36.39	5.91	3.60
Light + AIBN	10	5.4739	6.36	97.3	35.99	6.00	3.66
Light only	10	5.4664	6.35	97.4	36.02	N/A	N/A
Kinetic polymerisations of VAc with Spiro-XEP							
Conditions	Time (h)	VAc (g)	[VAc] (M)	RAFT (mg)	[RAFT] (mM)	AIBN (mg)	[AIBN] (mM)
Dark + AIBN	10	5.4674	6.35	187.7	36.05	5.91	3.60
Light + AIBN	10	5.4604	6.34	188.0	36.11	5.91	3.60

Dark + AIBN & light + AIBN (longer time)	48	5.4947	6.38	188.9	36.28	5.90	3.60

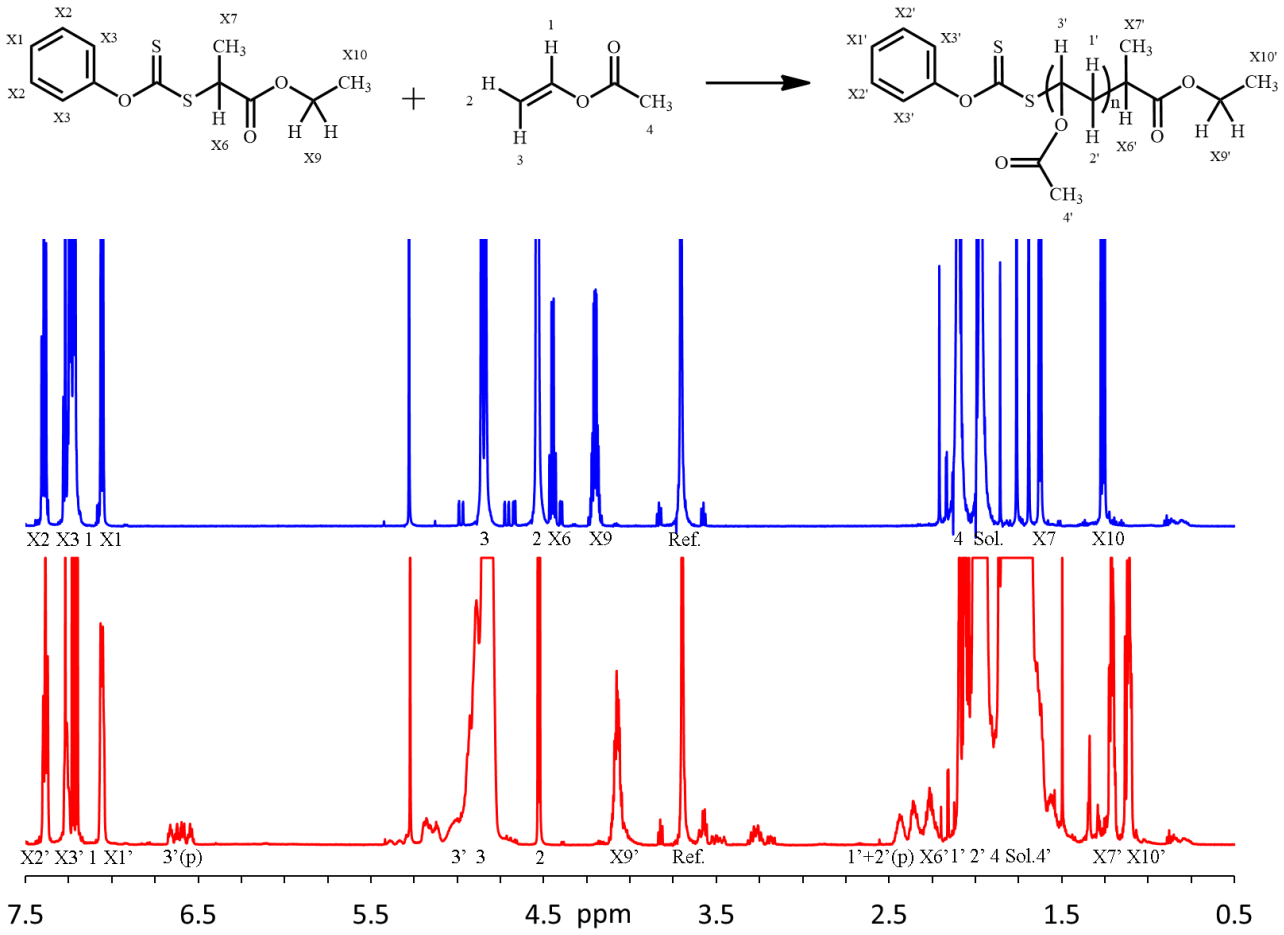

Figure 4.7: Exemplary ^{1}H NMR spectra for a polymerisation of VAc with PXEP with annotated proton peaks; top spectrum is from the t = 0 h sample, bottom spectrum is from the t = 10 h sample. Scheme for polymerisation with annotated peak shown at top.

$$\%\ monomer\ remaining\ = \frac{\frac{\int (Peaks\ 1+2)\ @\ t=x}{\int_{0.5pm}^{3ppm}(Aliphatic\ region)\ @\ t=x}}{\frac{\int (Peaks\ 1+2)\ @\ t=0}{\int_{0.5pm}^{3ppm}(Aliphatic\ region)\ @\ t=0}}$$

$$\therefore\ \%\ monomer\ conversion = 100 - \%\ monomer\ remaining$$

Equation 4.2: Ratio of proton resonances used to calculate conversion for polymerisations of VAc.

4.5.14 Synthesis of poly(VAc) macroinitiator with PXEP for use in kinetic chain extension experiments with VAc

PXEP (741.7 mg, 2.74 x 10^{-3} moles), VAc (5.484 g, 6.37 x 10^{-2} moles) and AIBN (44.8 mg, 2.73 x 10^{-4} moles) mixed to a total volume of 5 mL using acetonitrile. The resulting ratio of

[VAc]:[RAFT]:[AIBN] = 233.4 : 10 : 1 gives a theoretical M_n at 100 % conversion of 2000 g/mol. Polymerisation time was 18 h under dark conditions and the reaction temperature was 70 °C. Purified and dried as in section 4.5.7.2. M_n = 3250 g/mol, M_w = 3670 g/mol and Đ = 1.12. Conversion determined using the same formula and proton resonances as shown in section 4.5.13.

4.5.15 Kinetic chain extension polymerisations of VAc under standard conditions

These conditions were analogous to those used previously in section 4.5.8, with the poly(VAc) macroinitiator synthesised in section 4.5.14 used in place of PXEP. The ratio of reagents was maintained at [VAc] : [poly(VAc)] : [AIBN] = 1769.8 : 10 : 1 which gives a theoretical M_n at 100 % conversion of 18442 g/mol. All kinetic experiments conducted under these conditions used the quantities of reagents as shown in Table 4.5. The stock solution was made to a volume of 10 mL using acetonitrile as solvent and the reaction temperature was 70 °C. Polymers were recovered as per section 4.5.7.1. Conversion determined using the same formula and proton resonances as shown in section 4.5.13.

Table 4.5: Summary of reagents used in the kinetic chain extension polymerisations of VAc under standard conditions.

Kinetic polymerisations of VAc with poly(VAc) macroinitiator derived from PXEP							
Conditions	Time (h)	VAc (g)	[VAc] (M)	Poly(VAc) (g)	Poly(VAc) (mM)	AIBN (mg)	[AIBN] (mM)
Dark + AIBN	10	5.4772	6.36	1.1726	36.06	5.90	3.59
Light + AIBN	10	5.4025	6.28	1.1722	36.04	6.00	3.66
Light only	10	5.4729	6.36	1.1718	36.03	N/A	N/A

4.5.16 Synthesis of poly(VAc) macroinitiator with Spiro-XEP for use in kinetic chain extension experiments with VAc

Due to the incredibly low yield (< 20 %) of poly(VAc) when polymerised with Spiro-XEP, specific reactions were not run to synthesise a starting poly(VAc) macroinitiator. Instead the t = 10 h kinetic sample from the dark + AIBN kinetic reaction (section 4.5.13) was used in chain extension experiments with VAc. These kinetic samples were isolated and dried as in section 4.5.7.1. M_n = 1270 g/mol, M_w = 1550 g/mol and Đ = 1.22. Conversion determined using the same formula and proton resonances as shown in section 4.5.13.

4.5.17 Chain extension polymerisations of poly(VAc) derived from spiro-XEP under standard conditions

These conditions were analogous to those used previously in section 4.5.13, with the poly(VAc) macroinitiator described in section 4.5.16 used in place of PXEP. Poly(VAc) (49.0 mg, 3.86 x 10^{-5} moles), VAc (2.7334 g, 3.18 x 10^{-2} moles) and the appropriate amount of AIBN stock solution (in acetonitrile) to give 0.48 mg (2.96 x 10^{-6} moles) of AIBN. All reagents mixed to a total volume of 5 mL using acetonitrile. The resulting ratio of [VAc]:[RAFT]:[AIBN] = 10715 : 13 : 1 gives a theoretical M_n at 100 % conversion of 72058 g/mol. The polymerisation solution was divided in half; half was polymerised under dark + AIBN conditions whilst the other half was polymerised under light + AIBN conditions. In both cases polymerisation time was 18 h and the reaction temperature was 70 °C. Polymers were recovered as per section 4.5.7.1. Conversion determined using the same formula and proton resonances as shown in section 4.5.13.

4.5.18 Synthesis of poly(MA) macroinitiator with PXEP for use in block copolymer synthesis

PXEP (162.7 mg, 6.02 x 10^{-4} moles), MA (1.2037 g, 1.40 x 10^{-2} moles) and the appropriate amount of AIBN stock solution (in acetonitrile) to give 2.92 mg (1.78 x 10^{-5} moles) of AIBN. All reagents mixed to a total volume of 5 mL using acetonitrile. The resulting ratio of [MA]:[RAFT]:[AIBN] = 785.4 : 33.8 : 1 gives a theoretical M_n at 100 % conversion of 2000 g/mol. Polymerisation time was 6 h under dark conditions and the reaction temperature was 70 °C. Purified and dried as in section 4.5.7.2. M_n = 2320 g/mol, M_w = 2730 g/mol and Đ = 1.18. Conversion determined using the same formula and proton resonances as shown in section 4.5.8.

4.5.19 Synthesis of poly(VAc) macroinitiator with PXEP for use in block copolymer synthesis

PXEP (370.5 mg, 1.37 x 10^{-3} moles), VAc (2.7352 g, 3.18 x 10^{-2} moles) and AIBN (22.4 mg, 1.36 x 10^{-4} moles) mixed to a total volume of 5 mL using acetonitrile. The resulting ratio of [VAc]:[RAFT]:[AIBN] = 232.8 : 10 : 1 gives a theoretical Mn at 100 % conversion of 2000 g/mol. Polymerisation time was 6 h under dark conditions and the reaction temperature was 70 °C. Purified and dried as in section 4.5.7.2. M_n = 2670 g/mol, M_w = 3000 g/mol and Đ = 1.12. Conversion determined using the same formula and proton resonances as shown in section 4.5.13.

4.5.20 Synthesis of poly(MA-b-VAc) block copolymers with poly(MA) macroinitiator derived from PXEP

These conditions were analogous to those used previously in section 4.5.13, with the poly(MA) macroinitiator described in section 4.5.18 used in place of PXEP. Poly(MA) (300.5 mg, 1.3 x 10^{-4} moles), VAc (2.7325 g, 3.17 x 10^{-2} moles) and the appropriate amount of AIBN stock solution (in acetonitrile) to give 1.79 mg (1.09 x 10^{-5} moles) of AIBN. All reagents mixed to a total volume of 5 mL using acetonitrile. The resulting ratio of [VAc]:[poly(MA)]:[AIBN] = 2904.6 : 11.9 : 1 gives a theoretical M_n at 100 % conversion of 23743 g/mol. The polymerisation solution was divided in half; half was polymerised under dark + AIBN conditions whilst the other half was polymerised under light + AIBN conditions. In both cases polymerisation time was 18 h and the reaction temperature was 70 °C. Polymers were recovered as per section 4.5.7.1. Conversion determined using the same formula and proton resonances as shown in section 4.5.13.

4.5.21 Synthesis of poly(VAc-b-MA) block copolymers with poly(VAc) macroinitiator derived from PXEP

These conditions were analogous to those used previously in section 4.5.8, with the poly(VAc) macroinitiator described in section 4.5.19 used in place of PXEP. Poly(VAc) (144.2 mg, 5.39 x 10^{-5} moles), MA (1.2123 g, 1.41 x 10^{-2} moles) and the appropriate amount of AIBN stock solution (in acetonitrile) to give 0.23 mg (1.43 x 10^{-6} moles) of AIBN. All reagents mixed to a total volume of 5 mL using acetonitrile. The resulting ratio of [VAc]:[poly(MA)]:[AIBN] = 9875.5 : 37.8 : 1 gives a theoretical M_n at 100 % conversion of 25155 g/mol. The polymerisation solution was divided in half; half was polymerised under dark + AIBN conditions whilst the other half was polymerised under light + AIBN conditions. In both cases polymerisation time was 18 h and the reaction temperature was 70 °C. Polymers were recovered as per section 4.5.7.1. Conversion determined using the same formula and proton resonances as shown in section 4.5.8.

4.5.22 Synthesis of poly(Sty) macroinitiators for use in block copolymer synthesis

PXEP, Spiro-XEP and DECET were used to synthesise short poly(Sty) macroinitiators. The reagents used are given in Table 4.6, and they were mixed to a total volume of 5 mL using toluene. The resulting ratio of [Sty]:[RAFT]:[AIBN] gave a theoretical M_n at 100 % conversion of 2261, 2551 and 2793 g/mol with PXEP, Spiro-XEP and DECET respectively. Polymerisation time was 20 h under dark conditions and the reaction temperature was 70 °C. Purified and dried as in section 4.5.7.3. Conversion was determined by using a ratio of proton resonances as shown in Equation 4.3, with an

exemplary comparison of ^{1}H NMR spectra used for this purpose with annotated resonances shown in Figure 4.8.

Table 4.6: Summary of reagents used in the synthesis of poly(Sty) macroinitiators that were subsequently used in the synthesis of poly(Sty-b-MMA).

Synthesis of poly(Sty) macroinitiators for use in block copolymer synthesis									
RAFT agent	Time (h)	Sty (g)	[Sty] (M)	RAFT (g)	RAFT [M]	AIBN (mg)	[AIBN] (mM)	M_n (g/mol)	Đ
PXEP	20	2.2658	4.35	0.3077	0.228	12.4	15.11	1730	1.16
Spiro-XEP	20	2.2751	4.36	0.5942	0.228	12.6	15.35	1590	1.19
DECET	20	3.4021	6.53	0.4162	0.244	27.6	33.63	2710	1.10

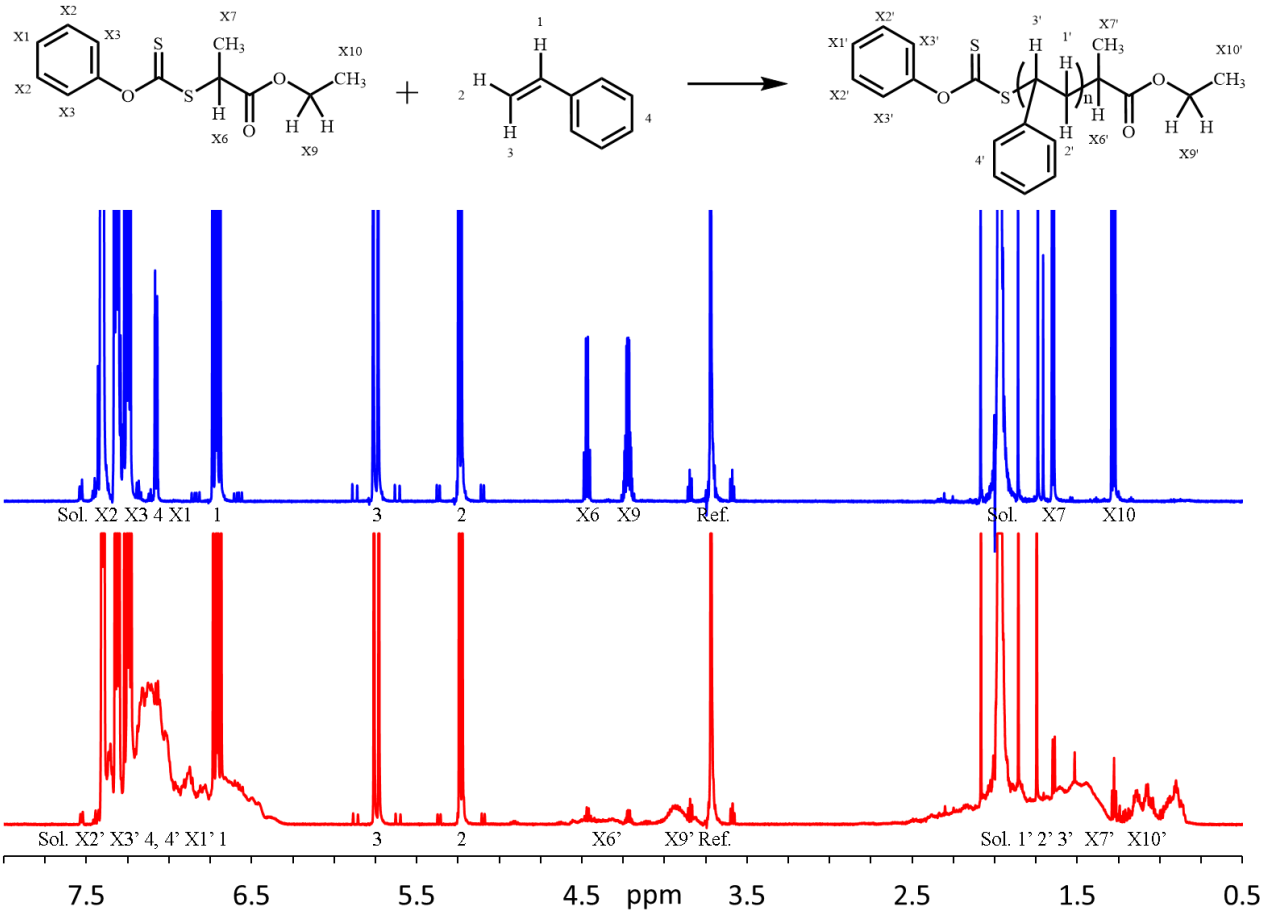

Figure 4.8: Exemplary ^{1}H NMR spectra for a polymerisation of Sty with PXEP with annotated proton peaks; top spectrum is from the t = 0 h sample, bottom spectrum is from the t = 20 h sample. Scheme for polymerisation with annotated peak shown at top.

$$\%\, monomer\ remaining\ = \frac{\frac{\int (Peaks\ 2+3)\ @\ t=x}{\int_{0.5pm}^{3ppm}(Aliphatic\ region)\ @\ t=x}}{\frac{\int (Peaks\ 2+3)\ @\ t=0}{\int_{0.5pm}^{3ppm}(Aliphatic\ region)\ @\ t=0}}$$

$$\therefore \%\ monomer\ conversion = 100 - \%\ monomer\ remaining$$

Equation 4.3: Ratio of proton resonances used to calculate conversion for polymerisations of Sty.

4.5.23 Synthesis of poly(Sty-b-MMA) block copolymers

The poly(Sty) macroinitiators described in section 4.5.22 were used, with the quantities of all reagents used listed in Table 4.7. All reagents mixed to a total volume of 5 mL using toluene. The polymerisation solutions were divided in half; half was polymerised under dark + AIBN conditions whilst the other half was polymerised under light + AIBN conditions. In both cases the reaction temperature was 70 °C. Under LED conditions, the reaction temperature was ~ 25 °C. All polymers were recovered as per section 4.5.7.3. Conversion was determined by using a ratio of proton resonances as shown in Equation 4.4, with an exemplary comparison of ^{1}H NMR spectra used for this purpose with annotated resonances shown in Figure 4.9.

Table 4.7: Summary of reagents used in the synthesis of poly(Sty-b-MMA) block copolymers.

PXEP poly(Sty) macroinitiator							
Conditions	Time (h)	MMA (g)	[MMA] (M)	Poly(Sty) (g)	Poly(Sty) (mM)	AIBN (mg)	[AIBN] (mM)
Dark + AIBN	20	0.5033	1.01	0.0341	3.94	0.64	0.79
Light + AIBN							
Dark + AIBN	20	1.5204	3.04	0.1004	11.61	0.96	1.17
Light + AIBN							
Spiro-XEP poly(Sty) macroinitiator							
Dark + AIBN	20	0.5028	1.00	0.0331	3.48	0.68	0.84
Light + AIBN							
Dark + AIBN	20	1.5114	3.02	0.1000	10.52	1.03	1.26
Light + AIBN							
DECET poly(Sty) macroinitiator							
Dark + AIBN	20	0.5239	1.05	0.0600	2.21	0.25	0.15
Light + AIBN							
LED	60	0.5054	1.01	0.0601	2.22	N/A	N/A

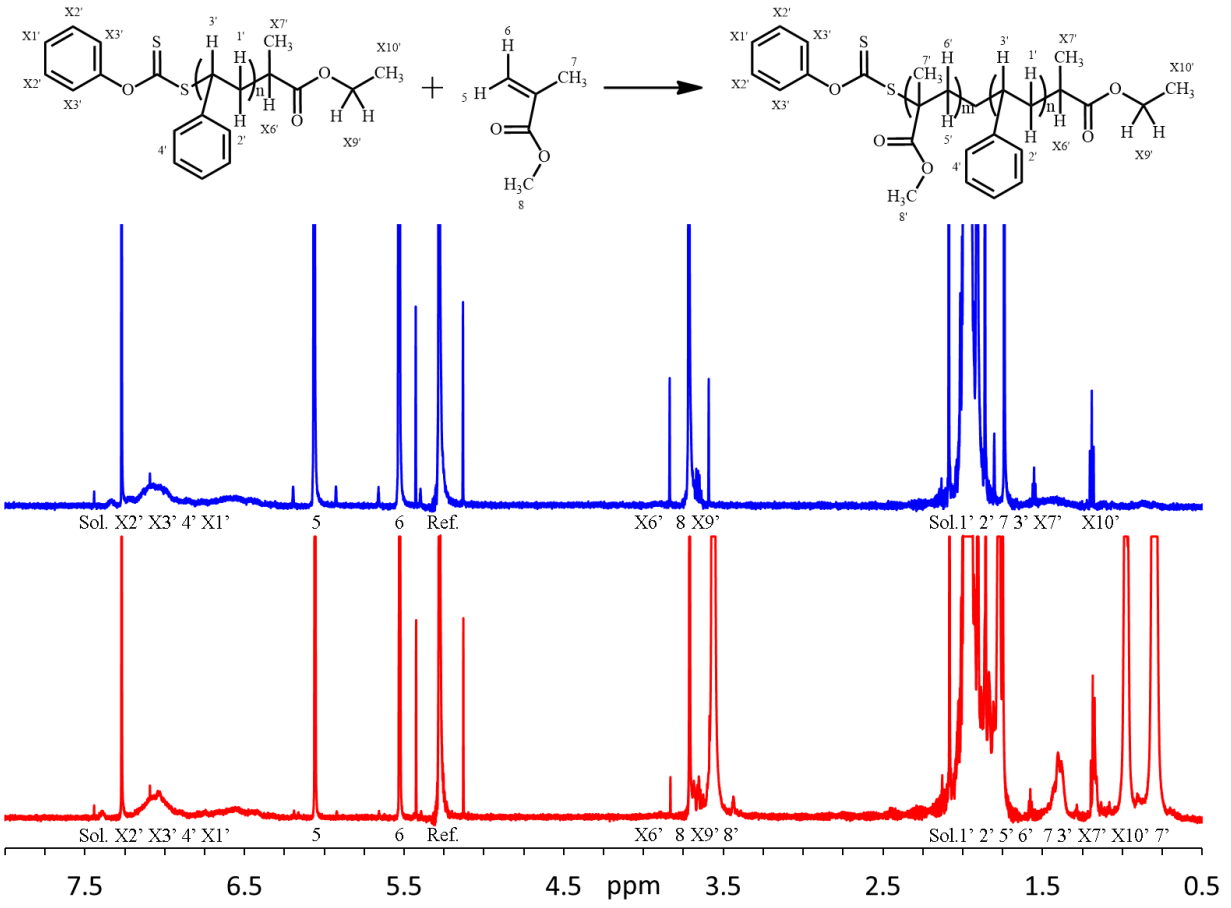

Figure 4.9: Exemplary ^{1}H NMR spectra for a polymerisation of MMA with poly(Sty) macroinitiator derived from PXEP with annotated proton peaks; top spectrum is from the t = 0 h sample, bottom spectrum is from the t = 20 h sample. Scheme for polymerisation with annotated peak shown at top.

$$\% \, conversion \; = \; \frac{\frac{\int (Peaks \; 5 + 6 + 8) \;\; @ \, t = x}{\int_{0.5pm}^{3ppm} (Aliphatic \; region) \;\; @ \, t = x}}{\frac{\int (Peaks \; 5 + 6 + 8) \;\; @ \, t = 0}{\int_{0.5pm}^{3ppm} (Aliphatic \; region) \;\; @ \, t = 0}}$$

$$\therefore \% \, monomer \; conversion = 100 - \% \, monomer \; remaining$$

Equation 4.4: Ratio of proton resonances used to calculate conversion for polymerisations of MMA.

4.5.24 Synthesis of poly(MA) macroinitiators for use in block copolymer synthesis

PXEP and DECET were used to synthesise short poly(MA) macroinitiators. The reagents used are given in Table 4.8, and they were mixed to a total volume of 5 mL using acetonitrile. The resulting ratio of [MA]:[RAFT]:[AIBN] gave a theoretical M_n at 100 % conversion of 2596 and 2699 g/mol with PXEP and DECET respectively. Polymerisation time was 6 h under dark conditions and the reaction temperature was 70 °C. Purified and dried as in section 4.5.7.2. Conversion determined using the same formula and proton resonances as shown in section 4.5.8.

Table 4.8: Summary of reagents used in the synthesis of poly(Sty) macroinitiators that were subsequently used in the synthesis of poly(Sty-b-MMA).

Synthesis of poly(MA) macroinitiators for use in block copolymer synthesis									
RAFT agent	Time (h)	MA (g)	[MA] (M)	RAFT (g)	RAFT [M]	AIBN (mg)	[AIBN] (mM)	M_n (g/mol)	Đ
PXEP	6	1.2037	2.80	0.1627	0.120	2.92	3.56	2320	1.18
DECET	6	2.4061	2.79	0.4567	0.121	5.83	3.56	2520	1.06

4.5.25 Synthesis of poly(MA-b-MMA) block copolymers

The poly(MA) macroinitiators described in section 4.5.24 were used, with the quantities of all reagents used listed in Table 4.9. All reagents mixed to a total volume of 5 mL using acetonitrile. The polymerisation solutions were divided in half; half was polymerised under dark + AIBN conditions whilst the other half was polymerised under light + AIBN conditions. In both cases the reaction temperature was 70 °C. Under LED conditions, the reaction temperature was ~ 25 °C. All polymers were recovered as per section 4.5.7.1. Conversion was determined by using a ratio of proton resonances as shown in Equation 4.5, with an exemplary comparison of ^{1}H NMR spectra used for this purpose with annotated resonances shown in Figure 4.10.

Table 4.9: Summary of reagents used in the synthesis of poly(Sty-b-MMA) block copolymers.

PXEP poly(MA) macroinitiator							
Conditions	Time (h)	MMA (g)	[MMA] (M)	Poly(Sty) (g)	Poly(Sty) (mM)	AIBN (mg)	[AIBN] (mM)
Dark + AIBN	10	0.5059	1.01	0.0534	4.61	0.72	0.88
Light + AIBN							
DECET poly(MA) macroinitiator							
Dark + AIBN	10	0.5038	1.01	0.0562	4.45	0.73	0.88
Light + AIBN							
LED	60	0.5036	0.97	0.0557	21.40	N/A	N/A

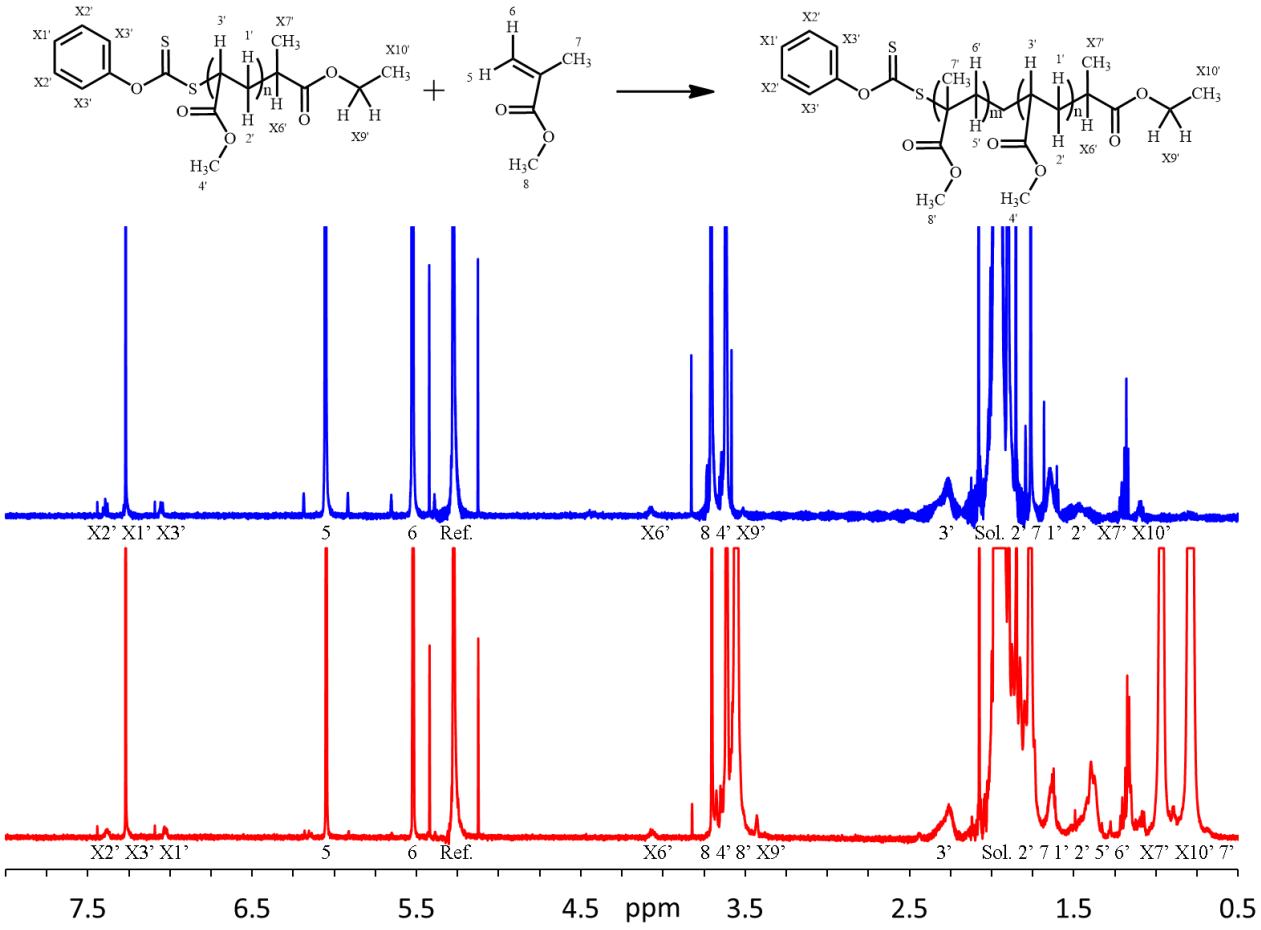

Figure 4.10: Exemplary ^{1}H NMR spectra for a polymerisation of MMA with poly(MA) macroinitiator derived from PXEP with annotated proton peaks; top spectrum is from the t = 0 h sample, bottom spectrum is from the t = 20 h sample. Scheme for polymerisation with annotated peak shown at top.

$$\% \, conversion \; = \; \frac{\frac{\int (Peaks \; 5 + 6 + 8) \;\; @ \; t = x}{\int_{0.5pm}^{3ppm} (Aliphatic \; region) \;\; @ \; t = x}}{\frac{\int (Peaks \; 5 + 6 + 8) \;\; @ \; t = 0}{\int_{0.5pm}^{3ppm} (Aliphatic \; region) \;\; @ \; t = 0}}$$

$$\therefore \% \, monomer \; conversion = 100 - \% \, monomer \; remaining$$

Equation 4.5: Ratio of proton resonances used to calculate conversion for polymerisations of MMA.

4.5.26 Control polymerisations under UV irradiation

The same conditions were used as described in section 4.5.8 and 4.5.13 however no RAFT agent or AIBN was added. All other parameters and post polymerisation proceedures were the same.

4.5.27 Control polymerisations under LED irradiation

Four individual monomer solutions (MA, MMA, Sty & VAc) were made up to 50 % (v/v) monomer concentration in acetonitrile in volumetric flasks, then transferred to Young's flasks and degassed as

described in section 4.5.2. The solutions were then irradiated in the LED reactor for a period of 12 h at room temperature, followed by recovery of samples as described in section 4.5.7.2.

4.6 Gel permeation chromatography (GPC) of polymer samples

4.6.1 Sample preparation and handling

All polymer samples including GPC standards were weighed by placing in pre-weighed glass scintillation vials, a quantity of ~ 7 to 10 mg was commonly used, with the appropriate amount of GPC grade THF added via micropipette in order to achieve a concentration of 2 mg/mL. The vial was then sealed and left to stand for at least 12 h, iideally for 24 h for GPC standards due to the large molecular weights of several of the standards. This was to allow for complete solvation and relaxation of the polymer chains in solution and was aided by agitation and shaking every few hours. The polymer solution was then transferred by glass pipette to a syringe with a PTFE plunger fitted with a 0.45 µm PTFE filter, and was then filtered directly into a GPC vial for analysis. It is important not to use conventional syringes with rubber plungers as these tend to contain a polymeric lubricant which introduces an impurity peak in the GPC traces.

4.6.2 Details of single detector system

The single detector system was comprised of a Waters 2690 Separation Module, a Waters 410 differential refractometer, with an Agilent guard column followed by two Agilent PLgel 5µm MiniMIX-C columns used in series and HPLC grade tetrahydrofuran as solvent. System parameters were as follows: 0.2 mL/min flow rate, both the detector and column temperatures were 25 °C and run time was 45 minutes with a 10 minute delay between samples. The system was calibrated using a series of narrow monodisperse polystyrene standards from Agilent with a Mp range (1320 – 990500 g/mol). A third order polynomial was fitted for the calibration curve of $\log_{10}$ Mp versus run time, which was approximately linear over the calibration range. Samples were run at a concentration of 2 mg/mL with an injection volume of 10 µL. M_n, M_w and Đ values were obtained by analysing the data using Waters Empower software. The resulting molecular weight values (M_n in polystyrene equivalents) were converted into PMMA equivalents followed by conversion into the molecular weights for the relevant monomer (MA and VAc) using the Mark-Houwink-Kuhn-Sakurada (MHKS) equation (Equation 2.54) and the parameters as determined by Gruendling *et al.* [7]. For block copolymers analysed on this system, the molecular weights were left as polystyrene equivalents. For a spectrum obtained with a THF blank, see Figure A5 in the Appendix. In regard to the uncertainty

in the values obtained, a 2500 g/mol polystyrene standard analysed 3 times over the course of a few days returned values that were within 10 g/mol of one another, which represents an error of ~ 0.5 %.

4.6.3 Details of dual detector GPC system

The dual detector system was comprised of a Waters Associates liquid chromatograph equipped with a Waters 2420 Refractive Index Detector (RID) and a Waters 2996 Photodiode Array Detector (PDA). Four Polymer Laboratories PLGel (3 x 5 μm Mixed-C and 1 x 3 μm Mixed-E) columns were used in series and HPLC grade tetrahydrofuran as solvent. System parameters were as follows: 1.0 mL/min flow rate, both the detector and column temperature was 35 °C and run time was 45 minutes with no delay between samples. The system was calibrated using a series of narrow monodisperse poly(methyl methacrylate) standards from Agilent. A third order polynomial was fitted for the calibration curve of $\log_{10}$ Mp versus run time, which was approximately linear over the calibration range (2 x 10^2 – 2 x 10^6 g/mol). Samples were run at a concentration of 2 mg/mL with an injection volume of 10 μL. M_n, M_w and Đ values were obtained by analysing the data using Waters Empower software and all molecular weight values are reported as PMMA equivalents. The calibration curve was used in processing RID data, but not PDA data as the samples pass through the PDA detector with a miniscule but variable delay. This makes application of the calibration curve not strictly valid. Furthermore, the PDA detector's main utility is in the detection of RAFT end groups which have two key absorbance peaks at unique wavelengths, at which the PMMA standards do not absorb.

4.6.4 Filtering and presentation of data

Data from the single detector GPC system was exported as a text format file and processed directly in Origin software, with the data presented being cut off slightly prior to the injection event and before any peaks of interest are present. This was done to maximise the size and impact of the plotted data and remove areas where nothing of interest was present. The RI data from the dual detector system was exported as a text format file and baseline corrected in Origin software. Due to the large file size and 3D nature of the PDA data, this was first imported into Microsoft Excel and only the data at the relevant wavelength corresponding to an absorbance from the RAFT group was selected from the large array. This data was then baseline corrected in Origin. The key reason behind the dual detector system data needing baseline correction lies in the way the two instruments are operated; the single detector system continuously pumps solvent at the same flow rate as when samples are run (0.2 mL/min), whilst the dual detector system undergoes an initial ramp from 0.1 mL/min up to 1.0 mL/min followed by period of flow at 1.0 mL/min to condition the column prior to sample injection. Such changes in operating pressure can cause baseline fluctuations.

4.6.5 Estimation of macroinitiator consumption using dual detector GPC data

The percentage of a macroinitior consumed during a block copolymerisation expeirment was estimated using the UV signal corresponding to the RAFT moiety as obtained from the dual detector GPC. Integration of the two peak areas as shown in Figure 4.11, and using Equation 4.6 the % of starting macroinitiator consumed was calculated.

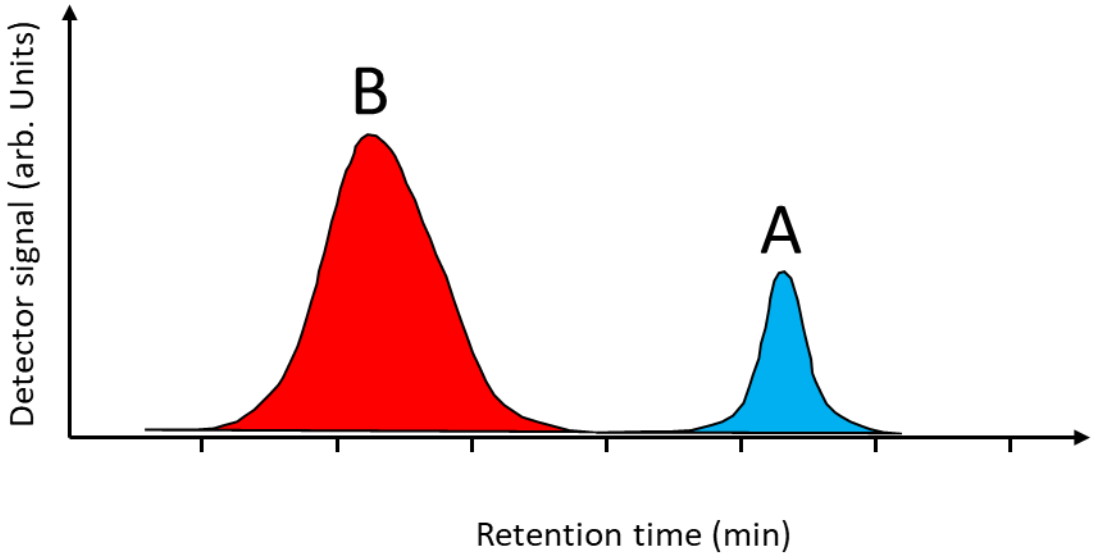

Figure 4.11: Generalised representation of two GPC peaks for integration.

$$\%\, macroinitiator\ consumed = \frac{Area\ B - Area\ A}{(Area\ A + Area\ B)} \times 100$$

Equation 4.6: General method for calculating the % of macroinitiator consumed during block copolymerisation.

4.7 Ultraviolet visible spectroscopy

4.7.1 Standard instrumentation and experimental setup

UV-Vis spectra of all samples were obtained using a Varian Cary 60 Spectrophotometer set to operate in absorbance mode, with a medium scan speed (600 nm/min), giving a resolution of 1 nm spacing between data points. In all experiments a quartz cuvette with a path length of 1 cm was used. Prior to each set of measurements being taken, a blank was first run with the same solvent (from the same bottle) as the samples to be measured were dissolved in, and the instrument then zeroed. This baseline was then automatically subtracted from data obtained in the subsequent runs by the Cary WinUV software.

4.7.2 Sample preparation for analysis of small molecules and polymers

For analysis of small molecules and polymers, a stock solution was made to a fixed concentration in a 5 mL volumetric flask. Further dilutions from this stock solution were done via micropipette by placing small aliquots of the stock solution into scintillation vials containing a pre-determined amount of the same solvent (also measured by micropipette) followed by rapid agitation to ensure mixing. In-between samples, the cuvette was rinsed twice with ethanol and dried with a stream of nitrogen.

4.7.3 Non-standard instrumentation and direct analysis of polymerisation mixtures

UV-Vis spectra of polymerisation mixture samples were obtained using a Thermo Scientific NanoDrop 1000 spectrophotometer. As per the standard operating procedure, the instrument was zeroed with water and then blanked with the solvent present within the polymerisation mixture (most commonly acetonitrile). The polymerisation solution was applied directly without dilution to the sensor in 3 µL aliquots via s micropipette. The path length is automatically fixed at 1 mm and spectra were taken with the normalisation and high absorbance modes enabled.

4.8 Equations used for calculating parameters from experimental data

4.8.1 Chain transfer constants for kinetic polymerisation samples

The chain transfer constants as a function of conversion and dispersity were estimated using the method of Goto & Fukuda [8], as shown in in Equation 4.7. D = dispersity, c = conversion, X_n = average chain length of polymer and C_{tr} = chain transfer constant.

$$D \approx 1 + \frac{1}{X_n} + \frac{2 - c}{c \cdot C_{tr}}$$

Equation 4.7: Approximation for estimating the chain transfer constant developed by Goto and Fukuda [8].

4.8.2 Estimating percentage of living chain ends in a macro-RAFT agent under ideal circumstances

The percentage of living chain ends for a given macroinitiator was estimated using Equation 4.8; this assumes the ideal case that there are no side reactions other than those associated with initiation and termination [9].

$$\%\ living\ ends = \frac{[RAFT]_0}{[RAFT]_0 + (d \cdot f \cdot [AIBN]_0 \cdot (1 - e^{(-kd \cdot t)}))}$$

Equation 4.8: Estimation for the percentage of living chain ends carrying the RAFT moiety.

Where d = the number of radicals consumed per termination event (set to 1), f = AIBN efficiency (set to 0.7) and k_d is the kinetic rate coefficient for AIBN dissociation (set to 1.683 x10^{-5} s^{-1}).

4.9 Predici model

4.9.1 Implementation of RAFT mechanism

The model used in this thesis was developed based on a simplified RAFT model which was kindly provided to the candidate by the author of Predici program, Dr. Michael Wulkow, via a collaboration with Dr. Graeme Moad at CSIRO, Clayton. Initially this simplified model featured a single step implementation of the pre-equilibrium and core equilibrium; both were changed to match the often-utilised reaction scheme as detailed by Vana *et al.* [10] with a few reactions removed and photolysis reactions added.

4.9.2 Implementation of photolysis reactions

The original model utilised a secondary "abstract" reactor and associated script and "dummy" species required to initialise it in the model, along with the flask reactor which houses the species used in the simulation. The initial model featured several scripts used to simulate a pulsed laser polymerisation with a periodic breakdown of initiator; these were removed due to not representing the constant irradiation used experimentally, and due to prohibitive simulation times of ~ 2 h for a reaction time of 6 h. The photolysis reactions were implemented such that each reaction has a defined kinetic rate coefficient which can be adjusted independently or modified with scripts. Removal of the "pulse" scripts gave much shorter simulation times of ~ 5 mins per 6 h experiment. It was necessary to retain the abstract reactor as this allowed a fictive species called "photon" to be added; this species required parameters for density, molecular weight and mass, which were all arbitrarily set. The concentration of photons was set to 1 M for simplicity, such that the kinetic rate coefficients chosen could be directly related to other parameters. Even though the "photon" species was in the separate "abstract" reactor, it could be used freely in constructing reactions from reaction modules which used species from the flask reactor. The "photon" species was required as there was no suitable reaction module with which to simulate the direct initiation of the monomer to form a macro-radical of chain length 1 (reaction 18, Scheme 4.12).

The forward reactions for the photolysis of the RAFT agent and pRAFT polymer were implemented with the pseudo 1st order rate coefficient of $k_{photons\text{-}RAFT}$ (Reactions 19 & 20, Scheme 4.12). The reverse reactions for the reaction of xanthate fragment radical (thiyl radical) with an R group or macro-radical was implemented as reactions 21 & 22, Scheme 4.12. The possibility that the xanthate

fragment radical will slowly add monomer to create a new propagating species (designated as pRAFT2) was also considered; this is expressed in reactions 23 & 24, Scheme 4.12. The termination of these radicals with both R group and macro-radicals was implemented in reactions 25 & 26, Scheme 4.12. All these reverse reactions were implemented with the possibility of using a fixed rate coefficient or a script to modify the kinetic rate coefficient as a function of the chain length of the macro-radicals reacting with the xanthate fragment radical.

In the case of recombination of a propagating xanthate radical (pRAFT2) with a macro-radical (reaction 26, Scheme 4.12), the length of the macro-radical was selected to be the determining factor, as realistically it can be expected to always be longer than the propagating xanthate radical. For the recombination of a propagating xanthate radical (pRAFT2) with an R group radical (reaction 25, Scheme 4.12), the length of the xanthate radical was used as the determining factor.

An explanation of how these scripts are structured, how the various elements of the scripts function along with the logic in how they were structured in the Predici model is given in section 4.9.3. A direct transcript of how these scripts were coded using Predici nomenclature can be found in section A1.2.1 in the Appendix.

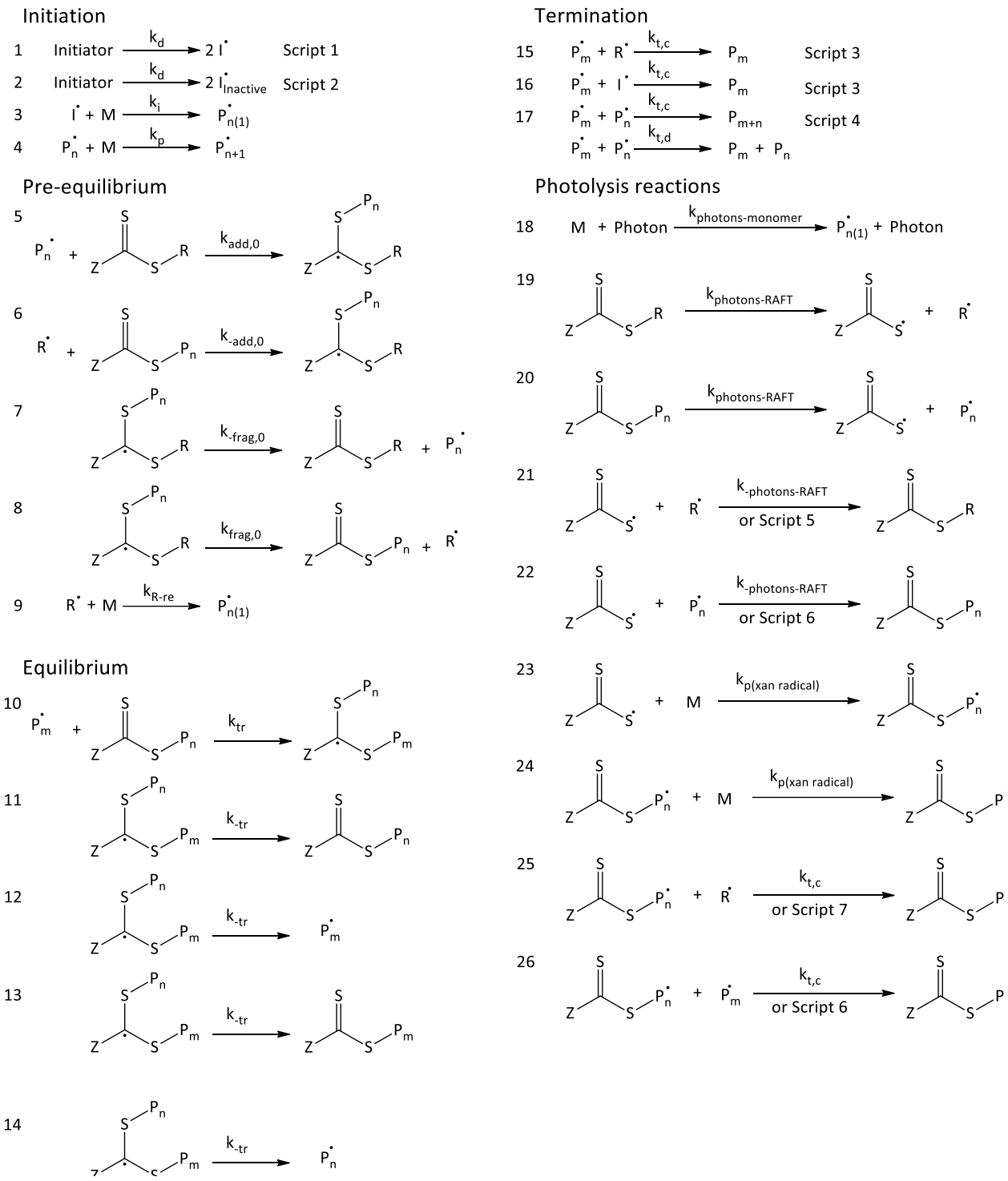

Scheme 4.12: Complete summary of all reactions comprising the Predici model.

4.9.3 Summary and explanation of Predici scripts

The following scripts correspond directly to the scripts as listed in the model summary (Scheme 4.12), for a summary of their implementation using Predici notation, please see Table A3 in the Appendix.

$$Result\ script\ 1 = k_d \cdot k_{photons-initiation} \cdot (f \cdot (1 - c))$$

Script 1 modifies the kinetic rate coefficient for the degradation of the initiator into primary initiator radicals. The k_p("photons-initiator") term is a multiplication factor that can be set to any number greater than 1 and simulates the enhanced breakdown rate due to direct photolysis of initiator. The f factor is the traditional efficiency factor, set to a number less than 1. The term (1 – c) where c is the factional conversion of monomer and simulates the linear decrease in efficiency of the initiator as a function of conversion. This is the same implementation as used by Theis *et al.* [11].

$$Result\ script\ 2 = k_d \cdot c \cdot k_{photons-initiation} \cdot (1 - f)$$

Script 2 mirrors script 1 and simulates the generation of the inactive radicals from initiator decomposition. The term (1-f0) is complementary to the efficiency factor f0 in script 1; it is required for balance such that the fraction of inactive radicals generated increases proportionally as the fraction of active radicals decreases. This is the same rationale for why the conversion (b) term is necessary as opposed to the (1-b) term; this is such that the number of inactive radicals increases as conversion increases and the number of active radicals drops.

In previous investigations involving the RAFT mechanism in Predici, various authors have utilised the unrealistic approach of a fixed value for the average termination rate coefficient for propagating radicals [12, 13] whilst others use the common chain length dependent expression [11, 14-17] as shown in Equation 4.9. Interestingly, occasionally both approaches are used depending on which polymerisation phenomenon was being investigated [13].

$$\langle k_t \rangle = k_t^0 \cdot {X_n}^{-\alpha}$$

Equation 4.9: Chain length dependent expression for the average rate coefficient for termination of propagating radicals.

Other authors have used a more comprehensive approach [15], as shown in Equation 2.23:

$$k_t^{i,i} = k_t^{1,1} \cdot {X_n}^{-\alpha_S} \quad for\ X_n \leq X_{n(cross)}$$
$$k_t^{i,i} = k_t^{1,1} \cdot (X_{n(cross)})^{-(\alpha_S - \alpha_L)} \cdot {X_n}^{-\alpha_L} = k_t^0 \cdot {X_n}^{-\alpha_l} \quad for\ X_n > X_{n(cross)}$$

Equation 4.10: Expression for the termination rate coefficient as a function of propagating chain length.

It is preferable to use the implementation as per Equation 4.9 or Equation 4.10, due to the observation that if the average rate of termination is implemented solely as a function of conversion, this approach neglects the significant influence of chain length. However, if the script for the rate coefficient is based on the chain length of the propagating radicals, then the effect of conversion is by default

included, as in the model, just as in reality, the chain length is critically linked to the overall conversion in the system.

$$Result\ script\ 3 = k_t^{1,1} \cdot {X_n}^{-\alpha_s} \quad if\ X_n \leq X_{n(cross)}$$
$$Result\ script\ 3 = k_t^{1,1} \cdot {X_n}^{-(\alpha_S - \alpha_l)} \cdot {X_n}^{-\alpha_l} \quad if\ X_n > X_{n(cross)}$$

Script 3 is a direct implementation of the chain length dependent expression for the average rate coefficient for termination of propagating radicals, which takes into account the two chain length regimes (Equation 4.10). The value of X_n is the number average chain length of the macro-radical species as they are the growing polymer chains in the model, with $X_{n(cross)}$ being the crossover chain length, with the α^s and α^l terms being the alpha values for the short and long chain length regimes respectively. Predici allows Boolean logic, hence this implementation allows two different results depending on if the condition (average chain length of macro-radicals > $X_{n(cross)}$) is met.

$$Result\ script\ 4\ (1) = k_t^{1,1} \cdot {X_n}^{-\alpha_s} \quad if\ X_n \leq X_{n(cross)}$$
$$Result\ script\ 4\ (1) = k_t^{1,1} \cdot {X_n}^{-(\alpha_S - \alpha_l)} \cdot {X_n}^{-\alpha_l} \quad if\ X_n > X_{n(cross)}$$
$$Result\ script\ 4\ (2) = 0$$

Script 4 is a replicate of script 3, however there are two expressions that are required by the nature of how the reaction is structured in Predici. The second term is the kinetic rate coefficient for termination by disproportionation, which in this case was set to zero. The validity of this assumption for the modelling of MA and VAc polymerisations can be found in sections 5.5.6 and 6.4.5 respectively.

$$Result\ script\ 5 = k_t^{1,1} \cdot f_{xan\ termination}$$

Script 5 allows for the modification of the kinetic rate coefficient for the reverse photolysis of the RAFT agent using a multiplication factor ("f(xan_termination)") as a function of the starting termination rate coefficient.

$$Result\ script\ 6 = k_t^{1,1} \cdot {X_n}^{-\alpha_s} \cdot f_{xan\ termination} \quad if\ X_n \leq X_{n(cross)}$$
$$Result\ script\ 6 = k_t^{1,1} \cdot {X_n}^{-(\alpha_S - \alpha_l)} \cdot {X_n}^{-\alpha_l} \cdot f_{xan\ termination} \quad if\ X_n > X_{n(cross)}$$

Script 6 allows for the chain length dependent implementation of the kinetic rate coefficient for the termination of the xanthate fragment radicals with propagating macro-radicals, including a multiplication factor ("f(xan_termination)") to account for the decreased reactivity of the xanthate fragment radicals. Structurally it is a replicate of script 3.

$$Result\ script\ 7 = k_t^{1,1} \cdot {X_n}^{-\alpha_s} \cdot f_{xan\ termination} \quad if\ X_n \leq X_{n(cross)}$$
$$Result\ script\ 7 = k_t^{1,1} \cdot {X_n}^{-(\alpha_S - \alpha_l)} \cdot {X_n}^{-\alpha_l} \cdot f_{xan\ termination} \quad if\ X_n > X_{n(cross)}$$

Script 7 allows for the chain length dependent implementation of the kinetic rate coefficient for the termination of the propagating xanthate fragment radicals with R group radicals, including a multiplication factor ("f(xan_termination)") to account for the potentially lowered reactivity of what amounts to a head-to-head termination event. In this script, X_n is the average chain length of the pRAFT2 radicals as this is the only polymeric radical in this reaction, hence the reactivity can be expected to be affected by the chain length of this species in an analogous fashion to the decrease in termination as a function of chain length implemented in previous scripts. Structurally it is a replicate of script 6.

Dispersity values in Predici are calculated based on a method of moments approach and the values of M_n, M_w and Đ can be recalled for all species within the program that are treated as distributions; this includes polymer and macro-radical species. Just as in the experimental samples, two types of polymer species exist in the model, both with their own M_n, M_w and Đ values. These are the living RAFT terminated polymer, designated as “pRAFT” and the non-RAFT terminated polymer, designated simply as “Polymer”. To compare simulated distributions and dispersity values to experimental values, scripts were written which calculate the overall M_n, M_w and Đ values, in a method that is sensitive to the relative concentrations of both species. The scripts for these can be found in Table A4 in the Appendix.

4.9.4 Numerical settings within Predici

The numerical settings used were essentially left unchanged from those of the original model, however the maximum step size was set to 250, which resulted in more data points taken especially early in the simulation, which gave smoother curves for the resulting data. A summary of the numerical settings used in shown in Figure 4.12.

Numerical option	Value
Actual stepsize (>0)	(not available)
Maximum stepsize (>0)	250
Initial stepsize (>0)	1.4142E-7
Scaling	1.00e-15
Implicit scaling	yes
Cut of negative concentrations	yes
Consistency check	yes
Solver	MEC(2) (stiff)
Error weighting according to distribution type	GPC (high disp.)
Chain-length strategy according to problem type	Combination, Addition, mild LCB
Accuracy (distributions) according to problem type	Mildly nonlinear

Figure 4.12: A screen capture showing the numerical settings used for all simulations.

4.10 References

1. Li, J., et al., *Visible Light-Induced Living Radical Polymerization of Butyl Acrylate: Photocatalyst-Free, Ultrafast, and Oxygen Tolerance.* Macromolecular Rapid Communications, 2017. **38**(13): p. n/a-n/a.
2. Norris, R.K. and S. Sternhell, *NMR Spectra of "p-nitrosophenol" and its methyl derivatives.* Aust. J. Chem, 1965. **19**: p. 841-860.
3. Shono, T., Y. Hayashi, and K. Shinra, *Nuclear Magnetic Resonances Studies of Nitrosonaphthols.* Bull. Chem. Soc. Jpn, 1971. **44**: p. 3179-3181.
4. Gaumont, A.C., L. Wazneh, and J.M. Denis, *Thiocyanohydrins, a new class of compounds, precursors of unstabilized thiocarbonyl derivatives.* Tetrahedron, 1991. **47**(27): p. 4927-4940.
5. *3528 SMD LED* 2011, ShenZhen Wayjun Technology Co., LTD. p. 1-11.
6. Keddie, D.J., et al., *Chain Transfer Kinetics of Acid/Base Switchable N-Aryl-N-Pyridyl Dithiocarbamate RAFT Agents in Methyl Acrylate, N-Vinylcarbazole and Vinyl Acetate Polymerization.* Macromolecules, 2012. **45**(10): p. 4205-4215.
7. Gruendling, T., et al., *Mark–Houwink Parameters for the Universal Calibration of Acrylate, Methacrylate and Vinyl Acetate Polymers Determined by Online Size-Exclusion Chromatography—Mass Spectrometry.* Macromolecular Chemistry and Physics, 2010. **211**(5): p. 520-528.
8. Goto, A. and T. Fukuda, *Kinetics of living radical polymerization.* Progress in Polymer Science, 2004. **29**(4): p. 329-385.
9. Moad, G. and C. Barner-Kowollik, *The Mechanism and Kinetics of the RAFT Process: Overview, Rates, Stabilities, Side Reactions, Product Spectrum and Outstanding Challenges*, in *Handbook of RAFT Polymerization*. 2008, Wiley-VCH Verlag GmbH & Co. KGaA. p. 51-104.
10. Vana, P., T.P. Davis, and C. Barner-Kowollik, *Kinetic Analysis of Reversible Addition Fragmentation Chain Transfer (RAFT) Polymerizations: Conditions for Inhibition, Retardation, and Optimum Living Polymerization.* Macromolecular Theory and Simulations, 2002. **11**(8): p. 823-835.

11. Theis, A., et al., *Access to Chain Length Dependent Termination Rate Coefficients of Methyl Acrylate via Reversible Addition−Fragmentation Chain Transfer Polymerization.* Macromolecules, 2005. **38**(7): p. 2595-2605.

12. Vana, P., T.P. Davis, and C. Barner-Kowollik, *Easy Access to Chain-Length-Dependent Termination Rate Coefficients Using RAFT Polymerization.* Macromolecular Rapid Communications, 2002. **23**(16): p. 952-956.

13. Theis, A., et al., *Probing the reaction kinetics of vinyl acetate free radical polymerization via living free radical polymerization (MADIX).* Polymer, 2006. **47**(4): p. 999-1010.

14. Theis, A., et al., *Mapping Chain Length and Conversion Dependent Termination Rate Coefficients in Methyl Acrylate Free Radical Polymerization.* Macromolecules, 2005. **38**(24): p. 10323-10327.

15. Johnston-Hall, G. and M.J. Monteiro, *Bimolecular radical termination: New perspectives and insights.* Journal of Polymer Science Part A: Polymer Chemistry, 2008. **46**(10): p. 3155-3173.

16. Buback, M., et al., *Chain-Length-Dependent Termination in Acrylate Radical Polymerization Studied via Pulsed-Laser-Initiated RAFT Polymerization.* Australian Journal of Chemistry, 2007. **60**(10): p. 779-787.

17. Barth, J., et al., *Chain-Length-Dependent Termination in Radical Polymerization of Acrylates.* Macromolecular Chemistry and Physics, 2011. **212**(13): p. 1366-1378.

5 Investigating the contribution of the photoiniferter effect on the RAFT polymerisation of methyl acrylate with a xanthate

5.1 Introduction

This chapter details the experimental and theoretical investigation of the photoiniferter effect as applied to the polymerisation of methyl acrylate (MA) under optimised RAFT conditions at 70 °C. MA is polymerised under 3 sets of conditions (dark + AIBN, light + AIBN, light only), where the UV light source (370nm, 2 mW/cm^2) has been chosen to overlap with the absorption spectrum of the RAFT agent 2-((phenoxycarbonothioyl)thio) ethyl propanoate, (PXEP)). These conditions are also applied to the chain extension of a poly(MA) macro-RAFT agent. This approach was taken as whilst plenty of literature has been concerned with the intricacies of the RAFT and photoiniferter mechanism with TCT compounds (Chapter 2, sections 2.3.3and 2.4.1), fewer investigations exist into the role of generative chain transfer in the photoiniferter mechanism when TCT compounds are utilised (Chapter 2, section 2.4.3). Even rarer still are investigations that concern themselves with directly comparing the kinetics and resulting polymers obtained when a TCT compound is used under typical RAFT conditions as opposed to under typical photo-iniferter conditions. The key differences are the presence of azo initiator and polymerisation at elevated temperatures (60 – 110 °C, RAFT conditions) or the complete absence of initiator (besides the TCT compound) at mild temperatures (20 – 35 °C, iniferter conditions). Suwier *et al.* polymerised styrene with the bi-functional iniferter tetra-ethylthiuram disulfide at 85 °C with 3 sets of reaction conditions; with AIBN as the sole radical source, with an equimolar quantity of TED and AIBN and with just TED [1]. Kinetically, the rates of polymerisation were AIBN ~ AIBN : TED (1:1) << TED. The evolution of M_n with TED as the sole radical source showed a large spike in M_n followed by a general decrease in M_n as a function of conversion, whilst for the AIBN : TED system the M_n remained largely constant as a function of conversion. Furthermore, dispersities in both cases remained constant at ~ 2, implying a chain transfer mechanism. This was compared to a room temperature polymerisation conducted with TED and initiated with irradiation by a UV lamp; the M_n increased linearly with conversion and the dispersity narrowed from ~ 2.5 to 2, characteristics associated with “living” behaviour. Cabannes-Boue *et al.* recently investigated the mechanism of the photo-RAFT / photoiniferter approach, where a dithiocarbamate was tested with a range of monomers (St, MMA, NVC & BA). Superior control over dispersity and molecular weight was observed under RAFT conditions with AIBN as initiator as opposed to room temperature irradiation with an LED light source [2]. However, very good control over BA polymerisation was seen under a range of photoiniferter conditions, including formation of

less dead polymer of low molecular weight. An area of interest lately is polymerisation-induced self-assembly (PISA), with the photo-RAFT/photoiniferter process often being utilised. Two recent studies compared the effects of temperature on this process; Tan *et al.* found no difference on the kinetics of the polymerisation of 2-hydroxypropyl methacrylate with a macro-RAFT agent using a commercially available photoinitiator in the temperature range 25 – 70 °C [3]. Blackman *et al.* found that extended irradiation of macro-initiators used in the PISA process either during their formation or subsequent chain extension led to loss of end group functionality. This manifested as different self-assembly behaviour and different resulting morphologies, whilst thermally chain extended polymers did not show this behaviour [4].

The drawback of these comparisons has been that except for the study by Tan *et al.*, the polymerisations done with radical initiator need to, by the very nature of most azo initiators, be conducted under elevated temperatures, whilst polymerisations conducted under iniferter conditions are always done at, or close to, room temperature. This makes a direct comparison between two experiments and elucidating the potential contribution from the photoiniferter (DC) and RAFT (DT) mechanisms problematic. Furthermore, almost all fundamental rate coefficients such as the rate of monomer propagation, temperature contributions to the various termination mechanisms and initiator degradation are strongly temperature dependent. To the best of the authors knowledge, only one such investigation exists in prior literature; this being the recent report by da M. Costa *et al.* on the acceleration of the RAFT process by commonly occurring light sources within a laboratory context, such as fluorescent lighting both in the room and in the fume hood in which the RAFT polymerisation is performed [5]. MMA and MA were polymerised under both "dark" and "light on" conditions at 70 °C with AIBN present, using 4-cyano-4-[(dodecylsulfanylthiocarbonyl)sulfanyl] pentanoic acid as the RAFT agent. An increase in the apparent polymerisation rate coefficient (k_{app}) ranging from a factor of ~ 3.2 to 1.2 was seen for MA, with the greatest increase at lower AIBN concentrations; this effect was less pronounced for MMA which showed enhancement factors of ~ 2.2 to 1.5.

To circumvent the experimental limitations of these previous studies, a comprehensive Predici model that includes all the features of conventional free radical polymerisation, the RAFT equilibrium and a range of potential photolysis effects was constructed. These include the effect of photolysis of the conventional free radical initiator AIBN, direct radical generation within the reaction mixture by photolysis of monomer and the core iniferter principle, namely the reversible photolysis of the RAFT agent. Scheme 5.1 shows a summary of the Predici model developed, where the "core model" consists of equations 1 – 4 and 15 – 17 (inclusive), representing the RAFT mechanism with AIBN initiation, with reactions 18 – 26 (inclusive) being the photolysis reactions.

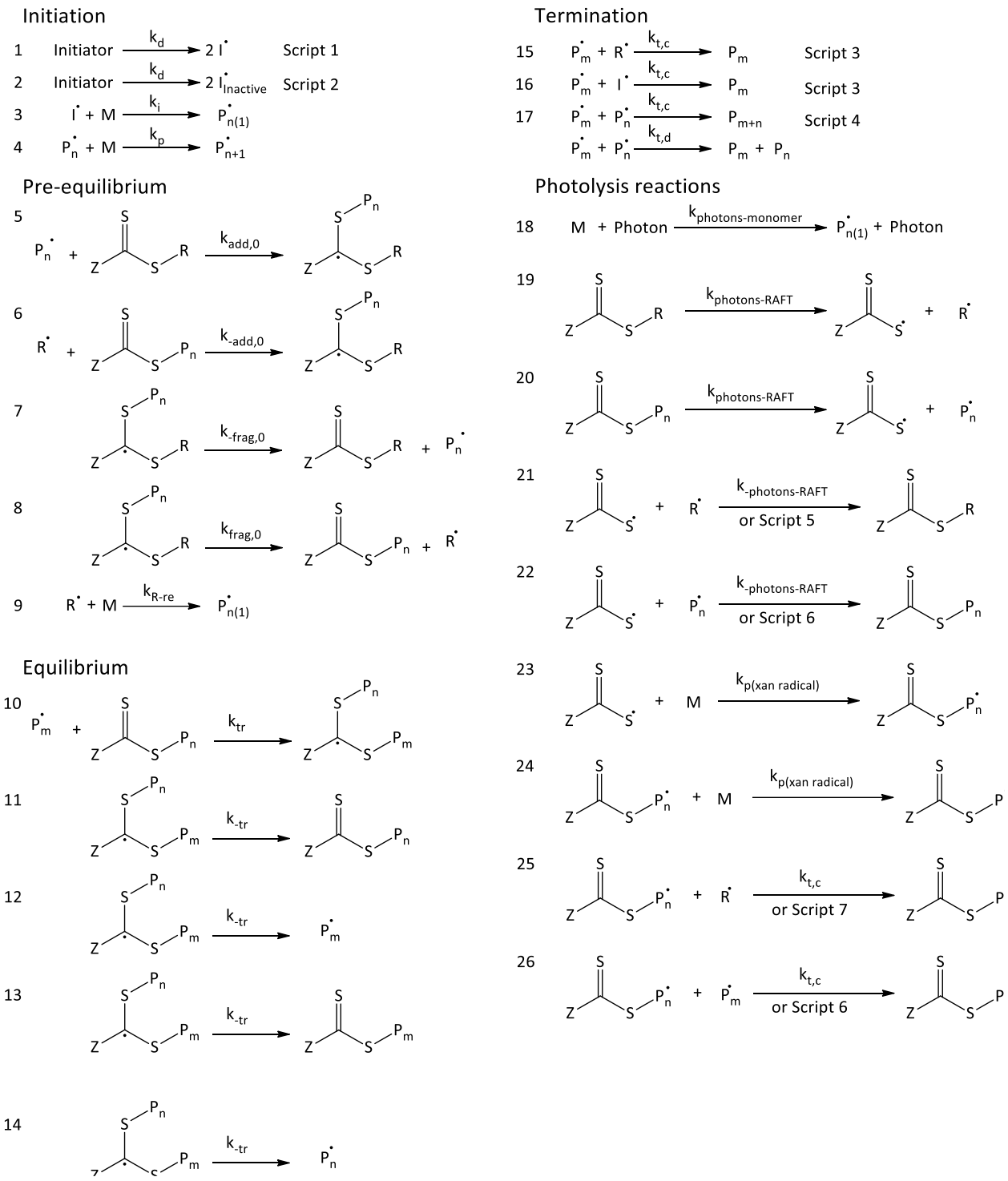

Scheme 5.1: Complete summary of all reactions comprising the Predici model.

To elucidate the mechanistic origins of the experimental phenomena seen under the three sets of polymerisation conditions, these possible photolysis scenarios are presented by means of sensitivity analysis of the model for the respective phenomena, where experimentally derived kinetic rate coefficients were used where possible. The simulated results are critically analysed on their realistic probability by comparison to literature precedent for the parameters used and by comparing the model

output to the experimental phenomena seen. The relative importance of degenerative chain transfer within iniferter polymerisation under these conditions is explored by selectively deactivating these reactions within the model. This understanding is required as these reactions are conducted with PXEP, which is a non-photochromic analogue of the photochromic RAFT agent (Spiro-XEP) tested under identical conditions in Chapter 7.

5.2 Experimental investigation into photolysis of reaction components used in kinetic MA polymerisations

5.2.1 Experimental procedures

Please refer to Chapter 4, sections 4.4 for relevant experimental procedures used in this section.

5.2.2 Analysis of UV-Vis absorption profiles for compounds utilised in MA polymerisation under UV irradiation

Photolysis of a compound in solution should only occur when there is overlap between its absorption spectrum and the emission spectrum of the light source used for irradiation. The overlap between both the strong absorption from PXEP (Figure 5.1, orange trace) and the faint absorption from AIBN (Figure 5.1, purple trace, inset) with the emission spectrum of the 6W UV lamp used (370nm, 2 mW/cm^2) (Figure 5.1, blue trace) indicates that photolysis of both compounds should theoretically be possible.

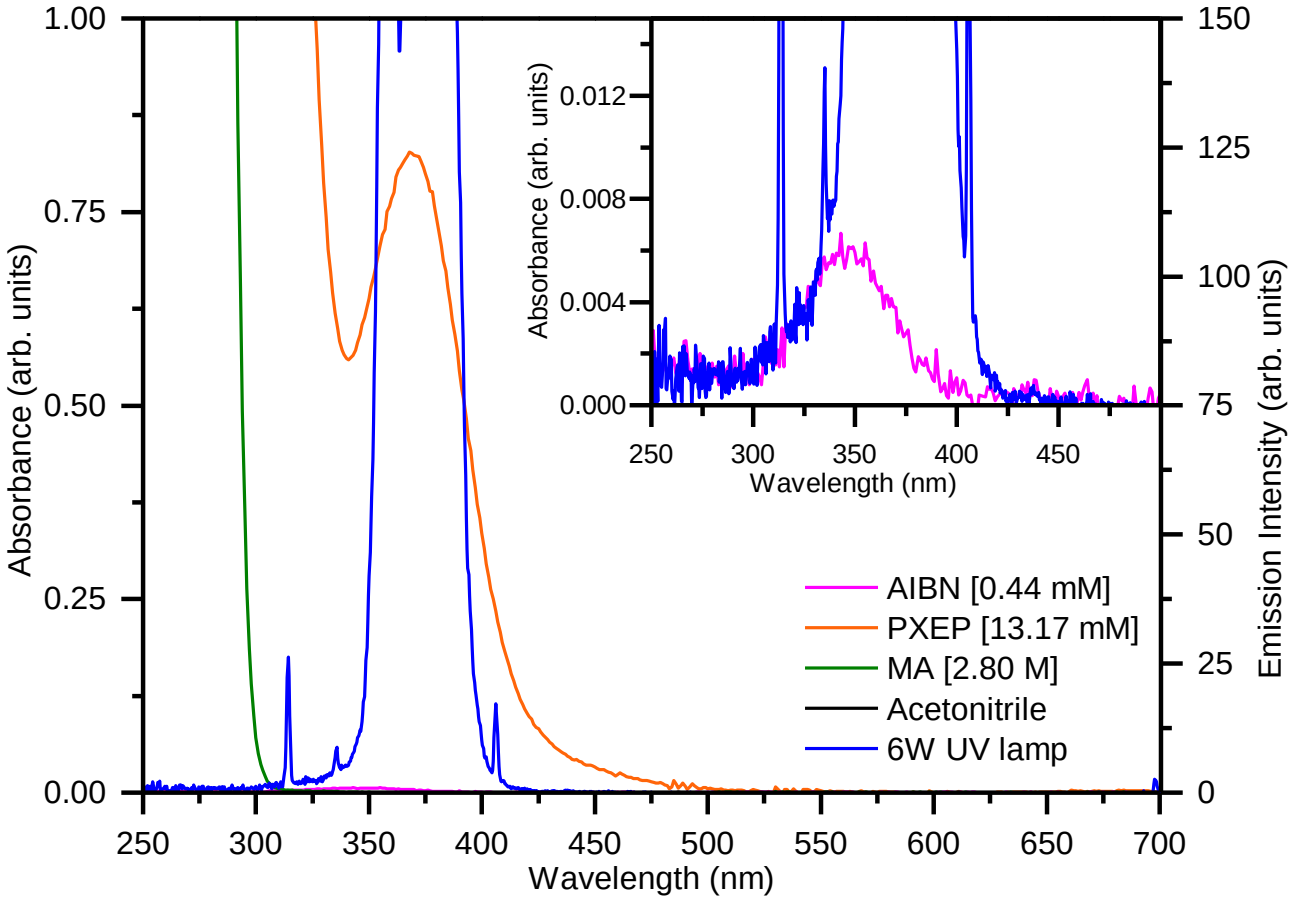

Figure 5.1 Superimposed UV-Vis spectra of AIBN, PXEP and MA at maximum experimental concentrations in acetonitrile used in kinetic experiments overlayed with emission spectrum of the 6W UV lamp (370nm, 2 mW/cm^2).

The absorption of acetonitrile is zero across the entire wavelength range where the UV lamp (370nm, 2 mW/cm^2) emits, as shown by the absorption profile which is essentially identical to the baseline (Figure 5.1, black trace). This indicates that there should not be any photolytic reactions originating from the solvent itself. Similarly, there is only minimal overlap between the absorption from the MA in acetonitrile (Figure 5.1, green trace) and the UV lamp (370nm, 2 mW/cm^2), indicating that direct photolytic initiation of the monomer should not occur.

5.2.3 Photolysis of monomer

To test for the effect of direct photopolymerisation of MA, a control experiment was conducted in the absence of both PXEP and AIBN, under irradiation for fixed period of 6 h which is equivalent to the duration of the kinetic experiments conducted later (section 5.3.2). A similar experiment in the absence of UV light but with the xanthate present was conducted; this was to determine whether the xanthate can function as a conventional thermal iniferter under the polymerisation conditions. These results are summarised in Table 5.1.

Table 5.1 Summary of control experiments conducted under MA polymerisation conditions; [MA] = 2.80 M, [AIBN] = 0, 70 °C, acetonitrile as solvent. UV irradiation (370nm, 2 mW/cm^2).

Entry	Time (h)	[PXEP] (M)	UV Light	% conversion by ^{1}H NMR	M_n (g/mol)	M_w (g/mol)	Đ
1	6	N/A	On	20.12	833900	1504730	1.80
2	10	1.35 x10^{-2}	Off	0.04	N/A	N/A	N/A

The result under UV irradiation (370nm, 2 mW/cm^2) (Table 5.1, entry 1) is consistent of what can be expected of a completely FRP process without any mediating agent, as evidenced by the high molecular weight, broad dispersity and associated noticeable increase in viscosity of the reaction mixture. This is also evidence that a seeming lack of overlap between the absorption spectrum of a monomer with the emission spectrum of light source used cannot guarantee the absence of polymerisation. The exact cause by which the radicals arise from to cause polymerisation is not important, insofar as both solvent and monomer are present in the same concentration in all kinetic experiments and thus this effect can be assumed to be constant in all cases. Indeed, it has been remarked that photopolymerisation of "*supposedly pure monomers using light sources such as sunlight or mercury lamps with Pyrex glass envelopes must be due to the presence of fortuitous traces of a sensitizer*" [6]. The second experiment (Table 5.1, entry 2) conclusively shows that without the presence of UV light, the xanthate is incapable of thermally dissociating to act as a thermal iniferter to any significant extent, as evidenced by conversion being essentially 0 and within experimental error. This also shows there are no extra sources of radicals capable of starting the polymerisation within the system that can become thermally active through simply heating the reaction mixture, such as direct thermal initiation of the MA monomer.

The potential effect of monomer photolysis is investigated in the Predici model in section 0.

5.2.4 Photolysis of AIBN

Along with being a ubiquitously used thermal initiator, AIBN is capable of absorbing in the UV region and undergoing photolysis in the form of both direct breaking of the C-N bond and isomerization around the nitrile group followed by conventional degradation [7-10]. Several studies have shown that the degradation products obtained by photolysis in solution are equivalent to those of conventional thermal degradation [8, 11]. This is sufficient evidence to say that UV photolysis in conjunction with conventional heating will increase the rate of AIBN degradation, which is represented by an effective increase in the kinetic rate coefficient for degradation (k_d).

To determine the values of k_d under both dark and UV irradiation experimental conditions, a solution containing AIBN (3.60 $x10^{-3}$ M), ethyl acetate (6.35 M) and acetonitrile was placed into Young's flasks and subjected to a normal polymerisation procedure. This ensured that both heat transfer and light intensity under UV irradiation were the same as during a normal kinetic polymerisation experiment, with the amount of AIBN degraded being determined by UV-Vis spectroscopy of the solutions before and after various reaction times. Due to the large spectral overlap that occurs between AIBN and the strong absorption from PXEP (Figure 5.1), PXEP was omitted from these experiments. Ethyl acetate was used in place of monomer as its lack of a vinyl bond prevents it from polymerising under irradiation while its structure gives it similar polarity to both MA and VAc monomers. These reaction conditions correspond to those employed for VAc polymerisation instead of those used for MA polymerisation; the reasons for this were twofold. Firstly, under MA conditions, the concentration of AIBN was much lower (4.00 $x10^{-4}$ M) which resulted in the AIBN peak having a starting absorbance that was too low for analysis by UV-Vis spectroscopy. Secondly, using the higher concentration meant a theoretically greater impact of the UV irradiation on the overall value of k_d, which means that the k_d determined would serve as a natural upper limit for use in the Predici modelling.

The peak attributed to the -N=N- bond in AIBN occurred at 345 nm which is consistent with previous reports by Osugi *et al.* for AIBN in benzene [9], and showed significant overlap with the emission wavelength of the UV lamp used (370nm, 2 mW/cm^2)(Figure 5.2, blue trace). In Figure 5.2, the traces in shades of red and green correspond to concentrations greater and lower than the starting concentration used during the degradation experiments, respectively. Across this range the calibration curve is perfectly linear (Figure 5.2, inset), giving an extinction coefficient for this absorbance of 12.375 M^{-1} cm^{-1}.

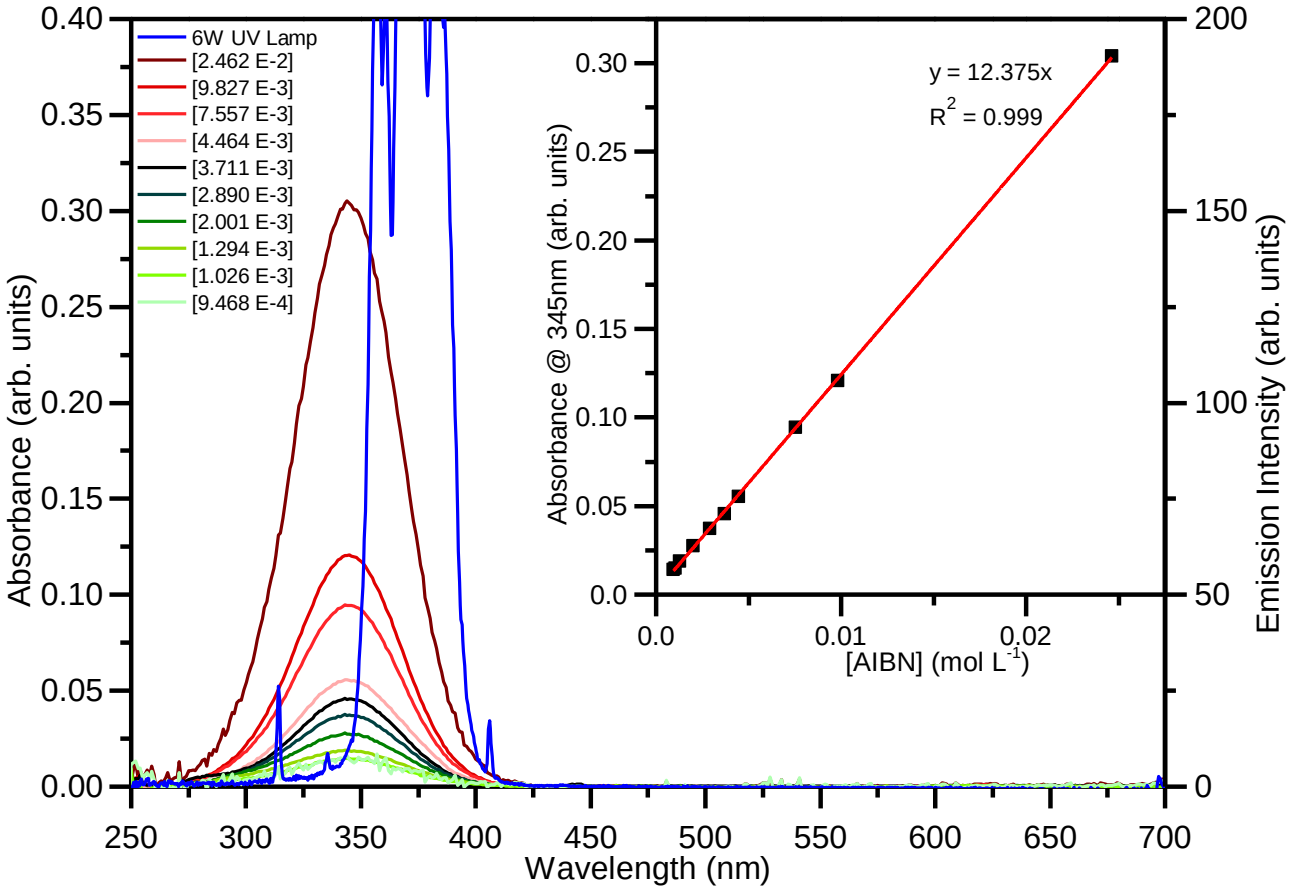

Figure 5.2: UV-Vis spectra of AIBN at various concentrations superimposed with emission spectrum from the 6W UV lamp (370nm, 2 mW/cm^2), and inset, calibration curve derived from the peak absorbance at 345 nm.

The UV-Vis spectra of solutions after given reactions times under both sets of conditions are shown in Figure 5.3. An overall decrease of the peak attributed to AIBN at 345 nm is accompanied by the appearance of a new peak at ~ 291 nm that increases in intensity as a function of reaction time under both reaction conditions. This peak is attributed to the formation of dimethyl-N-(2-cyanoisopropyl)-keteneimine (DKI) [9, 10] which is one of the by-products of AIBN degradation.

This peak was most likely responsible for the absorbance at the peak wavelength (345 nm) being slightly higher than prior to degradation for the first-time point (0.5 h) under dark conditions. This complicated the analysis slightly, as theoretically this would indicate that the % remaining of AIBN appears to increase above 100 % which is clearly impossible. For this reason, this data point was omitted from Figure 5.4 and from fitting the linear line of best fit to determine k_d from the pseudo first order kinetic plots (Figure 5.4, B) which were generated directly from the decrease in peak absorbance values obtained from Figure 5.3. In both cases, the origin was included as a data point and used as the intercept in the fitting procedure.

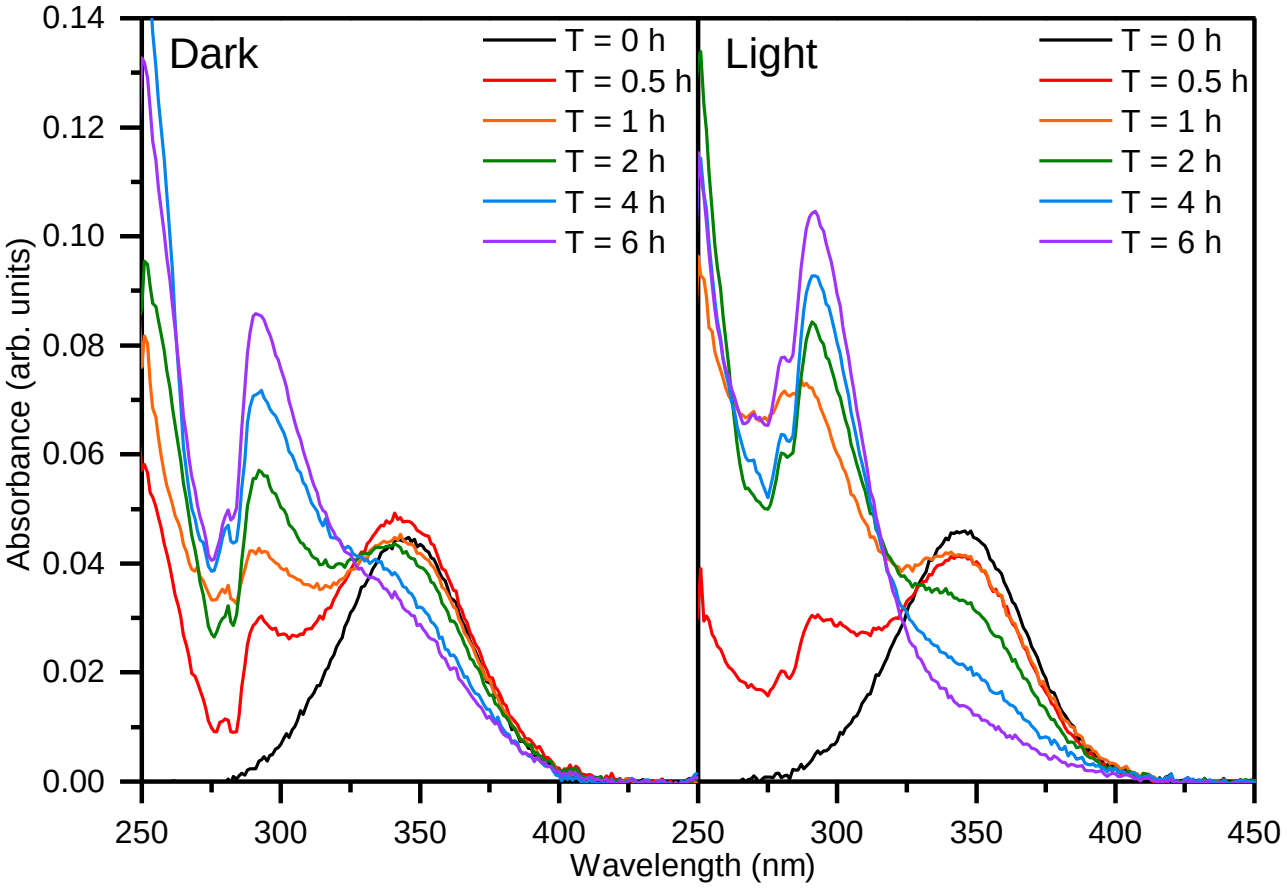

Figure 5.3: UV-Vis spectra of AIBN samples used in degradation studies at various time points; under dark + AIBN conditions (left) and under light conditions (right).

Using the kinetic parameters (E_a = 131.7 kJ mol^{-1}, A = 4.31 x10^{15} s^{-1}) as collated from literature by Moad & Solomon [12], the theoretical value of k_d at 70 °C (343.15 K) was found to equal 3.867 x10^{-5} s^{-1} and used as benchmark comparison. A value of 3.200 x10^{-5} s^{-1} in benzene is reported in the polymer handbook [13]; however it is known that for azo initiators the value of k_d can vary by as much as a factor of 2 at the same temperature depending on the nature of the solvent, with aromatic solvents giving higher k_d values [12]. Considering the value determined experimentally in this strongly polar solvent mixture is within a factor of ~ 2 of both the theoretical and the reported value in benzene, k_d = 1.6530 x10^{-5} is the value used within the simulations and within calculations. Furthermore, the effect of thermal affects such internal evaporation and condensation of solvent and monomer inside the Young's flask or simply the flask acting as a partial heat sink cannot be ruled out. This would naturally lead to an overall lower temperature of the solution and subsequently decrease the effective value of k_d determined. Irrespective of any potential contributions due to the DKI peak, if thermal effects were wholly responsible, the determined value of k_d equates to an internal solution temperature of 65.2 °C when the kinetic parameters from Moad & Solomon [12] are used. Even if the dark value of k_d is slightly underestimated by the method employed here, these effects are

also present during the photolysis case and should therefore be consistent. Finally, k_d being potentially marginally underestimated does not change the fundamental analysis and subsequent conclusions of the Predici modelling undertaken.

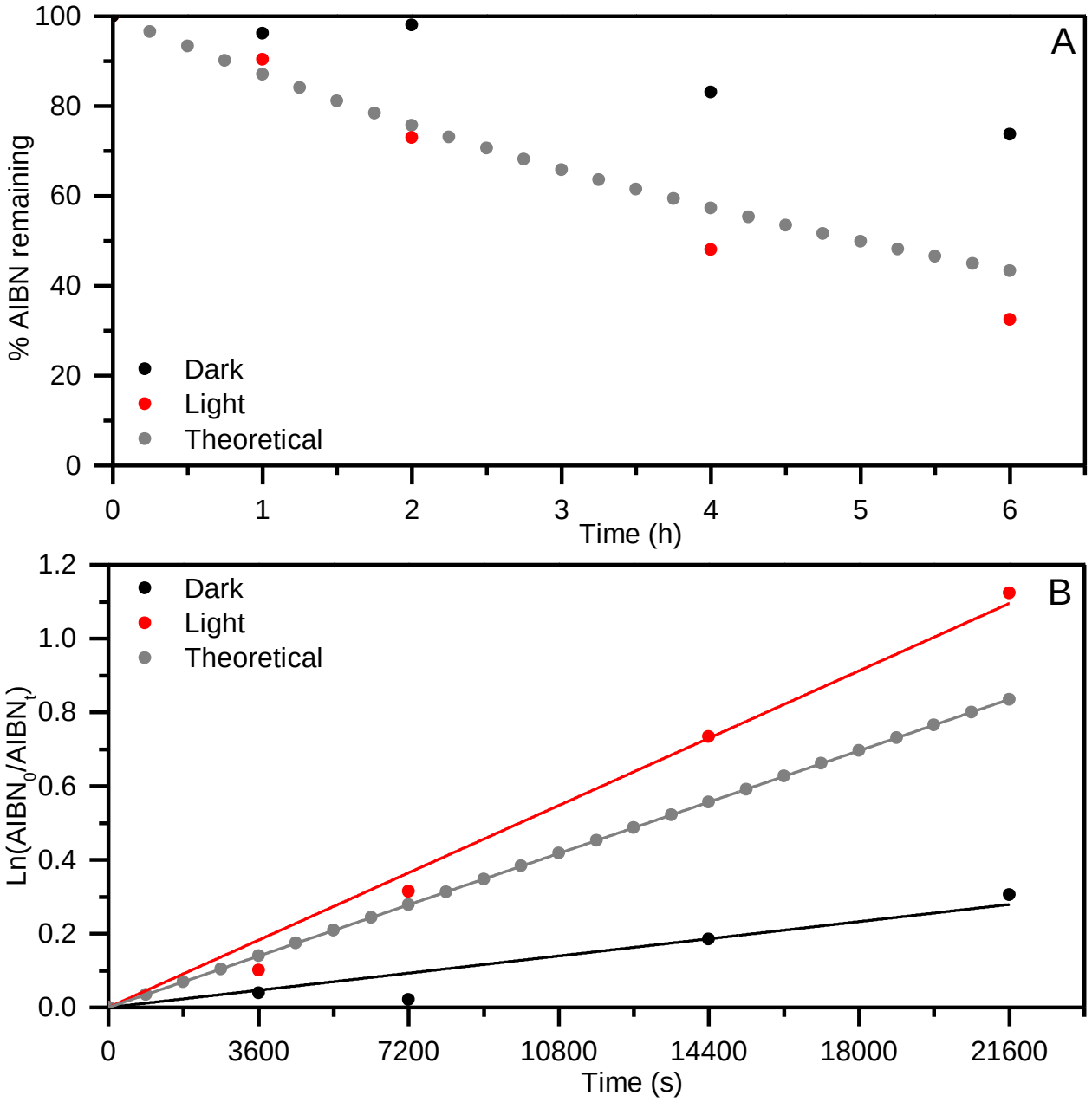

Figure 5.4: Percentage of starting AIBN concentration remaining as a function of time under the studied degradation conditions (70 °C) as calculated by UV-Vis absorbance data (A), 1st order kinetic plots corresponding to these conditions used to derive k_d values for use in the Predici model (B).

The impact of photolysis was found to increase the rate of AIBN degradation by a factor of 3.065, giving a k_d under photolysis conditions of 5.066 $x10^{-5}$ s^{-1}. It must be stressed that this is strictly a maximum upper value, as in the case of actual polymerisation there is PXEP present which has significant spectral overlap within the region where AIBN absorbs (Figure 5.1). Engel theorised that

the primary mode of photolysis of azo initiators is that of cis-trans isomerization; this was based on the observation that when the cis isomer is thermally stable, the quantum yield for initiator degradation was low (< 0.1) [7, 12]. Due due to AIBN having a modest quantum yield of 0.43 [14], which is a value potentially one to two orders of magnitude greater than for the quantum yield for the photolysis of TCT compounds. This suggests that despite its low concentration under MA polymerisation conditions, the photolysis of AIBN could be a potentially important reaction pathway. A comparison of all k_d values discussed is given in Table 5.2.

Table 5.2: Summary of k_d values.

Reaction conditions	k_d at 70 °C (x 10^{-5}) (s^{-1})	Ref.
Dark	1.653	This work
Light	5.066	This work
Theoretical	3.867	[12]
Reported (in benzene)	3.200	[13]

The potential effect of photolysis of AIBN is investigated in the Predici model in section 5.7.

5.2.5 Photolysis of PXEP

To study the photolytic degradation of PXEP, an equivalent concentration of 1.36 x10^{-2} Mas used in the polymerisation of MA was employed. To avoid polymerisation and remove any other potential affects of AIBN, MA monomer was substituted for ethyl acetate and AIBN was omitted due to spectral overlap. The calibration curve was created using concentrations of PXEP which encompassed all the concentrations utilised under MA polymerisation conditions and the higher starting concentration required for VAc polymerisations. The absorbance at 370 nm for the highest concentrations exceeds a value of 1.6 (Figure 5.5, black trace); this also manifests as a non-linear calibration curve at this absorbance or higher (Figure 5.5, inset). For this reason, the calibration curve was limited to values below 1.6 where in this range the calibration is almost perfectly linear, giving an extinction coefficient for this spin forbidden n → π* transition of 59.66 M^{-1} cm^{-1}, which is within the range for these weaker transitions [15]. The degradation was quantified by measuring the absorbance at 370 nm of the reaction mixture post UV exposure and normalising that to the pre-exposure absorbance value. It is possible that any degradation products may also absorb in this region, however no significant changes in peak shape or extra peaks were visible (Figure 5.6). This method of analysis is also consistent with that used within the literature [15, 16].

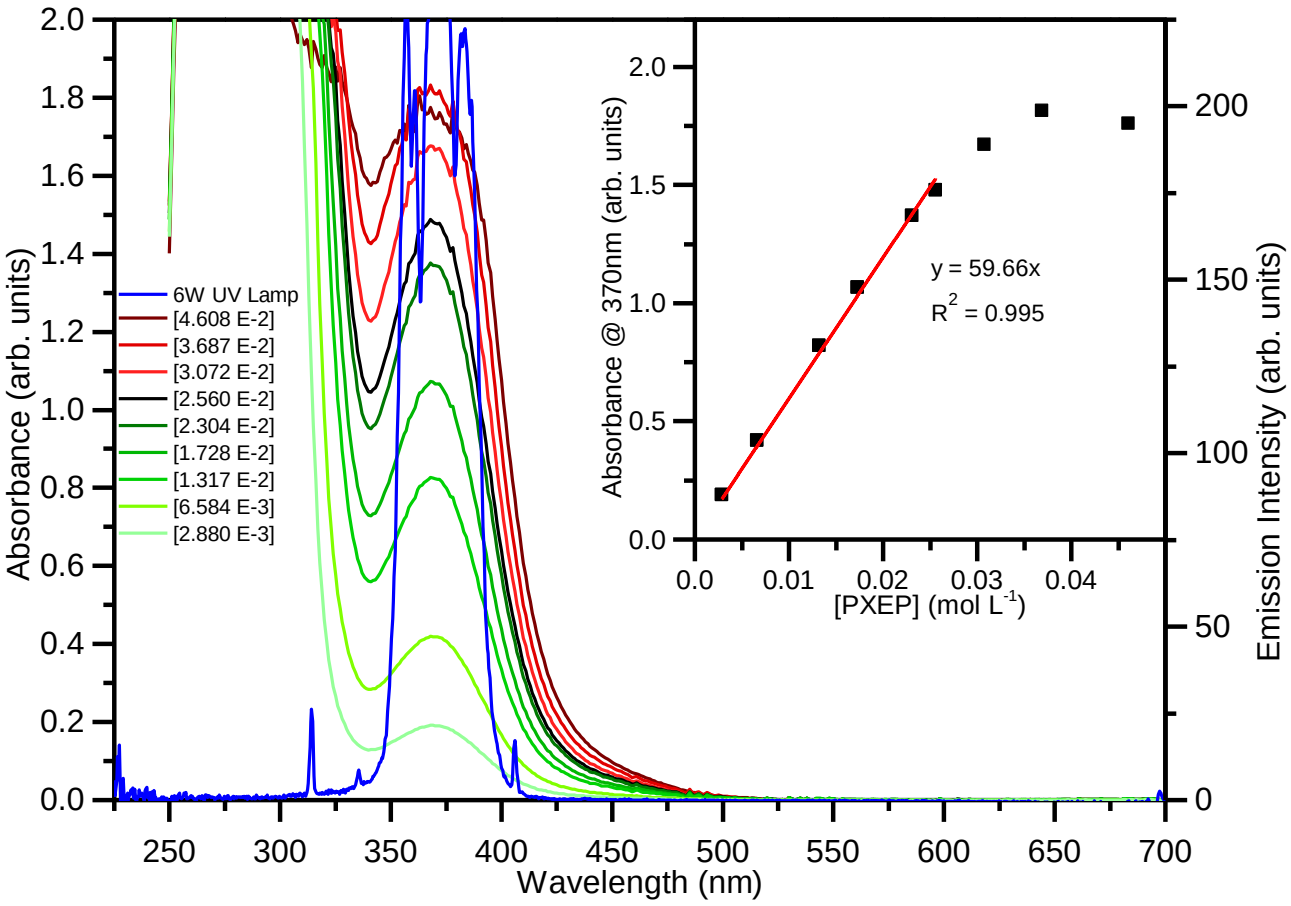

Figure 5.5: UV-Vis spectrum of PXEP at various concentrations superimposed with emission spectrum from the 6W UV lamp (370nm, 2 mW/cm^2), and inset, calibration derived from the peak absorbance at 370 nm.

There is a seemingly rapid minor degradation of around ~ 3 % which is followed by a slow linear increase in PXEP degraded until the 6 h mark (Figure 5.6, inset). Anomalously, the absorbance for the first-time point (Figure 5.6, T = 0.5 h, red trace) exceeds that of the starting solution. This potentially occurs due to a by-product of degradation having a similar absorption profile to PXEP, albeit with a higher extinction coefficient, in a similar way to what was observed for AIBN degradation. This is also supported by a slight red shift in the spectra for all degradation time points which is noticeable in the slope of the stronger $\pi \rightarrow \pi^*$ transition in the lower wavelength region (< 350 nm).

The degradation seen is most likely a qualitative combination of behaviours seen in literature; both Lu *et al.* [17] and McKenzie *et al.* [16] saw linear degradation as a function of time for a dithiobenzoate and a series of trithiocarbonates respectively. Ham *et al.* saw an abrupt initial degradation followed by a linear degradation rate for a xanthate with a secondary ethyl acetate R group [18]. Interestingly, McKenzie *et al.* report no degradation of a trithiocarbonate with a structurally analogous secondary R group whilst sometimes seeing a small increase above the starting absorbance values for certain trithiocarbonates investigated.

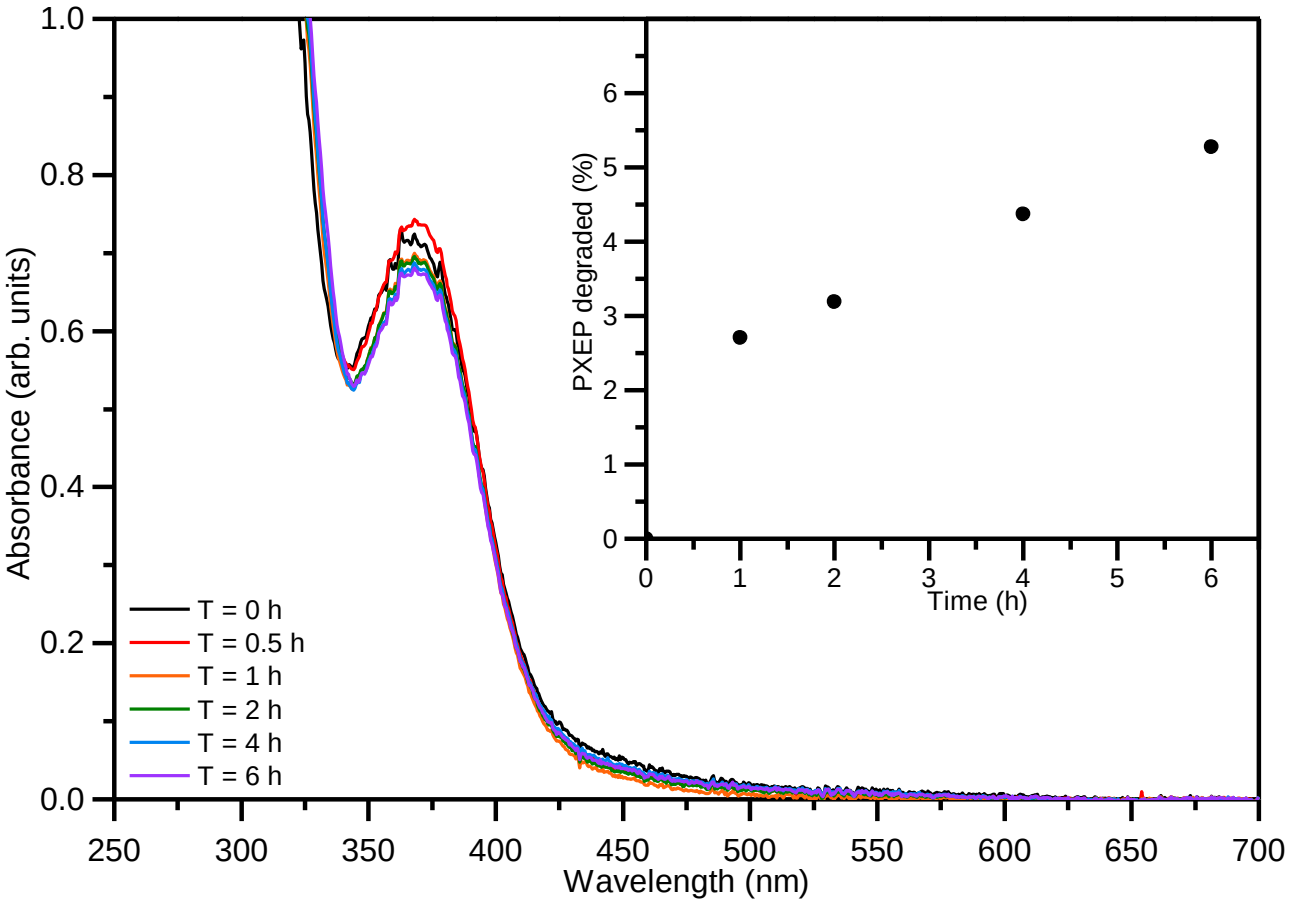

Figure 5.6: UV-Vis spectra of PXEP solutions after various times of heating at 70 °C with simultaneous irradiation with 6W UV lamp (370nm, 2 mW/cm^2), and inset, percentage of starting PXEP concentration degraded as a function of time derived from UV-Vis spectra absorbance at 370 nm. Starting [PXEP] = 1.36 x10^{-2} M.

The potential effect of the photolysis of PXEP is investigated in the Predici model in section 5.8.

5.3 Experimental studies of MA polymerisation

5.3.1 Experimental procedures

Please refer to Chapter 4, sections 4.5 for relevant experimental procedures used in this section.

The reaction conditions selected were taken directly from a previous publication by Keddie *et al.* [19], with the polymerisation of MA shown in Scheme 5.2. These conditions can be considered "typical" for RAFT polymerisation, initiated with a common thermal initiator (AIBN) at 70 °C and conducted in acetonitrile. Furthermore, these conditions give acceptable polymerisation rates and control over molecular weight, notwithstanding that the correct class of RAFT agent is selected. Finally, the performance of a series of RAFT agents has been benchmarked under these conditions;

this means that qualitative comparisons and inferences can be made between any novel RAFT agents utilised under these conditions and those tested previously.

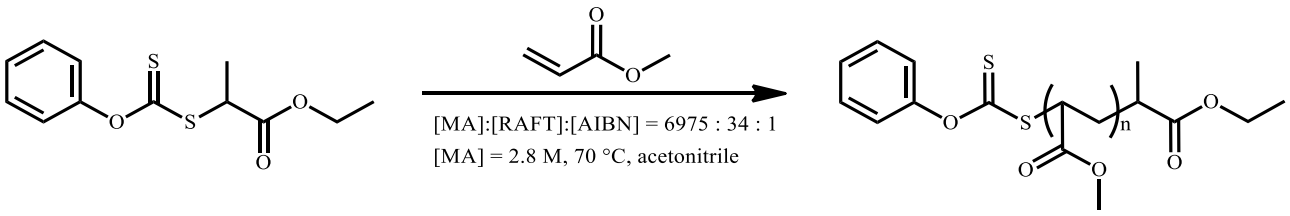

Scheme 5.2: Polymerisation of MA undertaken with PXEP under standard conditions.

Prior to investigating the effect of UV irradiation on MA polymerisation when the photochromic RAFT agent (spiro-XEP) is used, its effect in the presence of a non-photochromic analogue (PXEP) had to be tested. This conveniently also allowed for the investigation of the intricacies and mechanistic consequences of the photoiniferter effect under typical RAFT conditions.

Excluding ambient light is essential to ensure the rate of polymerisation under dark conditions is representative of the actual polymerisation rate prior to the addition of any external influences. Directly wrapping the Young's flasks in aluminium foil and covering the whole oil bath from light using aluminium foil were the two methods compared, with the latter method being chosen which was consistent with the approach taken by da M. Costa *et al.* [5]. This decision arose due to a comparison of kinetic experiments performed (Figure 5.7). When the flasks were directly covered in aluminium foil, this resulted in a slightly slower reaction with a non-zero intercept for conversion, and this can be attributed to a longer time required for the flask to reach thermal equilibrium. Indeed, regardless of the potential differences in the thermal mass of solution and associated exotherm at reaction start when conducting the polymerisation on different scales (~ 2 mL vs ~ 5 mL per flask), this effect is largely absent after 2 h.

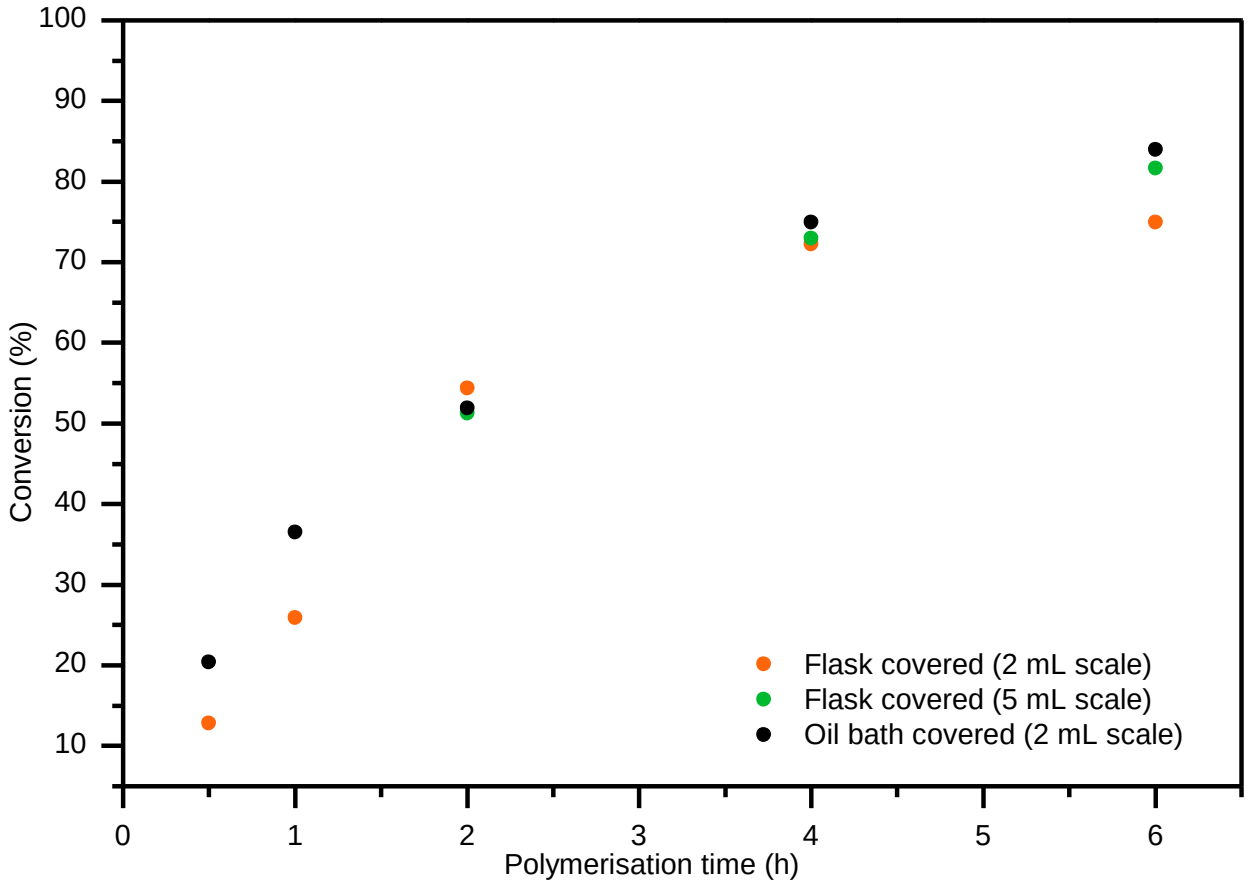

Figure 5.7: Kinetic experiments used to estimate the percentage error for MA polymerisation conducted at 70 °C with PXEP.

The percentage error associated with any conversion time point is hard determine accurately. The error associated with determination of conversion by ^{1}H NMR analysis can be considered under 1 %, as evidenced by the same polymerisation sample (stored in a freezer) being re-analysed 6 months apart and resulting in the same conversion being determined. The greater influence most likely comes from the time taken for the Young's flask to reach thermal equilibrium both when heating to start the reaction and cooling to bring it to a halt. This effect is likely greater for the lower conversion region (< 65 %) where the conversion versus time profile is much steeper; thus ± 5 % error for data in this region is likely realistic, with this error diminishing to lower values in the higher conversion region (> 65 %).

5.3.2 Kinetic studies of MA polymerisation

Figure 5.8 (A) shows the polymerisation kinetics under different conditions; in the dark + AIBN condition, a conversion of 84 % is obtained after 6 h which correlates very closely with the average conversion seen by Keddie *et al.* (between 78 – 85 %) when utilising less active RAFT agents under the same conditions. When UV light is applied (light + AIBN or light only) the polymerisation was

much faster, achieving an equivalent conversion of almost 90 % in just 1 h. This is followed by a gradual increase to essentially quantitative conversion (98 %) after 6 h in both cases. The almost perfect overlap between the light only and light + AIBN data sets between 1 and 6 h strongly implies that the contribution from AIBN breakdown is negligible to the kinetics seen. This is based on the fact if significantly different kinetics were to occur during shorter polymerisation times, this would naturally manifest as a deviation from the conversion versus time profile at higher conversions.

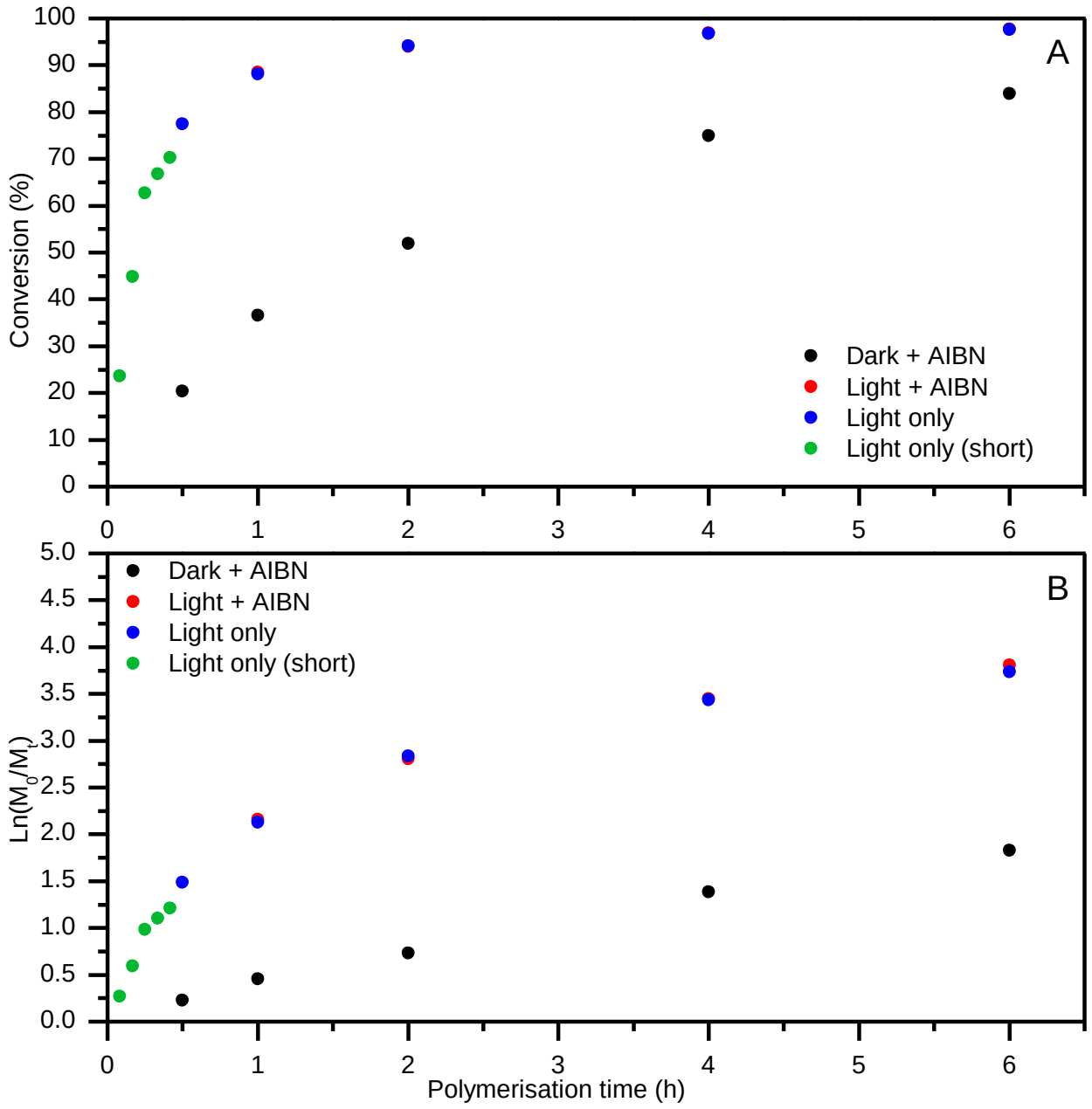

Figure 5.8: Conversion versus time plot (A) and 1st order kinetic plot (B) for MA polymerised under various conditions at 70 °C with PXEP.

Analysis of the pseudo first order kinetic plot (Figure 5.8, B) reveals that for the dark + AIBN case, the plot is reasonably linear. For a degenerative transfer (DT) mechanism such as RAFT this implies

that a steady state polymerisation is occurring where rates of initiation and termination are approximately equal and the number of radicals is essentially constant as a function of time [20, 21]. When short reaction times (< 1 h) were employed under irradiation in the absence of AIBN (Figure 5.8, light only (short)) the pseudo first order kinetic plot is once again essentially linear. As $Ln(M_o/M_t)$ is a function of $t^{2/3}$ under a dissociation combination (DC) mechanism instead of a function of t like for a DT mechanism [21, 22], this is strongly indicative of a DT mechanism being operative.

For the conditions where irradiation is used (light + AIBN and light only), a clear deviation from linearity is seen from 1 h onwards. This is not unexpected as after this point the reaction is essentially complete (> 95 % conversion) and the effects of monomer depletion become kinetically relevant.

The apparent rate coefficient of polymerisation (k_{app}) was calculated from the pseudo first order kinetic plots and the results are summarised in Table 5.3. Only the data up to ~ 85% conversion corresponding to an $Ln(M_0/M_t)$ value of ~ 2 was used as this was the linear region of the plots shown in Figure 5.8.

Table 5.3: Summary of calculated k_{app} values for the kinetic experiments shown in Figure 5.8 (B). UV irradiation (370nm, 2 mW/cm^2).

Conditions	k_{app} (h^{-1})	Error in k_{app} (+/-)	Enhancement factor
Dark + AIBN	0.32	0.01	1.00
Light only (1st 2 data points)	2.98	N/A	9.19
Light only (short)	3.25	0.17	10.03

The enhancement factor was calculated as a ratio between k_{app} for the dark + AIBN conditions and the conditions being tested, with the error used directly from the LINEST analysis. For the case where AIBN is absent, the value obtained for the light only (short) case can be considered more representative of the true polymerisation kinetics than the light only case due to more data points occurring within the lower conversion region. The calculated k_{app} for the light only (short) case being within experimental data for the light only value further supports the continuity in the kinetic data seen in Figure 5.8.

In terms of the photo enhancement seen, these results agree with the general trends seen by da M. Costa *et al.*, however the enhancement factors observed are much higher (max = 10.03 vs 3.13). This can be attributed to differences in experimental setup, namely the use of more intense light sources (6W UV lamp (370nm, 2 mW/cm^2) vs fluorescent fume hood lights) and different classes and concentrations of RAFT agent employed along with monomer concentration.

Despite the vastly accelerated polymerisation rates under UV irradiation, it is clear from Figure 5.9 that the evolution of the M_n under both light only and light + AIBN conditions is remarkably like that of the dark + AIBN conditions. This includes the initial spike in M_n and the associated positive deviation from the theoretically predicted M_n at low conversion, with good agreement at higher conversions (> 50%), Likewise, the dispersity values under UV irradiation conditions seem to fit the general trend set by the AIBN only data points, namely that they decrease as a function of conversion from ~ 1.55 to 1.25, with only a slight increase at very high conversions to a dispersity of around 1.29.

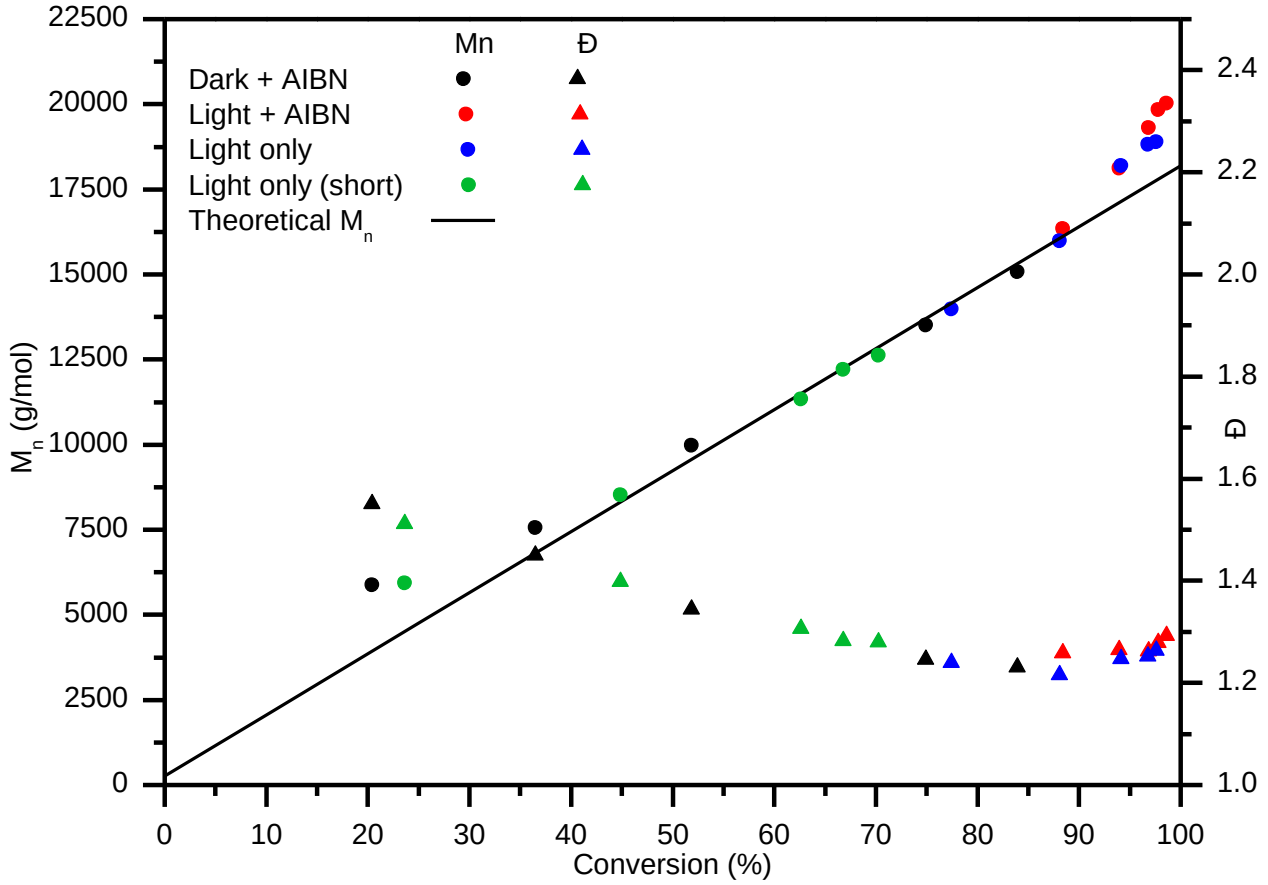

Figure 5.9: Evolution of molecular weight and dispersity as a function of conversion for MA polymerised under various conditions at 70 °C with PXEP.

Taken together, the evolution of M_n and dispersity indicate that the chain transfer rate of PXEP in this system is reasonably low, but still high enough to give control over the polymerisation. This is supported by the gradual consumption of PXEP as determined by ^{1}H NMR spectroscopy, which occurs under both dark + AIBN and light only (short) reaction conditions. This is evident from the faint resonance at 4.2 ppm attributed to unreacted PXEP still being present at the 1 h time point for the dark + AIBN case (Figure 5.10 (A), blue trace) which is also evident at the 5 min time point for the light only (short) case (Figure 5.10 (B), red trace). A similar trend of gradual if albeit severely

accelerated (relative to the dark + AIBN conditions) consumption of PXEP under light only conditions is visible from the ^{1}H NMR spectra (Figure 5.10 (B)). Overall these observations support the idea that slow consumption of PXEP is responsible for the hybrid behaviour seen which is typical when a MAM like MA is polymerised with a less active RAFT agent such as a xanthate or dithiocarbamate, with control over M_n being obtained once PXEP is fully consumed.

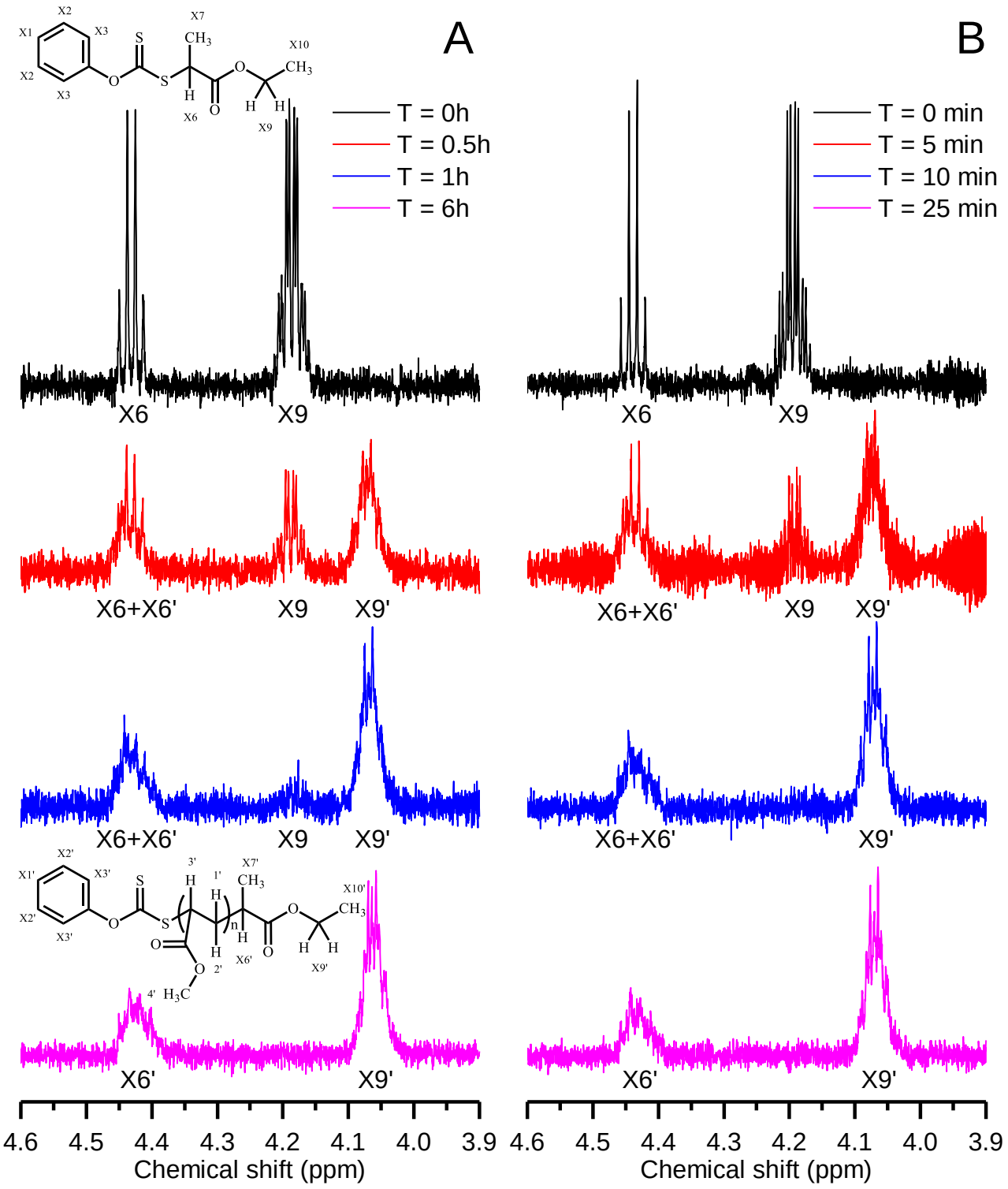

Figure 5.10: ^{1}H NMR spectra in the region of 3.9 – 5 ppm showing the resonances attributed to the starting PXEP and conversion into a poly(MA), obtained from analysis of kinetic polymerisation samples polymerised to various times under dark conditions (A) and light only (short) conditions (B).

The positive deviation from the theoretical M_n at high conversion under light only & light + AIBN conditions can arise due to degradation of the RAFT agent due to irreversible photolysis; this appears to be consistent with the degradation determined previously. This correlation of these two phenomena

and the nature of the kinetic rate coefficient for the reverse photolysis reaction is explored later in the Predici modelling in section 5.8.

Regardless of the reaction conditions used, a linear clustering of chain transfer constants as estimated by the method of Goto & Fukuda [23] was evident in Figure 5.11. This further supports the idea that the AIBN + light and light only conditions do not significantly disrupt the degenerative chain transfer mechanism of RAFT. This can be directly inferred as the parameters that govern the RAFT mechanism directly determine the chain transfer constant. The range of values determined for C_{tr} fit within the range of apparent chain transfer constants determined by Keddie *et al.* for dithiocarbamates that give similarly moderate control over MA polymerised under these conditions.

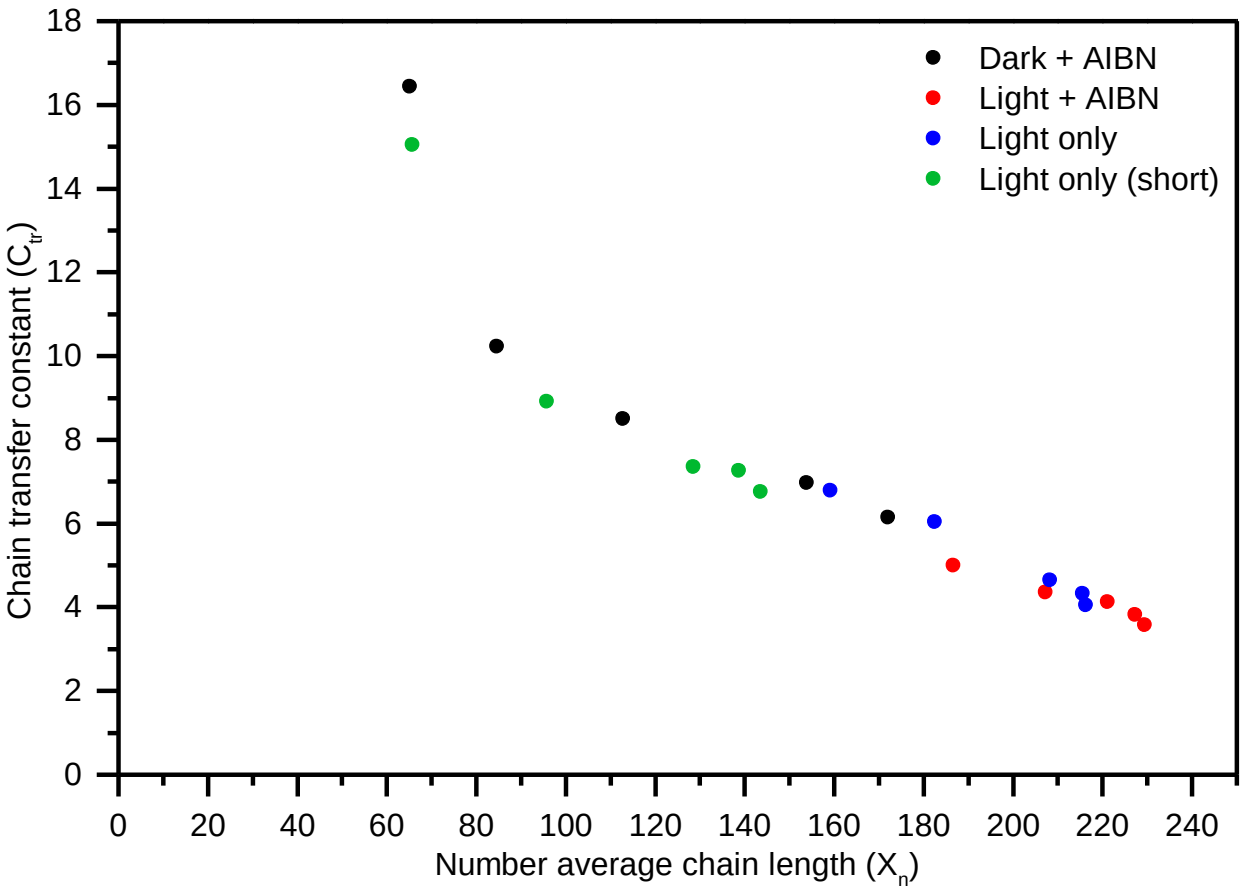

Figure 5.11: Chain transfer constants as estimated for PXEP when used in the polymerisation of MA under various conditions at 70 °C.

Overall, these observations are highly suggestive of the same degenerative transfer mechanism being operative under both the traditional RAFT conditions (dark + AIBN) and under irradiation conditions (light only & light + AIBN) for the majority of the duration of the polymerisation.

5.3.3 Kinetic studies of MA chain extension polymerisation

Owing to the gradual consumption of the RAFT agent seen under light only (short) conditions, it was imperative to investigate whether the polymerisation phenomena under irradiation conditions are a result of the photolysis of the initial R group on the RAFT agent as compared to polymer chains attached to the growing macro-RAFT agent. To this end, a low molecular weight poly(MA) macro-RAFT derived from PXEP was subjected to chain extension under identical conditions to those used in the previous section. The macro-RAFT agent was formed in the dark and had M_n = 2690 g/mol, Đ = 1.19 by GPC. Theoretically it had 98.59 % of all chain ends retaining the RAFT moiety, estimated using Equation 4.9, where a value greater than 95 % being considered indicative of a well-designed RAFT polymerisation [24]. Integration of proton resonances from the Z group (X2' & X3', Figure 5.12, inset) and from the R group (X10', Figure 5.12, inset) were compared and showed a 2 : 3 correspondence as expected. This indicates that on average both the R and Z group of the PXEP molecule were retained at either end of each polymer chain.

The UV-Vis absorption of the poly(MA) macroinitiator showed considerable overlap between then the weak spin forbidden n → π* transition and the output of the UV lamp (370nm, 2 mW/cm^2), indicating that it should also function as an efficient photoiniferter. Furthermore, the essentially unchanged peak position (369 nm for poly(MA) made with PXEP vs 370 nm for PXEP) supports the notion that incorporation of poly(MA) has not changed the electronic properties of the starting PXEP molecule, consistent with the idea that poly(MA) is structurally analogous to the starting R group.

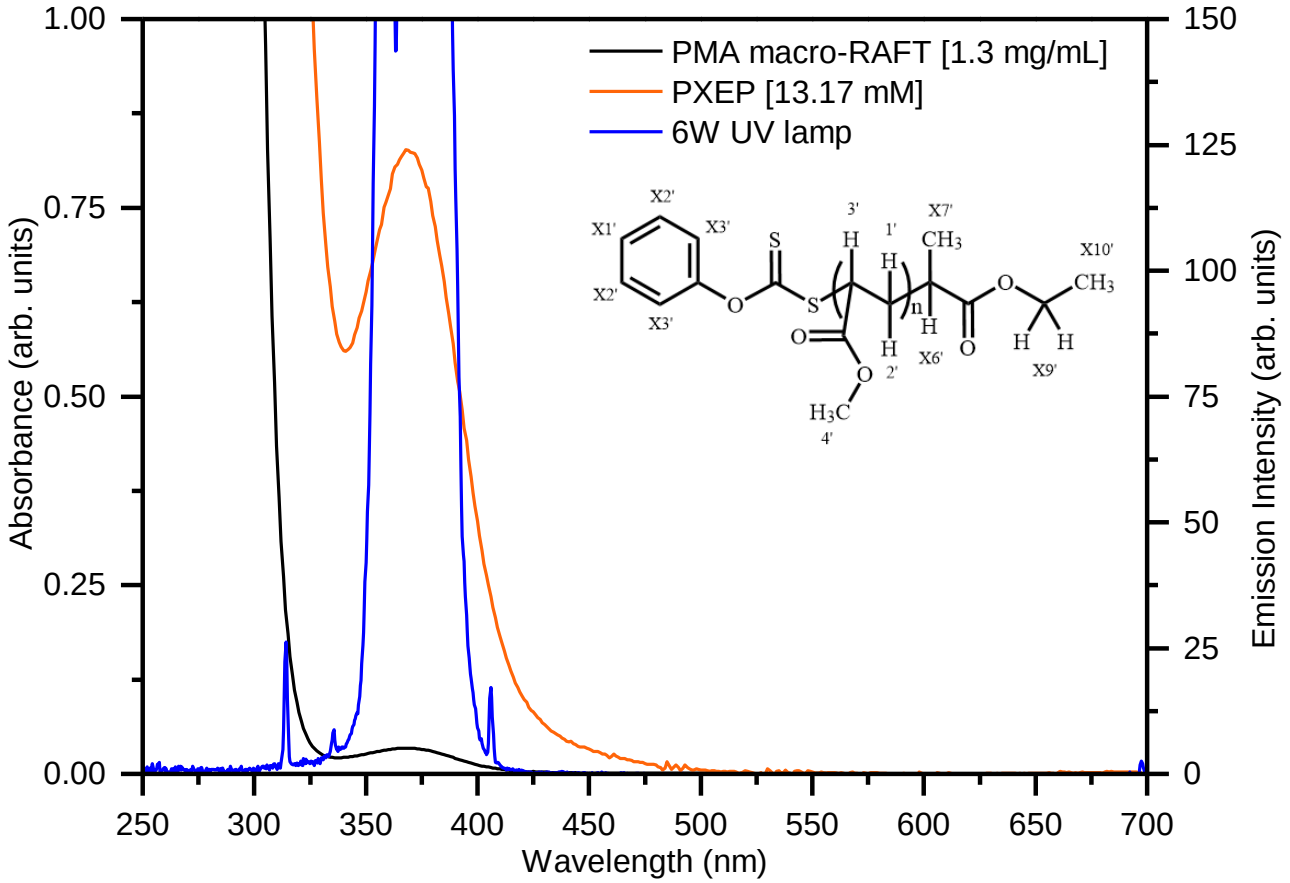

Figure 5.12: Comparison of the absorbance of the poly(MA) macro-RAFT agent used in chain extension kinetics superimposed with both the starting PXEP and the emission spectrum of the 6W UV lamp (370nm, 2 mW/cm^2).

Figure 5.13 (A) shows comparable trends to what was seen in the initial polymerisation; both the light + AIBN and light only kinetics are practically superimposable and are both much faster polymerisations than for the dark + AIBN conditions which are also very similar. This is supported by the pseudo first order kinetic plot (Figure 5.13 (B)) for the dark + AIBN conditions being essentially superimposable, with the resulting apparent rate coefficients of polymerisation being within experimental error (summarised in Table 5.4). The other two irradiation conditions yield similarly curved pseudo first order kinetic plots, once again due to high conversion being attained very rapidly. Due to the overwhelming similarities between the normal and chain extension kinetics under light only conditions, it can thus be concluded that the k_{app} and the subsequent enhancement factor are equivalent between the two experiments.

Table 5.4: Summary of calculated k_{app} values for kinetic chain extension experiments shown in Figure 5.13.

	Chain extension kinetics		Kinetics	
Condition	**k_{app} (h^{-1})**	**Error in k_{app} (+/-)**	**k_{app} (h^{-1})**	**Error in k_{app} (+/-)**
Dark + AIBN	0.29	0.03	0.32	0.04

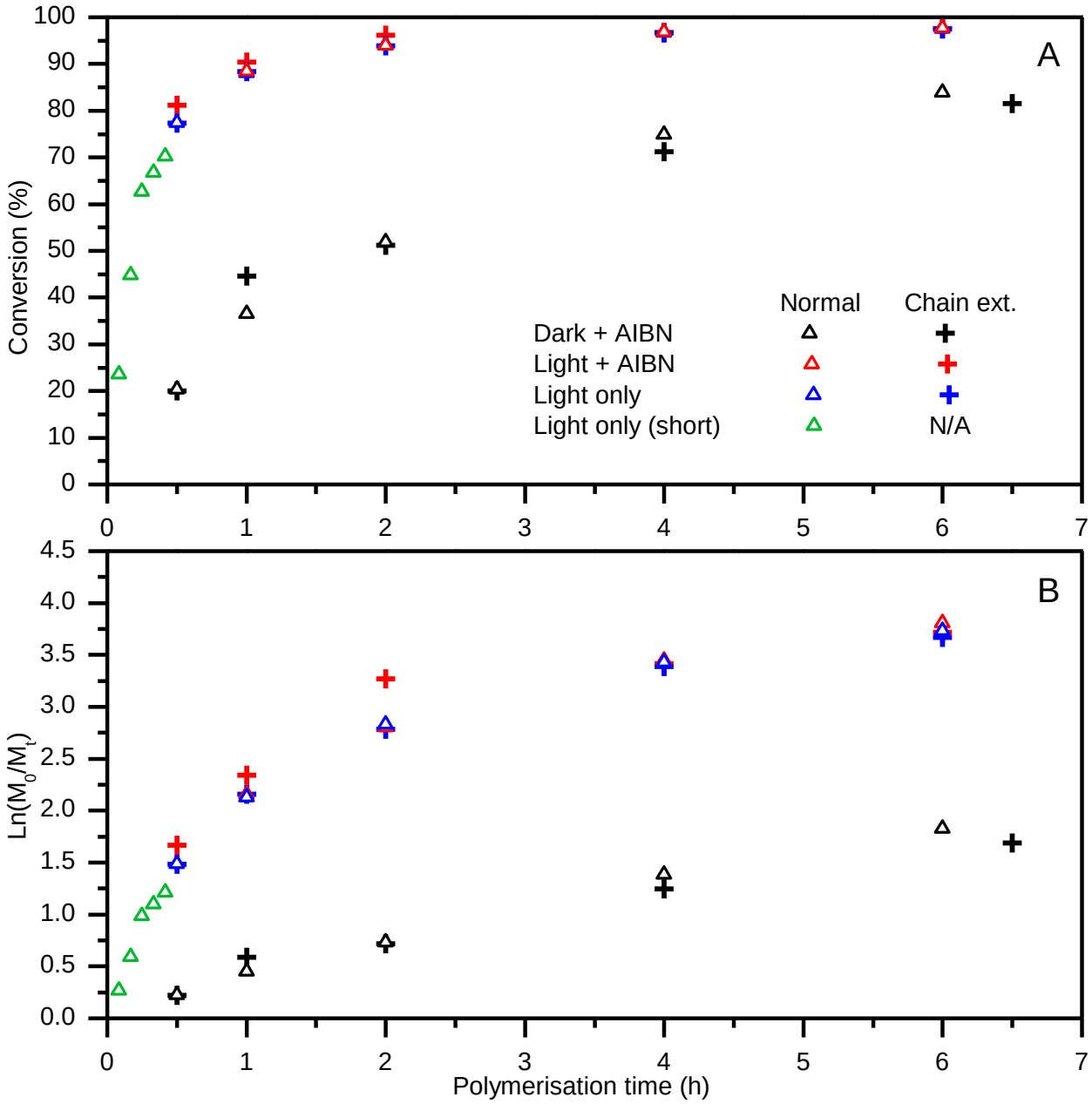

Figure 5.13: Conversion versus time plot (A) and 1st order kinetic plot (B) for MA chain extension polymerisations under various conditions at 70 °C with a poly(MA) macro-RAFT agent derived from PXEP.

Overall, this data is strongly supportive of the same reaction mechanisms being operative in both the conventional and chain extension polymerisations. This would also support the notion that incorporation of the poly(MA) segment to generate the macro-RAFT agent has not resulted in any significant changes to both the extinction coefficient and/or lower quantum yield for photolysis relative to the starting PXEP.

During chain extension, the evolution of M_n as a function of conversion under dark + AIBN conditions shows very good agreement to the theoretically predicted M_n and lower dispersity values throughout (Figure 5.14). This absence of hybrid behaviour is not surprising given that further chain

extension of a macro-RAFT agent with the same monomer effectively eliminates the RAFT pre-equilibrium. Once again, a positive deviation from the theoretical M_n under both sets of photolysis conditions along with slightly higher dispersity values can be attributed to degradation of the RAFT agent due to irreversible photolysis as described previously in section 5.3.2.

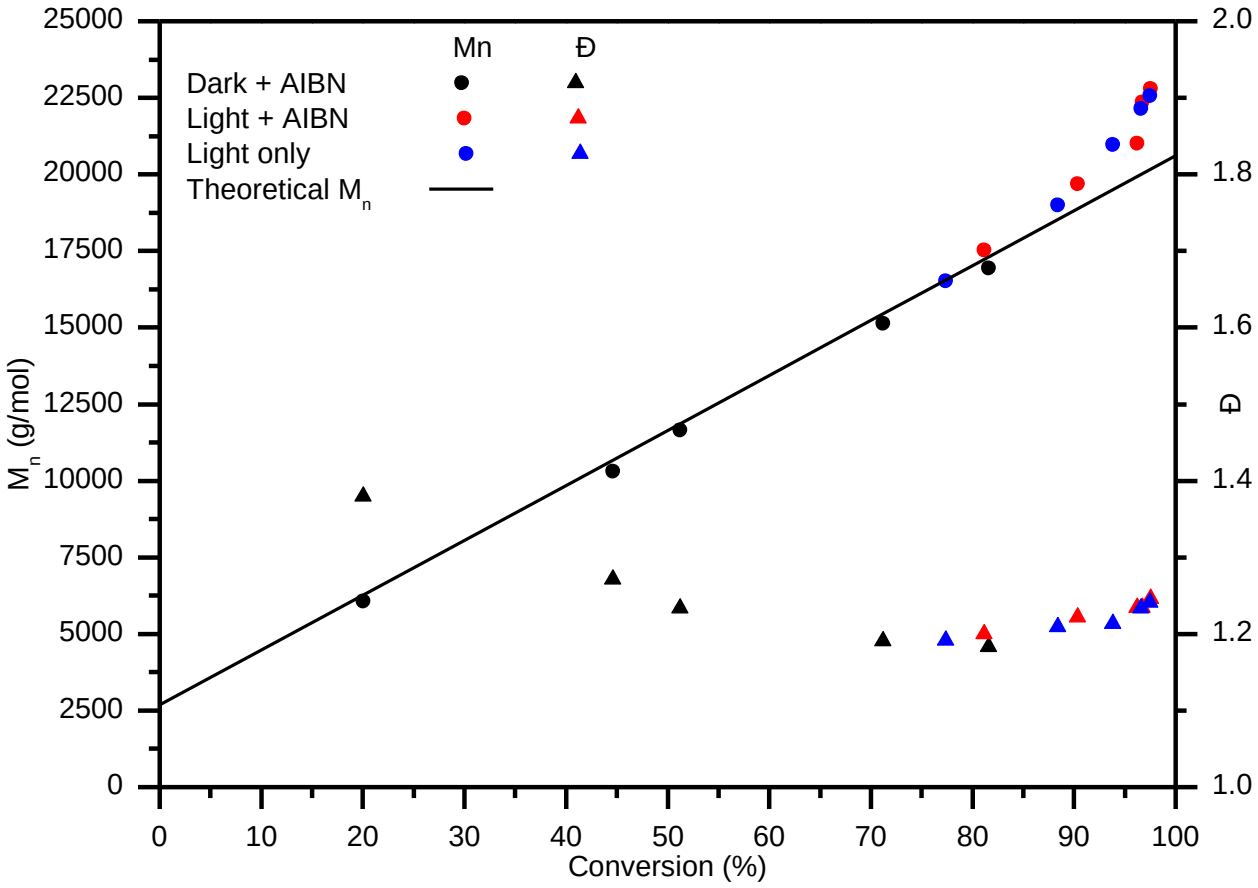

Figure 5.14: Evolution of molecular weight and dispersity as a function of conversion for MA chain extension polymerisations under various conditions at 70 °C with a poly(MA) macro-RAFT agent derived from PXEP.

Efficient chain extension as characterised by complete consumption of the starting macro-RAFT initiator and translation to higher molecular weights as a function of time; both are evident from the RI GPC plots for all polymerisation conditions shown in Figure 5.15. The GPC traces show no residual peaks or significant trailing in the low molecular weight region corresponding to the starting poly(MA) macro-initiator, which supports the notion of high chain end fidelity. The small peak centred on a retention time of ~ 31.5 minutes is an artefact that appears consistently in all traces, including a blank run featuring only filtered GPC grade THF (see Figure A5 in the Appendix).

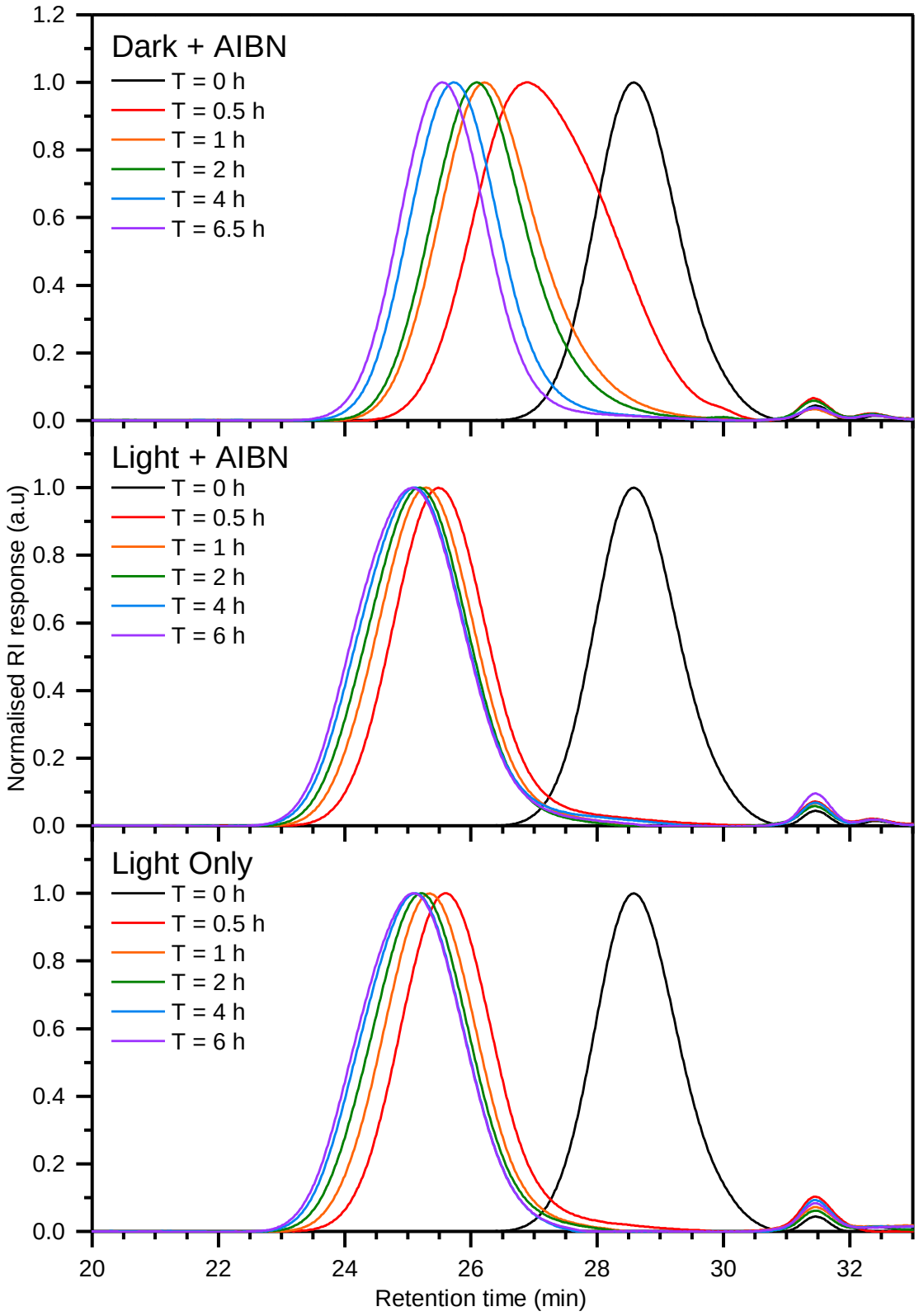

Figure 5.15: Normalised RID GPC traces for MA chain extension polymerisation samples at various time points, under various conditions at 70 °C with a poly(MA) macro-RAFT agent derived from PXEP.

Both conventional and chain extension polymerisation of MA using PXEP with 6W of UV irradiation shows marked acceleration of the polymerisation rate relative to the conventional case where dark +

AIBN conditions are employed. The RAFT mechanism appears to be active in all cases, with good control over dispersity and M_n being obtained. The exact nature of the photolysis induced enhancement in polymerisation rate is unclear; photolysis of monomer and reversible photolysis of the RAFT and macro-RAFT species via the iniferter mechanism are the primary possibilities. Experimentally it appears that photolysis of AIBN cannot be reason for the enhanced kinetics seen. All 3 scenarios are investigated with the aid of the Predici model in the subsequent sections.

5.4 Predici model development – implementation of RAFT and iniferter mechanisms

As explained in Chapter 2, section 2.6, a model can be made almost infinitely complex by including all possible reactions involving radical and non-radical species and combinations thereof. Based on multiple literature precedents and the added complexity of needing to incorporate a range of photolysis reactions, this model was designed to be comprehensive enough that all the key RAFT parameters can be manipulated, and the effect of various photolysis reactions studied. This model was summarised earlier in Scheme 4.12 in Chapter 4.

A description of the scripts pertaining to the implementation of certain kinetic rate coefficients is given in Chapter 4, section 4.9.3; a direct transcript of how these scripts were implemented is given in Table A3 in the Appendix. Table 5.5 summarises the species and their associated parameters used within the Predici model for simulations of MA polymerisations.

Table 5.5: Summary of species parameters and their concentrations as set in the model at t = 0 for modelling MA polymerisations.

Species name	Mol mass (g/mol)	Density (g/L)	Conc. (M)	Reactor
R	1.0113×10^2	1.000×10^3	0	Flask
Initiator	1.6421×10^2	1.000×10^3	4.041×10^{-4}	Flask
RAFT	2.7036×10^2	1.000×10^3	1.364×10^{-2}	Flask
I	6.911×10^1	1.000×10^3	0	Flask
I (Inactive)	6.911×10^1	1.000×10^3	0	Flask
Monomer	8.609×10^1	9.56×10^2	2.8188	Flask
Solvent	4.105×10^1	7.86×10^2	1.4215×10^1	Flask
Xanthate fragment	1.6923×10^2	1.000×10^3	0	Flask
Dummy	1.000	2.000	1.000	Abstract
Photon	1.000	2.000	1.000	Abstract

5.4.1 Omitted reactions and justifications thereof

5.4.1.1 Reaction of initiator derived radicals with RAFT agent and macro-RAFT agent

Since under the experimental conditions studied the ratio [AIBN]:[RAFT] ≈ 1 : 33 for MA and ≈ 1: 10 for VAc with a large excess of monomer in both cases, the reaction of initiator derived radicals with both the starting RAFT agent and growing macro-RAFT agent was omitted based on the statistical unlikeness of this being a significant pathway. This was the same justification suggested by Barner Kowollik *et al.* [25] in regards to this reaction.

5.4.1.2 Reversible and irreversible termination of the intermediate RAFT adduct radical

Stenzel *et al.* have reported retardation of polymerisation rate and lengthy inhibition in the polymerisation of vinyl acetate with a range of xanthates with analogous but not identical structures to PXEP; the Z groups used were a series of phenol and alkyl derivatives [26]. They theorised the inhibition periods seen could be attributed to the same potential factors as for dithiobenzoate mediated systems, namely irreversible and reversible termination of the RAFT adduct, along with slow fragmentation of the RAFT adduct radical. An alternate explanation was put forth in the *in silico* investigation by Coote & Radom [27] which uncovered a an alternate beta fragmentation pathway that results in the degradation of the xanthate adduct radical, leading to the formation of significantly less active radicals instead of the highly reactive PVAc propagating radical. Furthermore, the large K_{eq} values (~ 10^5 – 10^7) [28] that have been measured or theoretically calculated for dithiobenzoate systems are often thought to be primarily responsible for the phenomena of irreversible or reversible termination of the RAFT adduct radical. The values of K_{eq} for xanthate systems are significantly smaller (~10 – 10^2) [28] thus making these pathways seem unlikely; this was also the rationale used by Adamy *et al.* in their work which featured experimentally varying xanthate structure and subsequent modelling in Predici [29]. For these reasons, and that inhibition phenomena were not encountered experimentally during our investigations into the polymerisations being modelled, both reactions of the reversible and irreversible termination of the RAFT adduct radical were not included in the Predici model.

5.4.1.3 Chain transfer to monomer, polymer and solvent

These reactions were omitted for several reasons:

- For the case of the less reactive MA radicals the rate of chain transfer to various solvents is often orders of magnitude lower than other rate coefficients whilst for VAc it can be comparable in size to the rate of propagation [30]. There is however a very large spread of

values in the Polymer Data Handbook [13] in regards to these rate coefficients and the combinations of monomer and solvent for which they have been determined is somewhat limited [30].

- For the case of MA, chain transfer to polymer is known to occur and was taken into account when calculating the rate coefficient for propagation (see forthcoming section) however was not implemented directly as this adds a further level of complexity when dealing with populations of polymer species where there are midchain radicals present. For VAc, this process is thought not occur to any appreciable extent [31, 32], hence was not considered.
- Chain transfer to monomer was ignored for the same reason as transfer to polymer; the rate coefficients are often orders of magnitude smaller than the propagation rate coefficients and similarly, the spread of literature values is significant [30]. For the case of VAc, transfer to monomer was estimated by Monyatsi *et al.* to be 3 to 5 orders of magnitude lower than k_p [33].

Furthermore, there have been several investigations of various kinetic and mechanistic aspects of the polymerisations of both MA [34, 35] and VAc [36, 37] in Predici, and in every case the match between the modelling results and the experimental data was satisfactory, and none of these publications considered the phenomena listed above.

5.4.1.4 Reactions involving thiyl radicals generated during RAFT and macro-RAFT agent photolysis

Due to their relative abundance of RAFT agent (and thus macro-RAFT agent) compared to monomer and macro-radicals, the 1st reaction in Scheme 5.3 is not expected to be significant reaction pathway. Though the coupling of thiyl radicals from the photolysis of dithiocarbamates [38] and xanthates is known to occur [39] (reaction 2, Scheme 5.3), this reaction was not implemented in a reversible manner. This was due to the reasoning that the bis thiocarbonylthio disulfides would most likely have different photochemical properties to the parent xanthate, thus estimating appropriate kinetic rate coefficients for processes involving these species would be problematic. Insofar as bis thiocarbonylthio disulfides have sometimes been found to be stable to further photolysis [38], this coupling reaction is analogous to general degradation of the xanthate radical. A specific degradation reaction concerning the xanthate radical was not included, instead the accumulation of the xanthate radical was assumed to represent the degradation of the starting RAFT agent.

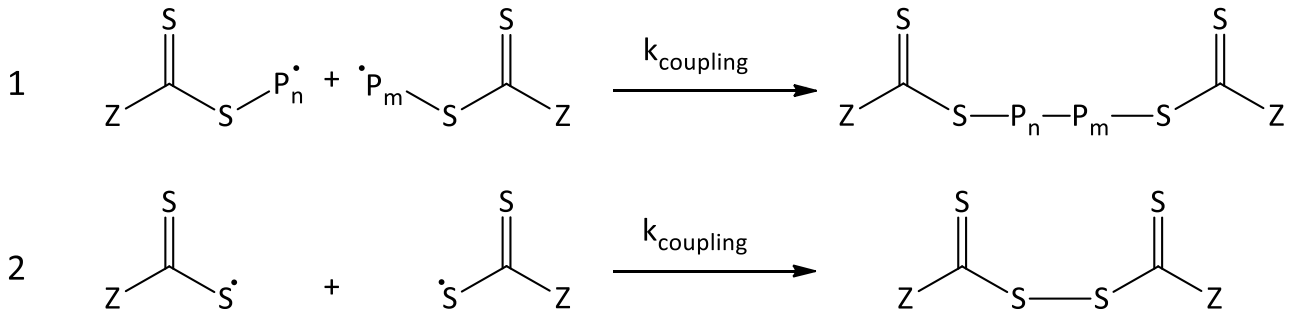

Scheme 5.3: Possible reactions involving the xanthate radical and pRAFT2 radical species which were omitted.

5.5 Predici model development – calculation, selection and testing of kinetic rate coefficients for baseline result

To ensure the best possible accuracy for the Predici model that was developed, the rate coefficients used in the model were determined per the following hierarchy:

1. Those that could be experimentally determined were done so as described previously in section 5.2.
2. Rate coefficients that could be calculated based on the relevant relationships established in the literature were done so, using the relevant experimental data.
3. Rate coefficients which did not fall into the first two categories were recalculated under experimental conditions using Arrhenius parameters obtained from the literature.
4. For rate coefficients that could not be calculated and for which there were multiple literature precedents, they were tested in turn and selected such that the closest match occurred between the experimental values and model outputs.
5. For circumstances where the previous procedure failed to give a sufficient fit between experimental and model output, the rate coefficients were fitted as closely as possible within reasonable limits, however this option was only used as a last resort.
6. Finally, for rate coefficients that had no literature precedents or only an approximate or theoretical value, several values including the logical “extremes” that these rate coefficients could conceivably take were tested.

This method was also the basis for the sensitivity analysis conducted when testing the various photolysis phenomena as described later.

5.5.1 Calculation of rate coefficient of 2-cyano-2-propyl radical (AIBN radical) addition to MA

The absolute experimentally derived rate constants (M^{-1} s^{-1}) and frequency factors ($log_{10}(A/ M^{-1} s^{-1})$ for the addition of various radicals to a range of mono and di-substituted alkenes (CH_2=CXY) at the listed temperature was taken from Table 1.0 in the comprehensive review by Fischer & Radom [40]. As the absolute rate constants were measured at various temperatures, it was necessary to reverse calculate the activation energies (E_a) by rearrangement of the Arrhenius equation. Since the exact value of "room temperature" is not specified within the text, using standard convention it was assumed to be equal to 22 °C (295.15 K) and the recommended frequency factors (L mol^{-1} s^{-1}) as given in the text were used. This lead to slight deviations (mostly < 1 kJ/mol) between the calculated E_a values to those listed in Table 2.0 in the review, even though they were supposedly also calculated from the same values as given in Table 1.0. The E_a for the addition of AIBN radicals to MA was found to be 29742 J/mol and the absolute rate constant at 70 °C (343.15 K) was calculated to be 939 M^{-1} s^{-1}, which was the value set for k_i in the model.

5.5.2 Calculation of the propagation rate coefficient for MA

The propagation rate coefficient (k_p) for MA under experimental conditions (70 °C, 2.79 M) was calculated in a two-stage procedure. Firstly, k_p in bulk MA at 70 °C was calculated using the Arrhenius equation using values for E_a of 17.3 kJ/mol and a frequency factor of 1.41 x 10^7 (L mol^{-1} s^{-1}) as recommended in the IUPAC guided review by Barner-Kowollik *et al.* [41], resulting in a value of k_p = 32798 L mol^{-1} s^{-1}. This report summarised k_p values determined via the PLP-SEC and PLP-MALDI techniques for bulk MA polymerisation in the range of – 28 to 60 °C. It was stressed that the derived Arrhenius parameters are for the propagation of secondary radicals present on the chain end in MA polymerisation, and thus give an overestimation of the actual "effective" k_p ($k_{p(eff)}$) seen under typical experimental conditions. This arises from the fact that acrylates are prone to the formation of tertiary midchain radicals due to inter and intra-molecular branching reactions and these show a marked decrease in reactivity [42-44]. $k_{p\ (eff)}$ was determined by applying Equation 5.1, as given in [41]. This is accounts for the decrease in the propagation rate coefficient as a function of monomer concentration seen for MA and the implication of monomer reaction orders greater than 1 [34].

$$k_{p\ (eff)} = \frac{k_p}{1 + \frac{k_{(bb)}}{k_{p\ (tert)} \cdot C_M}}$$

Equation 5.1 Determination of the effective propagation coefficient for MA polymerisation

Where $k_{p(eff)}$ is the effective kp (L mol^{-1} s^{-1}), k_p is the calculated k_p for secondary radicals (L mol^{-1} s^{-1}), $k_{(bb)}$ is the rate coefficient for the back biting reaction to form tertiary radicals (L mol^{-1} s^{-1}), $k_{p(tert)}$ is the rate coefficient for the propagation of tertiary radicals (L mol^{-1} s^{-1}) and C_m is the starting monomer concentration (mol L^{-1}). Values for $k_{(bb)}$ and $k_{p\ (tert)}$ have not been determined for MA, however have been for butyl acrylate (BA) which shows an almost identical fraction of midchain radical formation under identical PLP-SEC conditions [41]; this leads to the assumptions as given within this review that $k_{p(tert)} \approx k_p/1000$ and $k_{(bb)} \approx 100$ L mol^{-1} s^{-1} (at 60 °C). Using k_p = 32798 L mol^{-1} s^{-1}, $k_{p\ (tert)}$ = 32.798 L mol^{-1} s^{-1}, C_M = 2.79 mol L^{-1} gives a final value of $k_{p\ (eff)}$ = 15672 L mol^{-1} s^{-1} which was set as the value of k_p in the model. Even though the formation of midchain radicals was not explicitly put into the Predici model in the form of generating separate polymeric species with different reactivity, for kinetic considerations this is nevertheless an important correction to include due to the precedent for the occurrence of this phenomena under experimentally relevant conditions.

5.5.3 Selection of 1-ethoxycarbonyl ethyl radical (R group radical) addition rate coefficient to MA

The 1-ethoxycarbonyl ethyl radical derived from the fragmentation of the model xanthate has a structure that is essentially analogous to the structure of the propagating radical derived from MA (shown in Scheme 5.4). Based on this it was assumed that the rate of addition of the R group radical to MA monomer was identical to that of the effective rate of propagation, hence a value of $k_{R\text{-}re}$ = $k_{p(eff)}$ = 15672 L mol^{-1} s^{-1} was used. This is the same approach taken in various publications, and is a feature of the RAFT-CLD method [34].

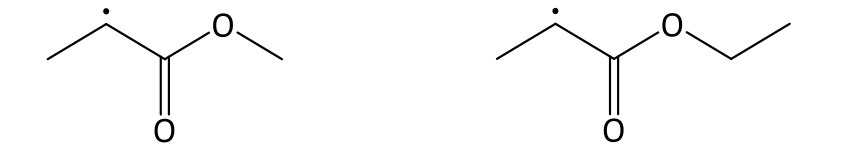

Methyl acrylate radical 1-ethoxycarbonyl ethyl radical (R group radical)

Scheme 5.4: Structural comparison of MA propagating radical and R group radical derived from PXEP.

5.5.4 Initiator efficiency factor (f) for AIBN breakdown

The values for the initiator efficiency of AIBN in MA polymerisations and the methods of implementation in simulations in Predici is summarised in Table 5.6; the approach utilising a linear decrease from f to 0 as a function of monomer conversion was implemented. Based on these literature precedents, f was set to 0.7 in the model.

Table 5.6: Implementations for AIBN breakdown in simulations of MA polymerisations.

Initiator efficiency model	f	Reference
Linear decrease from f to 0 at 100% monomer conversion	0.7	[34]
Constant efficiency of f	0.7	[34, 35]

5.5.5 Determination of k_d for AIBN degradation

The value of k_d for AIBN degradation was determined experimentally under both dark and irradiation conditions as described previously in section 5.2.4, with this value of 1.653 $x10^{-5}$ s^{-1} being used in the baseline model.

5.5.6 Selection of termination rate coefficients

The relative contribution of termination by disproportionation in MA has been disputed over the years, however more recent work has supported a preference for termination primarily by combination [45]. The value of kt_(disproportionation) was set to 0 to simulate termination solely by combination, as has been done by other authors when simulating the RAFT process in Predici [34, 46, 47]. As can be seen from Table 5.7, a range of implementations and values for the termination rate coefficient have been used in the past.

Table 5.7: Summary of termination values and implementation used for modelling MA polymerisations.

Termination model	$i_{, cross}$	$\log k_t^{1,1}$	α	Reference
Varied	~ 10	7.7 – 8.7	0.37 – 0.8	[48]
Varied	5	9.0	0.4	[34]
Varied	20	9.0	0.78 (short), 0.15 (long)	[35]
Varied	30	9.0	0.78 (short), 0.26 (long)	[49]
Varied	30	8.25	0.79 (short), 0.21 (long)	[50]
Fixed	N/A	9.0	N/A	[51]

The values of “alpha_short”, “alpha_long” and “i_cross” in the model were set to the values 0.79, 0.21 and 30 respectively, as determined most recently by Barth *et al.* [50]. The value of $k_t^{1,1}$ (“kt_1” in the model) is generally accepted to be equal to ~ 10^9, hence kt_1 was set to an initial value of 10^9 and the simulation tested to assess the kinetic behaviour; the other tested values of kt_1 are shown in Table 5.8. With the core model active, the other parameters in the model were set as shown in Table 5.8, with the parameters set as described previously, with the parameters relating to the RAFT mechanism explained in the forthcoming section.

Table 5.8: Summary of model parameters for baseline MA kinetic model, including parameters tested during each baseline simulation.

Parameter	Value	Units
ki	9.3900 x10^{2}	L mol^{-1} s^{-1}
kR-re	1.5672 x10^{4}	L mol^{-1} s^{-1}
kd	1.6530 x10^{-5}	s^{-1}
kp	1.5672 x10^{4}	L mol^{-1} s^{-1}
f	7.0000 x10^{-1}	N/A
alpha_short	7.9000 x10^{-1}	N/A
alpha_long	2.1000 x10^{-1}	N/A
i_cross	3.0000 x10^{1}	N/A
Termination parameters		
Simulation #	**Value of kt_1**	**Log (kt_1)**
B.1	9 x10^{9}	9.00
B.2	1.5849 x10^{9}	9.20
B.3	1.9953 x10^{9}	9.30
B.4	1.7783 x10^{9}	9.25

The starting value of $k_t^{1,1}$ = 1.0 x10^{9}, taken as a general guideline from literature, gives a conversion vs time profile that is higher compared to the experimental dark + AIBN data (sim B.1, Figure 5.16). Several higher values were tested (sim B.2 & B.3, Figure 5.16); adjusted to the marginally higher value of $k_t^{1,1}$ = 1.7783 x10^{9}, sim B.4 (Figure 5.16) yields a very close fit to the experimental data it is supposed to replicate. Furthermore, as can be seen from Figure 5.16 inset, the value of $k_t^{1,1}$ undergoes a rapid inflection as the average chain length of the macro-radicals exceeds that of the cross over length. Thus, the value of $k_t^{1,1}$ at t ~ 0 is essentially analogous to the value of k_t^0 and takes on a value of ~ 5.8 x10^{8} L mol^{-1} s^{-1} which is comparable to literature values within the scatter in values typically seen when this value is determined experimentally [37, 49]. The termination values used in all subsequent modelling was fixed to those parameters as shown for Sim B.4 in Table 5.8.

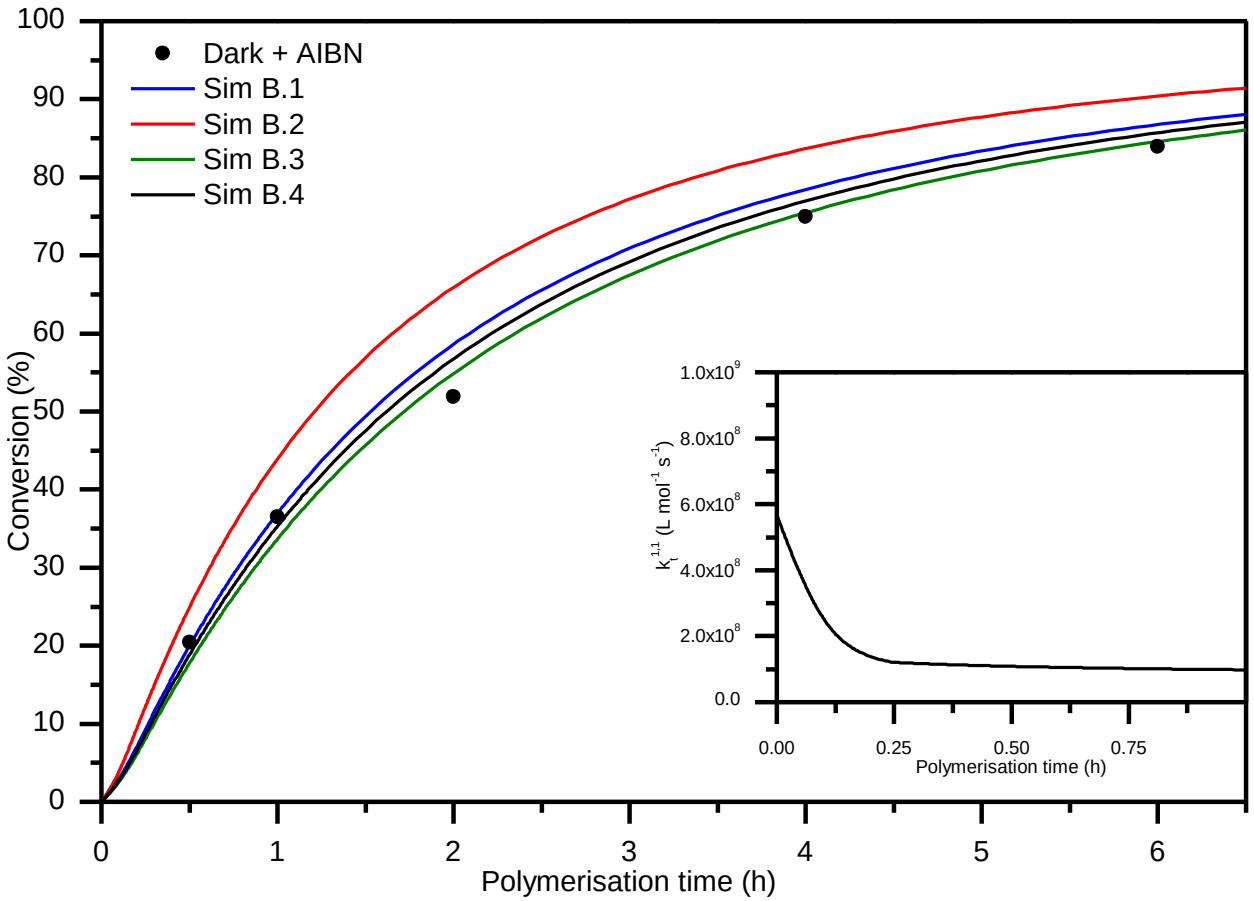

Figure 5.16: Comparison of kt_1 values and their effect on the simulated kinetics (conversion vs time) of the polymerisation of MA under dark + AIBN conditions, and inset, the value of kt_1 as a function of polymerisation time.

5.5.7 Parameters for RAFT pre-equilibrium & main equilibrium

As has been stated previously, the values of K_{eq} for xanthate systems lie in the range of ~10 – 10^2 [28]; for this reason, all values for fragmentation rate coefficients were set such that the value of K_{eq} for both sides of the pre-equilibrium and for the main equilibrium were equal to 100. Choosing the upper limit for this value will not have any kinetic consequences; Vana *et al.* proved that for "sensible" values of addition rate coefficients, differences in kinetic behaviour only manifest when $K_{eq} > 10^6$ [47].

Setting $k_p = k_{R\text{-}re}$ was based on the assumption of equal reactivities of both the R group radical and the propagating MA radical based on their similar structure. Logically this implies that that the pre-equilibrium RAFT adduct radical is expected to fragment with equal probability to both starting materials (RAFT agent + macro-radical) and products (R group radical + pRAFT).

The hybrid behaviour seen experimentally for the dark + AIBN conditions allows the value of the initial chain transfer constant ($C_{tr,0}$) to be estimated via Equation 5.2 [34].

$$X_n^0 \approx \frac{[M]_0}{C_{tr,0} \cdot [RAFT]_0} + 1$$

$$\therefore C_{tr,0} \approx \frac{[M]_0}{(x_n^0 - 1) \cdot [RAFT]_0}$$

Equation 5.2: Expression for the estimation of the initial chain transfer constant ($C_{tr,0}$).

The slight positive deviation from the expected M_n for the first two conversion points under dark + AIBN conditions appears non-linear in nature; when this is fitted with a quadratic equation the intercept at zero conversion results in a M_n value of 3800 g/mol, or a chain length of 44.15. Using Equation 5.2 gives a value for $C_{tr,0}$ = 4.79, which in this case is also equal to $C_{-tr,0}$. Using Equation 5.3 with the set value of k_p = 15672 L mol^{-1} s^{-1}, gives a value for both $k_{tr,0}$ and $k_{-tr,0}$ = 7.5038 x10^4 L mol^{-1} s^{-1}.

$$C_{tr,0} = \frac{k_{tr,0}}{k_p} \quad and \quad C_{-tr,0} = \frac{k_{-tr,0}}{k_{R-re}}$$

Equation 5.3: Definitions for chain transfer constants in the pre-equilibrium of the RAFT mechanism.

Obtaining the values of $k_{add,0}$ and $k_{-add,0}$ requires using Equation 5.4, with the partition coefficient (Ø) being set to 0.5 for the reason stated previously. This yields $k_{add,0}$ = $k_{-add,0}$ = 1.50078 x10^5 L mol^{-1} s^{-1}, with the corresponding values of $k_{frag,0}$ = $k_{-frag,0}$ = 1.50078 x10^5 L mol^{-1} s^{-1}

$$k_{tr,0} = k_{add,0} \cdot \frac{k_{frag,0}}{k_{frag,0} + k_{-frag,0}} = k_{add,0} \cdot \phi$$

$$k_{-tr,0} = k_{-add,0} \cdot \frac{k_{-frag,0}}{k_{frag,0} + k_{-frag,0}} = k_{-add,0} \cdot (1 - \phi)$$

Equation 5.4: Definitions of k_{add} and k_{-add} for the RAFT pre-equilibrium.

Equation 5.3 also applies for the determination of the values of k_{tr} and k_{-tr} for the main equilibrium; the values for C_{tr} have been determined previously (Figure 5.11). A range of parameters were tested to establish the best fit based several values calculated. The values of $k_{-tr,0}$ and thus k_{frag} for the main equilibrium need to be divide by a factor of 2 from the actual values determined; this is due to how the RAFT equilibrium is implemented in Predici [52, 53]. The values tested for the pre-equilibrium and equilibrium for testing of molecular weight control are compiled in Table 5.9, with the kinetic parameters set as those previously optimised. Simulation B.8 used values derived from an average of C_{tr} values calculated from the t = 0.5 and 1 h data points. Simulation B.9 used an estimated value of C_{tr} at a chain length of 0, which was calculated using a linear line of best fit to the C_{tr} values for the dark + AIBN conditions, with the first data point (t = 0.5 h, Ctr = 16.44) being omitted.

Table 5.9: Summary of model parameters for the RAFT pre-equilibrium and equilibrium for baseline kinetic model, including parameters tested during each simulation.

Parameter	Value	Units		
ki	9.3900 x10^{2}	M^{-1} s^{-1}		
kR-re	1.5672 x10^{4}	M^{-1} s^{-1}		
kd	1.6530 x10^{-5}	s^{-1}		
kp	1.5672 x10^{4}	M^{-1} s^{-1}		
f	7.0000 x10^{-1}	N/A		
alpha_short	7.9000 x10^{-1}	N/A		
alpha_long	2.1000 x10^{-1}	N/A		
i_cross	3.0000	N/A		
kt_1	1.7783 x10^{9}	M^{-1} s^{-1}		
Pre-equilibrium parameters				
kadd,0	1.50078 x10^{5}	M^{-1} s^{-1}		
k-add,0	1.50078 x10^{5}	M^{-1} s^{-1}		
kfrag,0	1.50078 x10^{3}	M^{-1} s^{-1}		
k-frag,0	1.50078 x10^{3}	M^{-1} s^{-1}		
Equilibrium parameters				
Simulation #	**Time point (h)**	**C_{tr}**	**kadd**	**kfrag**
B.5	0.5	1.6447 x10^{1}	5.1552 x10^{5}	2.5776 x10^{3}
B.6	1	1.0231 x10^{1}	3.2070 x10^{5}	1.6035 x10^{3}
B.7	6	6.1509	1.9279 x10^{5}	9.6397 x10^{2}
B.8	~ 0.75	1.3339 x10^{1}	4.1811 x10^{5}	2.0905 x10^{3}
B.9	~ 0	1.3884 x10^{1}	4.3518 x10^{5}	2.1759 x10^{3}

The higher than expected dispersity values early in the simulation (Figure 5.17) most likely occur due to the fact that Predici computes dispersity values based on a method of moments approach. At low conversions at the start of a reaction, this can be somewhat inaccurate due to large number of dormant chains in comparison with that of propagating chains. This was the same explanation as put forth by Wang & Zhu who saw similar initially high PDI values when simulating a generic RAFT polymerisation such as MA or St with a dithioester [54]. Irrespective of this fact, the simulations are mainly used to test kinetic behaviour, and in respect to dispersity values, relative trends can be compared as opposed to absolute values. All the simulations whose parameters are given in Table 5.9 are compared as a function of conversion in Figure 5.17. As expected, since the variation in parameters relating to the RAFT equilibrium is minor, there is no influence on the kinetics of the process.

Based on a reasonable fit with the experimental data, the parameters from sim B.6 were selected as the RAFT parameters for the baseline model of simulating the MA polymerisation under dark + AIBN conditions. and from this point on whenever the baseline simulation/result is discussed, it refers to sim B.6, using the parameters summarised in Table 5.10.

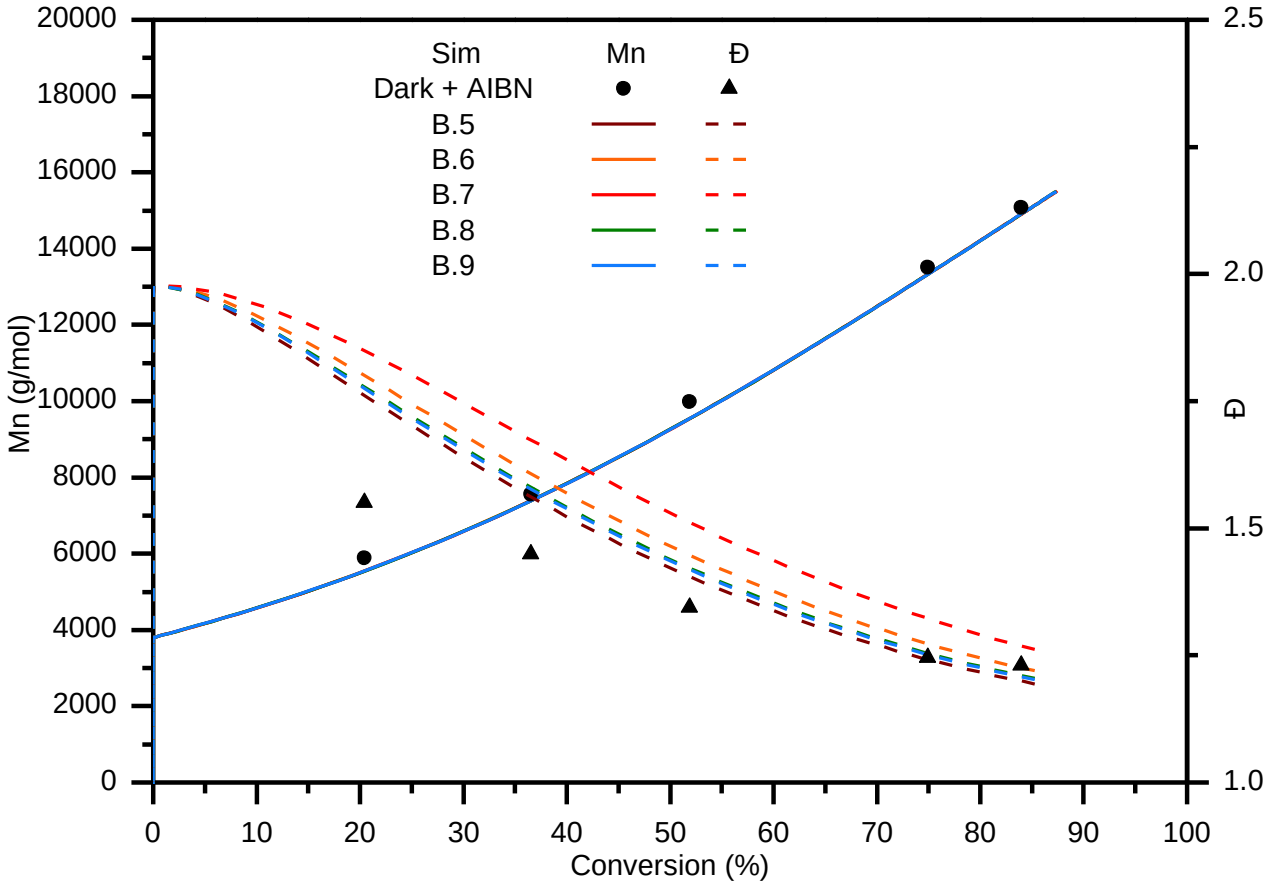

Figure 5.17: Comparison the effect of pre-equilibrium and equilibrium values on the overall dispersity values (overall dispersity vs conversion) of the polymerisation of MA under dark + AIBN conditions. Values tested are shown in Table 5.9.

Table 5.10: Finalised baseline parameters for modelling MA polymerisation under dark + AIBN conditions.

Parameter	Value	Units
ki	9.3900×10^{2}	$M^{-1} s^{-1}$
kR-re	1.5672×10^{4}	$M^{-1} s^{-1}$
kd	1.6530×10^{-5}	s^{-1}
kp	1.5672×10^{4}	$M^{-1} s^{-1}$
f	7.0000×10^{-1}	N/A
alpha_short	7.9000×10^{-1}	N/A
alpha_long	2.1000×10^{-1}	N/A
i_cross	3.0000×10^{1}	N/A
kt_1	1.7783×10^{9}	$M^{-1} s^{-1}$
Pre-equilibrium parameters		
kadd,0	1.50078×10^{5}	$M^{-1} s^{-1}$
k-add,0	1.50078×10^{5}	$M^{-1} s^{-1}$
kfrag,0	1.50078×10^{3}	$M^{-1} s^{-1}$
k-frag,0	1.50078×10^{3}	$M^{-1} s^{-1}$
Equilibrium parameters		
kadd	3.2070×10^{5}	$M^{-1} s^{-1}$
kfrag	1.6035×10^{3}	$M^{-1} s^{-1}$

5.6 Predici Results – Scenario 1: direct photolysis of monomer

Activating reaction 18 (Scheme 5.1) which is responsible for direct initiation of monomer and disabling all other sources of initiation within the model allowed the sensitivity of the model towards the kinetic rate coefficient of $k_{photons\text{-}monomer}$ to be tested. Determining what values are realistic for this parameter involved matching the conversion attained in the control experiments conducted in the absence of any RAFT agent but with UV irradiation which were described previously in section 5.2.3. This necessitated deactivating all reactions within the model except those responsible for a free-radical mechanism (only reactions 4, 17 & 18 were active, Scheme 5.1). A second higher value was also determined as a natural upper limit, this time with the RAFT mechanism active (reactions 4 – 17, 17 & 18 were active, Scheme 5.1). This arose from the fact that the RAFT mechanism significantly lowers the conversion achieved for a given value of $k_{photons\text{-}monomer}$ as compared to a solely free radical mechanism. This is a direct result of the RAFT mechanism lowering the M_n obtained which results in a larger termination rate coefficient (k_t) coupled with there being more termination reactions active within the model. The results are summarised in Table 5.11.

Table 5.11: Summary of simulations for determining the natural limits for the kinetic rate coefficient governing the direct initiation from monomer photolysis, $k_{photons\text{-}monomer}$.

Simulation	$k_{photons\text{-}monomer}$ (M^{-1} s^{-1})	Conversion with RAFT mechanism inactive (%)	Conversion with RAFT mechanism active (%)
1.A	1.60×10^{-12}	20.09	6.51
1.B	2.00×10^{-11}	45.71	20.76

Thus, the values of 1.60×10^{-12} and 2.00×10^{-11} M^{-1} s^{-1} are considered the realistic values for $k_{photons\text{-}monomer}$, however a range of higher values were also simulated to test whether the higher conversions seen could theoretically be attained via this initiation method, and if so, whether the control over the M_n and Đ would be retained. For this series of simulations, the baseline simulation which includes conventional initiation by breakdown of AIBN was active in all cases, which allows the light + AIBN experimental scenario to be modelled.

Table 5.12: Summary of $k_{photons\text{-}monomer}$ tested to simulate the effect of direct photolysis of monomer.

Simulation	$k_{photons\text{-}monomer}$ (M^{-1} s^{-1})
Baseline	N/A
1.1	1.6000×10^{-12}
1.2	2.0000×10^{-11}
1.3	1.0000×10^{-9}
1.4	1.0000×10^{-8}
1.5	1.0000×10^{-7}

The rate of generation of initiating radicals due to the breakdown of AIBN and photolysis of monomer can be calculated using Equation 5.6 and Equation 5.6 respectively. Since the initiating radicals in each case can be consumed in termination reactions, these rates represent an upper limit, however they still allow for a direct comparison of their relative contributions.

$$R_{i(AIBN)} = k_i \cdot [I^*] \cdot [M]$$
$$\therefore R_{i(AIBN)} = 2 \cdot f \cdot k_d \cdot [I_2]$$

Equation 5.5: Expression used to calculate the rate of initiation due to AIBN breakdown.

$$R_{i(photolysis-monomer)} = k_p \cdot [macro^*] * [M]$$
$$\therefore R_{i(photolysis-monomer)} = k_{photons-monomer} \cdot [Photon] \cdot [M]$$

Equation 5.6: Expression used to calculate the rate of initiation due to photolysis of monomer.

When the previously determined realistic values of $k_{photons\text{-}monomer}$ (listed in Table 5.11) are used in sims 1.1 & 1.2 (brown & orange curves respectively, Figure 5.18 (A)) this gives identical kinetic behaviour to the baseline model which does not feature photolysis of monomer (black curve, Figure 5.18 (A)). This behaviour is unsurprising when the relative rates of initiation are considered; Figure 5.18 (B) shows that the rate of initiation from photolysis of monomer in sims 1.1 & 1.2 is approximately 3 and 2 orders of magnitude smaller than from AIBN degradation respectively.

Higher values of $k_{photons\text{-}monomer}$ were tested to see if the observed kinetic behaviour could theoretically arise if photolysis of monomer occurred to a sufficient extent; only when the rate of initiation due to photolysis approaches or exceeds in magnitude the rate of initiation due to AIBN degradation (sims 1.3 – 1.5, Figure 5.18, B) does the rate of polymerisation increase noticeably (sims 1.3 – 1.5, Figure 5.18, A). Regardless of the value of $k_{photons\text{-}monomer}$ tested, all simulations showed essentially identical development of both M_n and dispersity as a function of conversion relative to the baseline model (for data, see Figure A8 in the Appendix.

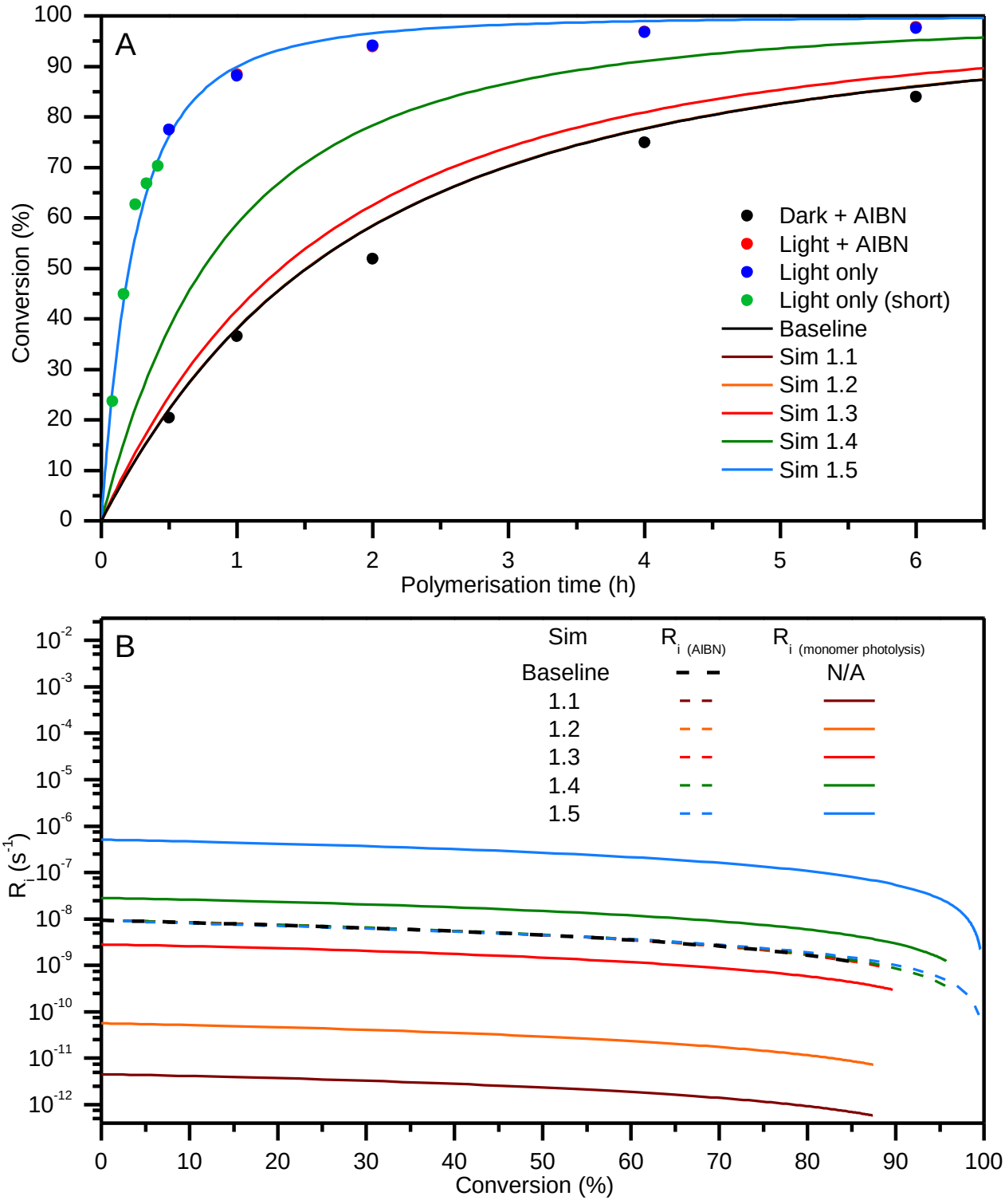

Figure 5.18: Comparison of conversion vs time plots for simulations 1.1 – 1.6 and experimental data (A) and calculated rates of initiation due to breakdown of AIBN and photolysis of monomer (B).

Overall this series of simulations support the experimental findings and imply that photolysis of monomer is not the reason for the increased kinetics seen under light + AIBN conditions.

5.7 Predici Results – Scenario 2: photolysis of AIBN

A series of simulations were run which used various multiplication factors (Table 5.13) to test whether an increased rate of AIBN degradation caused by photolysis could replicate the light + AIBN kinetics.

Table 5.13: Summary of k_d values tested to simulate the effect of photolytically accelerated degradation of AIBN.

Simulation	k_d (s^{-1})	Multiplication factor for k_d	$k_{photons\text{-}monomer}$ (M^{-1} s^{-1})
Baseline	1.6530×10^{-5}	1.00	**N/A**
2.1	5.0660×10^{-5}	3.06	1.60000×10^{-12}
2.2	5.0660×10^{-5}	3.06	2.0000×10^{-11}
2.3	8.2650×10^{-5}	5.00	**N/A**
2.4	2.4795×10^{-4}	15.00	**N/A**
2.5	4.9590×10^{-4}	30.00	**N/A**
2.6	1.6530×10^{-3}	100.00	**N/A**

The first two simulations (sims 2.1 & 2.2) employed the maximum value of k_d determined experimentally under UV irradiation (5.0660×10^{-5} s^{-1}). These simulations also tested the possibility of monomer photolysis occurring concurrently, with the values of $k_{photons\text{-}monomer}$ being set to the realistic values as determined previously in section 5.2.3.

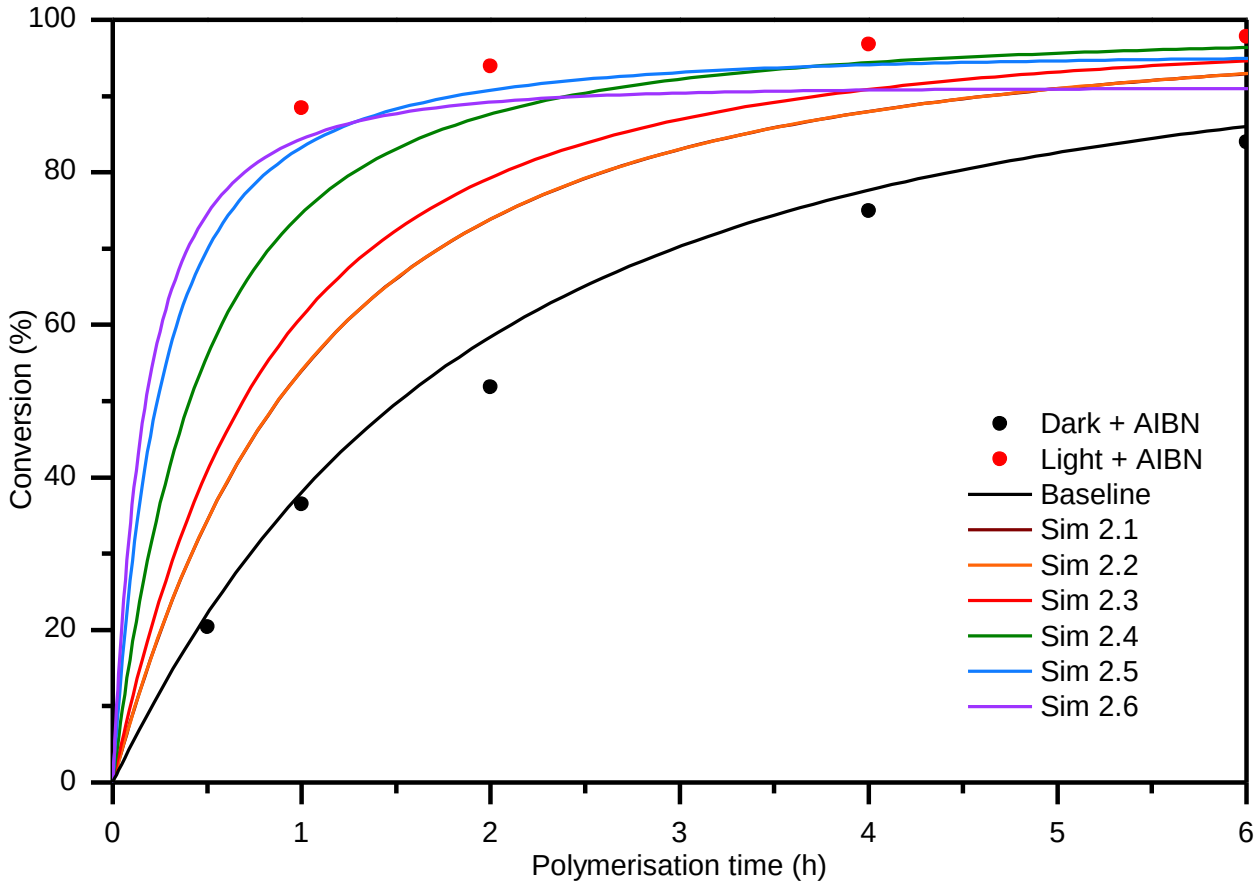

Figure 5.19: Comparison of conversion vs time plots for simulations 2.1 – 2.6.

Sims 2.1 & 2.2 (brown & orange curves respectively, Figure 5.19) both result in significantly faster kinetics relative to the baseline result (black curve, Figure 5.19), however cannot match the experimental data seen for the light + AIBN case. This confirms that photolysis of AIBN cannot be the reason for the increased kinetics seen under photolysis conditions, which logically confirms the experimental data which showed identical kinetics under both light only and light + AIBN conditions. Furthermore, the fact the kinetic curves for sims 2.1 & 2.2 are superimposed indicates that the kinetic contribution of monomer photolysis is negligible, which is consistent with the findings made previously in section 5.2.3.

Hypothetically higher rates of AIBN breakdown were tested, resulting in significantly faster kinetics as is evident from sims 2.3 – 2.6 (Figure 5.19). None of these hypothetical values of k_d can reproduce the kinetics of the light + AIBN result; the closest match to the initial rapid polymerisation occurs for a 100x greater k_d value (sim 2.6). Furthermore, as the value of k_d is increased, the final conversion attained eventually begins to decrease. This occurs due to both the concentration of AIBN and macro-radicals decreasing in tandem to essentially zero before the reaction finishes for the highest values of k_d tested; this was confirmed by the concentrations of these species within the model (see Figure A9

in the Appendix). This is not unexpected and has been classically referred to as a "dead end" polymerisation, where the polymerisation ceases when all the initiator has been consumed [55]. Regardless of the value of k_d tested, all simulations showed essentially identical development of both M_n and dispersity as a function of conversion relative to the baseline model (see Figure A10 in the Appendix).

By process of elimination, the previous simulations strongly indicate that photolysis of monomer and/or AIBN are both unable to account for the increased kinetics seen under irradiation, which only leaves reversible photolysis of the RAFT agent and the iniferter effect as the final scenario to consider.

5.8 Predici Results – Scenario 3: Reversible photolysis of RAFT species

As discussed previously within the literature review (section 2.4.4) and the introduction (section 5.1) light can photolyse the RAFT agent directly in a reversible manner, resulting in polymerisation in the presence of monomer. The reversible photolysis of the RAFT species as implemented by reactions 19 – 22 in Scheme 5.1 can be summarised as shown in Scheme 5.5.

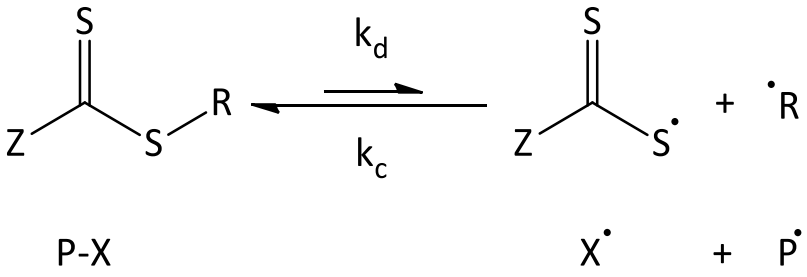

Scheme 5.5: Simplified representation of the reversible photolysis of the RAFT species, including corresponding representative RAFT species where P-X = initial RAFT agent, X* = xanthate radical and P* reactive propagating radical. Adapted from [22].

The kinetic coefficients in Scheme 5.5 are defined as being pseudo first order in nature, having units of s^{-1}, and are defined in relation to the parameters used in the model as:

$$k_d = k_{act} = k_{photons-RAFT}$$
$$k_c = k_{deact} \cdot [X^*] = k_{-photons-RAFT}$$

Equation 5.7: Definitions of the kinetic rate coefficients characterising the reversible photolysis of the RAFT agent

To investigate the contribution of the iniferter mechanism to the polymerisation behaviour seen, two main possible reaction mechanisms were considered:

1. Typical RAFT with iniferter contribution: the reactions governing the RAFT mechanism (reactions 4 – 15, Scheme 5.1) and the reversible dissociation of the RAFT species (reactions 19 – 22, Scheme 5.1) are active. Reactions 23 – 26 (Scheme 5.1) are activated or deactivated

depending on whether the xanthate fragment radical is considered active towards radical addition.

2. Typical iniferter mechanism without RAFT mechanism: the reactions governing the RAFT mechanism (reactions 4 – 15, Scheme 5.1) are inactive and reactions 19 – 22 (Scheme 5.1) are active to allow for the reversible dissociation of RAFT species. Once again, reactions 23 – 26 (Scheme 5.1) are activated or deactivated as required.

These two mechanistic possibilities are investigated in sections 5.8.1 and 5.8.2 respectively.

The light only and light only (short) experimental data was selected as the basis for simulating the reversible photolysis of RAFT species, as it represents the simplest case with ample data in the relevant low conversion range. Since both these experiments omitted AIBN, for all simulations in sections 5.8.1 and 5.8.2, conventional initiation by degradation of initiator and the subsequent reactions involving initiator radicals (initiation and termination) were disabled, unless explicitly stated otherwise. Similarly, for all simulations within sections 5.8.1 and 5.8.2, reaction 18 (Scheme 5.1) was active with $k_{photons\text{-}monomer}$ being set to 1.60 x10^{-12} (M^{-1} s^{-1}), which was included to represent the contribution due to photolysis of monomer as determined in sim 1.1.

As covered in more detail in Chapter 2 in section 2.4.2, the debate about the reactivity of thiyl radicals is ongoing, however the general consensus is that they are significantly less reactivate than conventional carbon or thiol radicals [56, 57], with this being explained by the existence of steric and spin factors upon recombination. [58]. Based on this it can be expected that termination reactions involving thiyl radicals with carbon centred radicals (R group, initiator derived or macro-radicals) will be primarily driven by the reactivity of the more reactive carbon centred radical. Hence scripts 5, 6 & 7 were written which modify the kinetic rate coefficients for the recombination reactions in the same chain length dependent manner as for the value of k_t between two macro-radicals.

Lalevée *et al.* have proposed an upper limit of ~ 10^3 M^{-1} s^{-1} as the rate coefficient of MMA addition to a range of thiyl radical species [57, 59]. Based on literature precedents, the assumption was made that the rate coefficient for recombination of thiyl radicals with other radical species ($k_{\text{-photons-RAFT}}$) will not exceed the rate coefficient for termination of other carbon centred radical species ($k_t^{1,1}$).

Based on these literature findings a range of simulations were undertaken with the following possibilities considered:

- That $k_{\text{-photons-RAFT}}$ is a fixed time and conversion independent value that is equal to either a factor of 1, 0.1 or 0.001 of the starting $k_t^{1,1}$ value.

- Conversely that $k_{-photons\text{-}RAFT}$ changes as a function of the chain length of the macro-radical species in solution in exactly the same way that k_t is chain length dependent, and that it equal to either a factor of 1, 0.1 or 0.001 the current value of k_t.
- For the two respective situations (fixed and varied $k_{-photons\text{-}RAFT}$), the possibility that the thiyl radical is inert ($k_{xanthate\text{-}prop}$ = 0 M^{-1} s^{-1}) along with being only moderately reactive towards monomer addition ($k_{xanthate\text{-}prop}$ = 10 or 100 M^{-1} s^{-1}) were considered. These values cover the common possibilities presented in literature, namely the common assumption that thiyl radicals are basically inert and the upper limit set by Lalevée *et al.* coupled with the consideration that MA is a less reactive towards radical addition than MMA. The kinetic rate coefficients for radical addition to MA are often at least an order of magnitude lower than to MMA, irrespective of the radical in question [40], hence the limit of 100 as opposed to 1000 M^{-1} s^{-1} being selected.
- In all circumstances, the assumption was made that value of the rate coefficient for the photolysis of the RAFT agent and the macro-RAFT species ($k_{photons\text{-}RAFT}$) was a fixed value. This was predicated on the assumption that the photochemical properties between the starting RAFT agent and the macro-RAFT species does not change. Furthermore, if this value were not fixed, there is no discernible way to ascribe how it should change and as function of which variable.

In the first simulation in each series of fixed parameter simulations, the value of $k_{-photons\ RAFT}$ was set equal to the starting value of $k_t^{1,1}$. The $k_{photons\ RAFT}$ kinetic rate coefficient was then optimised such that the kinetics match those of both the light + AIBN and light only experimental data points. The same equilibrium constant was maintained for subsequent simulations within each series where both kinetic rate coefficients were decreased relative to the initial simulation per the selection criteria described above.

A functionally equivalent approach was taken where $k_{-photons\ RAFT}$ effectively had variable values. For the first simulation in each series of varied parameter simulations, $f_{xan\text{-}termination}$ was set to 1, with $k_{photons\text{-}RAFT}$ being optimised to match both the light + AIBN and light only experimental data points. For the subsequent simulations within each series, the values for $k_{photons\text{-}RAFT}$ was decreased by the same order of magnitude as $f_{xan\text{-}termination}$. This ensure that the value of $K_{eq(photolysis)}$ was functionally the same in all cases, irrespective of the fact it changes as a function of conversion.

5.8.1 RAFT mechanism with iniferter contribution

For the first series of simulations the simplest case was considered, where the thiyl radical is inert and there is no propagation from this radical. The parameters for this series of simulations are summarised in Table 5.14.

Table 5.14: Parameters for simulations of reversible photolysis of RAFT species where $k_{p(xanthate\ fragment)} = 0$.

Simulation	$k_{photons\text{-}RAFT}$	$k_{-photons\text{-}RAFT}$	$f_{xan\text{-}termination}$	$K_{eq\ (photolysis)}$
3.0.1F (On)	3.5566	1.7783×10^{9}	N/A	2.000×10^{-9}
3.0.2F (On)	3.5566×10^{-1}	1.7783×10^{8}	N/A	2.000×10^{-9}
3.0.3F (On)	3.5566×10^{-3}	1.7783×10^{6}	N/A	2.000×10^{-9}
3.0.1V (On)	1.0000×10^{-1}	1.7783×10^{9} to 8.0293 x107	1.0000	5.623×10^{-11} to 1.245×10^{-9}
3.0.2V (On)	1.0000×10^{-2}	1.7783×10^{8} to 8.0293×10^{6}	1.0000×10^{-1}	5.623×10^{-11} to 1.245×10^{-9}
3.0.3V (On)	1.0000×10^{-4}	1.7783×10^{6} to 8.0293×10^{4}	1.0000×10^{-3}	5.623×10^{-11} to 1.243×10^{-9}

In Figure 5.20 (A) it can be seen that except for sim 3.0.3F (On) (red trace), all simulations can reproduce the experimental light only kinetics faithfully with minimal deviation. The simulations with fixed values for both $k_{photons\text{-}RAFT}$ and $k_{-photons\text{-}RAFT}$ show a gradual increase in overall reaction rate as both kinetic rate coefficients are decreased. This occurs as although the equilibrium coefficient for photolysis ($K_{eq(photolysis)}$) remains constant, the rate of recombination of active (P*) radicals and inactive thiyl radicals (X*) becomes orders of magnitude slower than the overall rate of termination (k_t) within the system. The difference between these two rate coefficients means that more monomers can add to the active species (P*) per photolysis cycle, thus increasing the overall polymerisation rate. This effect is much less pronounced for simulations where the value of $k_{-photons\text{-}RAFT}$ is varied, owing to the difference between k_t and $k_{-photons\text{-}RAFT}$ being proportionally smaller and accurately maintained as the desired factor ($f_{xan\text{-}termination}$) of k_t. Based on these results, discriminating which photolysis parameters are realistic cannot be undertaken from comparing kinetic profiles alone; analysis of the evolution of M_n and dispersity as a function of conversion is required.

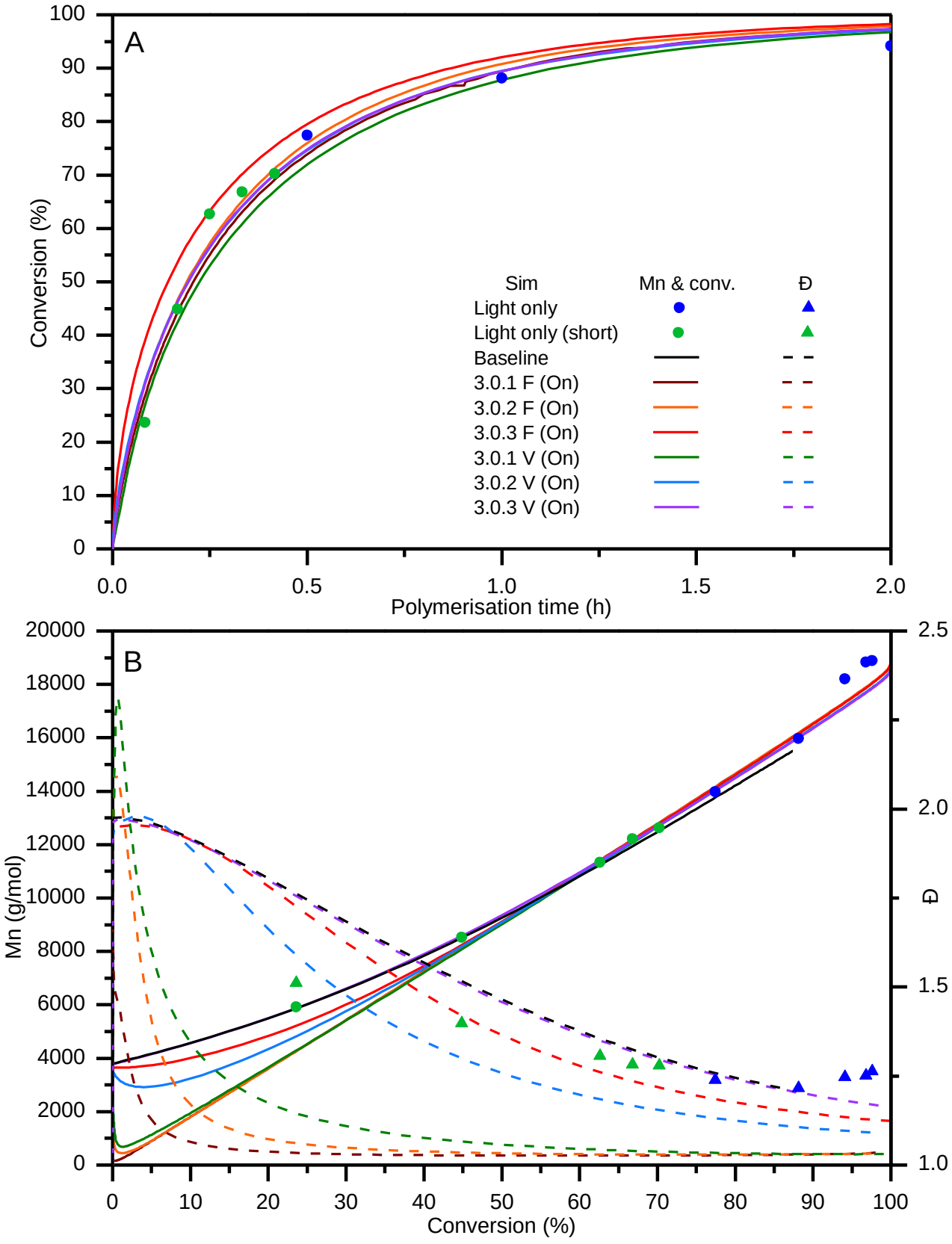

Figure 5.20: Comparison of conversion versus time (A) and evolution of molecular weight and dispersity as a function of conversion (B) for simulations concerning reversible photolysis of RAFT species where $k_{p(xan)} = 0$ to experimental data.

Inspection of Figure 5.20 (B) unsurprisingly reveals that simulations with the highest values of $k_{\text{-photons-RAFT}}$ (sims 3.0.1F (On), 3.0.2F (On) & 3.0.1V (On)) show the most control over both the M_n and dispersity. This results in an almost perfectly linear relationship between M_n and conversion which is unrealistic considering the hybrid behaviour seen experimentally which is adequately modelled in the baseline simulation (black trace, Figure 5.20 (B)). As the value of $k_{\text{-photons-RAFT}}$ is decreased in sims 3.0.2V (On) and 3.0.3F (On) (blue trace and red traces respectively, Figure 5.20 (B)), hybrid behaviour begins to manifest along with a dispersity profile that begins to resemble that of the baseline simulation. Once $k_{\text{-photons-RAFT}}$ is decreased by 3 orders of magnitude in sim 3.0.3V (On) (Figure 5.20 (B), purple trace) the evolution of M_n matches the experimental data very well including the positive deviation at higher conversions that is not seen in the baseline result. The evolution of dispersity remains essentially indistinguishable from the baseline result.

Two series of simulations were undertaken to investigate the possibility of both slow and fast propagation from the thiyl radical. This involved activating reactions 23 – 26 (Scheme 5.1) in the model and using $k_{p(\text{xanthate fragment})} = 10\ M^{-1}\ s^{-1}$ and $100\ M^{-1}\ s^{-1}$ respectively. There was no combination of values of both $k_{\text{photons RAFT}}$ and $k_{\text{-photons-RAFT}}$ that could satisfactorily reproduce the overall experimental kinetics seen for the light only (short) and light only case. Many of these simulations displayed very high dispersity values coupled with M_n versus conversion profiles that were significantly different to what was observed experimentally, and both these phenomena manifest due to an extra population of growing polymer chains that now exist because of propagation from the thiyl radical. For data from these simulations, see Figure A11and Figure A12 in the Appendix.

Compared critically to experimental data, the kinetic profiles from these three series of simulations strongly suggest that propagation from the thiyl radical is unlikely to be happening during the iniferter process. For the case where the thiyl radical is considered inert and the RAFT mechanism is active ($k_{p(\text{xanthate fragment})} = 0\ M^{-1}\ s^{-1}$, Table 5.14 and Figure 5.20), the simulations imply that the dissociation combination mechanism is primarily responsible for the increased kinetics seen by virtue of generating more initiating radicals, but not the control over the molecular weight and dispersity evolution. The importance of these two mechanisms is explored in detail in section 5.8.2 through investigation into the kinetic rate coefficients governing both RAFT and dissociation combination processes.

5.8.2 Comparison of RAFT and iniferter mechanisms in controlling polymerisation

Previously in section 5.8.1, the reactions that constitute the RAFT mechanism (reactions 4 – 15, Scheme 5.1) were always active within the model. To accurately determine whether the dissociation

combination mechanism could ever fully explain the experimental data, a series of comparisons was made, with the following rationale:

- For simulations where both the RAFT and iniferter mechanisms are operating (denoted with (ON) after sim #), deactivating the iniferter mechanism should have **no** negative consequences on the evolution of M_n and dispersity **if** the RAFT mechanism **is solely** responsible for the control seen.
- For simulations where the RAFT mechanism is deactivated (denoted with (Off) after sim #) and the iniferter mechanism is the **sole source** of control over M_n and dispersity, reactivating the RAFT mechanism should have **no** significant impact on the control seen.

Based on the conclusions from the previous section, the simulations from the series where $k_{p(xanthate\ fragment)} = 0\ M^{-1}\ s^{-1}$ which showed the closest match to the experimental data were investigated further. This involved selectively deactivating the RAFT mechanism and re-running the simulation with all other kinetic rate coefficients kept identical. In each series of simulations, one simulation for the (Off) case required parameters such that it matched the experimental data as closely as possible.

Keeping $k_{comb.}$ as a fixed value is the standard method within the literature [60, 61], so the effect of fixed values of $k_{-photons\text{-}RAFT}$ on the two mechanisms was tested initially. The parameters used are listed in Table 5.15 and the results are shown in Figure 5.21.

Table 5.15: Parameters for simulations comparing RAFT and iniferter mechanisms where $k_{p(xan)} = 0\ M^{-1}\ s^{-1}$ and $k_{-photons\text{-}RAFT}$ are fixed values.

Simulation	$k_{photons\ RAFT}$	$k_{-photons\ RAFT}$	$K_{eq\ (photolysis)}$
3.0.3F (On)/(Off)	3.5566×10^{-3}	1.7783×10^{6}	2.000×10^{-9}
3.0.4F (On)/(Off)	1.9600×10^{-2}	9.8000×10^{6}	2.000×10^{-9}

For the lowest value of $k_{-photons\text{-}RAFT}$ with the RAFT mechanism active (sim 3.0.3F (On), Figure 5.21, brown trace) it is evident that the overall control obtained is slightly too good, with the M_n and dispersity values being lower than the baseline model. Conversely, the same parameters with the RAFT mechanism deactivated (sim 3.0.3F (Off), Figure 5.21, blue trace) fail to control the molecular weight until a high conversion of ~ 70 % is reached, which is also reflected in the much higher dispersity at all conversion values.

Sim 3.0.2F (Off) (Figure 5.21, green trace) shows that solely employing the iniferter mechanism can reproduce the experimental data, however at lower conversions the M_n is significantly overestimated before being brought into line with the expected values and this has the corresponding effect of

increasing the dispersity beyond what is seen experimentally. Both results show that the iniferter mechanism by itself is incapable of reproducing the experimental data seen, and that the RAFT mechanism is primarily means of controlling the diversity and the molecular weight. With the RAFT mechanism active, the results indicate that if $k_{\text{-photons-RAFT}}$ is indeed a fixed value then it must be over 1000 times smaller than the starting value of k_t to reproduce the experimental data. This supports the literature findings that thiyl radicals are significantly less reactive towards termination with other radicals as compared to carbon centred radicals.

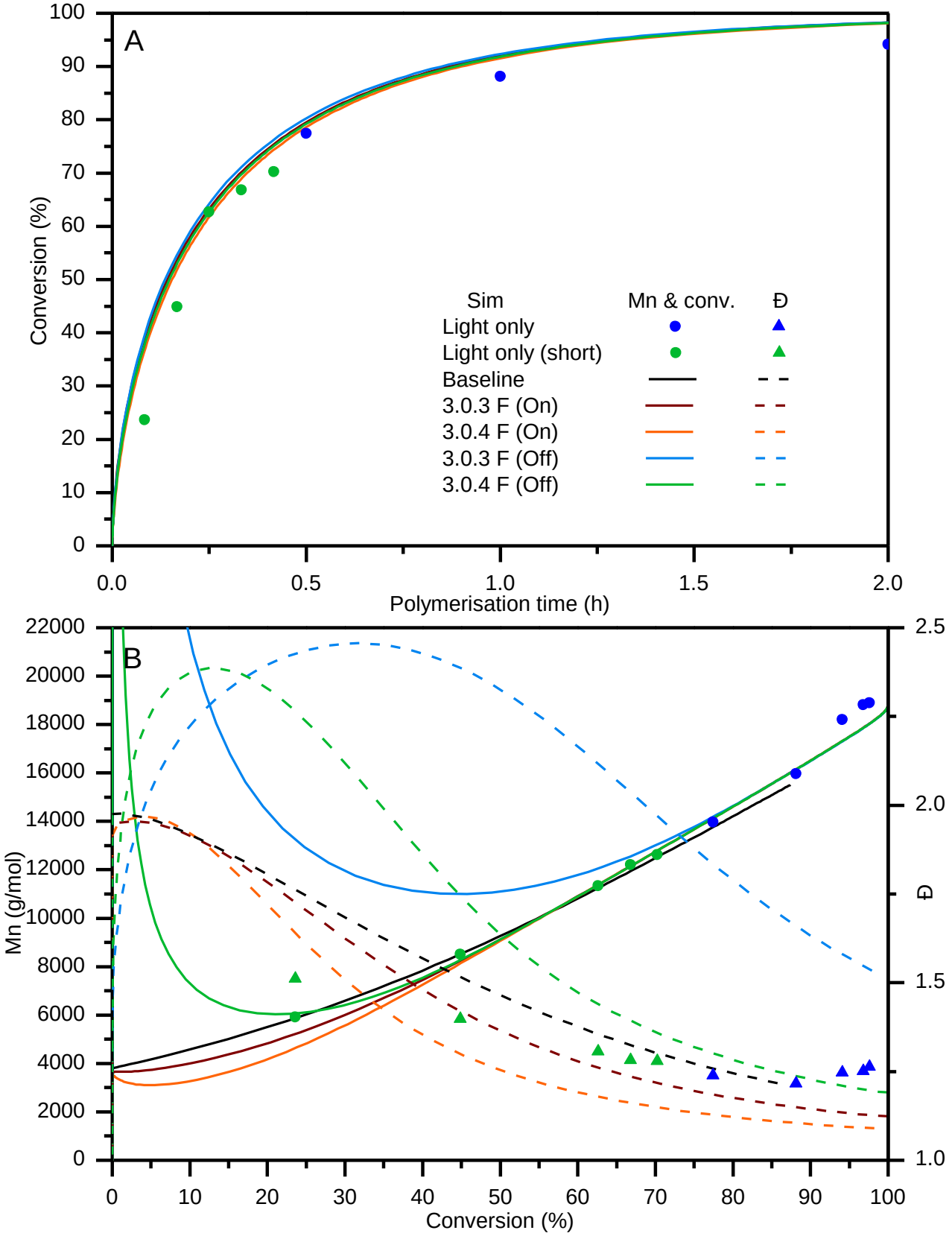

Figure 5.21: DT On/Off comparisons for the case when $k_{p(xan)}$ = 0, with $k_{\text{-photons-RAFT}}$ being fixed.

The non-conventional approach of employing varied values of $k_{\text{-photons-RAFT}}$ was also tested, with the parameters used in Table 5.16 and results shown in Figure 5.22.

Table 5.16: Parameters for simulations comparing RAFT and iniferter mechanisms where $k_{p(xan)}$ = 0 M^{-1} s^{-1} and $k_{-photons-RAFT}$ are varied values.

Simulation	$k_{photons\ RAFT}$	$k_{-photons\ RAFT}$	$f_{xan-termination}$	$K_{eq\ (photolysis)}$
3.0.2V (On)/(Off)	1.00 x10^{-2}	1.7783 x10^{8} to 8.0412 x10^{6}	0.1	5.623 x10^{-11} to 1.244 x10^{-9}
3.0.3V (On)	1.00 x10^{-4}	1.7783 x10^{6} to 8.0412 x10^{4}	0.001	5.623 x10^{-11} to 1.244 x10^{-9}
3.0.3V (Off)	1.00 x10^{-4}	1.7783 x10^{6} to 7.7052 x10^{4}	0.001	5.623 x10^{-11} to 1.298 x10^{-9}

Sim 3.0.3V (On) (orange trace) is the optimised case for the RAFT and iniferter combined mechanisms; when the RAFT mechanism is disabled (sim 3.0.3V (Off) (green trace) shows an increase in polymerisation rate (Figure 5.22, A). Sim 3.0.3V (Off) however completely fails to control the polymerisation (Figure 5.22, B), with the molecular weight always exceeding 50 kg/mol which also gives a correspondingly large dispersity value that increases with conversion.

Sim 3.0.2V (Off) (blue trace, Figure 5.22) shows an optimised scenario where the control is obtained solely from the iniferter mechanism; the initial spike in the M_n is smaller than for the optimised case utilising a fixed value of $k_{-photons-RAFT}$. Nevertheless, the dispersity values are higher than expected at all conversions. When the RAFT mechanism is turned on for these parameters (sim 3.0.2V (On), brown trace, Figure 5.22) there are no visible kinetic effects. The initial spike in molecular weight is absent with the molecular weight being underestimated at lower conversions; similarly, the dispersity values are noticeably smaller than the baseline result throughout.

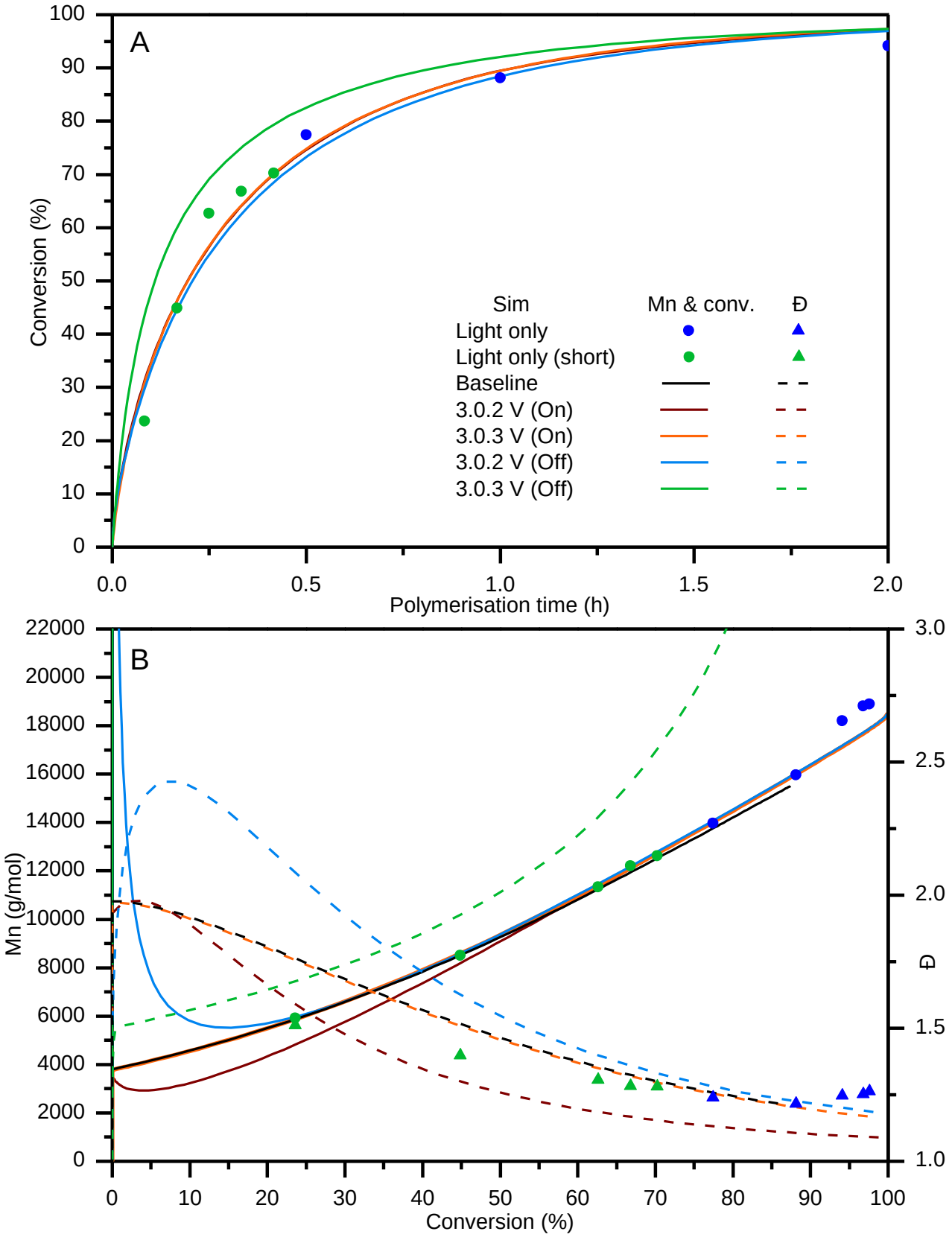

Figure 5.22: DT On/Off comparisons for the case when $k_{p(xan)} = 0$, with $k_{\text{-photons-RAFT}}$ being varied.

The control over both M_n and dispersity in these simulations of the iniferter process are a direct result of the value of k_{deact} as this value effectively describes the overall rate of recombination of both active (P*) and inactive (X*) species as defined previously. The values of k_{deact} were calculated for both series simulations undertaken using the concentrations of the xanthate radical as generated by the model.

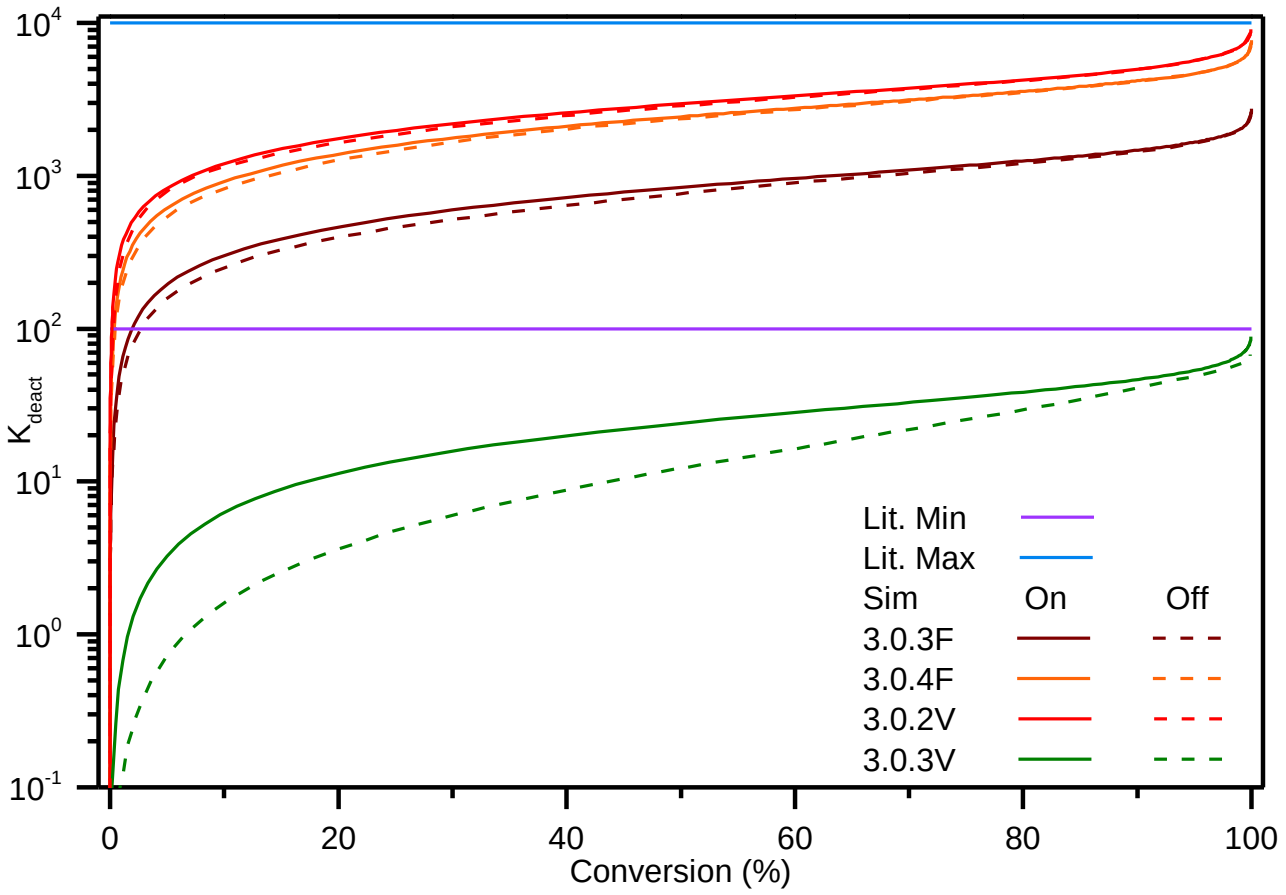

Figure 5.23: Values of k_{deact} for DT On/Off comparisons for the case when $k_{p(xan)} = 0$, with $k_{-photons-RAFT}$ being fixed.

According to Goto & Fukuda, most "successful" LRP systems occur when k_{deact} takes on values from 100 to 10000 [23]; Figure 5.23 supports the validity of this guideline as applied to the system studied here. Regardless of whether the RAFT mechanism is active or if $k_{-photons-RAFT}$ was a fixed or varied value, the simulations for which k_{deact} takes on values within the prescribed range show better control over both M_n and dispersity, with control increasing as the values of k_{deact} lie closer to the upper limit.

The fact that in all simulations the k_{deact} values start below the minimum literature guideline value is a direct result of the iniferter polymerisation mechanism, where there are no inert radicals (X*) present initially, hence k_{deact} is initially zero. The concentration of inert radicals due to photolysis increases with time until they are in sufficient abundance to recapture the growing polymer chains at a rate that allows the molecular weight to be brought under control. The effects of this mechanism

are directly reflected in the initial spike in M_n seen for all "Off" simulations, which is not identical in nature to the hybrid behaviour seen with the RAFT mechanism. This is because the RAFT agent is present at the start and the interaction between it and the growing macroradicals is primarily limited by the kinetic rate coefficient for initial addition, not its concentration.

Comparing all the simulations within this section shows that sim 3.0.3V (On) shows the best fit to both the M_n and dispersity of the light only (short) experimental data. The validity of this model can be tested further by comparing both the consumption and the degradation of the RAFT agent as a function of time to that which was experimentally determined under comparable conditions. Figure 5.24 (A) shows that both the baseline model and 3.0.3V (On) can quite accurately reproduce the disappearance of the starting RAFT agent under the respective experimental conditions they are designed to simulate. Sim 3.0.3V (On) slightly overestimates the percentage of RAFT degraded as compared to the experimental data, as shown in Figure 5.24 (B). These discrepancies most likely arise due to the assumption made that the accumulation of xanthate radicals in solution is directly correlated to the % of RAFT degraded, or that experimentally the degradation of the RAFT agent might occur differently in the presence of monomer.

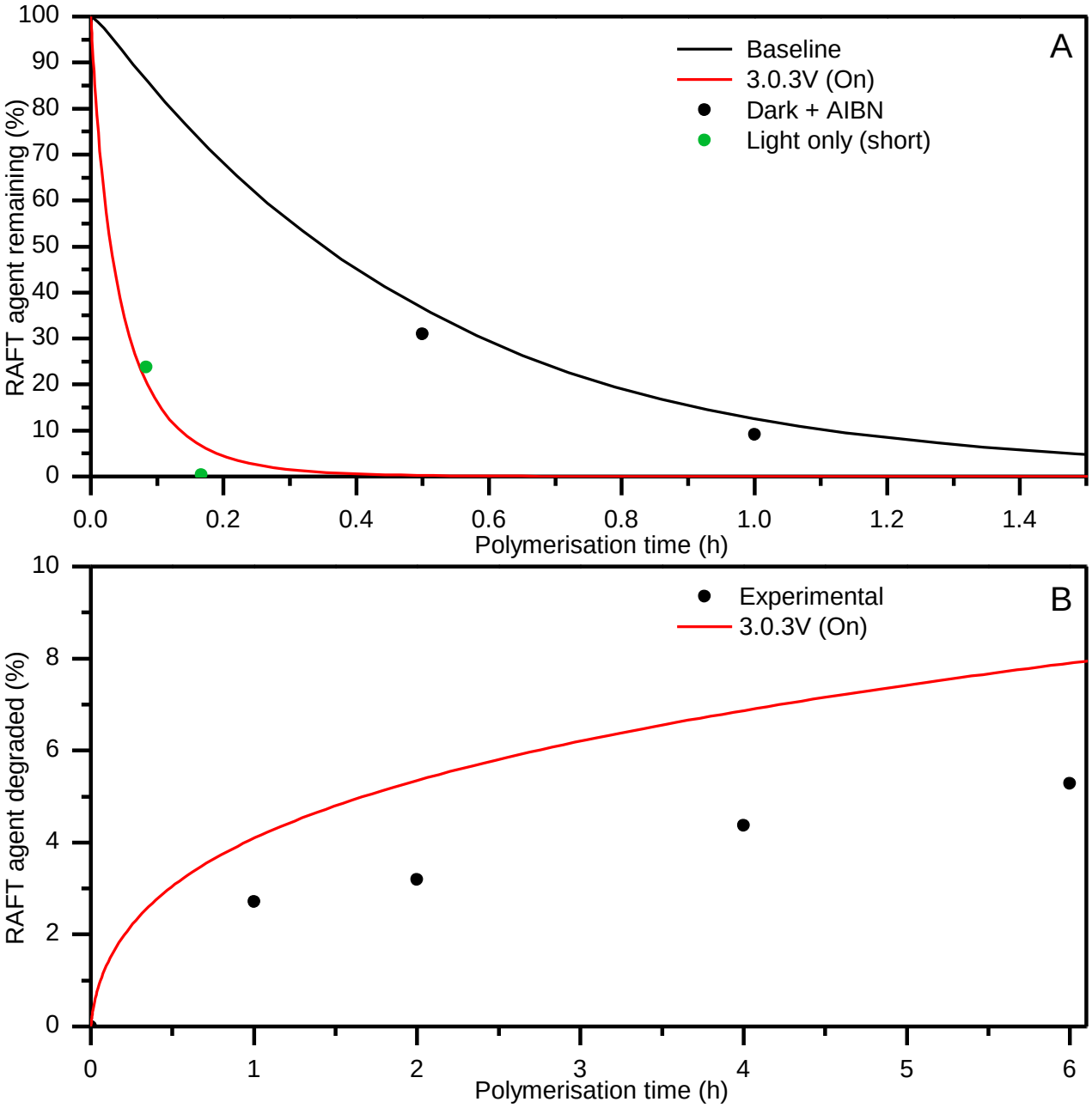

Figure 5.24: Comparisons between simulations and experimentally determined % RAFT remaining (A) and experimentally determined % RAFT degraded.

Taken holistically, the simulations within this section show quite conclusively that the control over molecular weight is dominated by the RAFT mechanism. The kinetic rate coefficients governing the iniferter mechanism in this case are not of sufficient magnitude to allow rapid enough interconversion between dormant and active radicals for this mechanism to be the sole method for molecular weight control. The primarily contribution of the iniferter mechanism in this case is simply the increase in polymerisation rate by generating initiating radicals in the form of R and macromolecular radicals.

5.8.3 Overall comparisons

As a final comparison, it was interesting to model the light + AIBN case but to consider the possibility that photolysis of monomer and AIBN is occurring simultaneously at the highest rates that were determined experimentally. Sim 3.0.3V (On) is the best descriptor for the light only and light only (short) experimental data and will be used as a basis for this comparison, with the parameters used given in Table 5.17.

Table 5.17: Kinetic rate coefficients used in final comparison of photolysis parameters.

Simulation	k_d	$k_{photons\text{-}monomer}$	$k_{photons\ RAFT}$
Baseline	1.6530×10^{-5}	N/A	N/A
3.0.3V (On)	N/A	1.60×10^{-12}	1.00×10^{-4}
3.0.3V (On, max)	5.0582×10^{-5}	2.00×10^{-11}	1.00×10^{-4}

The maximum rate of initiation due to photolysis of RAFT species was calculated using Equation 5.8Equation 5.6.

$$R_{i(photolysis-RAFT)} = k_{R-re} \cdot ([macro^*] + [R^*]) \cdot [M]$$
$$\therefore R_{i(photolysis-monomer)} = k_{photons-RAFT} \cdot ([RAFT] + [pRAFT])$$

Equation 5.8: Expression used to calculate the rate of initiation due to photolysis of RAFT species.

Even with the photolysis of AIBN and monomer being set to the maximum rate coefficients determined, the kinetic profiles for sim 3.0.3V (On) and sim 3.0.3V (On, max) are essentially identical as shown in Figure 5.25 (A). This can once again be understood in terms of the relative rates of initiation due to the different initiation pathways that are operative, and from Figure 5.25 (B) it is clear that photolysis of the RAFT agent is the dominant pathway. Photolysis of both AIBN and monomer have rates that are orders of magnitude lower than that of RAFT, which corroborates their minimal impact on the kinetics seen.

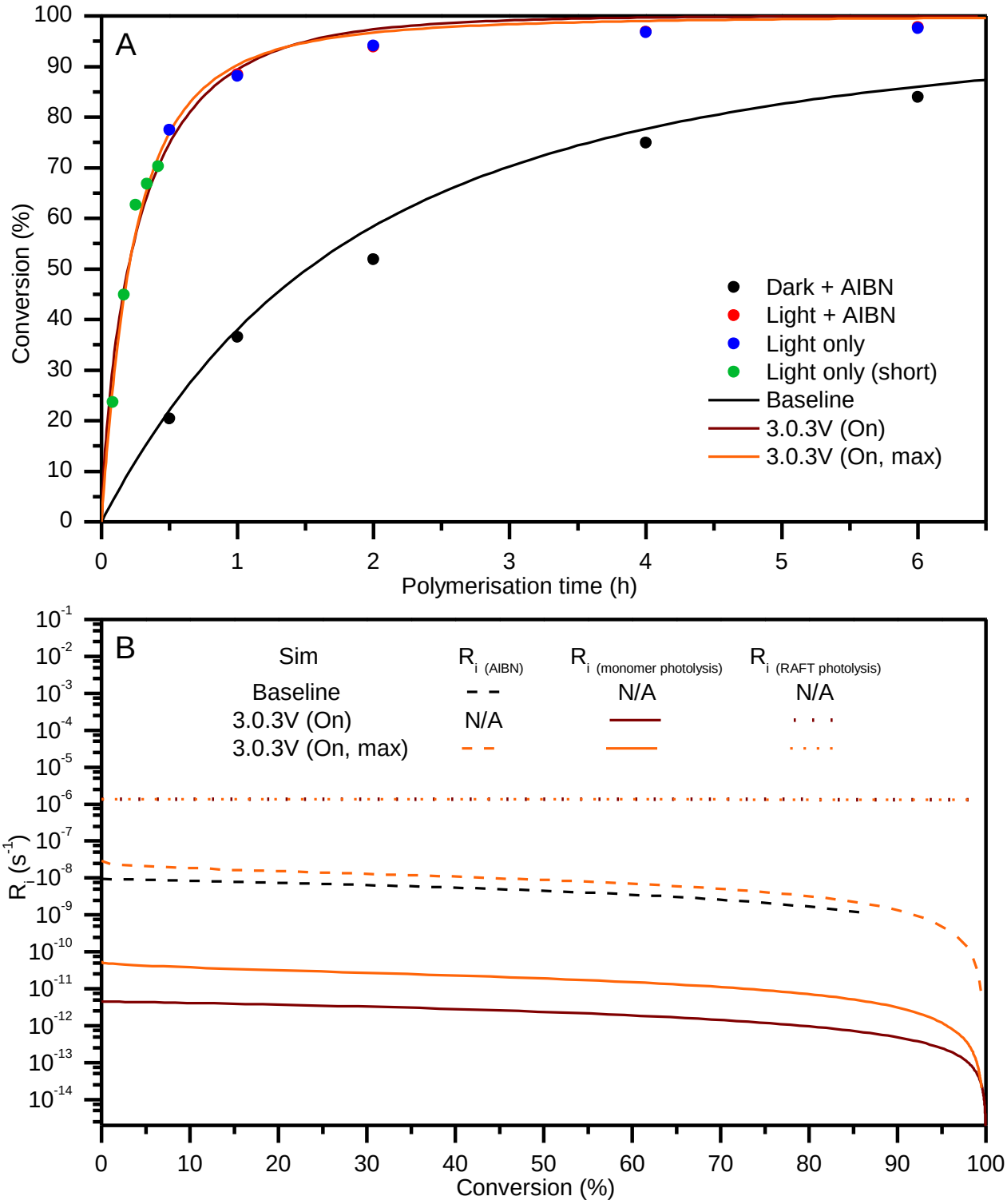

Figure 5.25: Overall kinetic comparisons for simulation 3.0.3V (On) with and without different initiation mechanisms active (A) and comparison of the relative rates of initiation due to those initiation mechanisms (B).

These results generally support the notion that the kinetic rate coefficient for a photoactive reaction is a combination of the following components:

- Overlap between the absorbance profile of the photoactive component and the output of the light source

- The concentration of the photoactive component in the reaction medium
- The quantum yield for the photochemical transformation

Thus, it is unsurprising that PXEP, which is ~ 34 times more abundant than AIBN and has the greatest absorbance in the UV region where the UV lamp (370nm, 2 mW/cm^2) emits (Figure 5.1) results in the largest kinetic rate coefficient for photolysis and thus has the largest contribution to initiation rate.

5.9 Conclusions

Experimental investigations provided the following conclusions:

- Polymerising MA under conditions that were optimised for RAFT polymerisation using PXEP as a chain transfer agent and AIBN as a thermal initiator resulted in hybrid behaviour but overall acceptable control over both molecular weight and dispersity.
- Conducting the same polymerisation both with and without AIBN present with exposure to a 6W UV lamp (370nm, 2 mW/cm^2) emitting at a peak emission wavelength of 370 nm resulted in an approximate 10-fold increase in polymerisation rate.
- The M_n and dispersity values all follow an incredibly similar pattern, regardless of the reaction conditions employed, thus implying that the same reaction mechanism is operating regardless of whether AIBN and/or UV light is present.

Modelling the experimental data in Predici provided the following conclusions:

- Supporting the experimental results, photolysis of AIBN leading to accelerated degradation and direct photolysis of monomer both cannot be responsible for the increased kinetics seen under irradiation conditions.
- Reversible photolysis of the RAFT agent via the iniferter mechanism was found to accurately recreate the kinetics under irradiation conditions only under the following circumstances:
    - The thiyl radical generated by photolysis was inert towards monomer addition.
    - That the kinetic rate coefficient for the termination of the thiyl radical with other radicals ($k_{\text{-photons-RAFT}}$) is between 2 and 3 orders of magnitude smaller than that of the average termination rate coefficient for carbon centred radicals in the system.
    - $k_{\text{-photons-RAFT}}$ can take a fixed value but a better fit to the experimental data occurs when this kinetic rate coefficient decreases as a function of the average chain length in the system in the same way as the average termination rate coefficient does.
    - Both these findings support the literature view that thiyl radicals are inherently less reactive than carbon centred radicals, and that the reactivity of the carbon centred

radicals in the system is the primary factor determining the kinetic rate coefficient for the termination of thiyl radicals between these two species.

- In the absence of the RAFT mechanism, there was no combination of kinetic rate coefficients for the iniferter mechanism that could satisfactorily recreate the evolution of M_n and dispersity as was seen experimentally. Conversely, with both the RAFT and iniferter mechanisms active, the experimental data could be recreated almost perfectly.

The conclusions from the modelling supported those made from the experimental data which suggested that the RAFT mechanism was active under all polymerisation conditions. This was further supported by essentially identical reaction rates and rate enhancement behaviour seen when irradiation was applied to a chain extension polymerisation conducted with a poly(MA) macroinitiator derived from PXEP.

5.10 References

1. Suwier, D.R., et al., *The iniferter technique in radical polymerization under UV and thermal conditions: a comparative study.* e-Polymers, 2002. **2**(25): p. 1-10.
2. Cabannes-Boue, B., et al., *Investigation into the mechanism of photo-mediated RAFT polymerization involving the reversible photolysis of the chain-transfer agent.* Polymer Chemistry, 2017. **8**(11): p. 1760-1770.
3. Tan, J., et al., *An insight into aqueous photoinitiated polymerization-induced self-assembly (photo-PISA) for the preparation of diblock copolymer nano-objects.* Polymer Chemistry, 2017. **8**(8): p. 1315-1327.
4. Blackman, L.D., et al., *Comparison of photo- and thermally initiated polymerization-induced self-assembly: a lack of end group fidelity drives the formation of higher order morphologies.* Polymer Chemistry, 2017. **8**(18): p. 2860-2871.
5. da M. Costa, L.P., et al., *Observed Photoenhancement of RAFT Polymerizations under Fume Hood Lighting.* ACS Macro Letters, 2016. **5**(11): p. 1287-1292.
6. Oster, G. and N. Yang, *Photopolymerization of vinyl monomers.* Chemical Reviews, 1968. **68**(2): p. 125-151.
7. Engel, P.S., *Mechanism of the thermal and photochemical decomposition of azoalkanes.* Chemical Reviews, 1980. **80**(2): p. 99-150.
8. Mill, T. and R.S. Stringham, *Photoisomerization of azoalkanes.* Tetrahedron Letters, 1969. **10**(23): p. 1853-1856.
9. Osugi, J., M. Sato, and M. Sasaki, *Kinetic studies on free radical reactions : I. Reaction of DPPH with free radicals formed by the photolysis of azo-bisisobutyronitrile.* The Review of Physical Chemistry of Japan, 1963. **33**(2): p. 53-64.
10. Moad, G., et al., *Measurements of Primary Radical Concentrations Generated by Pulsed Laser Photolysis Using Fluorescence Detection.* The Journal of Physical Chemistry A, 1999. **103**(33): p. 6580-6586.

11. Jaffe, A.B., K.J. Skinner, and M.J. McBride, *Solvent steric effects. II. Free-radical chemistry of azobisisobutyronitrile and azobis-3-cyano-3-pentane in viscous and crystalline media.* Journal of the American Chemical Society, 1972. **94**(24): p. 8510-8515.

12. Moad, G. and D.H. Solomon, *3 - Initiation*, in *The Chemistry of Radical Polymerization (Second Edition)*. 2005, Elsevier Science Ltd: Amsterdam. p. 49-166.

13. *Polymer Data Handbook*. 1999: Oxford University Press.

14. Back, R. and C. Sivertz, *The Photolysis of 2,2'-azo-bis-isobutyronitrile.* Canadian Journal of Chemistry, 1954. **32**(12): p. 1061-1067.

15. Skrabania, K., et al., *Examining the UV-vis absorption of RAFT chain transfer agents and their use for polymer analysis.* Polymer Chemistry, 2011. **2**(9): p. 2074-2083.

16. McKenzie, T.G., et al., *Investigation into the photolytic stability of RAFT agents and the implications for photopolymerization reactions.* Polymer Chemistry, 2016. **7**(25): p. 4246-4253.

17. Lu, L., et al., *Toward Rapid and Well-Controlled Ambient Temperature RAFT Polymerization under UV−Vis Radiation: Effect of Radiation Wave Range.* Macromolecules, 2006. **39**(11): p. 3770-3776.

18. Ham, M.K., et al., *Photoinitiated RAFT polymerization of vinyl acetate.* Journal of Polymer Science Part A: Polymer Chemistry, 2012. **50**(12): p. 2389-2397.

19. Keddie, D.J., et al., *Chain Transfer Kinetics of Acid/Base Switchable N-Aryl-N-Pyridyl Dithiocarbamate RAFT Agents in Methyl Acrylate, N-Vinylcarbazole and Vinyl Acetate Polymerization.* Macromolecules, 2012. **45**(10): p. 4205-4215.

20. Stenzel, M.H. and C. Barner-Kowollik, *The living dead - common misconceptions about reversible deactivation radical polymerization.* Materials Horizons, 2016. **3**(6): p. 471-477.

21. Fukuda, T., A. Goto, and Y. Tsujii, *Kinetics of Living Radical Polymerization*, in *Handbook of Radical Polymerization*. 2003, John Wiley & Sons, Inc. p. 407-462.

22. Moad, G. and D.H. Solomon, *9 - Living Radical Polymerization*, in *The Chemistry of Radical Polymerization (Second Edition)*. 2005, Elsevier Science Ltd: Amsterdam. p. 451-585.

23. Goto, A. and T. Fukuda, *Kinetics of living radical polymerization.* Progress in Polymer Science, 2004. **29**(4): p. 329-385.

24. Moad, G. and C. Barner-Kowollik, *The Mechanism and Kinetics of the RAFT Process: Overview, Rates, Stabilities, Side Reactions, Product Spectrum and Outstanding Challenges*, in *Handbook of RAFT Polymerization*. 2008, Wiley-VCH Verlag GmbH & Co. KGaA. p. 51-104.

25. Derboven, P., et al., *Chain Transfer in Degenerative RAFT Polymerization Revisited: A Comparative Study of Literature Methods.* Macromolecular Theory and Simulations, 2016. **25**(2): p. 104-115.

26. Stenzel, M.H., et al., *Xanthate Mediated Living Polymerization of Vinyl Acetate: A Systematic Variation in MADIX/RAFT Agent Structure.* Macromolecular Chemistry and Physics, 2003. **204**(9): p. 1160-1168.

27. Coote, M.L. and L. Radom, *Substituent Effects in Xanthate-Mediated Polymerization of Vinyl Acetate: Ab Initio Evidence for an Alternative Fragmentation Pathway.* Macromolecules, 2004. **37**(2): p. 590-596.

28. Coote, M.L., E.H. Krenske, and E.I. Izgorodina, *Quantum-Chemical Studies of RAFT Polymerization: Methodology, Structure-Reactivity Correlations and Kinetic Implications*, in *Handbook of RAFT Polymerization*. 2008, Wiley-VCH Verlag GmbH & Co. KGaA. p. 5-49.

29. Adamy, M., et al., *Influence of the Chemical Structure of MADIX Agents on the RAFT Polymerization of Styrene.* Macromolecules, 2003. **36**(7): p. 2293-2301.

30. Moad, G. and D.H. Solomon, *6 - Chain Transfer*, in *The Chemistry of Radical Polymerization (Second Edition)*. 2005, Elsevier Science Ltd: Amsterdam. p. 279-331.

31. Britton, D., F. Heatley, and P.A. Lovell, *Chain Transfer to Polymer in Free-Radical Bulk and Emulsion Polymerization of Vinyl Acetate Studied by NMR Spectroscopy.* Macromolecules, 1998. **31**(9): p. 2828-2837.

32. Barner-Kowollik, C., et al., *Critically Evaluated Rate Coefficients in Radical Polymerization – 8. Propagation Rate Coefficients for Vinyl Acetate in Bulk.* Macromolecular Chemistry and Physics, 2017. **218**(1): p. n/a-n/a.

33. Monyatsi, O., A.N. Nikitin, and R.A. Hutchinson, *Effect of Head-To-Head Addition on Vinyl Acetate Propagation Kinetics in Radical Polymerization.* Macromolecules, 2014. **47**(23): p. 8145-8153.

34. Theis, A., et al., *Access to Chain Length Dependent Termination Rate Coefficients of Methyl Acrylate via Reversible Addition−Fragmentation Chain Transfer Polymerization.* Macromolecules, 2005. **38**(7): p. 2595-2605.

35. Johnston-Hall, G. and M.J. Monteiro, *Bimolecular radical termination: New perspectives and insights.* Journal of Polymer Science Part A: Polymer Chemistry, 2008. **46**(10): p. 3155-3173.

36. Kattner, H. and M. Buback, *Chain-Length-Dependent Termination of Vinyl Acetate and Vinyl Pivalate Bulk Homopolymerizations Studied by SP-PLP-EPR.* Macromolecular Chemistry and Physics, 2014. **215**(12): p. 1180-1191.

37. Theis, A., et al., *Probing the reaction kinetics of vinyl acetate free radical polymerization via living free radical polymerization (MADIX).* Polymer, 2006. **47**(4): p. 999-1010.

38. Dika Manga, J., et al., *Mechanism of the polymerization of n-butyl acrylate initiated by N,N-diethyldithiocarbamate derivatives. Part 1. Photolysis of butyl-2-(N,N-diethyldithiocarbamyl)propionate and oligomerization of butyl acrylate.* Polymer International, 1998. **45**(1): p. 14-21.

39. Tazhe Veetil, A., et al., *Photochemistry of S-Phenacyl Xanthates.* The Journal of Organic Chemistry, 2011. **76**(20): p. 8232-8242.

40. Fischer, H. and L. Radom, *Factors Controlling the Addition of Carbon-Centered Radicals to Alkenes—An Experimental and Theoretical Perspective.* Angewandte Chemie International Edition, 2001. **40**(8): p. 1340-1371.

41. Barner-Kowollik, C., et al., *Critically evaluated rate coefficients in radical polymerization - 7. Secondary-radical propagation rate coefficients for methyl acrylate in the bulk.* Polymer Chemistry, 2014. **5**(1): p. 204-212.

42. Busch, M. and A. Wahl, *The significance of transfer reactions in pulsed laser polymerization experiments.* Macromolecular Theory and Simulations, 1998. **7**(2): p. 217-224.

43. Plessis, C., et al., *A Decrease in Effective Acrylate Propagation Rate Constants Caused by Intramolecular Chain Transfer.* Macromolecules, 2000. **33**(1): p. 4-7.

44. Nikitin, A.N., et al., *Determination of Propagation Rate Coefficient of Acrylates by Pulsed-Laser Polymerization in the Presence of Intramolecular Chain Transfer to Polymer.* Macromolecular Rapid Communications, 2003. **24**(13): p. 778-782.

45. Moad, G. and D.H. Solomon, *5 - Termination*, in *The Chemistry of Radical Polymerization (Second Edition)*. 2005, Elsevier Science Ltd: Amsterdam. p. 233-278.

46. Barner-Kowollik, C., et al., *Modeling the reversible addition–fragmentation chain transfer process in cumyl dithiobenzoate-mediated styrene homopolymerizations: Assessing rate coefficients for the addition–fragmentation equilibrium.* Journal of Polymer Science Part A: Polymer Chemistry, 2001. **39**(9): p. 1353-1365.

47. Vana, P., T.P. Davis, and C. Barner-Kowollik, *Kinetic Analysis of Reversible Addition Fragmentation Chain Transfer (RAFT) Polymerizations: Conditions for Inhibition, Retardation, and Optimum Living Polymerization.* Macromolecular Theory and Simulations, 2002. **11**(8): p. 823-835.

48. Theis, A., et al., *Mapping Chain Length and Conversion Dependent Termination Rate Coefficients in Methyl Acrylate Free Radical Polymerization.* Macromolecules, 2005. **38**(24): p. 10323-10327.

49. Buback, M., et al., *Chain-Length-Dependent Termination in Acrylate Radical Polymerization Studied via Pulsed-Laser-Initiated RAFT Polymerization.* Australian Journal of Chemistry, 2007. **60**(10): p. 779-787.

50. Barth, J., et al., *Chain-Length-Dependent Termination in Radical Polymerization of Acrylates.* Macromolecular Chemistry and Physics, 2011. **212**(13): p. 1366-1378.

51. Vana, P., T.P. Davis, and C. Barner-Kowollik, *Easy Access to Chain-Length-Dependent Termination Rate Coefficients Using RAFT Polymerization.* Macromolecular Rapid Communications, 2002. **23**(16): p. 952-956.

52. Wulkow, M., et al., *Implementing the reversible addition–fragmentation chain transfer process in PREDICI.* Journal of Polymer Science Part A: Polymer Chemistry, 2004. **42**(6): p. 1441-1448.

53. Wulkow, M., *Computer Aided Modeling of Polymer Reaction Engineering—The Status of Predici, I-Simulation.* Macromolecular Reaction Engineering, 2008. **2**(6): p. 461-494.

54. Wang, A.R. and S. Zhu, *Modeling the reversible addition–fragmentation transfer polymerization process.* Journal of Polymer Science Part A: Polymer Chemistry, 2003. **41**(11): p. 1553-1566.

55. Barner-Kowollik, C., P. Vana, and T.P. Davis, *The Kinetics of Free-Radical Polymerization*, in *Handbook of Radical Polymerization*. 2003, John Wiley & Sons, Inc. p. 187-261.

56. Lalevée, J., X. Allonas, and J.P. Fouassier, *A New Efficient Photoiniferter for Living Radical Photopolymerization.* Macromolecules, 2006. **39**(24): p. 8216-8218.

57. Lalevée, J., et al., *Controlled photopolymerization reactions: The reactivity of new photoiniferters.* Journal of Polymer Science Part A: Polymer Chemistry, 2007. **45**(12): p. 2436-2442.

58. Plyusnin, V.F., et al., *Optical spectroscopy of perfluorothiophenyl, perfluorothionaphthyl, xanthate and dithiophosphinate radicals.* Chemical Physics Letters, 2000. **325**(1): p. 153-162.

59. Lalevée, J., et al., *New Photoiniferters: Respective Role of the Initiating and Persistent Radicals.* Macromolecules, 2008. **41**(7): p. 2347-2352.

60. Rahane, S.B., S.M. Kilbey, and A.T. Metters, *Kinetic Modeling of Surface-Initiated Photoiniferter-Mediated Photopolymerization in Presence of Tetraethylthiuram Disulfide.* Macromolecules, 2008. **41**(24): p. 9612-9618.

61. Vivaldo-Lima, E. and A. de Jesús Mendoza-Fuentes, *Development Of A Kinetic Model For Iniferter Controlled/"Living" Free-Radical Polyerization Considering Diffusion-Controlled Effects.* Polymer Reaction Engineering, 2002. **10**(4): p. 193-226.

6 Investigating the contribution of the photoiniferter effect on the RAFT polymerisation of vinyl acetate using a xanthate

6.1 Introduction

This chapter details the experimental and theoretical investigation of the Iniferter effect as applied to the polymerisation of vinyl acetate (VAc) under conditions optimised for the RAFT process. As for the MA case in the previous chapter, VAc is polymerised under 3 sets of conditions, which are also applied to the chain extension of a poly(VAc) macro-RAFT agent. The comparisons between typical RAFT conditions with and without the iniferter contribution is valuable, as regardless of the technique employed, free radical polymerisation of vinyl acetate is problematic. This is due to the inherently unreactive nature of the monomer coupled with the extremely high reactivity of the VAc propagating radical [1]. Several mechanistic phenomena have been proposed to arise from this extreme difference between monomer and propagating radical reactivity, with various amounts of experimental evidence in support of each theory being found in the literature. A high rate of VAc radical termination has made determining the propagation rate coefficient for VAc difficult [2], however this does not result in a greater spread in the values obtained by the recommended PLP-SEC technique as compared to acrylates [3]. Backbiting to form midchain radicals such as occurs with acrylate monomers was proposed to also occur for VAc by Junkers *et al.* [2], however no such behaviour was subsequently detected by Kattner & Buback [4]. Non-insignificant rates of head to head monomer addition have also been detected and are known to affect the overall rate of propagation [5, 6], and their incidence has been shown to increase with increased reaction temperature [6, 7]. The differing reactivity between “head” and “tail” VAc radicals should affect their ability to undergo both bond formation and cleavage from RAFT/MADIX, ATRP or metal centred complexes changes, thus leading to typically poorer control over polymerisation relative to other monomers [6, 8].

Irrespective of the actual mechanisms responsible, the practical problems that arise during VAc polymerisation are both a broadening of the dispersity index at moderate conversions (typically > 40 %) when targeting molecular weights higher than around 10,000 g/mol. Furthermore, slowed polymerisation rates with polymerisation often halting before the majority of monomer is consumed are also observed [6]. Owing to the factors described, VAc is considered the archetypical LAM, thus investigations into RAFT polymerisation of this monomer have typically utilised xanthates [8-12] and sometimes dithiocarbamates [13].

Stenzel *et al.* reported retardation of the polymerisation rate and lengthy inhibition times in the polymerisation of vinyl acetate with a range of xanthates with analogous but not identical structures to PXEP; the Z groups used were a series of phenol and alkyl derivatives [9]. The dispersity values ranged from 1.08 to 1.71 depending on the xanthate used, however all samples were measured at approximately 25 % conversion. O-Ethyl-S-(1-ethoxycarbonyl) ethyl xanthate has been used by several groups to polymerise VAc via the routes of photoinitiation or the photoiniferter technique. This lead to varying degrees of success, with dispersities of 1.2 being obtained by both Chen *et al.* at a high conversion of 75 % [11] and Wang *et al.* at a low conversion of 28 % [12].Ding *et al.* used a series of xanthates under blue LED irradiation which showed oxygen tolerance and dispersity values under 1.4, even when targeting M_n values in excess of 35,000 g/mol and with high conversion [14].

Utilising a series of phosphonate functionalised xanthates, Dufils *et al.* achieved good control over dispersity ($D < 1.5$) only for low target M_n values ($M_n < 5000$ g/mol), otherwise dispersity values increased with increasing conversion [8]. The xanthate employed as a model compound in this work, PXEP, was first reported by Li *et al.* who concluded that it was unsuitable for VAc polymerisation after 2 single point experiments [10]. It is of interest to determine whether under different conditions it can be used successfully with VAc.

The same Predici model from the previous chapter is used to model the experimental results, appropriately adjusted for the different reaction conditions and kinetic parameters implemented. The modelling scenarios and subsequent analysis is repeated for the potential photolysis pathway. Mechanistic theories for the vast difference in polymerisation behaviour seen under light only conditions between the two monomers are put forth. Furthermore, the potential implications for RAFT polymerisations initiated via the photoiniferter mechanism are hypothesised based on this analysis.

6.2 Experimental investigation into photolysis of reaction components used in kinetic VAc polymerisations

6.2.1 Experimental procedures

Please refer to Chapter 4, sections 4.4 for relevant experimental procedures used in this section.

6.2.2 Analysis of UV-Vis absorption profiles for compounds utilised in VAc polymerisation under UV irradiation

Figure 6.1 shows the UV-Vis absorption profiles of the individual polymerisation components used in the polymerisation of VAc under experimental conditions. The black trace represents the

absorbance due to acetonitrile and once again this is analogous to the baseline. Unlike for the MA case, the absorbance profile for VAc does show some minor overlap with the emission spectrum of the UV lamp (370nm, 2 mW/cm^2), hence photolysis of VAc is expected to be a possibility. Furthermore, both PXEP and AIBN show stronger absorbances due to their increased concentration relative to the concentrations used in MA polymerisation.

Control experiments to test for the photolysis of each component were once again conducted and are presented in sections6.2.3, 6.2.4 and 6.2.5.

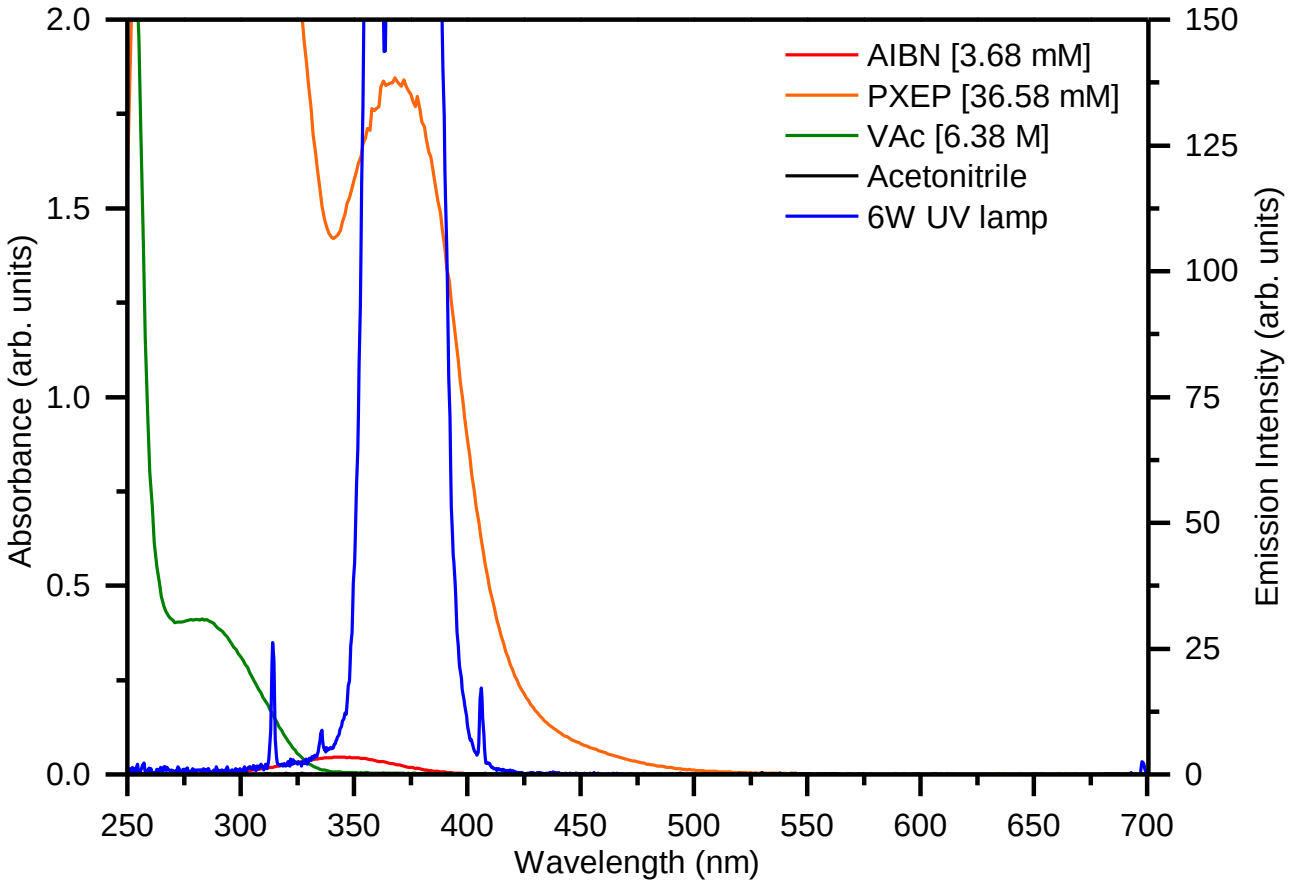

Figure 6.1 Comparison of the absorbance of vinyl acetate monomer in acetonitrile at various concentrations with emission spectrum of the 6W UV lamp (370nm, 2 mW/cm^2).

6.2.3 Photolysis of monomer

The ability of UV irradiation to initiate direct polymerisation of VAc along with the ability of PXEP to act as a thermal iniferter were tested under kinetic polymerisation conditions including a reaction time of 10 h, with AIBN absent. The results are shown in Table 6.1.

Table 6.1 Summary of control experiments conducted under VAc polymerisation conditions; [VAc] = 6.35 M, [AIBN] = 0, 70 °C, acetonitrile as solvent. UV irradiation (370nm, 2 mW/cm^2).

Entry	Time (h)	[PXEP] (M)	UV Light	% conversion by ^{1}H NMR	M_n (g/mol)	M_w (g/mol)	Đ
1	10	N/A	On	10.22	99100	184130	1.86
2	10	3.6 x10^{-2}	Off	0.25	N/A	N/A	N/A

Similar results to those obtained for MA were observed with UV irradiation (Table 6.1, entry 1); only minor conversion leading to polymer with broad dispersity and high molecular weight, characteristic of a free radical process occurring. Likewise, entry 2 (Table 6.1) once again shows that PXEP does not thermally dissociate to any appreciable extent and is incapable of initiating the polymerisation under these reaction conditions.

The potential effect of monomer photolysis is investigated in the Predici model in section 6.5.

6.2.4 Photolysis of AIBN

As explained previously in Chapter 5 section 5.2.4, this experiment used the reaction conditions employed for VAc kinetic polymerisations due to practical experimental considerations whilst also serving to provide an upper limit for the rate of degradation of AIBN under photolysis due to the higher concentration of AIBN employed. The results are summarised in Table 6.2Table 5.2.

Table 6.2: Summary of k_d values. UV irradiation (370nm, 2 mW/cm^2).

Reaction conditions	k_d at 70 °C (x 10^{-5}) (s^{-1})
Dark	1.653
Light	5.066

The potential effect of photolysis of AIBN is investigated in the Predici model in section 6.6.

6.2.5 Photolysis of PXEP

Under conditions identical to VAc polymerisation but with VAc replaced with ethyl acetate, the spectra of the solutions after irradiation at 70 °C for the given times is shown in Figure 6.2, with the percentage of the starting PXEP degraded being shown as a function of time (inset, Figure 6.2). Under these conditions, the absorbance values for all samples exceeded the linear range of the calibration curve, which necessitated the dilution of samples by a factor of 2 after degradation and prior to UV-Vis analysis. This is indicative that at these concentrations, intermolecular interactions between analyte molecules and thus potentially their derivative radical species could also be significant.

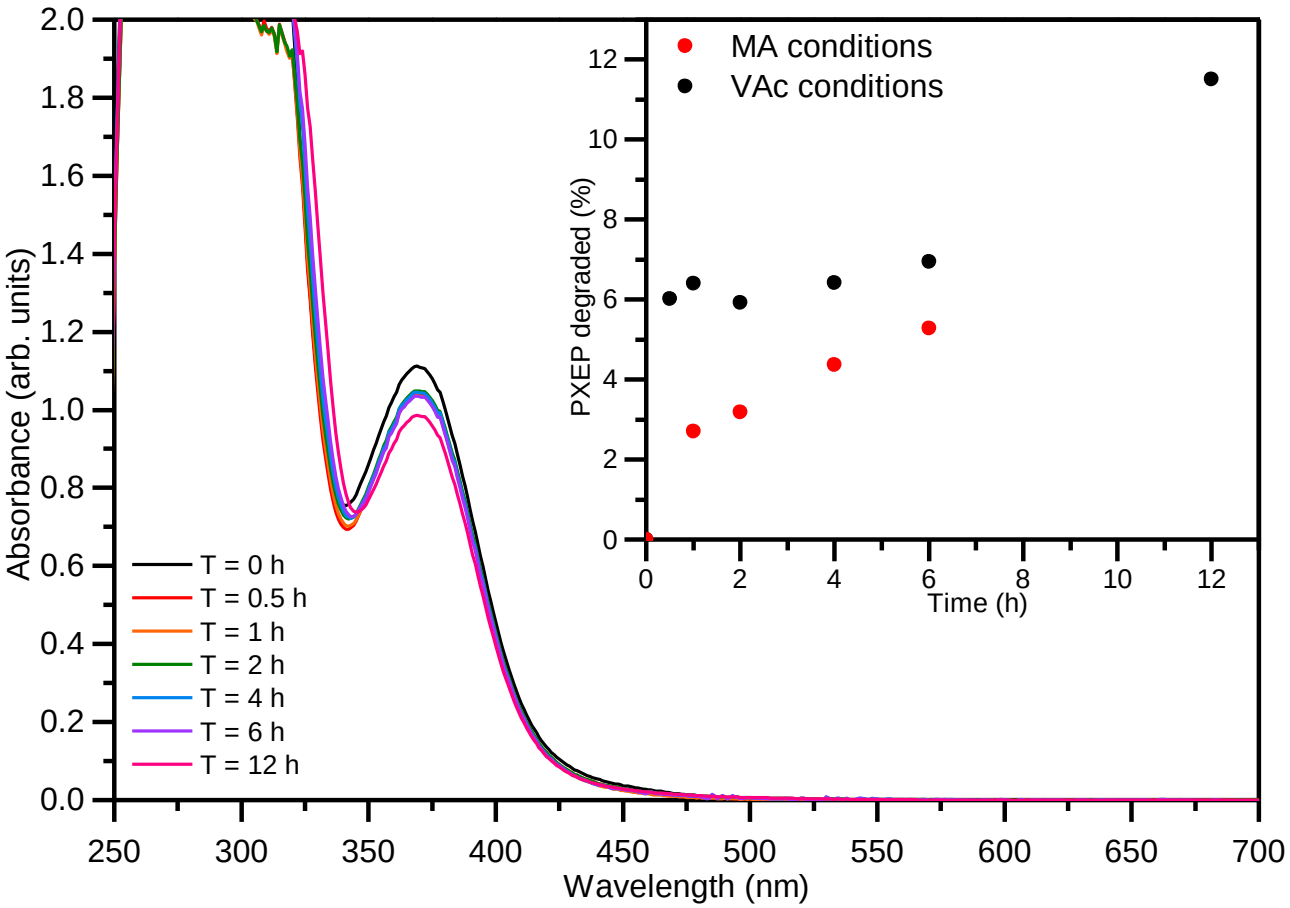

Figure 6.2: UV-Vis spectra of xanthate solutions after various times of heating at 70 °C with simultaneous irradiation with 6W UV lamp (370nm, 2 mW/cm^2), and inset, percentage of starting xanthate concentration degraded as a function of time derived from UV-Vis spectra absorbance at 370 nm.

The percentage of PXEP degraded as a function of irradiation time largely follows a similar trend as to what was seen previously under more dilute conditions for MA polymerisation (Figure 6.2, inset, red circles), however several notable differences. An initial spike is still seen, however the percentage degraded is approximately double (~ 6 % vs ~ 3%), followed by a slow linear increase and then a very large abrupt increase at the 12 h mark. There is also no point at which the absorbance of the solution after irradiation exceeds that of the starting solution.

These results imply that increasing the starting RAFT agent concentration is not beneficial to its stability under the irradiation conditions employed. This is somewhat contrary to the report by Wang *et al.* [15] who attributed an increase in the stability of a tertiary trithiocarbonate as arising from efficient degenerative chain transfer occurring only at higher concentrations.

The potential effect of the photolysis of PXEP is investigated in the Predici model in section 6.7.

6.3 Experimental studies of VAc polymerisation

6.3.1 Experimental procedures

Please refer to Chapter 4, sections 4.5 for relevant experimental procedures used in this section.

The conditions for VAc polymerisation were taken from the same publication by Keddie *et al.* [13] for the same reasons as described previously in Chapter 5, section 5.3.1, with the polymerisation of VAc shown in Scheme 6.1Scheme 5.2.

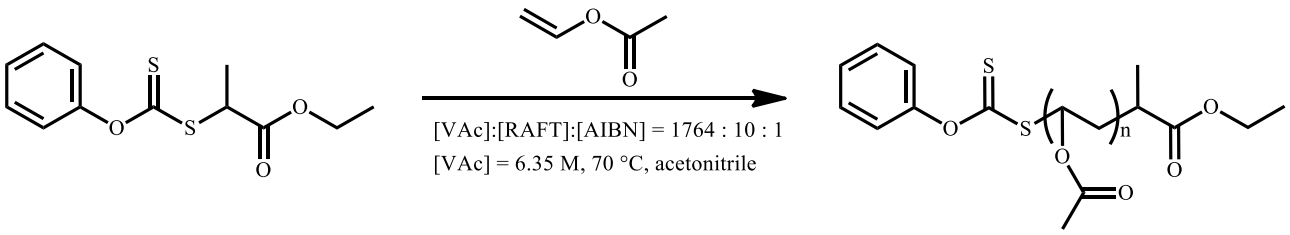

Scheme 6.1: Polymerisation of MA undertaken with PXEP under standard conditions.

Initially two polymerisations were run under Dark + AIBN conditions with the oil bath covered to gauge the reproducibility of the kinetics. As can be seen from Figure 6.3, the kinetic curves are essentially superimposable from the 2 h point onwards which consequently implies similar overlap at earlier time points despite only one reaction having data points in this region. From this it can be inferred that the ± 5 % error in conversion as determined for MA can also be considered an upper limit. This also reinforces the notion that erroneous thermal effects are minimised with the approach of wrapping the oil bath as opposed to wrapping individual flasks in order to exclude light.

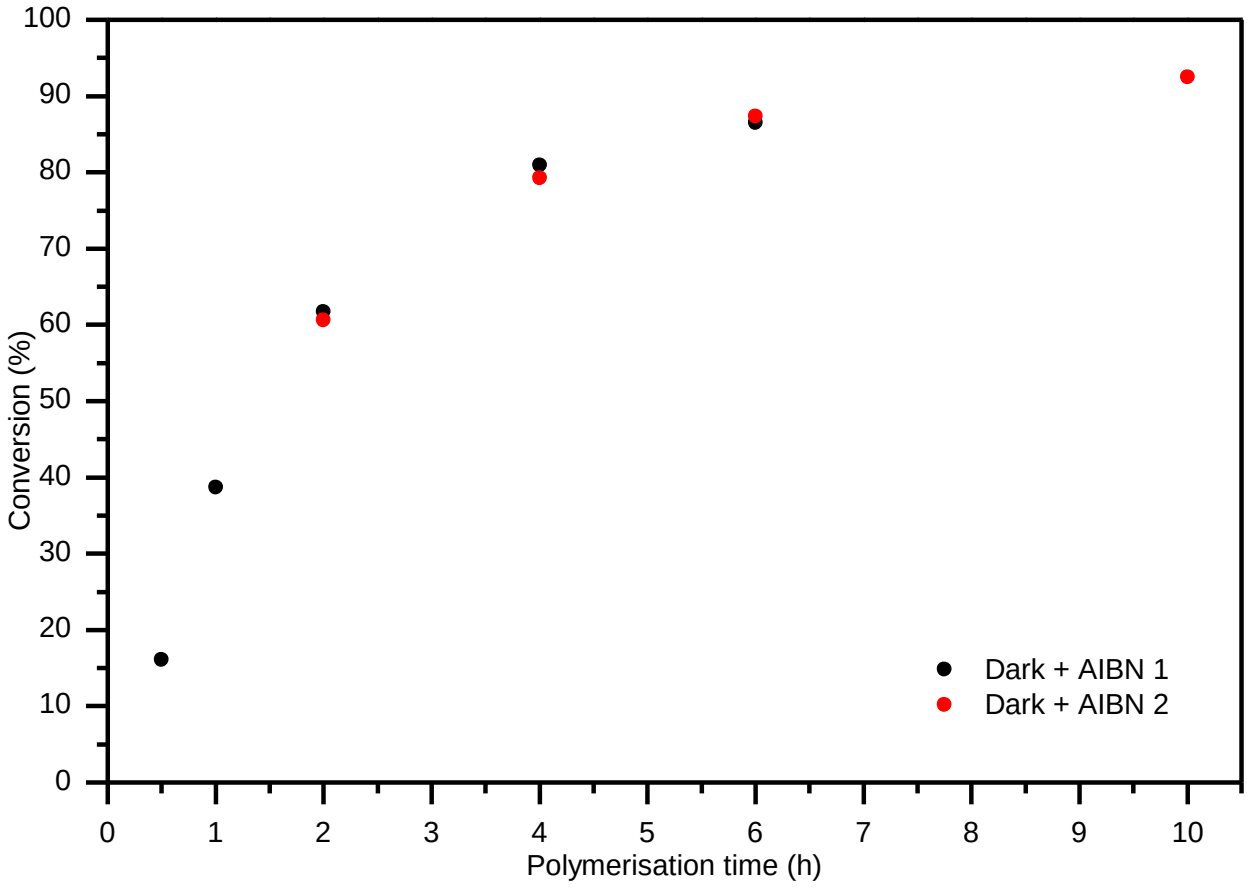

Figure 6.3: Kinetic experiments used to estimate the percentage error for VAc polymerisation conducted at 70 °C with PXEP.

6.3.2 Kinetic studies of VAc polymerisation

Figure 6.4 (A) shows the polymerisation kinetics under different conditions; under dark conditions the conversion attained at the 6 h mark is essentially identical to that obtained by Keddie *et al.* at the 10 h time point whilst using the least active RAFT agent in the series tested, having an apparent chain transfer constant of ~ 41. All other RAFT agents tested resulted in a negative correlation; the higher then chain transfer constant the lower the polymerisation rate. This implies that under these conditions, PXEP has a chain transfer coefficient that is lower than 41.

In striking contrast to MA, application of UV irradiation (light + AIBN) conditions only resulted in a modest increase in polymerisation rate as evidenced by slightly higher conversions that converge by the 4 h mark at around ~ 80 % conversion (Figure 6.4 (A)). Under light only conditions in the absence of AIBN leads to significantly slower kinetics, with a maximum conversion of only 60 % attained after 10 h. Thus, contrary to what was observed for MA, this data suggests that AIBN is the primary driver of the polymerisation rate, with UV irradiation only having a minor influence on the polymerisation rate.

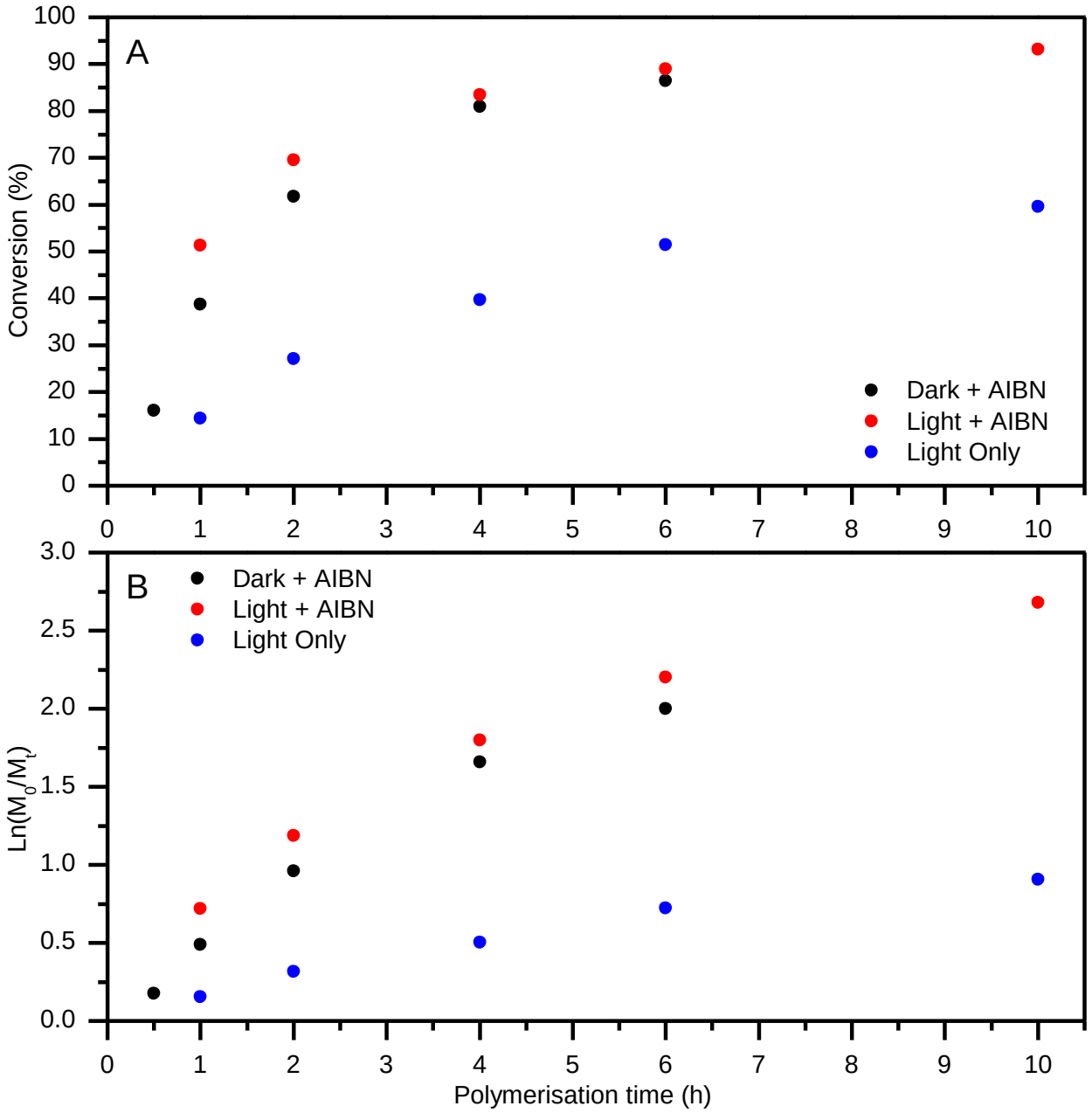

Figure 6.4: Conversion versus time plot (A) and 1st order kinetic plot (B) for VAc polymerised under various conditions at 70 °C with PXEP.

Concurrent with what was seen for MA, the pseudo first order kinetic plots for all reaction conditions are quite linear up to ~ 85 % conversion ($Ln(M_0/M_t)$ value of ~ 2) (Figure 6.4 (B)). This leads to the same conclusion, that the rates of initiation and termination are approximately equal over most of the polymerisation. Furthermore, just like for MA, this strongly suggests that a degenerative chain transfer mechanism is operative under all conditions utilised. The apparent kinetic rate coefficients of polymerisation (k_{app}) were calculated within this linear region, with the results summarised in Table 6.3. The enhancement factor was calculated by taking the ratio of the k_{app} value under a given experimental condition relative to the value for dark + AIBN conditions.

Table 6.3: Summary of calculated k_{app} values for the kinetic experiments shown in Figure 6.4 (B). UV irradiation (370nm, 2 mW/cm^2).

Conditions	k_{app} (h^{-1})	Error in k_{app} (+/-)	Enhancement factor
Dark + AIBN	0.43	0.02	1.00
Light + AIBN	0.49	0.04	1.14
Light only	0.13	0.01	0.30

Comparison of the apparent kinetic rate coefficients for the conditions featuring AIBN shows that under UV irradiation the polymerisation rate is only 14 % faster (enhancement factor of 1.14), with the k_{app} values being almost within error of one another. In the absence of AIBN, the k_{app} for the light only case is only 30 % of that for the dark + AIBN case, hence in this case it is not an enhancement factor as such. Comparisons to the work of da M. Costa *et al.* cannot be made due to VAc not being tested within this publication.

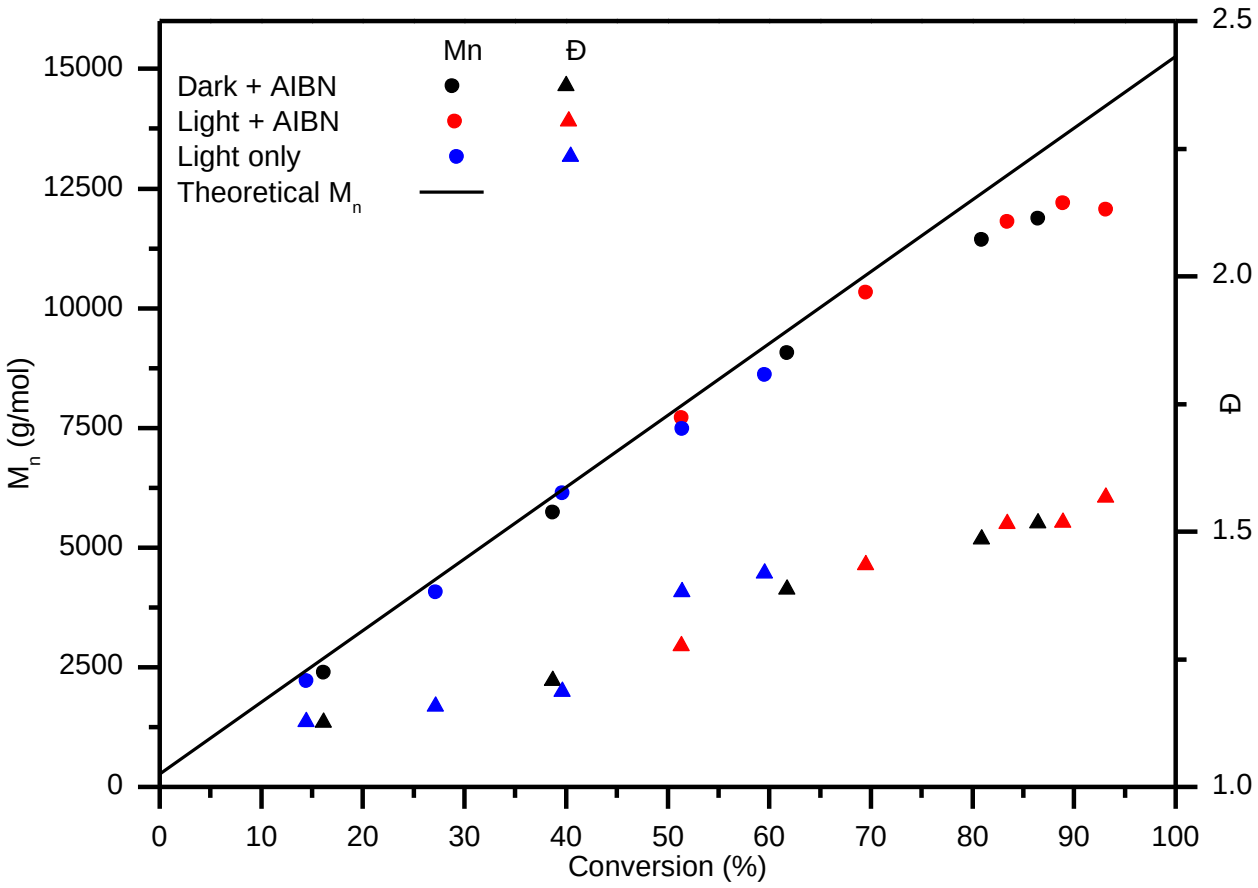

Figure 6.5: Evolution of molecular weight and dispersity as a function of conversion for VAc polymerised under various conditions at 70 °C with PXEP.

Figure 6.5 shows that under all reaction conditions there is close agreement between the theoretical and obtained molecular weight to moderately high (< 80 %) conversions, along with low dispersity

values under 1.25 for the first half of the reaction (< 50 % conversion). Coupled with a complete absence of hybrid behaviour, this is consistent with rapid capture of propagating radicals by PXEP during the pre-equilibrium stage followed by efficient fragmentation of the radical adduct to successfully release the re-initiating R group.

Regardless of the reaction conditions, at conversions exceeding 50 % the dispersity increases noticeably as a function of conversion. Concurrently at conversions exceeding 80 % there is also a noticeable negative deviation in the molecular weight. As explained in the introduction (section 6.1), there is no definitive explanation for both phenomena within the literature, however fundamentally these effects are a direct result of the very high reactivity of the PVAc propagating radical and low reactivity of the VAc monomer [1] which collectively results in chain transfer to polymer, monomer and head-to-head propagation [13].

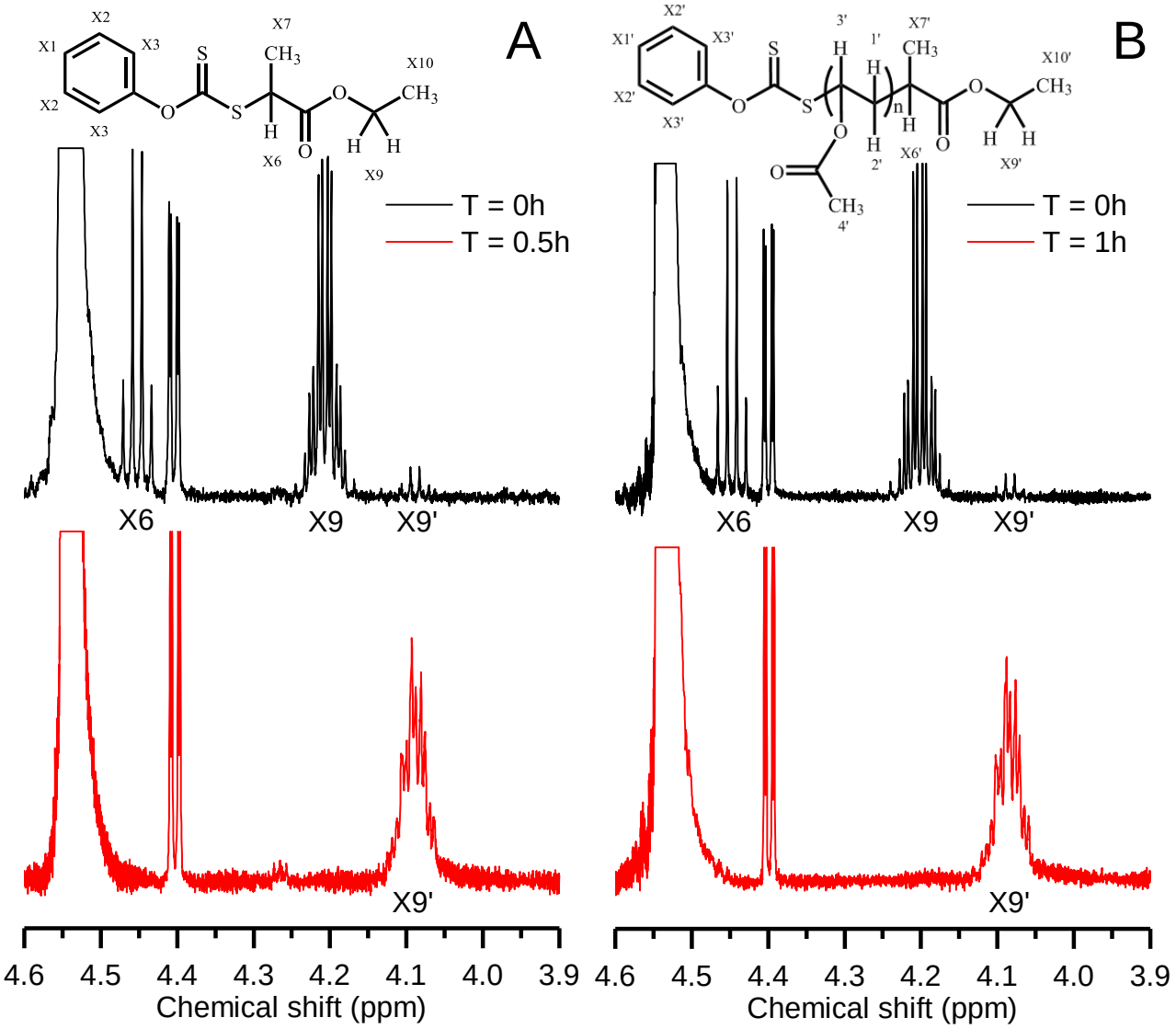

Figure 6.6: ^{1}H NMR spectra in the region of 3.9 – 5 ppm showing the resonances attributed to the starting PXEP and conversion into a poly(VAc), obtained from analysis of kinetic polymerisation samples polymerised to various times under dark conditions (A) and light only conditions (B).

Figure 6.6 shows that the consumption of PXEP is very rapid with the proton resonances attributed to the starting PXEP at 4.2 and 4.45 ppm being completely absent by the first-time point (0.5 & 1 h respectively) under both dark and light only conditions. This is strongly indicative that the chain transfer constant for PXEP under these conditions is higher than it was for the polymerisation of MA. This is confirmed in Figure 6.7, with the values for the chain transfer constant essentially all falling below the value of 41 predicted earlier by comparison to the results obtained by Keddie *et al.* [13]. There is a clear linear clustering of these values just as was seen for MA, with the sharp increase in the chain transfer constant at low chain lengths most likely being due to the limitations of this estimation method.

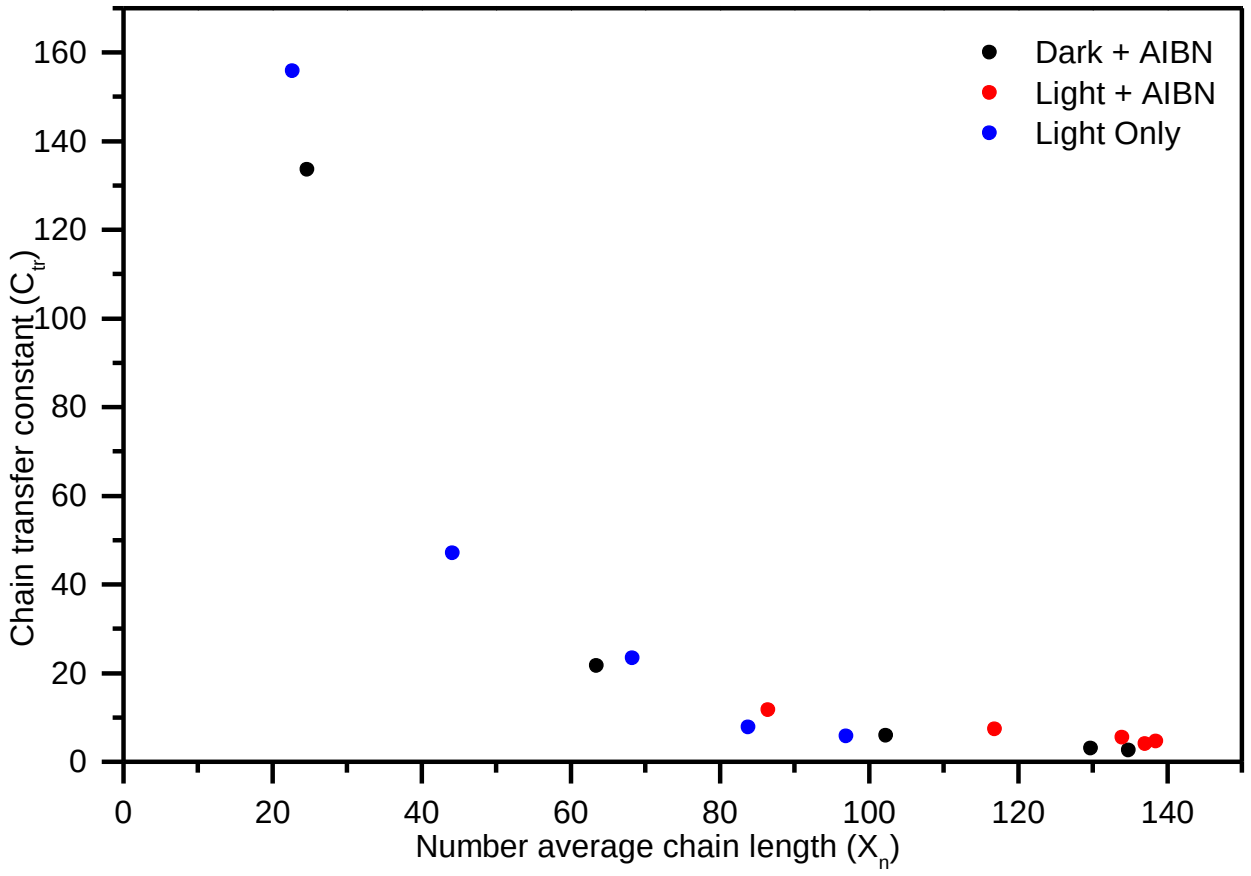

Figure 6.7: Chain transfer constants as estimated for PXEP when used in the polymerisation of VAc under various conditions at 70 °C.

Regardless of whether UV irradiation is employed, the remarkable continuity of both the evolution of M_n, dispersity and linear clustering of chain transfer values strongly suggests that just as for the polymerisation of MA, the polymerisation of VAc with PXEP proceeds via the RAFT mechanism.

Given that VAc is at the other end of the reactivity spectrum to MA, it was imperative to test whether the kinetic phenomena seen here also apply to the case of chain extension polymerisation. The rapid consumption of the starting PXEP seen should preclude any effects of the R group playing a crucial role in the process, as was a potential concern for MA.

6.3.3 Kinetic studies of VAc chain extension polymerisation

Chain extension experiments were conducted with a poly(VAc) macro-RAFT derived from PXEP that was synthesised in the dark and had an M_n of 2929 g/mol and $Đ$ = 1.13 by GPC, theoretically having 95.58 % of all chain ends retaining the RAFT moiety as estimated using Equation 4.9. The ratio of proton resonances from the phenol Z group (X2' & X3', Figure 6.8, inset) and proton resonances of the R group (X10', Figure 6.8 inset) were compared, and the correct 2:3 correspondence was found, indicating that on average each polymer chain retained both halves of the PXEP molecule.

Figure 6.8 shows that despite the incorporation of the polVAc block, the peak absorbance for this poly(VAc) macro-RAFT also occurred at 369 nm, which is essentially identical to the polyMA (369 nm) and starting PXEP (370 nm). This is evidence that that the poly(VAc) macro-RAFT agent should be capable of functioning as a macro-iniferter and undergoing chain extension under UV irradiation in the presence of more VAc monomer.

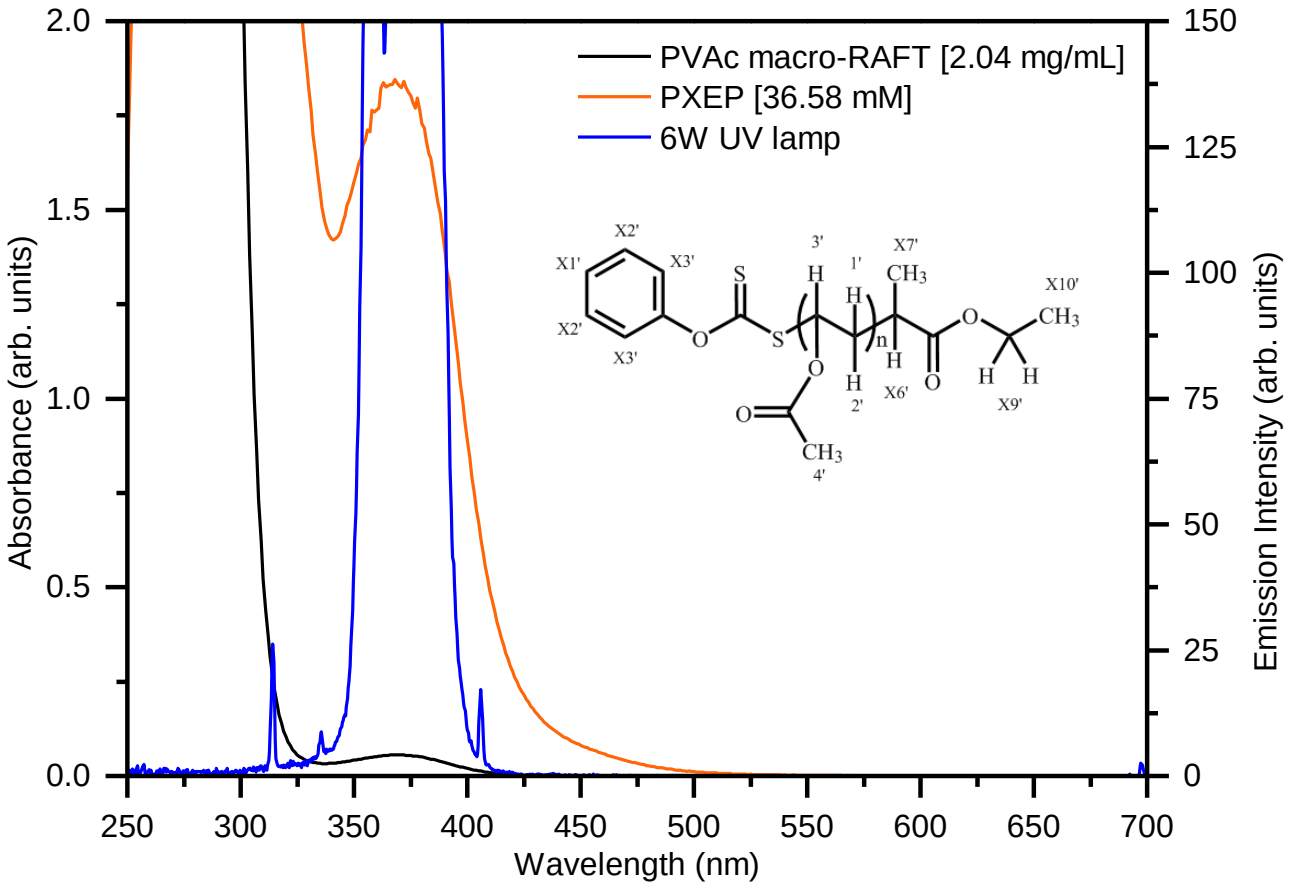

Figure 6.8: Comparison of the absorbance of the poly(VAc) macro-RAFT agent used in chain extension kinetics superimposed with the emission spectrum of the 6W UV lamp (370nm, 2 mW/cm^2).

Comparing the normal and chain extension kinetics, it is evident that the two do not match as closely as in the MA case, regardless of which reaction conditions are used (Figure 6.9, A). The light + AIBN and AIBN only kinetics are noticeably different for the chain extension case, being faster and slower respectively than in the conventional polymerisation. Chain extension kinetics with light only conditions are still significantly slower than those featuring AIBN and are slower than in the conventional case. The k_{app} values calculated for chain extension experiments are compared to the conventional k_{app} values in Table 6.4, and indeed appear to show that the differences seen are outside the error range of the respective experiments.

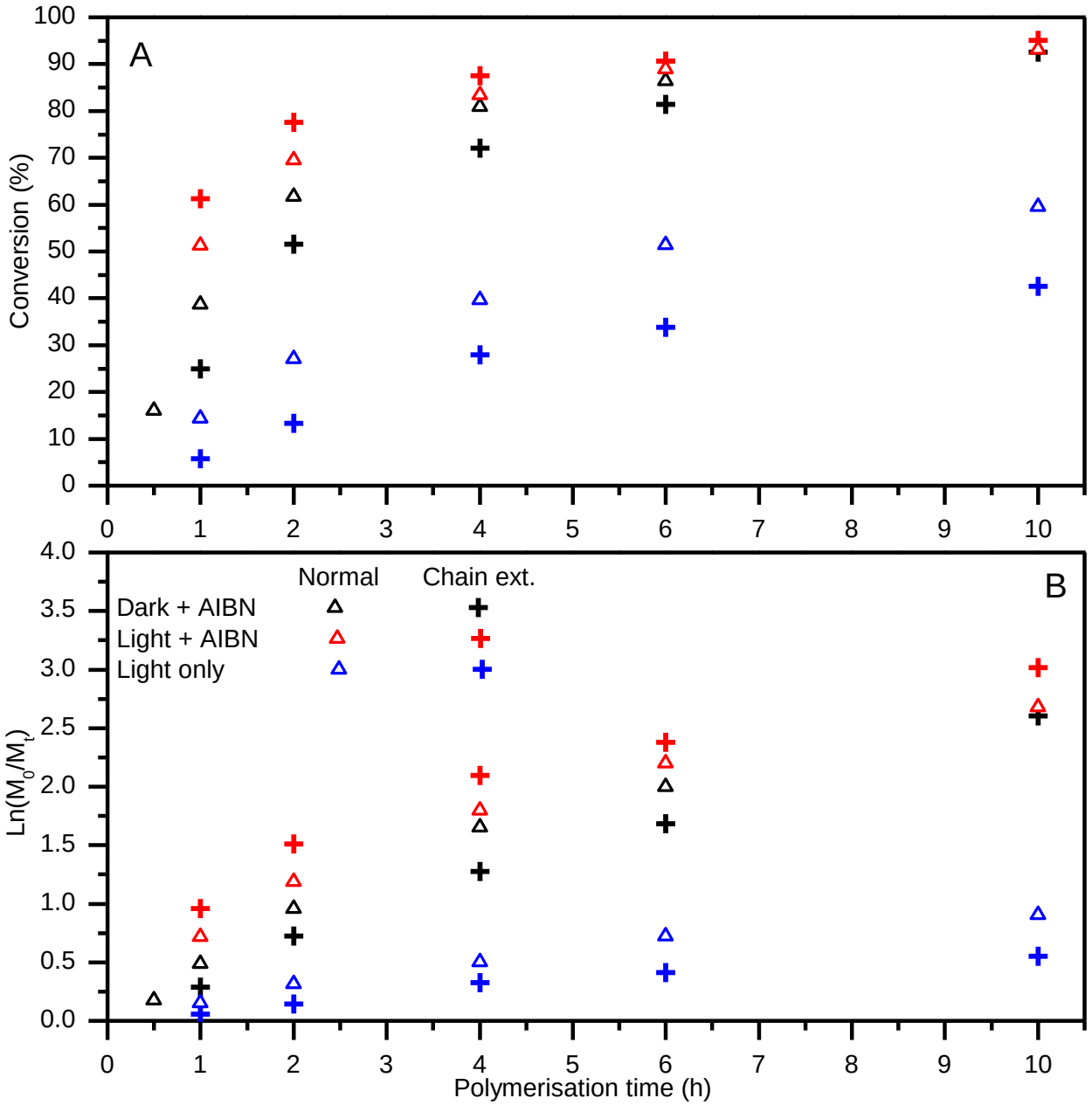

Figure 6.9: Conversion versus time plot (A) and 1st order kinetic plot (B) for VAc chain extension polymerisations under various conditions at 70 °C with a poly(VAc) macro-RAFT agent derived from PXEP.

It is possible that these differences arise due to the increased viscosity of the starting polymerisation mixture, which contains 2.66 times more macro-RAFT agent by concentration than for the MA case. Furthermore, despite not shifting the peak absorbance, it is possible that the incorporation of the poly(VAc) block will have altered the photochemical properties of the starting PXEP, as this has been observed previously with other RAFT agents by Ham *et al.* [16].

Table 6.4: Summary of calculated k_{app} values for kinetic chain extension experiments shown in

	Chain extension kinetics		Kinetics	
Condition	**k_{app} (h^{-1})**	**Error in k_{app} (+/-)**	**k_{app} (h^{-1})**	**Error in k_{app} (+/-)**
Dark + AIBN	0.30	0.01	0.43	0.02
Light + AIBN	0.80	0.06	0.49	0.04
Light only	0.062	0.004	0.13	0.01

Despite the similar trends seen kinetically, comparison of the experimentally obtained and theoretical M_n for the chain extension experiments reveals a significant discrepancy (Figure 6.10). Furthermore, the dispersity values increase significantly to almost 2 as the conversion increases.

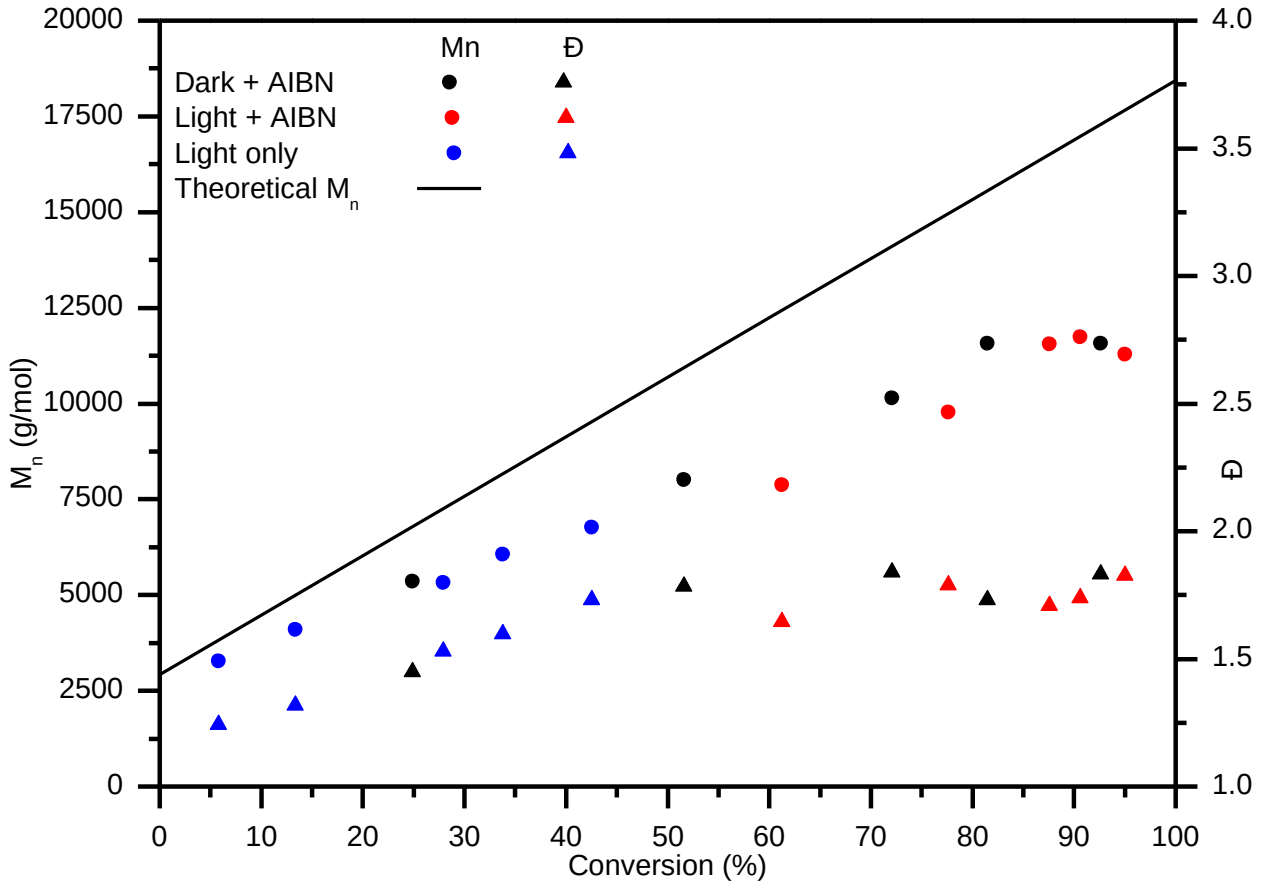

Figure 6.10: Evolution of molecular weight and dispersity as a function of conversion for VAc chain extension polymerisations under various conditions at 70 °C with a poly(VAc) macro-RAFT agent derived from PXEP.

Both these phenomena can arise due to the same factors as described previously for conventional VAc polymerisation. Another explanation is that the chain extension was not entirely successful. This is evidenced by the GPC traces showing an incomplete consumption of the starting poly(VAc) macro-initiator which manifests as tailing to lower molecular weights, regardless of the reaction conditions employed, as shown in Figure 6.11. Thus, when the complete peak is integrated this lowers the

measured M_n and increases the overall dispersity. Regardless, the main peak in each series of spectra shifts to progressively higher molecular weights (lower retention times) with increasing reaction times, which indicates that chain extension is occurring and is being moderated by the RAFT mechanism.

Similar phenomena were seen by Ham *et al.*, with the bimodal GPC distribution being attributed to the incomplete consumption of the starting PVAc macro-RAFT under UV irradiation [16]. A more comprehensive mechanistic explanation for the experimental results presented here is allusive; however, the most likely possibility being that the starting PVAc macro-RAFT contains a substantial percentage of dead chains that no longer contain a RAFT moiety. These can arise due to initiator derived chains that terminate before addition to the RAFT agent, or due to bimolecular termination between growing macro-radicals. It seems unlikely that photolytic stability of the PVAc macro-RAFT agent is to blame, given the literature precedent that shows these species readily undergo photolytic breakdown [14, 16, 17]. Interestingly, Shim *et al.* reported seemingly complete consumption of a series of PVAc macro initiators made under UV irradiation at 60 °C, when chain extension was conducted at 0 °C with the same irradiation method [17]. This potentially implies that problematic side reactions during the chain extension process are limited at lower temperatures [17].

Overall, the vast differences encountered between VAc and MA polymerisations lead to the conclusion that different photolysis pathways are dominant in both scenarios. The role of the various photolysis pathways are explored further within this chapter, with potential explanations explored for the differences seen between the two monomers.

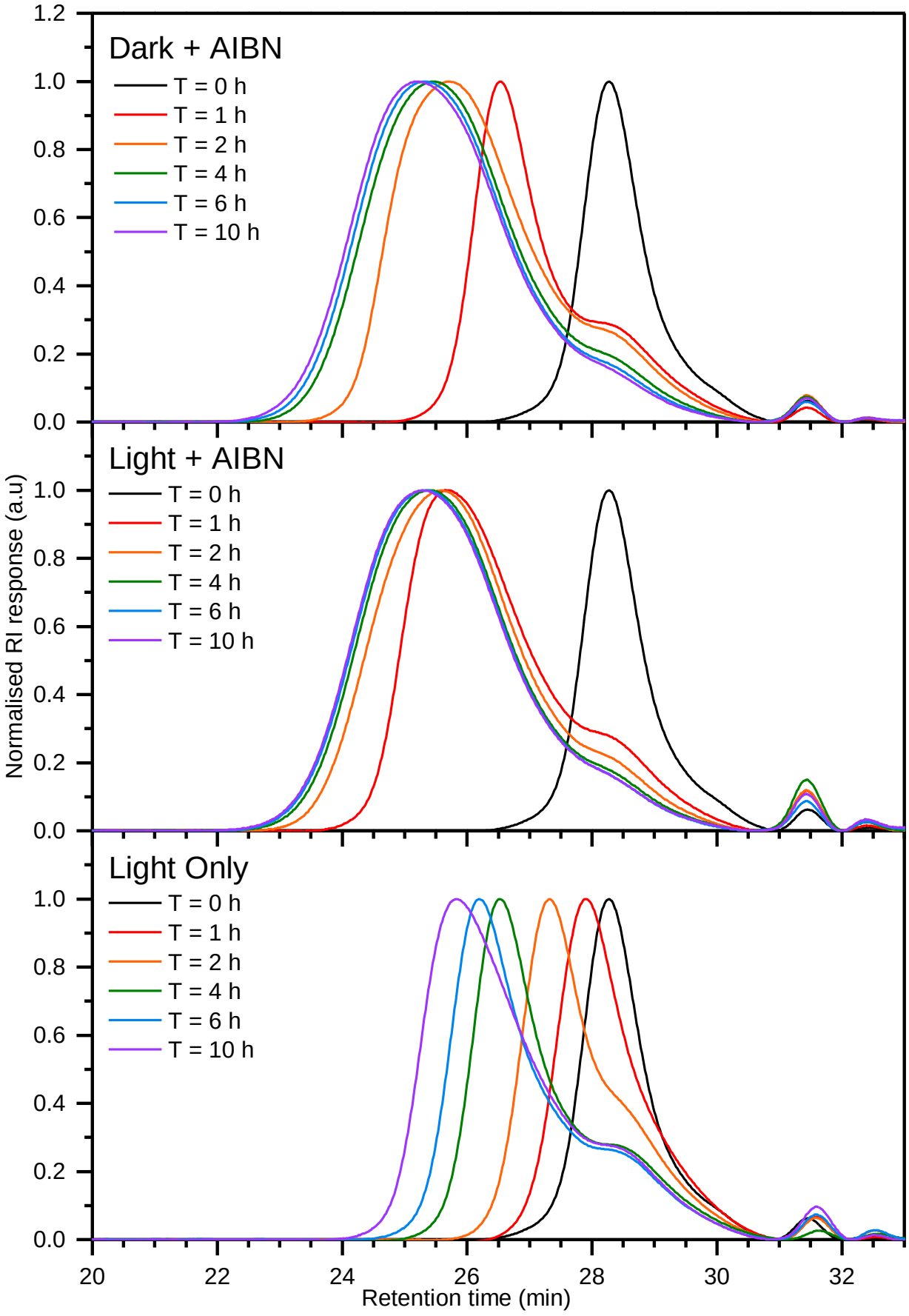

Figure 6.11: Normalised RID GPC traces for VAc chain extension polymerisation samples at various time points, under various conditions at 70 °C with a poly(VAc) macro-RAFT agent derived from PXEP.

6.4 Predici model development – calculation, selection and testing of kinetic rate coefficients

Table 6.5 summarises the initial values for all the species within the Predici model for simulations of VAc polymerisations, and the corresponding parameters used.

Table 6.5: Summary of species parameters and their concentrations as set in the model at t = 0 for modelling VAc polymerisations.

Species name	Mol mass (g/mol)	Density (g/L)	Conc. (M)	Reactor
R	101.1	1000	0	Flask
Initiator	164.2	1000	0.0036	Flask
RAFT	270.4	1000	0.03599	Flask
I	69.11	1000	0	Flask
I (Inactive)	69.11	1000	0	Flask
Monomer	86.09	934	6.3487	Flask
Sol	41.05	786	7.745	Flask
Xanthate fragment	169.2	1000	0	Flask
Dummy	1	2	1	Abstract
Photon	1	2	1	Abstract

6.4.1 Calculation of rate coefficient of 2-cyano-2-propyl radical (AIBN radical) addition to VAc

As for the case of MA, the absolute experimentally derived rate constants (M^{-1} s^{-1}) and frequency factors ($\log_{10}(A/ M^{-1} s^{-1})$ for the addition of AIBN radicals to vinyl acetate were taken from the Table 1.0 in the review by Fischer & Radom [18], with the activation energy recalculated in a similar fashion. The E_a for the addition of AIBN radicals to VAc was found to be 35503 J/mol and the absolute rate constant at 70 °C (343.15 K) was calculated to be 125 L M^{-1} s^{-1}, which was the value set for k_i in the model. This is significantly lower than the value for the addition of AIBN radicals to MA, which is entirely consistent with the significantly lower reactivity of the VAc monomer towards radical addition.

6.4.2 Calculation of the propagation rate coefficient for VAc

The propagation rate coefficient (k_p) for VAc under experimental conditions was calculated using the activation energy value (E_a of 20.40 kJ/mol) and frequency factor (1.35 x 10^7 L mol^{-1} s^{-1}) as recommended in the IUPAC review by Barner-Kowollik *et al.* [3]. Since VAc does not form tertiary propagating radicals to any appreciable extent, the calculated value of 10595 L mol^{-1} s^{-1} can be taken as accurate. Furthermore, the Arrhenius values given in the review cover the temperature range up to

70 °C and are said to encompass the kinetic effects associated with the non-negligible rate of head to head addition that occurs during VAc polymerisation.

6.4.3 Selection of 1-ethoxycarbonyl ethyl radical (R group radical) addition rate coefficient to VAc

Owing to the extra electron density from the oxygen adjacent to radical centre on the VAc radical, it is expected to have significantly different reactivity to the 1-ethoxycarbonyl ethyl radical (R group radical), hence the assumption that $k_p = k_{R\text{-}re}$ is not valid as it was for the MA case.

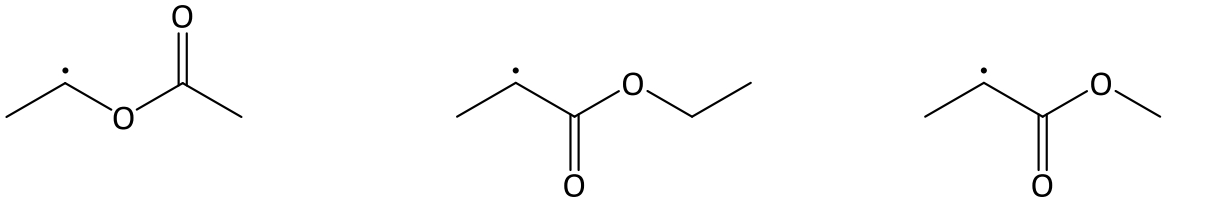

Scheme 6.2: Structural comparison of VAc propagating radical and R group radical derived from PXEP, and the MA propagating radical.

The value of $k_{R\text{-}re}$ was calculated using Equation 6.1:

$$r_1 = \frac{k_{11}}{k_{12}}$$

$$\therefore k_{12} = \frac{k_{11}}{r_1}$$

Equation 6.1 Relationship between reactivity ratios and propagation coefficients for two monomers.

Where r_1 = the reactivity ratio of MA, k_{11} = propagation rate coefficient of MA, k_{12} = rate coefficient for addition of VAc radical to a MA polymer chain end. The value of r_1 used for the calculation was the same as that used by Theis *et al.* [19], which was originally taken from a publication by Brar & Charan [20] who determined that $r_{MA} = r_1 = 7.28$ and $r_{VAc} = 0.04$ by the Kelen–Tüdős method. This is based on the previously employed assumption that the reactivity of the R group radical is essentially identical to the reactivity of a MA propagating radical based on their similar structure (Scheme 6.2). k_{11} was set to 15672 L mol^{-1} s^{-1} as calculated in the previous chapter, giving a value of $k_{11} = k_{R\text{-}re}$ = 2153 L mol^{-1} s^{-1}.

6.4.4 Initiator efficiency factor (f) & k_d for AIBN breakdown

Based on the literature precedents listed in Table 6.6, f was set to 0.5 in the model with a linear decrease from f to 0 as a function of monomer conversion being implemented, just as was the case for MA described in the previous chapter. The value of k_d determined experimentally under dark conditions as described previously in Chapter 5, section 5.2.4 was used. Hence $k_d = 1.653 \times 10^{-5}$ s^{-1} was used for the baseline calculations.

Table 6.6: Implementations for AIBN breakdown in simulations of VAc polymerisations.

Initiator efficiency model	f	Reference
Linear decrease from f to 0 at 100% monomer conversion	0.5	[19]
Constant efficiency of f	0.5	[19]

6.4.5 Selection of termination rate coefficients

Unlike for MA, there is no clear consensus within the literature as to the contribution of termination by disproportionation to the overall rate of termination during VAc polymerisation. Termination solely by disproportionation was used by Monyatsi *et al.* [5], with Hutchinson *et al.* also using this approach, however noting that the model was insensitive to the method of termination employed [21]. Conversely, termination solely by combination was implemented by Theis *et al.* [19], with Kattner *et al.* not specifying the mode of termination used in their work [4].

For consistency with the kinetic investigation of MA and in light of the lack of consensus within the literature, the contribution due to disproportionation was set to 0, with termination solely by combination being used within the Predici model. A range of termination rate coefficient values ($k_t^{1,1}$) and implementations employed in the literature are shown in Table 6.7; as for the MA case, the value of $k_t^{1,1}$ was set to 10^9 for the initial simulation with the other $k_t^{1,1}$ values tested being shown in Table 6.8.

Table 6.7: Summary of termination values and implementation used for modelling VAc polymerisations.

Termination model	$i_{, cross}$	$\log k_t^1$	α	Termination mode	Reference
Varied	N/A	8.65	0.16	Combination	[19]
Fixed	N/A	8.00	N/A	Combination	[19]
Varied	~ 20	9.18	0.57 (short), 0.16 (long)	N/A	[4]

Table 6.8: Summary of model parameters for baseline VAc kinetic model, including parameters tested during each baseline simulation.

Parameter	Value	Units
ki	1.2500 x10^{2}	L mol^{-1} s^{-1}
kR-re	2.1530 x10^{3}	L mol^{-1} s^{-1}
kd	1.6530 x10^{-5}	s^{-1}
kp	1.0595 x10^{4}	L mol^{-1} s^{-1}
f	5.0000 x10^{-1}	N/A
alpha_short	5.7000 x10^{-1}	N/A
alpha_long	1.6000 x10^{-1}	N/A
i_cross	2.0000 x10^{1}	N/A
Termination parameters		
Simulation #	**Value of kt_1**	**Log (kt_1)**
B.1	1.0000 x10^{9}	9.00
B.2	1.5000 x10^{9}	9.18

The simulation undertaken with the original estimate of kt_1 overestimates the polymerisation rate but only slightly (Figure 6.12, red trace). It is gratifying to note that using the literature parameters for the termination parameters yields a perfect fit to the experimental data (Figure 6.12, blue trace).

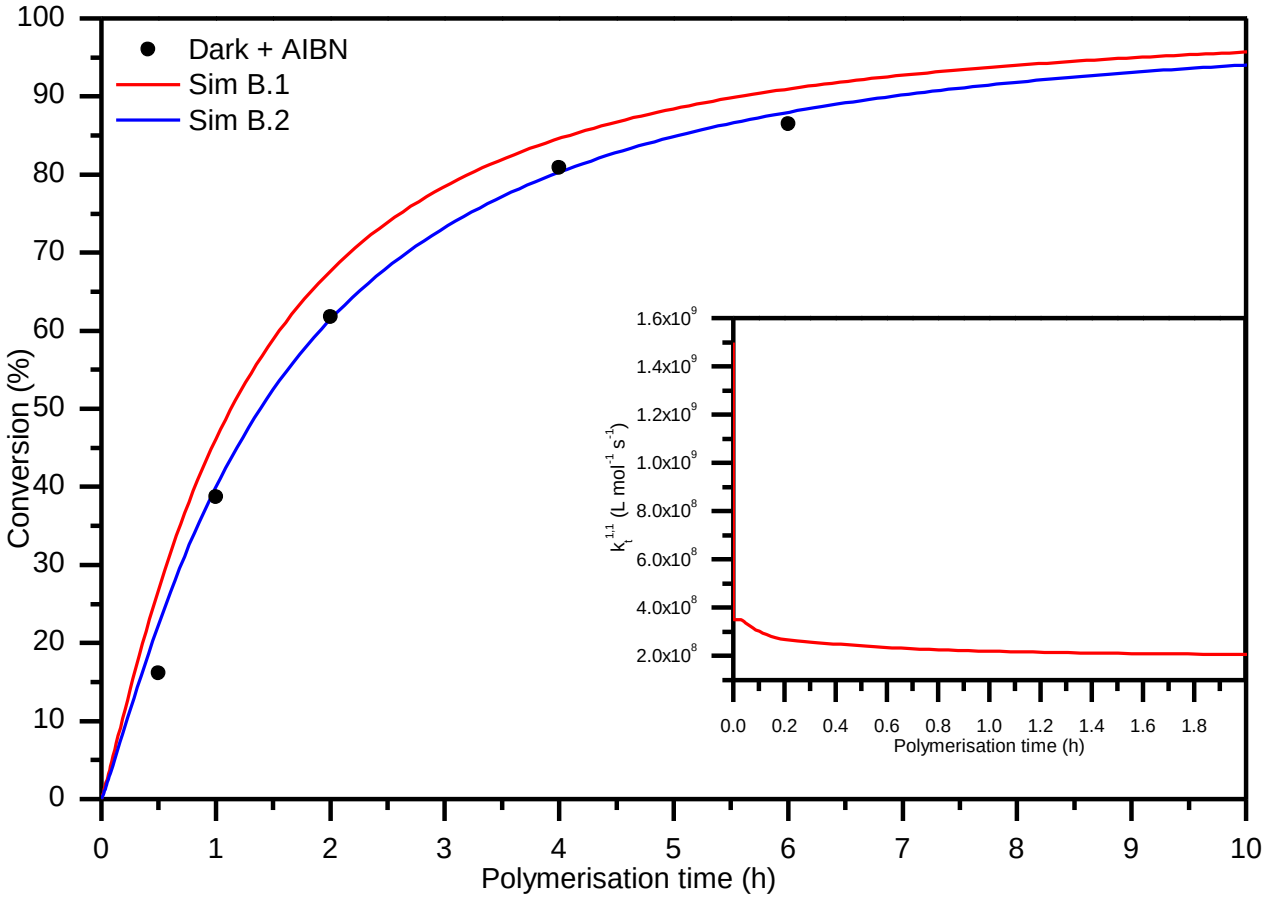

Figure 6.12: Comparison of kt_1 values and their effect on the simulated kinetics (conversion vs time) of the polymerisation of VAc under dark + AIBN conditions, and inset, the value of kt_1 as a function of polymerisation time.

6.4.6 Parameters for RAFT pre-equilibrium & main equilibrium

The kinetic rate coefficient for the R group adding VAc monomer ($k_{R\text{-}re}$) is equal to 2153 L mol^{-1} s^{-1}, which is approximately 20 % of the value of k_p for VAc. This implies that the R group radical is less reactive and thus more stable, and consequently should fragment preferentially from a PXEP adduct radical that also has an attached VAc propagating radical. As outlined by Theis *et al.* this naturally means that the partition coefficient for the pre-equilibrium must lie between 1 which corresponds to only fragmentation of the R group and 0.5 which corresponds to even fragmentation as occurs in the main equilibrium [19]. The partition coefficient was thus set to 0.75 in favor of fragmentation to the R group.

Despite the lack of obvious hybrid behaviour, the parameters for the both pre-equilibrium and main were calculated in the same manner as described previously in Chapter 5, section 5.5.7. The only difference being that the molecular weight versus conversion was fitted with a linear line of best fit to extrapolate the molecular weight at zero conversion.

C_{tr} values tested included a value at an approximate time of t = 0.75 with simulation B.4 used an estimated value of C_{tr} at a chain length of 0, which was calculated using a linear line of best fit to the C_{tr} values for the dark + AIBN conditions, with the first data point (t = 0.5 h, Ctr = 133.6) being omitted.

Table 6.9: Summary of model parameters for the RAFT pre-equilibrium and equilibrium for baseline kinetic model, including parameters tested during each simulation.

Parameter	**Value**	**Units**		
ki	9.39×10^{2}	$M^{-1} s^{-1}$		
kR-re	2.153×10^{3}	$M^{-1} s^{-1}$		
kd	1.653×10^{-5}	s^{-1}		
kp	1.0595×10^{4}	$M^{-1} s^{-1}$		
f	5.0×10^{-1}	N/A		
alpha_short	5.7×10^{-1}	N/A		
alpha_long	1.6×10^{-1}	N/A		
i_cross	2.0×10^{1}	N/A		
kt_1	1.5×10^{9}	$M^{-1} s^{-1}$		
Pre-equilibrium parameters				
kadd,0	4.53×10^{6}	$M^{-1} s^{-1}$		
k-add,0	4.53×10^{4}	$M^{-1} s^{-1}$		
kfrag,0	1.51×10^{6}	$M^{-1} s^{-1}$		
k-frag,0	1.51×10^{4}	$M^{-1} s^{-1}$		
Equilibrium parameters				
Simulation #	**Time point (h)**	**C_{tr}**	**k_{add}**	**k_{frag}**
B.3	~ 0	36.8	3.899×10^{5}	1.949×10^{3}
B.4	~ 0.75	24.63	2.609×10^{5}	1.304×10^{3}

The resulting simulations using parameters from Table 6.9 show a good agreement with the evolution of M_n, with sim B.3 corresponding to the higher chain transfer constant yielding a better match to the dispersity (Figure 6.13, brown trace). Once again for the same reasons as for MA, for forthcoming simulations the dispersity should be taken as a comparison relative to the baseline model as opposed to absolute values.

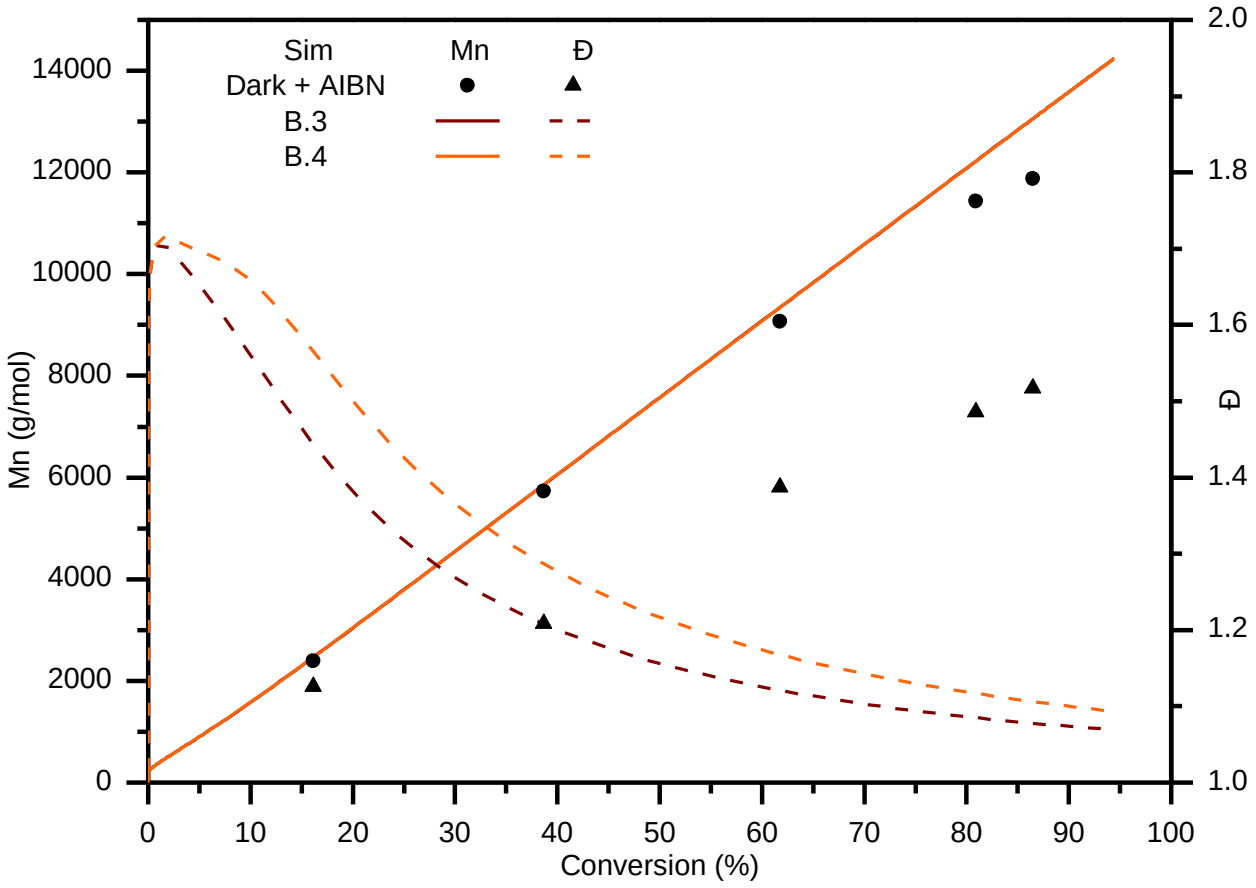

Figure 6.13: Comparison the effect of pre-equilibrium and equilibrium values on the overall dispersity values (overall dispersity vs conversion) of the polymerisation of VAc under dark + AIBN conditions. Values tested are shown in Table 6.9.

The parameters employed for simulation B.3 were selected as baseline model, and from this point every time the baseline model is used it refers to a simulation run with the parameters listed in Table 6.10.

Table 6.10: Finalised baseline parameters for modelling VAc polymerisation under dark + AIBN conditions.

Parameter	Value	Units
ki	9.39×10^{2}	$M^{-1} s^{-1}$
kR-re	2.153×10^{3}	$M^{-1} s^{-1}$
kd	1.653×10^{-5}	s^{-1}
kp	1.0595×10^{4}	$M^{-1} s^{-1}$
f	5.0×10^{-1}	N/A
alpha_short	5.7×10^{-1}	N/A
alpha_long	1.6×10^{-1}	N/A
i_cross	2.0×10^{1}	N/A
kt_1	1.5×10^{9}	$M^{-1} s^{-1}$
Pre-equilibrium parameters		
kadd,0	4.532×10^{6}	$M^{-1} s^{-1}$
k-add,0	4.532×10^{4}	$M^{-1} s^{-1}$
kfrag,0	1.511×10^{6}	$M^{-1} s^{-1}$
k-frag,0	1.511×10^{4}	$M^{-1} s^{-1}$
Equilibrium parameters		
kadd	3.899×10^{6}	$M^{-1} s^{-1}$
kfrag	1.949×10^{3}	$M^{-1} s^{-1}$

6.5 Predici Results – Scenario 1: Direct photolysis of monomer

The same approach was taken as previously in Chapter 5, section 5.7; reaction 18 which is responsible for direct initiation of monomer was activated and all other reactions responsible for initiation from other sources were disabled. Once again a free-radical mechanism (only reactions 4, 17 & 18 were active) was along with the RAFT mechanism being active (reactions 4 – 17, 17 & 18 were active) were considered.

Initially, the values of $k_{photons\text{-}monomer}$ which were determined for MA to yield comparable yields to the control experiments were used in sims 1.A and 1.B (Table 6.11) which gave higher conversion values than the control experiment (10.22 %, Table 6.1, entry 1).

To account for the vast difference between the starting monomer concentrations used in VAc and MA polymerisations, the values of $k_{photons\text{-}monomer}$ used in sims 1.A and 1.B were multiplied by a scaling factor as such:

$$Scaling\ factor = \frac{[MA]}{[VAc]} = \frac{2.79}{6.35}$$

$$\therefore Scaling\ factor = 0.44$$

The scaling factor works reasonably well, with the scaled $k_{photons\text{-}monomer}$ values from sims 1.A and 1.B being used in sims 1.C and 1.D which resulted in comparable yields (within 2 %) to the experimentally obtained value of 10.22 %. Further optimisation of the value of $k_{photons\text{-}monomer}$ resulted in sims 1.E and 1.F which are taken to be the natural limits that this value can be, as evidenced by close agreement between the yield obtained both with and without the RAFT mechanism active relative to the control experiment.

Table 6.11: Summary of simulations for determining the natural limits for the kinetic rate coefficient governing the direct initiation from monomer photolysis, $k_{photons\text{-}monomer}$.

Simulation	k(photons monomer) (M^{-1} s^{-1})	Conversion with RAFT mechanism inactive (%)	Conversion with RAFT mechanism active (%)
1.A	1.600×10^{-12}	16.79	3.98
1.B	2.000×10^{-11}	41.09	19.34
1.C	7.030×10^{-13}	12.06	2.31
1.D	8.787×10^{-12}	31.64	12.12
1.E	5.000×10^{-13}	10.46	1.79
1.F	7.000×10^{-12}	29.23	10.44

As per the MA case, the light + AIBN data was selected for modelling, which mean that for this series of simulations the baseline simulation which includes conventional initiation by breakdown of AIBN was active in all cases except for sim 1.4. The values determined as the natural limits for $k_{photons\text{-}monomer}$ (sims 1.E and1.F) were used initially for sims 1.1 & 1.2 (Table 6.12).

Table 6.12: Summary of $k_{photons\text{-}monomer}$ tested to simulate the effect of direct photolysis of monomer.

Simulation	$k_{photons\text{-}monomer}$ (M^{-1} s^{-1})	k_d (s^{-1})
Baseline	**N/A**	1.653×10^{-5}
1.1	5.0000×10^{-13}	1.653×10^{-5}
1.2	7.0000×10^{-12}	1.653×10^{-5}
1.3	8.0000×10^{-9}	1.653×10^{-5}
1.4	8.0000×10^{-9}	N/A

The kinetic curves for sims 1.1 and 1.2 (Figure 6.14 (A), brown and orange traces respectively) overlap perfectly with the baseline simulation (Figure 6.14 (A), black trace), indicating that monomer photolysis cannot realistically account for increased kinetics seen under light + AIBN conditions. This is further supported by sim 1.3 which required a value of $k_{photons\text{-}monomer}$ 3 orders of magnitude higher than the upper limit to match the light + AIBN experimental data. Furthermore, sim 1.4 shows that when AIBN initiation was turned off, the resulting kinetics are only marginally slower than the dark + AIBN kinetics and vastly faster than the light only experimental data. These findings are not surprising when the relative rates of initiation are compared; Figure 6.14 (B) shows that only for sims

1.3 and 1.4 does the rate of initiation due to monomer photolysis approach that due to AIBN degradation. Overall this quite conclusively shows that initiation of monomer is not the primary photolytic pathway for the enhanced kinetics seen.

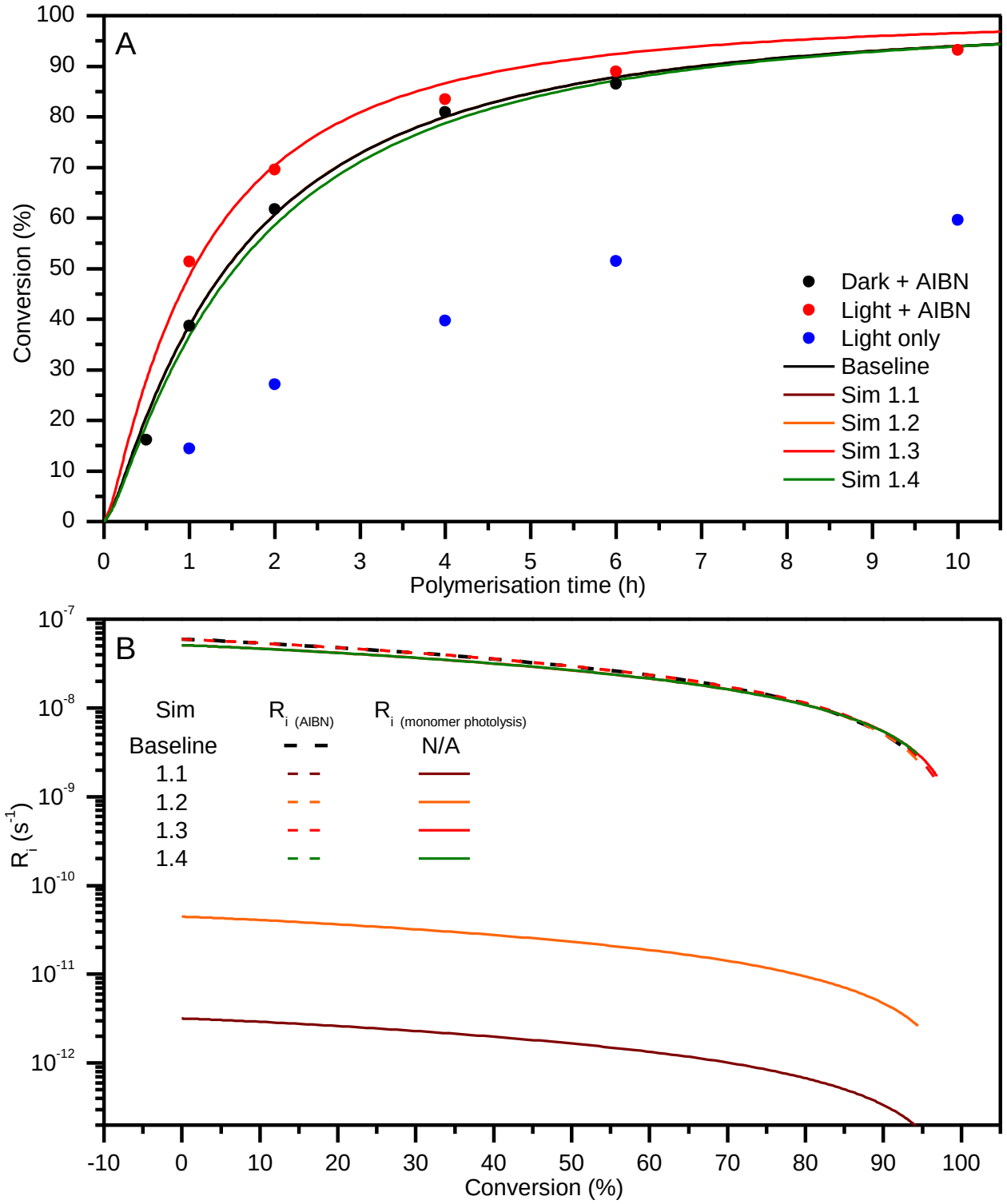

Figure 6.14: Comparison of conversion vs time plots for simulations 1.1 – 1.4 and experimental data (A) and calculated rates of initiation due to breakdown of AIBN and photolysis of monomer (B).

As was the case for MA, regardless of the value of $k_{photons\text{-}monomer}$ tested, all simulations showed essentially identical development of both M_n and dispersity as a function of conversion relative to the baseline model (see Figure A13 in the Appendix).

6.6 Predici Results – Scenario 2: Photolysis of AIBN

Testing only two values of k_d was required to deduce whether photolytically enhanced breakdown of AIBN could explain the faster kinetics seen under light + AIBN conditions. All simulations in this section had initiation due to monomer photolysis disabled besides sim 2.3 which used the upper limit value of $k_{photons\text{-}monomer}$ as deduced previously in section 6.5. These values are summarised in Table 6.13.

Table 6.13: Summary of kd values tested to simulate the effect of photolytically accelerated degradation of AIBN.

Simulation	k_d (s^{-1})	Multiplication factor for k_d	$k_{photons\text{-}monomer}$ (M^{-1} s^{-1})
Baseline	1.6530 x10^{-5}	1.00	N/A
2.1	5.0660 x10^{-5}	3.065	N/A
2.2	3.3060 x10^{-5}	2.00	N/A
2.3	3.3060 x10^{-5}	2.00	7E-12

The maximum value of k_d determined experimentally under UV irradiation was tested in sim 2.1; this resulted in faster kinetics than what was seen experimentally (Figure 6.15, brown trace). Upon decreasing k_d to 3.3060 x10^{-5} s^{-1} which corresponds to a 2-fold increase, this allowed sim 2.2 to accurately match the light + AIBN kinetics (Figure 6.15, red trace). Sim 2.3 gives an identical kinetic curve (Figure 6.15, orange trace) to that of sim 2.2, indicating that the maximum upper limit of monomer photolysis is essentially inconsequential to the polymerisation rate under these conditions.

The key differences between these findings and those for MA polymerisations most likely arise due to several factors. Firstly, under the fact maximum k_d value as determined experimentally, the concentration of AIBN is not depleted over the timescale of the reaction, even though the reaction is run for 10 h instead of 6 h as for MA. This is due to the increased overall concentration of AIBN in the starting reaction mixture as shown in Figure A14 in the Appendix. Secondly, the higher value of k_d determined under photolysis conditions should be treated strictly as an upper limit as it was determined under conditions that don't factor in the effects of the spectral overlap due to PXEP in the UV region.

Regardless of the parameters used, for sims 2.1 – 2.3, the evolution of molecular weight and dispersity values was identical to the baseline result, once again indicating no negative side effects from a higher rate of initiation. See Figure A15 in the Appendix for data.

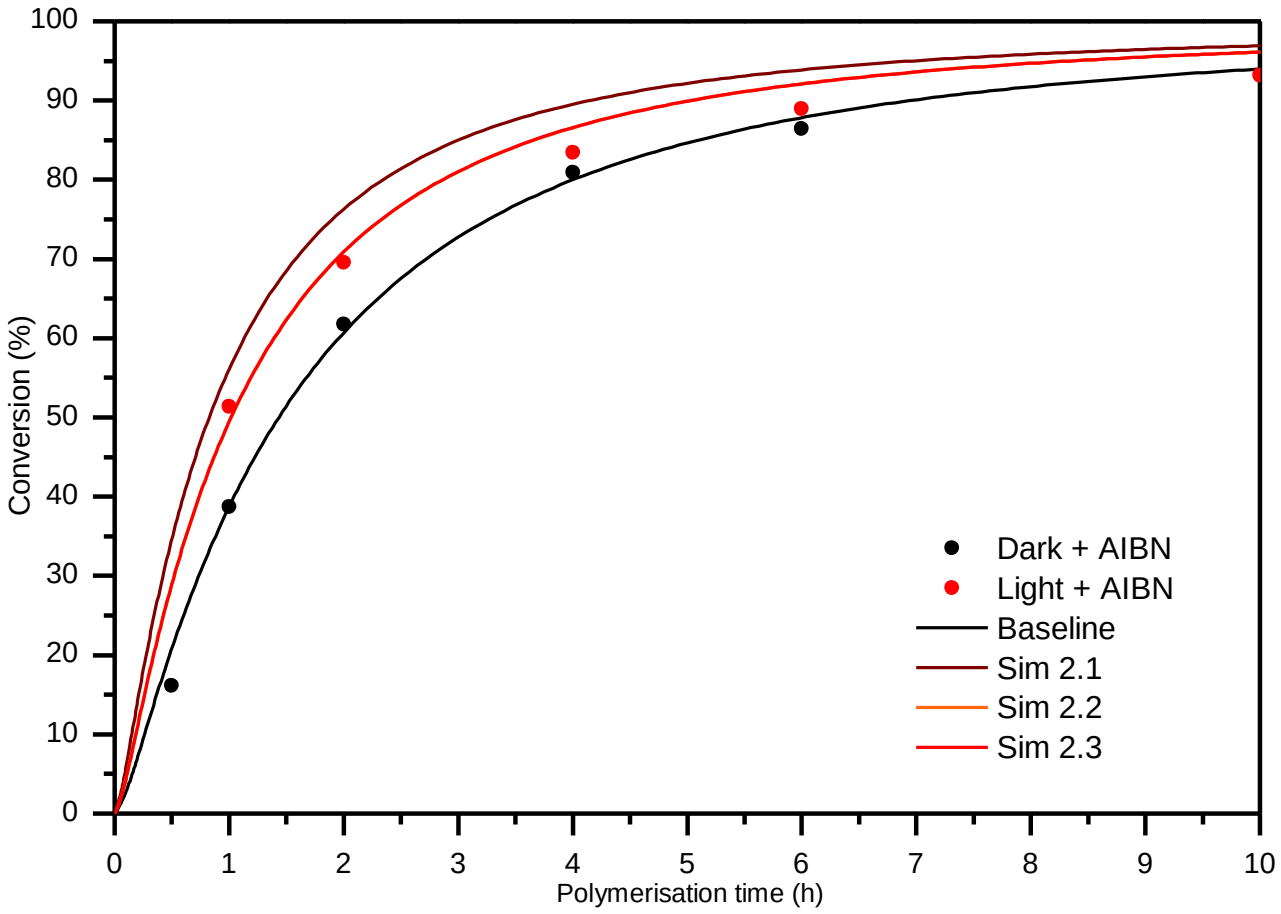

Figure 6.15: Comparison of conversion vs time plots for simulations 2.1 – 2.3 and experimental data.

6.7 Predici Results – Scenario 3: Reversible photolysis of RAFT species

The light only experimental data was chosen for modelling as it presents the simplest case where the initiation only occurs due to photolysis of RAFT agent and monomer; for all the simulations within this section $k_{photons\text{-}monomer}$ was set to the lower limit value of 5.00 x10^{-5} M^{-1} s^{-1}. The first series of simulations undertaken was once again the simplest case where the thiyl radical is considered inert; the parameters used are listed in Table 6.14.

Table 6.14: Parameters for simulations concerning reversible photolysis of RAFT species where kp(xanthate fragment) = 0.

Simulation	$k_{photons\text{-}RAFT}$	$k_{-photons\text{-}RAFT}$	$f_{xan\text{-}termination}$	$K_{eq\ (photolysis)}$
3.0.1F (On)	7.50×10^{-3}	1.50×10^{9}	N/A	5.00×10^{-12}
3.0.2F (On)	7.50×10^{-4}	1.50×10^{8}	N/A	5.00×10^{-12}
3.0.3F (On)	7.50×10^{-6}	1.50×10^{6}	N/A	5.00×10^{-12}
3.0.1V (On)	9.00×10^{-4}	1.50×10^{9} to 2.05×10^{8}	1.00	5.988×10^{-13} to 4.405×10^{-12}
3.0.2V (On)	9.00×10^{-5}	1.50×10^{8} to 2.04×10^{7}	1.00×10^{-1}	5.988×10^{-13} to 4.405×10^{-12}
3.0.3V (On)	9.00×10^{-7}	1.50×10^{6} to 2.04×10^{5}	1.00×10^{-3}	5.988×10^{-13} to 4.405×10^{-12}

As can be seen in Figure 6.16 (A), all simulations faithfully recreated the kinetics until the 6 h mark, at which point a deviation to higher conversions was seen until the end of the reaction. This most likely occurs due to the model being unable to faithfully reconstruct the more complex phenomena that manifest at higher conversions for VAc as was observed experimentally.

When $k_{-photons\text{-}RAFT}$ takes on a fixed value the kinetics appear slightly more rapid initially, while using a varied value for $k_{-photons\text{-}RAFT}$ can more accurately match the kinetics in the first 2 h. This suggests that just as for the MA case, the value of $k_{-photons\text{-}RAFT}$ most likely decreases in a similar fashion to the average k_t within the system.

Predictably just as for the MA simulations, the higher fixed and varied values of $k_{-photons\text{-}RAFT}$ give dispersity values which are underestimated relative to the baseline result. This implies that these parameters used in conjunction with the RAFT mechanism cannot be realistic as they give an unrealistic level of control. Only sims 3.0.3F (On) and 3.0.3V (On) (Figure 6.16 (B), red and purple traces respectively) provide an adequate match to the evolution of dispersity which is equal to that obtained with the baseline result. In all cases the evolution of M_n does not deviate from the baseline result (Figure 6.16 (B)).

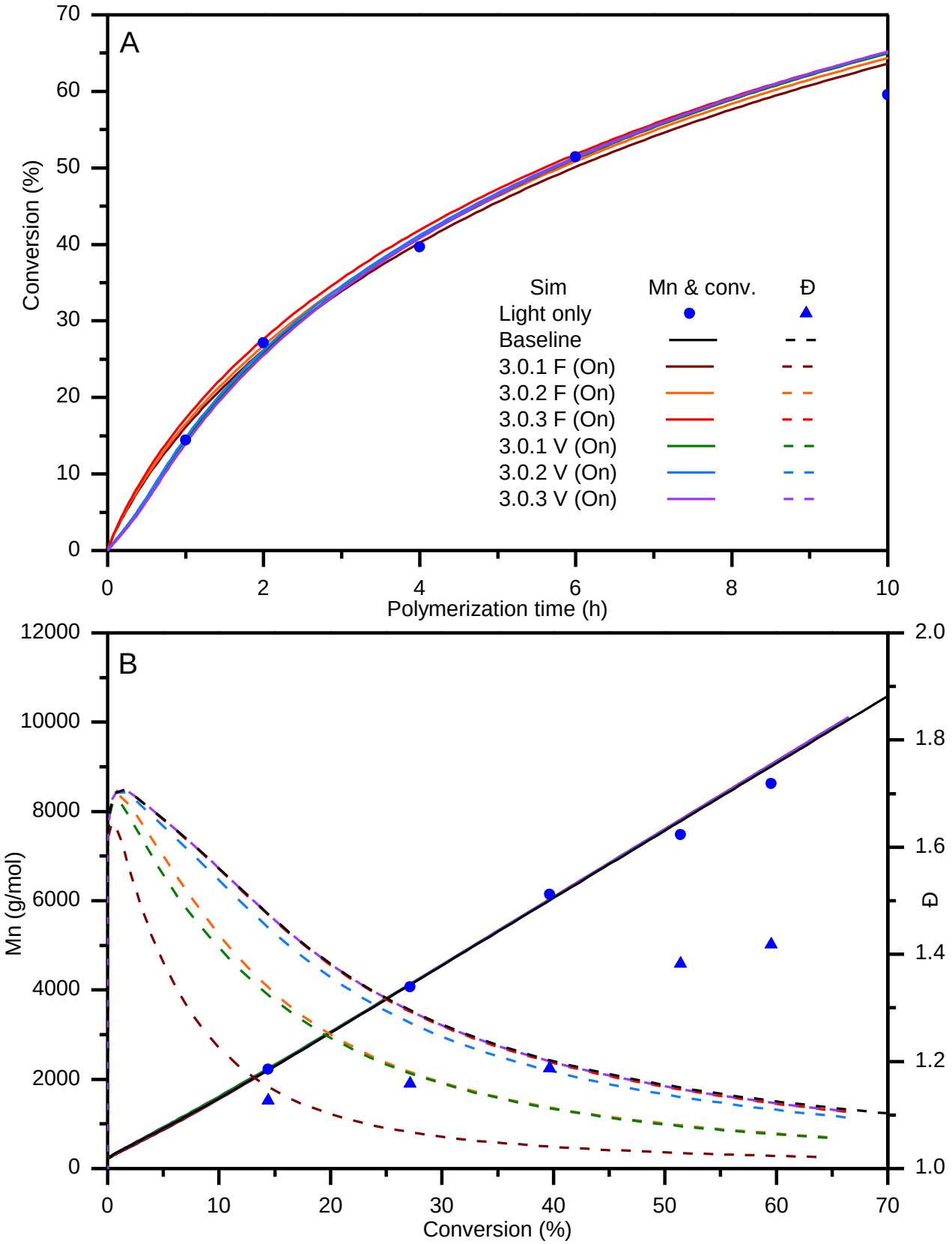

Figure 6.16: Comparison of conversion versus time (A) and evolution of molecular weight and dispersity as a function of conversion (B) for simulations concerning reversible photolysis of RAFT species where $kp_{xan\ frag}$ = 0 $M^{-1}\ s^{-1}$ to experimental data.

Regardless of the values set for the forward ($k_{photons\text{-}RAFT}$) and reverse ($k_{-photons\text{-}RAFT}$, both fixed and varied values) photolysis kinetic rate coefficients, setting the value of $k_{p(xan\ frag)}$ = 10 M^{-1} s^{-1} lead to kinetic profiles that were very linear as a function of time. The resulting kinetics could either match the very initial rate of polymerisation in the first 2 h but then significantly overestimate the conversion at later time points, or match the overall conversion attained at the 10 h mark but completely fail to match the overall kinetic profile. See Figure A16 in the Appendix. Based on these observations, simulations with $k_{p(xanthate\ fragment)}$ = 100 M^{-1} s^{-1} were not undertaken. Once again these results strongly imply that the thiyl radical derived from the photolysis of PXEP is unreactive towards the addition of monomer, regardless of whether it is highly reactive like MA or highly unreactive as for VAc.

6.7.1 Role of degenerative chain transfer in iniferter mechanism

The same approach was taken as used in the previous chapter to determine the role that the iniferter mechanism plays in controlling the evolution of both M_n and dispersity. The simulations from the previous section that gave the closest fit to the experimental data had the RAFT mechanism deactivated and the simulations re-run solely with the iniferter mechanism active. Furthermore, values for both $k_{photons\text{-}RAFT}$ and $k_{-photons\text{-}RAFT}$ which gave the closest fit to the experimental data with solely the iniferter mechanism active were also tested. For the case where $k_{-photons\text{-}RAFT}$ was fixed, the values tested are given in Table 6.15.

Table 6.15: Parameters for simulations comparing RAFT and iniferter mechanisms where kp(xan frag) = 0 M-1 s-1 and k -photons-RAFT are fixed values.

Simulation	$k_{photons\ RAFT}$	$k_{-photons\ RAFT}$	$K_{eq\ (photolysis)}$
3.0.1F (On)/(Off)	7.50 x10^{-36}	1.50 x10^{9}	5.00 x10^{-12}
3.0.3F (On)/(Off)	7.50 x10^{-6}	1.50 x10^{6}	5.00 x10^{-12}

Sim 3.0.1F (Off) (Figure 6.17 (B), purple trace) matches the experimentally obtained molecular weight, with only a slight spike seen initially. It simultaneously overestimates the dispersity at low conversions and underestimates it for most of the polymerisation. This scenario requires $k_{-photons\ RAFT}$ to be a higher value than k_t, implying that the thiyl radical is more reactive than the highly reactive VAc propagating radicals, which is completely unrealistic given literature precedent as explained previously in section 6.4.5. Sim 3.0.1F (On) (Figure 6.17, brown trace) once again shows that the RAFT mechanism provides greater control over the polymerisation and is indeed the dominant mechanism of control. This is further evidenced by sim 3.0.3F (Off) (Figure 6.17, blue trace) where without the RAFT mechanism the kinetics are faster due to the total lack of control over the molecular weight and dispersity which lowers the overall average value of k_t within the system.

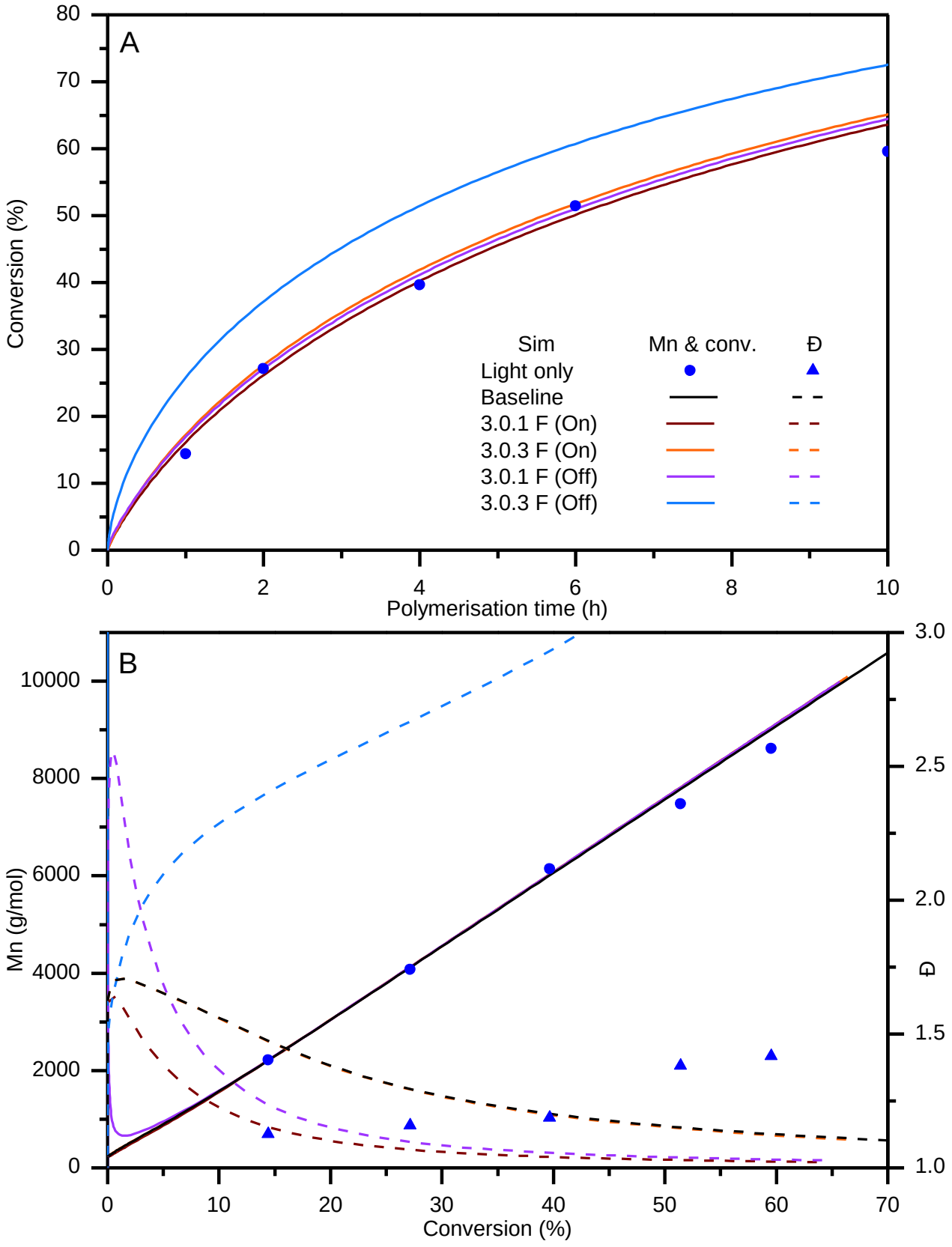

Figure 6.17: DT On/Off comparisons for the case when kp(xan) = 0, with k -photons-RAFT being fixed.

For the case where $k_{\text{-photons RAFT}}$ varies as a function of the value of k_t the parameters are listed in Table 6.16.

Table 6.16: Parameters for simulations comparing RAFT and iniferter mechanisms where kp(xan) = 0 M^{-1} s^{-1} and $k_{-photons-RAFT}$ are varied values.

Simulation	$k_{photons\ RAFT}$	$k_{-photons\ RAFT}$	$f_{xan-termination}$	$K_{eq\ (photolysis)}$
3.0.1V (On)	9.00×10^{-4}	1.50×10^{9} to 2.05×10^{8}	1.00	6.00×10^{-13} to 4.41×10^{-12}
3.0.1V (Off)	9.00×10^{-4}	1.50×10^{9} to 2.04×10^{8}	1.00	6.00×10^{-13} to 4.42×10^{-12}
3.0.3V (On)	9.00×10^{-7}	1.50×10^{6} to 2.04×10^{5}	01.00×10^{-3}	6.00×10^{-13} to 4.41×10^{-12}
3.0.3V (Off)	9.00×10^{-7}	1.50×10^{6} to 1.44×10^{5}	01.00×10^{-3}	5.981 E-13 to 6.25×10^{-12}

For the case where $k_{-photons\ RAFT}$ took on varied values, almost identical trends in the evolution of dispersity and molecular weights were seen for fixed values of $k_{-photons\ RAFT}$. Sim 3.0.1V (Off) represents the scenario with the highest realistic reactivity of the thiyl radical, namely where $k_{-photons\ RAFT}$ is directly equal to k_t. As seen in Figure 6.18 (B)(blue trace), in this case the iniferter mechanism fails to reproduce all aspects of the experimental data (conversion, M_n and dispersity) without the added control of the RAFT mechanism being active. This reinforces the conclusions derived for the MA case, namely that RAFT mechanism is the key to controlling the polymerisation with the iniferter mechanism simply providing an extra source of initiating radicals to increase the overall rate of polymerisation.

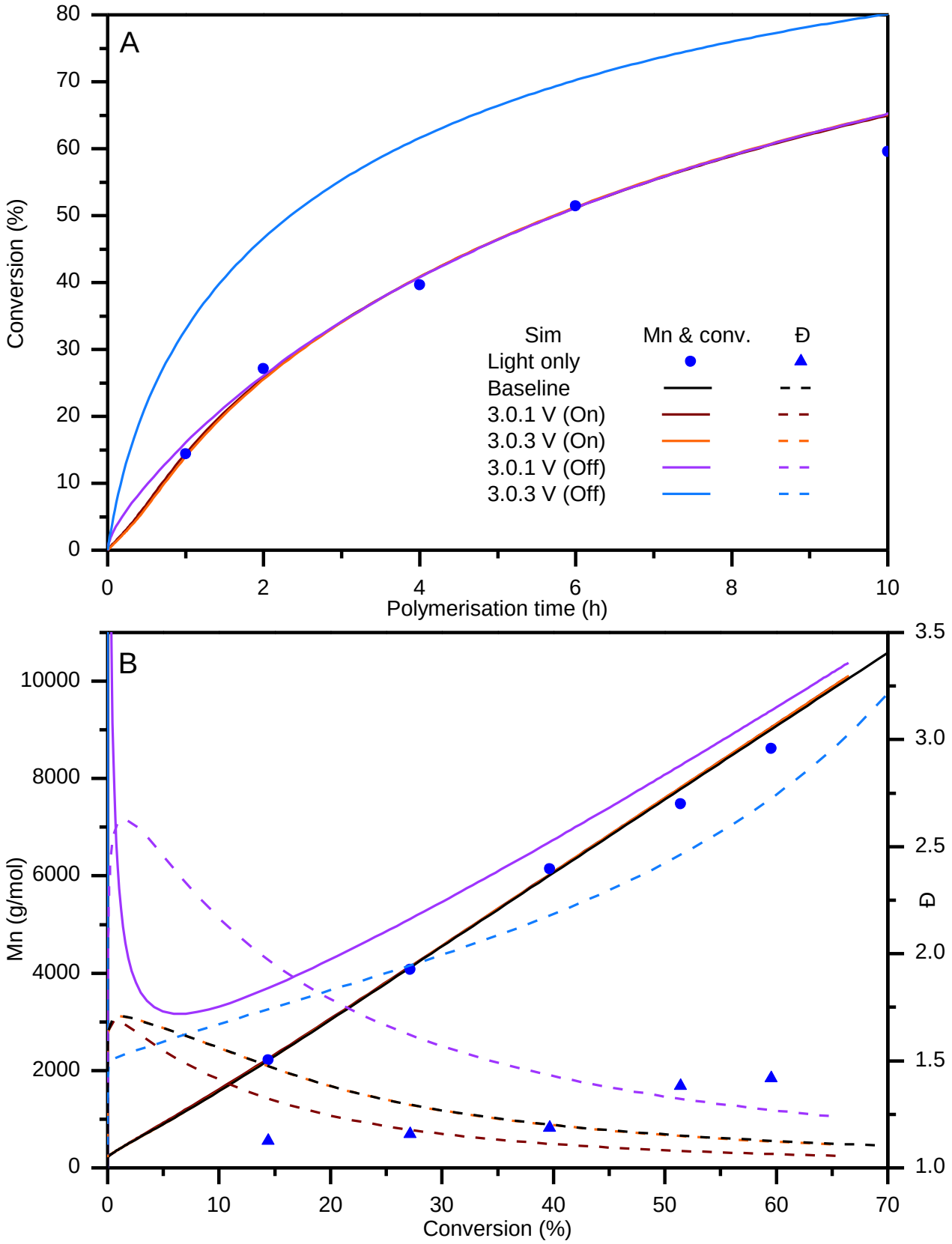

Figure 6.18: DT On/Off comparisons for the case when kp(xan) = 0, with k -photons-RAFT being varied.

The phenomena observed in Figure 6.17 and Figure 6.18 can be related to the values of k_{deact} that govern these simulations. Figure 6.19 shows clearly that simulations which the highest k_{deact} values

give the best control solely with the iniferter mechanism; this is consistent with what was found for the MA case. It is interesting that sim 3.0.3F (Off) (Figure 6.19, red trace) features k_{deact} values which exceed the plausible upper limit from literature; this is further evidence that in this case the $k_{-photons-RAFT}$ is an unrealistic value. Just as for the simulations of MA, the simulations that require the RAFT mechanism and give the best fits to the experimental data (sims 3.0.3V (On) and 3.0.3F (On)) have k_{deact} values which fall below the lower literature limit. This is consistent with the observations made previously that these simulations fail comprehensively to reproduce the experimental data when the RAFT mechanism is deactivated.

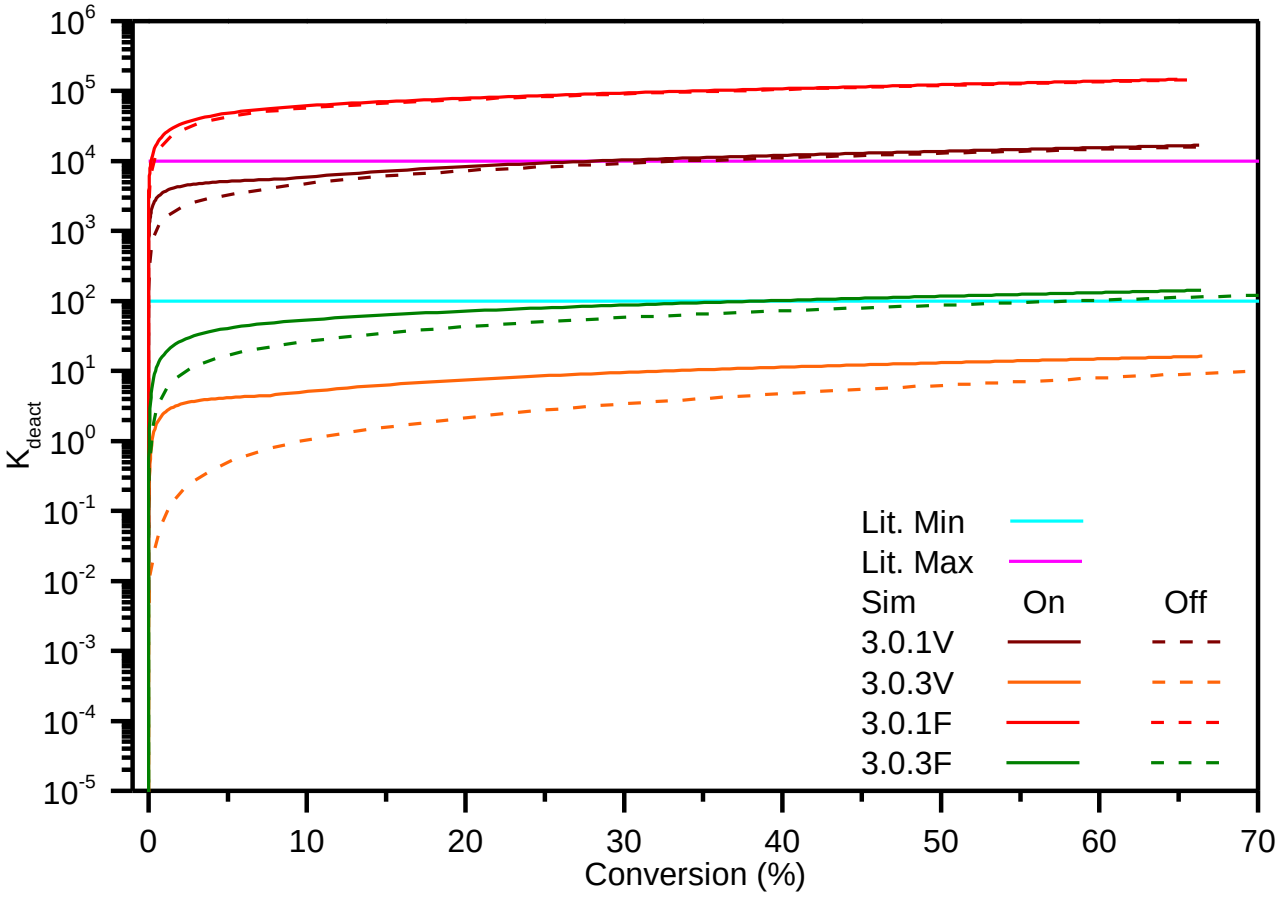

Figure 6.19: Values of k_{deact} for DT On/Off comparisons for the case when kp(xan) = 0, with k -photons-RAFT being fixed.

From the simulations undertaken in this section, sim 3.0.3V (On) was selected as the most realistic scenario to model the light only experimental data. The validity of this model could not be tested as rigorously as for the MA case due to PXEP being completely consumed by the 0.5 h time point under dark + AIBN conditions as evidenced by ^{1}H NMR (Figure 6.6, A). The baseline simulation recreates this quite well (Figure 6.20, A). Based on the continuinty seen in all aspects of the experimental data, a similar rate of consumption of PXEP under light only conditions can be assumed especially considering that it is entirely converted to the macro-RAFT species by the 1 h mark (Figure 6.6, B).

Sim 3.0.3V (On) results in around 10 % residual PXEP at the 0.5 h time point, with this discrepancy potentially arising from the extreme reactivity of the VAc radicals leading to greater consumption of PXEP in the time prior to analysis by ^{1}H NMR. There is slight evidence for this in Figure 6.6, where under both experimental conditions there are faint resonances from what is probably a single addtion of VAc to the starting RAFT agent seen in the ^{1}H NMR spectra for the 0 h time point samples.

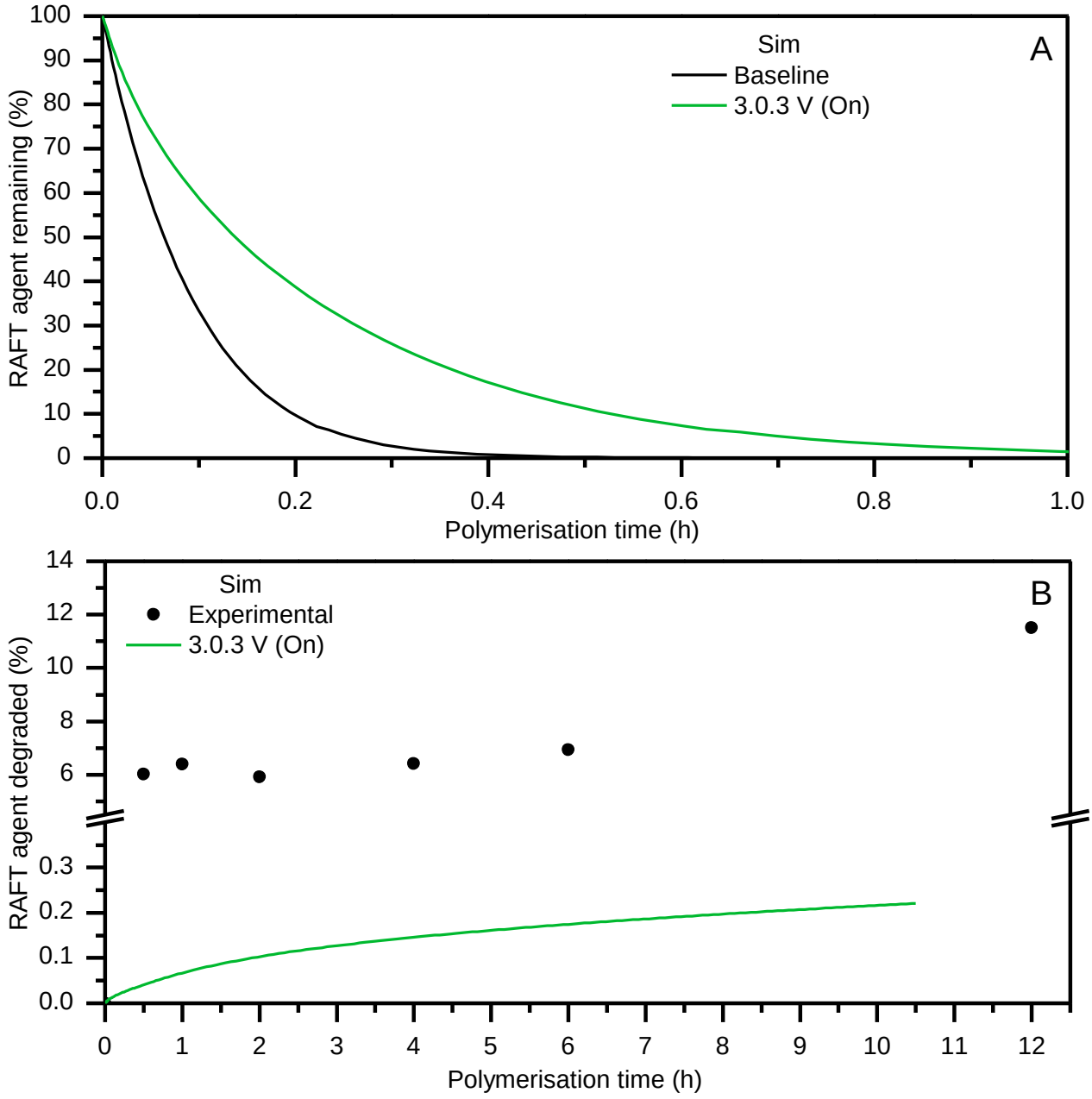

Figure 6.20: Overall kinetic comparisons for simulation 3.0.3V (On) with and without different initiation mechanisms active (A) and comparison of the relative rates of initiation due to those initiation mechanisms (B).

The greatest discrepancy between the simulated and experimental results can be seen in Figure 6.20 (B), where sim 3.0.3V (On) underestimates the percentage degradation of the RAFT agent by more than an order of magnitude at all time points. The most likely explanation for this behaviour is that

the photolytic stability of the starting PXEP and the poly(VAc) are significantly different due to the fundamental differences in the reactivity of the VAc and R group radicals.

6.7.2 Final comparisons

A simulation was undertaken which used kinetic rate coefficients that successfully recreated the light only experimental data with the added contribution of the upper limit for the photolysis of monomer. Parameters used in simulations for final comparisons are listed in Table 6.17.

Table 6.17: Kinetic rate coefficients used in final comparison of photolysis parameters.

Simulation	k_d	$k_{photons\text{-}monomer}$	$k_{photons\ RAFT}$
Baseline	1.6530×10^{-5}	N/A	N/A
4.0	1.6530×10^{-5}	7.00×10^{-12}	9.00×10^{-7}
4.1	3.3060×10^{-5}	5.00×10^{-13}	9.00×10^{-7}
3.0.3V (On)	N/A	5.00×10^{-13}	9.00×10^{-7}

Sim 4.0 reinforces the conclusions that both photolysis of monomer and the photolysis of the RAFT agent play only a minimal role on the kinetic behaviour seen as compared to the baseline simulation that only features initiation by breakdown of AIBN. This is evident by the near perfect overlap of the kinetic curves from sim 4.0 and the baseline simulation, shown in Figure 6.21 by the orange and black curves respectively.

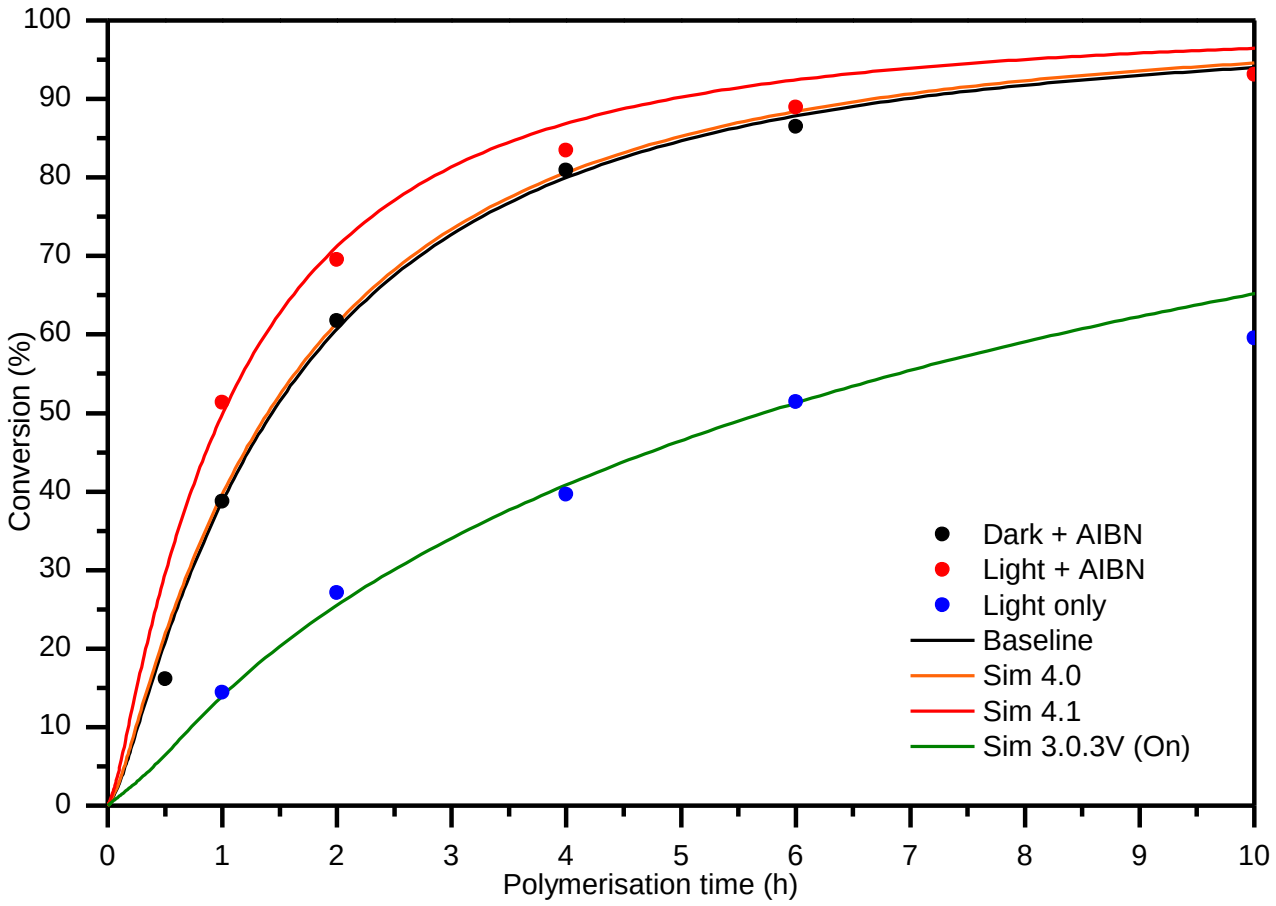

Figure 6.21:Overall kinetic comparisons for simulation 3.0.3V (On) with and without different initiation mechanisms active.

Further investigation of the contribution of the various initiation mechanisms (Figure 6.22) reveals that for all simulations except for sim 4.1 the contribution from RAFT photolysis is on the same order of magnitude as that from AIBN degradation. Howeverthe contribution from RAFT photolysis seems to exceed that of AIBN in the later stages of the polymerisation when conversion exceeds ~ 60 % in Sim 4.0 and ~ 75 % in Sim 4.1. This most likely occurs as even though AIBN is not depleted to less than 50 % of the starting concentration over the course of the polymerisation under the experimentally determined k_d (see Figure A14 in the Appendix), its initiation efficiency drops linearly to 0 as a function of conversion as per literature guidelines [19]. In both cases, the influence on kinetics at such a late stage in the polymerisation is almost non-existance due to the monomer being mostly consumed. For sim 4.1, initiation due to AIBN dominates up to a higher conversion of ~ 75 %. Once again, as for the MA case, the initiation due to photolysis of monomer is orders of magnitude lower, which supports the prior conclusion that regardless of the monomer this is not a significant kinetic contribution under the reaction conditions chosen.

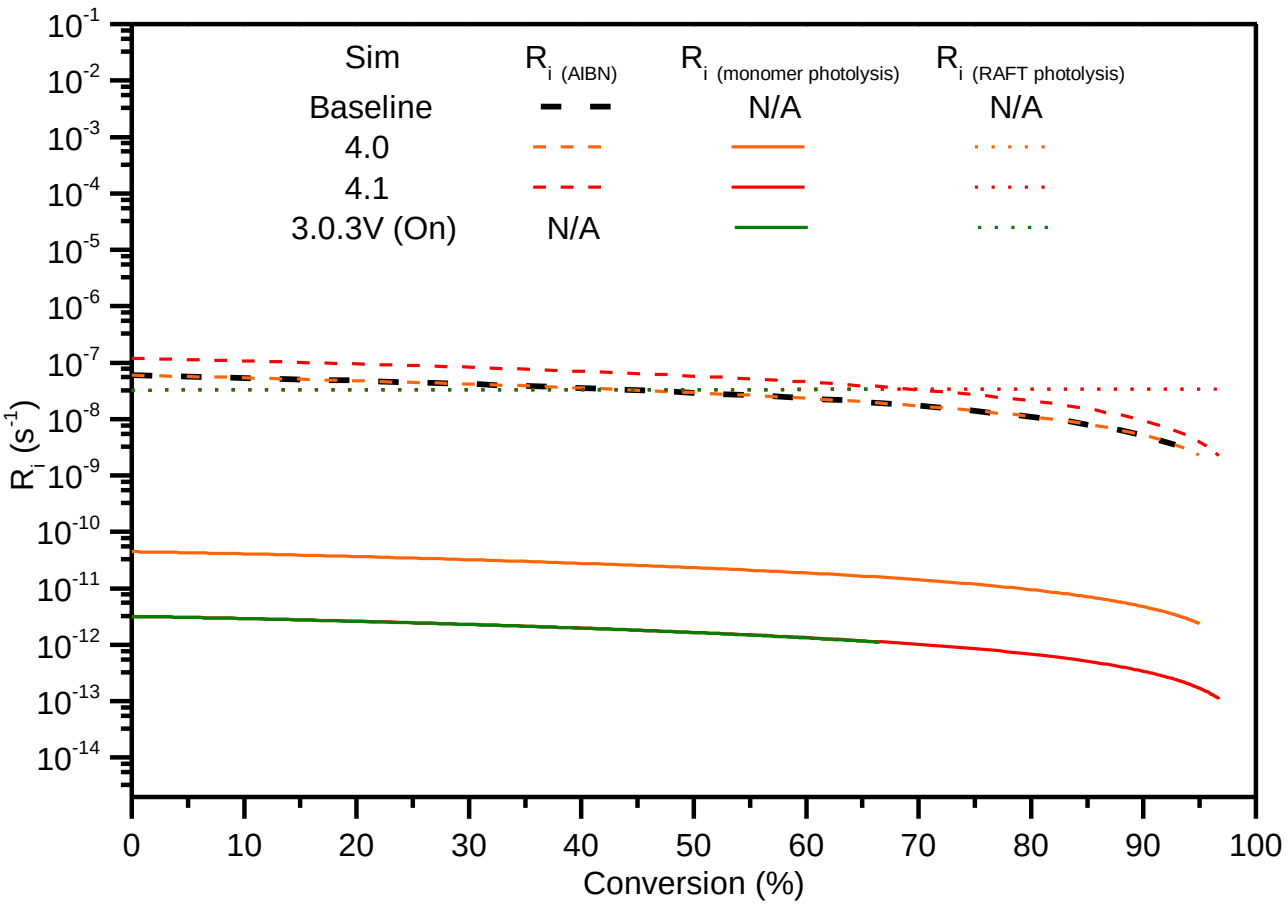

Figure 6.22: Comparison of the relative rates of initiation due to possible initiation mechanisms for simulations used as final comparisons.

6.8 VAc to MA comparisons & broader implications

The vast differences in the reaction conditions between the light only polymerisations for both MA and VAc are summarised in Table 6.18. Despite the higher concentrations of both monomer and RAFT agent which acts as a reversible photoinitiator, the VAc polymerisation under light only conditions is significantly slower. This is reflected in the value of $k_{photons\ RAFT}$ determined via modelling which describes the forward photolysis reaction in the DC mechanism; it is approximately 3 orders of magnitude lower for the VAc case. Potential explanations for this vastly different behaviour are explored further within this section. These values of $k_{dis.}$ nevertheless lie within the range reported in the literature for the photolysis of tetraethylthiuram disulfide; 2.2 $x10^{-6}$ s^{-1} to 1.45 $x10^{-5}$ s^{-1} depending on the solvent or monomer [22] along with 1.52 $x10^{-3}$ s^{-1} in the surface initiated polymerisation of MMA [23].

Table 6.18: Comparison of $k_{photons\ RAFT}$ parameters used to model the light only polymerisations for MA and VAc.

Monomer	[M] (M)	[RAFT] (M)	$k_{photons\ RAFT}$ (s^{-1})	k_{app} for light only (h^{-1})
MA	2.80	1.36×10^{-2}	1.00×10^{-4}	3.25
VAc	6.34	3.59×10^{-2}	9.00×10^{-7}	0.13

As has been derived previously in Chapter 2 section 2.1.2.4, the rate of polymerisation (R_p) including for RAFT systems where the DT mechanism is non-retarding is given by Equation 6.2.

$$R_p = k_p \cdot [M] \cdot [P^*]$$

Equation 6.2: Generalised expression for the rate of a free radical polymerisation.

As has been shown within this and the previous chapter, the experimental conditions employed led to unavoidable photolysis of monomer, however this gives an inconsequential contribution to the overall rate of polymerisation. Thus, for the analysis that follows the rate of initiation solely due to the reversible photolysis of the RAFT containing species will be considered.

In the first scenario, we will assume that the RAFT agent works like a conventional photoinitiator. For a photoinitiated polymerisation the rate of initiation is characterised by the light intensity absorbed (I_{Abs}), however when the combined term for the extinction coefficient (α), the path length (l) and initiator concentration ($[I_2]$) are small, the intensity of the incident radiation (I_0) becomes important and the rate of initiation can be simplified [24] as shown in Equation 6.3:

$$R_i = 2 \cdot \phi \cdot I_{Abs}$$
$$\therefore R_i \approx 2 \cdot \phi \cdot I_0 \cdot l \cdot \alpha \cdot [I_2]$$

Equation 6.3: Approximation for rate of initiation due to decomposition of photoinitiator.

The following assumptions are made:

- Conversion of the initial RAFT agent to a macro-RAFT species does not change the species extinction coefficient (α) or its quantum yield of photolysis (ϕ).
- The concentration of photoactive RAFT species does not change significantly over the duration of the reaction, i.e. that the degradation is limited to under 10 % of the starting RAFT agent concentration.
- The pathlength (l) and light intensity (I_0) remain constant.

Combining the terms that are assumed to be constant into a single term (A) and if steady state conditions are assumed, i.e. the rate of initiation and the rate of termination are equivalent, this gives Equation 6.4:

$$R_i = R_t$$
$$\therefore 2 \cdot \phi \cdot I_0 \cdot l \cdot \alpha \cdot [I_2] = 2 \cdot k_t \cdot [P_n^*]^2$$
$$\therefore A \cdot [I_2] = k_t \cdot [P_n^*]^2$$
$$\therefore [P_n^*] = \left(\frac{A \cdot [I_2]}{k_t}\right)^{1/2}$$

Equation 6.4: Concentration of propagating radicals as a function of fundamental parameters and photoinitiator concentration.

Combining Equation 6.4 with the expression for the rate of polymerisation (R_p) as shown previously yields Equation 6.5, where $[I_2]$ is equivalent to the RAFT agent concentration $[P-X]$.

$$R_p = \frac{k_p}{k_t^{1/2}} \cdot A^{1/2} \cdot [I_2]^{1/2} \cdot [M]$$

Equation 6.5: Equation for the rate of polymerisation of a photoinitiated FRP system.

Understanding the vast differences between the results obtained under light only experimental conditions for MA and VAc requires a consideration of the vastly different reactivities of the two monomers. This is directly reflected in Equation 6.5, where for a fixed initial concentration of monomer and RAFT agent the rate of polymerisation is expected to be directly related to the ratio $\frac{k_p}{k_t^{1/2}}$. A comparison of this ratio for several common vinyl monomers was undertaken, with the analysis limited to a chain length of 500 which corresponds to the approximate limit at which the gel effect becomes significant [25] with the kinetic rate coefficients used listed in Table 6.19.

Table 6.19: Summary of kinetic rate coefficients for commonly used monomers.

Monomer	α_s	α_l	i_{cross}	$k_t^{1,1}$ (M^{-1} s^{-1})	Ref. for $k_t^{1,1}$	k_p (70 °C) (M^{-1} s^{-1})	Ref. for k_p
MA	0.79	0.21	30	1.78 x10^9	Fitted in Predici	15672	[26]
VAc	0.57	0.16	20	1.50 x10^9	Fitted in Predici	10595	[3]
MMA	0.65	0.15	100	1.20 x10^9	[27]	1055	[28]
Sty	0.51	0.16	30	8.90 x10^8	[29]	480	[30]

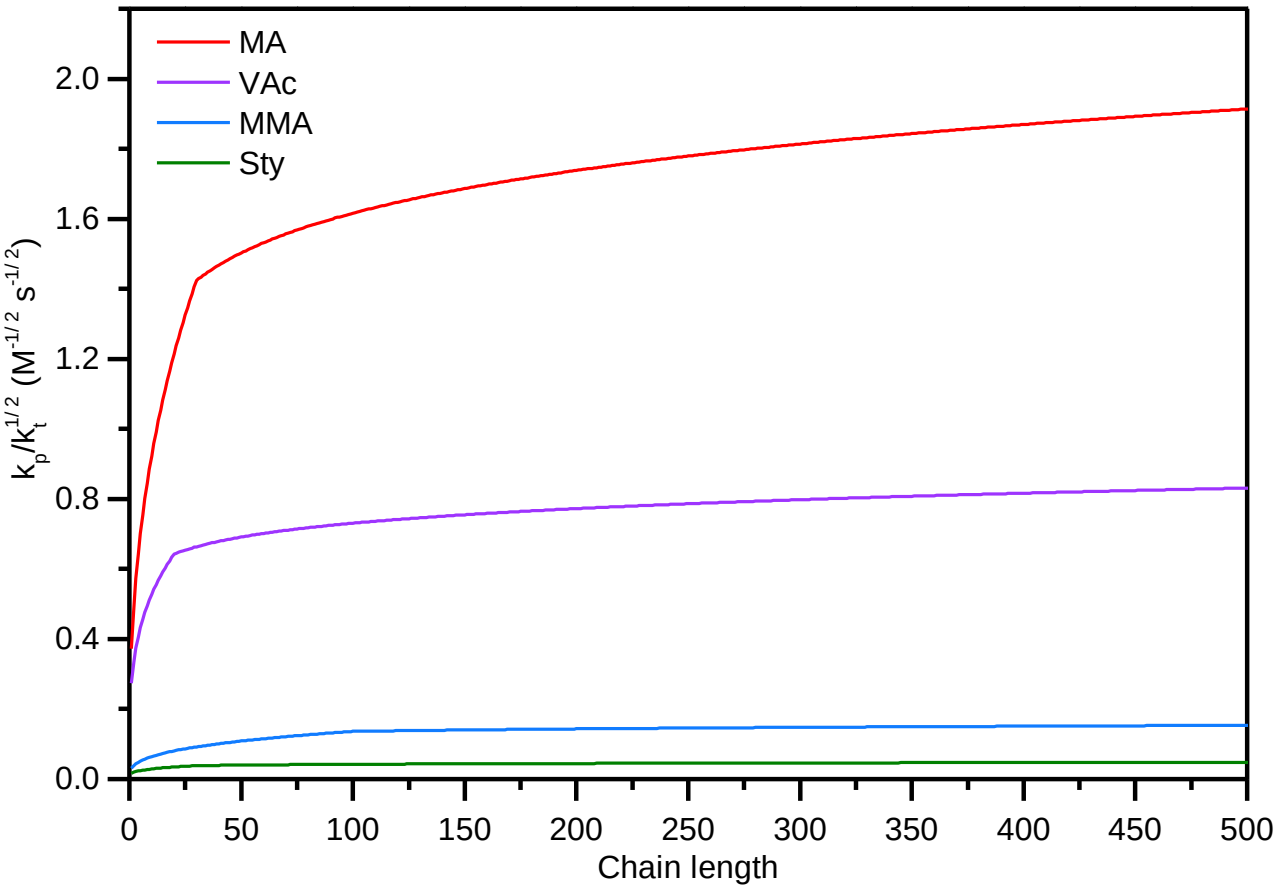

Figure 6.23: Comparison of k_p / $k_t^{1/2}$ values utilised in simulations of MA and VAc, with literature derived values used for Sty and MMA. Parameters used are given in Table 6.19.

Table 6.20: Comparison of polymerisation rate (R_p) as a function of monomer for a fixed concentration and identity of RAFT agent.

Entry	RAFT agent	Fastest → → → Slowest	Ref.
1	N/A	MA > VAc > MMA > Sty	Predicted, this work
2	BX	MA > MMA >> AN ~ VAc > St	[31]
3	BDC	MA > MMA ~ AN > Sty > VAc >> MAN	[32]

Based on the curves shown in Figure 6.23 and the assumptions outlined above, one would expect the polymerisation rate to follow the trend as per entry 1 in Table 6.20. Contrary to this, both Niwa *et al.* with bis(isopropylxanthatogen) disulfide [31] (entry 2, Table 6.20) and Otsu *et al.* with benzyl N,N-diethyldithiocarbamate [32] (entry 3, Table 6.20) showed varying rates of polymerisation as a function of monomer, where the concentration of RAFT agent was kept constant within each series of experiments. Niwa *et al.* also reported that the quantum yield for BX was greater in the presence of styrene than for MMA under all circumstances [31]. These results could potentially be complicated

by the fact that BX does not actually have an R group as such due to it being a symmetrical bis thiocarbonylthio disulfide. Indeed, both studies were undertaken prior to the current elucidation of the RAFT mechanism, with Niwa *et al.* proposing a mechanism of chain transfer to BX that only releases an inert radical in the process.

Both McKenzie *et al.* [33] and Ham *et al.* [16] showed that the photolytic stability of TCT compounds mirrored the radical stability of the R group as per the RAFT mechanism, for trithiocarbonates and xanthates respectively. Both results imply that monomers such as MMA which give stable radicals should facilitate efficient photolysis from a macro-RAFT agent. Xu *et al.* however found that fragmentation effciciency of trithiocarbonates with MMA was influenced by differing R groups effected the overall polymerisation in terms of both control and dispersity [34]. Considered holistically, these results show that the photopolymerisation behaviour of vinyl monomers seen with TCT compounds is more complicated and must result from a combination of multiple factors. Furthermore, it most likely supports the notion that the "A" constant in this analysis is not strictly constant and changes with the monomer used. This is further supported by the second scenario considered.

In the second scenario considered, we assume that the polymerisation follows the classical description of kinetics as outlined for a power law system by Fukuda *et al.* [35]; this assumes that no conventional initiation occurs besides that which arises from the reversible activation within a DC system. In this case the concentration of propagating radicals is given by Equation 6.6, where $[I]_0$ is the initial concentration of the RAFT agent and K is the equilibrium constant for interchange between active and inactive species, defined as $K_{eq} = \frac{k_{dis.}}{k_{comb.}}$ for a DC mechanism.

$$[P_n^*] = K_{eq} \cdot [I]_0 \cdot \left(3 \cdot k_t \cdot K_{eq}^2 \cdot [I]^2 \cdot t + [X^*]_0^3\right)^{-1/3}$$

Equation 6.6: Expression for the concentration of propagating radicals in the power law regime for a DC polymerisation system [35].

Since there are no thiyl radicals present initially $[X^*]_0 = 0$, Equation 6.6 combined with Equation 6.2 yields Equation 6.7.

$$R_p = \left(\frac{K_{eq} \cdot [I]_0}{3 \cdot k_t \cdot t}\right)^{\frac{1}{3}} \cdot [M] \cdot k_p$$

$$\therefore R_p = A \cdot \left(\frac{K_{eq}}{k_t}\right)^{\frac{1}{3}} \cdot [M] \cdot k_p \quad where\ A = \left(\frac{[I]_0}{3 \cdot t}\right)^{\frac{1}{3}}$$

Equation 6.7: Rate of polymerisation for a DT system under power law conditions with conventional initiation absent and initial concentration of stable radicals being zero.

Equation 6.7 shows that the equilibrium constant for the DC mechanism unsurprisingly plays a role in the kinetics. This is to be expected as values of $k_{dis.}$ and $k_{comb.}$ which comprise K_{eq} directly determine both the rate of interchange between active and inactive radical species and their average lifetime in the reaction. As has been discussed and shown within this and the previous chapter, the value of $k_{comb.}$ is at least 2 orders of magnitude lower than the termination rate coefficient k_t, which in turn changes as a function of chain length and the monomer used. The value for the dissociation rate coefficient $k_{dis.}$ is fundamentally expected to be governed by the same factors that determine the efficiency of a conventional photoinitiator. This amounts to the combined term $\phi \cdot I_0 \cdot l \cdot \alpha \cdot [I_2]$ as defined previously in Equation 6.4.

Considering the RAFT mechanism, the equilibrium constant was set to 100 for both monomers modelled, which is much too low to have any direct kinetic effects in regard to rate retardation. It has however been shown that the magnitude of the individual rate constants that make up the equilibrium constant are more important than the value of K itself [36]. For both MA and VAc it was concluded that the RAFT mechanism and not the DC mechanism gives control over the evolution of both M_n and dispersity. This means that the parameters governing the RAFT mechanism could potentially play a subtler role in explaining the vast difference between the light only polymerisation rates between the two monomers.

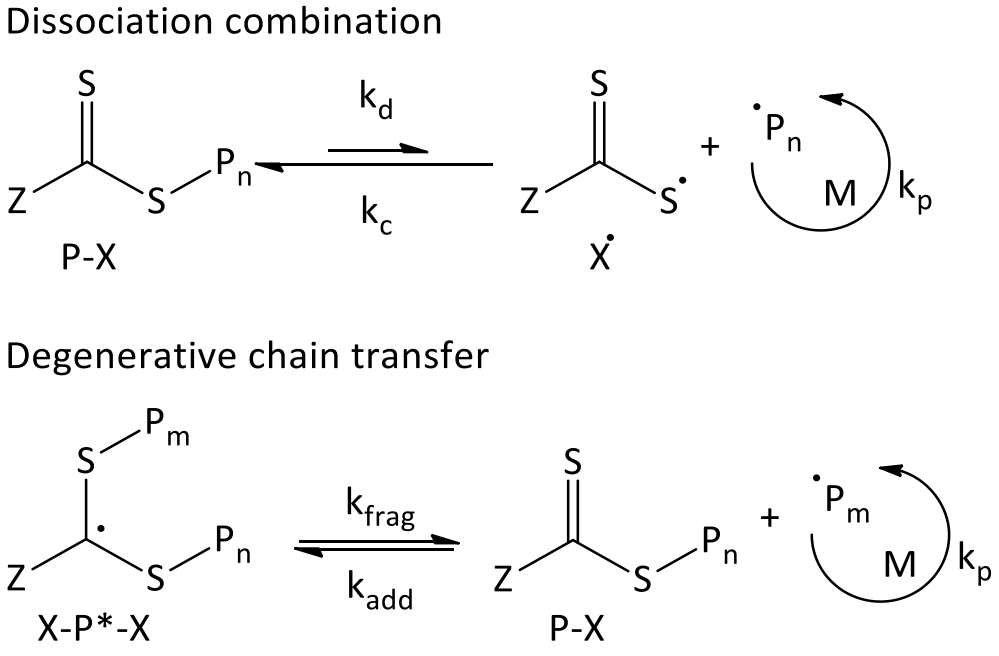

Scheme 6.3: Comparison of DC and DT polymerisation mechanisms with TCT compounds.

Based on Scheme 6.3 it is proposed that the selection of monomer and RAFT agent can have a kinetic influence when photolysis of the RAFT species is the key pathway for initiation via a reversible DC

mechanism. If the combination of monomer and RAFT agent results in an inefficient RAFT polymerisation, then this system is characterised by low k_{add} and high k_{frag} values which directly results in the RAFT equilibrium disfavouring the formation of the RAFT adduct radical. Conversely for a well-controlled RAFT polymerisation with higher overall values of k_{add} and lower values of k_{frag}, the overall ratio of RAFT adduct radicals relative to propagating macroradicals is expected to be much higher. A higher percentage of radicals being trapped as RAFT adduct radicals within a polymerisation should directly limit the amount of reversible photolysis to occur. This is a direct result of the fact that no literature precedent exists for the possibility of the RAFT adduct radicals (X-P*-X) to undergo photolysis. This hypothesis was tested by calculating the percentage of RAFT adduct radicals relative to macro-radicals for several simulations; the inert thiyl radicals (X*) were neglected in this calculation as these do not contain a growing macroradical capable of propagating after release.

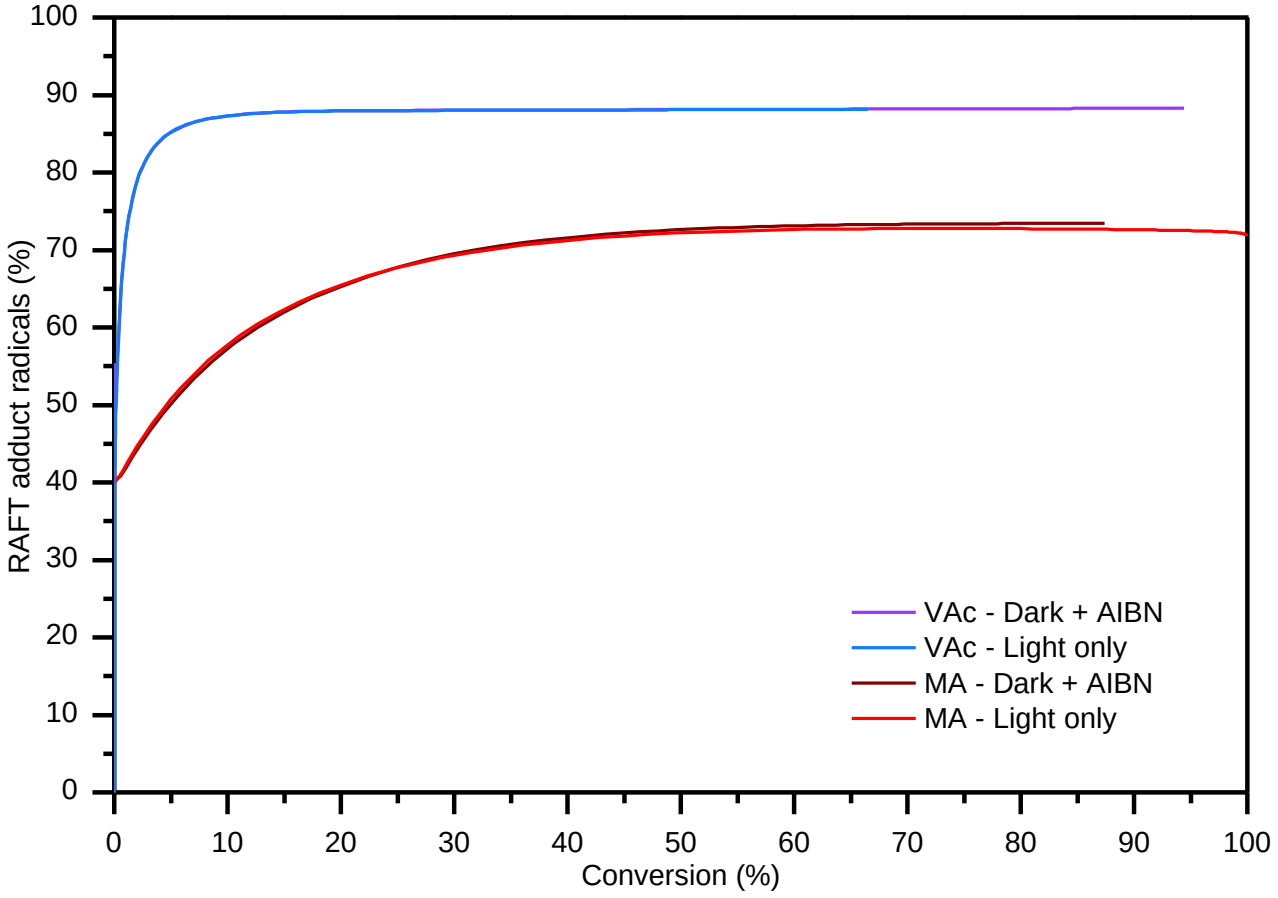

Figure 6.24: Comparison of ratios of RAFT radicals for simulated VAc and MA polymerisations initiated conventionally with AIBN and solely via photolysis of RAFT species (DC mechanism).

Figure 6.24 shows the percentage of radicals trapped as RAFT adduct radicals for the baseline simulations as well as for sims 3.0.3V (On) for both MA and VAc as these simulations best recreated the light only experimental data. The resulting traces appear to support the hypothesis put forth; in

both MA simulations the percentage of RAFT adduct radicals is significantly lower than for both VAc cases, with the percentage growing steadily as the RAFT agent is consumed.

Based on these findings and the conflicting literature precedents it is difficult to give absolute predictions as to how an individual monomer will behave in a photoinitiated RAFT polymerisation, however it can be expected that there will be several counteracting effects based on the activity of the RAFT agent and the reactivity of the propagating radicals. This is reaffirmed by the complex equation for the rate of polymerisation given by several literature sources [31, 37], shown in Equation 6.8. As stated previously, this was based on a kinetic scheme that did not include the full RAFT mechanism with reversible degenerative chain transfer. In Equation 6.8, $[P-X]$ is the RAFT agent/iniferter concentration, m is the number of active radicals released upon RAFT photolysis, σ is a constant, K_t is the average rate of termination, with all other parameters including $k_{dis.}, k_p, k_{R-re}$ are as defined previously for the RAFT mechanism.

$$R_p = \frac{[P-X]^{\frac{1}{2}} \cdot [M]}{\lambda} + \frac{[M]^2}{\mu}$$

$$Where: \quad \lambda = \frac{\left(\frac{K_t}{m \cdot k_{dis.}}\right)^{1/2}}{k_p} \quad and \quad \mu = \frac{\sigma \cdot K_t}{k_{R-re} \cdot k_p}$$

Equation 6.8: Rate of polymerisation for a photoiniferter polymerisation with chain transfer [31, 37].

In general, two main predictions can be made, with the concentration of RAFT agent, the light intensity and absorption at the photolysis wavelength are assumed to be constant for both cases.

Firstly, assuming the quantum yield for photolysis of TCT species remains the same regardless of the class of RAFT agent used, for any given monomer the possibility of photolytic rate enhancement should directly follow the RAFT agent reactivity. This should occur as a direct result of a greater percentage of radicals being trapped as the RAFT adduct radical for an overall greater time.

Secondly, for any given RAFT agent, the possibility of photolytic enhancement should decrease with the reactivity of the propagating radical being polymerised. This is a direct result of more reactive radicals both reacting faster to form the RAFT adduct radical and not favouring subsequent fragmenting. This means the ability of a monomer to undergo photolysis should increase from LAMs to MAMs as classified for RAFT. There is also the possibility that the conversion of an initial RAFT agent into a macro-RAFT species will alter its quantum yield or absorption wavelength which may influence the extent to which photolysis can occur. Furthermore, the overall rate of polymerisation will still be influenced by the overall $k_p/k_t^{1/2}$ ratio for a given type of monomer.

These predictions strongly imply that even for the case where photolytic initiation of monomer is entirely absent and reversible photolysis of RAFT species is solely the means of initiation, the fundamental limitations of the RAFT mechanism cannot be entirely avoided. It may however be possible, with clever reaction design, to potentially minimise these limitations. This idea as it relates to block copolymer synthesis is explored further in Chapter 8.

6.9 Conclusions

Experimental investigations provided the following conclusions:

- Polymerising VAc under conditions that were optimised for RAFT polymerisation using PXEP as a chain transfer agent and AIBN as a thermal initiator gave good control over molecular weight, with dispersity increasing beyond ~ 50 % conversion. This was attributed to the inherently problematic nature of polymerising VAc.
- Conducting the same polymerisation with exposure to a 6W UV lamp (370nm, 2 mW/cm^2) caused only a marginal increase in polymerisation of around 14 %. Without the presence of AIBN, under UV irradiation the polymerisation rate was significantly slower at around 30 % of the original rate attained in the dark.
- Just as for MA, the trends in experimental data including the evolution of M_n, dispersity and calculated chain transfer coefficient showed remarkably consistent trends regardless of the polymerisation conditions used. This once again strongly implied that the same reaction mechanism was active in all cases, regardless of whether or not UV irradiation was used.
- Chain extension experiments conducted under identical conditions with a poly(VAc) macroinitiator derived from PXEP gave different rates of polymerisation under all conditions. Notwithstanding, the same overall trend in increasing polymerisation rate was seen as follows: light only << AIBN + dark < light + AIBN.

Modelling the experimental data in Predici provided the following conclusions:

- Monomer photolysis cannot be solely responsible for the faster kinetics seen in the light + AIBN case. This was concluded as when the kinetic rate coefficients used in this simulation were used with AIBN initiation disabled, the resulting kinetics only marginally slower than with AIBN initiation active, and more importantly, were significantly faster than the light only kinetics.
- The experimentally determined upper limit of k_d for AIBN degradation under UV irradiation conditions resulted in faster simulated kinetics than the light + AIBN experimental data. A

lower value of k_d corresponding to an enhancement factor of 2 was found to adequately simulate the light + AIBN conditions, indicating that this is the key photolysis pathway responsible for the experimentally seen light + AIBN kinetics.

- Reversible photolysis of the RAFT agent via the iniferter mechanism was found to be the most plausible explanation for simulating the light only kinetics. The optimised kinetic rate coefficients for this process support the same findings as for the MA case previously articulated in Chapter 5, section 5.8. In brief the results support the following:
    - The thiyl radical is inert towards monomer addition.
    - The kinetic rate coefficient for the reversible termination between active radicals in the DC mechanism is varied in nature and is approximately 2 and 3 orders of magnitude smaller than the average termination rate coefficient for carbon centred radicals.
    - Degenerative chain transfer is responsible for molecular weight control under these reaction conditions.
    - The DC mechanism simply serves as another source of initiating radicals in the form of R and macro-radicals generated from the photolysis of RAFT and macro-RAFT species.
- Despite the much concentrations of both RAFT agent and monomer, the much slower polymerisation rate under light only conditions for VAc were attributed to several factors:
    - Inherent differences between the reactivity of the propagating radicals which manifests as different $k_p/k_t^{1/2}$ values which directly influence the polymerisation rate.
    - The reactivity of the RAFT agent towards radical addition and the reactivity of the propagating radicals manifested as greater percentage of the radicals within the system being trapped as RAFT adduct radicals. This in turn can potentially limit the overall rate of photolysis as this species is unable to undergo photolysis. Simulated concentrations of radical species from MA and VAc under both baseline and light only simulations seemed to support this assertion.
    - Based on the above observation it was predicted that the more active the RAFT agent towards radical addition and the more active the propagating radicals, the less photolysis should occur, all other factors being kept constant.

Overall, for both MA and VAc these results are essentially counter supportive of the conclusion made by Vana & Goto, namely that the DT mechanism only becomes significant when the parameters governing the DC mechanism are such that it is unable to control the molecular weight and dispersity

[38]. Thus, it appears that the combination of the properties of PXEP and the conditions tested allows the DT mechanism to dominate in favour of the DC mechanism.

These results strongly imply that a photochromic RAFT agent which can undergo reversible photolysis concurrently with a photochromic transformation on the Z group should not preclude its ability to manifest different polymerisation behaviour under a UV stimulus.

6.10 References

1. Harrisson, S., et al., *RAFT Polymerization of Vinyl Esters: Synthesis and Applications.* Polymers, 2014. **6**(5): p. 1437.
2. Junkers, T., D. Voll, and C. Barner-Kowollik, *Determination of vinyl acetate propagation rate coefficients via high frequency pulsed laser polymerization.* e-Polymers, 2009. **9**(1).
3. Barner-Kowollik, C., et al., *Critically Evaluated Rate Coefficients in Radical Polymerization – 8. Propagation Rate Coefficients for Vinyl Acetate in Bulk.* Macromolecular Chemistry and Physics, 2017. **218**(1): p. n/a-n/a.
4. Kattner, H. and M. Buback, *Chain-Length-Dependent Termination of Vinyl Acetate and Vinyl Pivalate Bulk Homopolymerizations Studied by SP-PLP-EPR.* Macromolecular Chemistry and Physics, 2014. **215**(12): p. 1180-1191.
5. Monyatsi, O., A.N. Nikitin, and R.A. Hutchinson, *Effect of Head-To-Head Addition on Vinyl Acetate Propagation Kinetics in Radical Polymerization.* Macromolecules, 2014. **47**(23): p. 8145-8153.
6. Morin, A.N., et al., *Effect of Head-to-Head Addition in Vinyl Acetate Controlled Radical Polymerization: Why Is Co(acac)2-Mediated Polymerization so Much Better?* Macromolecules, 2013. **46**(11): p. 4303-4312.
7. Kwak, Y., et al., *A Systematic Study on Activation Processes in Organotellurium-Mediated Living Radical Polymerizations of Styrene, Methyl Methacrylate, Methyl Acrylate, and Vinyl Acetate.* Macromolecules, 2006. **39**(14): p. 4671-4679.
8. Dufils, P.E., et al., *Phosphonate-terminated poly(vinyl acetate) synthesized by RAFT/MADIX polymerization.* Journal of Polymer Science Part A: Polymer Chemistry, 2012. **50**(10): p. 1997-2007.
9. Stenzel, M.H., et al., *Xanthate Mediated Living Polymerization of Vinyl Acetate: A Systematic Variation in MADIX/RAFT Agent Structure.* Macromolecular Chemistry and Physics, 2003. **204**(9): p. 1160-1168.
10. Li, J., et al., *Visible Light-Induced Living Radical Polymerization of Butyl Acrylate: Photocatalyst-Free, Ultrafast, and Oxygen Tolerance.* Macromolecular Rapid Communications, 2017. **38**(13): p. n/a-n/a.
11. Chen, M., et al., *Logic-Controlled Radical Polymerization with Heat and Light: Multiple-Stimuli Switching of Polymer Chain Growth via a Recyclable, Thermally Responsive Gel Photoredox Catalyst.* Journal of the American Chemical Society, 2017. **139**(6): p. 2257-2266.
12. Wang, J., et al., *Natural RAFT Polymerization: Recyclable-Catalyst-Aided, Opened-to-Air, and Sunlight-Photolyzed RAFT Polymerizations.* ACS Macro Letters, 2016. **5**(11): p. 1278-1282.

13. Keddie, D.J., et al., *Chain Transfer Kinetics of Acid/Base Switchable N-Aryl-N-Pyridyl Dithiocarbamate RAFT Agents in Methyl Acrylate, N-Vinylcarbazole and Vinyl Acetate Polymerization.* Macromolecules, 2012. **45**(10): p. 4205-4215.

14. Ding, C., et al., *Photocatalyst-Free and Blue Light-Induced RAFT Polymerization of Vinyl Acetate at Ambient Temperature.* Macromolecular Rapid Communications, 2015. **36**(24): p. 2181-2185.

15. Wang, H., et al., *Real-Time and in Situ Investigation of "Living"/Controlled Photopolymerization in the Presence of a Trithiocarbonate.* Macromolecules, 2013. **46**(7): p. 2576-2582.

16. Ham, M.K., et al., *Photoinitiated RAFT polymerization of vinyl acetate.* Journal of Polymer Science Part A: Polymer Chemistry, 2012. **50**(12): p. 2389-2397.

17. Shim, S.H., et al., *Simultaneous control over the molecular weight and tacticity of poly(vinyl acetate) using a low-temperature photoinitiated RAFT process in fluoroalcohols.* Polymer Chemistry, 2013. **4**(21): p. 5449-5455.

18. Fischer, H. and L. Radom, *Factors Controlling the Addition of Carbon-Centered Radicals to Alkenes—An Experimental and Theoretical Perspective.* Angewandte Chemie International Edition, 2001. **40**(8): p. 1340-1371.

19. Theis, A., et al., *Probing the reaction kinetics of vinyl acetate free radical polymerization via living free radical polymerization (MADIX).* Polymer, 2006. **47**(4): p. 999-1010.

20. Brar, A.S. and S. Charan, *Sequence determination of vinyl acetate–methyl acrylate copolymers by NMR spectroscopy.* Journal of Applied Polymer Science, 1994. **53**(13): p. 1813-1822.

21. Hutchinson, R.A., J.R. Richards, and M.T. Aronson, *Determination of Propagation Rate Coefficients by Pulsed-Laser Polymerization for Systems with Rapid Chain Growth: Vinyl Acetate.* Macromolecules, 1994. **27**(16): p. 4530-4537.

22. Van Kerckhoven, C., et al., *Dithiocarbamate telechelic polymers: Synthesis and block copolymerization.* Die Makromolekulare Chemie, 1991. **192**(1): p. 101-114.

23. Rahane, S.B., S.M. Kilbey, and A.T. Metters, *Kinetic Modeling of Surface-Initiated Photoiniferter-Mediated Photopolymerization in Presence of Tetraethylthiuram Disulfide.* Macromolecules, 2008. **41**(24): p. 9612-9618.

24. Moad, G. and D.H. Solomon, *3 - Initiation,* in *The Chemistry of Radical Polymerization (Second Edition).* 2005, Elsevier Science Ltd: Amsterdam. p. 49-166.

25. Johnston-Hall, G. and M.J. Monteiro, *Bimolecular radical termination: New perspectives and insights.* Journal of Polymer Science Part A: Polymer Chemistry, 2008. **46**(10): p. 3155-3173.

26. Barner-Kowollik, C., et al., *Critically evaluated rate coefficients in radical polymerization - 7. Secondary-radical propagation rate coefficients for methyl acrylate in the bulk.* Polymer Chemistry, 2014. **5**(1): p. 204-212.

27. Johnston-Hall, G., et al., *Accessing Chain Length Dependent Termination Rate Coefficients of Methyl Methacrylate (MMA) via the Reversible Addition Fragmentation Chain Transfer (RAFT) Process.* Macromolecular Chemistry and Physics, 2005. **206**(20): p. 2047-2053.

28. Beuermann, S., et al., *Critically evaluated rate coefficients for free-radical polymerization, 2.. Propagation rate coefficients for methyl methacrylate.* Macromolecular Chemistry and Physics, 1997. **198**(5): p. 1545-1560.

29. Kattner, H. and M. Buback, *Chain-Length-Dependent Termination of Styrene Bulk Homopolymerization Studied by SP−PLP−EPR.* Macromolecules, 2015. **48**(2): p. 309-315.

30. Buback, M., et al., *Critically evaluated rate coefficients for free-radical polymerization, 1. Propagation rate coefficient for styrene.* Macromolecular Chemistry and Physics, 1995. **196**(10): p. 3267-3280.

31. Niwa, M., T. Matsumoto, and H. Izumi, *Kinetics of the Photopolymerization of Vinyl Monomers by Bis(Isopropylxanthogen) Disulfide. Design of Block Copolymers.* Journal of Macromolecular Science: Part A - Chemistry, 1987. **24**(5): p. 567-585.

32. Otsu, T., et al., *Features of living radical polymerization of vinyl monomers in homogeneous system using N,N-diethyldithiocarbamate derivatives as photoiniferters.* European Polymer Journal, 1995. **31**(1): p. 67-78.

33. McKenzie, T.G., et al., *Investigation into the photolytic stability of RAFT agents and the implications for photopolymerization reactions.* Polymer Chemistry, 2016. **7**(25): p. 4246-4253.

34. Xu, J., et al., *Catalyst-Free Visible Light-Induced RAFT Photopolymerization*, in *Controlled Radical Polymerization: Mechanisms*. 2015, American Chemical Society. p. 247-267.

35. Fukuda, T., A. Goto, and Y. Tsujii, *Kinetics of Living Radical Polymerization*, in *Handbook of Radical Polymerization*. 2003, John Wiley & Sons, Inc. p. 407-462.

36. Vana, P., T.P. Davis, and C. Barner-Kowollik, *Kinetic Analysis of Reversible Addition Fragmentation Chain Transfer (RAFT) Polymerizations: Conditions for Inhibition, Retardation, and Optimum Living Polymerization.* Macromolecular Theory and Simulations, 2002. **11**(8): p. 823-835.

37. Niwa, M., et al., *Molecular design of block and graft copolymers by vinyl-substituted xanthates.* Die Makromolekulare Chemie, 1988. **189**(9): p. 2187-2199.

38. Vana, P. and A. Goto, *Kinetic Simulations of Reversible Chain Transfer Catalyzed Polymerization (RTCP): Guidelines to Optimum Molecular Weight Control.* Macromolecular Theory and Simulations, 2010. **19**(1): p. 24-35.

7 Kinetic investigations into the polymerisation of methyl acrylate and vinyl acetate with a spirooxazine based xanthate

7.1 Introduction

As shown in the review by Beija *et al.* [1], RAFT agents bearing photochromic or fluorescent moieties have primarily been limited to trithiocarbonates, dithiobenzoates and dithioesters, and as such have been used in the polymerisation of MAMs. It must be noted that most of these RAFT agents bear this functionality on the R group in order to synthesize polymers with photochromic or fluorescent functionality [1] rather than to impact the polymerisation. Despite their widespread use in polymer systems [2] and derivatisation into monomers for copolymerisation [3], spirooxazine functionalised initiators for use with RDRP techniques remain rare.

Such *et al.* pioneered the use of spirooxazines functionalised with ATRP functionality (SOX-ATRP 1 & 2, shown in Figure 7.) to allow the polymerisation of styrene [4] and methyl methacrylate [5] directly from the spirooxazine molecule in a controlled manner to create "tails" on the photochromic molecule in order to control the photochromic switching performance in solid polymers. [3, 6]. The SOX-RAFT agent shown in Figure 7. has been used by both Such *et al.* to polymerise styrene and butyl acrylate to form copolymers [6] and by Ercole *et al.* to synthesise a range of block copolymers with stimulus responsive segments [3].

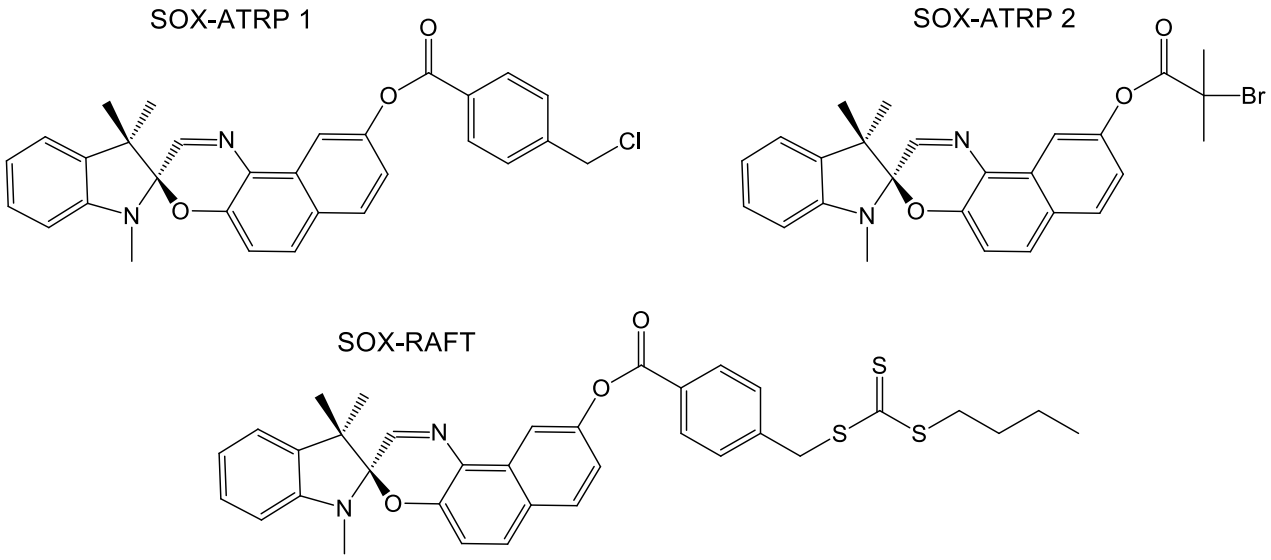

Figure 7.1: Spirooxazines functionalised with ATRP and RAFT functionality found in the literature.

The ability of the RDRP agents shown in Figure 7.1 to succeed in controlling polymerisations depends not only on their reactivity towards radical addition and subsequent fragmentation (in the

case of RAFT) or to re-cap the propagating radical (in the case of ATRP) but also on their resistance to photodegradation leading to structural changes within the molecule. Even though spirooxazines have been identified as being significantly more resistant to photodegradation processes than other spiro compounds , they are still liable to undergo degradation both in the dark [7] and under irradiation both in the presence [8] and absence of oxygen within polymer matrices [9], leading to a broad spectrum of degradation products as shown in Scheme 7.1.

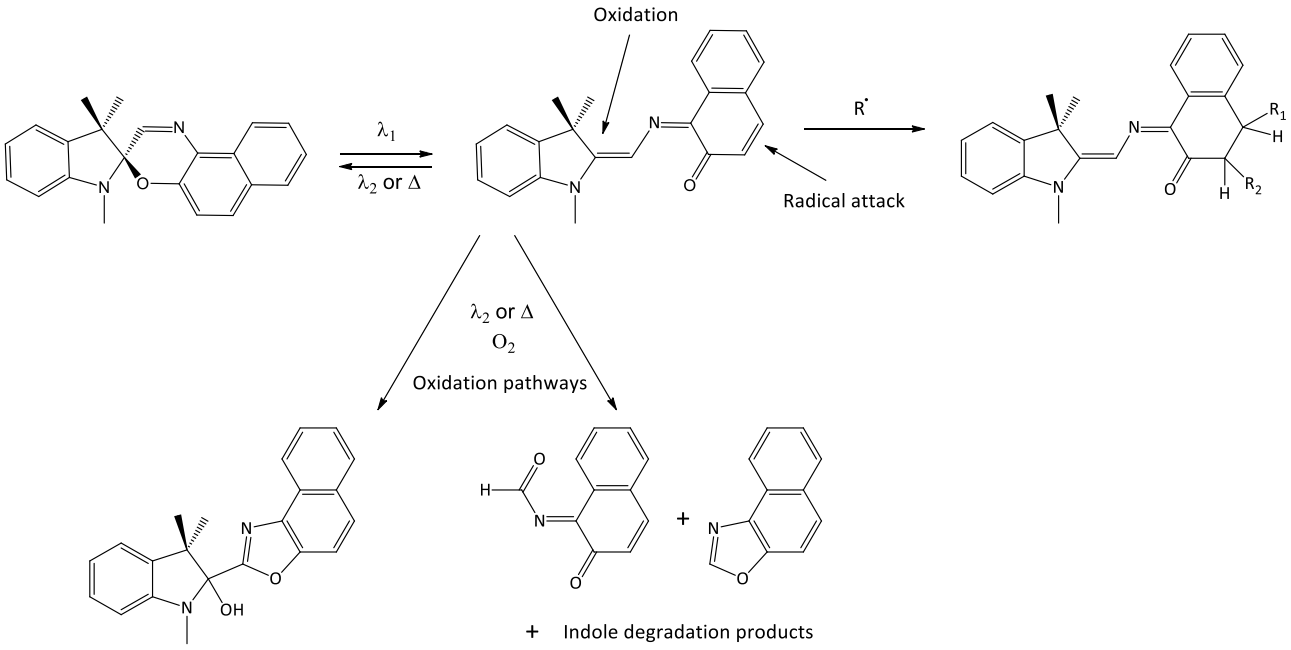

Scheme 7.1: Degradation pathways for spirooxazines. Adapted from [10].

This chapter details the experimental investigation of using a novel photochromic spirooxazine based xanthate (spiro-XEP) specifically designed, modelled and synthesised with the Z group bearing the spirooxazine moiety to influence its reactivity within the RAFT mechanism when exposed to UV light. As has been shown by the results of Chapters 5 and 6, UV exposure induces a range of photolysis pathways including reversible photolysis of the RAFT species via the photoiniferter mechanism (Scheme 7.2, blue box), with the reversible degenerative chain transfer (RAFT) mechanism (Scheme 7.2, red box) still dominating the polymerisation behaviour.

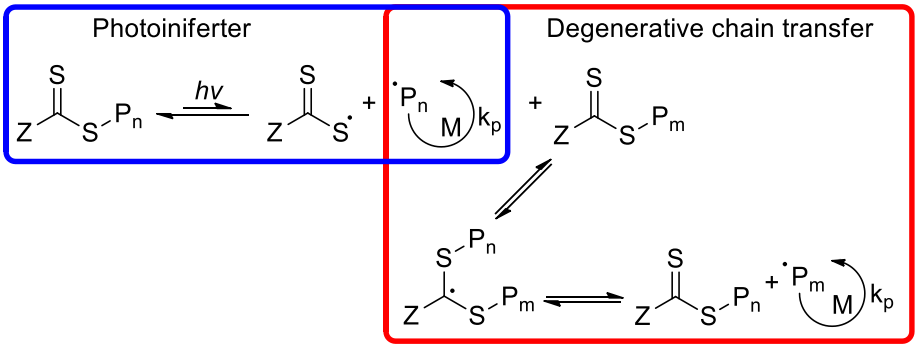

Scheme 7.2: Interplay between photoiniferter (blue box) and degenerative chain transfer (red box) mechanisms.

The polymerisation conditions for MA and VAc which were selected as a typical MAM and LAM respectively to evaluate the potential for universal RAFT agent using UV light as the stimuli are shown in Scheme 7.3. This allows the behaviour seen when UV light is applied to be compared with the results obtained with the non-photochromic analogue, PXEP, as previously explored in Chapters 5 and 6 under identical polymerisation conditions. These results are compared qualitatively to both a range of RAFT agents tested by Keddie *et al.* under the same reaction conditions used (minus the UV stimulus), and to the reactivity as predicted by the theoretical modelling presented in Chapter 3.

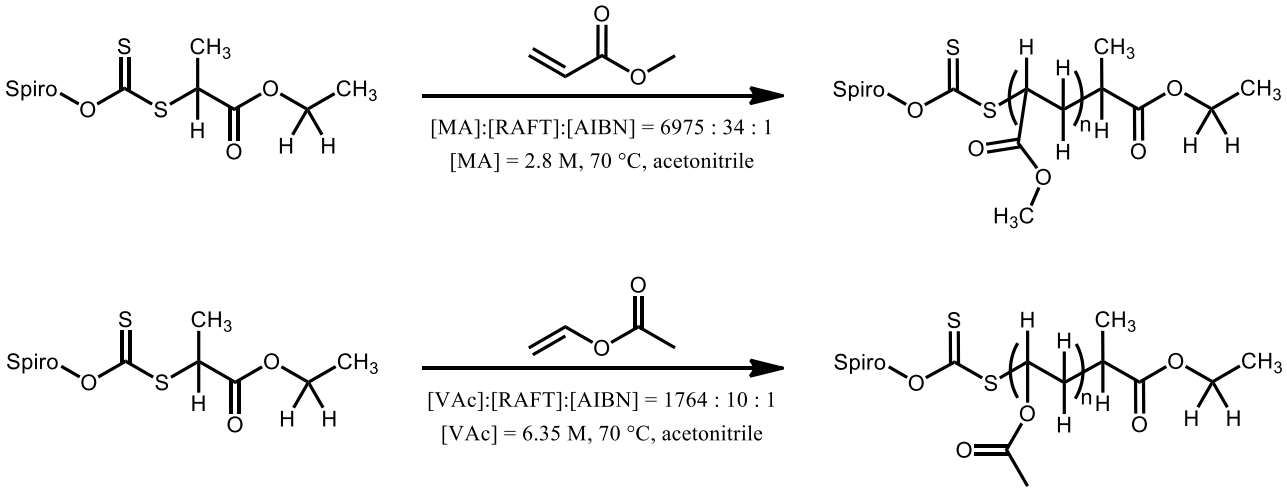

Scheme 7.3: Polymerisation conditions used in testing spiro-XEP with MA (top) and VAc (bottom).

The ability of spiro-XEP to generate macro-RAFT agents with living characteristics derived from both MA and VAc is investigated by chain extension with the respective monomers. Finally, potential causes for the range of intense colour changes seen with spiro-XEP under certain polymerisation conditions was investigated, with several possibilities and their overall potential mechanistic repercussions put forth.

7.2 Spectral characterization and control experiments with spiro-XEP

7.2.1 Experimental procedures

Please refer to Chapter 4, sections 4.5 for relevant experimental procedures used in this section.

7.2.2 Spectral characterization of spiro-XEP

As the spiro-XEP molecule is composed of both a parent spirooxazine molecule (spiro-OH) and a xanthate moiety, the UV-Vis absorption and the associated transitions are quite complex in nature as can be seen in Figure 7.2 (light green trace). The spiro-XEP appears to have a distinct peak ascribed to the $\pi \rightarrow \pi^*$ transition from the xanthate moiety which has the same peak absorbance (283 nm, Figure 7.2, light green trace) as seen for the non-photochromic analogue PXEP (Figure 7.2, light orange trace). Elucidation of the $n \rightarrow \pi^*$ transition from the xanthate moiety in spiro-XEP was not possible as the extinction coefficient for the spirooxazine ring opening absorbance in spiro-OH is significantly higher (8670 M^{-1} cm^{-1}) than that for the $n \rightarrow \pi^*$ transition from PXEP (59 M^{-1} cm^{-1}), with both transitions occurring in the same region. In the spiro-XEP molecule the spirooxazine ring opening peak appears to shift to 347 nm from 335 nm. The secondary broad peak from ~ 525 – 650 nm observed for spiro-XEP is attributed to a small fraction of the molecules existing in the open forms at room temperature under irradiation from ambient light (Figure 7.2, dark green trace). A summary of these transitions is shown in Table 7.1.

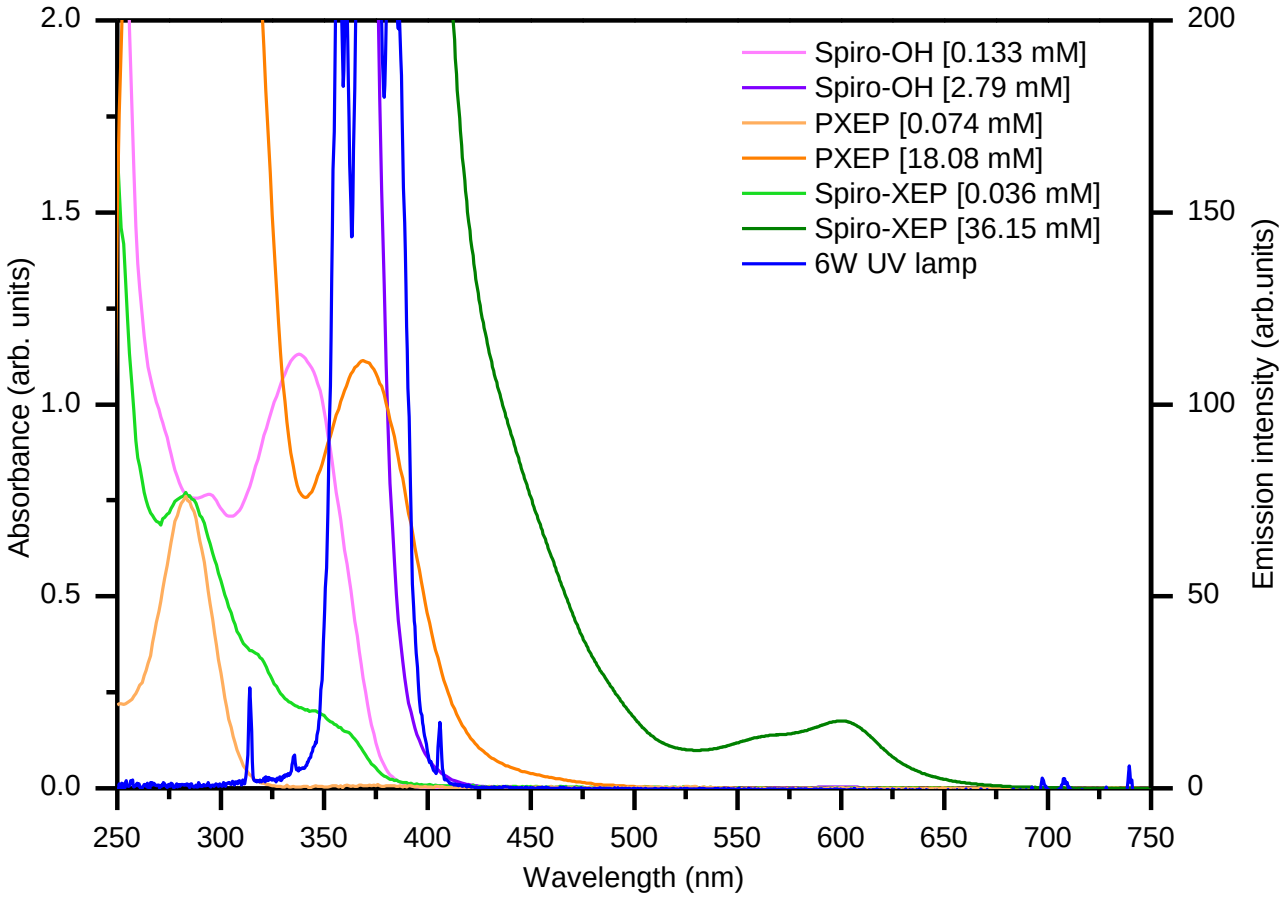

Figure 7.2: Comparison of the absorbance of Spiro-XEP, spiro-OH and PXEP (all in acetonitrile) at various concentrations with emission spectrum of the 6W UV lamp (370nm, 2 mW/cm^2).

Table 7.1: Summary of UV-Vis transitions for the compounds analysed in Figure 7.2.

Molecule	Peak (nm)	Extinction coefficient (M^{-1} cm^{-1})	Assigned transition
Spiro-XEP	283	21176	π → π* from C=S
	347	5526	Spirooxazine ring opening
PXEP	283	10904	π → π* from C=S
	370	59	n → π* from C=S
Spiro-OH	335	8670	Spirooxazine ring opening

As described previously, it is clear the transitions responsible for the photo-iniferter and spirooxazine switching behaviour will most likely be occurring simultaneously under 370 nm irradiation. Previous observations of photo switching behaviour both during purification by column chromatography and on TLC plates (see Chapter 4, section 4.3.8) indicates that spiro-XEP has not lost the photochromic properties of the parent spiro-OH molecule.

7.2.3 Control experiments

In Chapter 5 and 6 it was shown that in the absence of AIBN, XEP could act as a photoiniferter by the application of UV light, but did not function as a thermal iniferter. In an identical manner, the ability of spiro-XEP to act as both a thermal and photoiniferter compound was tested. Spiro-XEP also does not function as a thermal iniferter towards both MA and VAc to any appreciable extent, as evidenced by essentially zero conversion attained when both AIBN and UV irradiation are absent as sources of initiating radicals (entries 1 & 3 respectively, Table 7.2).

Table 7.2: Summary of control experiments conducted with spiro-XEP with both MA and VAc monomers: [MA] = 2.80 M, [VAc] = 6.35 M, [AIBN] = 0, 70 °C, polymerisation time = 10 h, acetonitrile as solvent. UV irradiation (370nm, 2 mW/cm^2).

Entry	Monomer	[Spiro-XEP] (mM)	UV Light	% conversion by ^{1}H NMR	M_n (g/mol)	M_w (g/mol)	Đ
1	MA	13.48	N	0.30	N/A	N/A	N/A
2	MA	13.48	Y	92.06	18170	22560	1.24
3	VAc	35.99	N	0.00	N/A	N/A	N/A
4	VAc	35.99	Y	2.10	800	1000	1.24

Under UV irradiation, poly(MA) is formed and results in high conversion, analogous to what was seen when PXEP was used. The molecular weight agrees well with the theoretical Mn at high conversion, and the dispersity (1.24) indicates that spiro-XEP can function as a suitable photoiniferter for MA and maintain control of the polymerisation.

Only marginal conversion is seen when VAc is used, which is contrary to what was observed for PXEP. This initial result indicates that spiro-XEP is a poor photoiniferter for VAc, however the kinetics of polymerising VAc are explored further in section 7.4.

7.3 Kinetic studies of MA polymerisation

The same experimental conditions as those used in Chapter 5 (section 5.3) are used here to allow a direct comparison between the polymerisation behaviour of spiro-XEP and the non-photochromic analogue PXEP. For full details of the experimental conditions, please refer to Chapter 4, section 4.5. Polymerisation of MA with spiro-XEP is shown in Scheme 7.4.

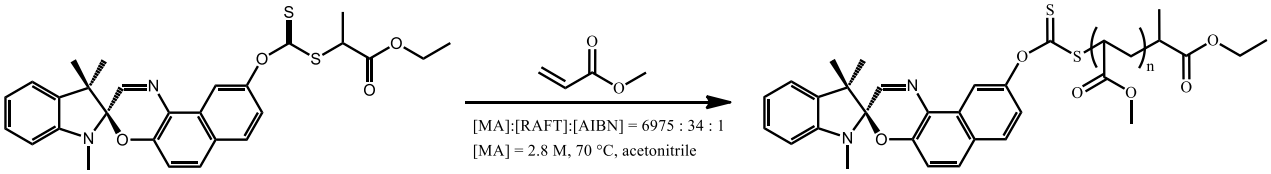

Scheme 7.4: Polymerisation of MA undertaken with spiro-XEP under standard conditions

As can be seen in Figure 7.3 (A), which shows the polymerisation kinetics, conversions of 76 % and 94 % were obtained after 6 h dark + AIBN and light + AIBN conditions, respectively. These are slightly lower than the conversions seen with PXEP, (84 % and 99 % respectively) under identical conditions. Under dark + AIBN conditions, there is a slight plateauing of conversion seen by the 6 h point which did not occur with PXEP.

Under light + AIBN conditions, a marked increase in polymerisation rate is evident (Figure 7.3, A). Analysis of the pseudo first order kinetic plot (Figure 7.3, B) reveals that under dark + AIBN conditions, the rate of polymerisation (k_{app} = 0.30 h^{-1}) is within error of the rate seen for PXEP (k_{app} = 0.32 h^{-1}), indicating that spiro-XEP does not induce any retardation into the polymerisation despite its vastly different structure. Under light + AIBN conditions, the increase in polymerisation rate to k_{app} = 0.80 h^{-1} equates to an enhancement factor of 2.67, which is distinctly less than that seen for PXEP (10.03) under light only conditions which were shown to be representative of light + AIBN conditions (see Chapter 5, section 5.3.2). Results summarised in Table 7.3.

Table 7.3: Comparison of calculated k_{app} values for the kinetic experiments shown in Figure 7.3 (B). UV irradiation (370nm, 2 mW/cm^2).

Conditions	k_{app} (h^{-1})	Error in k_{app} (+/-)	Enhancement factor
Dark + AIBN	0.30	0.01	1.00
Light + AIBN	0.80	0.04	2.67

This significantly different enhancement by UV irradiation is indicative of the photoiniferter pathway for spiro-XEP being less efficient than for PXEP which is probably related to the photochromic nature of this molecule. As shown previously, the overlap in the absorption at around 370 nm which may be due to a competitive absorption between the spirooxazine Z group to undergo ring opening and the C-S bond cleavage, subsequently reducing the photo-iniferter efficiency.

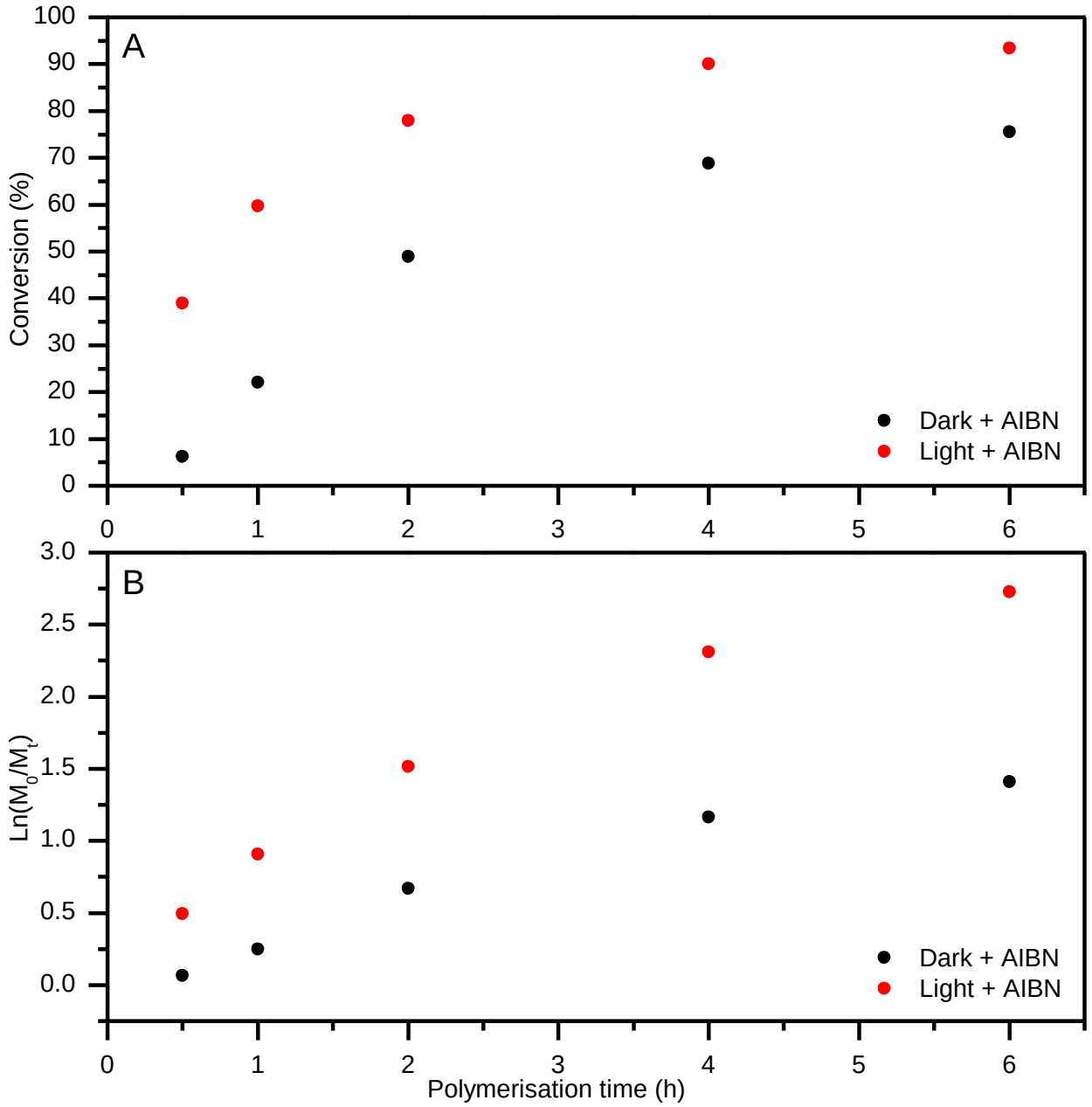

Figure 7.3: Conversion versus time plot (A) and 1st order kinetic plot (B) for MA polymerised under various conditions at 70 °C with Spiro-XEP.

There is close agreement between the experimentally obtained number average molecular weight under both dark and light + AIBN conditions and the theoretical M_n, as can be seen in Figure 7.4. With spiro-XEP the extent of the hybrid behaviour seen at low conversion is smaller than that seen for PXEP, as evidenced by an estimated M_n of 2100 g/mol at zero conversion, which is lower than that estimated for PXEP at 3800 g/mol. This indicates an overall faster establishment of the main RAFT equilibrium which results in a better level of control over the polymerisation. The control experiment under light only conditions for MA had an extended reaction time of 10 h and fits the general trend for both M_n and dispersity obtained under both dark and light + AIBN conditions.

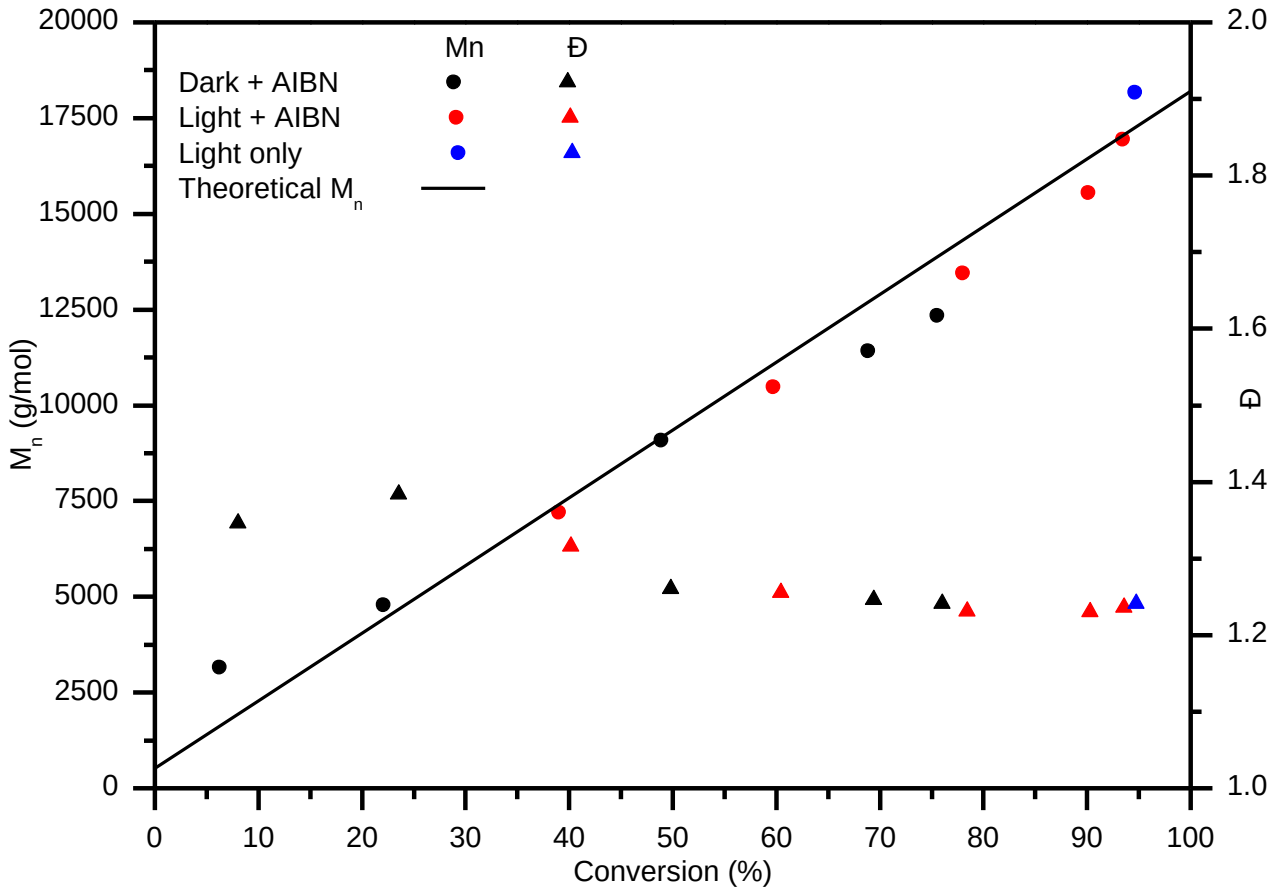

Figure 7.4: Evolution of molecular weight and dispersity as a function of conversion for MA polymerised under various conditions at 70 °C with spiro-XEP.

Similar to what was seen with PXEP, there was gradual consumption of the spiro-XEP agent during MA polymerisations. This was determined by ^{1}H NMR where resonances attributed to the starting spiro-XEP (labelled d & f in Figure 7.5) were still present after 1 h of polymerisation under dark + AIBN conditions (Figure 7.5, blue trace). As seen by the disappearance of the resonance f along with the broadening of resonances d that occurs as spiro-XEP is consumed, spiro-XEP was completely consumed by the 2 h point (Figure 7.5, magenta trace) which corresponds to 49 % monomer conversion. Under light + AIBN conditions, spiro-XEP is completely consumed by the 0.5 h time point, which corresponds to 39 % monomer conversion; this fits the general trend seen with dark + AIBN conditions. The resonances attributed to the impurities (labelled Imp. in Figure 7.5) are seen to also disappear quite rapidly, being completely absent after 1 h of polymerisation. As these impurities were identified as being primarily a symmetrical trithiocarbonate and a symmetrical disulfide, it unsurprising that they are rapidly consumed, owing the higher reactivity of trithiocarbonates towards radical addition. Under photolysis, the disulfide may simply function as a source of initiating radicals without any detriment or contribution to the chain transfer process. The trithiocarbonate potentially introduces a separate population of polymer chains with a more reactive

RAFT moiety, and the implications of this are potentially more significant in the polymerisation of VAc than for MA. This is explored further in the chain experiments conducted with spiro-XEP and VAc in section 7.4.1.

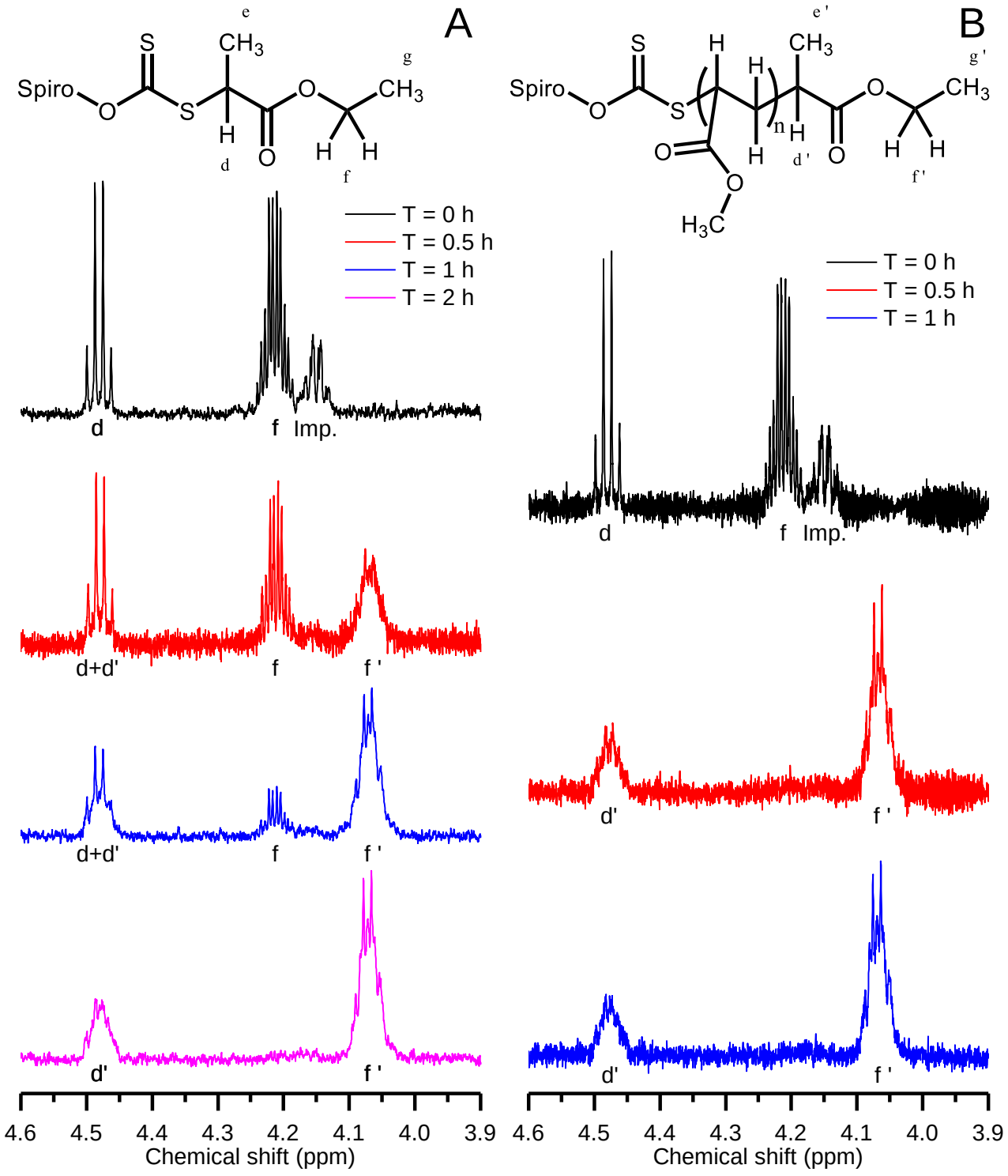

Figure 7.5: ^{1}H NMR spectra in the region of 3.9 – 4.6 ppm showing the resonances attributed to the starting spiro-XEP and conversion into a poly(MA), obtained from analysis of kinetic polymerisation samples polymerised to various times under dark conditions (A) and light + AIBN conditions (B).

There is no significant difference in the dispersity of the polymers obtained under dark + AIBN and light + AIBN conditions, with both reaction conditions giving data that appears to follow the same general trend. The dispersity values start out broader (D ~ 1.4) early in the polymerisation (< 30 % conv.) and become narrower as the polymerisation progresses. The dispersities obtained at higher conversions (> 75 %) are very similar to those obtained with PXEP at similar conversion values. These results indicate that the spiro-XEP compound does not undergo noticeable changes in its reactivity towards radical addition or fragmentation under UV irradiation. This is further supported by the estimated apparent chain transfer constants for spiro-XEP conforming very closely to those obtained with PXEP under equivalent reaction conditions, as shown in Figure 7.6.

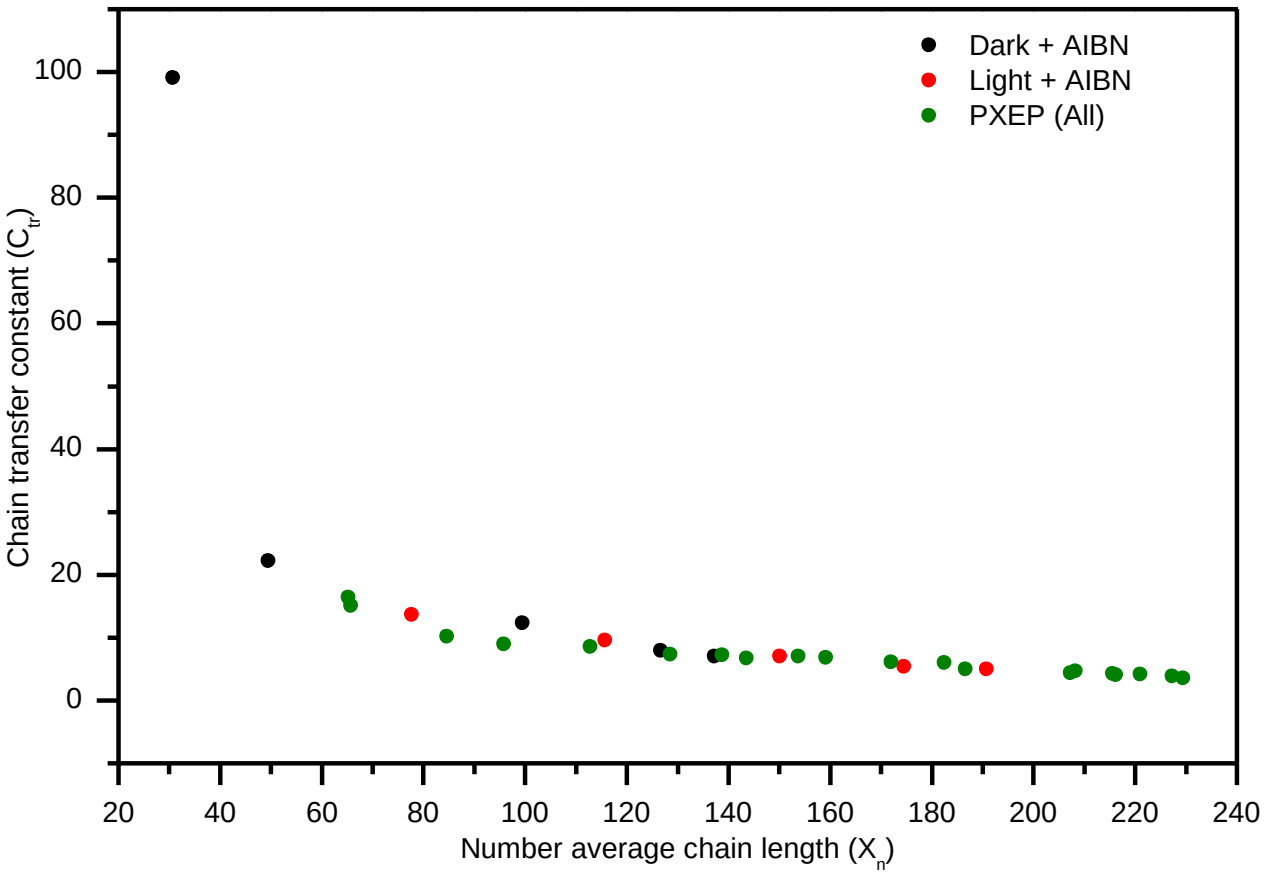

Figure 7.6: Chain transfer constants as estimated for spiro-XEP when used in the polymerisation of MA under various conditions at 70 °C.

Based on the conclusions from chapters 5 & 6 that showed equivalent kinetics of both normal and chain extension experiments under equivalent conditions for each respective monomer (MA and VAc) with PXEP, kinetic chain extension experiments were not conducted with spiro-XEP.

7.3.1 Chain extension of poly(MA)

The ability of spiro-XEP to generate living polymers capable of chain extension was investigated with a poly(MA) macro-RAFT derived from spiro-XEP that was synthesised under light + AIBN conditions and had an M_n of 2300 g/mol and Đ = 1.17 by GPC, theoretically having over 98 % of all chain ends retaining the RAFT moiety as estimated using Equation 4.9. Successful chain extension and essentially complete consumption of the starting macroinitiator was seen under both dark + AIBN and light + AIBN conditions as shown in Figure 7.7 (black and red traces respectively), with no significant overlap with the RI peak from the starting macroinitiator (Figure 7.7, grey trace).

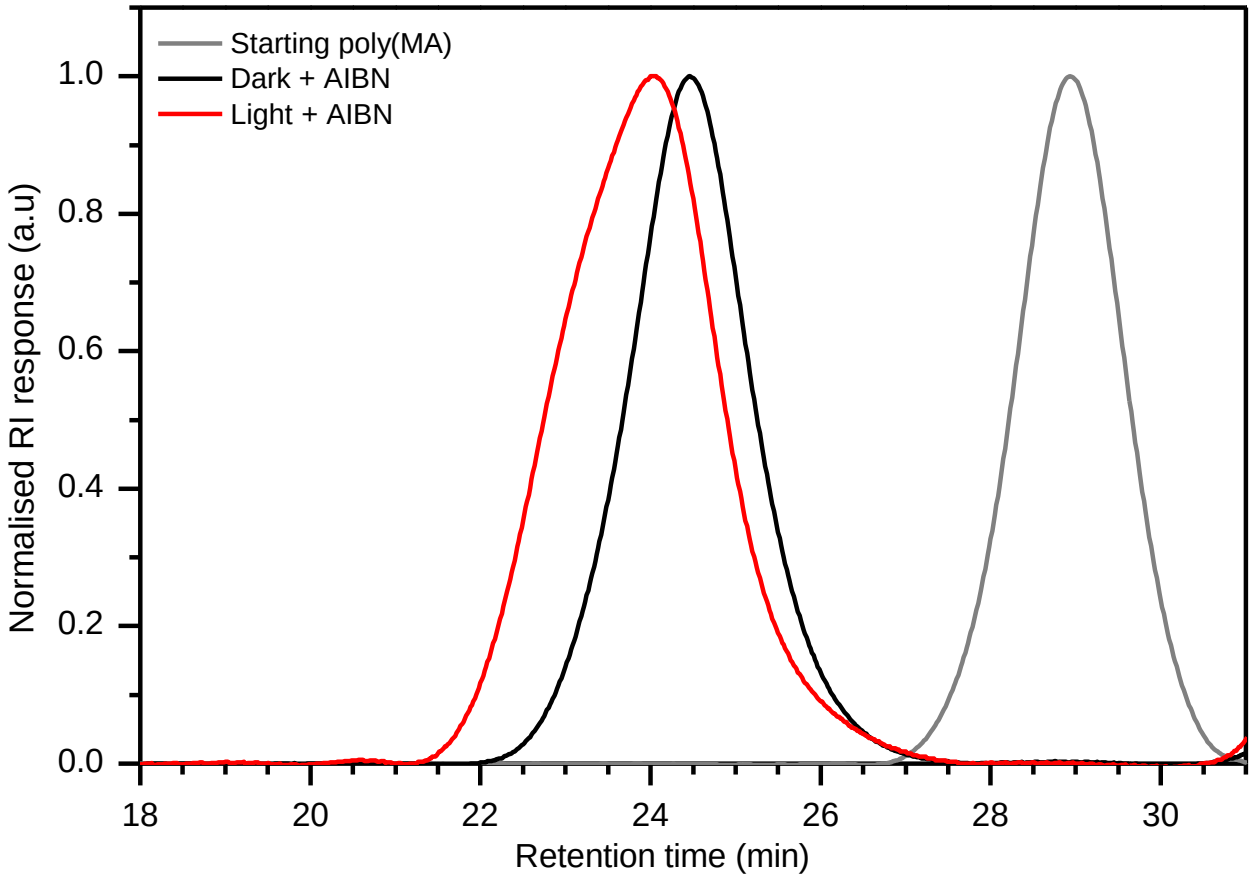

Figure 7.7: Normalised RID GPC traces for MA chain extension polymerisation samples under different conditions at 70 °C with a poly(MA) macro-RAFT agent derived from spiro-XEP.

The resulting M_n of the chain extended poly(MA-b-MA) was 32480 g/mol and 43720 g/mol under dark and light + AIBN conditions respectively, compared to the theoretical value of 35,000 g/mol at 100 % conversion. The larger discrepancy under light + AIBN conditions could indicate the presence of secondary polymer species resulting from either termination by recombination or irreversible photolysis, with the former being more likely and supported by the peak broadening seen towards higher molecular weights (lower retention times) in Figure 7.7 (red trace). Irrespective of this, these

results show that spiro-XEP can be used to synthesise poly(MA) macroinitiators with living characteristics. These results are summarised in Table 7.4.

Table 7.4: Summary of characterization poly (MA-b-MA) chain extension polymers corresponding to GPC traces in Figure 7.7. Solvent is acetonitrile, [MA] = 2.79 M, temperature = 70 °C, polymerisation time = 18 h. UV irradiation (370nm, 2 mW/cm^2).

Synthesis of poly(MA-b-MA)			(g mol^{-1})		
Sample	UV Light	% conv.	M_n	M_w	Đ
poly(MA)	N	98.1	2300	2700	1.17
Dark + AIBN	N	84.6	32480	39230	1.21
Light + AIBN	Y	96.1	43720	58460	1.34

Overall the results obtained with the polymerisation of MA indicate that under these reaction conditions, spiro-XEP does not show significant differences in performance as a RAFT agent with the application of UV irradiation.

7.4 Vinyl acetate polymerisation

Once again, the same experimental conditions as those used in Chapter 6 (section 6.3) are used here to allow a direct comparison between the polymerisation behaviour of spiro-XEP and the non-photochromic analogue PXEP. For full details, please refer to Chapter 4, section 4.5. Polymerisation of VAc with spiro-XEP is shown in Scheme 7.5.

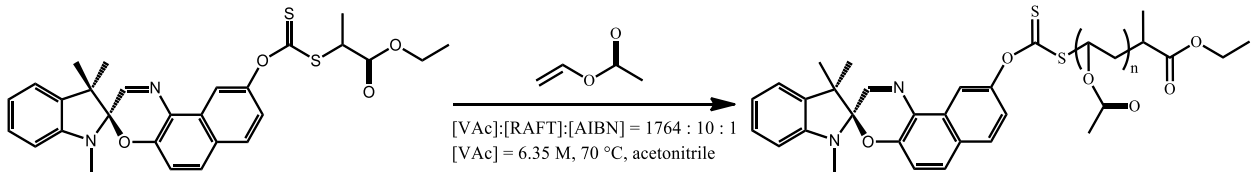

Scheme 7.5: Polymerisation of VAc undertaken with Spiro-XEP under standard conditions.

Figure 7.8 (A) shows the polymerisation kinetics under both dark + AIBN and light + AIBN conditions are essentially identical for the first 10 h, with the conversion values forming a single series of overlapping data points. Only at much longer reaction times of 24 & 48 h is there a difference between dark + AIBN and light + AIBN conditions, with the conversion being higher with the application of UV light.

It is evident that regardless of the reaction conditions, the conversion attained at any time point with spiro-XEP is significantly lower than that attained with PXEP. For example, spiro-XEP shows only

5.6 % conversion under both reaction conditions at 6 h, compared with 86.5 % for PXEP under dark + AIBN conditions at the same time point.

As shown in Figure 7.8 (B), the pseudo first order kinetics show a clear deviation from linearity under both reaction conditions after 10 hours, indicating a non-steady state radical concentration. AIBN radicals were found to be predominant initiating species in the polymerisation of VAc (see Chapter 6, section 6.7.2), hence the depletion of AIBN at extended reaction times is theorised to be the primary cause of this change in apparent polymerisation rate. The quantity of AIBN remaining under dark + AIBN conditions was estimated using the k_d determined experimentally (see Chapter 5, section 5.2.4) and under light + AIBN conditions using the k_d value determined by Predici modelling (see Chapter 5, section 6.6). A shown in Table 7.5, at the 10 h point there is still at least 30 % AIBN remaining under both reaction conditions, with disparity between the quantity remaining under different reaction conditions shrinking due to the exponential degradation kinetics. Nevertheless, it is clear that by the 48 hour time point there is practically no AIBN remaining to sustain the polymerisation.

Table 7.5: Comparison of estimated % of AIBN remaining under different reaction conditions used in VAc polymerisation.

Conditions	**kd (s^{-1}) (x 10^{-5})**	**AIBN remaining (% of original)**		
		After 10 h	**After 24 h**	**After 48 h**
Dark + AIBN	1.653	55.2	24.0	5.75
Light + AIBN	3.306	30.4	5.75	0.33

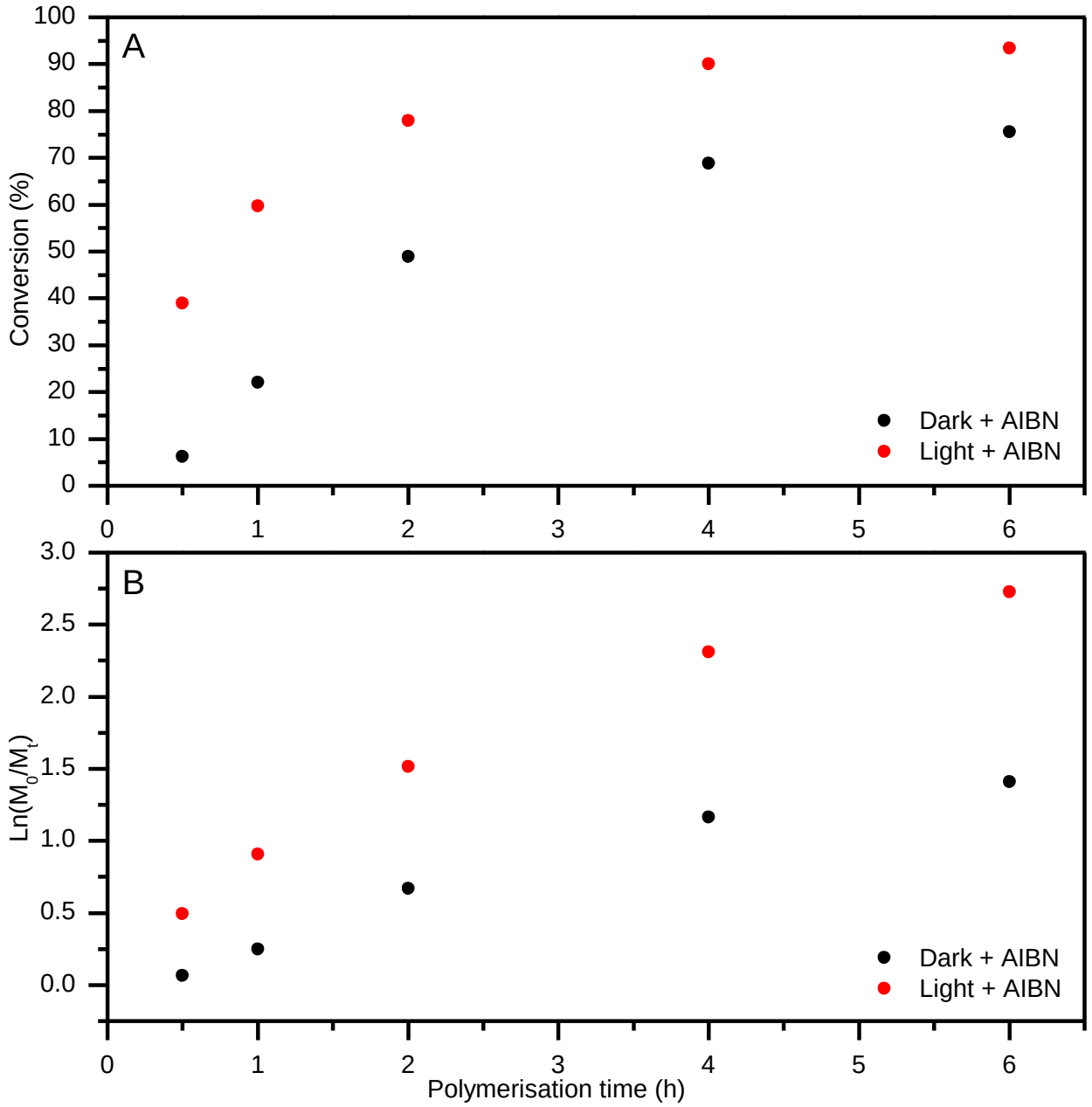

Figure 7.8: Conversion versus time plot (A) and 1st order kinetic plot (B) for VAc polymerised under various conditions at 70 °C with Spiro-XEP.

K_{app} values determined from the first 10 hours of polymerisation are the same within error for both experimental conditions, confirming that UV irradiation did not have any kinetic effect until the majority of AIBN was degraded after which the primary source of initiating radicals became photolysis of the spiro-XEP derived growing chains. Quantitatively, the retardation in polymerisation rate with spiro-XEP gives a polymerisation rate of only ~ 2 % of that obtained with PXEP under equivalent reaction conditions. These results are summarised in Table 7.6.

With PXEP, the apparent polymerisation rate (k_{app}) under light only conditions was only 30 % of the rate obtained with dark + AIBN conditions; due to this and the extraordinarily slow rate of

polymerisation seen with spiro-XEP under light + AIBN conditions, kinetics under light only conditions were not attempted with spiro-XEP. At the equivalent time of 10 h, the single point control experiment under light only conditions gave a conversion of 2.9 % versus an average of 8.5 % under both conditions featuring AIBN. This result indicates that the reduced polymerisation rate under light only conditions seen with PXEP is also replicated with spiro-XEP.

Table 7.6: Comparison of calculated k_{app} values for the kinetic experiments shown in

Conditions	k_{app} (h^{-1})	Error in k_{app} (+/-)	Enhancement factor
Dark + AIBN	0.0092	0.0001	1.00
Light + AIBN	0.0089	0.0004	~ 1.00

Despite the significant retardation in polymerisation rate, analysis of Figure 7.9 reveals that the polymerisation was controlled under both reaction conditions, as evidenced by the number average molecular weight increasing with conversion and remaining only slightly under the theoretically expected M_n. The dispersity values for all but one sample are under 1.2, indicating that narrow if albeit very short polymer chains were formed. There is no broadening of dispersity as was seen with PXEP, however this is most likely simply due to the conversion and M_n being too low for this effect to occur.

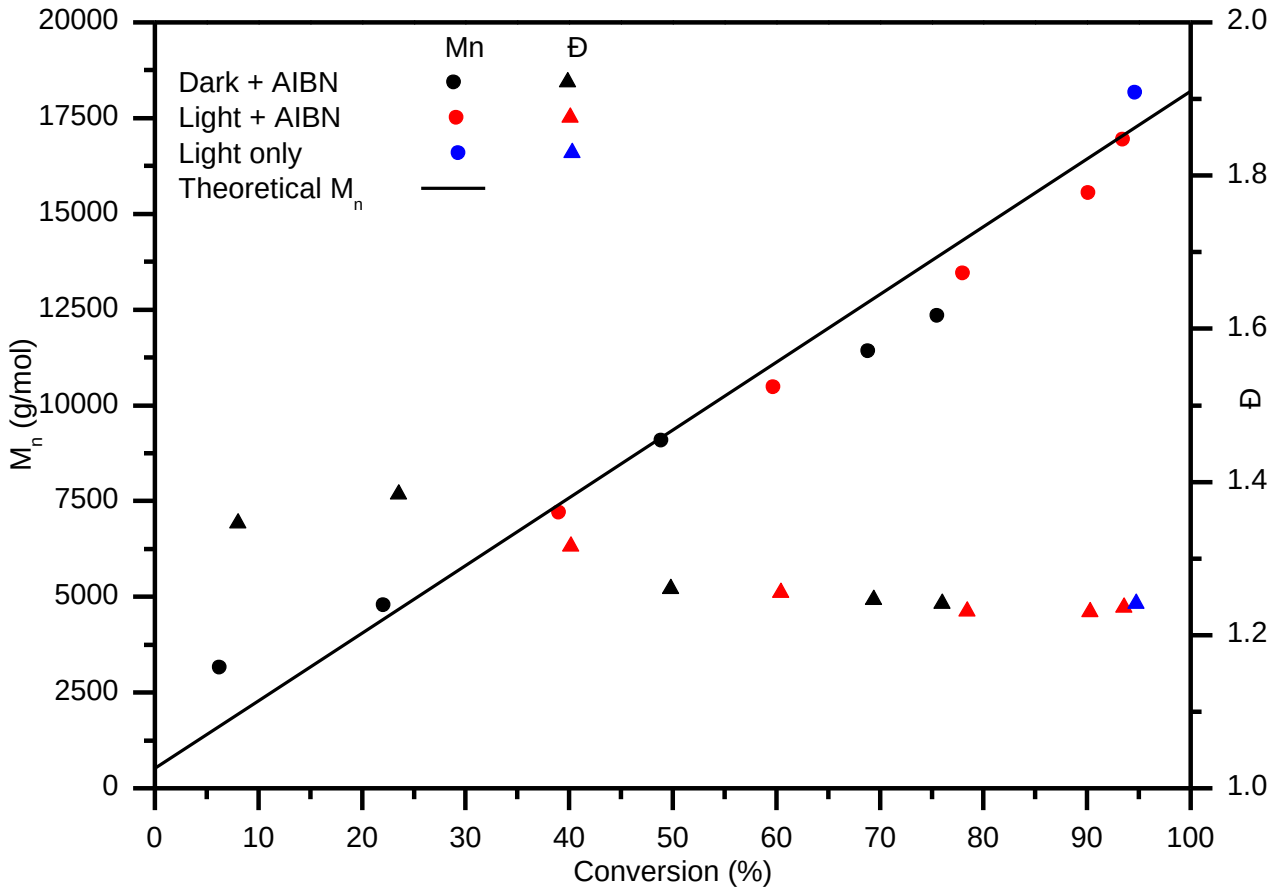

Figure 7.9: Evolution of molecular weight and dispersity as a function of conversion for VAc polymerised under various conditions at 70 °C with spiro-XEP.

Comparing the estimated chain transfer constants for spiro-XEP under dark + AIBN and light + AIBN conditions reveals that they appear to form a continuous trend (Figure 7.10, red & black data points). The possibility of spiro-XEP having a higher chain transfer constant compared with PXEP is hoever supported by the general trend reported by Keddie *et al.* [11] whereupon as the C_{tr} value for a RAFT agent increased, the overall conversion of VAc under identical dark + AIBN conditions decreased. The most active RAFT agent tested, cyanomethyl (4-Cyanophenyl)(pyridin-4-yl) carbamodithioate in that study had a C_{tr} value estimated to be in excess of 320 and attained only 20 % conversion after 14 h, which is comparable to the behaviour seen here with spiro-XEP.

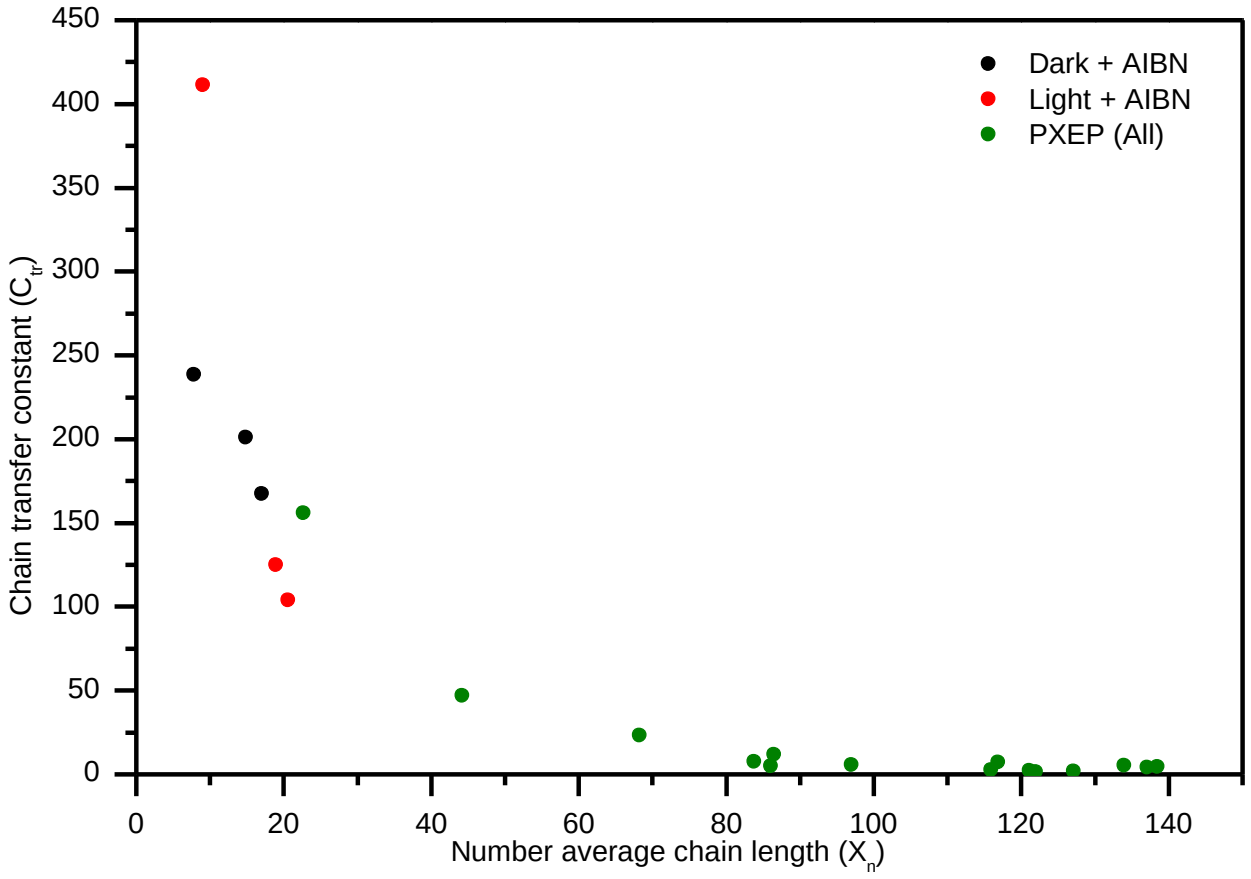

Figure 7.10: Chain transfer constants as estimated for spiro-XEP when used in the polymerisation of VAc under various conditions at 70 °C.

The estimated C_{tr} being the same under both dark + AIBN and light + AIBN conditions is corroborated by ^{1}H NMR resonances corresponding to the spiro-XEP agent decreasing in intensity at approximately the same rate (Figure 7.11, A & B), indicating very similar rates of consumption of spiro-XEP under both reaction conditions. Keddie *et al.* [11] report that the RAFT agent cyanomethyl (4-Cyanophenyl)(pyridin-4-yl) carbamodithioate, which showed comparable retardation to spiro-XEP, was completely consumed when ~ 1.5 % conversion of VAc was attained. This is consistent with the ^{1}H NMR resonances of the 2 h polymerisation samples (Figure 7.11, blue traces) showing trace spiro-XEP remaining which correspond to ~ 2 % VAc conversion. The behaviour seen here with spiro-XEP could also be influenced by the presence of the estimated 10 mole % trithiocarbonate impurity, as trithiocarbonates are known to inhibit the polymerisation of VAc [12]. Potential evidence for this exists in Figure 7.11, where the F' resonance is clearly composed of several distinct resonances arising from several distinct species. The overall broad nature of this resonance implies the bulk of the signal arises from a poly(VAc) species featuring multiple insertions of VAc monomer, however the sharp and well defined nature of the overtone resonances imply they arise from a species more akin in structure to the starting RAFT agent. One such possible species could arise from a single

insertion of VAc monomer into the trithiocarbonate impurity, which should in theory restrict any further insertions of VAc due to this being the mechanism by which highly active RAFT agents can retard a polymerisation.

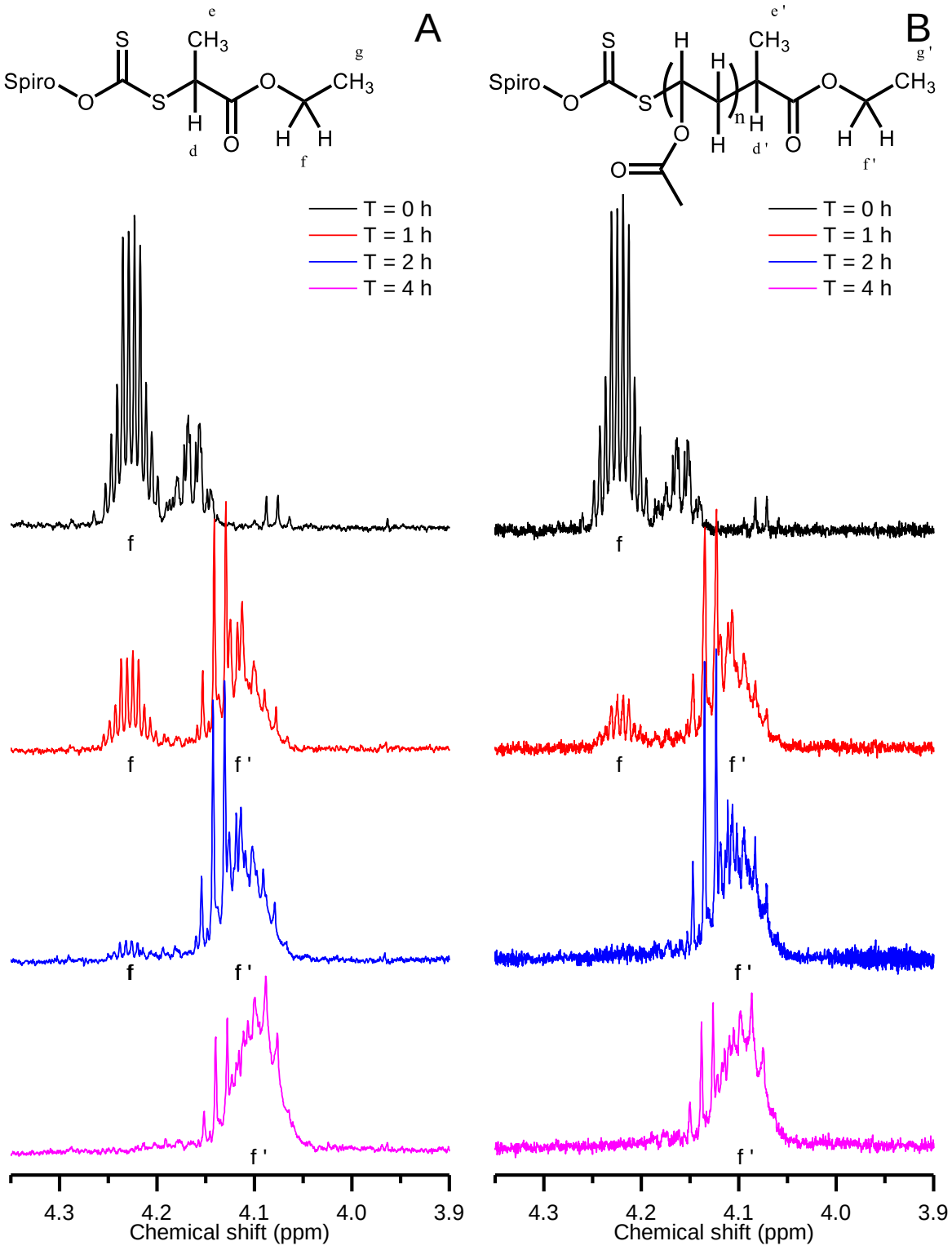

Figure 7.11: ^{1}H NMR spectra in the region of 3.9 – 4.6 ppm showing the resonances attributed to the starting spiro-XEP and conversion into a poly(VAc), obtained from analysis of kinetic polymerisation samples polymerised to various times under dark conditions (A) and light + AIBN conditions (B).

7.4.1 Chain extension of poly(VAc)

Based on the polymerisation behaviour seen with spiro-XEP and VAc, it was imperative to test whether the rate retardation seen was caused by a feature of the main equilibrium, or the pre-equilibrium reaction of the RAFT mechanism. Furthermore, as it was known that the starting spiro-XEP contained approximately 10 mole % of a trithiocarbonate impurity, isolating a purified poly(VAc) and subjecting that to chain extension under identical polymerisation conditions would allow this potential cause of rate retardation to be eliminated.

The chain extension experiments used the T = 10 h sample made under dark + AIBN conditions as a poly(VAc) macro-RAFT. This had an M_n of 1300 g/mol and Đ = 1.17 by GPC, theoretically having 97 % of all chain ends retaining the RAFT moiety as estimated using Equation 4.9.

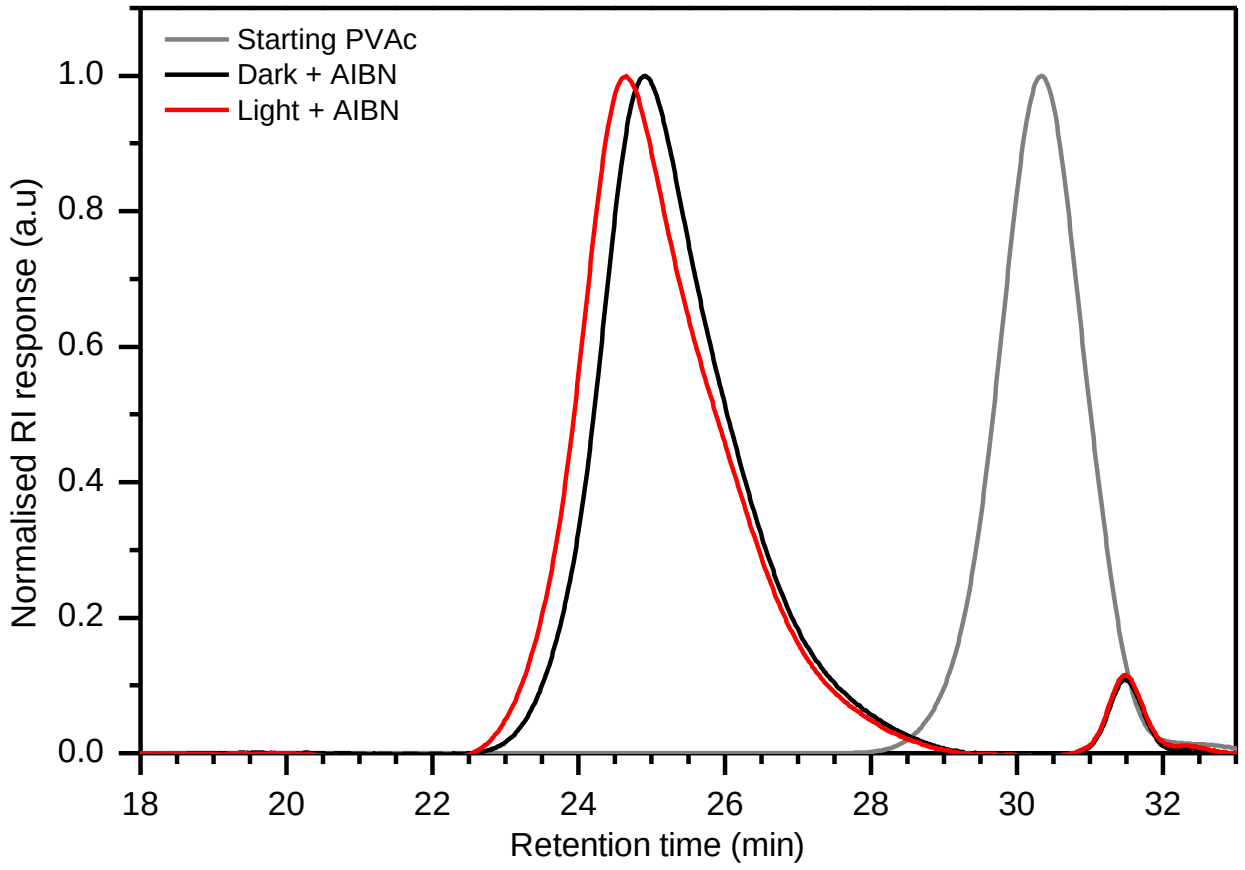

Figure 7.12: Normalised RID GPC traces for VAc chain extension polymerisation samples under different conditions at 70 °C with a poly(VAc) macro-RAFT agent derived from spiro-XEP.

Due to its low molecular weight, the narrow peak seen for the starting poly(VAc) macroinitiator (Figure 7.12, grey trace) overlaps with the consistent artefact seen at a retention time of ~ 31.5 mins (see Figure A5 in the Appendix). Both chain extended polymers show a large shift to lower retention

times and minimal overlap with the starting macroinitiator peak (Figure 7.12, red and black traces), which suggests high consumption of this starting species.

The overall molecular weights obtained are 15790 g/mol and 17660 g/mol under dark + AIBN and light + AIBN conditions respectively. The dispersity values for these polymers increased to over 1.4 in both cases, which is consistent with what was seen for kinetic polymerisations of VAc with PXEP under identical conditions once the M_n exceeded approximately 6000 g/mol. These findings are summarised in Table 7.7. The M_n is overestimated by 37 % and 39 % under dark + AIBN and light + AIBN conditions respectively, however this most likely arises due to the factors explained previously in Chapter 6, section 6.1.

Table 7.7: Summary of characterization poly (VAc-b-VAc) chain extension polymers corresponding to GPC traces in Figure 7.12. Solvent is acetonitrile, [VAc] = 6.35 M, temperature = 70 °C, polymerisation time = 10 h poly(VAc) and 18 h (chain extension). UV irradiation (370nm, 2 mW/cm^2).

Synthesis of poly(VAc-b-VAc)			(g mol^{-1})		
Sample	UV Light	% conv.	M_n	M_w	Đ
poly(VAc)	N	8.6	1300	1520	1.17
Dark + AIBN	N	15.6	15790	22340	1.42
Light + AIBN	Y	17.3	17660	25820	1.46

There appears to be a slight increase in conversion when UV irradiation is applied, however, under both polymerisation conditions the conversion is below 20 % after 18 h, meaning that the rate retardation persists during chain extension. The estimated K_{app} for the chain extension polymerisations supports this, with the apparent polymerisation rates being 0.0094 h^{-1} and 0.010 h^{-1} under dark + AIBN and light + AIBN conditions respectively. These results are within error of the rates calculated for the kinetic polymerisations of VAc as shown in Table 7.6 under equivalent polymerisation conditions. The important conclusion from this is that the retardation of the polymerisation rate with VAc is not due to the RAFT pre-equilibrium reaction which involves the consumption of the starting spiro-XEP or impurities present within the spiro-XEP agent. Instead, it appears that the retardation in polymerisation rate results from the inherent reactivity of this compound towards VAc radical addition and the subsequent effects this has within the RAFT mechanism. Furthermore, successful chain extension confirms that although the polymerisations proceed very slowly, VAc polymerised with spiro-XEP retains living characteristics.

7.5 Conclusions from MA and VAc polymerisations

The spiro-XEP demonstrated that it was able to polymerise both MAMs (MA) and LAMs (VAc), although polymerisation of VAc was very slow and was retarded compared with the non-photochromic analogue, PXEP. Under both light and dark conditions, control was retained, and the chains showed living character through subsequent chain extension reactions.

However, while spiro-XEP shows an enhanced polymerisation rate for MA under light +AIBN conditions compared to dark + AIBN conditions, the enhancement was not as great as demonstrated for the non-photochromic PXEP. This is probably due to overlap of the UV light source output with the absorption spectra from both the spirooxazine ring opening and C-S photoiniferter transitions, therefore leading to a potentially lowered quantum yield for the photoiniferter pathway.

There was no significant difference in the polymerisation rates for VAc under light or dark conditions.

The conclusions of the polymerisation behaviour of MA and VAc seen with spiro-XEP are summarised in Table 7.8.

Table 7.8: Key points of polymerisation behaviour seen for MA and VAc with spiro-XEP.

Methyl acrylate				
	M_n	Đ	Conversion	Polymerisation rate coefficient (K_{app}, h^{-1})
Dark + AIBN	12300 g/mol max, close agreement to theoretical M_n	1.38 – 1.24, decreasing with conversion	75.5 % after 6 h	0.30
Light + AIBN	16900 g/mol max, close agreement to theoretical M_n	1.32 – 1.24, decreasing with conversion	93.5 % after 6 h	0.80, giving an enhancement factor of 2.67
Vinyl acetate				
	M_n	Đ	Conversion	Polymerisation rate (K_{app}, h^{-1})
Dark + AIBN	1990 g/mol, underestimated compared to theoretical M_n	1.07 – 1.15, increasing with conversion	11.9 % after 48 h	0.0092
Light + AIBN	2290 g/mol, underestimated compared to theoretical M_n	1.07 – 1.17, increasing with conversion	14.7 % after 48 h	0.0089, within error of the value obtained for dark + AIBN conditions

7.6 Thermochromic & photochromic colour changes seen with spiro-XEP – comparison of monomer and solvent effects, potential explanations and mechanistic implications

The different rates of polymerisation of VAc seen with spiro-XEP and PXEP must be due to the substitution of the standard phenol Z group for the photochromic spirooxazine Z group. Several mechanistic explanations for the drastically reduced polymerisation rate of VAc seen with spiro-XEP can be correlated with the colour changes that were observed during various experiments conducted with this compound.

Spiro-XEP in acetonitrile displays thermochromic behaviour in acetonitrile; upon heating to 70 °C a darkening of the solution was observed immediately as shown in Figure 7.13. This change is fully reversible, with the solutions returning to their original colour upon cooling, which is consistent with other spirooxazine derivatives based on the spiro-OH parent compound [13, 14].

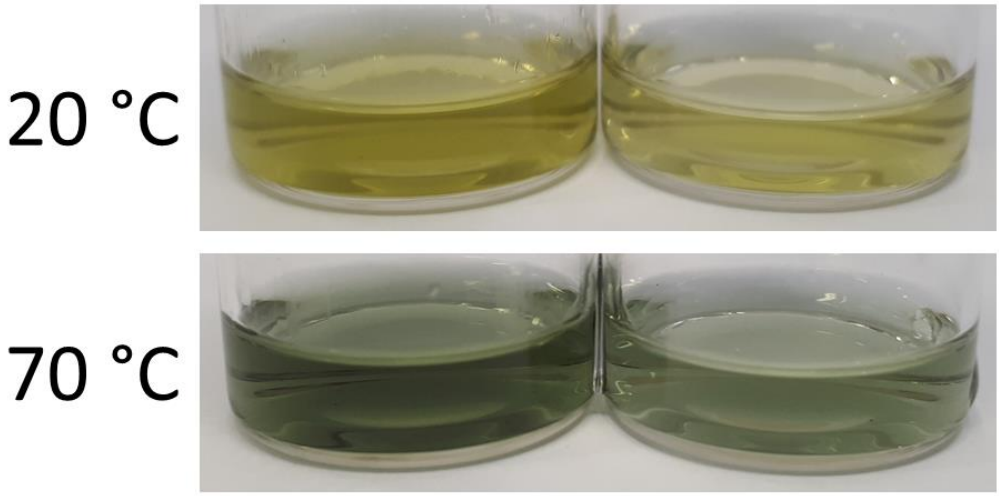

Figure 7.13: Spiro-XEP in acetonitrile [36.15 mM] (left), [18.07 mM] (right) both at room temperature (~ 20 °C) (top) and straight after heating to 70 °C in a water bath (bottom).

During the polymerisation of VAc, the solution first turned green, similar to that shown upon heating in acetonitrile, however this changed to brown after 10 minutes before turning a deep red after 30 minutes. During the polymerisation of MA, the green colour developed and then gradually became pink over the course of the polymerisation. The colour changes seen during the polymerisations with both monomers persisted when the reaction mixtures were cooled down first to room temperature and ~ -10 °C in a freezer. The difference between the colour intensity for dark + AIBN and light + AIBN conditions at equivalent time points is visually apparent for MA polymerisation samples (Figure 7.14. C & D respectively), which is not the case for the VAc samples (Figure 7.14, A & B respectively).

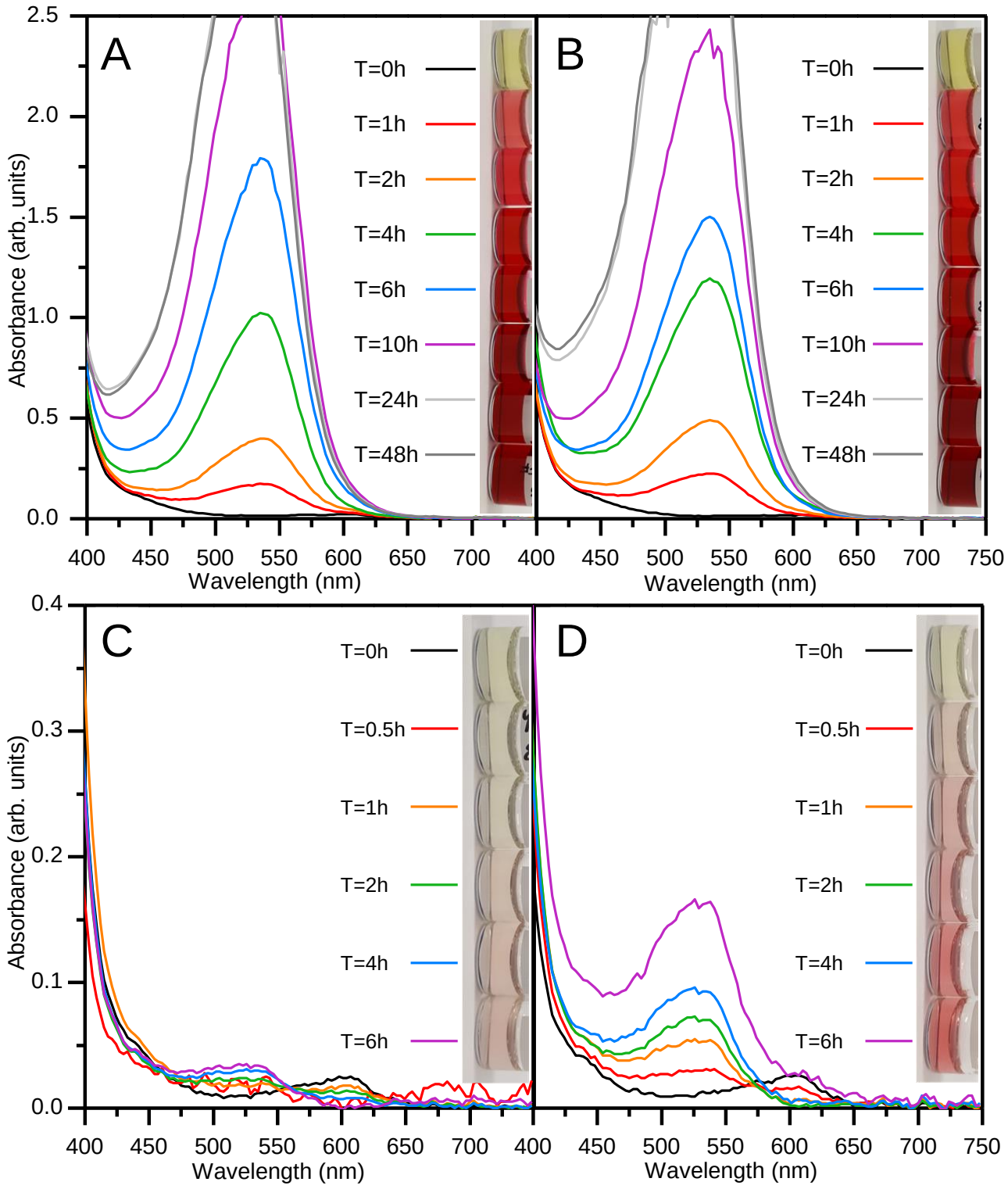

Figure 7.14: UV-Vis spectra of kinetic polymerisation reaction mixture samples (shown inset) with spiro-XEP: MA under dark + AIBN (A) and light + AIBN conditions (B). VAc under dark + AIBN (C) and light + AIBN conditions (D).

The control experiments previously conducted without AIBN (data given in Table 7.2) in which the polymerisation solutions were exposed to UV irradiation (light only conditions) and gave measurable conversion showed a colour change to red (Figure 7.15). The dark only control samples (that did not give any conversion) visually appeared unchanged; this was confirmed by the absence of any extra

spectral features and overlapping spectra for samples before (T = 0 h) and after heating in the dark with monomers for 10 h (Figure 7.15). From these results it is evident that AIBN radicals were not responsible for the colour changes seen; instead polymer formation from the spiro-XEP agent appears to be important. Furthermore, just as for the kinetic samples analysed in Figure 7.14, the control experiments conducted with VAc show more vivid colour changes than those with MA (Figure 7.15), indicating that the nature of the monomer used plays a role. In Figure 7.15 the peak absorbance wavelength was 526 nm for MA and 535 nm for VAc samples which suggests that similar species are responsible for the colours seen.

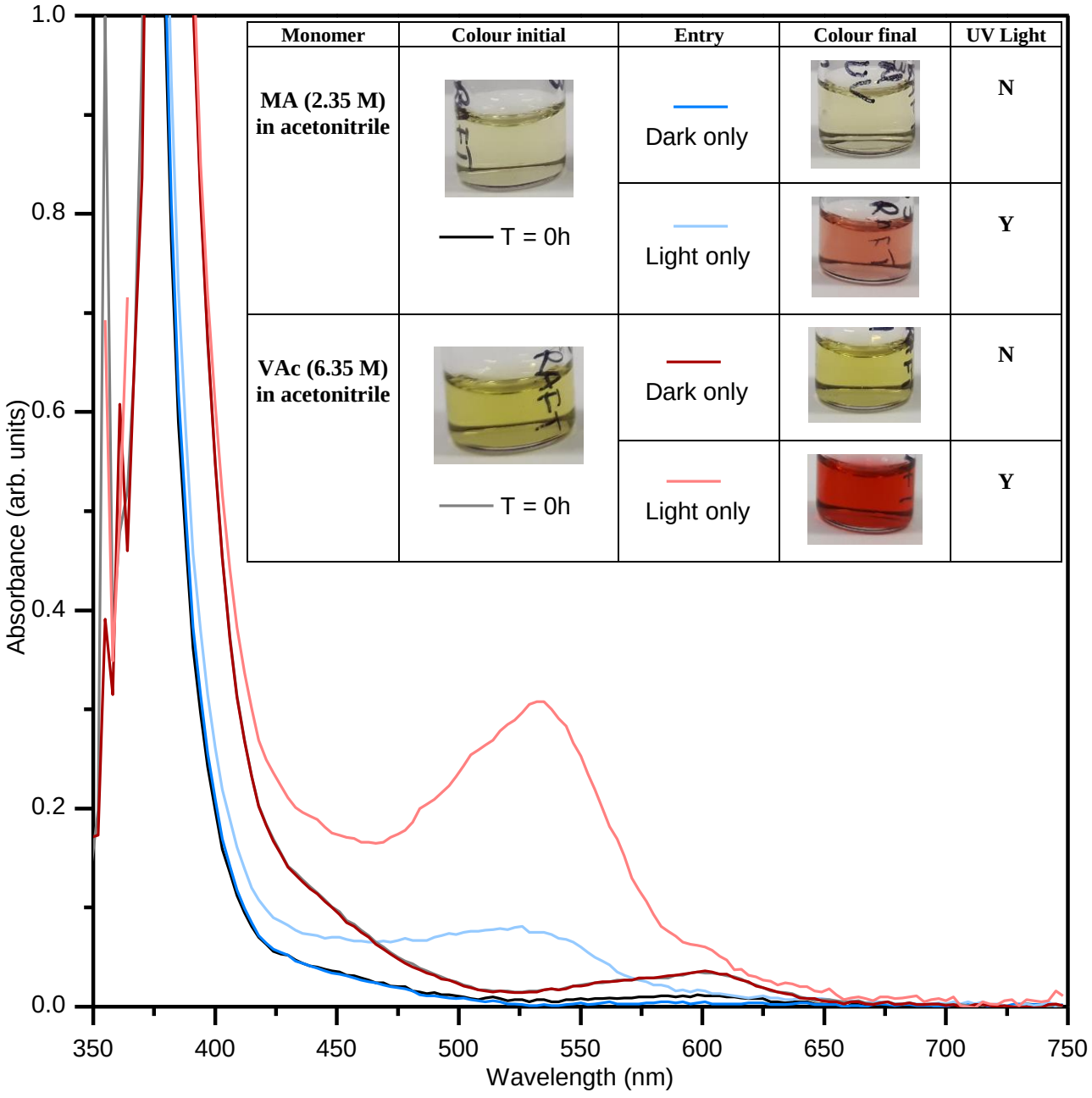

Figure 7.15: UV-Vis spectra of reaction mixture samples of control experiments conducted with MA and VAc without AIBN. Inset: images of samples corresponding to data shown along with a summary of reaction conditions, reaction time = 10 h in all cases.

The peak absorbance values from Figure 7.14 were normalised by concentration of spiro-XEP to account for the different starting concentrations of spiro-XEP which were ~ 2.65 x higher in VAc experiments relative to MA experiments. This allowed a qualitative comparison of the peak absorbance values for both monomers as a function of several variables, as shown in Figure 7.16.

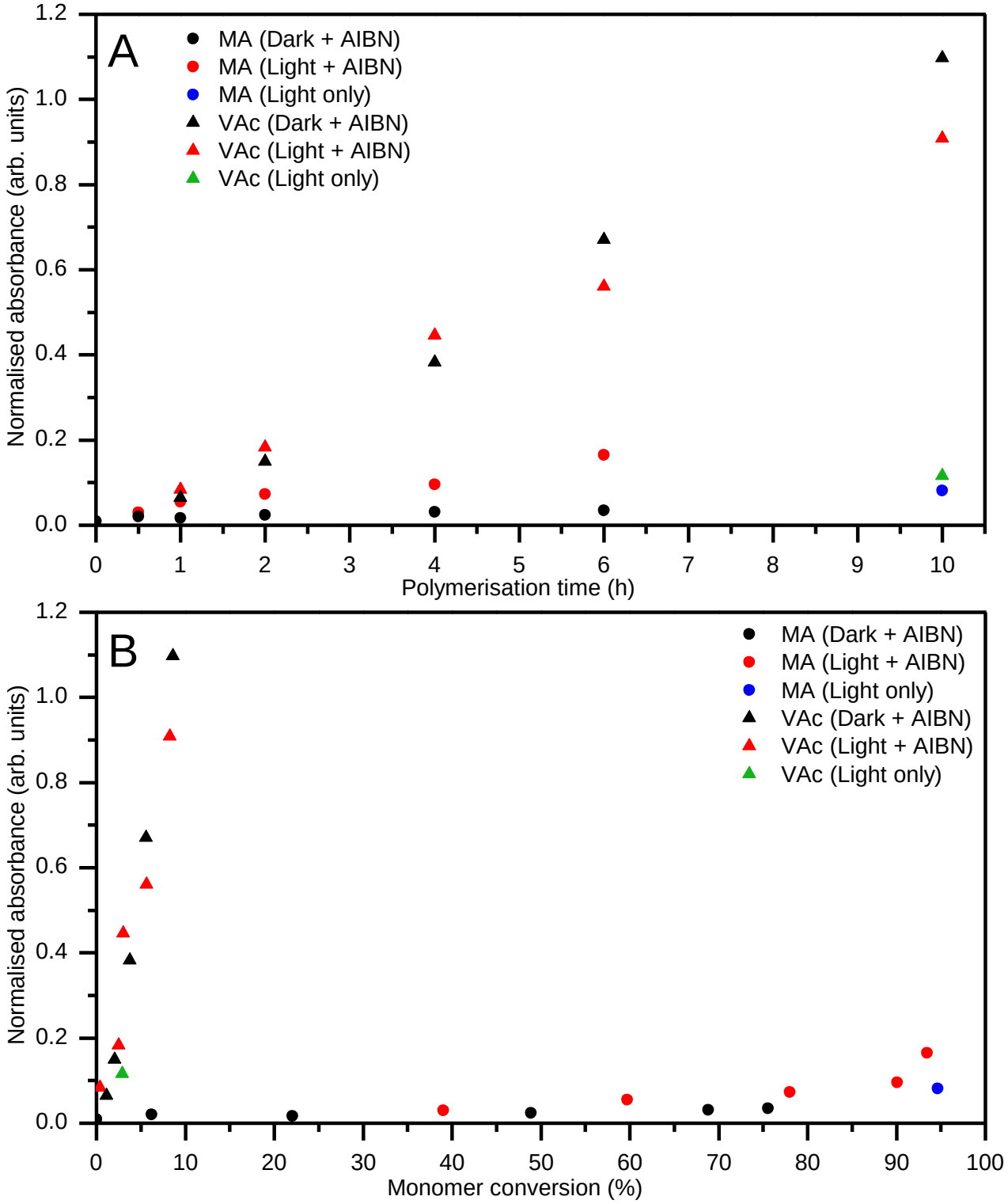

Figure 7.16: Normalised absorbance at peak wavelength (526 nm for MA, 535 nm for VAc) vs polymerisation time (A) and vs monomer conversion (B).

For MA and VAc polymerisations featuring AIBN there is a linear correlation between the peak absorbance and both polymerisation time (Figure 7.16, A) and monomer conversion (Figure 7.16, B). For the control experiments conducted without AIBN under light only conditions, only the MA sample (Figure 7.16, A, blue circle) aligns with the general trend set by the MA kinetic samples (Figure 7.16, A, red and black circles) as a function of polymerisation time; the VAc control (Figure 7.16, A, green triangle) and VAc kinetic samples (Figure 7.16, A, red and black triangles) do not align with one another.

Figure 7.16 (B) shows that for both monomers the absorbance increases in a linear fashion as conversion increases and that this relationship distinctly segregates all experiments by the monomer used. It is evident that the increase in absorbance is much more significantly impacted by conversion for VAc (Figure 7.16, B, triangles) than for MA (Figure 7.16, B, circles).

The linear correlations between the conversion attained and the intensity of the colour change seen which were distinctly separated by monomer type raises three possible explanations for this phenomenon. Firstly, that the presence of a polymer "tail" attached to the spiro-XEP is altering the spiro-XEP molecule in such a way as to change its electronic and thus spectral properties, and that this is related to the molecular weight of the tethered polymer. Secondly, that the spirooxazine Z group is causing the RAFT adduct to be exceptionally stable, thus effectively trapping the RAFT adduct radical by "locking" the spirooxazine in an open merocyanine form. Thirdly, that this is a radical driven process whereby radicals are reacting in some way with the spiro-XEP molecule outside the addition and fragmentation or photoiniferter processes that occur at the RAFT moiety.

7.6.1 Polymer tail explanation

To test whether the presence of a monomer "tail" was required for the colour change to occur, another series of control experiments was conducted under all 3 polymerisation conditions (dark + AIBN, light + AIBN and light only), however this time in the absence of any monomer. The same reaction time of 10 h and concentration of spiro-XEP as that used in the kinetic polymerisations of VAc was employed to maximise any potential colour changes seen. Two solvent systems were used; pure acetonitrile and the other a mixture of ethyl acetate in place of VAc but at the same molar percentage as VAc (giving 64 : 36 (v/v) ethyl acetate : acetonitrile) in order to mimic the polarity of the VAc system.

As shown in Figure 7.17, the dark + AIBN samples changed to a mild orange colour, with the spectral profile being almost being identical for both solvent systems (Figure 7.17, dark blue and brown traces). The pure acetonitrile solvent system showed the greatest colour change to dark red with both

light + AIBN and light only conditions, having a higher absorbance in the ~ 530 nm region (Figure 7.17, blue and light blue traces respectively) than the equivalent reaction conditions in the acetonitrile ethyl acetate mixture (Figure 7.17, red and light red traces). As acetonitrile is more polar than ethyl acetate, this indicates that the process leading to the colour change in the absence of monomer radicals favours a more polar solvent system.

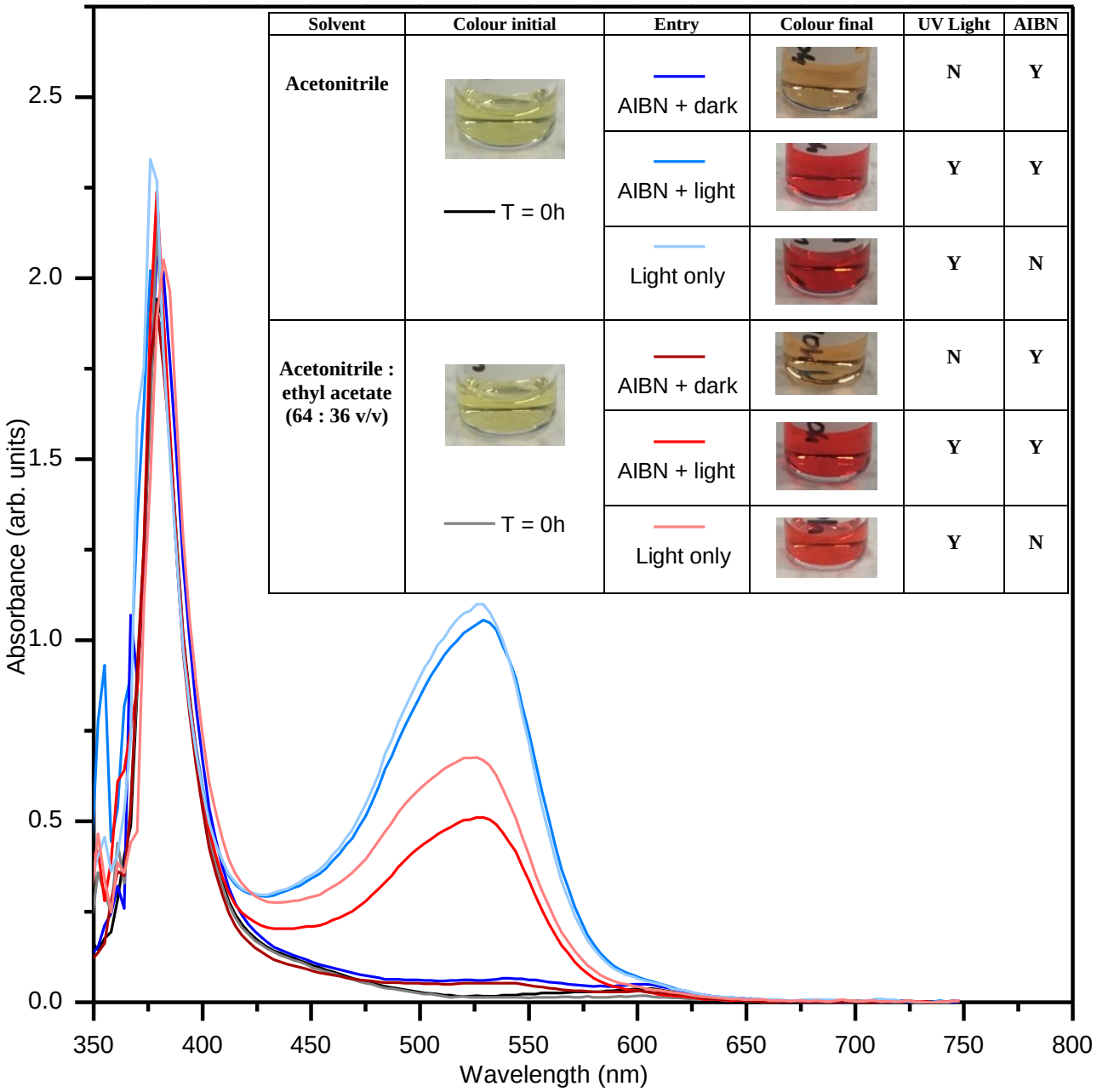

Figure 7.17: UV-Vis spectra of reaction mixture samples of control experiments conducted in the absence of monomers. Inset: images of samples corresponding to data shown along with a summary of reaction conditions, reaction time = 10 h in all cases.

Given the evidence from this series of control experiments, it can be concluded that the process leading to the formation of the coloured species does not require the conversion of spiro-XEP to a

macro-RAFT species. Instead, a simple radical source is required, whether through the breakdown of a conventional radical initiator like AIBN or direct photolysis of spiro-XEP.

The colour changes seen during polymerisations with spiro-XEP are unique insofar that similar behaviour has not been reported with other spirooxazine based RDRP agents used during polymerisations, the conditions of which are summarised in Table 7.9.

Table 7.9: Summary of polymerisation conditions used with spirooxazine based RDRP agents found in literature.

RAFT agent	RAFT agent : Initiator : Monomer	Monomer	Ref.
SOX-RAFT	1 : 0.05 : 250	NIPAM	[3]
Poly(NIPAM)-SOX-RAFT	1 : 0.05 : 92	NAM	[3]
SOX-RAFT	1 : 0.05 : 81	n-BA	[6]
SOX-RAFT	1 : N/A : 102	Sty	[6]
SOX-RAFT	1 : N/A : 200	Sty	[6]
Poly(sty)-SOX-RAFT	1 : 0.05 : 100	n-BA	[6]
Poly(sty)-SOX-RAFT	1 : 0.05 : 200	n-BA	[6]
Poly(n-BA)-SOX-RAFT	1 : 0.05 : 100	Sty	[6]
Poly(n-BA)-SOX-RAFT	1 : N/A : 100	Sty	[6]
ATRP initiator	**ATRP initiator : Catalyst : Ligand : Monomer**	**Monomers**	**Ref.**
SOX-ATRP 1	1 : 1 : 2 : 100	Sty	[4]
SOX-ATRP 2	1 : 1 : 2 : 100	MMA	[5]

The occurrence of red colouration was absent in all cases where polymers derived from both the SOX-RAFT agent [6] and from the SOX-ATRP agents [4, 5] along with the parent spiro-OH compound functionalised with oligomeric tails [15] were incorporated into plastic ophthalmic lenses. In all cases the photochromic polymer conjugates were mixed and polymerised in a standardised formulation of a 1 : 4 wt ratio of poly(ethylene glycol) 400 dimethacrylate (9G) and 2,2′-bis[4-methacryloxyethoxy]phenyl]propane, initiated with 0.4 wt % AIBN [4-6, 15]. This gives a ratio of 1 : 20 : 1935 of the photochromic derivative : AIBN : total monomers.

One of the key differences between the VAc polymerisations undertaken with spiro-XEP and those listed in Table 7.9 is that the SOX-RAFT agent is a trithiocarbonate and is thus expected to be significantly more reactive towards radical addition than spiro-XEP which is a xanthate. Trithiocarbonates typically have kinetic rate coefficients for radical addition which are orders of magnitude greater than xanthates [12] which inherently means that for a spirooxazine based trithiocarbonate any propagating radicals are more likely to add to the RAFT moiety instead of the

other potentially reactive sites on the spirooxazine moiety. Such reactions would lead to potential by-products, as is discussed later in section 7.6.3.

Furthermore, all the monomers polymerised with the SOX-RAFT agent are MAMs which yield propagating radicals much less reactive than the highly reactive VAc radical. The lens formulations described [3-6] do feature more AIBN than photochromic additive by molar equivalents, however the photochromics are by design shielded from the bulk of the reaction mixture by encapsulation due to their polymer "tails". Furthermore, once again the monomers used are in a large excess to AIBN and will form comparatively unreactive radicals due to both being methacrylate derivatives.

7.6.2 Trapped RAFT adduct radical explanation

As shown in Scheme 7.6, it is possible the spiro-XEP molecule is being "trapped" or locked in the open state as a RAFT adduct radical. It can be speculated that such an adduct radical could be stabilised by delocalisation throughout the merocyanine isomers and subsequently change the spectral properties of the photochromic moiety.

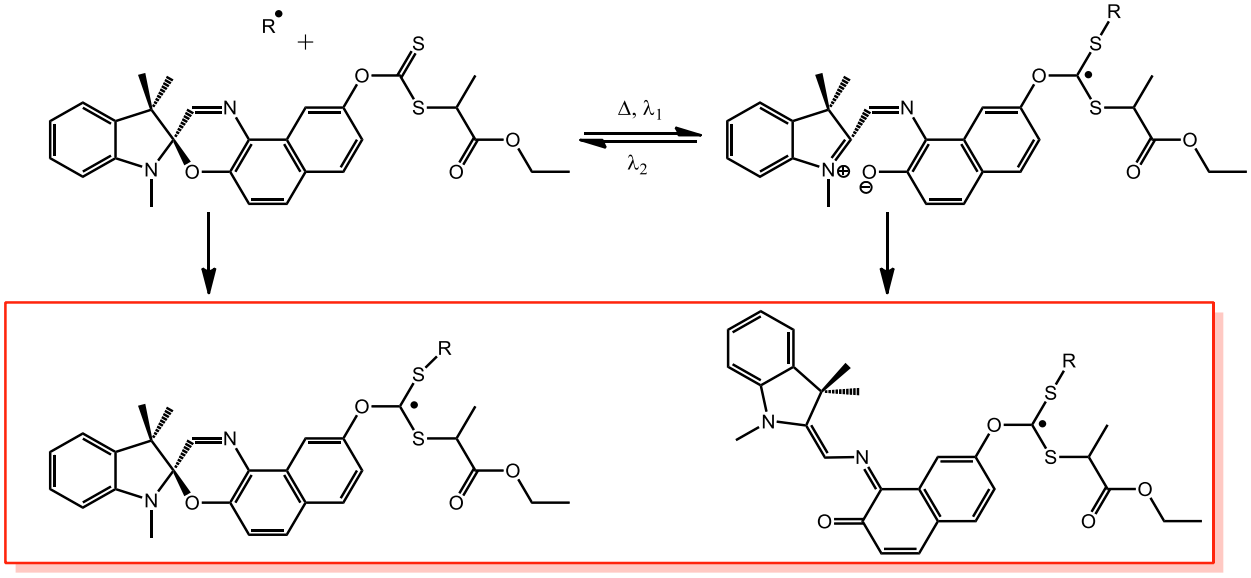

Scheme 7.6: Potential reactions leading to the formation of a highly coloured RAFT adduct radical from spiro-XEP (highlighted in red).

The higher absorbances seen with VAc could correspond to higher RAFT adduct radical concentrations; it was shown via Predici modelling of the polymerisations with PXEP that VAc leads to a higher percentage of radicals within the polymerisation mixture existing as the RAFT adduct radical (see Chapter 6, section 6.7). However, based on the Predici simulations, the percentage of the RAFT species existing as RAFT adduct radicals was calculated to be 2.86 $x10^{-4}$ % for VAc and 1.43 $x10^{-4}$ % for MA, with the remainder existing as dormant RAFT capped polymers. For VAc

polymerisations, the resulting absolute concentration of RAFT adduct radicals is predicted to be 1.03 $x10^{-7}$ M. Thus if the concentration of RAFT adduct radicals with spiro-XEP is on the same order of magnitude, with the optical pathlength for all UV-Vis measurements presented within this section (7.6) being 1 mm and assuming an absorbance of 1 is obtained, this means that the trapped RAFT adduct radical would have an extinction coefficient of ~ 9.71 $x10^{7}$ M^{-1} cm^{-1}. As this is unrealistic, the possibility that the colour arises due to the RAFT adduct radical is highly unlikely.

Given the reactive nature of radical species, it seems unlikely that such a radical adduct would survive the isolationg and purification process that the poly(MA) and poly(VAc) macroinitiators were subjected to (detailed previously in Chapter 4, section 4.5.7.2.) prior to chain extension experiments. However these macroinitiators did retain their intense colour through the purification process, which could be analysed when they were reconstituted into the chain extension reaction mixtures as shown in Figure 7.18. The possibility that the colour arises from the trapped RAFT adduct radical is highly unlikely considering that the isolation of such a radical species has also never been reported in the literature.

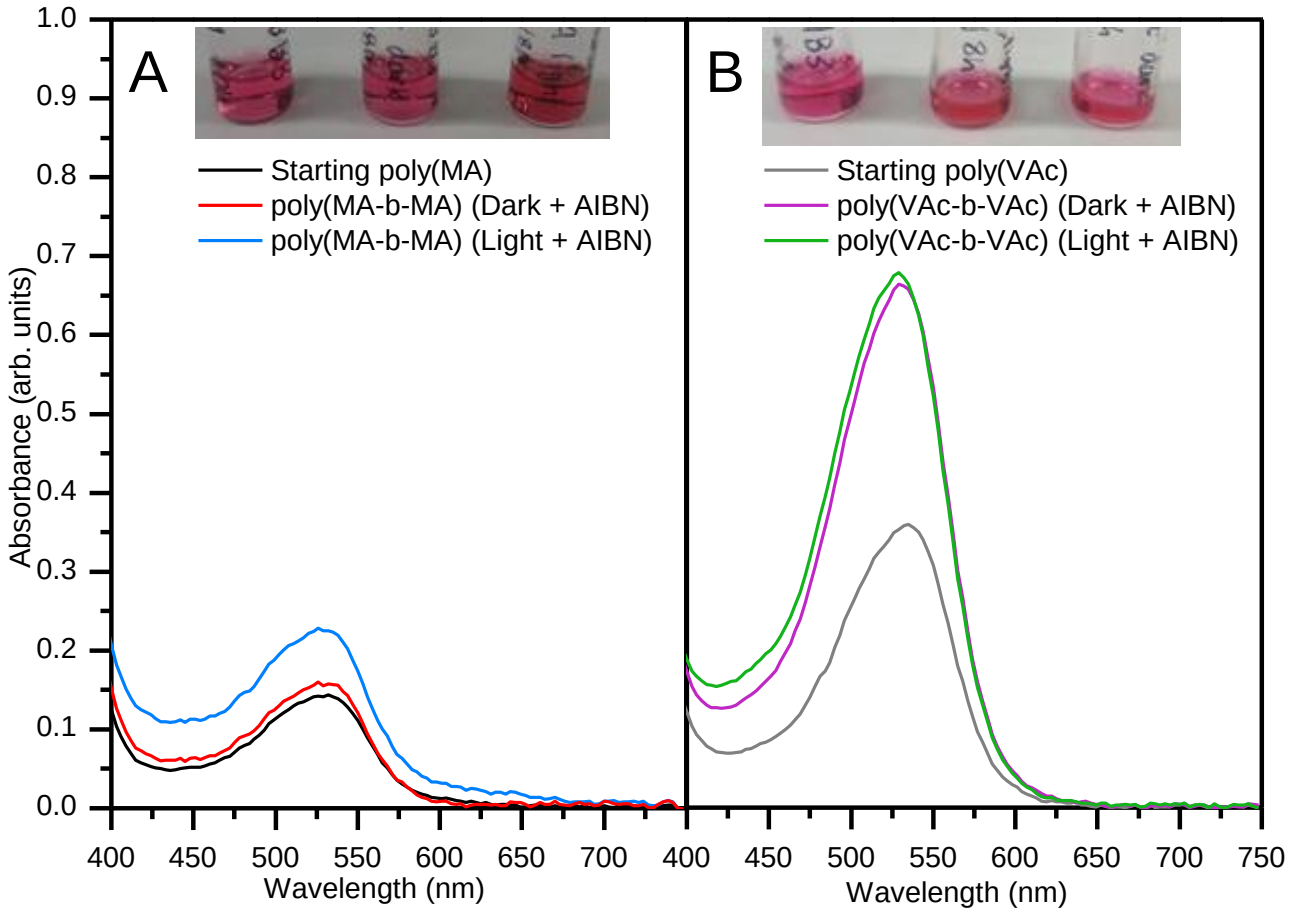

Figure 7.18: UV-Vis spectra of reaction mixture samples of MA chain extension (A) and VAc chain extension (B) experiments conducted with macroinitiators derived from spiro-XEP, with samples shown inset.

7.6.3 Non-reversible degradation of spirooxazine moiety explanation

The third possible explanation is that the colour changes seen arise from the degradation of the spirooxazine moiety, with several such possibilities having literature precedent. As applied to spiro-XEP, their structures are shown in Figure 7.19.

Free Radical Adducts (FRAs) of the form of FRAs 1 in Figure 7.19 have been reported to form by the addition of radicals derived from AIBN or di-tert-butyl peroxide across the 5'=6' bond in the merocyanine structure [16]. The process occurs predominantly at the 6' position but can also occur at the 5' position, with the radicals then terminating by hydrogen abstraction. These products were found to be intensely red in colour, having absorption maxima in the range 518 – 556 nm, with very large extinction coefficients ranging from 14,000 – 57,000 M^{-1} cm^{-1}. The formation of FRAs was associated with a loss in photochromic activity, however they were found to bleach when exposed to air and irradiated with visible light.

The second (FRAs 2) structure is proposed to arise based on the finding that spirooxazines can undergo the C-O bond breaking process by the formation of a bi-radical species via a homolytic process [17, 18] as opposed to heteroltyic cleavage which leads to the charge separated zwitterionic isomers. This thus leads to the possibility of the diradical species coupling with free radicals such as those formed from the photolysis of the R group, MA or especially VAc. Various mechanisms relying on the presence of the diradical species in conjunction with molecular oxygen are proposed to lead to the formation of both the oxidised and the cleaved forms of the degradation products [8]. The oxidised form is known to occur after irradiation in aerated acetonitrile as reported by Malatesta *et al.* [16] and within polymer matrices which are assumed to be largely free of oxygen [9]. Malatesta *et al.* later showed that in the presence of an electron acceptor this process can occur in the dark via a thermal route [7].

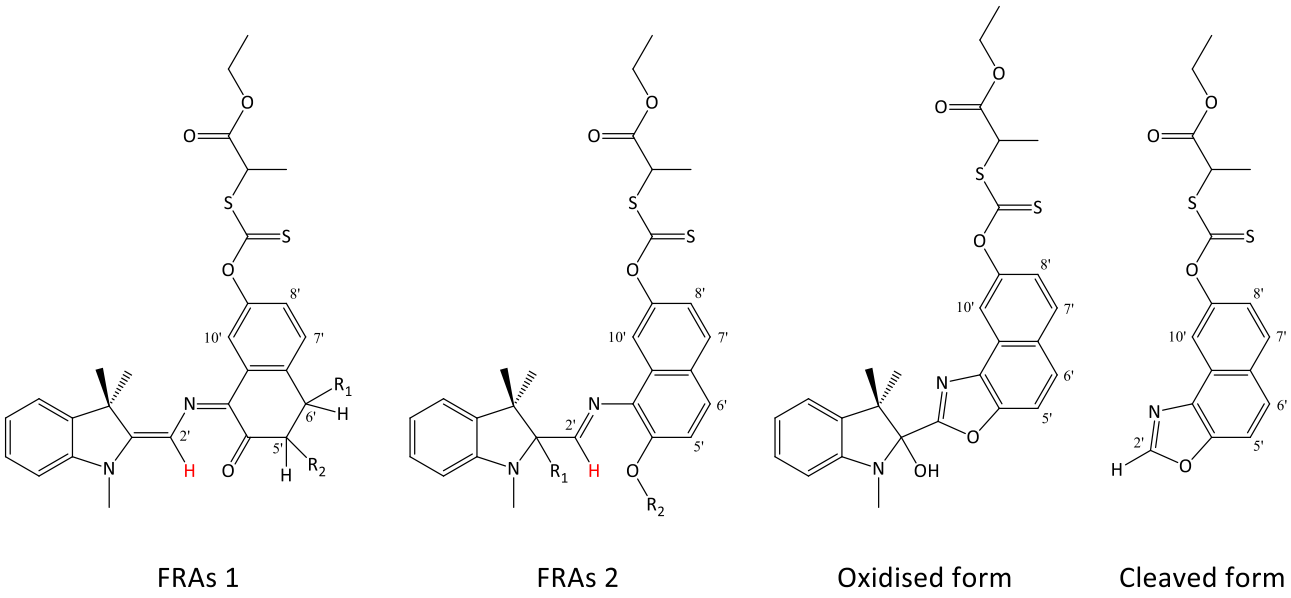

Figure 7.19: Possible by-products generated from reaction of spiro-XEP with radical species. All shown in the most likely TTC isomer.

^{1}H NMR analysis of the acetonitrile reaction mixtures run under light + AIBN and light only conditions (Figure 7.20) after removal of volatiles reveals extra resonances (marked with asterisks) that support the hypothesis that the oxidised form of spiro-XEP is forming. Relative to the resonances from the N-CH_3 group, the integrations for the resonances attributed to protons 4, 6', 2' 7' and 10' are 80 – 85 % as compared to the starting spiro-XEP, with the new resonances (marked with asterisks) integrating for a complimentary 15 – 20 %. There is no decrease in the integration values for the 5' and 8' resonances, however this is due to overlap of resonances from the by-products as evident from resonances broadening and visibly overlapping with others. For the MA + light only sample, the resonances in the aromatic region closely match those seen under both light only and light + AIBN conditions. This implies the formation of similar by-products; however, their abundance could not be estimated due to the resonances used as references (those from the methyl groups present on the indole) showed significant overlap with resonances attributed to the poly(MA).

For the control experiment with VAc, the resonances attributed to the 4, 2' and 10' protons show only a 5 – 15 % decrease in integration, however completely different resonances between 6.6 – 6.9 ppm are seen to form along with those previously seen under all other experimental conditions. These new resonances integrate for a ~ 50 % of the value of the other aromatic resonances attributed to single protons, which potentially implies the formation of significant quantities of this other by-product. Overall this supports that theory that with VAc present, other unique by-products are formed which most likely arise due to the presence of highly reactive VAc radicals.

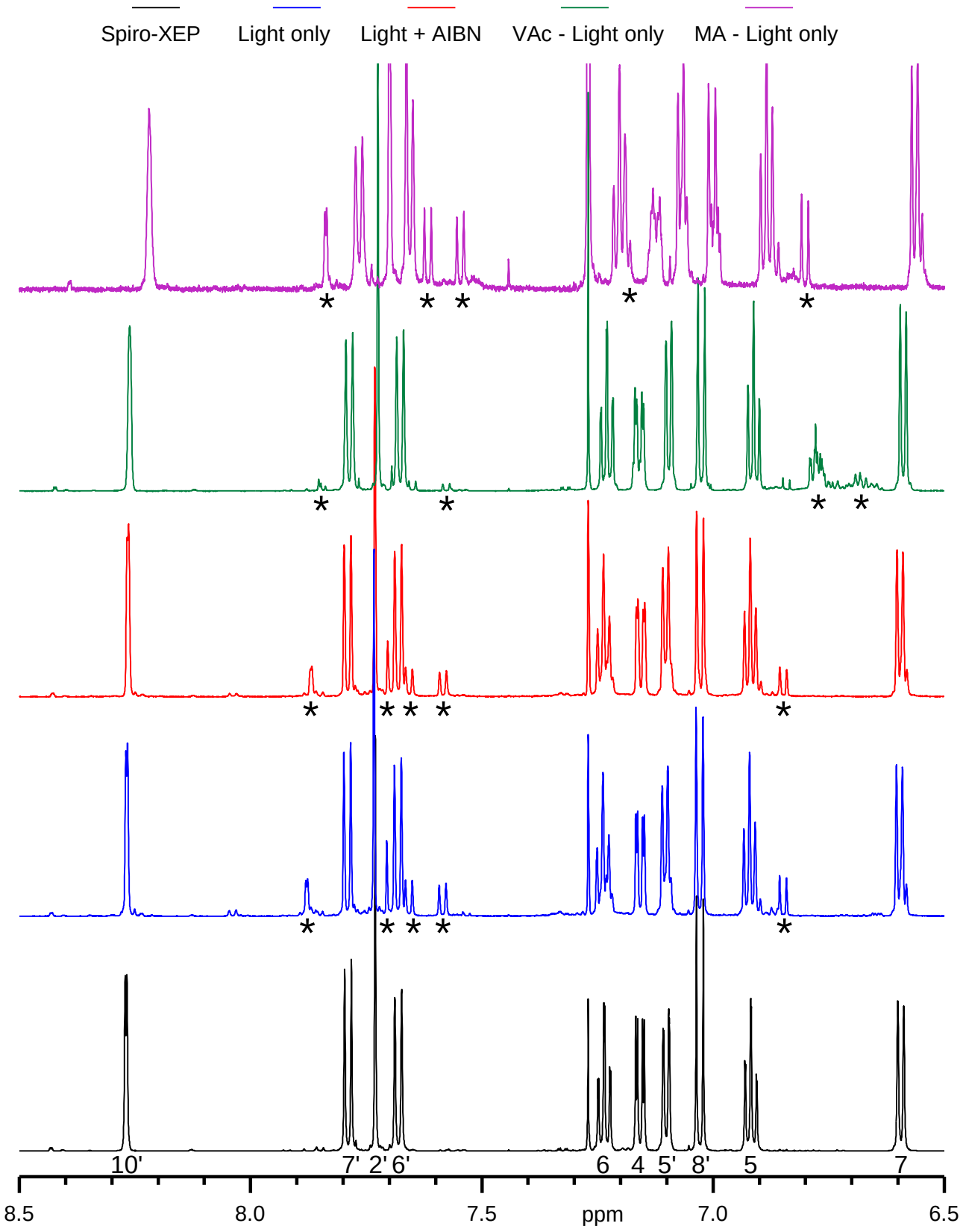

Figure 7.20: Comparison of ^{1}H NMR spectra showing the aromatic region for samples after control experiments (coloured traces) and spiro-XEP prior (black trace).

Regardless of whether they are from the FRAs [16] or from spirooxazines functionalised with oligomeric tails [15] which were locked open as a combination of TTC and CTC isomers [19], the resonance from the proton at the 2' position (marked in red, Figure 7.19) is always significantly downshifted by around 2 ppm relative to the 10' resonance. This makes the 2' resonance very distinct, as the 10' resonance is usually the most downshifted in a ^{1}H NMR spectrum of these compounds in their closed spirooxazine form. There are no resonances attributed to the 2' protons seen in Figure 7.21, with the most downshifted resonances being those attributed to the 10' proton which remains unchanged in its position relative to that seen for the starting spiro-XEP (Figure 7.21, black trace). This is key additional evidence against both the "polymer tail" and "trapped RAFT adduct" explanations.

Further support of the oxidised form of spiro-XEP being generated during irradiation is the presence of a new broad resonance which is typical of a hydroxyl group; this is seen for the light only, light + AIBN and MA + light only samples (Figure 7.21, blue, red and purple traces respectively, marked with an asterisk). This was not seen for the VAc + light only case, further supporting the hypothesis that the coloured by-products are potentially different to those obtained under the other reaction conditions tested.

As was previously shown by ^{1}H NMR analysis (see Figure 7.11), during VAc polymerisations spiro-XEP was consumed over ~ 2 h under light + AIBN and ~ 4 h under dark + AIBN conditions, during which the polymerisation mixture darkened to a deep red colour (Figure 7.14, A & B). Considering the ^{1}H NMR spectra shown in Figure 7.20 and Figure 7.21, this indicates that by whichever mechanism the coloured species is being generated, it is happening in tandem with the consumption and conversion of spiro-XEP into the macro-RAFT species.

Using the conservative estimate that 10 % of the spirooxazine moiety is irreversibly degraded under light only conditions with VAc (based on Figure 7.20 and Figure 7.21), this gives the concentration of the colour causing species to be ~ 3.60 x10^{-3} M. Using the same assumptions and calculation method as in section 7.6.2, the extinction coefficient for this degraded spirooxazine species is estimated to be 2.78 x10^{3} M^{-1} cm^{-1}. This is well within the range of extinction coefficients typically seen for transitions of both spirooxazine degradation products [16] and RAFT agents [20].

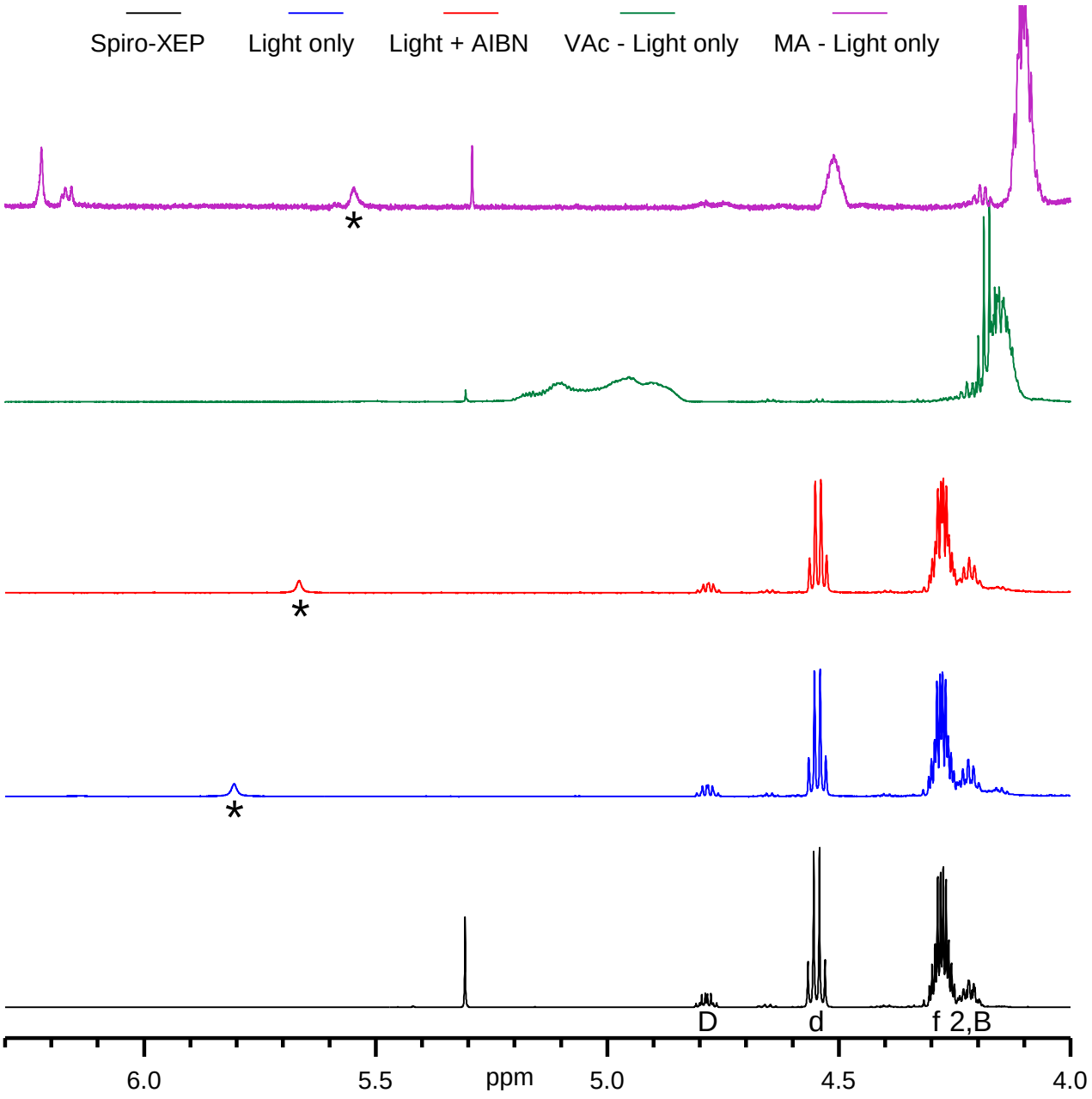

Figure 7.21: Comparison of ^{1}H NMR spectra for samples after control experiments (coloured traces) and spiro-XEP prior (black trace).

Taken holistically, the data suggests that post the colouration process to dark red, the spiro-XEP no longer has the original spirooxazine structure and instead has a structure more akin to a permanently open merocyanine form. For this reason, the new red coloured form of spiro-XEP can be expected to have different reactivity towards radical addition and potentially radical fragmentation. The *ab initio* modelling results showed that the open form of spiro-XEP has a ΔH_{frag} value comparable to a trithiocarbonate, meaning it is expected to retard the polymerisation of unstable propagating radicals such as those of VAc, whilst simultaneously not retarding the polymerisation of MAMs such as MA. Thus, it seems plausible that the red coloured form of the spiro-XEP could be responsible for the

significantly retarded rate of polymerisation seen when it is used in VAc polymerisation, whilst no such was seen with MA polymerisations.

7.7 Conclusions

Spiro-XEP was able to control the polymerisation of MA under both dark + AIBN and light + AIBN conditions, giving polymers with low dispersities (D < 1.25) and close agreement between obtained and expected molecular weights. Under equivalent reaction conditions a spiro-XEP poly(MA) macroinitiator was successfully chain extended to yield higher molecular weight poly(MA) polymers. There was no evidence to suggest that UV irradiation changes the reactivity of the spiro-XEP compound in the context of the RAFT mechanism. Instead, a conventional enhancement in the rate of polymerisation by a factor of 2.67 x, attributed to the photoiniferter effect was observed, however this was significantly decreased relative to the non-photochromic analogue PXEP which showed an enhancement factor of 10 x. This difference was attributed to competitive absorption by the spirooxazine moiety leading to photochromic ring opening and the absorption by the RAFT moiety leading to the photoiniferter effect.

When utilised with VAc, spiro-XEP showed significant retardation of polymerisation rate which was only ~ 2 % the rate obtained with the non-photochromic analogue PXEP under equivalent reaction conditions. Unlike for PXEP which showed a modest increase in polymerisation rate of ~ 15 %, application of UV light with spiro-XEP had no impact on the rate of polymerisation. Notwithstanding, the poly(VAc) polymers generated showed good agreement between obtained and expected molecular weights and had narrow dispersities (D < 1.2). Furthermore, the retardation in polymerisation rate also applied to chain extension experiments conducted with purified poly(VAc) macroinitiators, which nevertheless allowed successful chain extension to form narrow dispersity high molecular weight poly(VAc).

A range of colour changes in the polymerisation mixtures and resulting polymers from green to dark red were seen with MA, however this was much more striking with VAc. These changes were found to persist upon isolation of the polymers by removal of volatiles, and the absorbances were found to linearly correlate with monomer conversion. Furthermore, it was deduced that these colour changes could be induced when spiro-XEP was exposed to both thermally generated AIBN derived radicals and by direct photolysis of spiro-XEP. It is speculated that these colour changes are directly related to the rate retardation seen with VAc, due to this colour most likely being associated with a permanently open form of the spiro-XEP structure. The exact structure of the highly coloured red

species was not conclusively identified; however, evidence supports the formation of an oxidised open spirooxazine structure.

7.8 References

1. Beija, M., M.T. Charreyre, and J.M.G. Martinho, *Dye-labelled polymer chains at specific sites: Synthesis by living/controlled polymerization.* Progress in Polymer Science, 2011. **36**(4): p. 568-602.
2. Malic, N., et al., *Controlling Molecular Mobility in Polymer Matrices: Synchronizing Switching Speeds of Multiple Photochromic Dyes.* Macromolecules, 2010. **43**(20): p. 8488-8501.
3. Ercole, F., et al., *The application of a photochromic probe to monitor the self-assembly of thermosensitive block copolymers.* Soft Matter, 2011. **7**(6): p. 2687-2696.
4. Such, G.K., R.A. Evans, and T.P. Davis, *Control of Photochromism through Local Environment Effects Using Living Radical Polymerization (ATRP).* Macromolecules, 2004. **37**(26): p. 9664-9666.
5. Such, G.K., R.A. Evans, and T.P. Davis, *Tailoring Photochromic Performance of Polymer-Dye Conjugates Using Living Radical Polymerization (ATRP).* Molecular Crystals and Liquid Crystals, 2005. **430**(1): p. 273-279.
6. Such, G.K., R.A. Evans, and T.P. Davis, *The Use of Block Copolymers to Systematically Modify Photochromic Behavior.* Macromolecules, 2006. **39**(26): p. 9562-9570.
7. Malatesta, V., R. Millini, and L. Montanari, *Key Intermediate Product of Oxidative Degradation of Photochromic Spirooxazines. X-ray Crystal Structure and Electron Spin Resonance Analysis of Its 7,7,8,8-Tetracyanoquinodimethane Ion-Radical Salt.* Journal of the American Chemical Society, 1995. **117**(23): p. 6258-6264.
8. Malatesta, V., *Photodegradation of Organic Photochromes*, in *Organic Photochromic and Thermochromic Compounds - Volume 2 - Physicochemical Studies, Biological Applications and Thermochromism*, J.C. Crano and R.J. Guglielmetti, Editors. 2002, Kluwer Academic Publishers: New York. p. 65-166.
9. Baillet, G., G. Giusti, and R.J. Guglielmetti, *Study of the Fatigue Process and Yellowing of Polymeric Films Containing Spirooxazine Photochromic Compounds*. Vol. 68. 1995. 1220-1225.
10. Such, G., et al., *Factors Influencing Photochromism of Spiro-Compounds Within Polymeric Matrices.* Journal of Macromolecular Science, Part C, 2003. **43**(4): p. 547-579.
11. Keddie, D.J., et al., *Chain Transfer Kinetics of Acid/Base Switchable N-Aryl-N-Pyridyl Dithiocarbamate RAFT Agents in Methyl Acrylate, N-Vinylcarbazole and Vinyl Acetate Polymerization.* Macromolecules, 2012. **45**(10): p. 4205-4215.
12. Coote, M.L., E.H. Krenske, and E.I. Izgorodina, *Quantum-Chemical Studies of RAFT Polymerization: Methodology, Structure-Reactivity Correlations and Kinetic Implications*, in *Handbook of RAFT Polymerization*. 2008, Wiley-VCH Verlag GmbH & Co. KGaA. p. 5-49.
13. Suh, H.J., et al., *The crystalline-state photochromism, thermochromism and X-ray structural characterization of a new spiroxazine.* Dyes and Pigments, 2003. **57**(2): p. 149-159.

14. Li, Y., et al., *Thermo- and Acid-Responsive Photochromic Spironaphthoxazine-Containing Organogelators.* Chemistry – A European Journal, 2010. **16**(29): p. 8690-8698.

15. Evans, R.A., et al., *The generic enhancement of photochromic dye switching speeds in a rigid polymer matrix.* Nature Materials, 2005. **4**: p. 249.

16. Malatesta, V., et al., *Reductive Degradation of Photochromic Spiro-Oxazines. Reaction of the Merocyanine Forms with Free Radicals.* The Journal of Organic Chemistry, 1995. **60**(17): p. 5446-5448.

17. Baillet, G., *Dealkylation of N-substituted Indolinospironaphthoxazine Photochromic Compounds Under UV Irradiation.* Journal of Photochemistry and Photobiology A: Chemistry, 1994. **83**(2): p. 147-151.

18. Alberti, A., *EPR and Radical Processes*, in *Organic Photochromic and Thermochromic Compounds - Volume 2 - Physicochemical Studies, Biological Applications and Thermochromism*, J.C. Crano and R.J. Guglielmetti, Editors. 2002, Kluwer Academic Publishers: New York. p. 211-239.

19. Yee, L.H., et al., *Photochromic Spirooxazines Functionalized with Oligomers: Investigation of Core−Oligomer Interactions and Photomerocyanine Isomer Interconversion Using NMR Spectroscopy and DFT.* The Journal of Organic Chemistry, 2010. **75**(9): p. 2851-2860.

20. Skrabania, K., et al., *Examining the UV-vis absorption of RAFT chain transfer agents and their use for polymer analysis.* Polymer Chemistry, 2011. **2**(9): p. 2074-2083.

8 Copolymers by the photo-RAFT method: effect of RAFT agent class and wavelength of irradiation on overcoming the monomer sequence limitations of the RAFT mechanism

8.1 Introduction

This chapter details the experimental investigations into how the reversible photolysis of macro-RAFT species via the iniferter mechanism can be applied to overcoming the limitations of monomer sequence in block copolymer synthesis imposed by the RAFT mechanism. The synthesis of poly(LAM-b-MAM) type copolymers is attempted, with the identity of the monomers comprising the two blocks being varied in their reactivity to test the extent to which photolysis effects this reaction. This includes the synthesis of poly(MAM1-b-MAM2) copolymers where the second block (MAM2) is still of the MAM class, however has less reactive radicals and in this circumstance behaves more "LAM like" relative to the first block (MAM1). The specific monomers tested include MA and VAc, MMA and Sty. The synthesis attempted includes poly(MA-b-VAc), poly(VAc-b-MA), poly(Sty-b-MMA) and poly(MA-b-MMA) block copolymers. The exemplary synthesis of poly(MMA-b-X) where X = MA or Sty and the likely products formed under the mechanisms operating are shown in Figure 22.

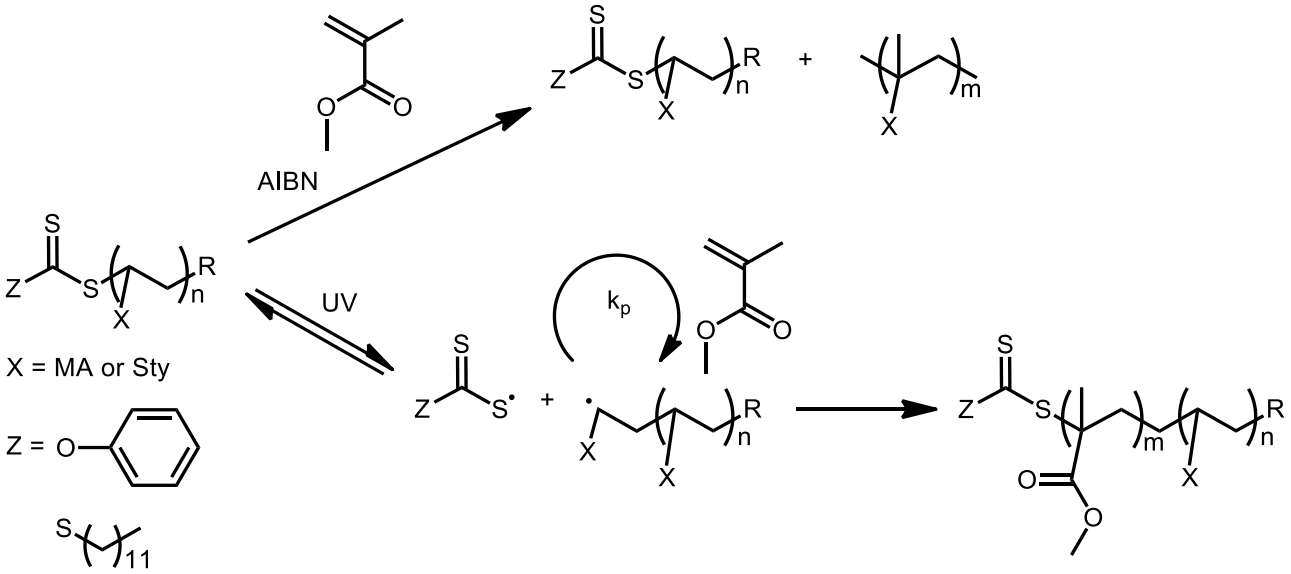

Figure 22: Expected products for the chain extension of poly(X) (X=MA or Sty) with MMA via conventional initiation and the RAFT mechanism (top) and the photoiniferter method (bottom).

Due to MA and VAc having very disparate reactivities in both their monomer and propagating radical forms, the synthesis of poly(MA-b-VAc) and poly(VAc-b-MA) presents the opportunity of testing the limits of this approach. The monomer sequence in poly(MA-b-VAc) is "allowed" as per the RAFT mechanism; the highly reactive VAc radicals will rapidly form the RAFT adduct radical with the poly(MA) macroinitiator. This is followed by preferential fragmentation of the more stable and less reactive poly(MA) propagating radical which can then reinitiate polymerisation by adding VAc monomer.

Conversely, the sequence in poly(VAc-b-MA) is expected to result in a mechanism that functions as a free radical polymerisation of MA with little to no formation of the desired copolymer product. This would be a result of the low reactivity of MA oligomeric radicals not adding rapidly to the poly(VAc) macroinitiator. However the more important consideration is that even if addition occurs and the RAFT adduct radical is formed, it is expected that the MA oligomeric chain would fragment preferentially instead of the poly(VAc) chain, thus preventing the formation of the desired copolymer.

Combinations of MA, MMA and Sty monomers and the synthesis poly(Sty-b-MMA) and poly(MA-b-MMA) block copolymers provides insight into the photoiniferter process when the difference between monomer and propagating radical reactivities is a lot less extreme than between MA and VAc.

Macro-RAFT agents derived from PXEP and Spiro-XEP are used, along with ones synthesised using S-1-dodecyl-S'-((2-ethoxycarbonyl)-ethyl) trithiocarbonate (henceforth referred to as DECET). Macro-RAFT agents based on DECET present a unique opportunity to study both how the radical trapping ability of the macro-RAFT species and irradiation wavelength potentially influence the success of the photolysis reaction.

Furthermore, based on the successful chain extension of poly(MA), poly(VAc) and macroinitiators derived from Spiro-XEP as shown in Chapter 7, the possibility of Spiro-XEP providing an advantage in synthesising block copolymers with unconventional block sequences was investigated. Comparing block copolymers synthesised with both Spiro-XEP and the nonphotochromic analogue PXEP allows deduction of whether UV irradiation causes any tangible mechanistic effects via switching of the photochromic Z group beyond simply enabling the photoiniferter effect to occur.

8.2 Experimental procedures

Please refer to Chapter 4, sections 4.5 for relevant experimental procedures used in the synthesis of macroinitiators and copolymers within this section. For polymer samples analysed on the single detector GPC system, the molecular weights are given directly as polystyrene equivalents. For

polymer samples analysed on the dual detector GPC system, the molecular weights are given directly as polymethyl methacrylate equivalents. In both cases the molecular weight data analysed came from the refractive index (RI) detector.

For samples analysed on the dual detector GPC system, very large data sets were obtained from the photodiode array (PDA) detector in the 250 – 400 nm range; only data at 305 nm corresponding to absorbance by the RAFT moiety was used.

All samples prepared for analysis and analysed on the single detector GPC system were done so by the candidate. Approximately two thirds of the samples prepared for analysis and analysed on the dual detector GPC system were done so by Dr. Guoxin Li at CSIRO, Clayton. All subsequent data processing of raw data into GPC traces as utilised within this thesis along with interpretation of the results was done so by the candidate.

8.3 Copolymers of MA and VAc with PXEP – limitations of monomer order

Firstly, the synthesis of poly(MA-b-VAc) which is allowed under RAFT monomer guidelines was under taken. A short poly(MA) macroinitiator was synthesised from PXEP using the same conditions as employed previously for the kinetic polymerisations of MA in Chapter 5. Similarly, the conditions for the polymerisation of VAc to form the poly(MA-b-VAc) copolymer were the same as those used for the kinetic polymerisation of VAc in Chapter 6. The ratio of PXEP/macroinitiator to the monomers was adjusted such that the theoretical M_n at 100 % conversion was 2000 g/mol for both poly(MA) and poly(VAc) macroinitiators. Similarly, the target M_n for both poly(MA-b-VAc) and poly(VAc-b-MA) copolymers was 25,000 g/mol. As the same 6 W UV lamp (370nm, 2 mW/cm^2) was used for irradiation, overlap with the n $\rightarrow$ π^* transition was guaranteed, a shown previously for poly(MA) and poly(VAc) macroinitiators in Chapter 5 (section 5.3.3) and Chapter 6 (section 6.3.3) respectively.

The GPC trace of the starting poly(MA) shows both the RI and PDA peak are symmetrical and gaussian in shape while being almost superimposable (Figure 8.1, A), with both features implying high chain end fidelity of the macroinitiator which is consistent with the theoretically predicted value of 99.4 % retention of the RAFT moiety as estimated using Equation 4.9. The polymers obtained from the synthesis of poly(MA-b-VAc) under all reaction conditions result in a single monomodal RI peak at lower retention times as can be seen in Figure 8.1 (B, C & D). Similarly, under all reaction conditions the PDA peak appears to overlap only minimally with the position of the peak corresponding to the starting poly(MA) macroinitiator, indicating its high consumption over the

course of the reaction. Both results support the successful formation of poly(MA-b-VAc) block copolymers under both dark + AIBN and light + AIBN conditions.

It is evident that in all copolymer spectra the PDA peak from the RAFT moiety matches the RI peak more poorly than for the starting macroinitiator. This discrepancy most likely arises due to the inter detector delay and the fact the intensity of the PDA signal is proportional to the number of RAFT end groups while the intensity of the RI signal is proportional to the number of monomer units[1]. Hence if the RAFT groups are not evenly distributed amongst all molecular weights, for example, if dead chains are present, then differences in the two signals can be expected. At lower polymer dispersities these factors do not lead to significant differences between the RI and PDA traces, however for polymers with large dispersities these factors manifest as large discrepancies between the signals from the two detectors. This discrepancy is seen in spectra for various block copolymers throughout this chapter and can be attributed to the same cause. Furthermore, this phenomenon is wholly consistent with the spectra obtained for various narrow and broad block copolymers made from both different monomers and RAFT agents that were analysed on this GPC system in the past [2].

The reverse synthesis of poly(VAc-b-MA) which under RAFT monomer guidelines should not be possible was attempted by first polymerising a short poly(VAc) macroinitiator from PXEP using the same conditions as employed previously for the kinetic polymerisations of VAc in Chapter 6. Similarly, the conditions for the polymerisation of MA to form the poly(VAc-b-MA) copolymer were the same as those used for the kinetic polymerisation of MA in Chapter 5.

The starting poly(VAc) macroinitiator suffers from slight tailing towards lower molecular weights as can be seen from both the RI and PDA traces in Figure 8.1 (B); this is consistent with what was seen during chain extension experiments in Chapter 6. The predicted chain end fidelity of the poly(VAc) macroinitiator is 97.9 % as estimated using Equation 4.9, meaning the success of failure of the chain extension process is not expected to be limited by the availability of living chain ends.

For all reaction conditions, similar bimodal RI distributions are seen (Figure 8.1, E, F & G). The larger intensity peak corresponds to polymer formed during the chain extension process, with the smaller peak at higher retention times closely matching the RI peak from the original poly(VAc) macroinitiator. Unlike the RI detector, the response from the PDA detector is not biased towards high molecular weight polymers as explained previously. Thus, irrespective of the relatively small RI peak corresponding to the starting poly(VAc), the PDA spectra are dominated by the peak from the RAFT moiety present on the starting poly(VAc). This shows conclusively that most of the RAFT terminated polymer remain essentially unextended regardless of the conditions used. The secondary PDA peak at lower retention times is not symmetrical; this shows that the RAFT moiety is preferentially located

on the shorter block copolymers, and consequently that photolysis of the RAFT capped poly(VAc) chain ends was slow and gradual, leading to new block copolymer chains being initiated over the course of the polymerisation.

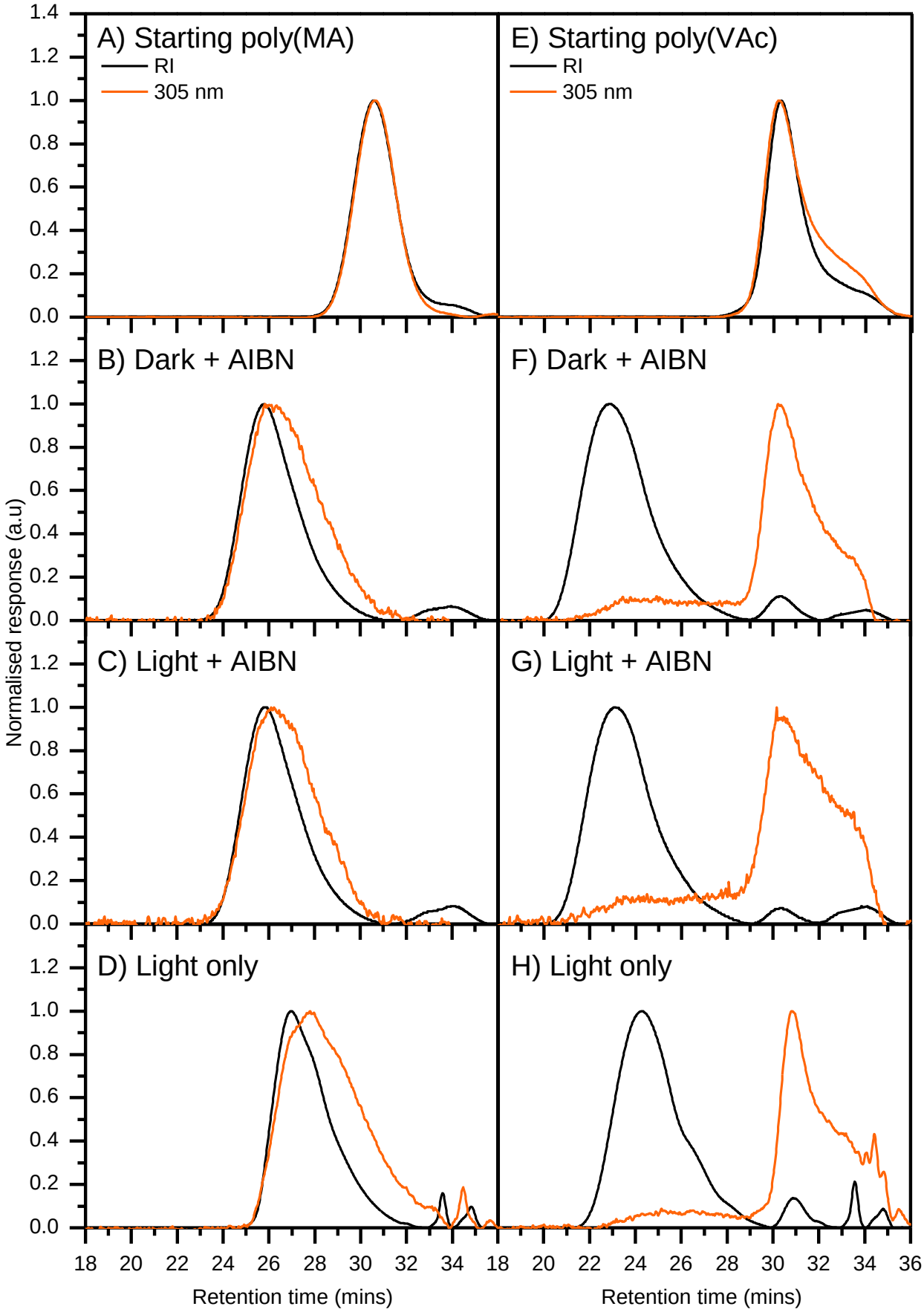

Figure 8.1: Compiled GPC traces for the attempted synthesis of poly(MA-b-VAc) copolymers (A-C) and poly(VAc-b-MA) (D-F) using macro-initiators derived from PXEP under different reaction conditions.

The finding that UV irradiation plays seemingly a minimal role on the molecular weight distributions in the synthesis of poly(MA-b-VAc) is strongly supported by the essentially identical conversion, molecular weights and dispersity values obtained under both dark + AIBN and light + AIBN conditions as shown in Table 8.1. Under dark + AIBN conditions, an estimated 80.6 % of the starting poly(MA) macroinitiator is consumed after only 62.5 % monomer conversion; with UV irradiation this increases marginally to 84.7 % without affecting monomer conversion. This indicates an efficient fragmentation favouring the release of the poly(MA) fragment from the poly(MA)-RAFT-poly(VAc) adduct radical, as expected by the RAFT mechanism. This is also reflected in the M_n values obtained, which are only marginally higher than the expected ~ 15.5 kg/mol at the conversion attained.

Under light only conditions the conversion is lower than for both conditions featuring AIBN, with the percentage of starting macroinitiator consumed being less than half of that obtained when AIBN is present. This suggests that under light only conditions, photolysis of the poly(MA) macroinitiator is reasonably efficient, however this ceases to be the case after conversion into the poly(MA-b-VAc) copolymer with a terminal VAc unit. The reasonably high dispersity values obtained for the block copolymers most likely stems from the same factors as for the broadening seen during VAc polymerisation as described previously in Chapter 6.

Table 8.1: Summary of experimental conditions and characterization of resulting poly (MA-b-VAc) copolymers corresponding to GPC traces (A – D) in Figure 8.1. UV irradiation (370nm, 2 mW/cm^2).

Synthesis of poly(MA-b-VAc)			(g mol^{-1})			% macroinitiator consumed
Sample	UV Light	% conv.	M_n	M_w	Đ	
poly(MA)	N	94.7	2410	2820	1.17	N/A
Dark + AIBN	N	62.6	18440	30160	1.60	80.6
Light + AIBN	Y	62.5	18680	29090	1.56	84.7
Light only	Y	47.8	13040	22270	1.71	38.0

These results are largely consistent with both the experimental findings and subsequent Predici modelling undertaken in Chapter 6 for the polymerisation of VAc under identical reaction conditions. There is however an influence from the starting poly(MA) macroinitiator that introduces some polymerisation behaviour similar to that seen in MA kinetic polymerisations described in Chapter 5. The key findings suggest that thermal breakdown of AIBN is still the primary source of initiation, however with UV photolysis gives a much higher conversion than what is expected if solely VAc like polymerisation behaviour were to be expected, indicating that photolysis of the starting poly(MA) macroinitiator also plays a non-insignificant role in the initiation rate. This can only result when the consumption of the starting poly(MA) macroinitiator is relatively rapid, thus converting it to the much

less photolytically labile poly(MA-b-VAc) where there is a terminal VAc unit. If this were not the case, a larger discrepancy in conversion between light + AIBN and dark + AIBN conditions would be expected.

Characterisation of the polymers formed in the attempted synthesis of poly(VAc-b-MA) (Table 8.2) largely supports the assertion that minimal chain extension occurred, with the M_n of the smaller peaks only increasing by around 300 g/mol relative to the starting poly(VAc) macroinitiator which corresponds to the addition of only ~ 4 monomer units. This is further supported by only ~ 20 % of poly(VAc) being consumed under both reaction conditions featuring AIBN, and around 11 % for light only conditions. The M_n of the larger molecular weight peaks under all conditions is ~ 10 x lower than for the control experiment conducted in the absence of any RAFT species which yields a polymer with an M_n of 834,000 g/mol. This indicates that even though only minimal consumption of the starting poly(VAc) occurs, degenerative chain transfer is still readily occurring.

Table 8.2: Summary of experimental conditions and characterization of resulting polymers corresponding to GPC traces (E – H) in Figure 8.1. UV irradiation (370nm, 2 mW/cm^2).

Synthesis of poly(VAc-b-MA)			(g mol^{-1})				% macroinitiator consumed
Sample	UV Light	% conv.	M_n	M_w	Đ	Peak	
poly(VAc)	N	68.2	2500	3040	1.16		N/A
Dark + AIBN	N	92.9	88840	215060	2.42	L	20.2
			2820	3020	1.07	S	
Light + AIBN	Y	98.3	77710	181950	2.34	L	18.7
			2860	3020	1.06	S	
Light only	Y	93.8	69210	145920	2.11	L	11.2
			N/A	N/A		S	

There are only marginal differences in the conversion attained (all > 90 %) under all 3 reaction conditions investigated, meaning that the rate of polymerisation earlier at earlier reaction times cannot be inferred. Regardless of whether AIBN or photolysis of RAFT species is the dominant pathway for generation of initiating radicals, the influence of the RAFT mechanism is minimal on both the molecular weight and conversion obtained. The poly(VAc) macroinitiator when converted to a poly(VAc-b-MA) copolymer with a terminal MA unit this is expected to undergo rapid photolysis. Collectively, these results strongly imply that the poly(VAc)-RAFT-poly(MA) adduct radical is fragmenting preferentially to release the poly(MA) radical as expected. This coupled with the poor photolytic properties of the poly(VAc) macroinitiator prevent the efficient synthesis of poly(VAc-b-MA) via the photoiniferter RAFT approach.

These results imply that the absolute difference in propagating radical reactivity between MA and VAc and the subsequent consequences this has on the RAFT mechanism was too great to be overcome by the application of the photoiniferter effect under the reaction conditions tested. These results are consistent with a recent result by Xu *et al.* who succeeded in inserting a single VAc unit into a trithiocarbonate based styrene - N-phenylmaleimide dimer under photoiniferter conditions, noting that further propagation was impossible due to the inability of the VAc radical to fragment from the trithiocarbonate [3]. This does not occur under the reaction conditions employed here due to the PXEP being of much lower stability as both a RAFT agent and as a RAFT adduct radical relative to a trithiocarbonate.

Coupled with the Predici modelling previously undertaken, these results strongly suggest that monomers from the "MAM" end of the reactivity spectrum are prime candidates for allowing the photolysis of RAFT species via the iniferter mechanism to be the primary source of initiating species. Thus, even though the RAFT mechanism is operative and overall control obtained is via degenerative chain transfer, focusing on MAMs in block copolymer synthesis should allow the consumption of the starting macroinitiator via photolysis. Once it is consumed, the subsequent propagation steps to form the desired block copolymer should be allowed by the RAFT mechanism as the terminal chain ends are now capped with the secondary monomer in the desired block sequence.

To test this theory, the next series of experiments still focused on forcing the monomer order from more "LAM like" monomers to more "MAM like" monomers, however Sty and MMA were used due to the difference in propagating radical reactivity and stability being significantly less than between MA and VAc.

8.4 Synthesis of poly(Sty-b-MMA) – comparison of RAFT agent class, monomer concentration and photolysis wavelength

Investigating the possibility of Spiro-XEP providing a mechanistic advantage over PXEP under UV irradiation was explored through the attempted synthesis of poly(Sty-b-MMA) copolymers using poly(Sty) macroinitiators derived from both RAFT agents. Furthermore, by keeping the targeted molecular weight of the block copolymers constant, the effect of monomer and macroinitiator concentration was investigated to see whether the overall polymerisation rate and concentration of photoactive species plays a role in the products formed. This was undertaken in light of several literature findings indicating the lowering the concentration of photoactive species is beneficial both in the synthesis of block copolymers via the photoiniferter method [4] and during photoinitiated single monomer unit (SUMI) work [5]. MMA concentrations of both 1 M and 3 M were tested.

5.4.1 Analysis of UV-Vis absorption profiles for compounds utilised in polymerisation of poly(Sty-b-MMA) block copolymers under UV irradiation

As was tested for poly(MA) and pol(VAc) macroinitiators in previous chapters, the ability of the UV lamp to stimulate the n → π* transition of the macroinitiators derived from Spiro-XEP and PXEP was investigated by UV-Vis analysis. The strong overlap between the emission spectrum of the UV lamp (370nm, 2 mW/cm^2) and the absorption spectrum of both macroinitiators (Figure 8.2, orange & green traces) indicates that the photoiniferter effect should occur readily.

Similarly, the possible effect of direct photolysis of monomer was investigated. The overlap between the UV lamp (370nm, 2 mW/cm^2) and the MMA was minimal at both experimental concentrations tested (Figure 8.2, red & brown traces). Control experiments in the absence of any initiator or RAFT agent were conducted under UV irradiation for 22 h., with the results summarised in Table 8.3.

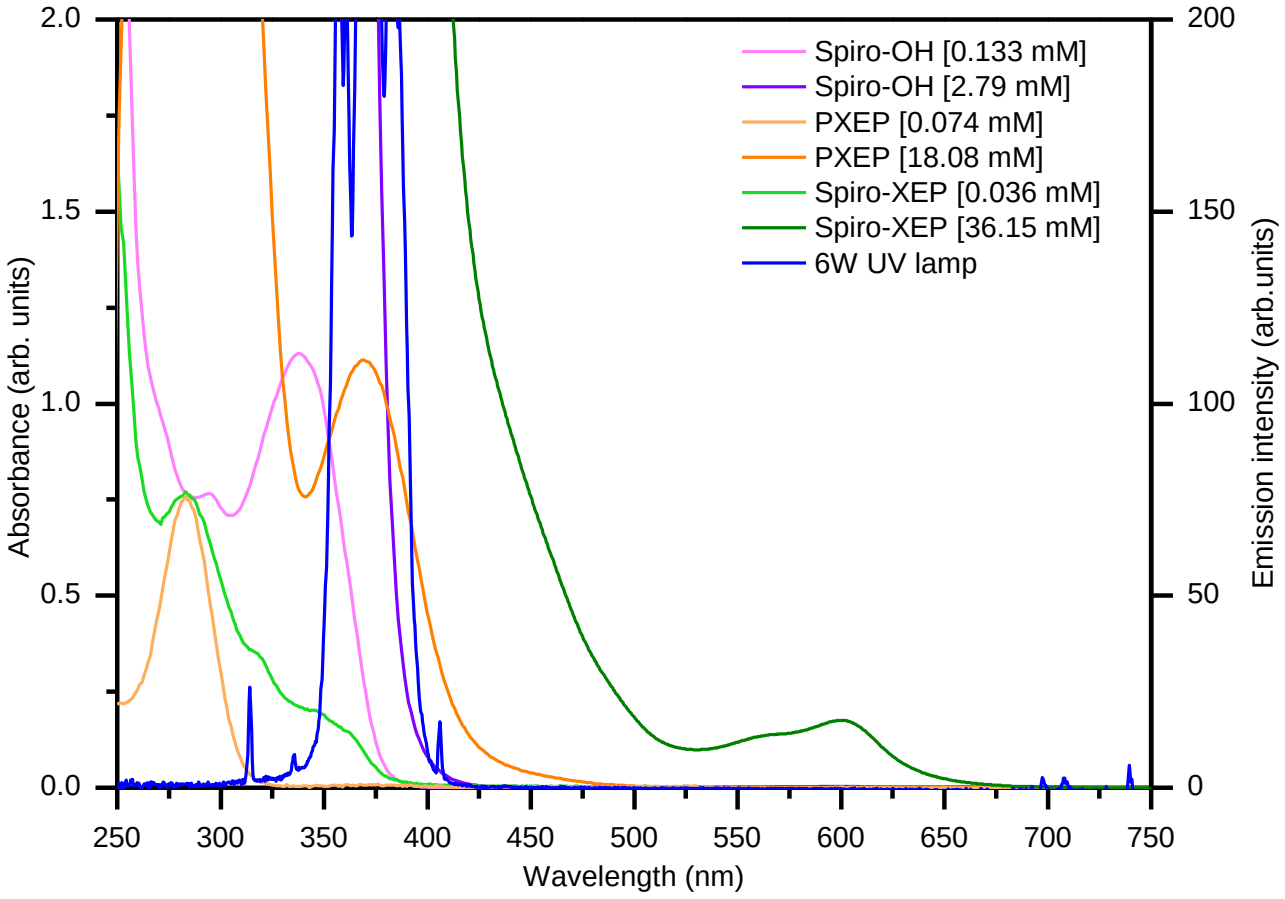

Figure 8.2: Superimposed UV-Vis spectra of macroinitiators and MMA at experimental concentrations in toluene used in kinetic experiments overlayed with the emission spectrum of the 6W UV lamp (370nm, 2 mW/cm^2).

It was observed that upon completion of the control experiments, the 3M reaction mixture had a higher viscosity than for the 1M case; based on this observation it can be expected that the average

rate of termination (R_t) in the 3M reaction should be smaller than for the 1M reaction. As the average kinetic chain length is defined as the ratio of R_p to R_t [6], this logically should manifest as a higher average kinetic chain length due to an increase in R_p and decrease in R_t under the higher MMA concentration. Curiously the reverse occurred, as can be seen in Table 8.3.

Table 8.3: Summary of control experiments conducted under poly(Sty-b-MMA) polymerisation conditions with UV irradiation (370nm, 2 mW/cm^2); [RAFT] = 0, [AIBN] = 0, 70 °C, toluene as solvent, reaction time = 22 h.

Entry	[MMA] (M)	% conv. by ^{1}H NMR	M_n (g/mol)	M_w (g/mol)	Đ
1	1.0	16.0	817090	1243310	1.52
2	3.0	18.9	233260	511870	2.19

The dispersity values obtained for the 1M and 3M correspond closely with the values expected if termination by combination (D = 1.5) and disproportionation (D = 2.0) were occurring respectively [6]. Thus, the resulting molecular weights can be understood as most likely arising due to the higher viscosity of the reaction mixture leading to the disproportionation mechanism being favoured. This theory is supported by the work of Nakamura & Yamago who found poly(MMA) primary terminates by disproportionation, however this significantly decreases as a function of temperature which was speculatively attributed to lower solution viscosities occurring at higher temperatures [7].

8.4.2 Comparison of Spiro-XEP, PXEP and monomer concentration

The poly(Sty) macroinitiators synthesised with both PXEP and Spiro-XEP are both predicted to have a high chain end fidelity of 96.8 %. Using 1M MMA and a Spiro-XEP macroinitiator under dark + AIBN conditions results in a bimodal molecular weight distribution (Figure 8.3, A, red trace). The RI spectrum shows only partial consumption of the starting macroinitiator and a large broad peak at much lower retention times, indicating incomplete chain extension. For light + AIBN conditions the result is significantly different in that the starting macroinitiator peak is largely absent, with the secondary peak occurring at a much lower retention time and appearing to have a lower molecular weight shoulder (Figure 8.3, A, blue trace).

Using a PXEP macroinitiator under identical conditions essentially reproduces these results (Figure 8.3, C). One subtle difference is that under light + AIBN conditions the peak appears more Gaussian in shape and shifts to a higher retention time, which results in partial overlap with the original macroinitiator peak position (Figure 8.3, C, blue trace).

The 3M experiments expose significant differences in the block copolymers obtained using Spiro-XEP and PXEP derived macroinitiators. When a Spiro-XEP macroinitiator is used, bimodal distributions are obtained under both dark + AIBN and light + AIBN reaction conditions (Figure 8.3,

B), showing incomplete consumption of the starting macroinitiator. Under light + AIBN conditions the larger peak at lower retention time has a complex shape and appears to be comprised of 3 or 4 separate peaks including a distinct high molecular weight shoulder. This is indicative of significant termination by combination of growing polymer chains having occurred. Using dark + AIBN conditions, these effects are absent with the higher molecular weight peak retaining a largely symmetrical shape similar to what has been seen previously under 1M conditions (Figure 8.3, B, red trace).

With the PXEP macroinitiator, a slightly asymmetrical monomodal distribution seeming to favour lower molecular weights is obtained with light + AIBN conditions, however the peak does not exhibit the same broadness and complex features as was seen with the Spiro-XEP macroinitiator (Figure 8.3, D, blue trace). As has been consistently observed in all other experiments within this section for dark + AIBN conditions, a similar bimodal distribution featuring the peak from the unreacted macroinitiator and a higher molecular weight peak was again observed (Figure 8.3, D, red trace).

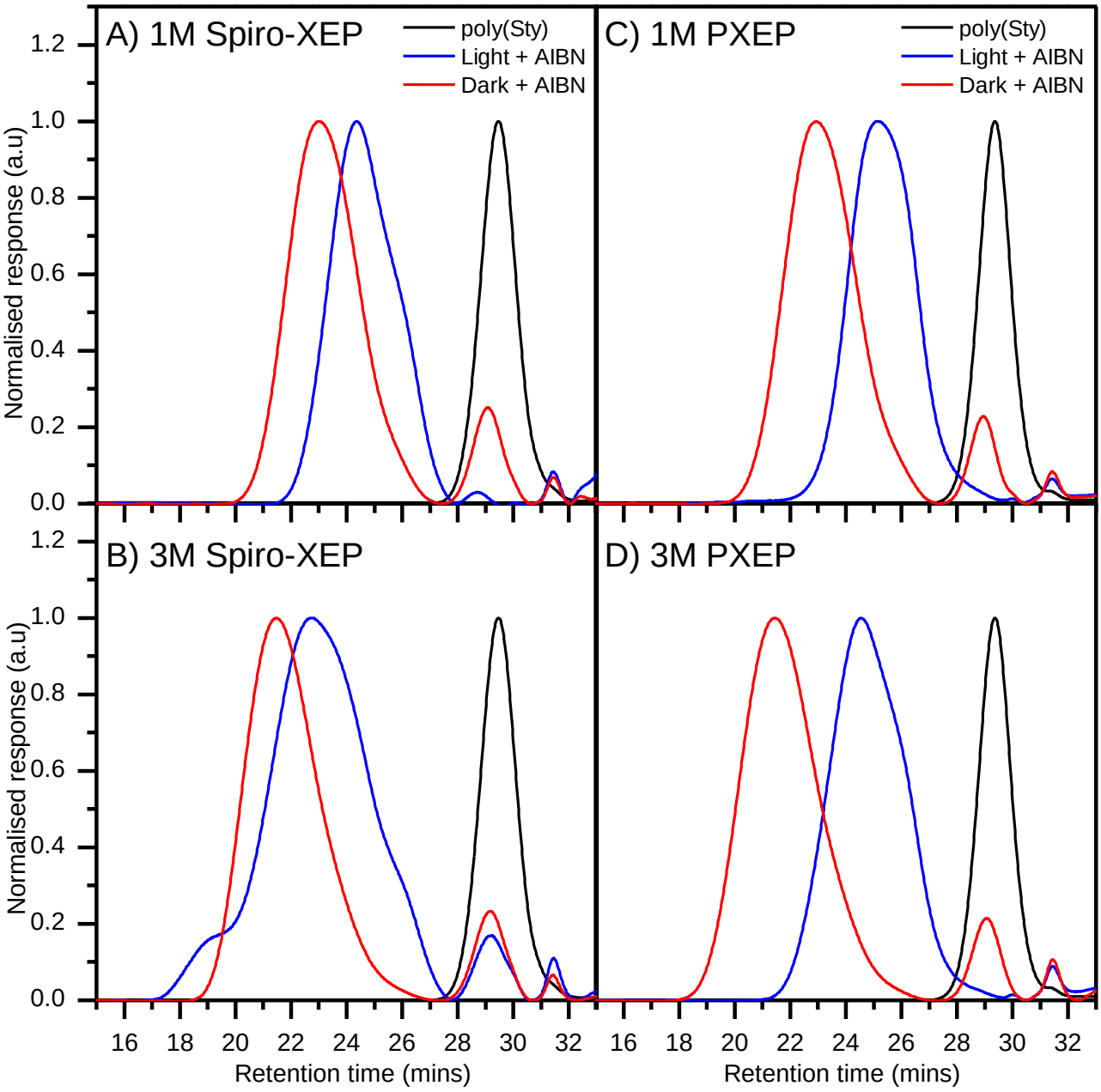

Figure 8.3: Comparison RI GPC traces for poly(Sty-b-MMA) copolymers synthesised with Spiro-XEP and PXEP under both 1M and 3M monomer concentrations. Spectra obtained on the single detector GPC system.

Based on these results there must be significant mechanistic differences between polymerisations conducted with and without UV irradiation under both MMA concentrations. Molecular weight analysis of the 1M reactions (Table 8.4) reveals that irrespective of whether PXEP or Spiro-XEP macroinitiators are used under dark + AIBN conditions, the molecular weight of the starting macroinitiator peak does not increase by more than ~ 600 g/mol. Since this is equivalent to ~ 7 MMA monomers, this suggests that the starting macroinitiators are essentially unreacted with only a small percentage chain extending. Similarly, the conversion attained is identical within experimental error for both reaction conditions, with a 20 % higher conversion under light + AIBN conditions. At the 75

% conversion attained under these conditions, theoretical M_n is expected to be 20,600 g/mol; the M_n PXEP given by is closer than that from Spiro-XEP. These results show that the efficiency of the photoiniferter reaction is practically identical in both cases and that any potential photo-switching of the Spiro-XEP has minimal consequences overall. Given the vast differences in the polymerisation rate of VAc between PXEP and Spiro-XEP and the almost identical rate when applied to MA, this result suggests that rate differences between the two RAFT agents are monomer and condition specific.

Table 8.4: Characterisation of poly(Sty-b-MMA) copolymers made with PXEP and Spiro-XEP with [MMA] = 1M, polymers corresponding to GPC traces (A & C) in Figure 8.3. Dark + AIBN and Light + AIBN conditions: 80 °C. UV irradiation (370nm, 2 mW/cm^2).

Synthesis of poly(Sty-b-MMA) with PXEP			(g mol^{-1})			
Sample	UV Light	% conv.	M_n	M_w	Đ	Peak
poly(Sty)	N	62.5	1730	2020	1.17	
Dark + AIBN	N	55.7	99100	184130	1.86	L
			2360	2570	1.09	S
Light + AIBN	Y	75.6	18740	28740	1.53	
Synthesis of poly(Sty-b-MMA) with Spiro-XEP			(g mol-1)			
Sample	UV Light	% conv.	M_n	M_w	Đ	Peak
poly(Sty)	N	61.5	1590	1900	1.20	
Dark + AIBN	N	55.7	62460	107880	1.73	L
			2130	2360	1.11	S
Light + AIBN	Y	75.2	27910	44260	1.59	L
			2740	2850	1.04	S

Table 8.5: Characterisation of poly(Sty-b-MMA) copolymers made with PXEP and Spiro-XEP with [MMA] = 3M, polymers corresponding to GPC traces (B & D) in Figure 8.3. Dark + AIBN and Light + AIBN conditions: 80 °C. UV irradiation (370nm, 2 mW/cm^2).

Synthesis of poly(Sty-b-MMA) with PXEP			(g mol^{-1})			
Sample	UV Light	% conv.	M_n	M_w	Đ	Peak
poly(Sty)	N	62.5	1730	2020	1.17	
Dark + AIBN	N	75.1	141220	287750	2.04	L
			2210	2410	1.10	S
Light + AIBN	Y	96.3	22960	42460	1.85	
Synthesis of poly(Sty-b-MMA) with Spiro-XEP			(g mol^{-1})			
Sample	UV Light	% conv.	M_n	M_w	Đ	Peak
poly(Sty)	N	61.5	1590	1900	1.20	
Dark + AIBN	N	72.0	138240	263950	1.91	L
			2030	2260	1.11	S
Light + AIBN	Y	91.9	55940	206210	3.69	L
			1960	2180	1.11	S

The molecular weight analysis for 3M conditions shows that under all reaction conditions for both Spiro-XEP and PXEP macroinitiators the molecular weights obtained for the larger peaks were higher than under 1M conditions (Table 8.5). Interestingly, this is the opposite trend to that seen in the control experiments, which implies that the molecular weight is moderated by the chain transfer process to an extent such that it potentially alters the termination pathway that is dominant, however this was not confirmed. Despite the 3-fold increase in the concentration of both monomer and photosensitive macroinitiator, the conversion in the same timeframe consistently increased by ~ 20 % under equivalent reaction conditions for both macroinitiators. This further supports the idea that a xanthate moiety with terminal MAM units is prone to photolysis and thus the reversible photolysis of RAFT species plays a significant role in generating initiating radicals under these conditions.

The results obtained for the PXEP macroinitiator under light + AIBN conditions show the dispersity of the peak is much higher under 3M conditions at 1.85 vs 1.53 under 1M conditions. This is despite the higher conversion under 3M conditions; all other factors being constant, the dispersity should narrow at higher conversion as per the RAFT mechanism. Based on these results it was concluded that poly(Sty) macroinitiators synthesised with Spiro-XEP show no advantage over ones derived from PXEP, hence further studies with Spiro-XEP were not pursued.

To gain a deeper understanding of the success of the chain extension process, the block copolymers formed with the PXEP macroinitiator were analysed further using multiwavelength detection to track the distribution of the RAFT moiety as shown in Figure 8.4. For the starting poly(Sty) macroinitiator there is perfect overlap between the RI and PDA detector response at 305 nm corresponding to an absorption from the RAFT moiety; this strict overlap is indicative of high chain end fidelity. For both monomer concentrations the bimodal distributions seen with the RI detector for dark + AIBN conditions show only one substantial peak in the PDA trace centred around the RI peak from the starting macroinitiator (Figure 8.4, B & E, orange traces). This shows that minimal chain extension occurred and that in both cases the second larger RI peaks correspond to predominantly free radical derived poly(MMA) homopolymer. This was confirmed when the two respective PDA peaks were integrated, giving an estimated 2.9 % and 1.9 % consumption of the starting poly(Sty) macroinitiator for 1 and 3 M reaction conditions respectively.

As expected based on the monomodal RI distributions, an inverse result was obtained with both concentrations tested under light + AIBN conditions. Under photolysis conditions, both RI and PDA traces are monomodal (Figure 8.4, C & F), with the PDA traces showing that most of the RAFT species are retained on the starting macroinitiator (Figure 8.4, C & F, orange traces). This confirms the successful formation of the poly(Sty-b-MMA) polymer, which is supported by an estimated 91.8

% and 95.8 % consumption of the starting poly(Sty) macroinitiator for 1 and 3 M reaction conditions respectively.

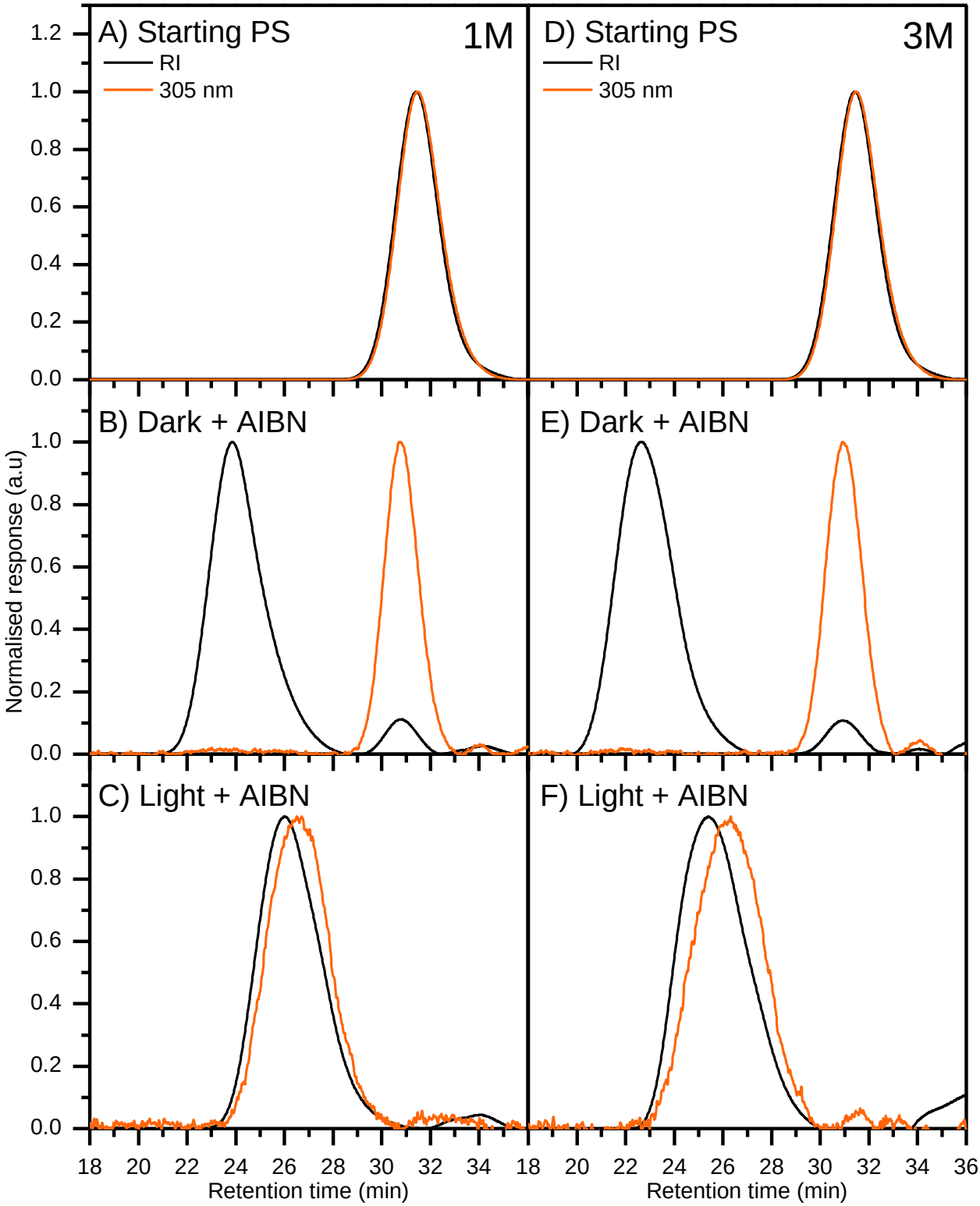

Figure 8.4: Comparison RI & PDA GPC traces for poly(Sty-b-MMA) copolymers synthesised with PXEP under both 1M and 3M monomer concentrations under different reaction conditions.

Based on these results it can be concluded that an increased concentration of photoactive species and monomer in the reaction mixture is detrimental to obtaining monodisperse poly(Sty-b-MMA) block copolymers. Further testing with more dilute MMA concentrations were not undertaken as this would require even longer irradiation times than the currently used 20 h which could become problematic regarding RAFT agent degradation. Consequently, if higher molecular weight block copolymers were desired this would require lowering the concentration of photoactive species even further, thus compounding this problem.

These findings are consistent with the general trends as reported by both Niwa *et al.* [8] and Ajayaghosh [9] for studies of conventional photoiniferter polymerisations undertaken with a range of RAFT agents and several monomers including Sty and MMA. Based on the estimated consumption of the poly(Sty) macroinitiator, these results exceed those reported previously in the literature for poly(Sty-b-MMA) block copolymers derived from a range of dithiocarbamates [10] [11].

In general, this behaviour can be explained in terms of the initiator efficiency (ϕ) and the fraction of propagating radicals terminated by the "primary" radicals (β), defined as the radicals arising from the photolysis of the RAFT agent [9]. Both authors found that for a fixed [RAFT], ϕ increased with increasing monomer concentration whilst simultaneously β decreased and conversely, for a fixed [M], ϕ decreased whilst β increases [8, 9]. This could occur as at higher RAFT concentrations the occurrence of chain transfer is increased even if the kinetic rate constant for this reaction is not. As per the predictions made in Chapter 6, this could decrease the rate of photolysis due to a greater percentage of the RAFT species being effectively trapped as the RAFT adduct radical. Ajayaghosh theorised that the decreased probability of primary radical termination at higher monomer concentrations means termination by combination and disproportionation pathways will be favoured [9]; the molecular weight distribution obtained under photolysis conditions with Spiro-XEP at the higher MMA concentration support this assertion. Interestingly, the only reported successful formation of poly(Sty-b-MMA) without photoiniferter conditions was achieved using benzyl dithioacetate in a starve fed emulsion polymerisation system, which implies lowering the active radical concentration is beneficial in overcoming this mechanistic limitation [12].

These mechanistic considerations are likely to only be crucial when attempting to synthesise block copolymers with a block sequence contrary to those recommended for RAFT. For example, Nakayama *et al.* found that varying the concentration of styrene in the formation of poly(ethylene glycol-b-Sty) using benzyl N,N-diethyldithiocarbamate as the starting iniferter played no role in the success of the reaction. In all cases the poly(ethylene glycol) macroinitiator was completely

consumed within 10 minutes of irradiation [13], with only the molecular weight of the resulting block copolymer changing with monomer concentration.

8.4.3 Synthesis of poly(Sty-b-MMA) copolymers with DECET: effect of RAFT agent class and irradiation wavelength

Xanthates are not typically used for the polymerisation of MAMs such as MMA due to generally having lower chain transfer constants than trithiocarbonates or dithioesters [14, 15]. It was imperative to test whether the photoiniferter effect allowing the synthesis of poly(Sty-b-MMA) block copolymers is a result of xanthates being used or simply a unique property of RAFT terminated poly(Sty) chain ends being able to undergo efficient photolysis. The rest of this chapter aims to explore these two questions. If a trithiocarbonate could be utilised successfully under photolysis conditions, it should in principle allow the formation of narrower dispersity poly(Sty-b-MMA) and poly(MA-b-MMA) copolymers. To test this, the trithiocarbonate DECET as first synthesised by Ponnusamy *et al.* [16] (structure shown in Figure 8.5) was chosen for the synthesis of the starting poly(Sty) macroinitiator.

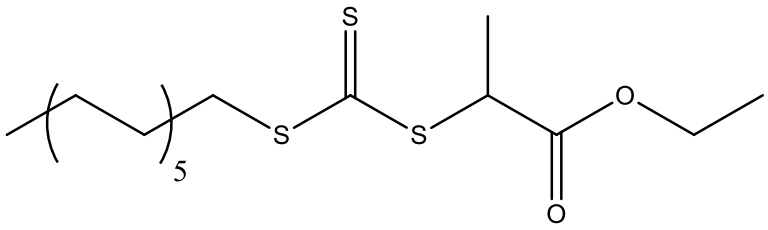

Figure 8.5: Structure of S-1-dodecyl-S'-((2-ethoxycarbonyl)-ethyl) trithiocarbonate (DECET).

DECET was selected as it has an identical R group to PXEP and Spiro-XEP means its reinitiating efficiency to both MA and Sty are identical, which precluded any difficulties and differences in the synthesis of the starting macroinitiators. Being a trithiocarbonate the change in electron density around the central RAFT moiety not only makes it inherently better at trapping radicals relative to PXEP, but also changes the absorbance wavelength and extinction coefficient of the n → π* and π → π* molecular transitions. This means the weak n → π* molecular transition for trithiocarbonates typically occurs well into the visible region at between 420 – 500 nm which corresponds to blue light [17]. This has led to trithiocarbonates being utilised with blue LED irradiation in several photoiniferter studies [18, 19] with the added advantage that the reactions can be run at room temperature [20], thus avoiding potentially harmful side reactions favoured at higher temperatures [21]. For this purpose, a blue LED reactor (471 nm)was constructed by winding an LED strip on the inside of a beaker; for full details please see section 4.4.4 in Chapter 4.

As can be seen in Figure 8.6, both the poly(Sty) and poly(MA) macroinitiators derived from DECET (Figure 8.6, red & orange traces respectively) have n → π* molecular transitions with maxima at 437 nm and 432 nm respectively. These features are similar to the absorption profile of DECET itself (Figure 8.6, green traces), which has a π → π* molecular transition at 433nm ± 1nm and a n → π* molecular transition at 306 ± 1nm. For a summary of the extinction coefficients which were determined for these transitions, see Table A8 in the Appendix.

For both macroinitiators, the emission profile for the 6W UV lamp overlaps with both the n → π* and the π → π* transitions, meaning realistically both photolysis pathways are likely to be active with UV irradiation (Figure 8.6, blue trace). Utilising the LED light source (471 nm), there is only overlap with the weaker n → π* transitions for both macroinitiators (Figure 8.6, light blue trace).

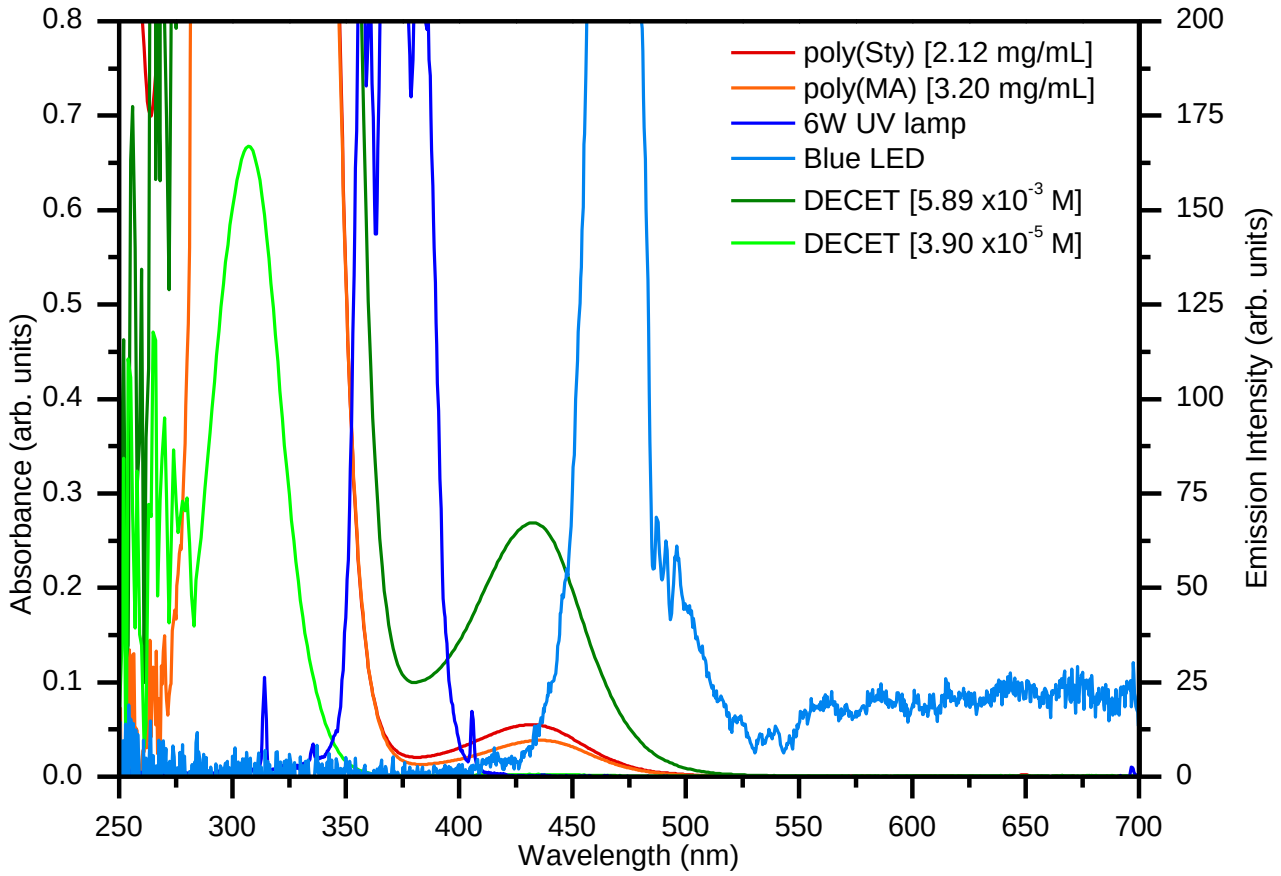

Figure 8.6: Comparison of DECET derived macroinitiators with both UV lamp (370nm, 2 mW/cm^2) and LED light (471 nm) soures used.

As a control experiment, MMA at 50 % (v/v) monomer concentration in acetonitrile was irradiated in the LED reactor (471 nm) for a period of 12 h at room temperature. This resulted in zero conversion as determined by ^{1}H NMR and no peaks were detected in the GPC trace obtained from rinsing the reaction vessel with THF after volatiles were removed under vacuum. For a complete summary of control experiments with other monomers, see Table A9 in the Appendix.

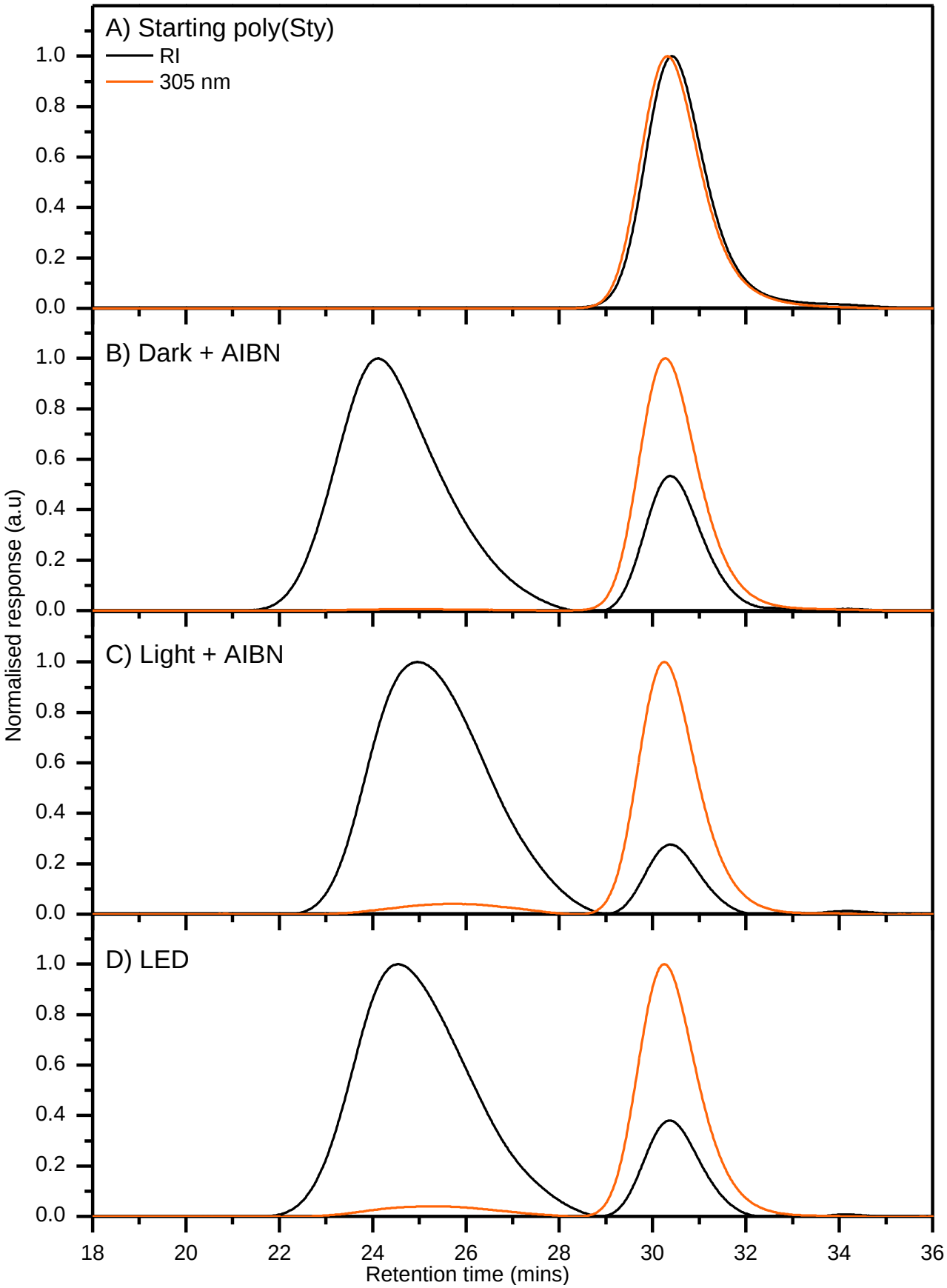

Figure 8.7: Compiled GPC traces for poly(Sty-b-MMA) copolymers synthesised with DECET under a range of reaction conditions.

The poly(Sty) macroinitiator made with DECET gave RI and PDA traces that showed very close agreement (Figure 8.7, A), indicating a high chain end fidelity which is consistent with the theoretical value of 93.6 % as estimated using Equation 4.9. With dark + AIBN conditions, the RI spectra were bimodal in nature, with the peak corresponding to the starting macroinitiator being largely retained, indicating its low consumption and thus poor chain extension. This was supported by the PDA trace being essentially flat in the region where the secondary peak appears in RID trace, with the solitary monomodal peak corresponding to starting macroinitiator (Figure 8.7, B). With UV irradiation, the RI distribution was once again bimodal, however the secondary larger peak occurred at a lower retention time and the peak from the starting macroinitiator was proportionally smaller in intensity. These two factors indicate a higher overall consumption of the macroinitiator; this is supported by the PDA trace being noticeably bimodal with a small peak which has the same width and position as the larger RI peak (Figure 8.7, C). The RI and PDA spectra obtained with LED irradiation conditions were almost identical to those obtained with light + AIBN conditions.

Under dark + AIBN and light + AIBN conditions, the percentage conversion obtained was ~ 10 and 4 % larger than when a PXEP derived macroinitiator was used; this is surprising given the identity of the RAFT agent should not influence conversion under most circumstances. There is a smaller increase in conversion with UV irradiation in this case (14.7 %) than what was observed for the PXEP derived macroinitiator (19.9 %). This is most likely due to the much greater overlap of the UV output with the n $\rightarrow$ π^* molecular transition in PXEP as opposed to in DECET where the overlap is only partial (Figure 8.6).

Under both LED irradiation at room temperature (~ 25 °C) and with light + AIBN at 70 °C only 7.2 % of the starting macroinitiator was consumed in both cases, while the conversion was 64.4 % and 79.0 % respectively. The k_p value for MMA at 25 °C (323 M^{-1} s^{-1}) is 3.26 times smaller than at 70 °C (1055 M^{-1} s^{-1}), however the reaction time at 25 °C was selected to be 3 times longer than at 70 °C (60 h vs 20 h respectively) to effectively counteract this. Mechanistically, these observations strongly imply that overall the product of the quantum yield and irradiation intensity must be similar with both UV and LED irradiation, however the subsequent reactions involving the radicals generated must ultimately lead to the differences seen. Analysis of the resulting molecular weights as shown in Table 8.6 supports this theory; despite the lower conversion under LED conditions the molecular weight for the larger peak is 7700 g/mol greater.

Overall it is apparent that photolysis of the terminal poly(Sty) unit is possible when the n $\rightarrow$ π^* transition is stimulated in PXEP under irradiation from a 6W 370 nm light, yielding successful formation of poly(Sty-b-MMA) copolymers. Stimulating both the $\pi \rightarrow \pi^*$ and n $\rightarrow$ π^* transition with

the same UV light or just the n → π* transition with a 471 nm LED of a poly(Sty) macro-initiator derived from DECET fails to cleanly yield poly(Sty-b-MMA) copolymers.

Table 8.6: Summary of experimental conditions and characterization of resulting poly (Sty-b-MMA) copolymers corresponding to GPC traces in Figure 8.7. Dark + AIBN and Light + AIBN conditions: 80 °C. UV irradiation (370nm, 2 mW/cm^2). LED irradiation at 25 °C, peak intensity at 471 nm.

Synthesis of poly(Sty-b-MMA) with DECET			(g mol^{-1})				% macroinitiator consumed
Sample	UV Light	% conv.	M_n	M_w	Đ	Peak	
poly(Sty)	N	94.3	930	1040	1.12		N/A
Dark + AIBN	N	64.3	60090	94740	1.58	L	1.1
			N/A	N/A	N/A	S	
Light + AIBN	Y	79.0	37990	57010	1.50	L	7.2
			3200	3420	1.07	S	
LED	Y	64.4	45710	71570	1.57	L	7.3
			3200	3450	1.08	S	

8.5 Synthesis of poly(MA-b-MMA) – influence of RAFT agent class, photolysis wavelength and monomer concentration

To test whether the phenomena seen in the previous section are unique to poly(Sty) macroinitiators, a further two poly(MA) macroinitiators where synthesised with both PXEP and DECET and the synthesis of poly(MA-b-MMA) was attempted with the same experimental conditions as used previously.

8.5.1 Analysis of poly(MA-b-MMA) copolymers made with PXEP

The RI and PDA spectra from the starting poly(MA) macroinitiator made with PXEP showed a slight discrepancy at the longest retention times, however the correspondence between the two spectra was still very good (Figure 8.8, A). This is unexpected, as under the reaction conditions chosen for its synthesis the theoretical chain end fidelity should be very high at 99.4 % as estimated using Equation 4.9. A monomodal PDA distribution centred over the RI peak from the starting macroinitiator with a bimodal RI distribution was seen in the synthesis of poly(MA-b-MMA) as can be seen in Figure 8.8, B. This is entirely consistent with results obtained previously under dark + AIBN conditions in the synthesis of poly(Sty-b-MMA) with both PXEP and DECET. This confirms that inefficient fragmentation to fragment the poly(MMA) radical from the poly(MA)-RAFT-poly(MMA) adduct radical is the cause, as expected per the RAFT mechanism given the much higher stability and subsequently lower reactivity of the MMA radical relative to the MA radical. This is supported by only an estimated 1 % of the starting macroinitiator being consumed. Data summarised in Table 8.7.

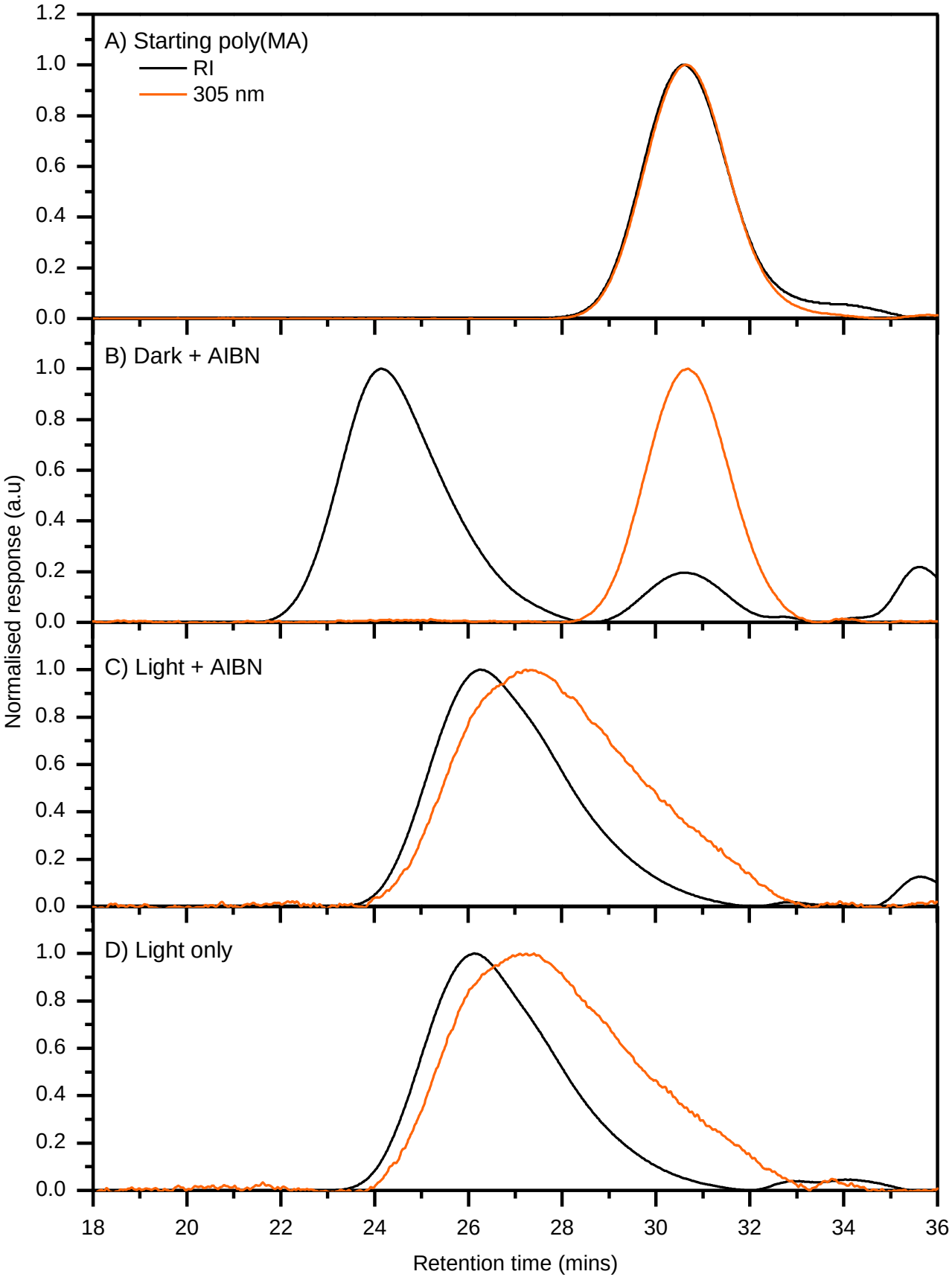

Figure 8.8: Compiled GPC traces for poly(MA-b-MMA) copolymers synthesised with PXEP under a range of reaction conditions.

Table 8.7: Characterisation of poly(MA-b-MMA) copolymers made with PXEP with [MMA] = 1M, polymers corresponding to GPC traces in Figure 8.7. Dark + AIBN and Light + AIBN conditions: 80 °C. UV irradiation (370nm, 2 mW/cm^2).

Synthesis of poly(MA-b-MMA) with PXEP			(g mol^{-1})				% macroinitiator consumed
Sample	UV Light	% conv.	M_n	M_w	Đ	Peak	
poly(MA)	N	94.70	2410	2820	1.17		N/A
Dark + AIBN	N	47.46	59150	91780	1.55	L	1.3
			2630	3120	1.19	S	
Light + AIBN	Y	75.72	15050	25600	1.70		52.5
Light only	Y	71.75	16260	28060	1.73		52.5

Light + AIBN conditions appear to yield the desired the poly(MA-b-MMA) copolymer and this is supported by both the PDA and RI peaks showing translation to lower retention times, however the PDA peak overlaps quite significantly with the position of the PDA peak from the starting macroinitiator (Figure 8.8, C). This is reflected in only 52.5 % of the starting macroinitiator being consumed, which is significantly lower than when the poly(Sty) case was used, at 91.8 %. The dispersity values also reflect this, being 1.70 and 1.53 for the poly(MA) and poly(Sty) macroinitiators respectively. Interestingly the conversion obtained under UV photolysis is essentially identical at 75 % for both cases. These slight differences can arise due to the concentrations of macroinitiator being slightly different to match the molecular weight, being 3.38 mM and 4.42 mM for the poly(Sty) and poly(MA) macroinitiators respectively. Overall it is evident that the formation of poly(MA-b-MMA) was less successful than the formation of poly(Sty-b-MMA) under comparable reaction conditions.

8.5.2 Synthesis of poly(MA-b-MMA) copolymers with DECET: effect of RAFT agent class and irradiation wavelength

Similarly, for the synthesis of poly(MA-b-MMA) with DECET, the resulting molecular weight distributions are strikingly alike to those obtained for poly(Sty-b-MMA) also made with DECET. The starting poly(MA) macroinitiator made with DECET has a theoretical chain end fidelity of 99.4 % as estimated using Equation 4.9, and this is supported by the narrow and symmetrical Gaussian peaks seen for both the RI and PDA spectra in Figure 8.9, A. Under all reaction conditions employed, bimodal molecular weight distributions were obtained using the RI detector (Figure 8.9, B-D). Unlike what was observed for poly(MA-b-MMA) with PXEP, the PDA traces for both light + AIBN and LED reaction conditions show a complete absence of a peak corresponding to the RAFT moiety at higher molecular weights (Figure 8.9, B-D). This indicates a total failure to form the desired poly(MA-b-MMA) copolymer that retains the RAFT moiety; this is reflected in less than 1 % of the poly(MA) macroinitiator being consumed under light + AIBN conditions (Table 8.8).

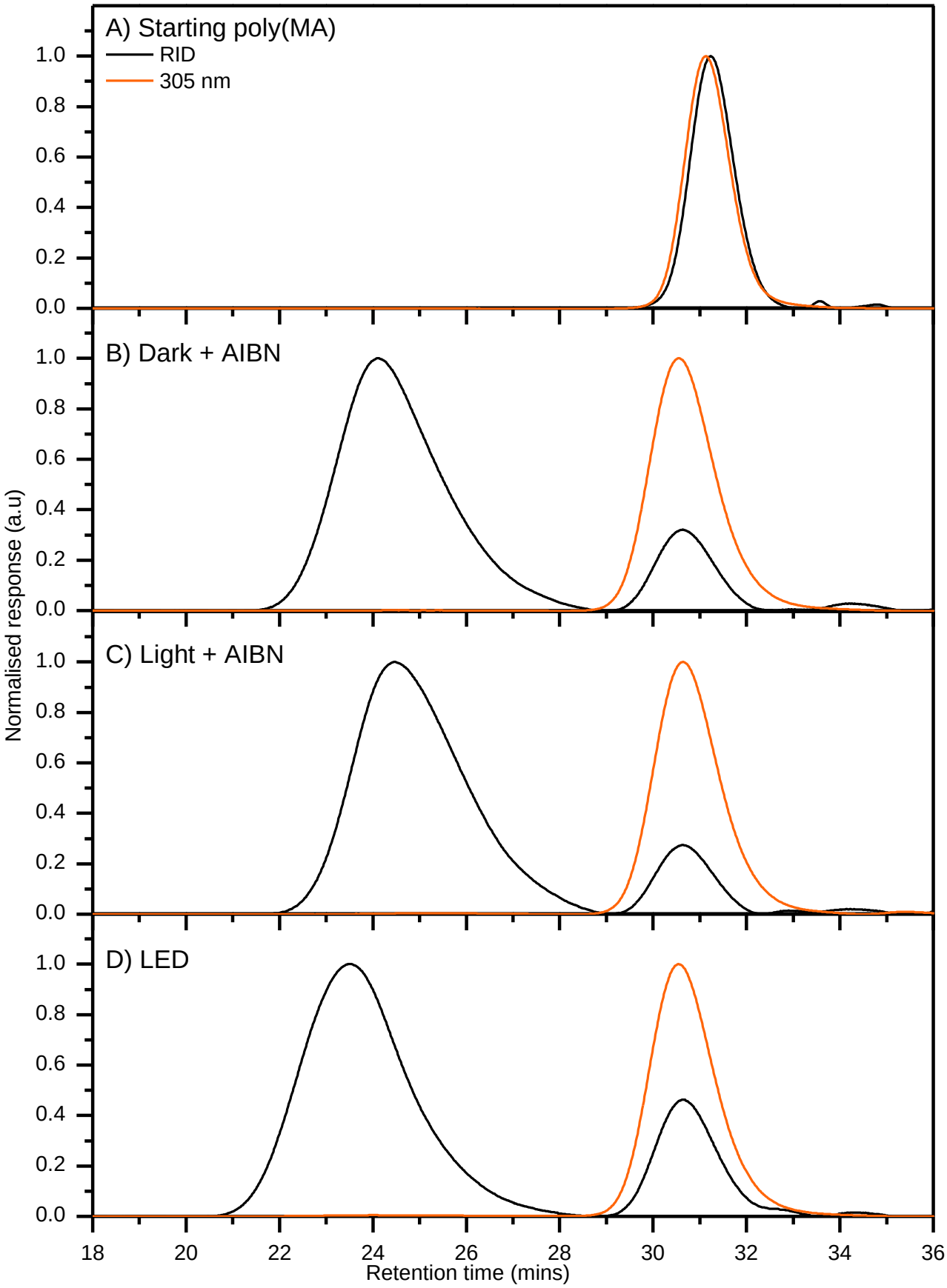

Figure 8.9: Compiled GPC traces for poly(MA-b-MMA) copolymers synthesised with DECET under a range of reaction conditions.

Table 8.8: Summary of experimental conditions and characterization of resulting poly (MA-b-MMA) copolymers corresponding to GPC traces in Figure 8.9. Reaction time =10 h. Dark + AIBN and Light + AIBN conditions: 80 °C. UV irradiation (370nm, 2 mW/cm^2). LED irradiation at 25 °C, peak intensity at 471 nm.

Synthesis of poly(MA-b-MMA) with DECET			(g mol^{-1})				% macroinitiator consumed
Sample	UV Light	% conv.	M_n	M_w	Đ	Peak	
poly(MA)	N	92.97	1990	2260	1.13		N/A
Dark + AIBN	N	45.21	58710	93660	1.60	L	0.0
			2810	3060	1.09	S	
Light + AIBN	Y	50.79	46860	73020	1.56	L	0.5
			2860	3070	1.07	S	
LED	Y	31.82	89120	156920	1.76	L	1.0
			2620	2970	1.13	S	

It must be noted that for the reactions containing AIBN, the reaction time was decreased by 50 % to 10 h (Table 8.8). Nevertheless, if consumption of the starting poly(MA) macroinitiator were to occur, it should still be evident as within this timeframe more than 45 % monomer conversion was attained under both dark and light + AIBN conditions. Under LED conditions, the reaction time was identical (60 h) to that used in the poly(Sty-b-MMA) polymerisation. The comparative conversion is much smaller for the poly(MA-b-MMA) case, being 31.8 % as compared to 64.4 % for poly(Sty-b-MMA), with DECET used for the starting macroinitiators in both cases. This result is a more severe example of the differences in conversion between the two macroinitiators which was also seen for the comparison made with PXEP for the same copolymers being synthesised. These results directly imply that there must be a significant difference in either the quantum yield of photolysis, the re-initiating efficiency of the Sty radical vs MA radical or the ability to ability of photolysis to occur due to preferential formation of the non-photolyzable RAFT abduct radical as theorised previously in Chapter 6.

These results are somewhat contrary when compared to those of McKenzie *et al.* who reported that trithiocarbonates with propanoic acid (analogous to the MA radical) and benzyl (analogous to the Sty radical) R groups both showed almost no degradation after extended periods of photolysis with blue LEDs [22]. This was despite that at the same concentration, the trithiocarbonate with the propanoic acid R group had approximately twice the absorbance intensity for the n → π* transition being photolysed.

These results indicate that there is a complex effect of UV irradiation on conversion, the consumption of the starting macroinitiator and the combination of the radical trapping ability of the RAFT agent along with the reactivity of the propagating radical derived from the initial macroinitiator. As the reactivity of the propagating radical increases from Sty to MA with the same class of RAFT agent,

the comparative increase in yield under UV irradiation relative to dark + AIBN conditions decreases, whilst simultaneously the consumption of the starting macroinitiator decreases. When switching the class of RAFT agent from the less active xanthate PXEP to the more active trithiocarbonate DECET for the same starting macroinitiator the same effects are seen. These effects are compounded and manifest in the poorest performance when the synthesis of poly(MA-b-MMA) was attempted with DECET.

These findings reinforce the conclusions reached in Chapter 6, namely that combinations of monomer and RAFT agent that favour the formation of the RAFT abduct radical species seem to decrease the ability of UV to influence the reaction rate by disallowing the efficient photolysis of RAFT containing species.

8.6 Conclusions

- Under conditions that yielded well controlled polymerisation of VAc, using a poly(MA) macroinitiator derived from PXEP gives poly(MA-b-VAc) block copolymers regardless of whether UV irradiation was used in conjunction with conventional initiation by thermal breakdown of AIBN.
- Under conditions that gave controlled polymerisation of MA, reversing the monomer order to form poly(VAc-b-MA) block copolymers is unsuccessful under all conditions used. This is attributed to the inability of the photoiniferter mechanism to effectively overcome the limitations of the RAFT mechanism which prevent successful fragmentation of the VAc propagating radical after the formation of the MA-RAFT-VAc adduct radical.
- The synthesis of poly(Sty-b-MMA) with both PXEP and Spiro-XEP under UV irradiation should ideally be undertaken with MMA concentrations of 1M or less as this minimises the dispersity of the resulting block copolymers. This is attributed to the reduced negative effects associated with a high concentration of radical species and high viscosities which prevent homogenisation of the reaction mixture.
- Overall, Spiro-XEP was inferior to PXEP as evidenced by PXEP giving narrower dispersity poly(Sty-b-MMA) block copolymers.

UV irradiation can overcome the limitations of the RAFT mechanism to allow the synthesis of both poly(Sty-b-MMA) and poly(MA-b-MMA) block copolymers when PXEP is used. Using DECET for synthesis of poly(Sty) and poly(MA) macroinitiators leads to macroinitiator that chain extend in a much poorer fashion when compared directly to the same macroinitiators derived from PXEP. Furthermore, the results indicate that photolysis of the poly(MA) macroinitiators is less successful

relative to poly(Sty) macroinitiators, regardless of whether PXEP or DECET are used to form the starting macroinitiator.

Using UV irradiation which overlaps with both molecular transitions in DECET gave marginally the same results as increasing the irradiation wavelength to only stimulate the n → π* transition with DECET by employing blue LEDs (471 nm). These results most likely occur due to the stronger influence of the degenerative chain transfer mechanism that is expected to occur when DECET is used, primarily due to the far superior radical trapping abilities of trithiocarbonates relative to xanthates.

Taken holistically, these results strongly support the idea that when attempting the synthesis of block copolymers of the general poly(LAM-b-MAM) form, the RAFT agent chosen should be of the lowest activity possible whilst still allowing the synthesis of a relatively narrow starting poly(LAM) block with good chain end fidelity. Furthermore, the difference in radical stability and thus reactivity between the LAM and MAM block cannot be too great. The limitations of this approach are likely specific to the RAFT agent and monomer combination and probably need to be experimentally determined; the effect of irradiation wavelength and light intensity also needs to be explored further. Considering the findings presented here, it appears that in retrospect the early successes of researchers in the iniferter field at producing block copolymers of the poly(LAM-b-MAM) can most likely be attributed due to the RAFT agents selected being of generally lower activity, namely xanthates [8] and dithiocarbamates [10, 11, 23].

8.7 References

1. Gavrilov, M. and M.J. Monteiro, *Derivation of the molecular weight distributions from size exclusion chromatography.* European Polymer Journal, 2015. **65**: p. 191-196.
2. Gardiner, J., et al., *4-Halogeno-3,5-dimethyl-1H-pyrazole-1-carbodithioates: versatile reversible addition fragmentation chain transfer agents with broad applicability.* Polymer International, 2017. **66**(11): p. 1438-1447.
3. Xu, J., et al., *Synthesis of Discrete Oligomers by Sequential PET-RAFT Single-Unit Monomer Insertion.* Angewandte Chemie International Edition, 2017: p. n/a-n/a.
4. Niwa, M., Y. Sako, and M. Shimizu, *Block Polymerizations of Vinyl Monomers Initiated by Telechelicisopropyl Xanthate-Terminated Polymers as Macrophotoinitiator. Design Of Block Copolymers. 2.* Journal of Macromolecular Science: Part A - Chemistry, 1987. **24**(11): p. 1315-1332.
5. Haven, J.J., et al. *RAFT 20 years later - RAFT-synthesis of uniform, sequence-defined (co)polymers*. in *Reversible Deactivation Radical Polymerization: From Mechanisms to Materials and Applications*. 2018. Washington, DC: American Chemical Society.
6. Moad, G. and D.H. Solomon, *5 - Termination*, in *The Chemistry of Radical Polymerization (Second Edition)*. 2005, Elsevier Science Ltd: Amsterdam. p. 233-278.

7. Nakamura, Y. and S. Yamago, *Termination Mechanism in the Radical Polymerization of Methyl Methacrylate and Styrene Determined by the Reaction of Structurally Well-Defined Polymer End Radicals.* Macromolecules, 2015. **48**(18): p. 6450-6456.

8. Niwa, M., T. Matsumoto, and H. Izumi, *Kinetics of the Photopolymerization of Vinyl Monomers by Bis(Isopropylxanthogen) Disulfide. Design of Block Copolymers.* Journal of Macromolecular Science: Part A - Chemistry, 1987. **24**(5): p. 567-585.

9. Ajayaghosh, A., *Macrophotoinitiator containing pendent xanthate chromophore: photopolymerization of methyl methacrylate and evaluation of kinetic parameters.* Polymer, 1995. **36**(10): p. 2049-2053.

10. Otsu, T. and A. Kuriyama, *Living mono- and biradical polymerizations in homogeneous system synthesis of AB and ABA type block copolymers.* Polymer Bulletin, 1984. **11**(2): p. 135-142.

11. Turner, S.R. and R.W. Blevins, *Photoinitiated block copolymer formation using dithiocarbamate free radical chemistry.* Macromolecules, 1990. **23**(6): p. 1856-1859.

12. Moad, G., et al., *Living free radical polymerization with reversible addition – fragmentation chain transfer (the life of RAFT).* Polymer International, 2000. **49**(9): p. 993-1001.

13. Nakayama, Y., et al., *Preparation of poly(ethylene glycol)–polystyrene block copolymers using photochemistry of dithiocarbamate as a reduced cell-adhesive coating material.* Biomaterials, 1999. **20**(10): p. 963-970.

14. Destarac, M., *On the Critical Role of RAFT Agent Design in Reversible Addition-Fragmentation Chain Transfer (RAFT) Polymerization.* Polymer Reviews, 2011. **51**(2): p. 163-187.

15. Moad, G. and C. Barner-Kowollik, *The Mechanism and Kinetics of the RAFT Process: Overview, Rates, Stabilities, Side Reactions, Product Spectrum and Outstanding Challenges*, in *Handbook of RAFT Polymerization*. 2008, Wiley-VCH Verlag GmbH & Co. KGaA. p. 51-104.

16. Ponnusamy, K., R.P. Babu, and R. Dhamodharan, *Synthesis of block and graft copolymers of styrene by raft polymerization, using dodecyl-based trithiocarbonates as initiators and chain transfer agents.* Journal of Polymer Science Part A: Polymer Chemistry, 2013. **51**(5): p. 1066-1078.

17. Skrabania, K., et al., *Examining the UV-vis absorption of RAFT chain transfer agents and their use for polymer analysis.* Polymer Chemistry, 2011. **2**(9): p. 2074-2083.

18. Tan, J., et al., *Facile Preparation of CO2-Responsive Polymer Nano-Objects via Aqueous Photoinitiated Polymerization-Induced Self-Assembly (Photo-PISA).* Macromolecular Rapid Communications, 2017. **38**(13): p. n/a-n/a.

19. Rubens, M., P. Latsrisaeng, and T. Junkers, *Visible light-induced iniferter polymerization of methacrylates enhanced by continuous flow.* Polymer Chemistry, 2017.

20. Li, J., et al., *Photo-induced reversible addition-fragmentation chain transfer (RAFT) polymerization of acrylonitrile at ambient temperature: A simple system to obtain high-molecular-weight polyacrylonitrile.* Reactive and Functional Polymers, 2017. **113**: p. 1-5.

21. Lewis, R., et al., *Ultra-fast aqueous polymerisation of acrylamides by high power visible light direct photoactivation RAFT polymerisation.* Polymer Chemistry, 2017.

22. McKenzie, T.G., et al., *Investigation into the photolytic stability of RAFT agents and the implications for photopolymerization reactions.* Polymer Chemistry, 2016. **7**(25): p. 4246-4253.

23. Lambrinos, P., et al., *The mechanism of the polymerization of n.butyl acrylate initiated with N,N-diethyl dithiocarbamate derivatives.* European Polymer Journal, 1990. **26**(10): p. 1125-1135.

9 Summary and Future Work

A pair of spiro-dithiocarbamates with the RAFT moiety on the indole half of the spirooxazine and a pair of spiro-xanthates with RAFT moiety on the naphthalene half of the spirooxazine were designed as candidate molecules to test whether RAFT agent reactivity can be influenced by a photoswitchable Z group. DFT simulations of a series of conventional RAFT agents established a linear correlation between LUMO energy and the natural charge on the sulfur in the C=S bond of the RAFT moiety, which is indicative of trends in RAFT agent reactivity. Differing electronic properties and in turn reactivity of the RAFT moiety was indicated by all spiro-RAFT agents aligning with this trend while in the closed spirooxazine form, however, each showed a marked deviation from the linear trend when in the open merocyanine form. Thermodynamic parameters that can qualitatively predict RAFT agent reactivity were computed for a spiro-xanthate and spiro-dithiocarbamate via *ab initio* molecular orbital theory calculations. These parameters predicted the spiro-xanthate should be sufficiently reactive towards radical addition to control the polymerisation of both MAMs and LAMs in both the open and closed forms, however the spiro-dithiocarbamate would be reactive enough to control MAMs only when in the open form. Both spiro-RAFT agents were expected to allow fragmentation of LAMs in their closed form but were expected to retard LAM polymerisation by preventing radical fragmentation when in the open form. A photochromic xanthate (spiro-XEP) and its non-photochromic xanthate analogue (PXEP) were synthesised for comparative testing purposes.

Polymerisation of MA with PXEP under dark + AIBN conditions resulted in an apparent polymerisation rate coefficient of 0.32 h^{-1}, with this increasing by a factor of 10 under UV irradiation irrespective of the presence of AIBN. This kinetic behaviour was replicated during chain extension experiments with a poly(MA) macroinitiator, indicating that this behaviour was not influenced by the RAFT pre-equilibrium. In the absence of monomer, UV irradiation was found to lead to accelerated decomposition of AIBN and to permanent degradation of PXEP. Modelling in Predici showed that under polymerisations with UV irradiation, reversible photolysis of RAFT terminated species was the primary source of initiating radicals and thus the reason behind the increased polymerisation rate, with other photolysis pathways playing a minor role. Spiro-XEP gave the same apparent polymerisation rate under dark + AIBN conditions as PXEP, however a smaller enhancement factor of 2.67x under UV irradiation with AIBN present. This was attributed to competitive absorption of UV photons by the spirooxazine and RAFT moieties. Spiro-XEP also gave living polymers as shown by successful chain extension to form poly(MA-b-MA) under both dark + AIBN and light + AIBN conditions.

The Predici modelling showed that in both MA and VAc polymerisations the RAFT mechanism is the means of control of both molecular weight and dispersity, with the photoiniferter effect being unable to account for the experimentally observed evolution of both these variables. The modelling also strongly suggested that the thiyl radical generated from the photoiniferter effect appears to be inert towards monomer addition and is only responsible for reversible termination.

Polymerisation of VAc with PXEP under dark + AIBN, light + AIBN and light only conditions resulted in apparent polymerisation rates of 0.43, 0.49 and 0.13 h^{-1} respectively. Polymerisation rates for chain extension experiments under equivalent conditions showed the same kinetic trends however overall the rates were different, and this was rationalised to occur due to the increased viscosity of the reaction mixtures. Modelling in Predici showed that UV irradiation increased the decomposition rate of AIBN by a factor of 2, with this being the primary source of initiating radicals and thus responsible for the modest 1.15x increase in polymerisation rate. Spiro-XEP showed significant retardation of the apparent polymerisation rate under both dark + AIBN and light + AIBN conditions, being ~ 0.0092 h^{-1} which is only 2.1 % of the rate obtained with PXEP under equivalent conditions. Similar polymerisation rates were observed when spiro-XEP was used in the successful chain extension to form poly(VAc-b-VAc) under both polymerisation conditions.

Polymerisation solutions containing spiro-XEP changed colour to red; this behaviour was found to linearly depend on monomer conversion and be much more pronounced with VAc. Exposing spiro-XEP to a thermal radical source in the dark as well as during UV irradiation with no monomers present gave similar results. In all cases these changes were found to be non-reversible and persisted in the purified polymers. It was proposed that this is due to a permanently open form of the spiro-XEP structure generated from radical induced degradation of the spirooxazine moiety. This altered RAFT agent structure could thus be an explanation of the rate retardation seen during VAc polymerisations.

The synthesis of copolymers such as poly(VAc-b-MA), which have block orders “forbidden” by the RAFT mechanism was attempted under photoiniferter conditions with PXEP, however was not successful. Conversely, poly(MA-b-VAc) copolymers were formed under all reaction conditions tested. UV irradiation was required for the successful synthesis of poly(Sty-b-MMA) and poly(MA-b-MMA) copolymers, however thermal initiation was found to lead to bimodal molecular weight distributions. Furthermore, using PXEP as the starting RAFT agent in both cases gave better results than a trithiocarbonate (DECET) under equivalent conditions. Irrespective of the RAFT agent used, poly(Sty) was determined to lead to more uniform copolymers than poly(MA). Thus, it was concluded

that less active RAFT agents are required as this allows a greater contribution from the photoiniferter effect to consume the starting macroinitiator.

9.1 Future Work

The complexity of the relationship between the Z functional photochromic part of the photochromic RAFT agent and the photoiniferter effect are inherent challenges in achieving a photoswitchable RAFT agent. The use of narrow spectrum illumination sources can potentially separate the activation of the photochromic from the iniferter effect, although the latter is primarily only a source of radicals and does not negatively impact the ability to polymerise different monomers as required.

A potential alternate method of switching the spiro-XEP agent is to use the ability of spirooxazines to undergo reversible switching by protonation. This would allow 100% of the spiro-RAFT to be in the switched merocyanine form as required and thus give a definite comparison between the polymerisation behaviour of the open merocyanine and closed spirooxazine forms. Quantification of the thermochromic effect seen with spiro-XEP and selection of appropriate reaction conditions including method and type of initiator would be required to achieve this.

Further investigation into the formation and identification of the red coloured by-products under both light only and dark + AIBN conditions could potentially lead to an elucidation of the mechanism by which they are generated. This would be of interest for future work with spirooxazine based RAFT agents that are expected to be used in the polymerisation of monomers which give highly reactive propagating radicals, such as VAc. Understanding the degradation process could potentially allow for the design and synthesis of new spirooxazine based RAFT agents that are more resistant to degradation.

Finally, polymerisation of monomers such as NVP and NVC which are of intermediate reactivity would give a more comprehensive appraisal of the applicability of spiro-XEP.

Appendix

A1.1 Supplementary data for Chapter 3

Table A1: Summary of calculated parameters for RAFT agents modelled using DFT in Spartan.

		Energy (eV)		Dipole (Debye)	Bond lengths (Å)				Natural charges				
Z Group	R Group	HOMO	LUMO		C-Z	C=S	C-S	S-R	"Z" atom	C in C=S	S in C=S	S in C-S-R	"R" atom
1	3	-5.83	-2.30	3.93	1.48	1.653	1.771	1.890	-0.124	-0.333	0.016	0.374	-0.264
1	7	-5.88	-2.18	2.35	1.48	1.655	1.766	1.845	-0.113	-0.338	0.039	0.376	-0.595
2	3	-6.11	-1.89	1.44	1.77	1.645	1.777	1.877	0.365	-0.572	-0.031	0.349	0.174
2	7	-6.24	-1.83	0.44	1.77	1.651	1.775	1.855	0.373	-0.581	-0.058	0.362	-0.593
4	1	-6.21	-2.13	4.75	1.51	1.639	1.764	1.876	-0.725	-0.347	0.017	0.383	-0.264
4	3	-6.02	-1.93	3.51	1.50	1.646	1.765	1.880	-0.732	-0.327	0.005	0.374	0.146
4	7	-6.08	-1.88	2.00	1.51	1.647	1.758	1.849	-0.723	-0.342	-0.037	0.379	-0.602
1	1	-6.14	-2.59	3.49	1.47	1.649	1.779	1.900	-0.134	-0.329	0.041	0.368	-0.270
1	2	-5.73	-2.18	5.04	1.48	1.654	1.770	1.912	-0.124	-0.328	0.010	0.345	-0.163
2	1	-6.37	-2.07	3.18	1.75	1.651	1.775	1.891	0.385	-0.589	-0.010	0.391	-0.280
2	2	-6.01	-1.76	1.12	1.78	1.651	1.772	1.905	0.361	-0.574	-0.058	0.348	-0.142
3	1	-6.33	-2.23	4.85	1.39	1.647	1.790	1.873	-0.406	-0.137	-0.026	0.342	-0.258
3	2	-5.92	-1.88	2.22	1.40	1.651	1.777	1.897	-0.405	-0.136	-0.055	0.310	-0.145
5	4	-6.46	-1.66	3.66	1.34	1.638	1.771	1.867	-0.517	-0.028	-0.035	0.371	-0.487
5	5	-6.59	-1.70	4.59	1.34	1.643	1.780	1.854	-0.504	-0.026	-0.077	0.363	-0.493
5	6	-6.55	-1.73	3.47	1.34	1.637	1.772	1.854	-0.516	-0.031	-0.030	0.378	-0.711
6	4	-6.49	-1.51	3.75	1.32	1.646	1.775	1.865	-0.526	-0.006	-0.079	0.365	-0.487
6	5	-6.34	-1.33	2.66	1.33	1.648	1.784	1.830	-0.516	0.000	-0.109	0.340	-0.072
6	6	-6.58	-1.59	3.54	1.32	1.645	1.776	1.852	-0.526	-0.009	-0.074	0.371	-0.711
7	4	-5.69	-1.41	5.61	1.35	1.664	1.808	1.876	-0.439	-0.122	-0.095	0.306	-0.484
7	5	-5.33	-1.17	4.33	1.35	1.671	1.829	1.854	-0.410	-0.108	-0.137	0.242	-0.055
7	6	-6.12	-1.07	5.65	1.35	1.673	1.814	1.839	-0.428	-0.106	-0.174	0.302	-0.693
Spiro-di.(Closed)	5	-5.54	-2.00	3.53	1.37	1.653	1.795	1.870	-0.463	-0.139	-0.018	0.302	-0.491
Spiro-di.(Open)	5	-5.22	-2.77	4.24	1.41	1.649	1.762	1.862	-0.416	-0.188	0.021	0.421	-0.470
Spiro-di.(Closed)	6	-5.59	-1.81	5.22	1.36	1.654	1.822	1.832	-0.451	-0.123	-0.064	0.316	-0.703
Spiro-di.(Open)	6	-5.44	-3.01	3.95	1.40	1.648	1.769	1.853	-0.417	-0.185	0.028	0.419	-0.716
Spiro-xan.(Closed)	5	-5.43	-1.76	5.27	1.34	1.642	1.768	1.867	-0.514	-0.021	-0.057	0.358	-0.475
Spiro-xan.(Open)	5	-5.22	-2.58	5.74	1.34	1.642	1.791	1.833	-0.487	-0.012	-0.063	0.318	-0.064
Spiro-xan.(Closed)	6	-5.33	-1.75	3.92	1.34	1.638	1.773	1.853	-0.514	-0.028	-0.034	0.375	-0.710
Spiro-xan.(Open)	6	-5.30	-2.67	5.31	1.34	1.643	1.791	1.844	-0.482	-0.018	-0.065	0.349	-0.699

A1.1.1 Assessment study on comparison of *ab initio* levels of theory for computation of spiro-RAFT agents

Comparisons of the key parameters RSE, ΔH_{stab}.and ΔH_{frag}.calculated using different levels of *ab initio* theory for the CSIRO RAFT agents in both their netural and protonated forms along with the Z = methyl prototypical RAFT agent are shown below.

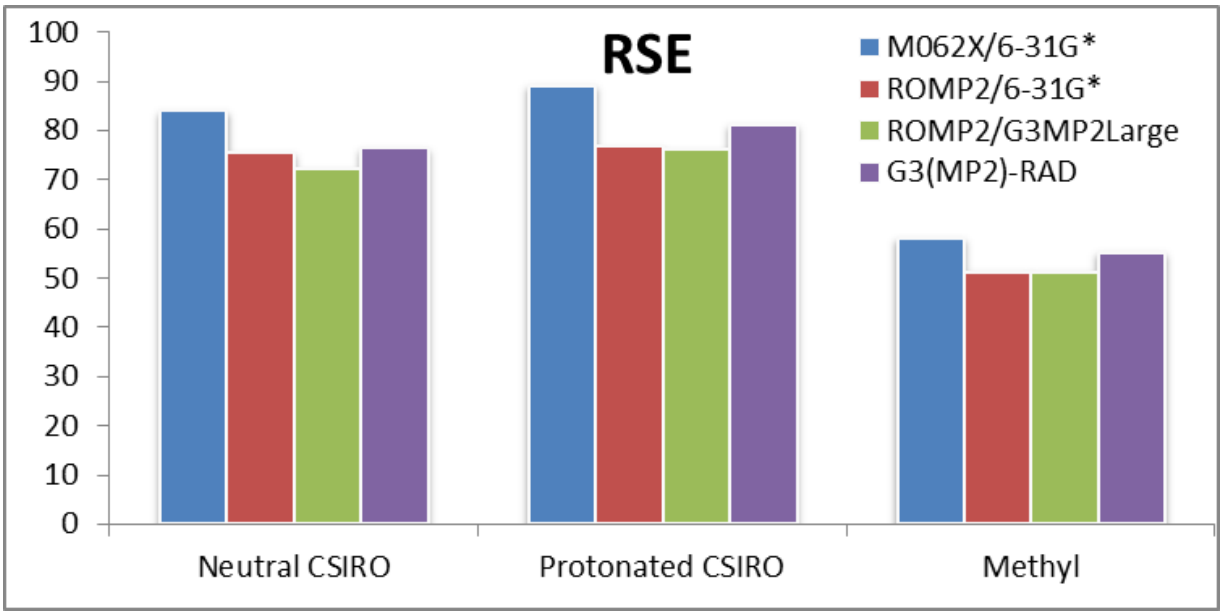

Figure A1: Assesement on levels of theory for calculation of RSE.

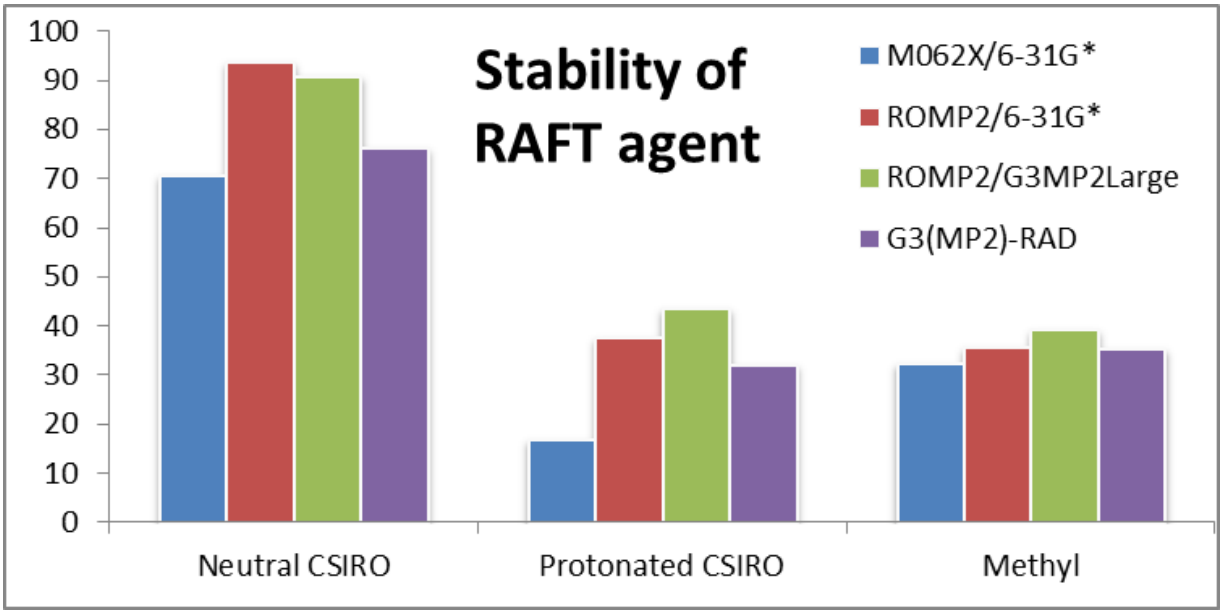

Figure A2: Assesement on levels of theory for calculation of ΔH_{stab}.

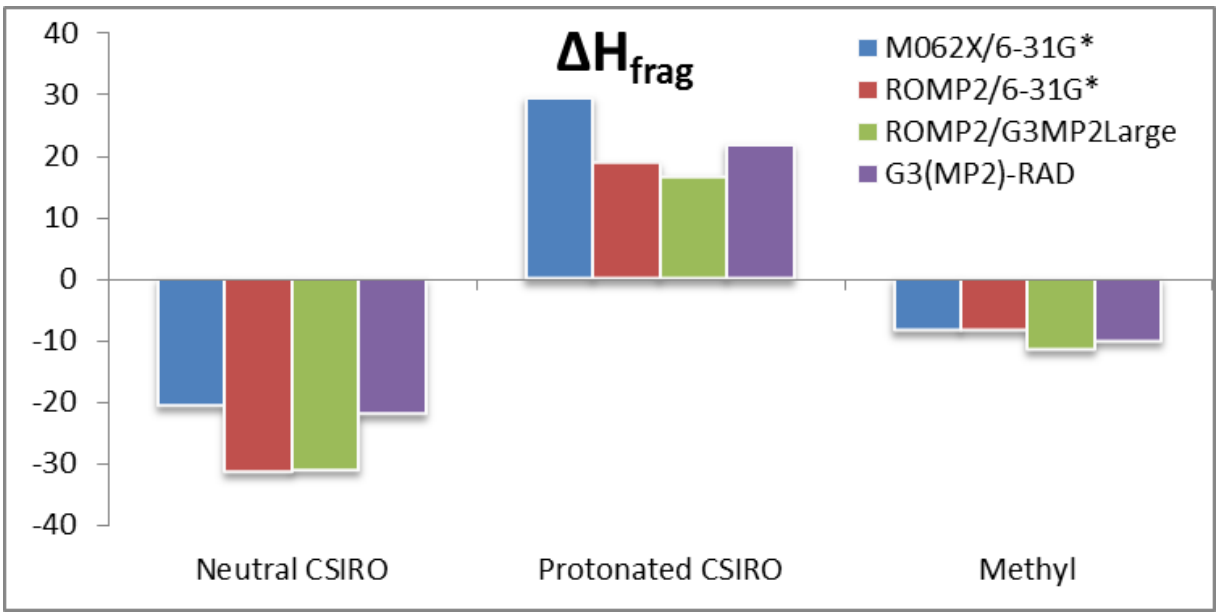

Figure A3: Assesement on levels of theory for calculation of ΔH_{frag}.

Table A2: Enthalpy at 0K using various levels of theory (kJ/mol).

	M062X/6-31G*	ROMP2/6-31G*	ROMP2/G3MP2Large	G3(MP2)-RAD
Stability of RAFT agent				
Neutral CSIRO	70.7	93.7	90.9	76.2
Protonated CSIRO	16.9	37.5	43.6	32.1
Methyl	32.3	35.6	39.2	35.4
RSE				
Neutral CSIRO	84.1	75.6	72.4	76.5
Protonated CSIRO	89.3	76.8	76.3	81.4
Methyl	58.2	51.4	51.3	55.4
ΔH_{frag}				
Neutral CSIRO	-20.6	-31.4	-31.1	-22.0
Protonated CSIRO	29.6	19.0	16.7	21.9
Methyl	-8.4	-8.4	-11.4	-10.1
R^2	0.96	0.97	0.96	1
MAD	5.9	5.2	6.5	
MAX	15	17	15	

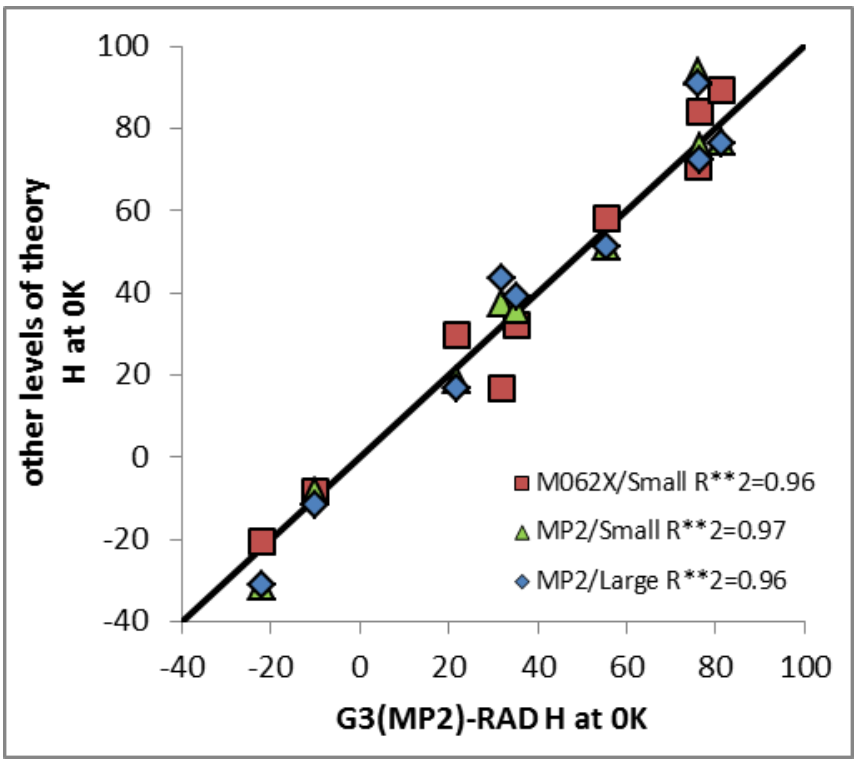

Figure A4: Correlation shown between levels of theory.

All the data above shows that the M062X/6-31G* should be appropriate for the replacement of G3(MP2)-RAD for the study of the large photochromic RAFT agents.

A1.2 Supplementary data for Chapter 4

A1.2.1 Details for the attempted synthesis of cyanomethyl (phenoxycarbonothioyl) xanthate

Method A: Phenol (0.4972 g, 5.31 $x10^{-3}$ moles, 1.00 eq.) was dissolved in 3.2 mL of dimethyl sulfoxide (DMSO), then treated drop wise with potassium hydroxide solution (30 W/V, 0.99 mL, 5.29 $x10^{-3}$ moles, 1.00 eq.) and left to stir for 1 h. Carbon disulfide (CS_2) (0.482 mL, 7.98 $x10^{-3}$ moles, 1.51eq.) was added drop wise which gave a gradual colour change of the reaction mixture to dark red; this was left to stir for 4 h. Chloroacetonitrile (0.336 mL, 5.31 $x10^{-3}$ moles, 1.00 eq.) was added dropwise which gave a change back to a yellow colour; left to stir for 20 h. After washing with brine and extraction with diethyl ether, analysis of the organic extracts by TLC showed the only coloured products to be more polar than the starting phenol.

Method B: Phenol (0.5079 g, 5.40 $x10^{-3}$ moles, 1.00 eq.) along with potassium tert-butoxide (0.7427 g, 6.62 $x10^{-3}$ moles, 1.23 eq.) was dissolved in 3.2 mL of dry dimethylformamide and left to stir for 1 h. CS_2 (0.48 mL, 7.95 $x10^{-3}$ moles, 1.47 eq.) was added drop wise which gave a gradual colour change of the reaction mixture to dark orange; this was left to stir for 3 h. Chloroacetonitrile (0.336 mL, 5.31 $x10^{-3}$ moles, 0.98 eq.) was added dropwise which gave a change to dark red; left to stir for

20 h. Same as for method A, after washing with brine and extraction with diethyl ether, analysis of the organic extracts by TLC showed the only coloured products to be more polar than the starting phenol.

Method C: Phenol (0.4987 g, 5.23 $x10^{-3}$ moles, 1.00 eq.) was dissolved in 5.0 mL of DMSO, then treated drop wise with potassium hydroxide solution (30 W/V, 0.99 mL, 5.29 $x10^{-3}$ moles, 1.00 eq.) and left to stir for 2 h. Carbon disulfide (CS_2) (0.35 mL, 5.80 $x10^{-3}$ moles, 1.09 eq.) was added drop wise which gave a gradual colour change of the reaction mixture to dark red; this was left to stir for 18 h. Bromoacetonitrile (0.408 mL, 5.86 $x10^{-3}$ moles, 1.10 eq.) was added dropwise and left to stir for 48 h. After washing with brine and extraction with chloroform, analysis of the organic extracts by TLC showed all components to be more polar than the starting phenol.

Method D: Phenol (0.5119 g, 5.44 $x10^{-3}$ moles, 1.00 eq.) along with potassium tert-butoxide (0.6841 g, 6.10 $x10^{-3}$ moles, 1.12 eq.) was dissolved in 10 mL of dry toluene and left to stir for 4 h. CS_2 (0.35 mL, 7.95 $x10^{-3}$ moles, 1.06 eq.) was added drop wise and left to stir for 16 h, after which point the reaction mixture had turned orange. Bromoacetonitrile (0.4 mL, 5.74 $x10^{-3}$ moles, 1.06 eq.) was added dropwise which gave a change to dark red; left to stir for 48 h. Same as for method A, after washing with brine and extraction with toluene, analysis of the organic extracts by TLC showed the only coloured products to be more polar than the starting phenol.

A1.2.2 Details for the attempted synthesis of N-H terminated spirooxazine by debenzylation of 1-benzyl-3,3-trimethylspiro[indoline-2,3'-[3H]naphtha[2,1-b][1,4]oxazine]

Methods A & B: Into a 25 mL round bottom flask equipped with a stirrer bar, benzylated spirooxazine mixed with Pd on C (10 % w/w) followed by addition of the ~ 10 mL of the desired solvent. The reaction vessel was then sealed with a suba seal, and reaction mixture sparged with ~ 2 L of hydrogen gas, before being equipped with a balloon providing a positive pressure of hydrogen gas and left to stir for the specified time at room temperature. Reactions were halted by exposure to air, filtering through a short pipette column filled with celite, followed by removal of solvent under vacuum.

Method C: Same general procedure as for methods A & B, however after filtration through celite, the reaction mixture was stirred rapidly for 10 mins with saturated sodium bicarbonate solution to neutralise the acetic acid catalyst. The mixture was then extracted with chloroform, dried with sodium sulfate, filtered and dried under vacuum.

Method D: Benzylated spirooxazine (43.5 mg, 1.08 $x10^{-4}$ moles, 1 eq.) dissolved with rapid stirring in 3 mL of DMSO, to which a suspension of k tert-butoxide (137.3 mg, 1.22 $x10^{-3}$ moles, 11.38 eq.)

in 6 mL DMSO added dropwise, with an immediate colour change to black seen. Left to stir under ambient conditions for 5 h, then the reaction was halted by washing with 10 mL of saturated ammonium chloride solution. This was extracted with 3x 10 mL of diethyl ether and 2x 20 mL of chloroform. Organic extracts combined, dried with sodium sulfate, filtered under gravity and dried under vacuum.

Method E: Benzylated spirooxazine (0.85 g, 2.14 $x10^{-3}$ moles, 1 eq.) dissolved with rapid stirring in 15 mL of DMSO, to which a suspension of k tert-butoxide (0.2356 g, 2.10 $x10^{-3}$ moles, 0.98 eq.) in 10 mL of DMSO was added dropwise. Added a further 5 mL of DMSO with 25 mL of THF to aid the solubility of the benzylated spirooxazine. The round bottom flask was then sealed with a suba seal, and reaction mixture sparged with ~ 2 L of oxygen gas and left under a positive pressure of oxygen for the duration of the reaction. Unreacted benzylated spirooxazine remaining as determined by TLC was observed after 12 h, necessitating further additions of k tert-butoxide (0.2408 g, 2.14 $x10^{-3}$ moles, 1.00 eq.) and (0.7040 g, 6.27 $x10^{-3}$ moles, 2.93 eq.) after 12 and 36 h respectively. After a total reaction time of 72 h, the reaction was washed with brine, and extracted twice with chloroform to give a bright red organic layer. The orange aqueous layer (pH ~ 10 by pH strips) was acidified dropwise by the addition of 1M HCl until a pH of ~ 1 was reached, which allowed extraction of the bright orange colour into the chloroform layer. Both red and orange organic fractions were dried with sodium sulfate, filtered under gravity and the solvent removed under vacuum.

A1.2.3 Blank GPC trace obtained with single detector GPC system

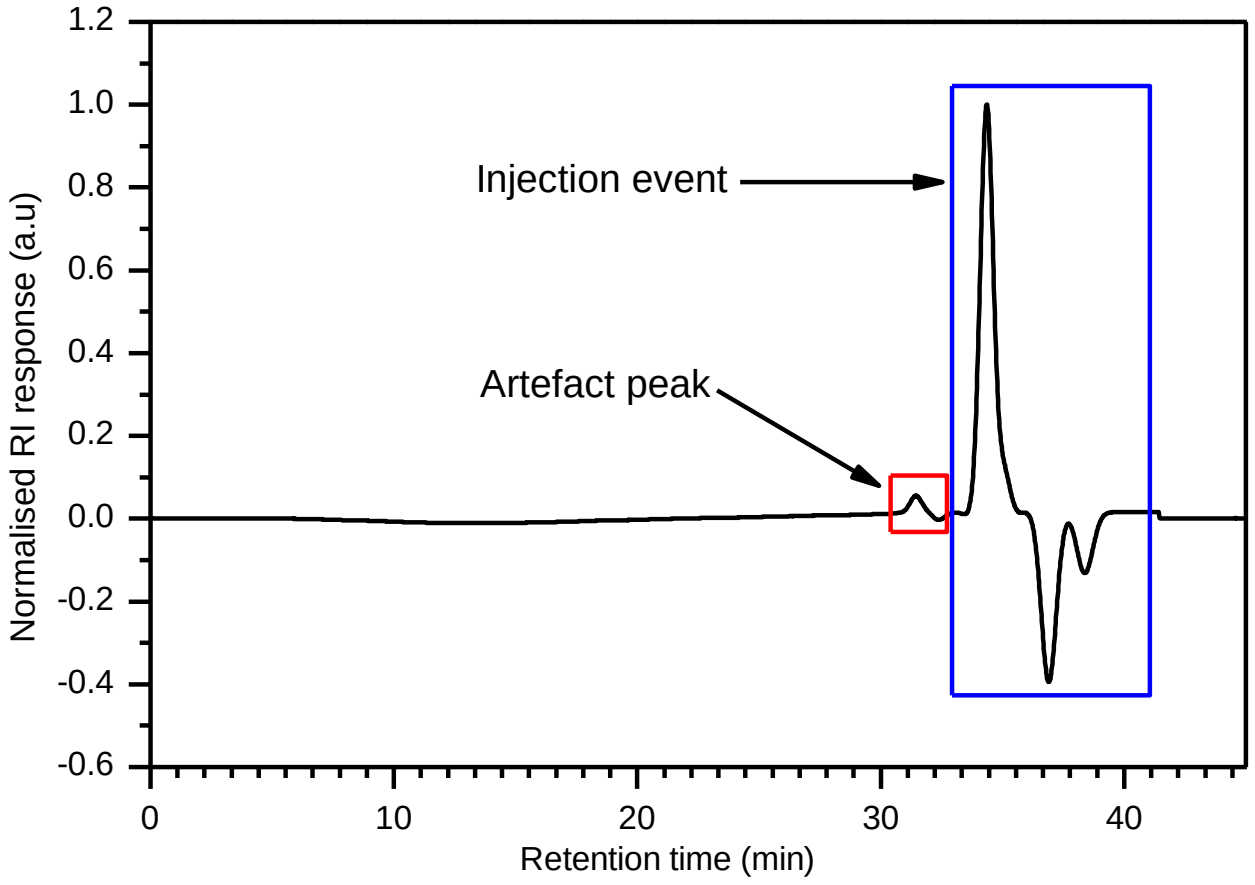

Figure A5: GPC trace of a sample of mobile phase (THF) under standard analysis condtions.

The artefact peak shown in Figure A5 (red box) has a peak retention time of 31.45 minutes, meaning that is sometimes overlaps with the spectra obtained when analysing low molecular weight macroinitiatiors used in chain extension experiments.

A1.2.4 Details for LEDs used in LED photochemical reactor

Figure A10 and Figure A7 (ShenZhen Wayjun Technology Co., LTD.) show detailed characterization information for the same type of LEDs as used to make the blue LED photochemical reactor. The peak wavelength of the LED reactor was found to be 471 nm using the same characterization method as described previously (section 4.4.1) for the UV lamp.

4. BLUE 3528 SMD LED

PART NO	Chip		Lens Color
	Material	Emitted Color	
LED-1210BVC	InGaN	Blue ■	WATER CLEAR

Absolute Maximum Ratings (Ta = 25℃)

Items	Symbol	Absolute maximum Rating	Unit
Power Dissipation	PD	150	mW
Forward Current(DC)	IF	50	mA
Peak Forward Current *	IFP	200	mA
Reverse Voltage	VR	5	V
Operation Temperature	Topr	-40 ~ +95	℃
Storage Temperature	Tstg	-40 ~ +100	℃
Soldering Temperature	Tsol	Reflow Soldering:240℃/10sec Hand Soldering: 350℃/3sec	

*Pulse width≦0.1msec duty≦1/10

Figure A6 Electric characterization data for blue 3528 SMD LEDs. Obtained from [1].

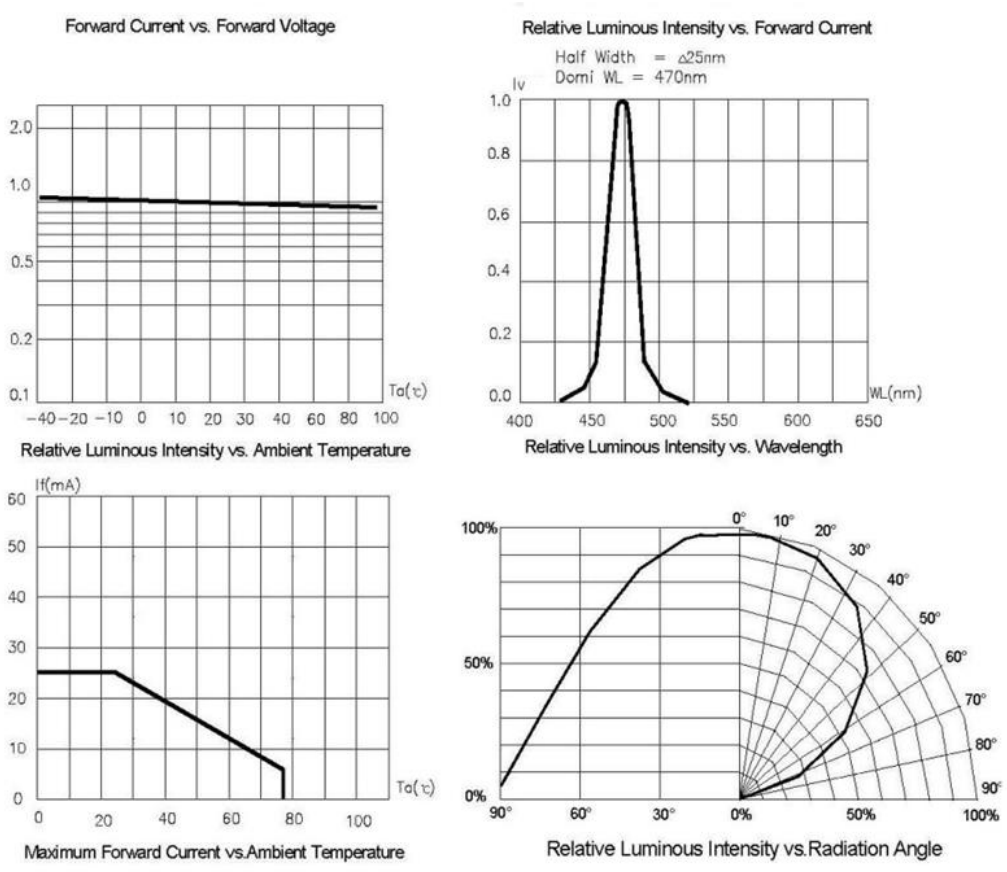

Figure A7: Spectral characterization data for blue 3528 SMD LEDs. Obtained from [1].

A1.2.1 Direct transcripts of Predici scripts

Table A3:Predici scripts used for modification of kinetic rate coefficients.

Script name	Actual script
1	a = getkp(“kd”) b = getx(“monomer”) c = getkp(“photons-initiator”) f0 = getkp(“f”) result1 = a * c * (f0 * (1 – b))
2	a = getkp(“kd”) b = getx(“monomer”) c = getkp(“photons-initiator”) f0 = getkp(“f”) result1 = a * b * c * (1 - f0)
3	k1 = arg1 // kt1 = getkp("kt_1") b = getmn("macro-radical") c = 86.09 d = (b/c) e = getkp("alpha_short") f = getkp("alpha_long") g = getkp("i_cross") i = (b/c) // result1 = kt1*(d^(-e)) if (d > g) result1 = kt1*(g^(-(e-f)))*(i^(-f))
4	k1 = arg1 k2 = arg2 // kt1 = getkp("kt_1") b = getmn("macro-radical") c = 86.09 d = (b/c) e = getkp("alpha_short") f = getkp("alpha_long") g = getkp("i_cross") h = getkp("kt_(disproportionation)") i = (b/c) // result1 = kt1*(d^(-e)) if (d > g) result1 = kt1*(g^(-(e-f)))*(i^(-f)) result2 = h
5	k1 = arg1 //

	kt1 = getkp("kt_1") a = getkp("f(xan_termination)") // result1 = kt1*a
6	k1 = arg1 // kt1 = getkp("kt_1") b = getmn("macro-radical") c = 86.09 d = (b/c) e = getkp("alpha_short") f = getkp("alpha_long") g = getkp("i_cross") h = getkp("f(xan_termination)") i = (b/c) // result1 = kt1*h*(d^(-e)) if (d > g) result1 = h*kt1*(g^(-(e-f)))*(i^(-f))
7	k1 = arg1 // kt1 = getkp("kt_1") b = getmn("pRAFT2") c = 86.09 d = (b/c) e = getkp("alpha_short") f = getkp("alpha_long") g = getkp("i_cross") h = getkp("f(xan_termination)") i = (b/c) // result1 = kt1*h*(d^(-e)) if (d > g) result1 = h*kt1*(g^(-(e-f)))*(i^(-f))

Table A4: Summary of scripts written for analysis of combined molecular weight distributions of various polymer species.

Script name	Actual script
Mn Overall (complex).fun	a = getmy("Polymer",0) / (getmy("Polymer",0) + getmy("pRAFT,0))) * getmn("Polymer") b = getmy("pRAFT",0) / (getmy("Polymer",0) + getmy("pRAFT,0))) * getmn("pRAFT") result1 = a + b
Mw overall (complex).fun	a = getmy("Polymer",0) / (getmy("Polymer",0) + getmy("pRAFT,0))) * getmw("Polymer") b = getmy("pRAFT",0) / (getmy("Polymer",0) + getmy("pRAFT,0))) *

	getmw("pRAFT") result1 = a + b
PDI Overall (complex).fun	a = (getmy("Polymer",0) / (getmy("Polymer",0) + getmy("pRAFT,0))) * getmw("Polymer")) b = (getmy("pRAFT",0) / (getmy("Polymer",0) + getmy("pRAFT,0))) * getmw("pRAFT")) c = (getmy("Polymer",0) / (getmy("Polymer",0) + getmy("pRAFT,0))) * getmn("Polymer")) d = (getmy("pRAFT",0) / (getmy("Polymer",0) + getmy("pRAFT,0))) * getmn("pRAFT")) result1 = (a + b) / (c + d)

A1.1 Supplementary data for Chapter 5

A1.1.1 Photolysis of monomer simulations

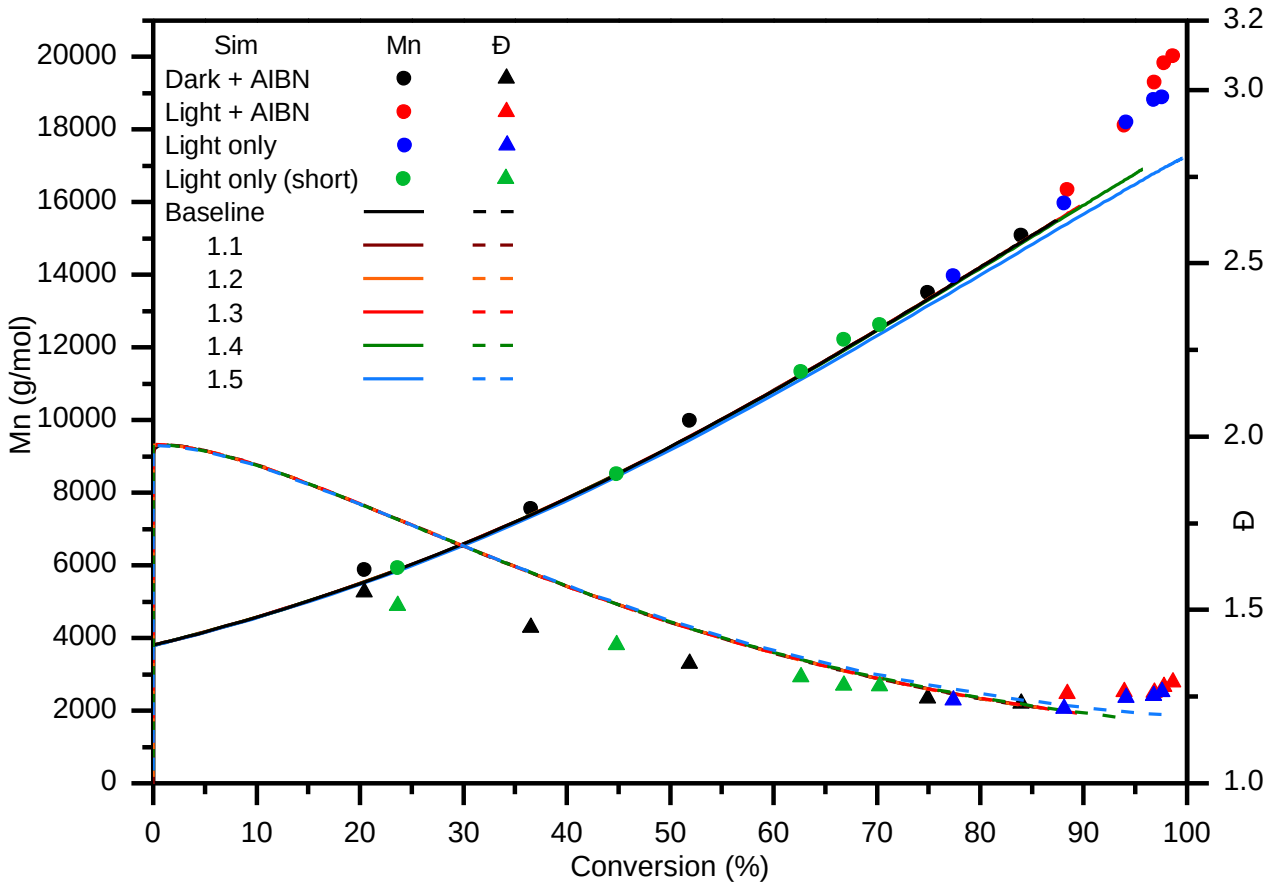

Figure A8: Comparison of evolution of molecular weight and dispersity as a function of conversion for simulations 1.1 – 1.6 and experimental data.

A1.1.2 Photolysis of AIBN simulations

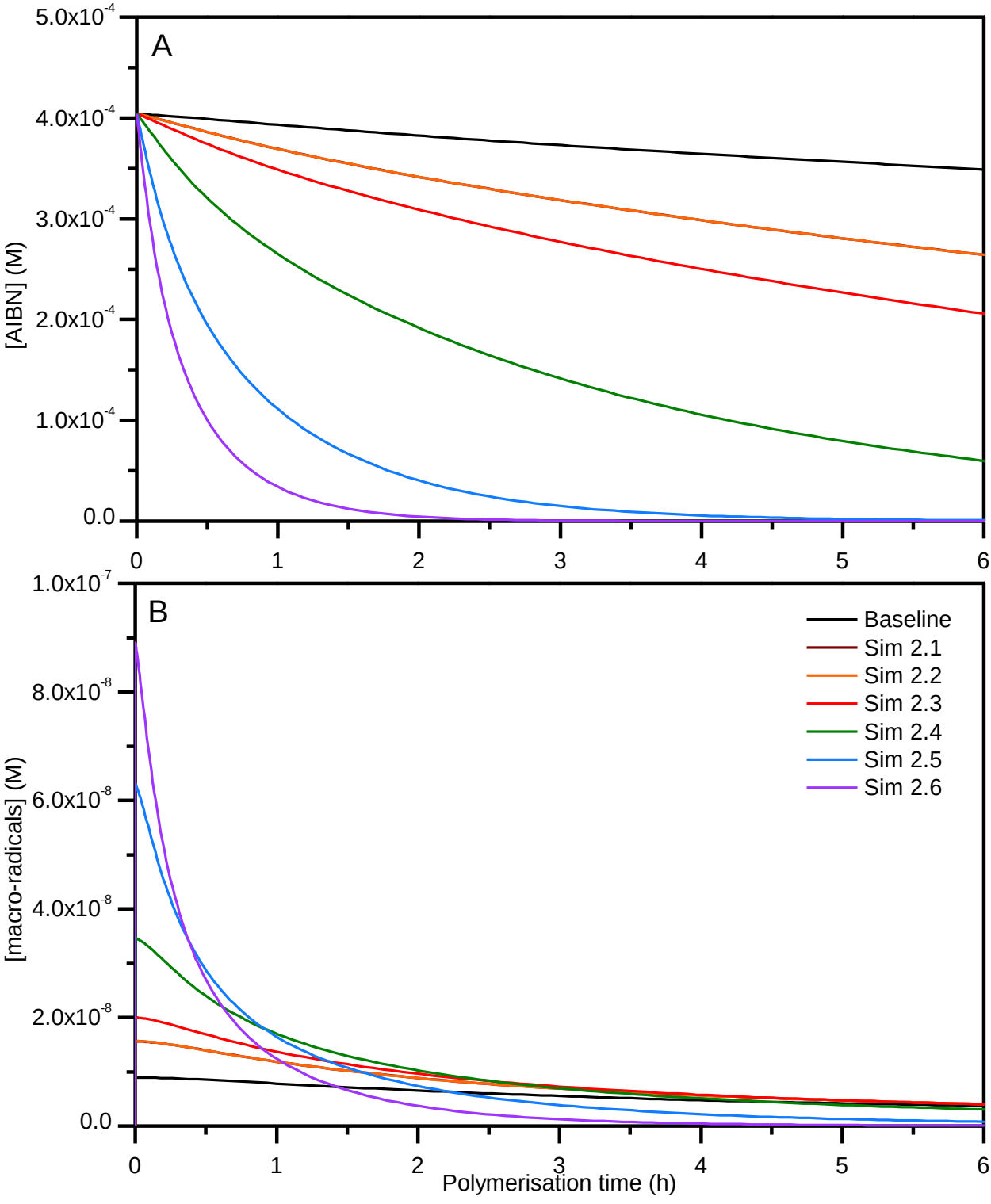

Figure A9: Simulated concentrations of AIBN (A) and macro-radicals (B) vs time for simulations 2.1 – 2.6.

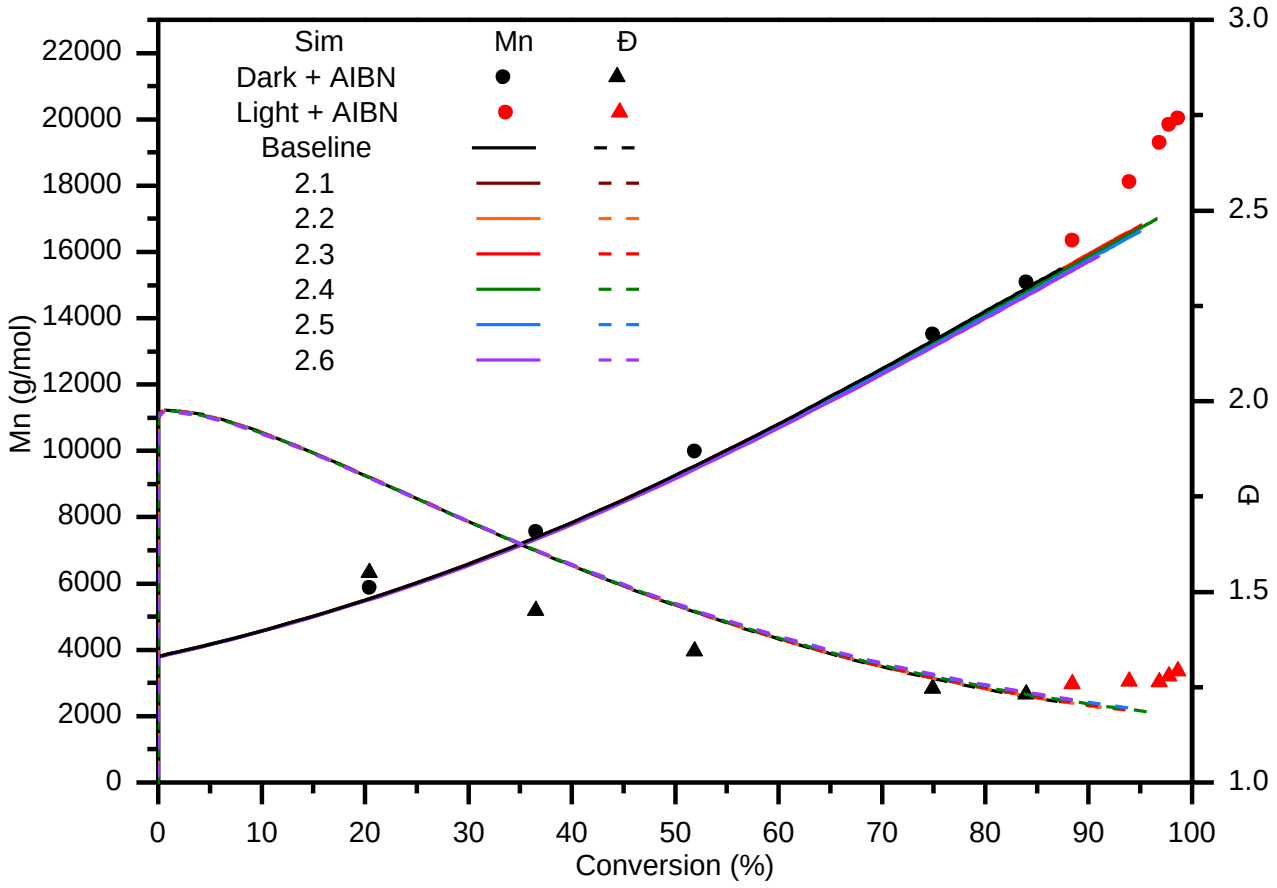

Figure A10: Comparison of evolution of molecular weight and dispersity as a function of conversion for simulations 2.1 – 2.6 and experimental data.

A1.1.3 Photolysis of RAFT agent simulations

Table A5: Parameters for simulations of reversible photolysis of RAFT species where $k_{p(xan)}$ = 10 M^{-1} s^{-1}.

Simulation	$k_{photons\ RAFT}$	$k_{-photons-RAFT}$	$f_{xan-termination}$	$K_{eq(photolysis)}$
3.10.1F (On)	1.7783 E -01	1.7783 E+09	N/A	1.000 E-10
3.10.2F (On)	1.7783 E -02	1.7783 E +08	N/A	1.000 E-10
3.10.3F (On)	1.7783 E -04	1.7783 E +06	N/A	1.000 E-10
3.10.1V (On)	1.0000 E-02	1.7783 E+09 to 8.0627 E+07	1.0000 E+00	5.623 E-12 to 1.240 E-10
3.10.2V (On)	1.0000 E-03	1.7783 E+08 to 8.0627 E+06	1.0000 E-01	5.623 E-12 to 1.240 E-10
3.10.3V (On)	5.0000 E-05	1.7783 E+06 to 8.0627 E+04	1.0000 E-03	5.623 E-12 to 1.240 E-10

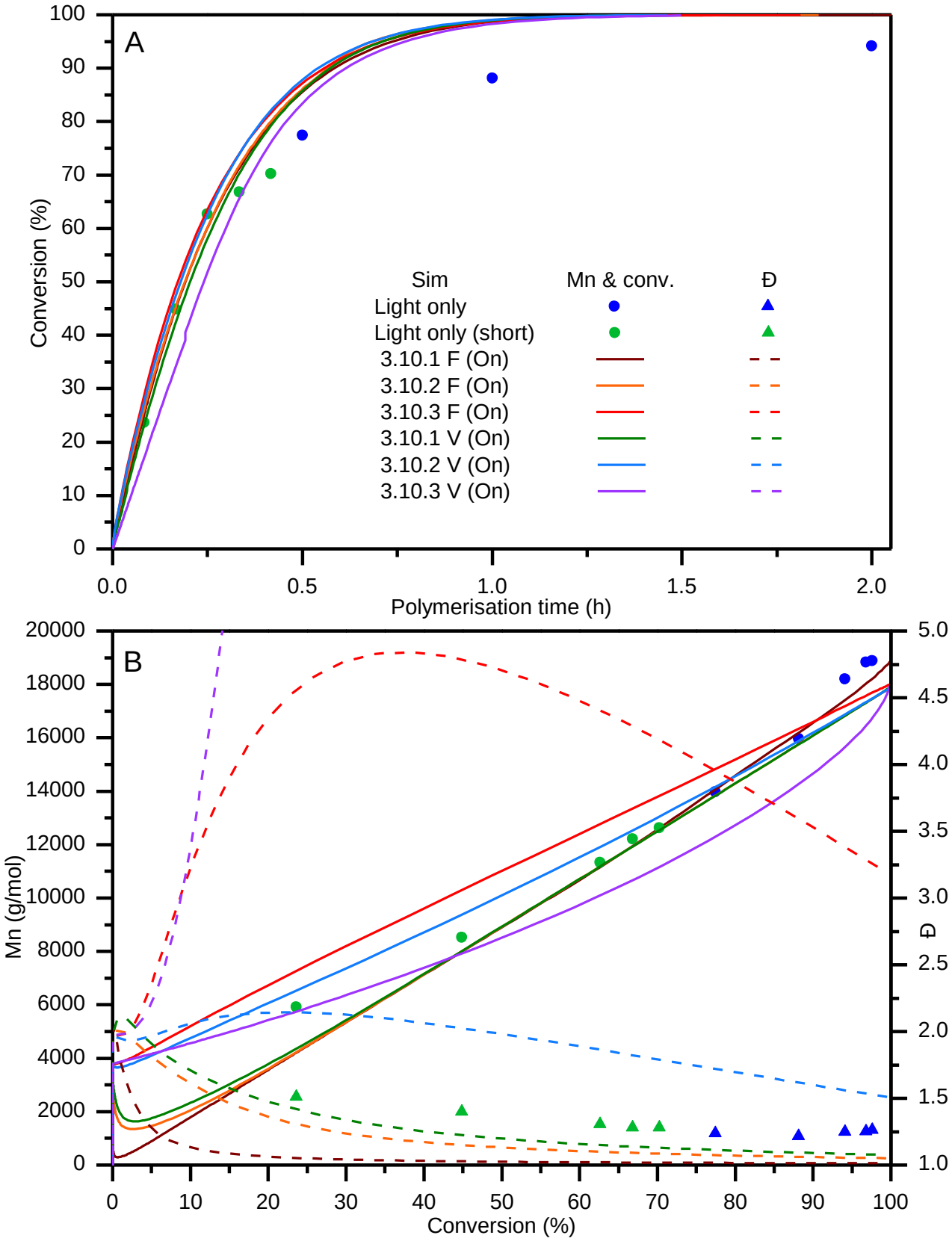

Figure A11: Comparison of conversion versus time (A) and evolution of molecular weight and dispersity as a function of conversion (B) for simulations concerning reversible photolysis of RAFT species where $k_{p(xan)} = 10$ to experimental data.

Table A6: Parameters for simulations of reversible photolysis of RAFT species where $k_{p(xan)}$ = 100.

Simulation	**$k_{photons\ RAFT}$**	**$k_{-photons-RAFT}$**	**$f_{xan-termination}$**	**$K_{eq(photolysis)}$**
3.100.1F (On)	4.4458 E-03	1.7783 E+09	N/A	2.500 E-11
3.100.2F (On)	4.4458 E-04	1.7783 E+08	N/A	2.500 E-11
3.100.1V (On)	5.0000 E-04	1.7783 E+09 to 7.7889 E+07	1.0000 E+00	2.812 E-13 to 6.248 E-12
3.100.2V (On)	5.0000 E-05	1.7783 E+08 to 7.7889 E+06	1.0000 E-01	2.812 E-13 to 6.248 E-12

Simulations corresponding to a fixed value of $k_{-photons-RAFT}$ of 1.7783 $x10^{6}$, and for the variable case, where $f_{xan-termination}$ was 1.00 $x10^{-3}$ were not successfully completed as they resulted in a computation time of over 3 hours corresponding to a reaction time of only ~ 250 seconds within the simulation. The conversion attained was only ~ 10 %, with over 5500 variables most likely being responsible for the heavy computational load encountered, along with the unrealistic overall dispersity values were more than 50 in both cases.

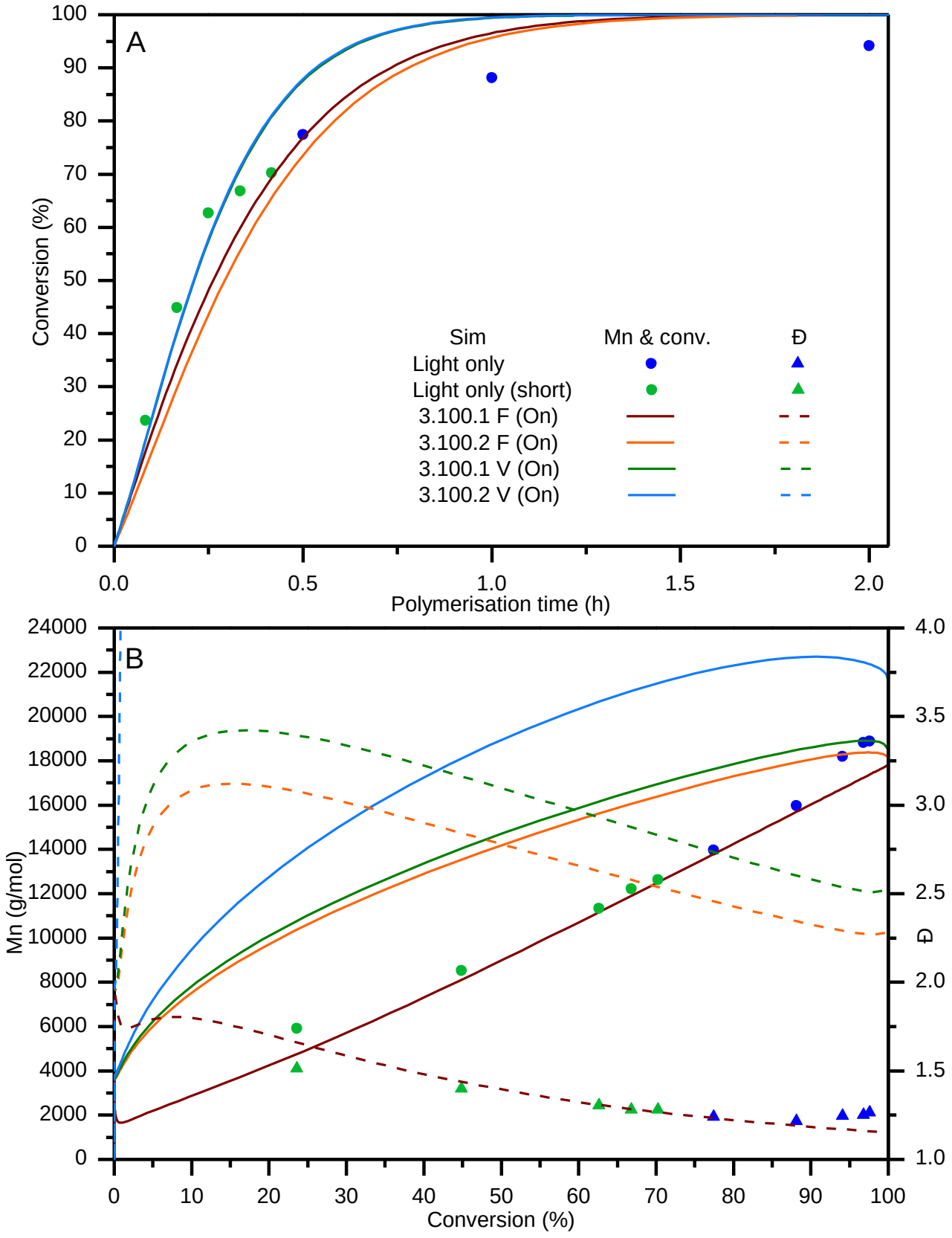

Figure A12: Comparison of conversion versus time (A) and evolution of molecular weight and dispersity as a function of conversion (B) for simulations concerning reversible photolysis of RAFT species where kp(xanthate fragment) = 100 to experimental data.

A1.2 Summplementary data for Chapter 6

A1.2.1 Photolysis of monomer simulations

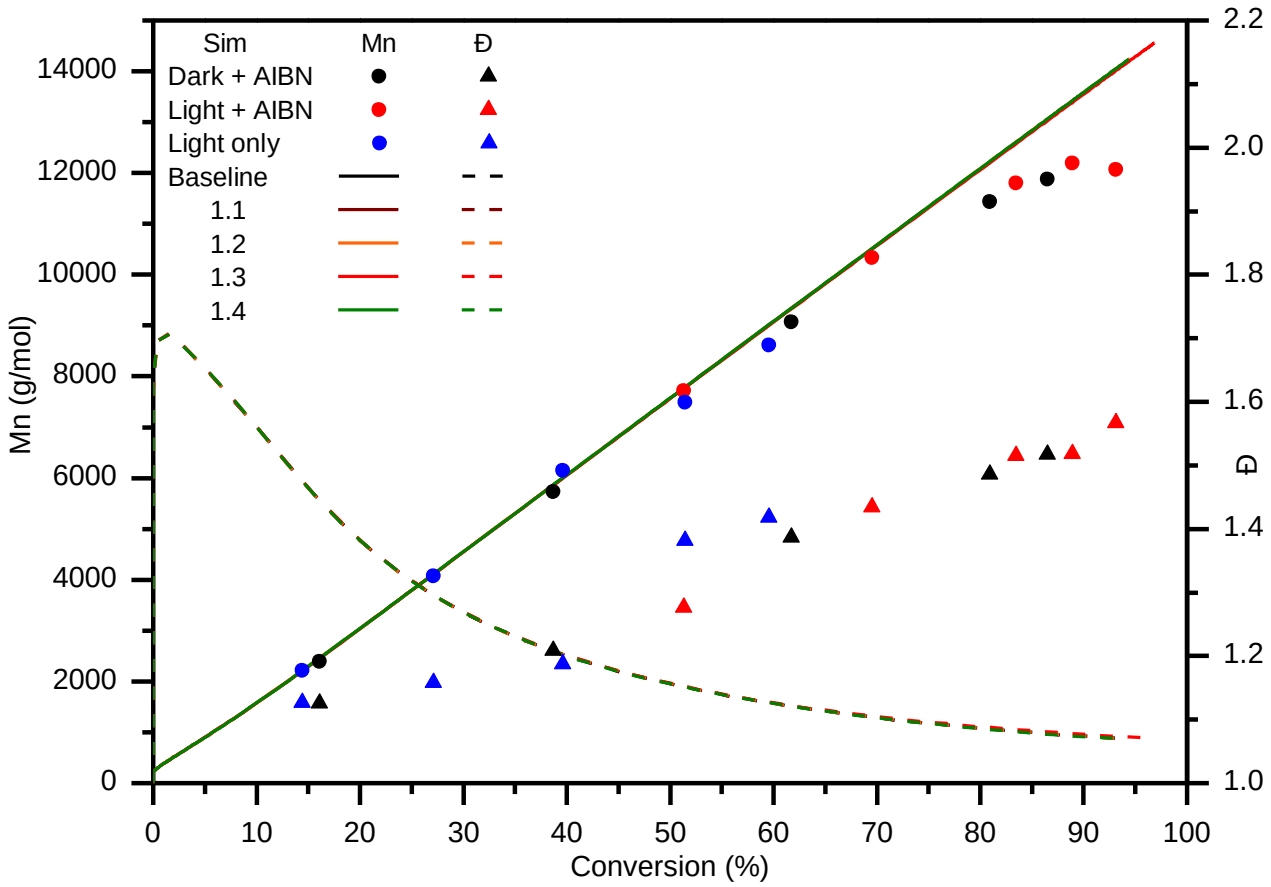

Figure A13: Comparison of evolution of molecular weight and dispersity as a function of conversion for simulations 1.1 – 1.4 and experimental data.

A1.2.2 Photolysis of AIBN simulations

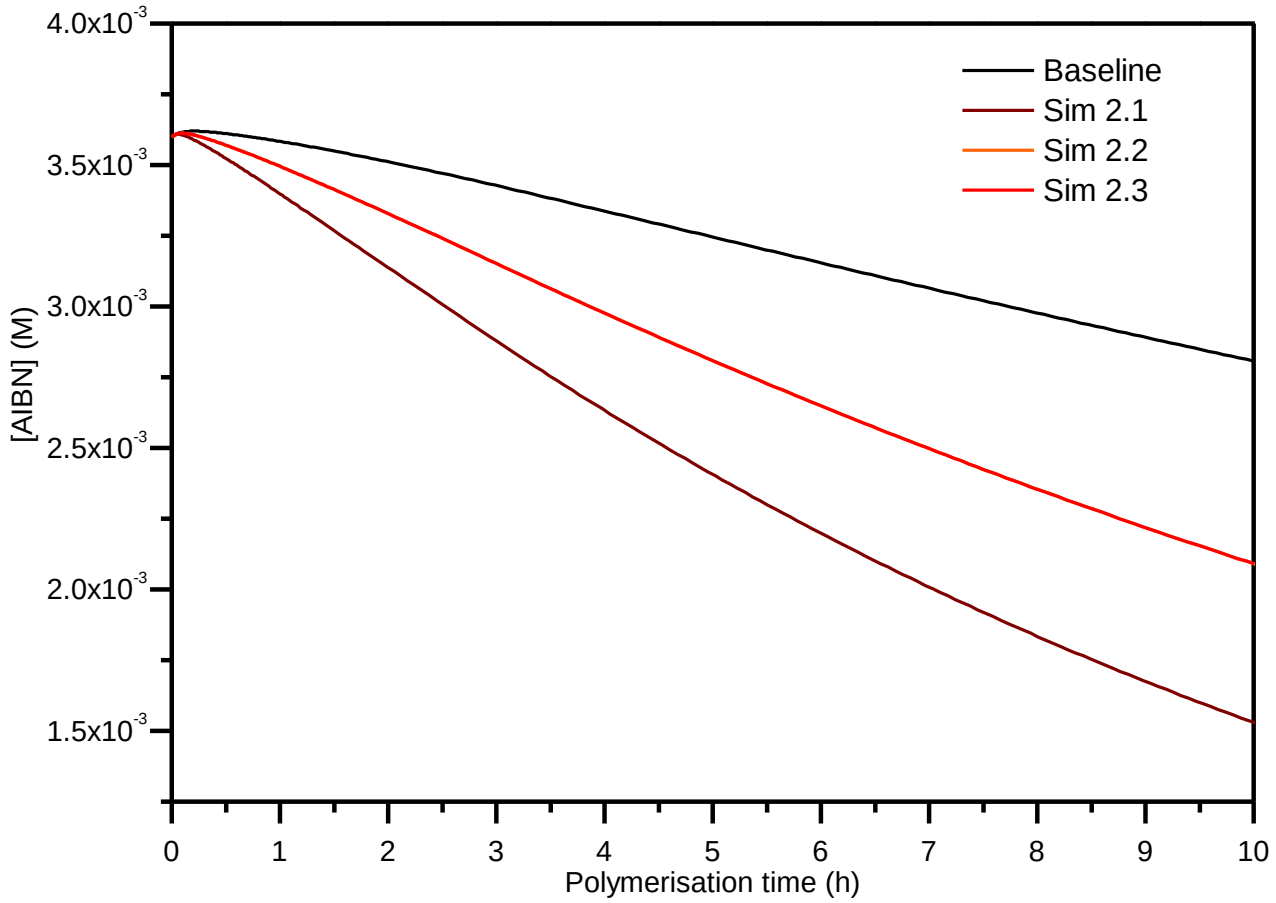

Figure A14: Simulated concentrations of AIBN vs time for simulations 2.1 – 2.3.

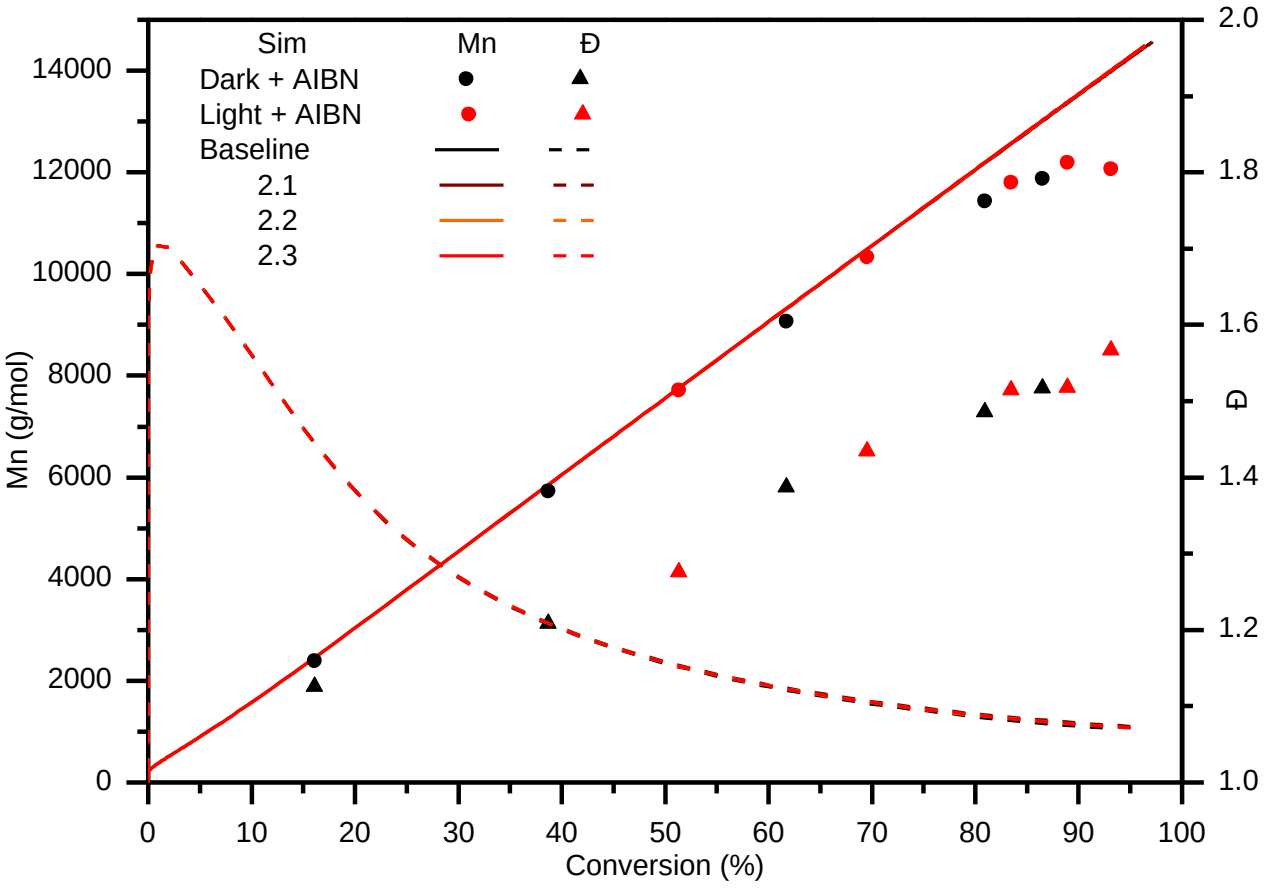

Figure A15: Comparison of evolution of molecular weight and dispersity as a function of conversion for simulations 2.1 – 2.3 and experimental data.

A1.2.3 Photolysis of RAFT agent simulations

Table A7: Parameters for simulations of reversible photolysis of RAFT species where $k_{p(xan)}$ = 10 M^{-1} s^{-1}.

Simulation	$k_{photons\ RAFT}$	$k_{-photons-RAFT}$	$f_{xan-termination}$	$K_{eq(photolysis)}$
3.10.1F (On)(S)	3.750 E-05	1.50E+09	N/A	2.50 E-14
3.10.1F (On)(F)	1.500 E-04	1.50E+09	N/A	1.00 E-13
3.10.2F (On)(S)	3.750 E-06	1.50E+08	N/A	2.50 E-14
3.10.2F (On)(F)	1.500 E-05	1.50E+08	N/A	1.00 E-13
3.10.1V (On)	6.000 E-06	1.50E+09 to 2.0605 E+09	1.00	4.000 E-15 to 2.912 E-14

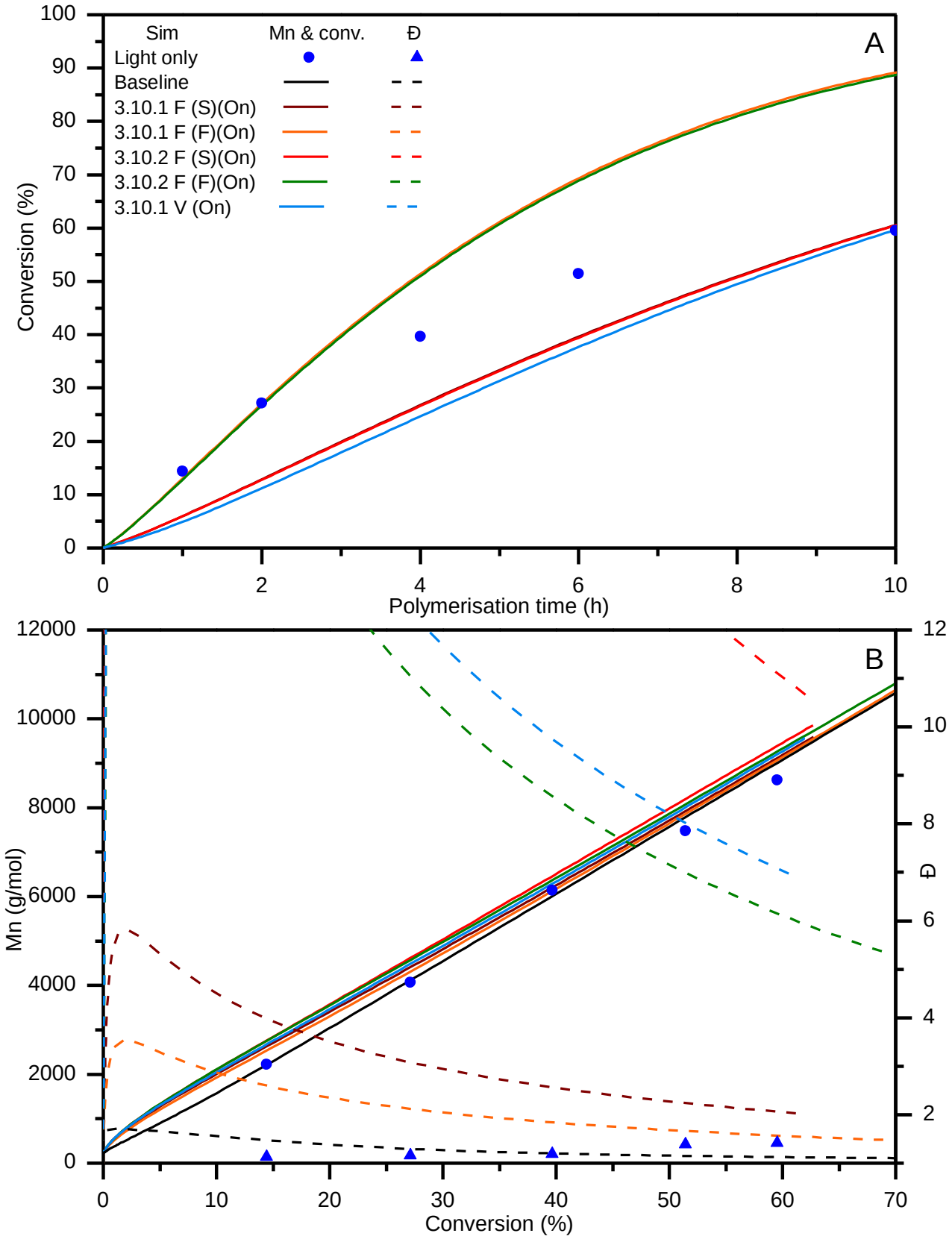

Figure A16: Comparison of conversion versus time (A) and evolution of molecular weight and dispersity as a function of conversion (B) for simulations concerning reversible photolysis of RAFT species where of $k_{p(xan\ frag)}$ = 10 M^{-1} s^{-1} to experimental data.

A1.3 Supplementary data for Chapter 8

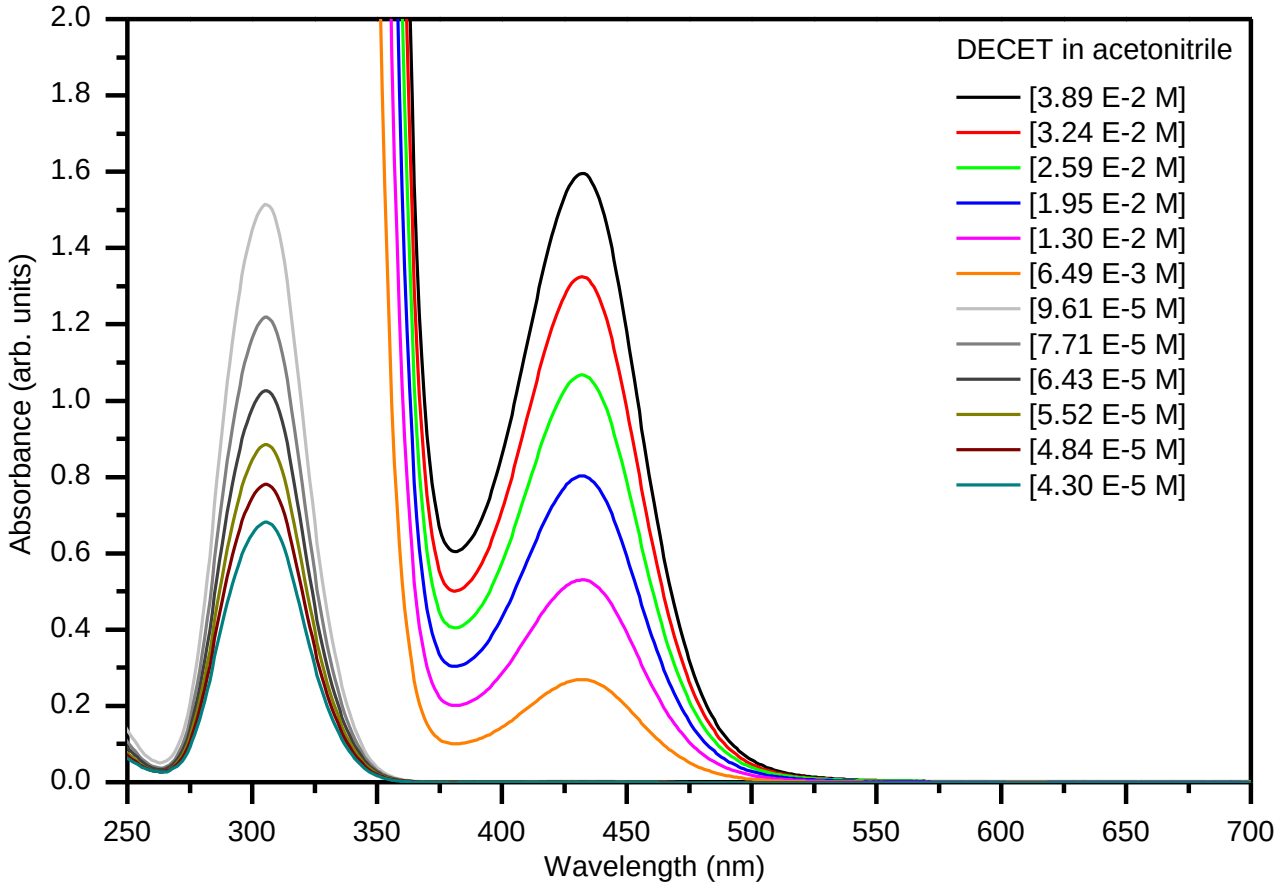

Figure A17: UV-Vis absorption spectra of DECET in acetonitrile at various concentrations used to calculate extinction coefficients for molecular transitions.

The extinction coefficients for the π → π* and n → π* molecular transitions were determined from Figure A17 and Figure A18. The results are summarised in Table A8. The ± 1nm deviation in peak maxima and differences in extinction coefficients for both transitions most likely arise from solvent interactions.

Table A8: Molecular transitions and extinction coefficients determined for PXEP and DECET.

Transition	RAFT agent	Peak (nm)	Extinction coefficient (M^{-1} cm^{-1})	Solvent
n → π*	PXEP	370	59.66	Acetonitrile
n → π*	DECET	432	40.99	Acetonitrile
n → π*	DECET	433	45.19	Toluene
π → π*	DECET	305	15870.87	Acetonitrile
π → π*	DECET	307	16757.93	Toluene

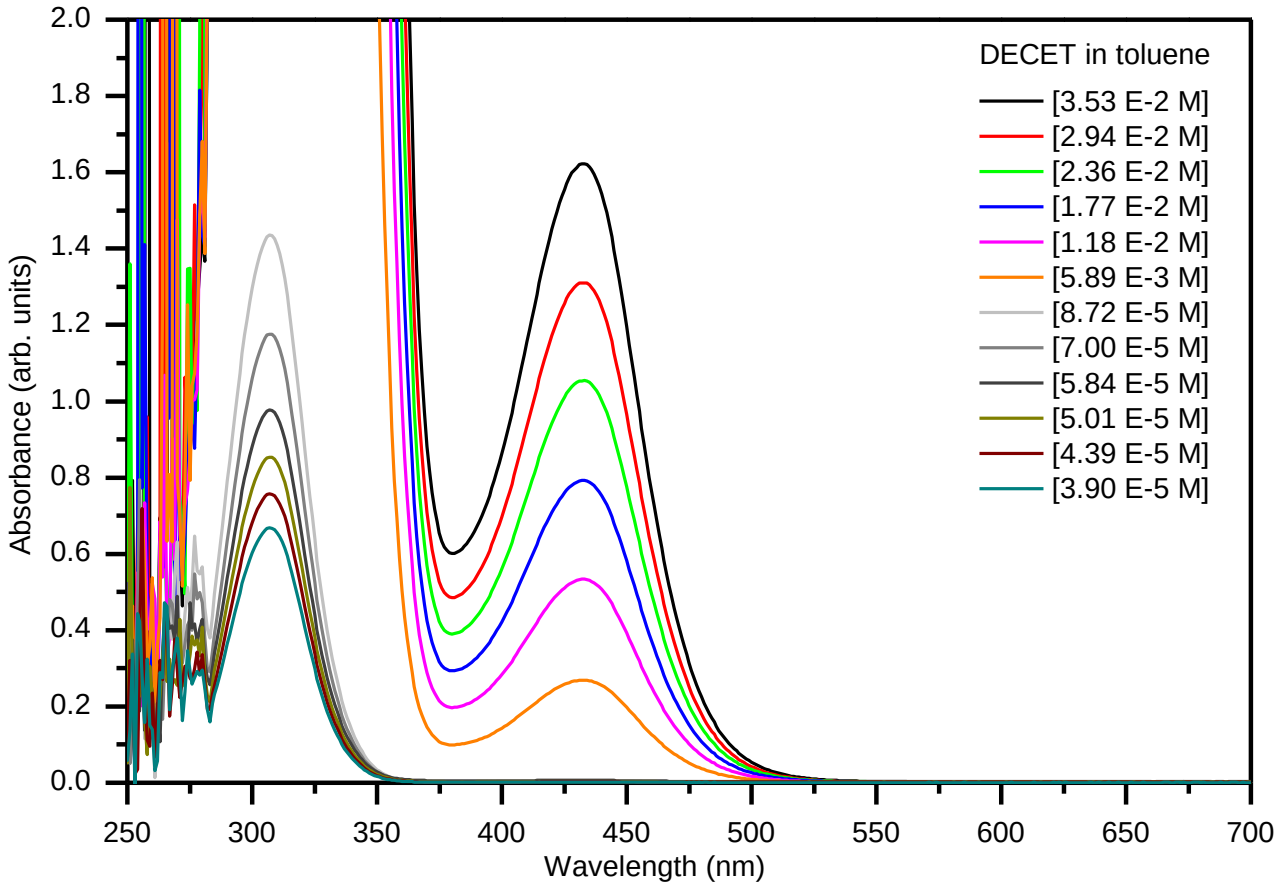

Figure A18: UV-Vis absorption spectra of DECET in toluene at various concentrations used to calculate extinction coefficients for molecular transitions.

Table A9: Summary of control experiments conducted with 470 nm LED reactor; temperature ~ 25 °C, reaction time = 12 h.

Entry	Monomer	[Monomer] (% v/v)	% conv. by ^{1}H NMR	M_n (g mol^{-1})	M_w (g mol^{-1})	Đ
1	MMA	50.03	0	N/A	N/A	N/A
2	Sty	50.04	0	425800	846900	1.99
3	MA	50.18	0.95	1519500	2408500	1.58
4	VAc	50.11	0.30	N/A	N/A	N/A

A1.4 References

1. *3528 SMD LED* 2011, ShenZhen Wayjun Technology Co., LTD. p. 1-11.